医療福祉機器技術
Ｅ－０７２

平成７年度
新エネルギー・産業技術総合開発機構
提案公募型・最先端分野研究開発事業
研究成果報告書

神経機能材料開発に関する基盤研究

平成９年３月

大阪工業技術研究所

010010678-0

医療福祉機器技術
Ｅ－０７２

平成７年度
新エネルギー・産業技術総合開発機構
提案公募型・最先端分野研究開発事業
研究成果報告書

神経機能材料開発に関する基盤研究

1998. 6. 25

平成９年３月

大阪工業技術研究所

（様式－２）

平成７年度　新エネルギー・産業技術総合開発機構委託業務　研究成果報告書概要

作成年月日	平成９年３月３１日
分野／ プロジェクト番号	分野：医療福祉機器分野　　番号：Ｅ－０７２
研究機関名	通商産業省　工業技術院　大阪工業技術研究所
代表者部署・役職	有機機能材料部　高分子表面化学研究室　室長
代表者氏名	田口　隆久 田口
プロジェクト名	神経機能材料開発のための基盤研究
研究期間	平成７年１１月１日 ～ 平成９年３月３１日
研究の目的	脳神経系の修復・代替を目指す人工神経の開発は、急速な高齢化の進行する我が国の緊急かつ重要な最先端研究課題である。本研究においては、次の３課題に焦点を合わせ、神経機能材料開発のための基盤研究を行う。第１課題は、神経繊維伸長活性を持つ蛋白質の機能部位解明、第２課題は、シナプス伝達機能制御に関与する分子群の解明、第３課題は、人工デバイスと脳神経細胞の界面調製とする。
成果の要旨	第１課題では、新規神経繊維伸長活性因子の発見と遺伝子クローニングに成功し、この因子の機能部位を解明した。第２課題では、活動依存的シナプス形成機構の解析し、さらに長期的増強現象のin vitro解析を試み、この現象を誘導する因子の存在を発見した。また、このような現象に並行する、シナプス活動に伴う神経細胞形態変化を見出した。さらに、神経機能制御分子の海洋微生物ライブラリーからのスクリーニングを行うとともに材料化に寄与する光制御ペプチド機能材料の開発に成功した。第３課題では、リソグラフィー技術を用いたパターニングとこれを用いた細胞接着性制御に成功した。
成果発表・特許等の状況	本研究の成果は、２３件の論文発表、２８件の口頭発表によって広く公開された。また、１件の特許を申請中である。
今後の予定	本研究の成果をもとに提案した、平成９年度通産省工業技術院産業科学技術先導研究「脳神経細胞工学の基盤研究」が採択されたので、この研究を通じてより応用に近づく技術開発を進めて行く。

（様式－３）

Summary of New Energy and Industrial Technology Development Organization Entrusted R&D Report for FY 1996

Date of preparation	31, March 1997
Field/ Project number	Field/ Medical and welfare equipment Technology E－０７２
Research organization	Osaka National Research Institute Agency of Industrial Science and Technology Ministry of International Trade and Industry
Post of the research coordinator	Department of Organic Materials Polymer Surface chemistry Section
Name of the research coordinator	Takahisa TAGUCHI (signature) T. Taguchi
Title of the project	Basic research for neuroactive materials
Duration of the project	November 1, 1995 ～ March 31, 1997
Purpose of the project	Development of neuroacitive materials to improve neuronal defects is one of the most important subjects in Japan that will soon become a aging society. In this project, basic research for neuroactive molecule was perfomed to develop technology for neuronal regeneration, regulation of synaptic activity and interface between artificial surface and living neurons.
Summary of the results	A novel neurite promoting factor was discoverd and its cDNA was cloned. Mutagenesis in vitro showed that a functional region of this factor located in a polypeptide of less than 50 aminoacids. Using neuronal culture, synapse formation was found to depend on two modes of activities and long-lasting synaptic potentiation was demonstrated to depend on a macromolecules released from pre- or postsynaptic neurons. To regulate nervous activities, photoactivated caged-peptide was developed and confirmed to change in affinity to its receptor. Neurons were cultured on substrates paterned by microlithography..
Publication,patents, etc.	The results were open as 23 papers and 26 oral presentation One patent was applied.
Future plans	The leading research for neurotechnology that had been planed based on the results of this project, started in FY 1997 to develop advanced neuronal engineering and neuroactive materials.

まえがき

医療福祉分野における重点課題となっている各種人工臓器開発の中で人工神経開発は、他の人工臓器の場合に較べ大きく様相が異なる。すなわち、人工神経の場合には、一個の細胞が機能ユニットであり、かつ、複数の神経細胞からなるのネットワークの中ではじめて神経機能が発現する、という二重性を克服しなければならない。このことは、単一細胞での構造機能解析と細胞間情報伝達システム、すなわち、シナプスの構造機能解析の両者から得られる分子メカニズムをもとに、その機能を代行できるシステムの構築とそれを実現する神経機能材料開発を行う必要があることを意味している。

一方、我が国社会の高齢化が２０１５年にピークを迎えることは周知の事実であり、このような状況に対応するための様々な角度からの方策を立案・実施することは、優先度の高い緊急の課題である。

この様な状況を勘案し、本研究においては、人工神経開発を最終的目標とし、それに近づくための神経機能材料開発に関する基盤研究を緊急に開始することを目的とする。広範な分野を含むこの分野の研究開発の推進するための先導的役割を担う本プロジェクトにおいては、神経機能の修復・代替機能を持つ機能性材料の創製のための基盤研究を次の３課題に絞り集中的な研究を遂行した。

第一の課題は、神経修復材料の開発を目指した、神経繊維伸長を促進する材料開発のための基盤研究である。中枢神経系の細胞は、発生後の再生・増殖は困難であり、この事実が神経系の疾患・障害からの回復を困難にしてきた。しかしながら、神経系は、発生過程においては、細胞増殖を繰り返し、神経繊維を伸長させて神経回路網を形成する能力を有している。また、最近の研究から、生後の中枢神経の再生も困難ではあるが不可能ではないことが示されている。本プロジェクトの提案者によるこれまでの研究から、除神経筋の抽出液中に中枢神経の神経繊維伸長を促進する蛋白質が存在することが明らかになっている。本課題においては、その蛋白質の構造解析を分子生物学的手法で行い、さらに、機能に必須な部位を解明し、その部分をペプチド化するこにより低分子化し、人工神経開発のための材料としての応用可能性を確立することを目指したものである。

第二の課題は、神経活動賦活化材料の開発を目指した、シナプス伝達効率を制御する材料開発のための基盤研究である。大脳皮質や海馬等で解析が進んでいる長期増強現象のようなシナプス伝達効率の変化は脳神経系の機能、特に記憶・学習等の高次機能、の発現に必須のメカニズムと考えられおり、最近で

は分子生物学の進歩とも相まって物質的基盤の解明も進んできた。本課題は、培養神経細胞を用いてシナプス伝達効率変化を解析し、これに関与する新規シナプス伝達制御分子の同定・構造解析を試みる。機能分子を材料化する際に重要になる分子の機能発現制御手法の研究も行い材料開発の基盤を確立する。さらに、シナプス部位内部での情報伝達過程を解析することによりさらに多様な制御原理の開発を目指したものである。

　第三の課題は、神経機能の代替・修復を行う、生体内神経組織に導入可能な電子デバイスの開発を目指した、神経細胞と人工基板とのインターフェース材料開発のための基盤研究である。主にマイクロリソグラフィーの手法を応用し、人工基板の神経細胞との適合性と基板上のパターニング手法を検討し、よい結果を得られた材料を用いて神経活動モニター機能と神経細胞刺激機能を組み込んだ基板の開発へつなぐ研究を目指したものである。

（次ページの補足説明図参照）

ＮＥＤＯ提案公募型・最先端分野研究開発プロジェクト

神経機能材料開発のための基盤研究

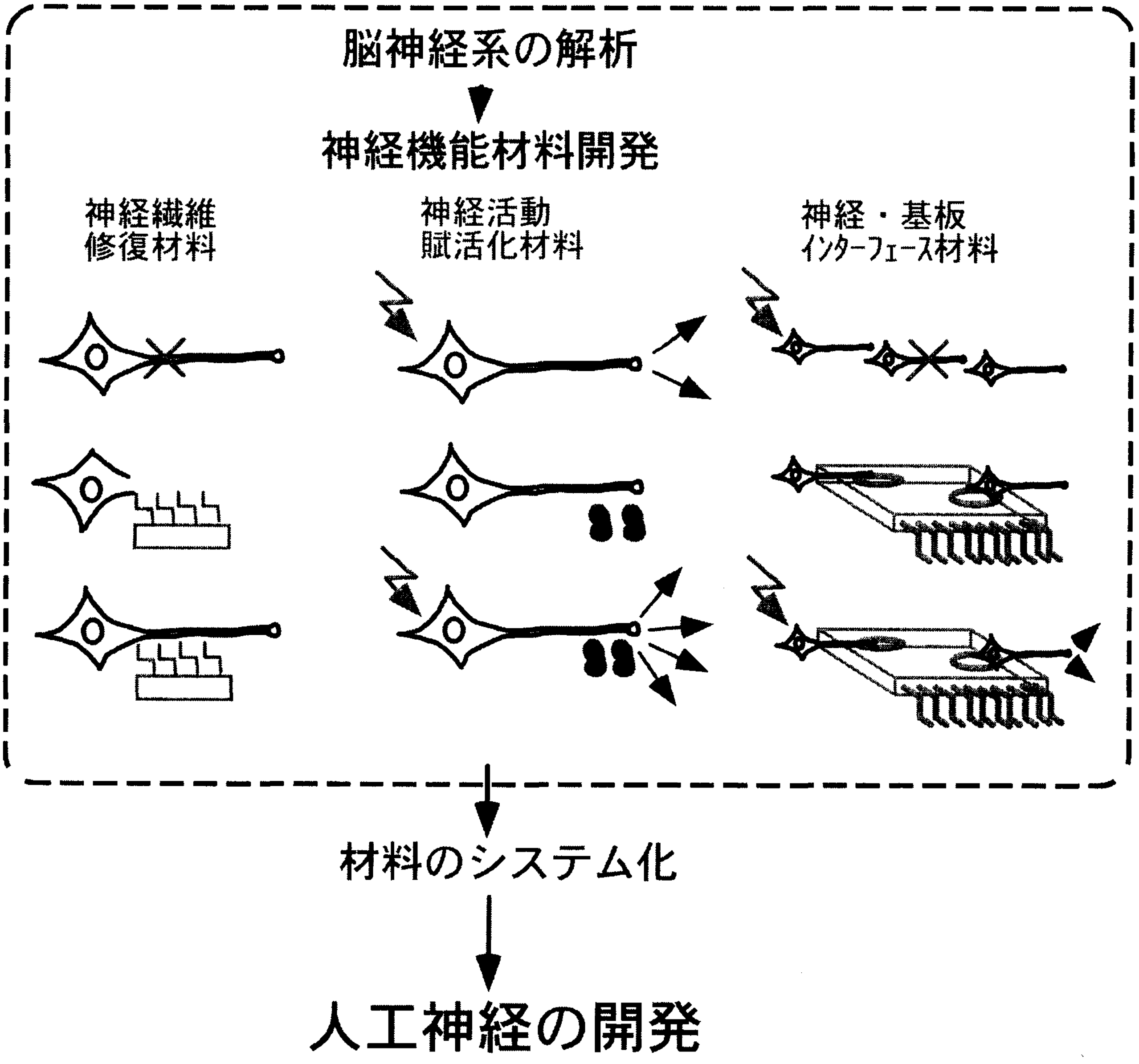

脳神経系の解析

神経機能材料開発

神経繊維
修復材料

神経活動
賦活化材料

神経・基板
インターフェース材料

材料のシステム化

人工神経の開発

研究チーム名簿

研究代表者　田口隆久　通商産業省工業技術院大阪工業技術研究所
有機機能材料部高分子表面化学研究室・室長

共同研究参加研究者

大阪工業技術研究所側

田口隆久	有機機能材料部高分子表面化学研究室
湯元　昇	有機機能材料部生体分子工学研究室
茂里　康	有機機能材料部生体分子工学研究室
田中孝治	材料物理部セラミック材料研究室

ＮＥＤＯ派遣研究員

岡本賢一	平成７年１１月１日～平成８年９月３０日
エレナ・イワノバ	平成７年１２月１日～平成９年３月３１日
谷口弘志	平成８年１月１日～平成９年３月３１日
上垣浩一	平成８年４月１日～平成８年９月３０日
吉田邦人	平成８年１０月１日～平成９年３月３１日
清水まゆみ	平成８年１０月２１日～平成９年３月３１日

目　次

ページ

表紙 …… 1

概要（和文） …… 2

概要（英文） …… 3

まえがき …… 4

目次 …… 8

第１章　神経修復材料 …… 9

- １－１　神経繊維伸長活性を有する新規蛋白質の発見 …… 9
- １－２　神経繊維伸長蛋白質のcDNAクローニング …… 13
- １－３　神経繊維伸長蛋白質の活性部位解析 …… 16

第２章　神経活動賦活化材料 …… 19

- ２－１　活動依存的シナプス形成の解析 …… 19
- ２－２　サイレントシナプスの発見とシナプス成熟過程解析　24
- ２－３　長期的増強現象の in vitro 解析 …… 34
- ２－４　長期的増強を誘導する分子の発見 …… 43
- ２－５　シナプス活動に伴う神経細胞形態変化の解析 …… 47
- ２－６　神経機能制御分子の解析　59
- ２－７　神経機能制御分子の海洋微生物ライブラリーからのスクリーニング …… 63
- ２－８　光制御ペプチド機能材料の開発 …… 67

第３章　神経細胞人工基板インターフェース材料 …… 71

- ３－１　リソグラフィー技術を用いたパターニングと培養神経細胞接着性制御 …… 71
- ３－２　培養基板表面処理による微生物物質生産制御 …… 76

第４章　結論と今後の予定 …… 78

第５章　成果発表 …… 83

第６章　購入機器一覧 …… 92

あとがき …… 94

添付資料 …… 95

第１章　神経修復材料

１－１　神経繊維伸長活性を有する新規蛋白質の発見

標的組織由来の神経栄養因子として，運動神経細胞に作用する骨格筋由来の神経繊維誘導因子の存在が古くから予測されていたが，その同定はいまだなされていなかった。Hendersonらにより，胚時期のニワトリ骨格筋細胞を用いて条件付けした培養液中に神経繊維伸長促進活性が存在することが，脊髄神経細胞の初代解離培養系を用いて示された。さらに、彼らは，ヒヨコの座骨神経を除神経すると，その神経に支配されていた下腿部骨格筋の抽出液に含まれる神経繊維伸長促進活性が上昇することを示した。一方、田口らにより，この除神経筋抽出液にはニワトリ胚由来の脳神経細胞に対しても繊維誘導活性が存在することが示された。注目すべき点は，この誘導活性が終脳神経細胞に対して特異的に観察された点である。

まず、この除神経筋由来の因子の特性解析を行った。神経繊維伸長活性を持つ蛋白質は３種類に分類される。すなわち、神経栄養因子のような拡散性の分子、ラミニンのような細胞外マトリックス結合性分子、イムノグロブリンスーパーファミリーのような膜蛋白質である。本研究の対象は筋抽出液であるため、３番目の可能性は除外される。拡散性分子と結合性分子の可能性について、培養神経細胞系を用い検討した。図１に示したように、除神経筋抽出液に含まれる活性因子は、培養基質接着性の分子であり、さらに興味深いことに、この因子は培養細胞添加以前に培養基質に接着していることが機能発現に必要である。すなわち、神経細胞が培養基質に付着した後にこの因子を培養液中に加えても効果がないと言うことである。我々が注目している神経突起伸長活性を担う分子に基質接着性を有することは、この分子の解析に大変有利である。この点を

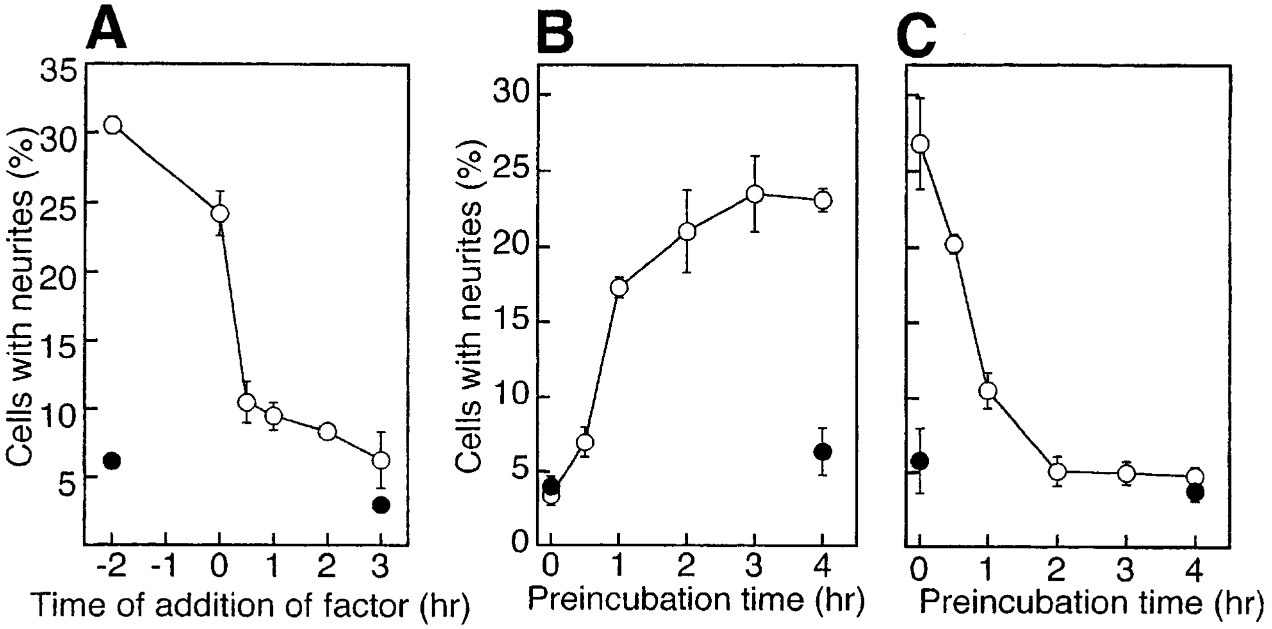

図１　神経繊維伸長活性を担う分子の培養基質接着性

Ａ：分子の添加時期と細胞添加時期（ｔ＝０）の関係

Ｂ：培養前処理の影響（培養基質）、Ｃ：培養善処理の影響（培養液）

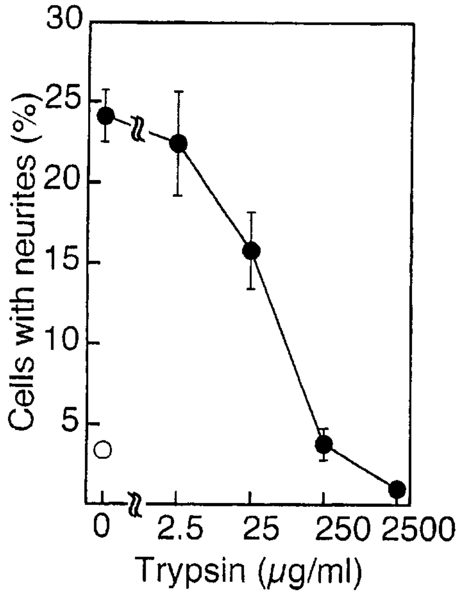

図２　トリプシン処理の神経繊維伸長活性への影響

生かしてこの分子が糖蛋白質であることを明らかにした。図２に示したように、培養皿に接着させた抽出液をプロテアーゼで処理すると、神経繊維伸長活性がなくなった。さらに、糖に結合するレクチンの一種であるコンカナバリンＡを培養基質に接着した分子に結合させると活性が阻害され、接合部位特異的な糖でこの結合を切り離すと活性が回復した。この結果は、我々が注目している活性を担う分子が糖鎖を持った蛋白質であることを示している。糖蛋白質、あるいは、糖蛋白質部分は細胞外に存在するため、目的の蛋白質が細胞外に分泌されていることが強く示唆された。（図３参照）

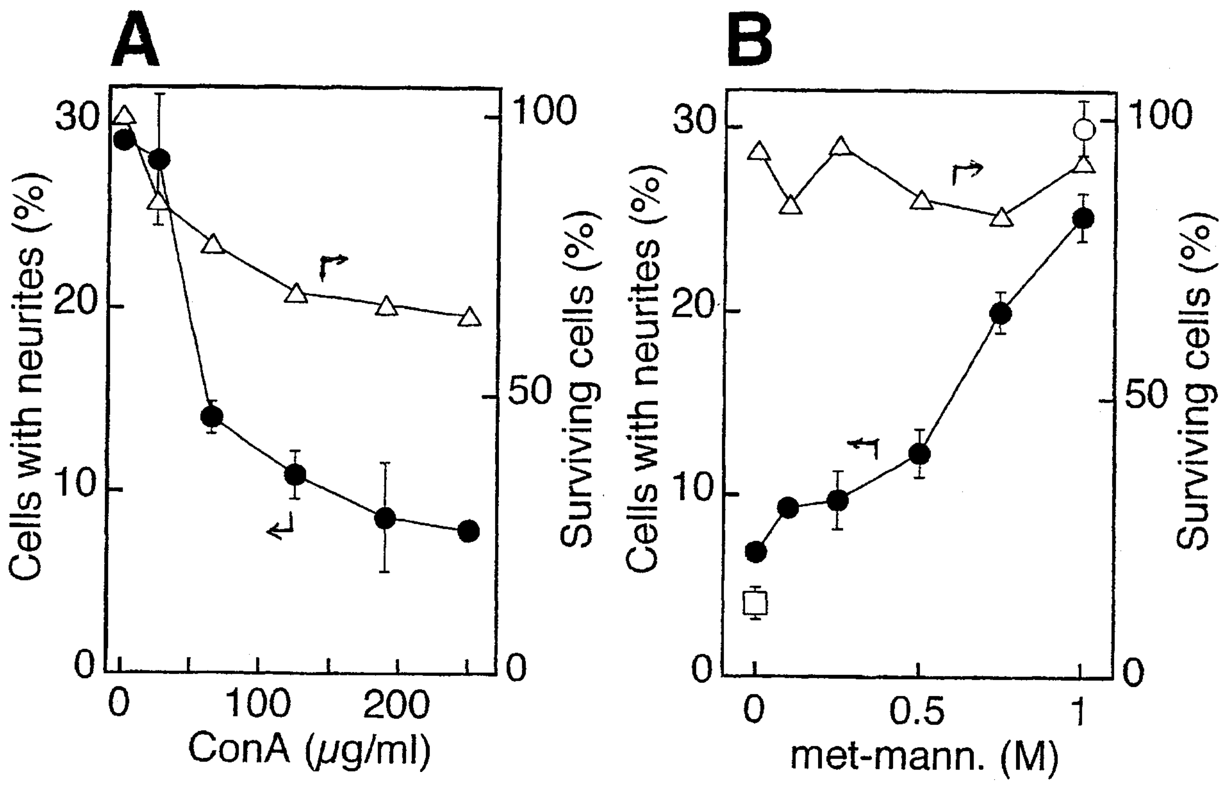

図３　レクチン処理の神経繊維伸長活性への影響

Ａ：コンカナバリンＡ処理の影響

Ｂ：コンカナバリンＡの効果のαメチルマンノシドによる阻害

さらに、この分子を同定・解析するために、神経繊維伸長活性を阻害するモノクローナル抗体の調製を行った。部分精製した除神経筋抽出液蛋白質を抗原とてマウスを免疫し、その脾臓細胞からハイブリドーマを調製し、活性阻害を指標にスクリーニングを行ったところ５種類のクローンが得られた（図４）。その中でも、4D2a と命名された抗体が最も阻害効果が顕著であった。

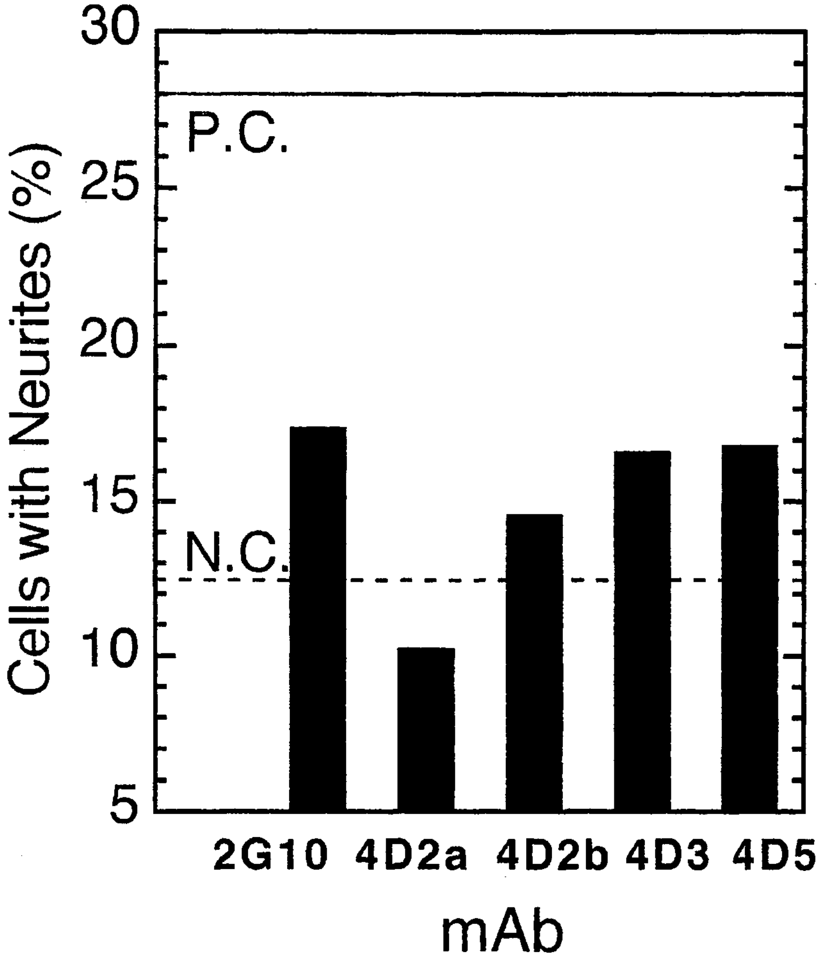

図４　モノクローナル抗体による神経繊維伸長活性阻害

１－３　神経繊維伸長蛋白質の活性部位解析

クローニングしたニューロクレシン cDNA から大腸菌で発現させた組換え蛋白質の神経突起誘導活性は，ニワトリ胚脳神経系の初代解離培養系において終脳特異的に観察される（図８）。

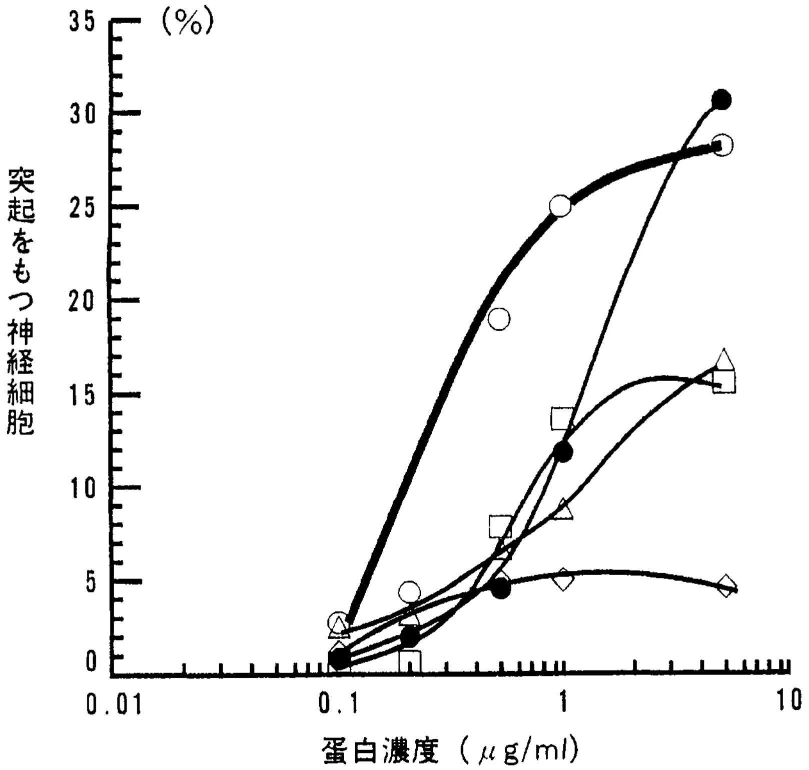

図８　組換えニューロクレシン活性の脳領野特異性

○：終脳、　●：筋抽出液の終脳細胞への影響　□：菱脳　△：間脳

◇：中脳

この活性はカルボキシル末端（Ｃ末端）30kD 領域だけを発現させた場合にも観察され，突起伸長活性に必須な領域はＣ末端に近い部分にあると考えられる。また、大腸菌で発現させた組換え蛋白質にも活性があることから、この活性に糖鎖は必須でないと言うことができる。したがって、限定された部位のアミノ酸配列が活性に重要である。

そこで、活性に必須なアミノ酸配列を検索する目的で、cDNA に人工突然変異を導入した。適当な位置の制限酵素切断による欠損突然変異体 cDNA の作製と適当なＰＣＲプライマーによる欠損変異体増幅 cDNA の作製とそれらのベクターへの組み込み・蛋白発現によって変異体蛋白質を得た。それらの蛋白質の神経突起伸長活性をニワトリ胚終脳神経細胞培養系でアッセイした。それらの

結果をまとめたのが図９である。１１種類の人工変異体を調製し、それぞれに対応する組換え蛋白質を発現し、精製した。この組換え蛋白質はグルタチオン－Ｓ－トランスフェラーゼとの融合蛋白質として発現されるため、グルタチオンを結合させたアフィニティークロマトグラフィーカラムで精製することができる。それぞれの蛋白質の神経繊維伸長活性を調べたところ、図９の塗りつぶし棒で示した変異体には活性があり、縦縞の棒には活性がなかった。それぞれの欠損部位が対応するようにならべると、核酸の番号で１８４１～１９２１の部位が欠損すると活性を失うと考えられる。この長さは、アミノ酸に換算すると２６残基となり、人工合成可能なペプチドの長さにまで活性部位を絞り込むことができた。

残念ながら、人工合成したこのアミノ酸は培養基質への接着が難しく、直接的な活性部位の証明はまだできていない。

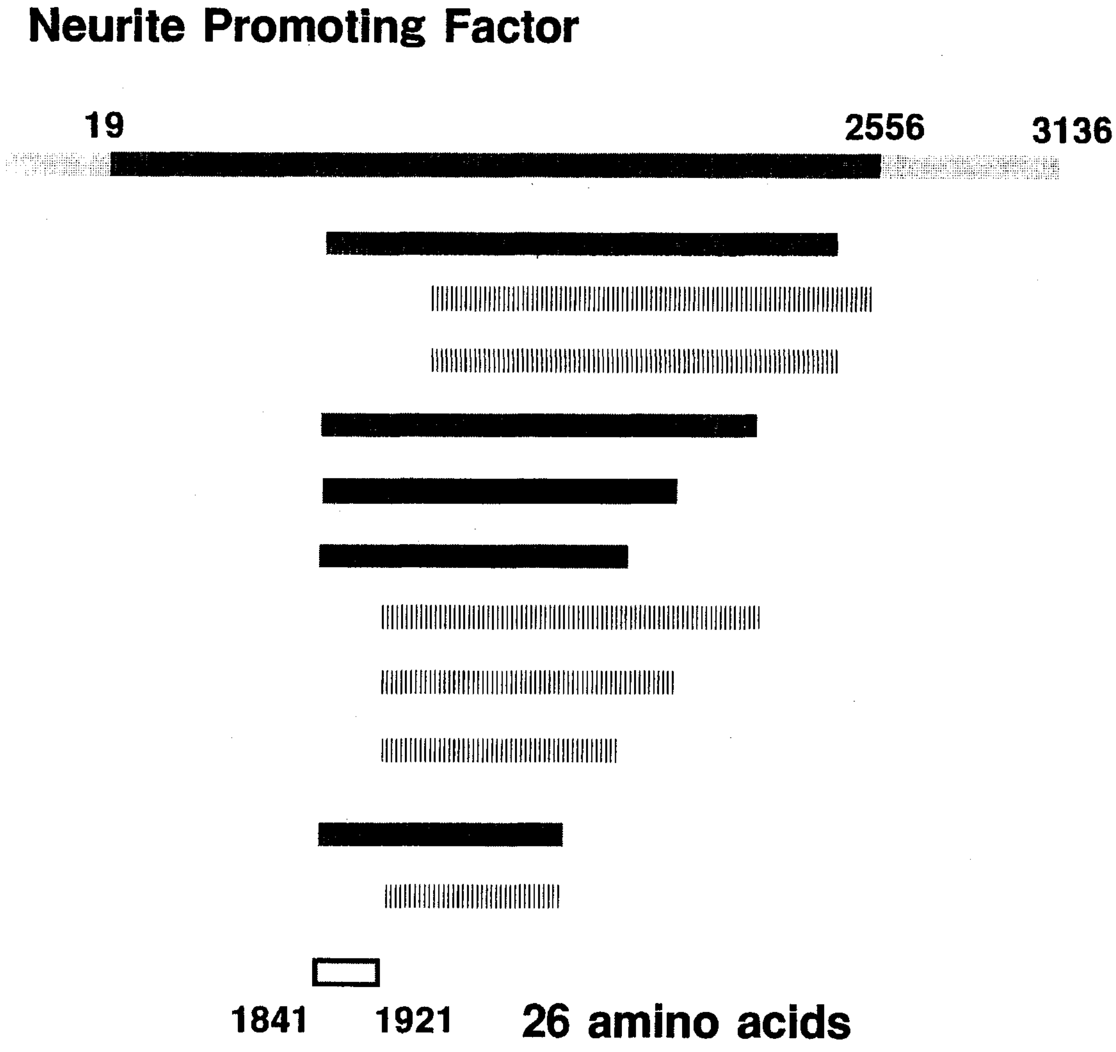
Neurite Promoting Factor
19
2556
3136
1841
1921
26 amino acids

図９　ニューロクレシンの活性部位検索
塗りつぶした領域が活性のあった変異蛋白、縦縞の領域が活性のなかった変異蛋白

第２章　神経活動賦活化材料

２－１　活動依存的シナプス形成の解析

神経細胞は、発生の過程で増殖を終えたあと適当な場所に移動し、分化してシナプス形成を行う。このシナプス形成によって初めて脳神経回路網が形成される。シナプス形成過程を詳細に追跡し解析するためには、脳組織そのものを使うことは困難である。そこで、我々は大脳神経細胞の解離培養系を開発し、これを用いてシナプス形成過程を解析してきた。これまでに、ニワトリ胚大脳神経細胞を用いたこの培養系において、胚令等価日数、すなわち、胚令と培養日数を合計した値、にしたがってシナプス形成が進行することを示した。このことは、培養系という人工的な環境に大脳神経細胞を移しても細胞の発生プログラムは同じ時計にしたがって進むことを示唆しており、この系が発生過程の解析に適していることを示している。この培養系においては、胚令１０日の神経細胞を用いた場合、培養３日目からシナプス形成が始まり、培養７日目にかけてシナプス入力頻度とシナプス入力振幅が急速に増加する。この過程はシナプス部位の成熟過程と見なすことができるため、この過程に対する神経細胞自身の活動の重要性が示唆される。このような活動を解析することは、その活動によって変化する分子群の解析につながり、この成果はシナプス形成制御に関与する機能分子の同定に直結するものと期待される。

シナプスは神経細胞の形成する回路網における情報伝達において本質的役割を果たす。このシナプスにおける神経伝達物質を介した情報伝達効率の制御が、脳の高次機能の発現に寄与していると考えられている。この効率制御機構についてはいくつかの提案があるが、確定したものはない。したがって、この機構の解明とそれに続く機能分子の解明は、シナプス伝達制御を通じた神経機能材料

の開発に結びつく。本章の神経賦活化材料もそのひとつである。

本項目では、シナプス形成機構とシナプス伝達効率制御機構の類似性に着目し、シナプス形成機構の解析から機能分子の同定に資する情報を得るための研究を行った。前述した急速なシナプス形成期（培養５日目から７日目）における神経活動依存的シナプス伝達増強の解析を実施した。培養系はニワトリ胚（胚令１０日）の大脳神経細胞を用い、パッチクランプ法により誘起シナプス後電流値を測定した。培養日数５－７の間、神経活動を抑制する薬剤、テトロドトキシン（ＴＴＸ）とシアノニトロキノキサリンディオン（ＣＮＱＸ）を培地に加えシナプス形成に対する影響を解析した。前者は神経軸索のナトリウムイオンチャネルを阻害し、後者はシナプス後膜に存在するグルタミン酸受容体に拮抗する。したがって、ＴＴＸは神経軸索の伝導を阻害し、ＣＮＱＸはシナプス伝達を阻害する。言い換えれば、後者は非ＮＭＤＡ型受容体を介したすべてのシナプス伝達を遮断するのに対し、前者は伝導に伴わないシナプス伝達物質（グルタミン酸）放出によるシナプス伝達は阻害しない。

この２種類の薬剤で処理すると、対照群に比較し誘起シナプス後電流の増大が有意に抑制された。さらに、抑制の程度は、ＴＴＸで阻害した場合に較べ、ＣＮＱＸの場合の方が顕著であった（図１０）。

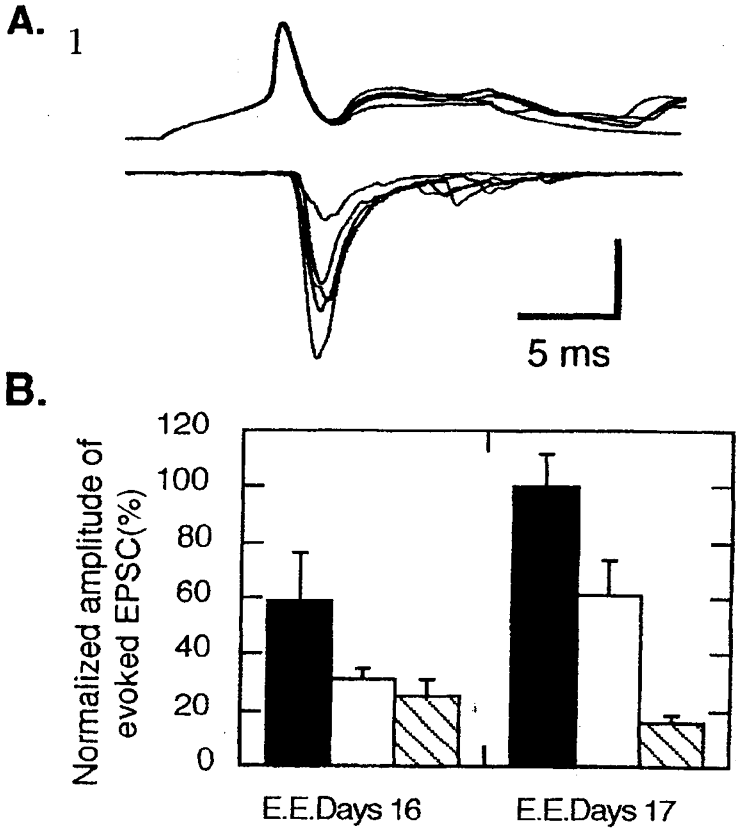

図１０　活動を阻害した時の誘起シナプス後電流の大きさ

Ａ：電流波形の例、Ｂ：クロは対照実験、白はＴＴＸ添加、斜線はＣＮＱＸ添加、E.E.Days 16,17 はそれぞれ培養６日目と７日目を示す。

対照群、ＴＴＸ処理、ＣＮＱＸ処理のそれぞれのシナプス後電流の波形を詳細に調べると、波形の大きさは変化しても形そのものは変わらない、すなわち、波形は相似形になっていることを明らかにした。より定量的に解析するために、各波形の上昇時定数と下降時定数を計測し比較したが、有意な差は認められなかった（図１１）。この結果は、シナプス伝達効率の上昇がシナプス後膜に存在する受容体の種類の変化によるものではないことを示している。もし、シナプス後膜の受容体の種類が変化しチャネル特性が変わればこれらの値に変化が生じるはずである。また、シナプス小胞内の神経伝達物質の濃度の変化、あるいは、一度に放出されるシナプス小胞の個数の変化によってシナプス前膜から放出される伝達物質密度の時間変化が変わった場合にもこれらの値に影響が出るため、この結果はシナプス前膜のこの様な変化の可能性も否定している。

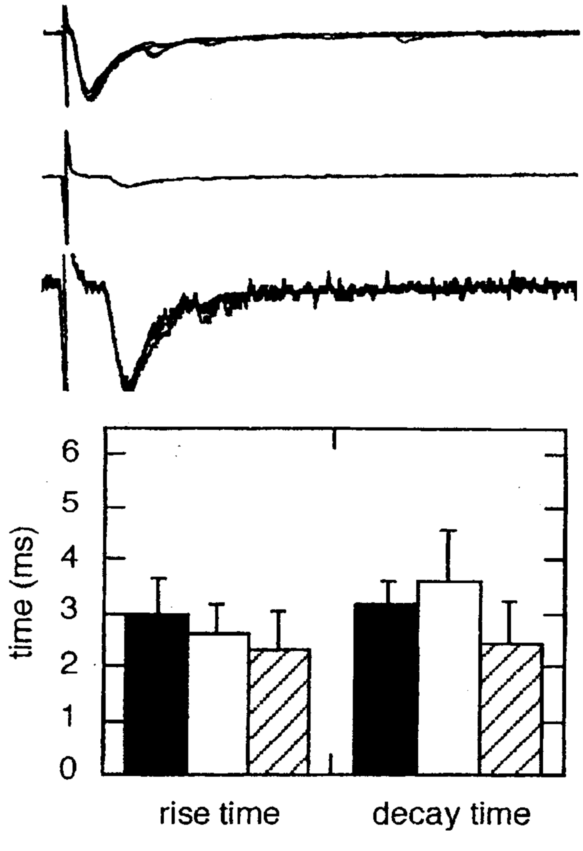

図１１　誘起シナプス後電流の波形解析

一番上のトレース：対照実験、中段のトレース：阻害後の電流、下段のトレース：中段のトレースの縦軸を拡大した図、グラフ：各波形の上昇、下降時定数、クロ；対照実験、白；ＴＴＸ添加、斜線；ＣＮＱＸ添加

図１０の結果に示された、ＴＴＸとＣＮＱＸの阻害効果の差は何に起因するのであろうか。この点を解明するために、微小シナプス後電流の大きさの変化について検討を加えた。その結果、対照群に較べると両者とも減少したが、両者の差は有意ではなかった（図１２）。

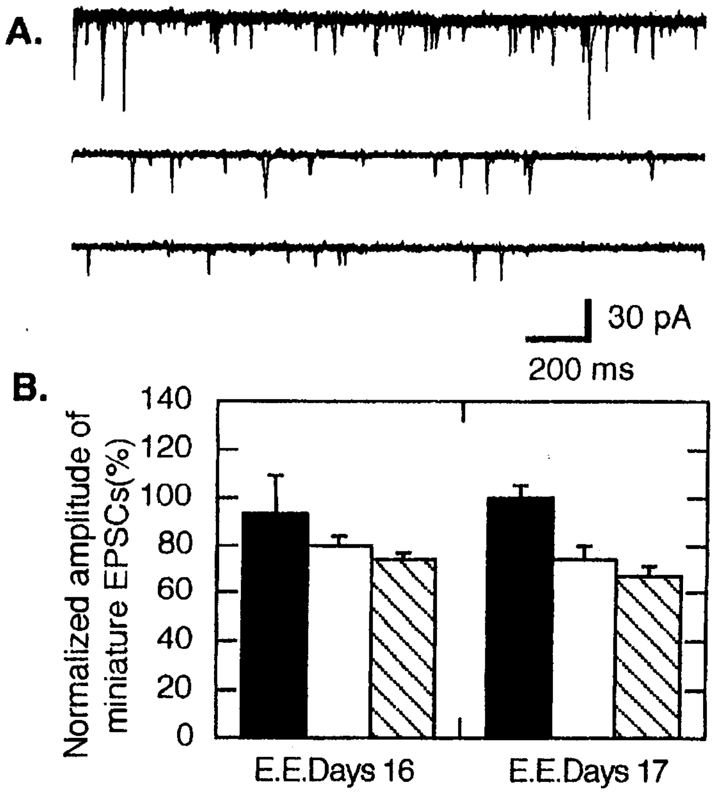

図１２　微小シナプス後電流の解析
トレースの例（上；対照、中；ＴＴＸ、下；ＣＮＱＸ）
グラフ：微小シナプス後電流の大きさの解析（クロ；対照実験、白；ＴＴＸ添加、斜線；ＣＮＱＸ添加）

この微小シナプス後電流は、シナプス前膜より偶発的に放出される１個のシナプス小胞に含まれる神経伝達物質により誘起されるシナプス電流である。したがって、個々のシナプス部位における機能、すなわち、シナプス前膜からの伝達物質放出機構やシナプス後膜上の受容体機能は、両阻害剤処理で差がないということである。

図１０と１２に示された、シナプス形成過程における活動依存性の差はどのように解釈できるのであろうか。我々は、図１３にしめした新しい解釈で統一的な理解が可能であることを示した。すなわち、ひとつの神経細胞からもう一つに神経軸索が伸びてシナプスを作る場合、局所的に観察すると、シナプス部位は、最小単位のシナプス伝達機構を有するユニットが複数個集まって形成されており、個々のユニットの機構の成熟とユニットの個数の増加は別のメカニ

ズムに支配されている。ここで、ＴＴＸに感受性のある神経活動は前者の成熟機構に関与し、ＣＮＱＸに感受性のある神経活動は、さらに、後者の個数の増加機構にも関与している。このように考えると、上記の実験事実を矛盾なく説明できる。ここでのべたユニットをシナプス接点（ synaptic contact ）と呼ぶことも提唱している。この考え方を図１３に示した。ＴＴＸに阻害されず、ＣＮＱＸに阻害される活動が、シナプス接点の数の増加に寄与すると結論される。このような活動の例として、自発的シナプス伝達があるが、この現象がどのような経路で接点数増加につながるか、は今後の課題である。このメカニズムが解明されれば、シナプス活動制御の新しい手法やそのための神経機能材料の開発にすぐに結びつくことが期待されている。

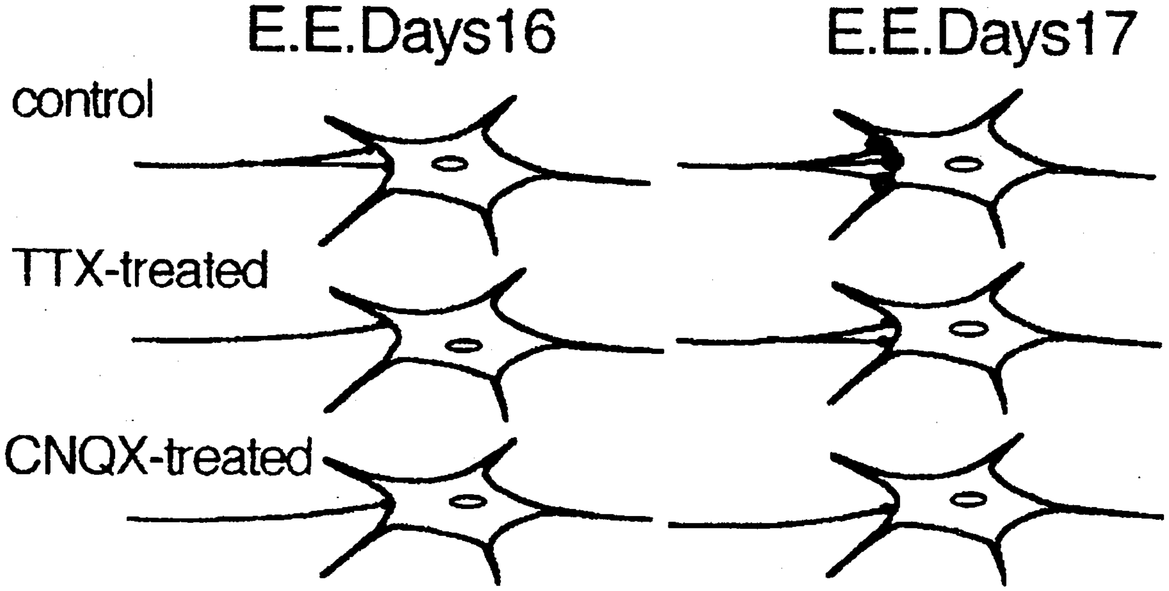
E.E.Days16
E.E.Days17
control
TTX-treated
CNQX-treated

図１３　神経活動依存的シナプス形成の説明図

２－２　サイレントシナプスの発見とシナプス成熟過程解析

我々が開発したニワトリ胚大脳神経細胞培養系においては、興奮性と抑制性の両方のシナプスが観察されている。前者はグルタミン酸、後者はガンマアミノ酪酸（ＧＡＢＡ）を神経伝達物質としている。脳内の情報処理においてはグルタミン酸受容体の関与するシナプスが重要な働きをしているが、このこのタイプのシナプスにも多様性がある。グルタミン酸受容体には、大別すると、３種類、すなわち、ＮＭＤＡ型受容体、ＡＭＰＡ型受容体、代謝型受容体が知られている。前２者は、グルタミン酸を受容すると受容体内部に存在するイオンチャネルを開き細胞を脱分極させる働きをする受容体である。最近、ひとつのシナプスにこのＮＭＤＡ型受容体とＡＭＰＡ型受容体の両者が存在するデュアルコンポーネントシナプス（ＤＣシナプス）があり、これがシナプス機能に重要な働きがあるという見方が出てきた。我々の培養神経細胞においてはＡＭＰＡ型受容体のシナプスは確認されていたが、このＤＣシナプスの存在は未確認であった。

ニワトリ胚（胚令１０日）から調製した大脳神経細胞を７日間培養した系においてホールセルパッチクランプ法を用いてシナプス電流を記録・解析した。静止膜電位に近いマイナス６０ｍＶで自発性興奮性シナプス後電流（ｓＥＰＳＣ）を測定すると、鋭いピークの内向き電流が観察された。これまでの解析からこれはＡＭＰＡ型受容体を介した電流である（図１４）。

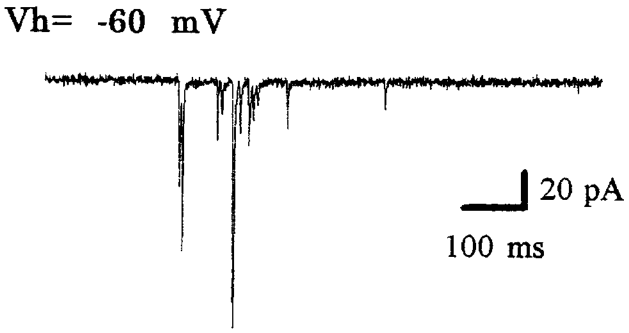

図１４　自発性シナプス後電流波形

次に、固定膜電位をプラス６０ｍＶにして記録を取ると、逆転電位の関係で今度は外向き電流が記録される。もしＡＭＰＡ型受容体だけがシナプスに存在するなら、図１４とミラーイメージになる鋭いピークのｓＥＰＳＣが記録されるはずであるが、実際はピークの立ち上がりは鋭いにもかかわらず下降相は緩やかなカーブを描いた（図１５上）。これはＡＭＰＡ型受容体以外の受容体の存在を示唆しており、この特性からＮＭＤＡ型受容体の共存が示唆される。ＮＭＤＡ型受容体に対する特異的アンタゴニストであるＡＰ５を作用させると、予想通り緩やかな下降相が消え、鋭いピークが現れた（図１５下）。これらの結果は、我々の培養系の興奮性シナプスはＤＣシナプスであることを示している。このことを確認するために誘起興奮性シナプス後電流を記録し解析した（図１６）。黒丸で示した値がＮＭＤＡ型受容体による誘起興奮性シナプス後電流であるが、マイナスの膜電位での阻害というこの受容体の特性が現れている。この抑制は、細胞外マグネシウムイオンのチャネル阻害効果に起因する。

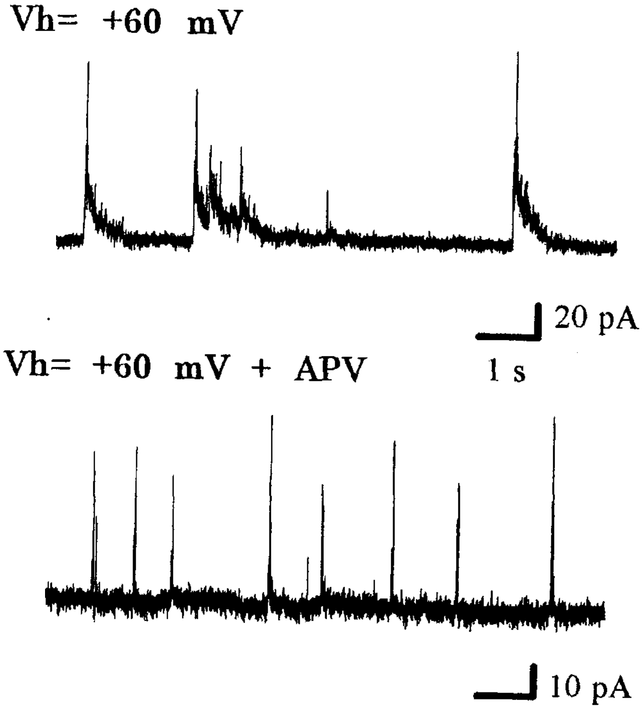

図１５　脱分極下での自発性シナプス後電流波形

図１５からも推測されるようにほぼすべてのシナプスがＤＣシナプスである。しかし、前項で述べたように、シナプス部位は複数のシナプス接点から構成されると考えられる。ｓＥＰＳＣや誘起興奮性シナプス後電流の記録では、ひとつのシナプス前細胞からの入力はすべて同時に合算して記録されるため、ＡＭＰＡ型受容体とＮＭＤＡ型受容体とが同一接点に存在するのか、それぞれ別個の接点に存在するのか、は区別がつかない。そこで微小興奮性シナプス後電流（ｍＥＰＳＣ）の解析を行った（図１７）。この手法で記録されるひとつのｍＥＰＳＣはひとつの接点に対応する。測定はすべて膜電位をマイナス６０ｍＶに固定して行った。通常はこの条件ではＮＭＤＡ型受容体を通る電流は記録できないが、細胞外マグネシウムイオンを除いてこれを可能にした。早い初期下降相と早い後半の上昇相が認められる対照実験結果に対し、マグネシウムイオンを除くと、早い下降相＋遅い上昇相の点や遅い下降相＋遅い上昇相の点が現れる。これらの点は、同一接点内に両方の受容体を有するもの、同一接点内にＮＭＤＡ型受容体のみを有するものにそれぞれ対応する。

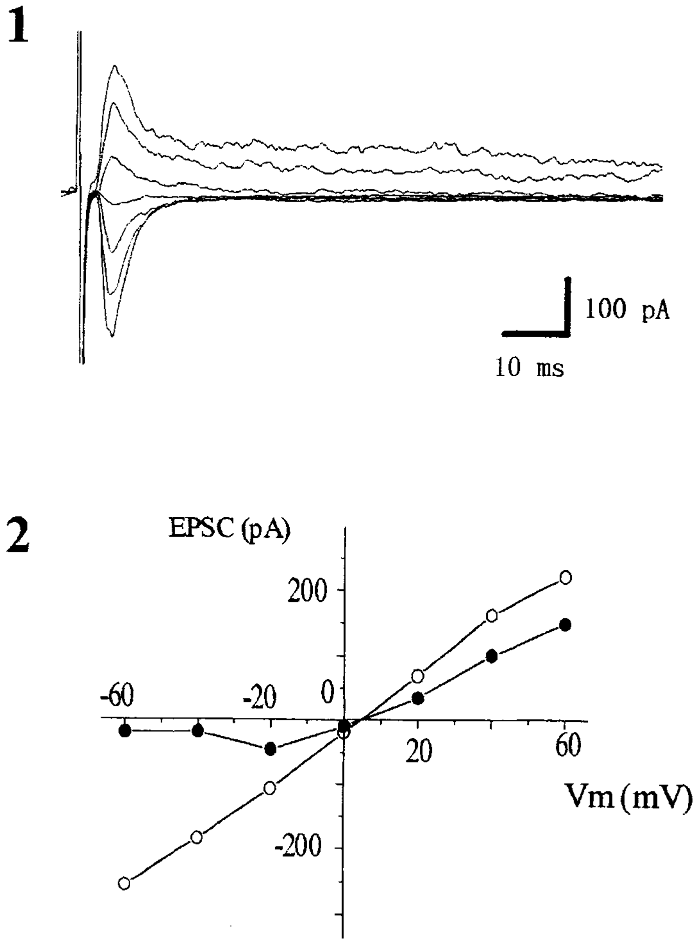

図１６　ＤＣシナプスの電流電圧関係

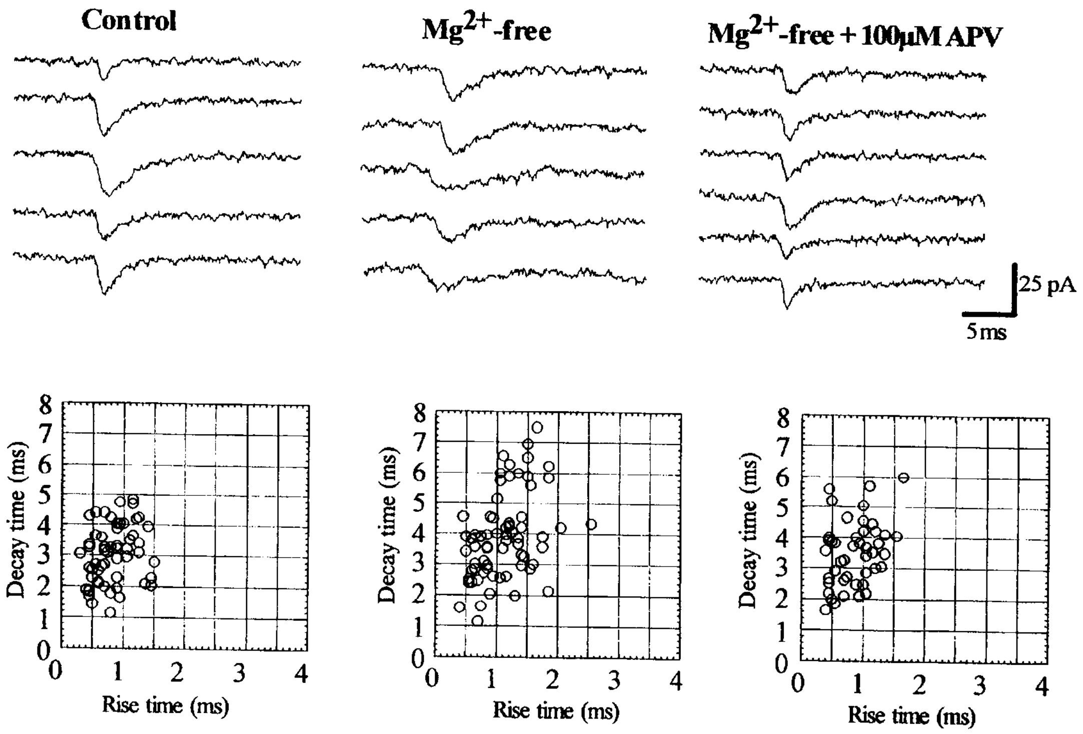

図１７　ＤＣシナプスの微小シナプス後電流解析

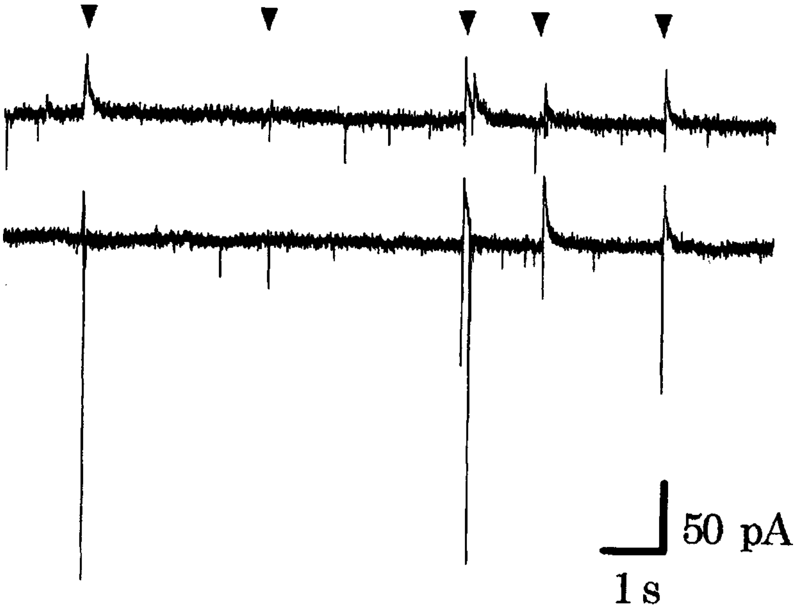

図１９　若い神経細胞と発生の進んだ細胞での自発的シナプス後電流
上：若い細胞、下：発生の進んだ細胞

この興奮性シナプスの活動による内向き電流は、発生の進んだ段階では主にＡＭＰＡ型受容体を介したものであるが、前述の様に、このシナプスはＤＣシナプスであり、ＮＭＤＡ型受容体も共存している。図１９の解析ではＮＭＤＡ型受容体の発生に関する情報は得られないので、別な解析を行った。

若い細胞（この場合は胚令６日の大脳神経細胞を５日間培養）と発生の進んだ細胞（胚令１０日の神経細胞を７日間培養）とに同時にホールセルパッチクランプを行い、両者へのｓＥＰＳＣを記録した（図２０）。静止膜電位に近い値に固定した場合、前項でも述べたように、若い細胞の方には殆どシナプス入力がなく、一方、発生の進んだ細胞では、大きく鋭いｓが観測された（図２０左）。これまでは、この状況から、このような若い細胞にはシナプスが形成されないと考えてきたが、驚いたことに固定膜電位をプラス６０ｍＶにするとｓＥＰＳＣが記録された（図２０中、右）。この図の上下の電流ピークを比較すると、若い方への入力時には必ずもう一方への入力も存在する。このことは、培養系の中の神経細胞回路網の活動が同期して起こっており、これに伴うシナプス入力が観測されていることを示している。すなわち、若い方の細胞で観測

された入力は、細胞表面の受容体がたまたま活性化されたされたことによる電流ではなく、シナプスの構造の中の受容体のシナプス前膜からの伝達物質放出による活性化によるものであることを示唆している。

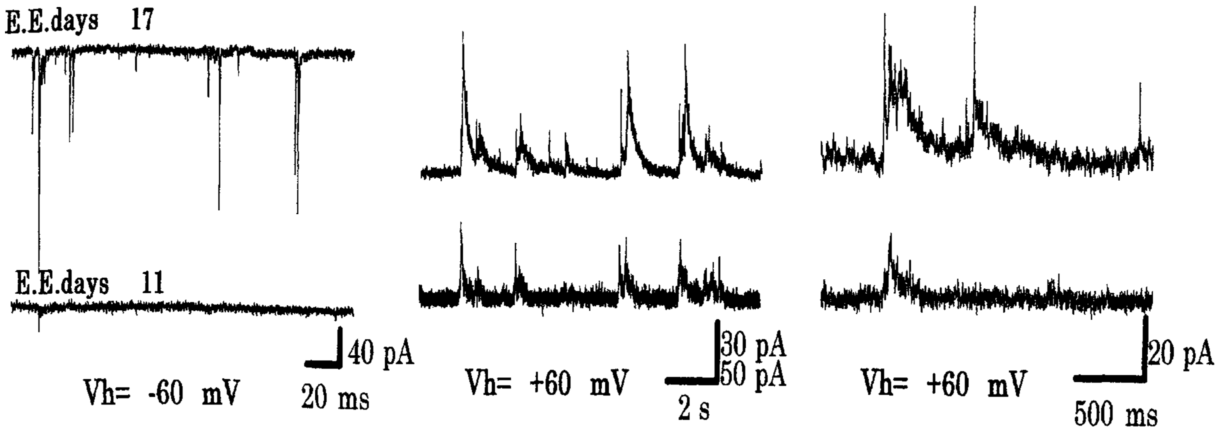

図２０　サイレントシナプスの検出
左：静止膜電位付近での記録、中：脱分極下での記録、右：脱分極下での記録の拡大トレース

この点をより確実にするために、誘起ＥＰＳＣによるシナプス電流解析を行った（図２１）。これにより、マイナス６０ｍＶでは応答せず、プラス６０ｍＶではじめて応答するシナプスの存在が明確になった。

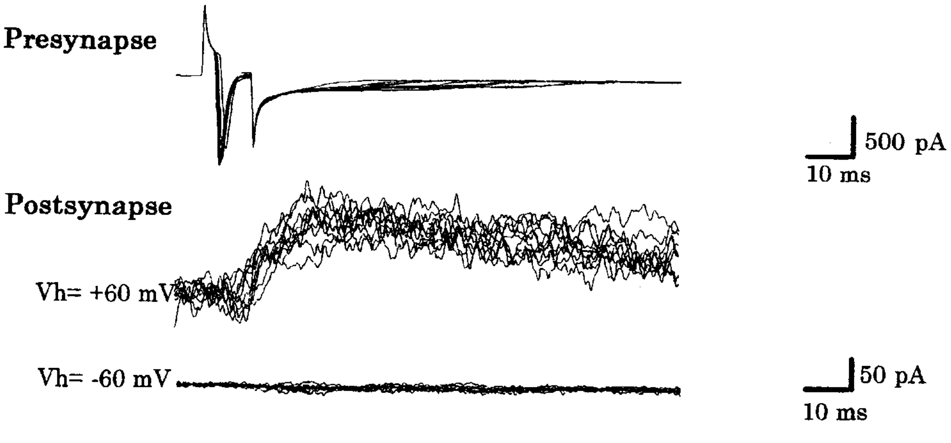

図２１　誘起シナプス後電流によるサイレントシナプスの確認

この若い細胞に形成されるシナプスを詳細に解析すると、発生の進んだ細胞では早い上昇相とまちまちな下降相の電流波形が主であるが、若い細胞のシナプスでは殆どが遅い上昇相と下降相の波形であった。これはＮＭＤＡ型受容体のシナプス応答に特徴的である（図２２）。

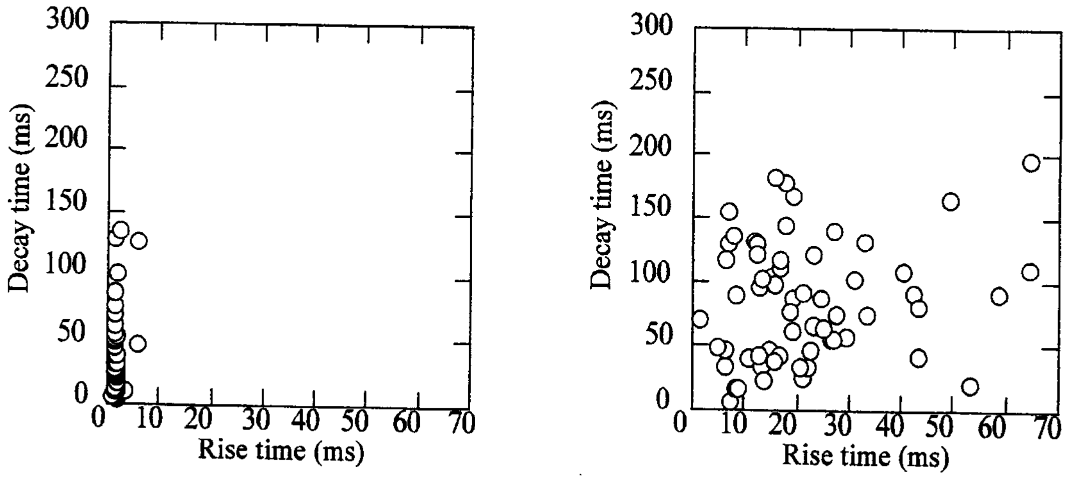

図２２　シナプス電流波形解析
左：発生の進んだ神経細胞、右：若い神経細胞

そこで、この受容体の特異的拮抗阻害剤を用いた検討をするとこの応答は完全に消滅した（図２３）。このことは、若い神経細胞に形成されるこのシナプスに存在し機能する受容体はＮＭＤＡ型だけであることを明確に示している。この型のシナプスはサイレントシナプスと呼ばれる。

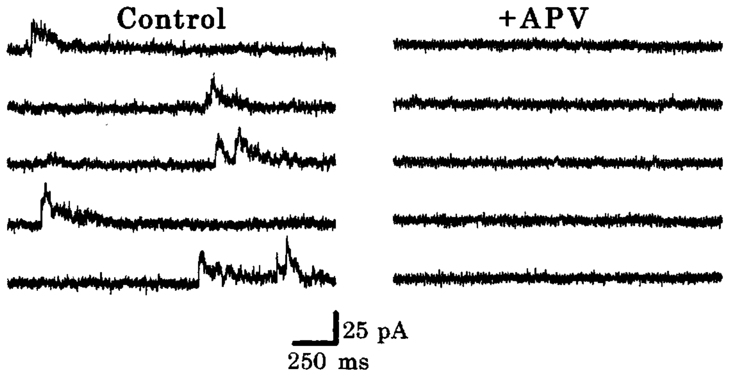

図２３　サイレントシナプスのＮＭＤＡ受容体依存性

これらの結果から、我々のニワトリ胚大脳神経細胞の培養系におけるシナプスは、まず、サイレントシナプスが形成され、それがデュアルコンポーネントシナプスに変わることによって成熟する。この様式を図２４に模式的に示した

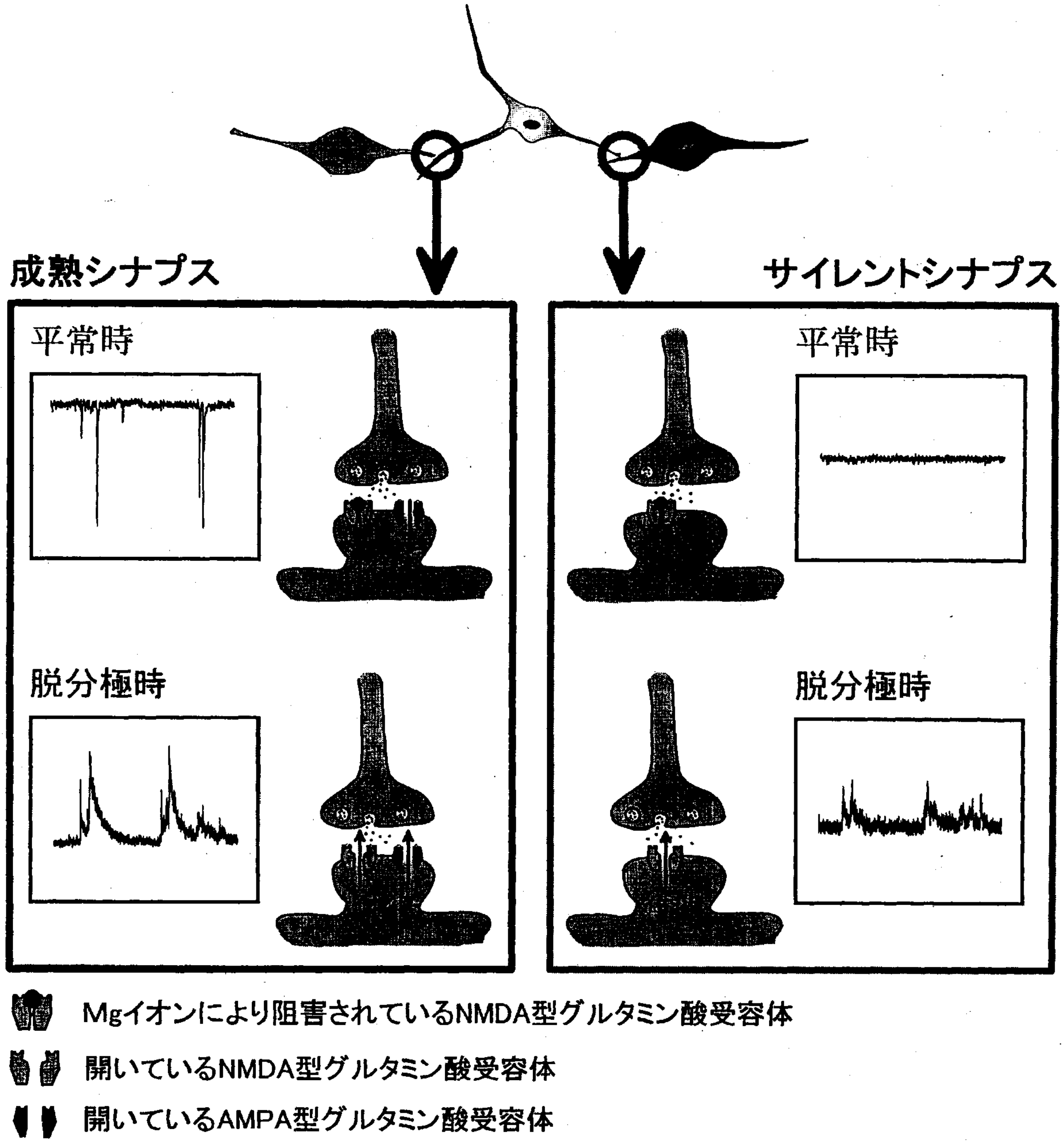
成熟シナプス
サイレントシナプス
平常時
脱分極時
平常時
脱分極時
Mgイオンにより阻害されているNMDA型グルタミン酸受容体
開いているNMDA型グルタミン酸受容体
開いているAMPA型グルタミン酸受容体

図２４　サイレントシナプスを介したシナプス形成過程

このシナプスの型の変換はどのように進行するのであろうか。もっとも簡単な考え方が遺伝子発現調節である。すなわち、若い時期にはＮＭＤＡ型受容体のみが発現されており、発生が進むにつれてＡＭＰＡ型受容体も発現されるようになる、という様式でる。そこで、若い神経細胞の表面の膜をアウトサイドーアウトパッチクランプという手法を用いて細胞表面にあるグルタミン酸受容体を解析した（図２５）。この結果は、サイレントシナプスしか作れない若い細胞の表面には、両方の受容体が機能できる形で存在することを示している。

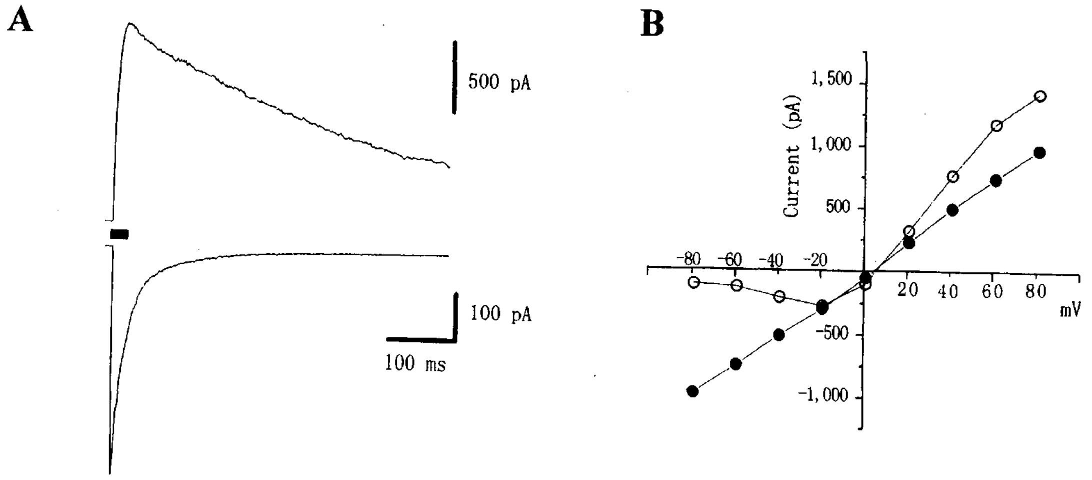

図２５　若い神経細胞表面のグルタミン酸受容体解析

したがって、遺伝子発現調節でシナプスの成熟が進行するのではなく、シナプス直下への受容体の組み込み機構により調節されている可能性が高くなってきた。細胞内骨格の動態と結びついた細胞膜受容体の動きがあり、ＡＭＰＡ型受容体がサイレントシナプス接点に移動してシナプスの成熟が加速されると様式を仮定しているが、この証明は今後の課題である。しかし、この仕組みが分子レベルで解明されれば、シナプス伝達効率の制御手法の開発に弾みがつくことは間違いなく、神経活動賦活化材料のモデルとなる機能分子解明につながることが大いに期待される。

２－３　長期的増強現象の in vitro 解析

脳の高次機能の発現は脳神経回路網の動的特性の変化である。この変化を誘導する機構の詳細はまだ不明であるが、シナプスにおける伝達効率の可塑的変化が重要な役割を果たしていると考えられている。したがって、この機構の分子的理解が脳の高次機能の理解を飛躍的に深めることは確実であるが、それだけではなく、シナプス機能の活性化を中心とした神経活動賦活化のための手法開発も大きく前進させるものと考えられる。このシナプスの可塑的変化にはいくつかの様式が知られているが、最も解析の進んでいる現象が長期増強現象（Long-term potentiation, LTP）である。

本項目においては、このＬＴＰ発現の分子機構を理解するための基礎となる個々の神経細胞の特性、単一シナプスにおける可塑的な変化の詳細な研究を行った。この研究では、我々の開発したニワトリ胚大脳解離培養系においても脳高次機能に不可欠なシナプス伝達効率の可塑的長期変化が起こり得るかどうか検討し、この可塑性の分子メカニズムを解析可能な系の確立をめざした。

実験は、胚齢１０日目のニワトリ胚から取り出した神経細胞を培養して６－８日目のものを用い、比較的容易に記録できる自発性シナプス後電流（spontaneous excitatory post synaptic current; sEPSC）の振幅を記録した。sEPSCは、２つのニューロンから同期して観測されるものに着目した。これは記録を取っているニューロンに共通のシナプス前細胞の発火により引き起こされるものであるので、誘導EPSCに相当するものと考えられる。まず、Mg^{2+}を含む通常の記録外液下で３分間のsEPSCを記録した。その後、記録外液をMg^{2+}を含まない記録外液に置換した。Mg^{2+}非存在下では、sEPSCの頻度が増大し、NMDA型グルタミン酸受容体による時定数の遅い電流成分が増加した。カレントクランプモードで１５分間放置した後、通常の記録外液に再置換してsEPSCを記録した。１５分間のMg^{2+}除去により、sEPSCの振幅は増大し、記録外液を通常のものに再置換した後もこの変化は少なくとも1時間30分以上の長期にわたって持続することを確認した。この実験の模式図を図２６に示す。

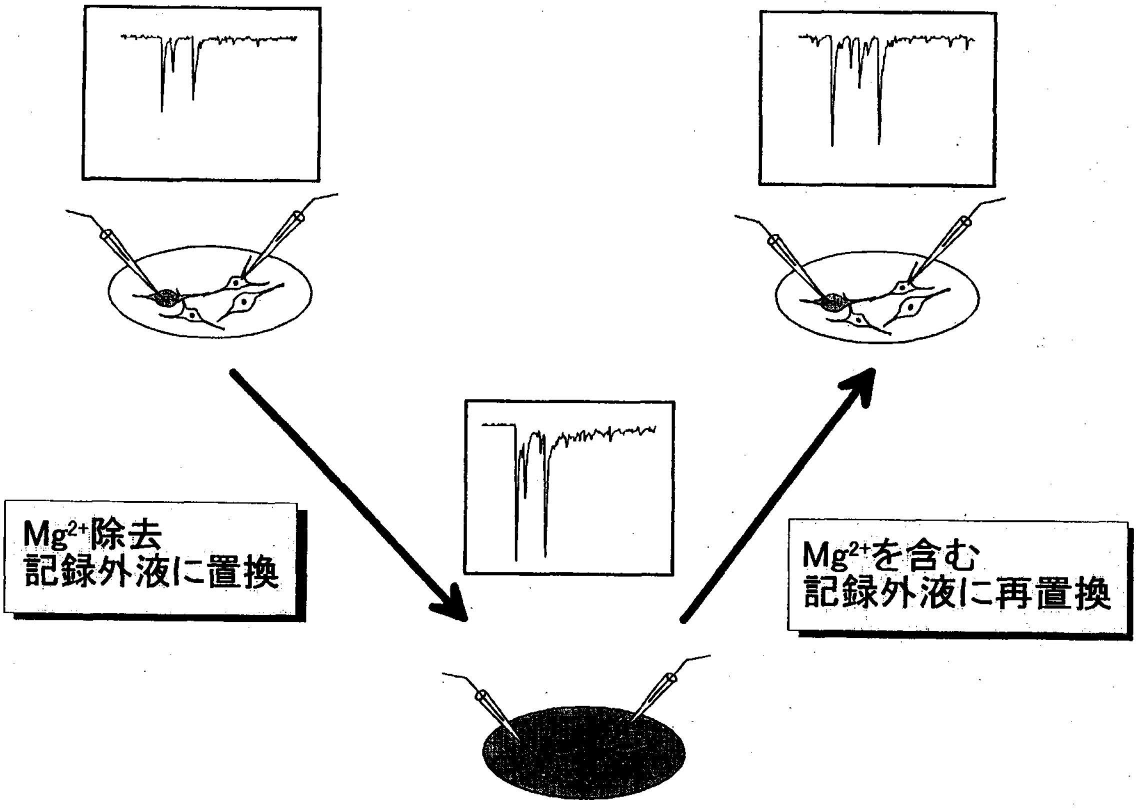
Mg²⁺除去
記録外液に置換
Mg²⁺を含む
記録外液に再置換

図２６　マグネシウムイオン除去によるシナプス伝達増強実験の模式図

この実験で得られた sEPSC の電流波形を図２７に示した。マグネシウムイオン除去時にこの電流が増大し（図２７Ｂ）、記録外液を再置換後もこの増大が続いていること（図２７Ｃ）が確認できる。

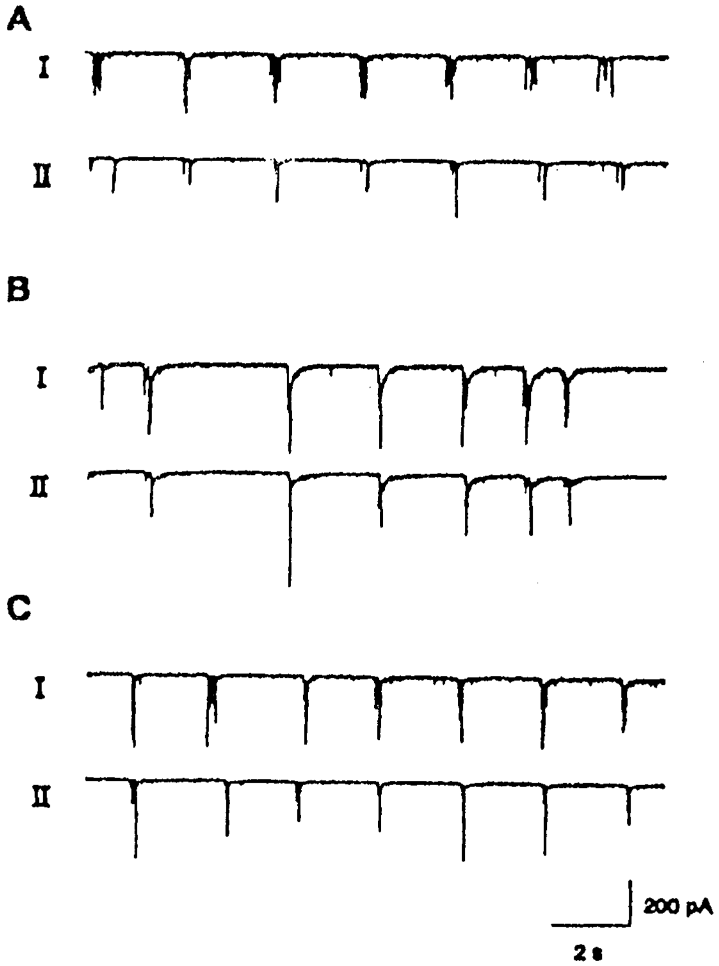

図２７　マグネシウムイオン除去によるシナプス伝達増強
Ａ：除去前、Ｂ：除去中、Ｃ：除去後

マグネシウムイオンの除去は２つの効果が期待される。すなわち、カルシウムチャネルに対する抑制効果をのぞき、細胞内へのカルシウム流入を促進する効果と静止膜電位下ではマグネシウムイオンの阻害効果で活性のないＮＭＤＡ型グルタミン酸受容体を活性化する効果である。特に、後者のＮＭＤＡ型グルタミン酸受容体の活性化は、よく研究されているラット海馬Ｃａ１領域で観察されるＬＴＰの誘導に必須であり、最も注目されている現象のひとつである。実際にこの受容体がマグネシウムイオン除去中に活性化されていることは図２７の電流ピークを拡大により確認できる（図２８）。図２８の一番上の波形がマグネシウム除去前であり、中段の波形が除去の中波形である。後者の各ピークは下がり際（右側）の曲線の勾配が緩くなっている。これが、開口時間の長いこの受容体の特性をよく表しており、この受容体の阻害剤、ＡＰ５を加えるとこの部分が消失する。

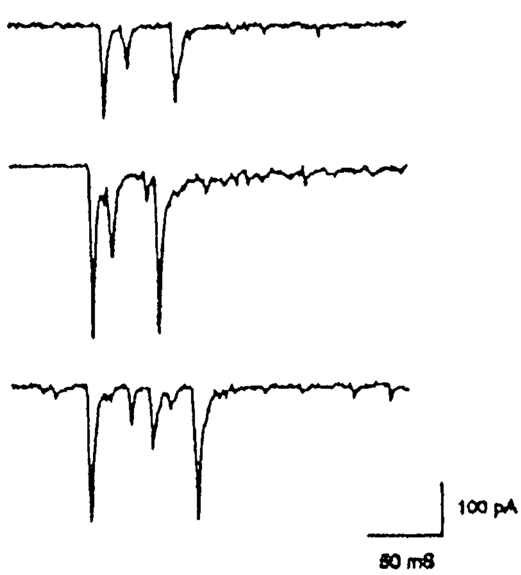

図２８　電流波形の詳細な解析
上：除去前、中：除去中、下：除去後

増強の時間経過は次の図２９に示した。

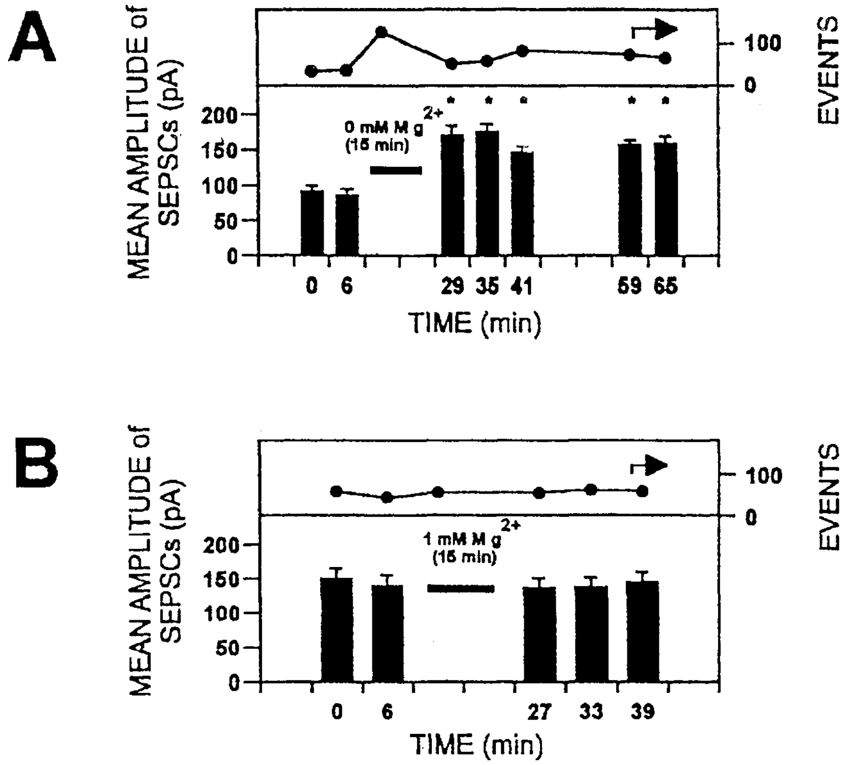

図２９　マグネシウムイオン除去によるシナプス伝達増強の時間経過
A：マグネシウムイオン除去、B：対照実験

増強の前後におけるsEPSCの大きさの分布を示すヒストグラムは図３０に示した。左側がマグネシウムイオン除去処理をした場合の結果で、右側がそれをしなかった対照実験の結果である。

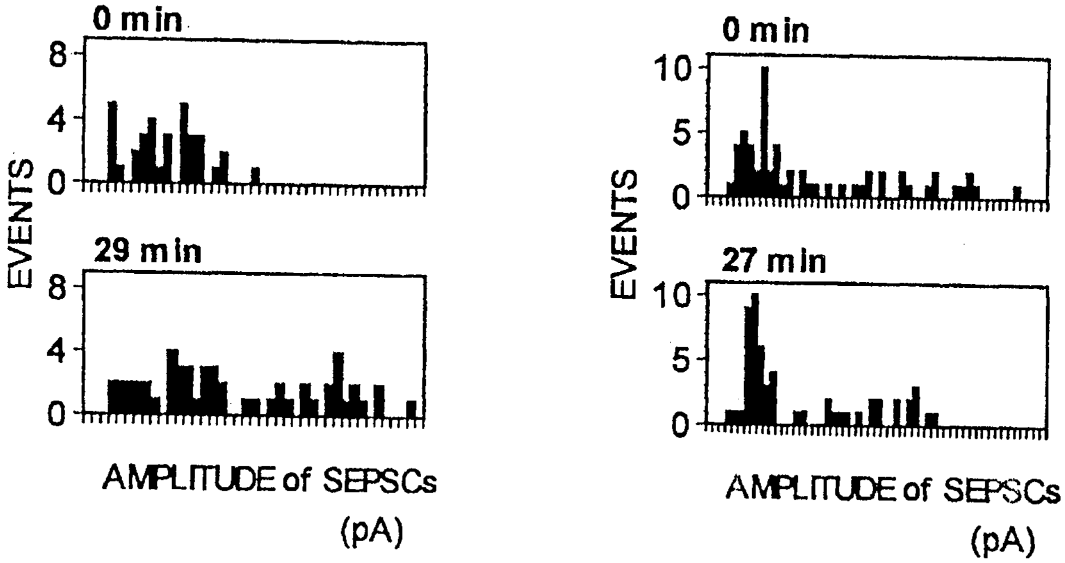

図３０　マグネシウムイオン除去によるシナプス伝達増強による電流強度のヒストグラム
０ minは除去前、２７ minは除去後。

また、CNQX，TTXをMg2+のない記録外液中に加えてシナプス伝達を阻害すると、sEPSCの振幅は変化しないことから、sEPSCの増強はシナプス活動に依存したものであり、イオン環境の変化によるアーティファクトでないことをことを確認した（図３１）

NMDA型グルタミン酸受容体の拮抗阻害薬であるD,L-APVにより、この長期的SEPSC振幅増加は顕著に抑えられた。一方NMDA型グルタミン酸受容体を阻害しないL-APVはこの増強を抑制しなかった。このことから、NMDA型グルタミン酸受容体が活性化することがSEPSCの増強に必須である可能性が示唆された（図３２）。

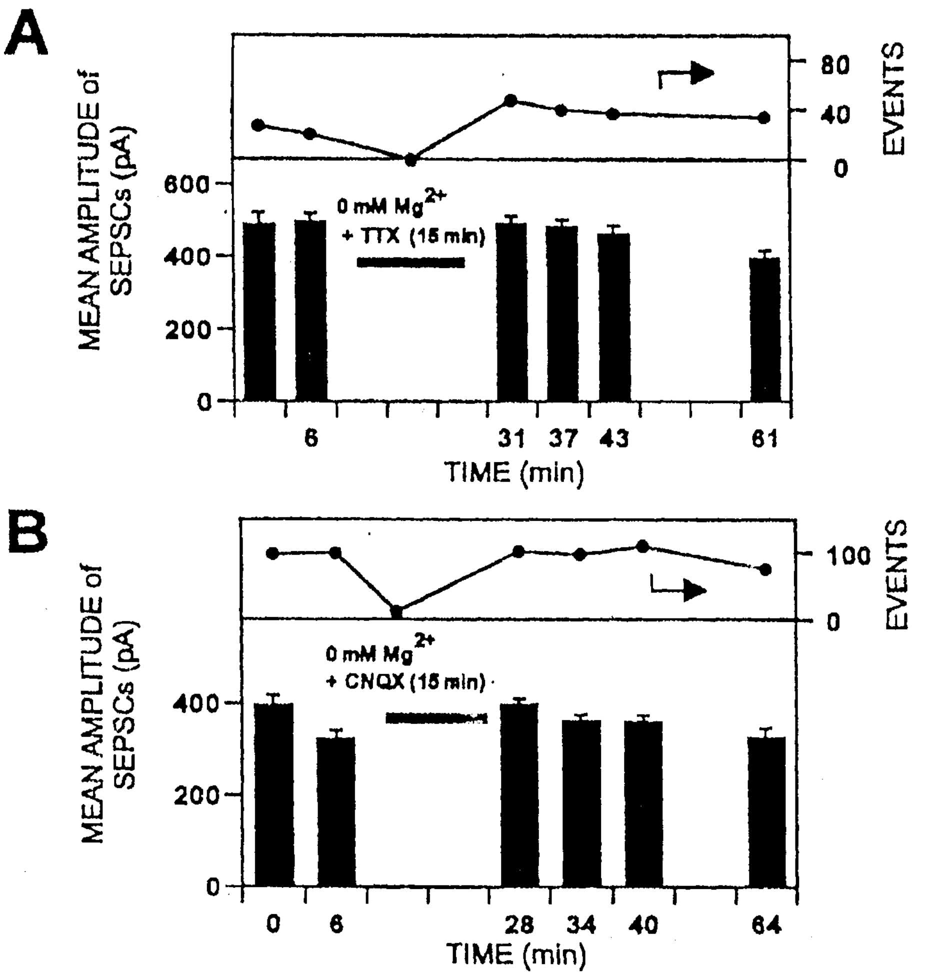

図３１　マグネシウムイオン除去によるシナプス伝達増強の阻害
Ａ：ＴＴＸ添加、Ｂ：ＣＮＱＸ添加

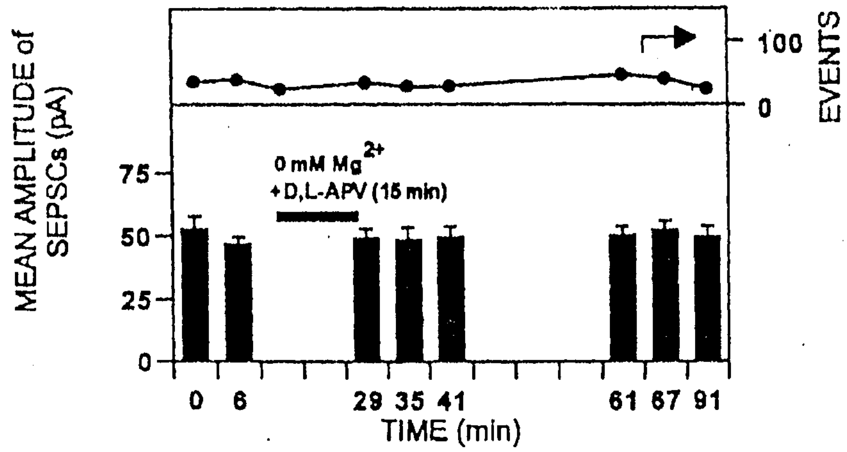

図３２　マグネシウムイオン除去によるシナプス伝達増強のＮＭＤＡ受容体拮抗阻害剤による抑制

さらに、蛋白翻訳阻害剤である cycloheximide、RNA 合成阻害剤である actinomycin D も SEPSC の振幅上昇を抑えた。何らかの mRNA、タンパク質が新規に合成されることが SEPSC の増強をに必須であることが明らかになった。１５分間という比較的短時間の間にこの増強に必須なタンパク質の合成が行われる可能性が示唆された（図３３）

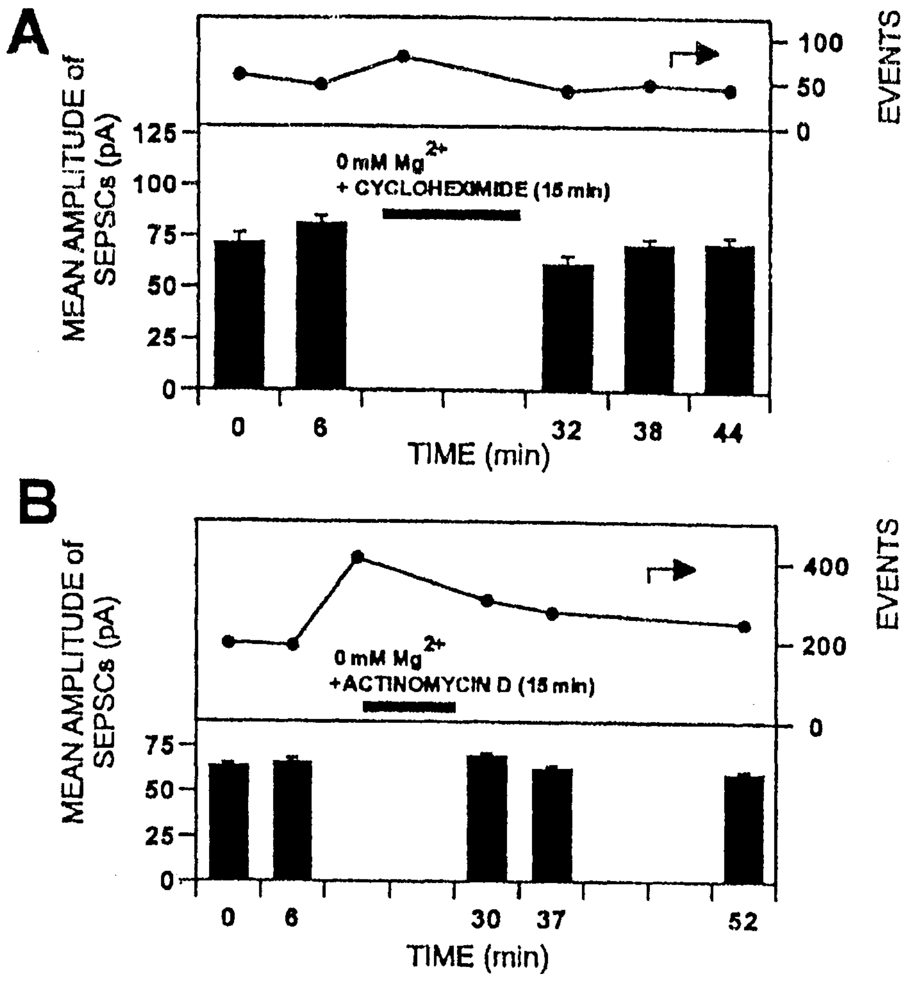

図３３　マグネシウムイオン除去によるシナプス伝達増強の遺伝子発現依存性
Ａ：翻訳阻害剤による抑制、Ｂ：転写阻害剤による抑制

マグネシウムイオン除去による増強の前後で、TTX存在下でミニアチュアシナプス後電流を解析し（図３４）、その頻度が増大することを確かめた（図３５）。このことは、自発性シナプス後電流の増大には、少なくともシナプス部位の数の増大が重要であることを示している。このメカニズムには、サイレントシナプスの活性化を含む可能性がある。

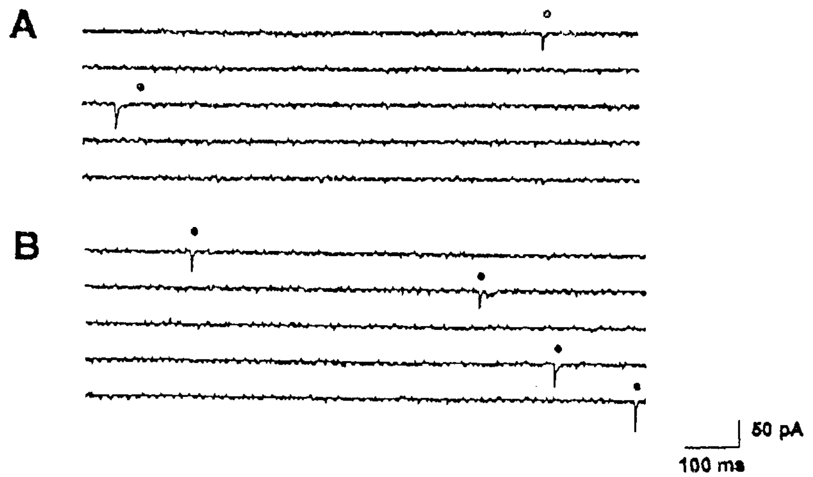

図３４　マグネシウムイオン除去によるシナプス伝達増強後の微小シナプス後電流
A：増強前、B：増強後

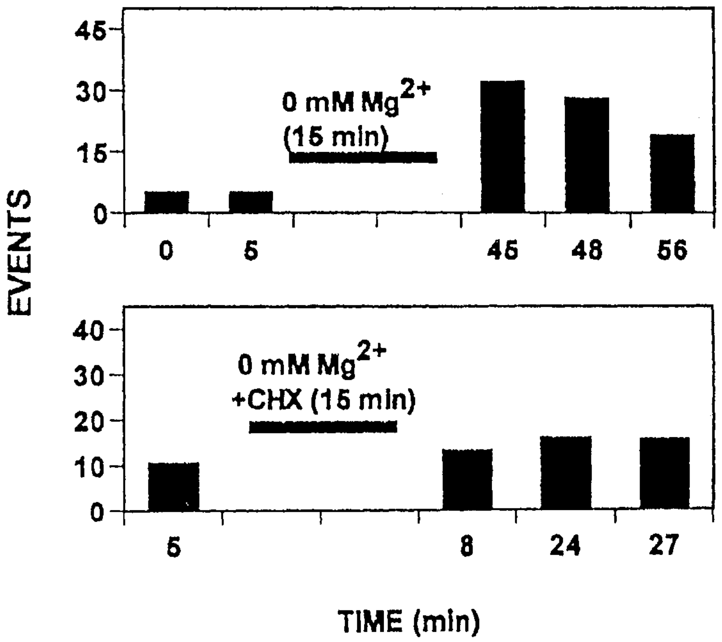

図３５　マグネシウムイオン除去によるシナプス伝達増強後の微小シナプス後電流の頻度解析
上：通常の操作、下：翻訳阻害剤存在下での操作

シナプスの伝達物資放出機能には、細胞内の膜輸送現象が密接に関与することが予想される。このことから、培養細胞を用いて細胞膜の動態をレーザー共焦点顕微鏡を用いて観察した結果、カルシウム依存的な新たな膜輸送機構を明らかにし、さらには、この機構にリン酸化酵素が関与することもその阻害剤を用いて示すことができた。

本項目の研究から、我々の開発した大脳神経細胞の培養系においてもシナプスの可塑的現象の解析が可能であることが示された。この解析においてはsEPSCのみを解析したが、さらに詳細な解析には誘起EPSCの解析が必要である。培養神経細胞はホールセルクランプ法に対する耐性がやや弱いため、長期変化を記録するには若干問題点が残っている。この点を克服し、より精密な解析を目指して行く。

本研究から、従来考えられていたよりも短い時間経過で遺伝子発現が要求されることは明らかになった。短すぎるとの批判はあるが、この結果の再現性は充分にあり確かな実験事実である。さらに、最近の、酵素反応、細胞内物質輸送の生化学的、細胞生物学的研究の成果を考えると１５分という時間は決して短すぎると言うことはない。我々のこの系での研究を進めることにより、シナプス機能の可塑的変化を説明する新たな分子メカニズムが明らかになるものと期待される。

蛋白合成がこの長期的増強現象に関与すると言うことは、増強誘導期間中に新たな蛋白質が合成されているということであり、この蛋白質の同定に成功はシナプス機能活性化に有用な物質の発見に結びつく。

２－４　長期的増強を誘導する分子の発見

前項で述べたように、我々の開発した神経細胞培養系においてシナプス伝達の可塑的変化の解析が可能になった。この系で解析された長期的増強現象の誘導にはシナプス活動を必要とし、さらに、シナプス後膜に存在するNMDA型グルタミン酸受容体の活性化が要求される。その結果起こる増強においてはシナプス接点の数が増加している可能性が出てきた。接点の増加はシナプス前膜と後膜の両者の変化を含む可能性があり、その場合にはシナプス後膜から前膜への何らかの情報伝達が必要になる。そこで次に、この増強現象に伴い、何らかの拡散性因子が放出されている可能性について検討を加えた。増強を誘導したマグネシウムイオンを含まない記録外液を採取し、1mMのマグネシウムイオンを加えて通常の記録外液とイオン組成が同じになるように調整し、条件付けしたマグネシウムイオン除去記録外液 (CM) を準備した別の培養皿の培養神経細胞に対しホールセル記録を行い、シナプス伝達の存在を確認した後そこにこのＣＭを添加すると、sEPSCの振幅が上昇した。この実験を模式的に示した（図３６）。

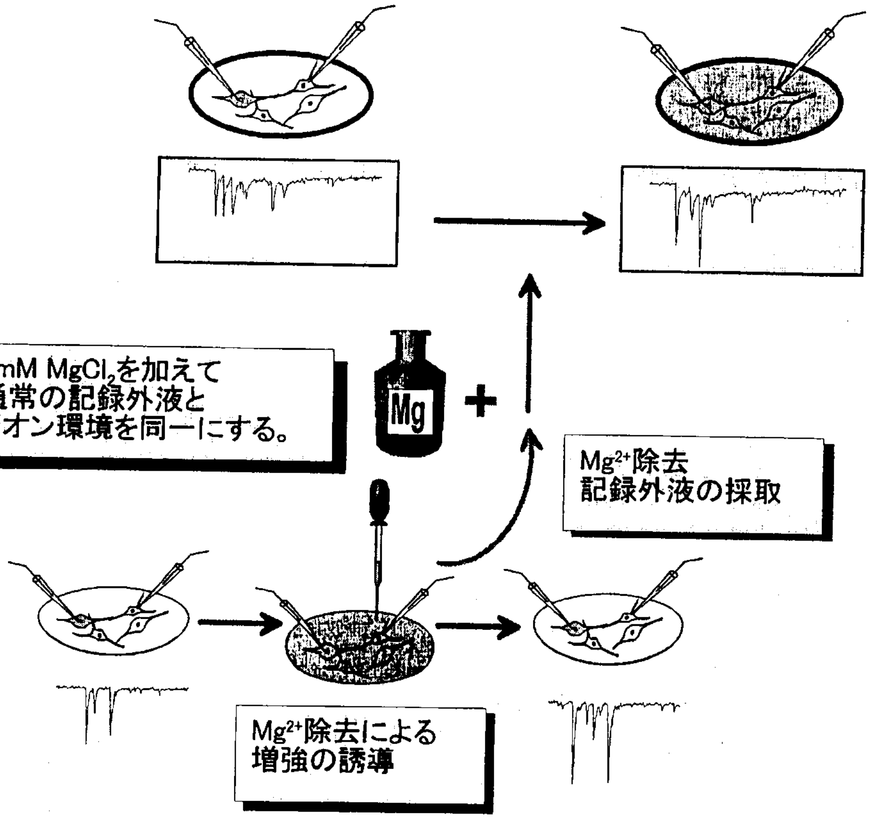
1mM MgCl$_2$を加えて
通常の記録外液と
イオン環境を同一にする。
Mg
+
Mg^{2+}除去
記録外液の採取
Mg^{2+}除去による
増強の誘導

図３６　条件付け培地を用いた実験の模式図

この増強は３０分以上にわたり継続し、さらに、培養系を灌流し、ＣＭの成分を除いた後も増強が持続した（図３７）。興味深いことに、蛋白合成阻害剤を加えた状況でもこの増強は誘導された。マグネシウムイオン除去による誘導の場合、この処理を１５分間行う必要があったが、ＣＭの添加の場合は、添加後直ぐに増強が観測された。したがって、これまでに得られている結果を総合すると、次のような増強機構が推定される。マグネシウム除去処理によりNMDA型グルタミン酸受容体が活性化され、ここから流入した細胞外カルシウムイオンにより細胞内情報伝達系が作動し、遺伝子発現・蛋白合成が誘導され、それに基ずく情報伝達分子が細胞外に放出される。この放出分子がシナプス前細胞の変化を促し機能するシナプス接点の数が増大し増強現象が起こる。この機構の情報伝達分子は、ＣＭに含まれシナプス伝達効率の上昇を誘導する分子と同じものであると考えられる。

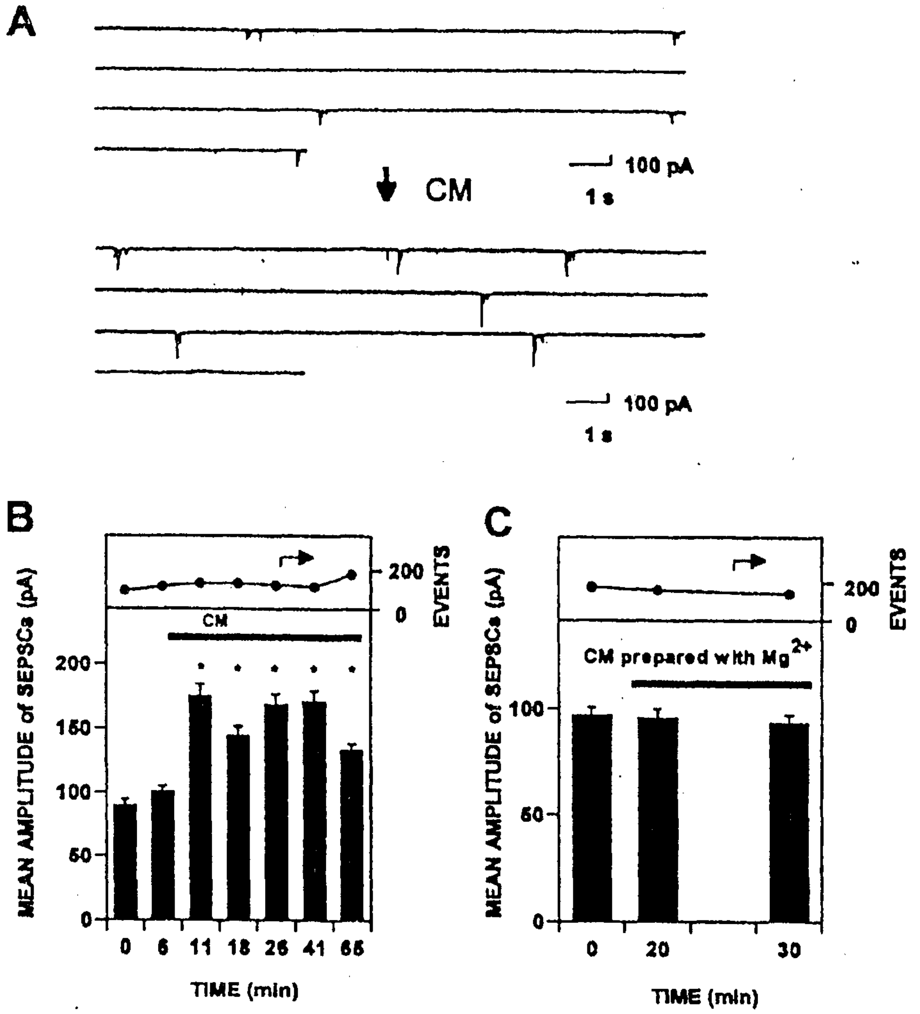

図３７　条件付け培地を用いたシナプス伝達増強

Ａ：電流記録、Ｂ：電流値増大の時間経過、Ｃ：対照実験

この分子の詳細については今後も解析を継続する予定であるが、３０ＫＤの限界ポアサイズを持つフィルターで濃縮したＣＭにも同様の増強誘導能があり、これ以下の部分は増強を誘導しなかったという実験結果、および、ＣＭを９０℃、２０分間加熱したものは増強誘導活性を失ったという実験結果が既に得られている。ことから、ＣＭに含まれる因子がタンパク質であることが示唆されている。また、対照実験としてマグネシウムイオン除去による増強の誘導を行わない場合の記録外液を別の培養皿のニューロンに添加した場合は増強が起こらないことも確認した。

この誘導因子の発見は、シナプス伝達制御に役立つ神経機能分子の解明につながる。この分子の発見は神経活動賦活化材料の開発に現実性を与え、今後の神経機能材料への応用が大いに期待される。

さらに、ハチ毒の一種である、ＭＣＤペプチド（マストパラン含有細胞内分泌顆粒減少ペプチド）が、ラット海馬Ｃａ１領域で長期増強を引き起こすことが分かり、この作用がＧ蛋白質を介して作用することも分かってきた。このような神経機能性ペプチドも神経機能材料創製のモデル分子のひとつである。

このようなシナプス機能解析の結果は、総合すると、シナプス形成、シナプス機能変化には共通の分子・細胞メカニズムが存在し、どちらにおいても機能する（有効な）シナプス接点の数の調節に依存するという仮説に矛盾しない。この我々の仮説を「有効シナプス接点仮説（ Functional synaptic contact hypothesis ）」と呼ぶ（図３８）。

有効接点仮説

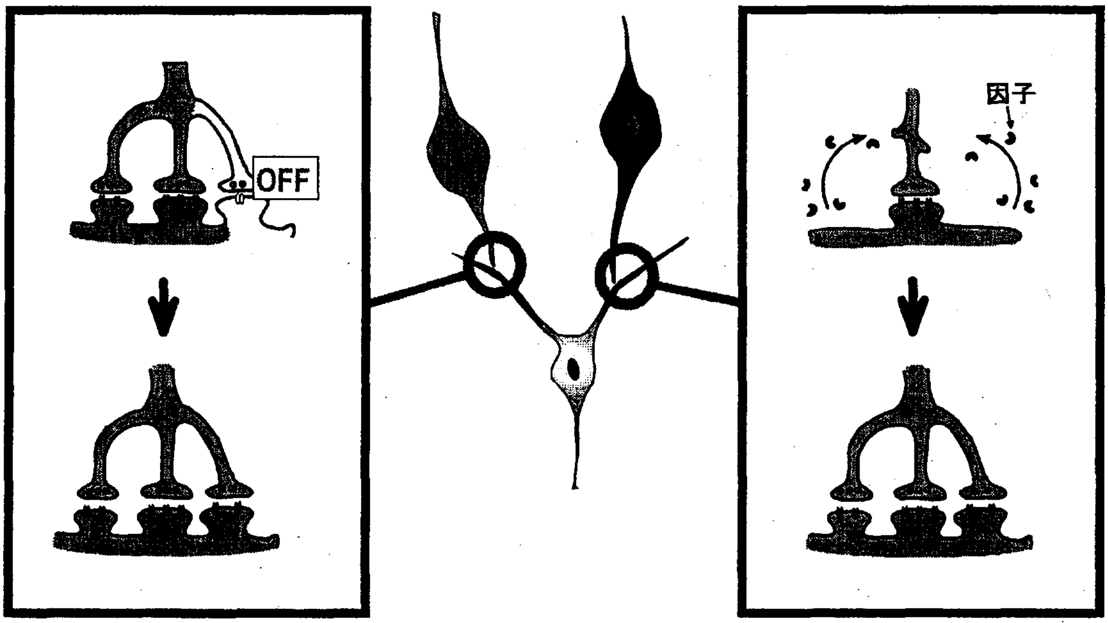

図３８　有効シナプス接点仮説の説明図

２－５　シナプス活動に伴う神経細胞形態変化の解析

シナプス可塑性は、記憶学習などの脳高次機能に重要な役割を果たすと考えられているが、その発現メカニズムに関してはまだ解析が進んでいない。前項で述べたように、我々は、本研究等の成果から、有効シナプス接点仮説を作業仮説として提唱している。この仮説に従えば、シナプスの機能変化に伴う神経細胞形態変化、特にシナプス部位の局所的細胞形態変化、が観測される可能性がある。この解明は複雑な脳組織を用いたのでは計測不可能であるので、より単純な培養細胞系の活用が有効である。前述のように我々はすでに大脳神経細胞の解離培養系を用いてシナプス形成やシナプス伝達の可塑的変化の電気計測に成功している。本研究では、この系を用いて神経細胞のシナプス部位形態変化を計測し、可塑性メカニズムの関連を解析する。

神経細胞内分子可視化・操作技術を開発するために、まずシナプス伝達の可塑的変化に伴うニューロン形態変化を解析できる系を開発する必要がある。これには複雑な脳組織を用いたのでは計測不可能である。そこで大脳神経細胞の解離培養系を用いた方法を検討した。この培養系においては、血清を加えて培養するため培養日数の増加に伴い神経細胞の他にグリア細胞（主にアストロ細胞）が増殖する。神経細胞の微細構造を解析するためには、大脳神経細胞の純粋培養系を方が好ましいため、まず、この系の開発を試みた。神経細胞のみの培養系を調製するこれまでの方法は、細胞の増殖を阻害するＤＮＡ合成阻害剤であるシトシンアラビノフラノシド（ AraC ）を添加しグリア細胞の増殖を抑制するものである。この方法を用いると確かにグリア細胞の存在しない培養系が調製できるが、使用する AraC の微妙な濃度変化で神経細胞にも致死的影響を与える。したがって、一見正常にみえる純粋培養系の神経細胞においても、そのすべての機能が正常であるとの保証はない。事実、我々の以前の研究においても、 AraC によってグリア細胞を除去した神経細胞培養系においてシナプス形成が約５０％抑制された結果が得られている。別な純粋培養系では抑制は起こらないという結果が出ており、これは AraC の副作用である可能性が高い。

そこで本研究では、新たなグリア細胞の除去法を開発した。細胞培養系においては神経細胞もグリア細胞も培養基板に接着して成長する。この接着は、ポリリジンを塗布した培養気質に吸着した血清中の蛋白質（フィブロネクチンなど）を介していると考えられる。もし、この接着の様式が神経細胞とグリア細胞で異なっていれば、この接着力を制御することによって、一方の細胞をはが

すことができる。これまでの研究から、細胞接着に係わる蛋白質の接着部位の構造（アミノ酸配列）はかなりよく調べられている。そこで、その配列を含んだペプチドを合成（図３９）し、培養系に添加した。

#1	H-Arg-Gly-Asp-OH	RGD -containing peptide
#2	H-Arg-Gly-Asp-Ser-OH	
#3	H-Gly-Arg-Gly-Asp-Ser-Pro-NH_2	
#4	H-Gly-Ala-Cys-Arg-Gly-Asp-Cys-Leu-Ala-NH_2	
#5	H-Gly-Ala-Gly-Arg-Gly-Asp-Ser-Leu-Ala-NH_2	
#6	H-Gly-Ala-Cys-Gly-Arg-Gly-Asp-Ser-Pro-Cys-Gly-Ala-NH_2	
#7	H-Gly-Ala-Gly-Gly-Arg-Gly-Asp-Ser-Pro-Gly-Gly-Ala-NH_2	
#8	H-Leu-Gly-Thr-Ile-Pro-Gly-NH_2	laminin LGTIPG
#9	H-Pro-Asp-Ser-Gly-Arg-NH_2	laminin PDSGR
#10	H-Tyr-Ile-Gly-Ser-Arg-Cys-NH_2	laminin YIGSR
#11	H-Arg-Glu-Asp-Val-NH_2	fibronectin ⅢCS; REDV site
#12	H-Gly-Val-Lys-Gly-Asp-Lys-Gly-Asn-Pro-Gly-Trp-Pro-Gly-Ala-Pro-NH_2	collagen type Ⅱ IV-H1
#13	H-Asp-Gly-Glu-Ala-NH_2	collagen type Ⅰ DGEA site

図３９　用いられたペプチドのアミノ酸配列

このペプチドの中では、ＲＧＤ配列を含むペプチドにグリア細胞を選択的に除去する活性が存在した。さらに興味深いことに、単なるＲＧＤペプチドよりもより長いペプチド、さらには、ＲＧＤ部分の側鎖構造の自由度を制限したペプチドの方が高い活性を示した。図４０にこのペプチドを添加し調製した選択培養系の写真をしめした。（図４０上は、ペプチドを加えなかった対照実験の結果である）

そこでまず神経細胞の発達に伴って、神経線維上のスパイン様突起構造の密度の変化を測定した。その結果培養７日目からスパイン様突起構造の神経線維に対する密度は上昇し、培養１０日目でそのピークに達した（図４３）。そのピーク時のスパイン密度はラット海馬の解離培養系のスパイン密度の役２倍であった。しかしながらラット脳海馬スライス上で測定されたスパイン密度に比べるとその約１／５だった。本実験のような解離培養系では、細胞間の密度がどうしても二次元的で低くなるため、スパインの測定例が少ないが、これまでに測定されたスパイン密度としてはもっとも高密度であるといえる。このことは本実験で用いた解離培養系がシナプスの形態変化の測定に極めて適しており、二次元的には生体脳の細胞密度にかなり近づいていることを示唆している。

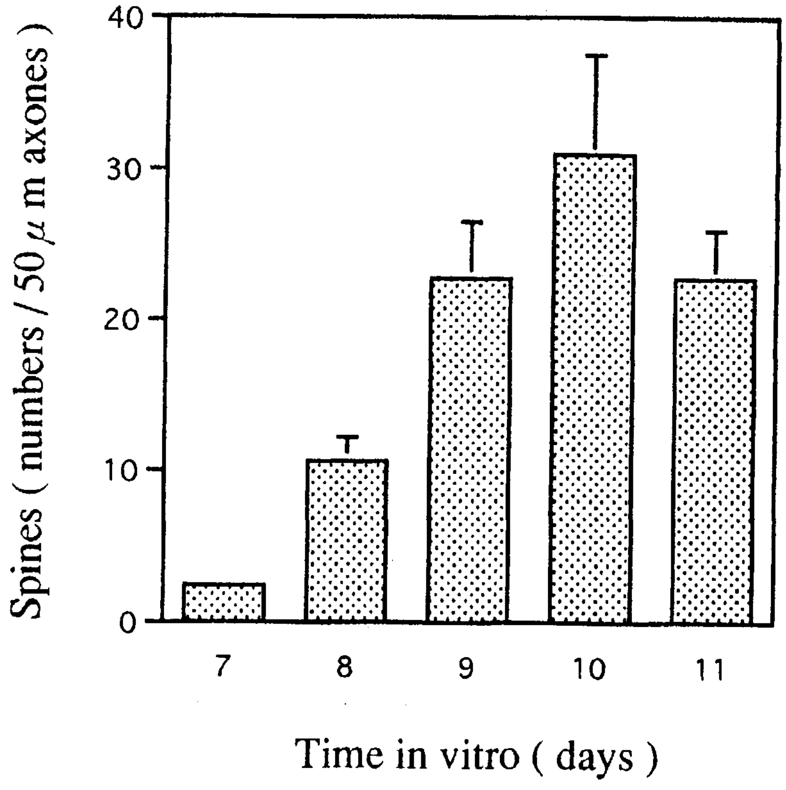

図４３　スパイン密度の発生に伴う変化

次に神経細胞の発達に伴うスパイン様突起構造の時間的な形態変化を計測した。その結果培養７日目のスパインヘッドレスの突起は、その構造を大きく変化させていることが分かった。一方、培養１０日目のスパインヘッドの存在する突起は、時間的な構造変化がほとんど観察されなかった。このことは通常の条件下の突起では、スパイン完成後はあまり構造的に変化しないことを示唆している。

以上の結果を踏まえて、シナプス伝達の長期増強に伴うスパイン形態の変化を測定した。シナプス伝達の長期増強の誘因は、前述の細胞外液のマグネシウムイオンを除去することによって行った。その結果、スパイン密度がまだ低い培養７日目のスパイン様突起構造は、このマグネシウムイオンの除去によって、その突起部分が伸長した。また培養１０日目のスパインヘッドを持った突起では、そのヘッド部分の面積が大きくなった。

次にこの現象が実際の脳組織上で生ずる現象か調べるために、脳スライスを使用した。胚齢１３日から１５日の深麻酔したヒヨコを断頭し、５％ＣＯ２／９５％Ｏ２に飽和させ、氷冷したクレブス溶液中で十分に冷やした（２分）。丁寧に大脳を取り出し、マイクロスライサーを用いて厚さ３００μｍのスライスを切り出した。ＩＭＨＶ領域を含むスライスは、３７度に加温し、５％ＣＯ２／９５％Ｏ２で飽和させたクレブス溶液中で１時間インキュベートし、実験に使用した。

脳スライスにおいても培養細胞と同様のスパイン像が観察され（図４６）、この密度が個体の発生に伴って変化することを確認した（図４５）

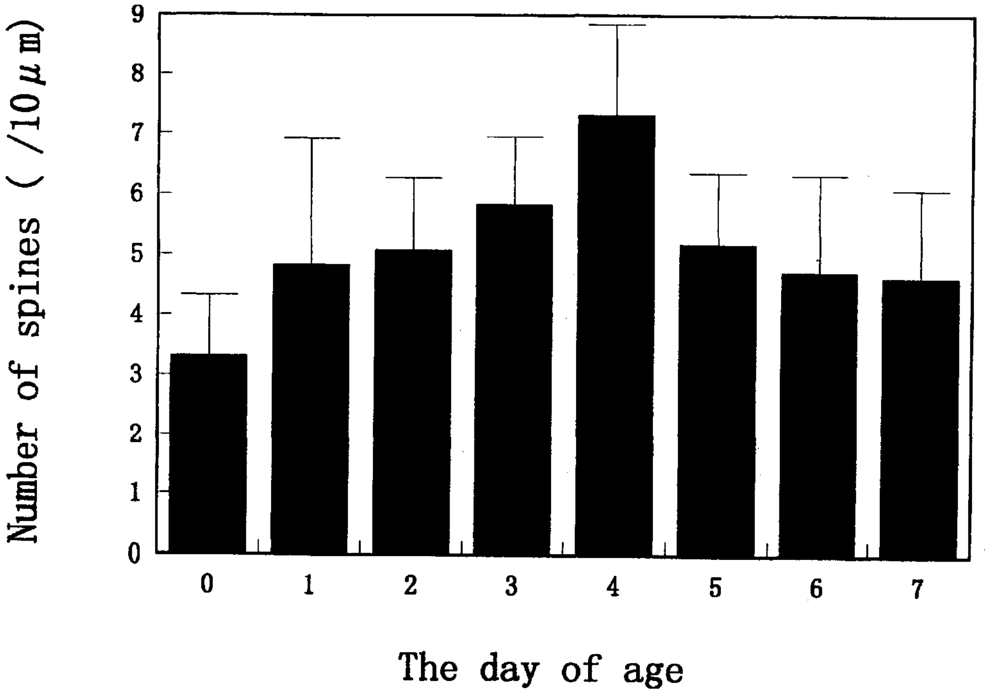

図４５　脳スライスにおけるスパイン密度の発生に伴う変化

この項に示した研究から、我々が有効シナプス接点仮説で予測したシナプス伝達効率変化に伴う形態変化を支持する結果が得られた。この結果は画期的なものであるが、それだけに慎重に裏付け証拠を集める必要がある。

この事実が充分に確認されればシナプス機能に結びつく単一細胞レベル、分子レベルの研究が大きく進展する可能性が高く、また、その結果としてシナプス機能を制御し、神経活動賦活化材料開発に役立つ分子の発見が現実のものとなる。

２－６　神経機能制御分子の解析

神経活動は電気的活動にその特徴がある。「電気的活動」とは、細胞の内から外、あるいはその逆、に流れる電流を伴う活動のことである。この電流が神経細胞内の情報伝搬や神経細胞間の情報伝達において主要な役割を果たす。この電流の本質はイオン流であり、これは細胞内外に形成されたイオン濃度勾配を駆動力とする電気化学ポテンシャルに流れである。流れるイオン種としては、ナトリウムイオン、カリウムイオン、塩素イオン、水素イオン、カルシウムイオンが主なものである。このイオン流は電荷を持った粒子の流れであるため細胞を取り巻き疎水性コアを持つ生体膜は通過することができない。そこで細胞はイオンを選択的に刺激応答的に通過させる構造を進化の過程で発達させてきた。この構造がチャネル蛋白質や受容体蛋白質である。

チャネル蛋白質は膜貫通型の蛋白質でその構造内、あるいはサブユニットの集合体の中に、文字通り、イオンの通る溝を形成することができる。この溝は構造的にイオンの透過に関して選択性をしめし、外側の環境、例えば膜電位、カルシウムイオン濃度、ｐＨ、の変化によりコンダクタンスや開確率を変化させる。また、リン酸化等の蛋白修飾やＧ蛋白質の会合等によってもチャネル活性が制御される。

神経細胞はこのチャネル蛋白質や受容体蛋白質の活性を広範に活用して複雑な情報処理機構を機能させている。したがって、このチャネル蛋白質はもっとも重要な神経機能分子のひとつである。この蛋白質の活性制御手法や活性制御分子の開発はすぐに神経活動賦活化材料開発に結びつく。近年の遺伝子工学技術の進歩により多くのチャネル蛋白質の一次構造、すなわち、アミノ酸配列は明らかになったが、まだ構造機能相関の解明には至っていない。そこで本研究では、チャネル蛋白質を機能面から解析しその特徴の理解を試みた。

形成収縮胞は低浸透圧下で棲息する下等真核生物に見られる細胞内小器官であり、水を細胞質から集めて細胞外へと放出する。この機構には多くの種類のチャネル蛋白質の関与が予想される。これらを解析するために、細胞性粘菌 *Dictyostelium discoideum* から収縮胞に富む膜分画を水性二相分配法によって調製し（図４９）、脂質人工二重膜に組み込んで単一チャネル電流の解析を行った。シス側 300mM／トランス側 100mM の非対象ＫＣｌ溶液中で逆転電位 -20.4 ｍＶ（$\mathrm{PK}^{+}/\mathrm{PCl} = 7$）、コンダクタンス 102pS のンチャネルを観察した（図５０）。このチャネルはバースト期と静止期からなり、バースト期における平

バースト期における開確率はトランス側の電位を負にすると減少して0に漸近し、正の電位で増加して約0.6に漸近した（図５１）。このチャネルはmM以下の濃度のキニンや30mMのTEA$^+$によってブロックされた。開確率の電位依存性は両側の溶液中のＫＣｌ濃度に大きく依存した。このチャネルの収縮胞における役割について知るために、粘菌細胞に対するキニンの効果について調べた。低張条件下においてキニンを与えると、細胞は丸くなり、収縮胞の肥大化が見られた。収縮胞の収縮頻度は低下し、またその低浸透圧耐性は低下した。キニン存在下で収縮胞が収縮するのと同期して、偽足様の細胞膜の突起が伸びるのが観察された。これらの結果を総合すると、このチャネルは収縮胞の正常な機能に重要な役割を果たしている可能性を示している。

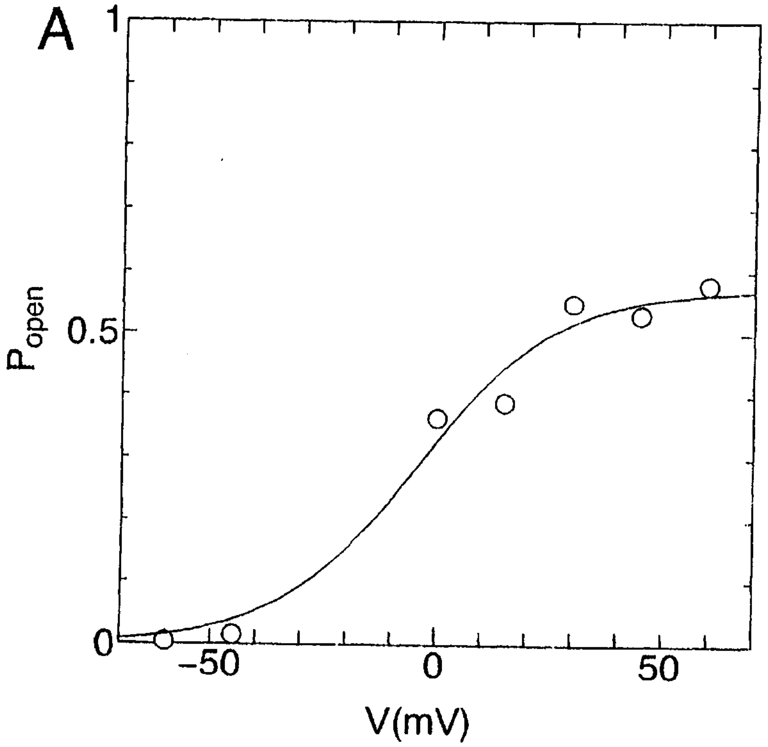

図５１　チャネル開確率の膜電位依存性

ここで解析されたカリウムチャネルは従来知られているものとはことなる新しいタイプであった。細胞の形態変化にも関与しているこの蛋白質の機能は、神経細胞の機能解析の面からも興味深い。同種の蛋白質の神経系での存在を検討する必要がある。また、このチャネルの構造面での情報を増やすために遺伝子クローニングも重要な今後の課題となる。

２－７　神経機能制御分子の海洋微生物ライブラリーからのスクリーニング

神経機能材料のモデルになる機能分子を神経系の機能解析から発見するという研究戦略は最も正統なものであるが、有効な機能分子を短期間に数多く見出すには効率にかける面がある。そこで本項目では、微生物ライブラリー解析技術を導入して、その微生物の産生・分泌する低分子の解析を試みた。

神経伝達の初期の課程は細胞膜でおこり、伝達物質が形質膜上の受容体を変化させ、形質膜のイオンチャンネルを開く。神経伝達物質としてはアミン類、アミノ酸類の低分子性物質のほか、ペプチド性の物質も知られており、現在までに１００種類近くの神経ペプチドが確認されている。細胞での情報伝達を観察するためには、伝達を担う物質を細胞に導入する必要があるが、ペプチドはタンパク質より分子量が小さく、合成、標識化、細胞への導入が容易であるため、実験系に有用である。この神経ペプチドの中に微生物に対して殺菌作用を示すものの存在が報告され、神経伝達と抗菌作用の初期のメカニズムが類似しているのではないかと考えられている。したがって抗菌ペプチドは神経ペプチドの作用メカニズム解明に応用できる可能性がある。抗菌ペプチドは動物、植物界に広く存在し、微生物自体にも他の微生物に対する抗菌ペプチドを放出するものがある。このことは逆に抗菌ペプチドが神経ペプチドの作用メカニズム解明に応用できる可能性を示している。

そこで本項目では新規神経機能性ペプチドを探索するため、最近新分野として研究活動が盛んになりつつある海洋微生物に着目し、これらが生産する新規の抗菌ペプチドについて検討した。太平洋、日本海およびオホーツク海の海水または生物から採取された未同定の海洋微生物から抗菌ペプチドの精製を試みた。採取された４９１株の海洋微生物のうち、Staphylococcus aureus、Staphylococcus epidermidis、Proteus vulgaris、Proteus mirabilis、Eschericia coli、Enterobacter cloacae、Enterococcus faecalis、Candida albicans、Bacillus subtilis、Aeromonas hydrophila、Vibrio anguillarumの１１種類の微生物に対して抗菌作用を示したものは１２６株あり、１２株の培養液の抗菌活性はトリプシン処理によって著しく減少した。したがって１２種類の微生物がペプチド・タンパク性の抗菌物質を生産すると考えられ、そのうちNo.１１５株の培養液のS. epidermidisに対する抗菌活性はトリプシン処理による減少が顕著であった。

培養液の組成を0.4%トリプトン、0.2%イースト抽出物、0.1%グルコース、

0.01%塩化カルシウム、0.02%リン酸水素二カリウム、0.01%臭化カリウム、75%海水とした場合に抗菌活性が強く、この組成が抗菌物質生産に適していることがわかった。この液でNo. １１５株を振とう培養した後、遠心分離して菌細胞を除き、得られた上清を熱処理後、減圧濃縮した。これにアセトンを加えて75%とし、アセトン層と水層を分離した。

アセトン層についてペプチド性の抗菌物質の分離法を検討した。まず分画分子量1000の透析膜で低分子物質を除去し、次に分画分子量12,000-14,000の膜を用いて再び透析を行い、膜を通過する成分を集めた。この画分に硫酸アンモニウムを90%飽和になるように加えて塩析を行い、沈でん画分をシリカ系C18カラムを用いた高速液体クロマトグラフィーで分離した。溶出液は0.1%トリフルオロ酢酸（A液）と80%アセトニトリル（B液）とした。第一段階のクロマトグラフィーではB液濃度をステップワイズ状に上昇させ、大まかな分離を行った。すなわち、20%、30%、100%B液で溶出する物質を採集し、それぞれAP20、AP30、AP100画分とした。第二段階ではそれぞれの画分をB液濃度をグラジエント状に上昇させて溶出した。その結果、AP20のクロマトグラフィーでは2画分（AP20□、AP20□）、AP30では2画分（AP30□、AP30□）、AP100では1画分（AP100□）に活性が認められた。これら活性画分のうち、AP30□をさらにゆるやかなグラジエント状で溶出すると、さらに多数のピークに分離され、2つのピーク（AP30□a、AP30□b）に活性が認められた（図５２）。

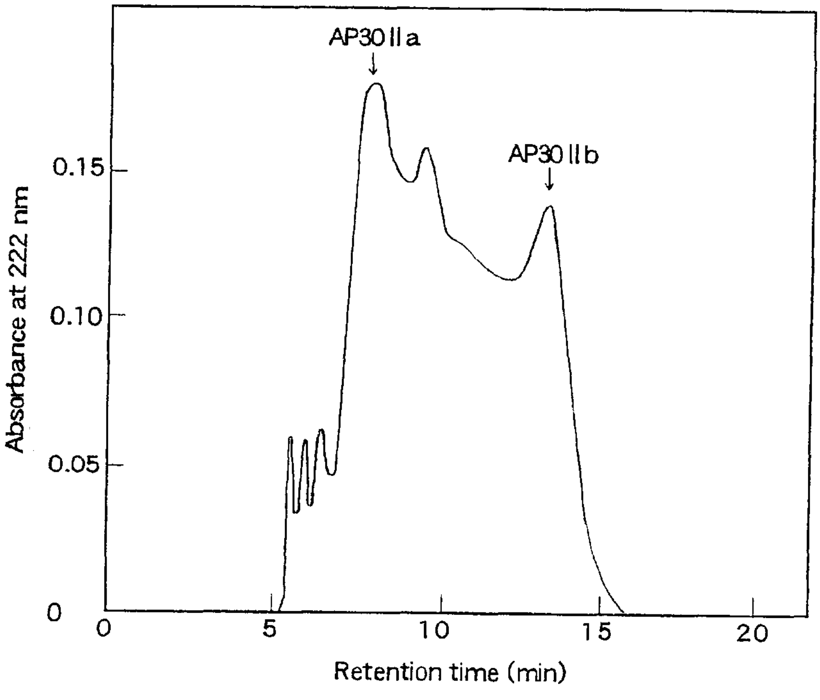

図５２　高速液体クロマトグラフィーによる分離

AP30□bについてレーザーイオン化飛行型質量分析計で分析すると、分子量1100付近に2つのピークを認めた（図５３）。両ピークの分子量の差は約23であり、Naイオンの結合型と非結合型であると考えられた。

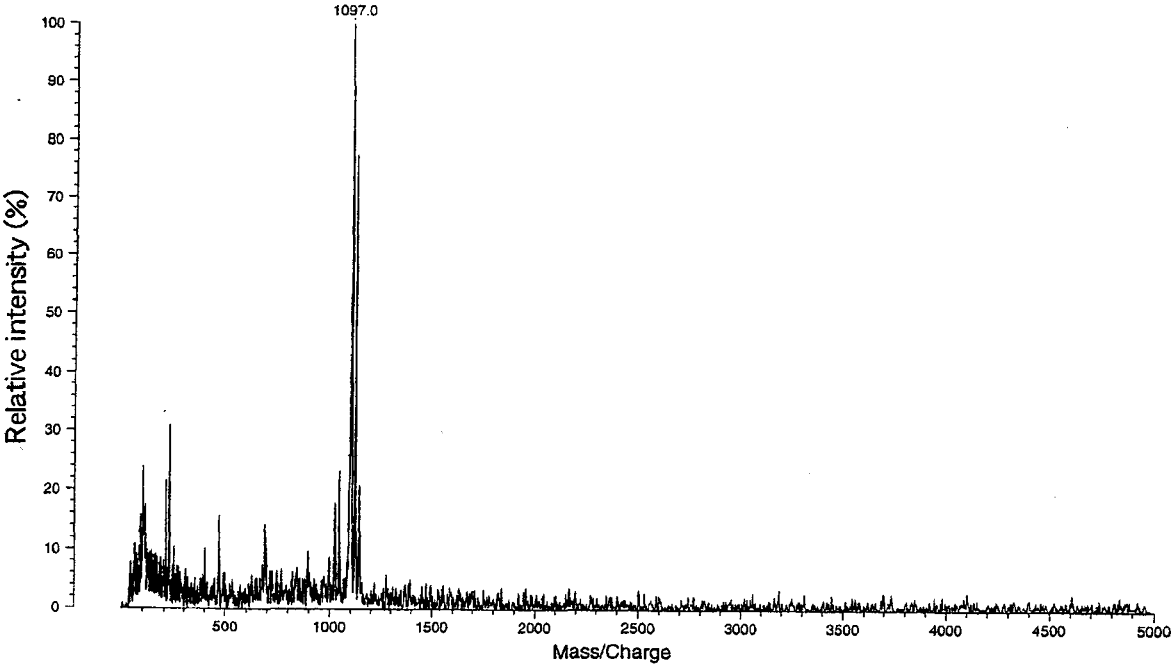

図５３　ＴＯＦ－ＭＡＳＳによる質量分析

したがってAP30□b画分は単一物質で、アミノ酸数個からなる物質と推察された。以上の抗菌物質の精製過程を図５４にまとめ、活性が存在する画分を下線で示した。本研究ではアセトン抽出画分について重点的に精製法を検討し、この画分に少なくとも6種類の抗菌物質が存在することがわかり、その他水画分にも抗菌活性が認められた。したがってこの微生物はペプチド性のものを含む多種類の抗菌物質を合成して菌体外に放出することがわかり、抗菌ペプチドの獲得に有用であることを確認した。

図５４　海洋微生物分泌物質精製のフローチャート

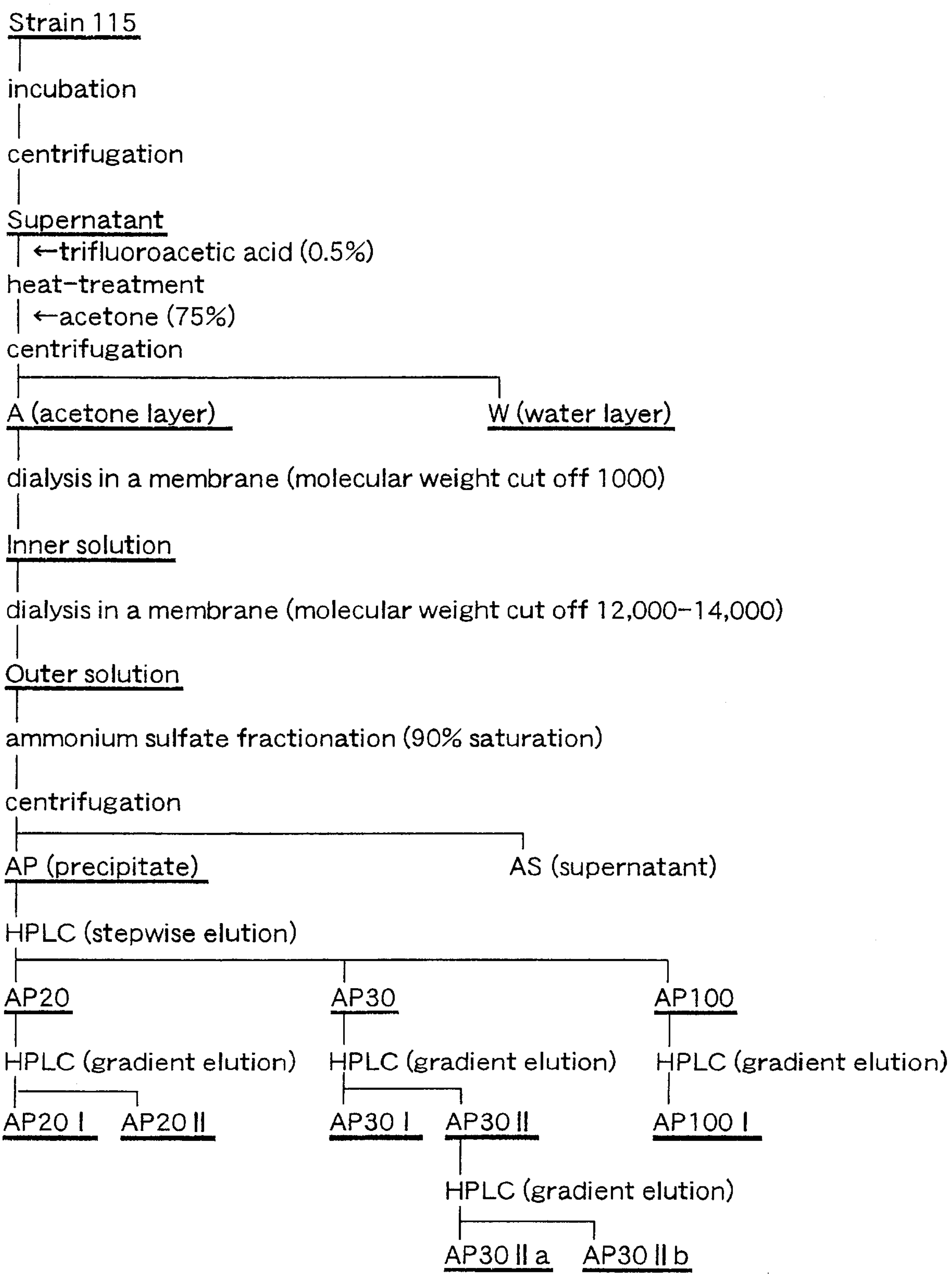
Strain 115
incubation
centrifugation
Supernatant
←trifluoroacetic acid (0.5%)
heat-treatment
←acetone (75%)
centrifugation
A (acetone layer)
W (water layer)
dialysis in a membrane (molecular weight cut off 1000)
Inner solution
dialysis in a membrane (molecular weight cut off 12,000-14,000)
Outer solution
ammonium sulfate fractionation (90% saturation)
centrifugation
AP (precipitate)
AS (supernatant)
HPLC (stepwise elution)
AP20
AP30
AP100
HPLC (gradient elution)
HPLC (gradient elution)
HPLC (gradient elution)
AP20 I
AP20 II
AP30 I
AP30 II
AP100 I
HPLC (gradient elution)
AP30 II a
AP30 II b

このように、海洋微生物のライブラリーを用いたスクリーニングを導入することによって神経機能材料開発に有用な分子を見出すことができた。本項目においては、精製の容易さから分泌物質のスクリーニングを実施したが、菌体内に有用物質が含まれている可能性も高い。この解析は研究期間の関係上実施できなかったが、ライブラリーの菌体は凍結保存してあるため、今後の研究で解析を進めて行きたい。

2－8　光制御ペプチド機能材料の開発

分子レベルでの精密な機能設計が可能なバイオ材料に対する大きな期待が寄せられており、とりわけ天然の枠にとらわれないバイオ材料の開発が課題となっている。これは神経機能材料開発にも必要不可欠の技術である。ペプチドは４０以下のアミノ酸が重合した高分子で蛋白質に較べて小型の分子である。神経機能発現に最も関連の深い分子は蛋白質であるが、その蛋白質の機能発現に係わる部位は数個から数１０個のアミノ酸で構成される構造であることが多い。したがって、ペプチドで機能性蛋白質の機能を実現することは充分に可能である。さらに、ペプチドは人工合成が容易であるため神経機能材料の素材として優れた特質を備えている。したがって、ペプチドの材料化技術は神経機能材料開発に必須の技術である。

神経系蛋白質の機能制御を低分子であるペプチドが担う例も多数報告されており、そのペプチド自身が即神経機能材料になる可能性もある。そのようなペプチドの例として３６個のアミノ酸の重合体である神経ペプチドＹがある。本項目では、このペプチドをモデル分子として用い、このペプチドの活性を光で制御する新しい手法の開発を行った。

ケージドＡＴＰやケージドＣａ$^{2+}$等、紫外光照射によりその生理活性を制御できるケージド化合物は、時間・空間的に高分解能が要求される実験に多用され、現在も多種類の化合物が合成されている。しかしながら、蛋白質・ペプチドのケージド化合物は、報告数が極めて少なく、また報告された調製法（化学修飾による方法、サプレッサーｔＲＮＡを用いる方法、液相中の有機合成的方法）は、ケージド化の部位や量の制御、収量、操作の煩雑さ等の点において問題が多く、ケージドペプチド・蛋白質の一般的な調製法にはなっていない。

本項目では、光感応基を側鎖に持つ新規なチロシン誘導体（図５５）を新たに合成し、Ｆｍｏｃ固相合成法によってペプチドに組み込むことにより、任意の位置に光感応基を持つペプチドが合成できることを明らかにした。

ケージドペプチド中の光感応基は、紫外光照射により容易に脱保護する事ができ、保護基のはずれた目的ペプチドを生成する。図５６にケージド神経ペプチド（ケージドＮＰＹ）を紫外線照射し、高速液体クロマトグラフ（ＨＰＬＣ）によりその光反応生成物を分析した結果を示す。光照射により、無保護の神経ペプチドＹ（ＮＰＹ）が生成していることが確認された。

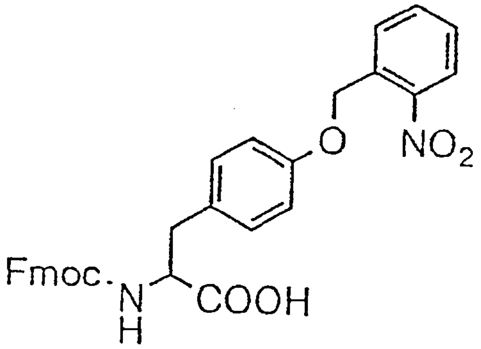
NO2
O
Fmoc
N
H
COOH

図５５　光感受性アミノ酸（チロシン）

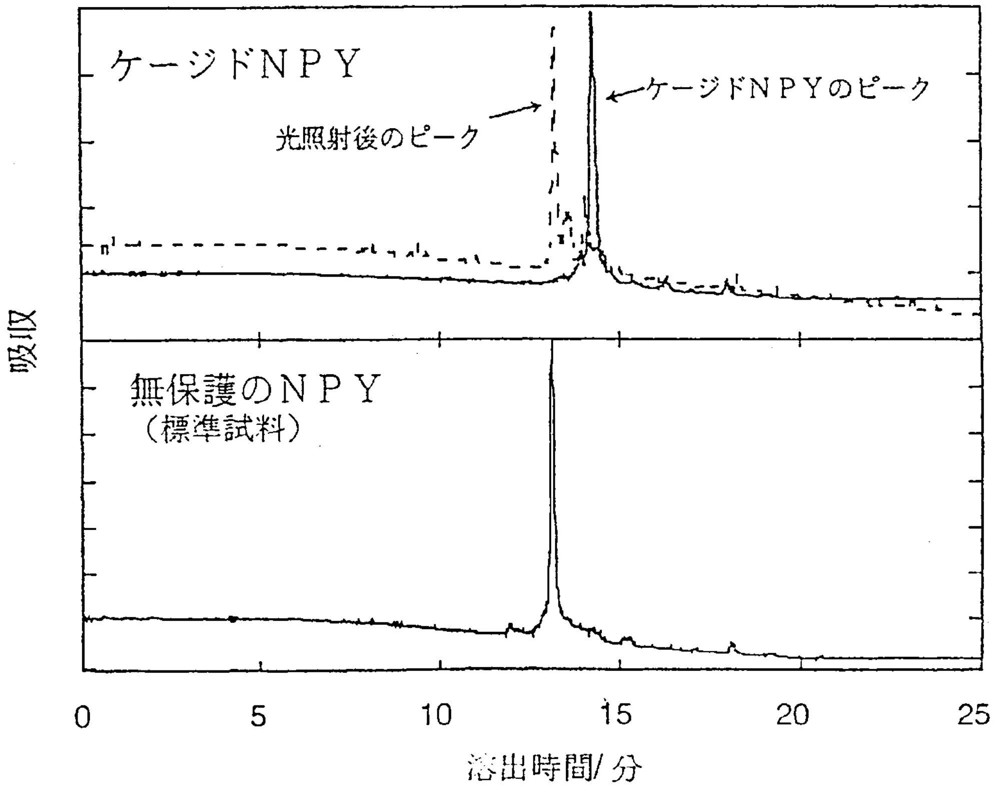

図５６　光照射によるケージドアミノ酸の正常アミノ酸への転換

ところでケージド化合物には、光照射により保護基が脱保護できると共に、生理活性が変化する性質が求められる。そこで、神経ペプチドY（NPY）のケージドペプチドを合成し、その生理活性を求めてみたところ、生理活性発現に重要と示唆されてきた部位に光感応基を導入した場合に生理活性が制御できることを見いだした（図57）。

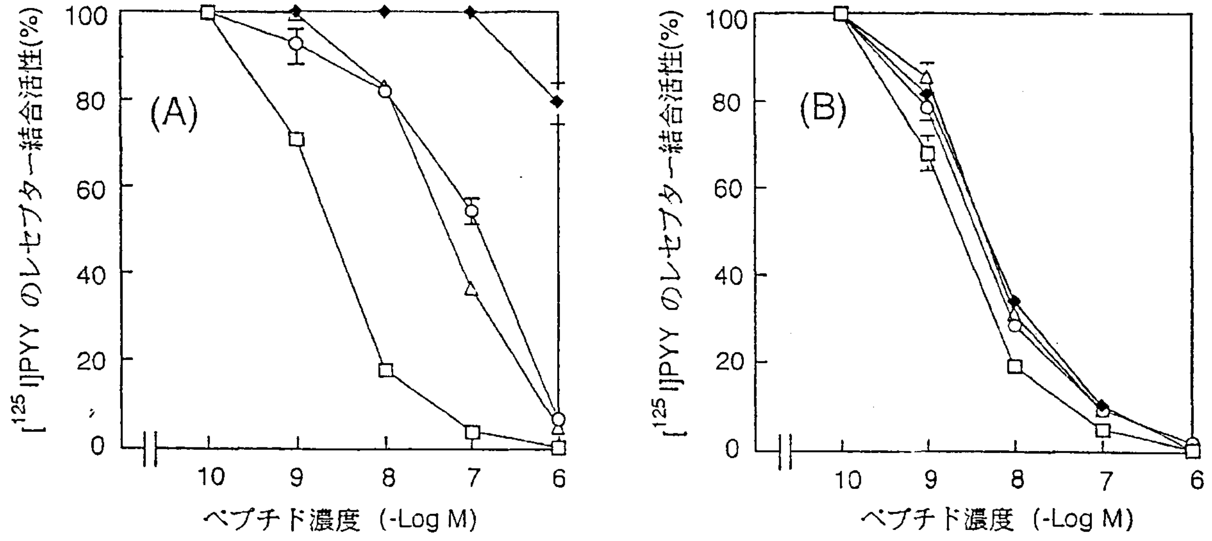

図57　ケージドアミノ酸を組み込んだニューロペプチドYの受容体への結合能変化
A：光照射前、B：照射後、□はノーマルペプチド、残りはケージドペプチド、ケージドペプチドの中でも◆が最も大きな結合能変化を示した。

脳神経細胞内情報伝達系を制御できる分子として、ペプチドが多く見いだされているが、我々の結果は、それらペプチド性の機能分子をケージド化できることを示している。今後、ケージドペプチドを用いて情報伝達を細胞の任意の場所と時間でオン、オフすることにより、複雑な神経細胞内情報伝達機構の解明に新しい展開を与えるとともに、活性制御の容易な神経機能材料開発に活用されるのは間違いないと考えられる。

第３章　神経細胞人工基板インターフェース材料

３－１　リソグラフィー技術を用いたパターニングと培養神経細胞接着性制御

神経細胞に対する損傷が軽微な場合には、再生・修復手法を開発することによって正常な神経細胞へ回復可能であるが、重い損傷の場合は神経細胞の細胞死を防ぐことは困難になる。このような状況で脳神経系の正常な機能を回復するためのひとつの手法が人工素子による機能代替である。これを実現するためにまず解決しなければならない問題点は、生きた神経細胞と人工基板とのマッチングをとることである。すなわち、神経細胞と人工基板のインターフェースの開発が重要である。本課題では、特に人工基板の作製法の開発とその人工基板を使ってのインターフェース材料の研究開発を中心に行った。この人工基板作製とインターフェース材料開発の足がかりとするために、神経細胞を基板上にパターン化する方法を開発した。

神経細胞・人工基板インターフェース材料を開発するために、神経細胞を基板上にパターン化する方法を検討した。まず、半導体製造に用いられているフォトリソグラフィ法を用いて作製した樹脂パターンを基板に形成後、樹脂表面の親疎水性を制御し、用いた樹脂への細胞接着性を検討した。この目的に適したシステマティックな処理法を独自に考案した（図５８）。この方法によりネガ型とポジ型の両方のパターニング、基板表面の光感受性樹脂、フォトレジストへの生理活性分子の固定化が容易になった（図５９）。しかし、この光感受性樹脂の親疎水性を変化させるだけでは、基板表面のパターンに完全に沿った形で細胞を固定化することは困難であった（図６０）。

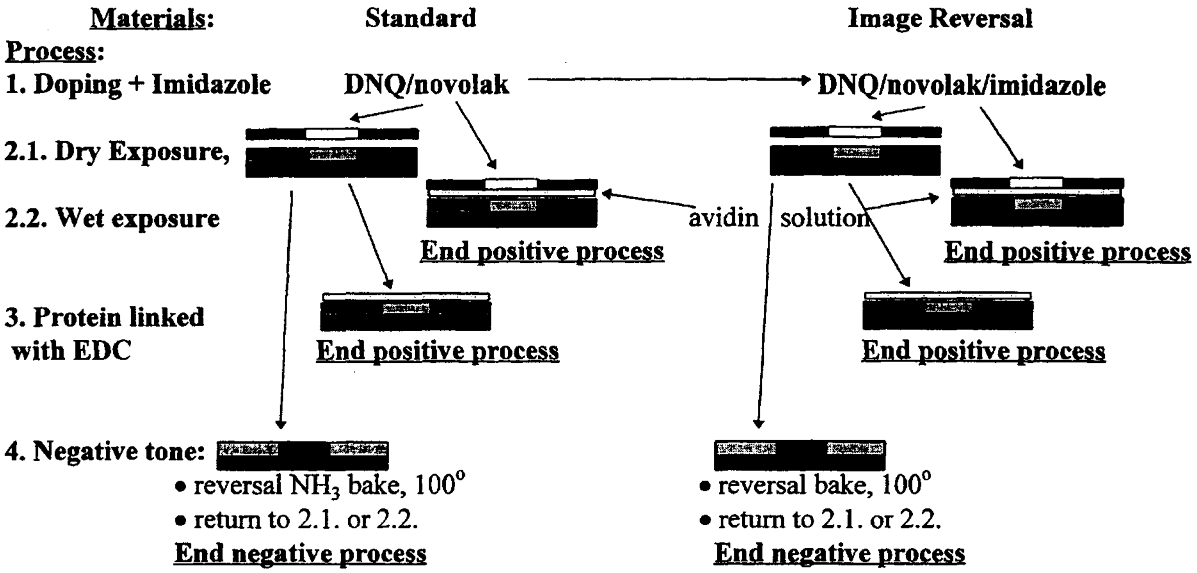
Materials:
Standard
Image Reversal
Process:
1. Doping + Imidazole
DNQ/novolak
DNQ/novolak/imidazole
2.1. Dry Exposure,
2.2. Wet exposure
avidin solution
End positive process
End positive process
3. Protein linked with EDC
End positive process
End positive process
4. Negative tone:
• reversal NH3 bake, 100°
• return to 2.1. or 2.2.
End negative process
• reversal bake, 100°
• return to 2.1. or 2.2.
End negative process

図５８　リソグラフィー法によるシステマティックな基板表面処置と分子架橋

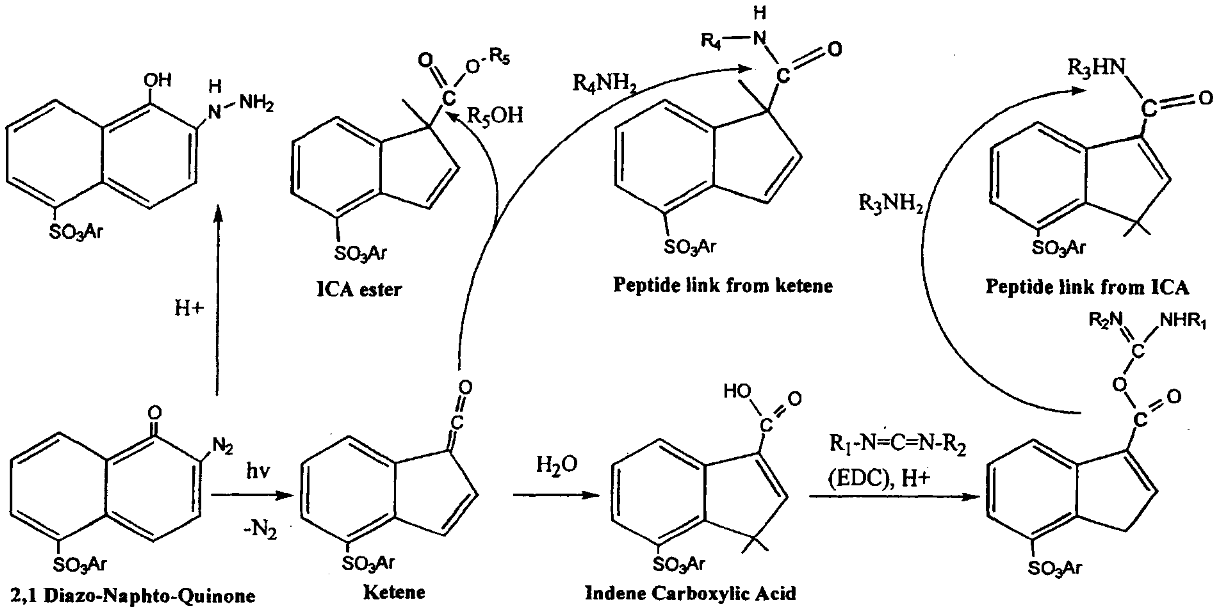
OH
H
N
NH2
SO3Ar
H+
O
R5
R5OH
ICA ester
H
R4
N
O
R4NH2
Peptide link from ketene
R3HN
O
R3NH2
Peptide link from ICA
R2N
NHR1
O
N2
hv
-N2
2,1 Diazo-Naphto-Quinone
Ketene
H2O
HO
Indene Carboxylic Acid
R1-N=C=N-R2
(EDC), H+

図５９　基板表面親疎水性制御と分子架橋の反応図

３－２　培養基板表面処理による微生物物質生産制御

この項目の研究は、当初の研究計画には含まれていない。前項のフォトレジストを塗布した基板への神経細胞の接着性制御に関する研究の過程で、この表面への海洋微生物の接着が観察され、さらに、接着した微生物からの抗生物質分泌が促進された。この海洋微生物は、前章で述べた神経機能制御分子のスクリーニングに用いられたものである。したがって、ここで認められた新しい現象は、微生物による神経機能分子の大量調製に応用可能である。

ガラス表面をもつ容器で微生物を培養した場合は、フォトレジスト表面の容器で培養した場合に較べて抗生物質産生活性が低かった。さらに、フォトレジスト表面でも、それに対する光処理の程度で微生物の抗生物質産生活性が影響された（図６４）。

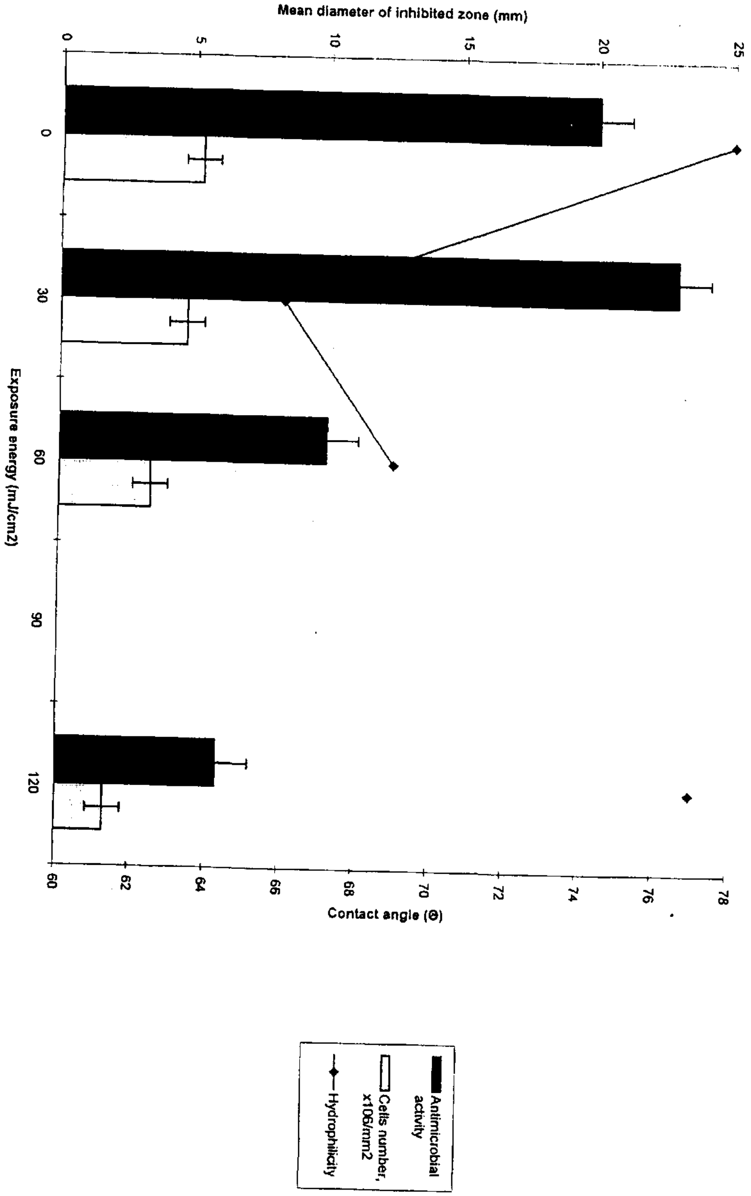

図６４　表面処理基板上での海洋微生物培養
白：微生物密度、黒：抗生物質活性、折れ線：接触角

すなわち、最も活性の高かったのは、短い光照射で処理した場合で、この処理の場合が最も表面の親水性が高かった。基板表面の微生物の数はむしろやや減少しているので、微生物個々の活性が上昇していると考えられる。

このような結果は、神経機能材料の微生物による生産効率を表面の物理化学的性質の制御で上昇させることが可能であることを示している。神経機能材料が実用化される段階においては有用な技術となることが期待される。

第４章　結論と今後の予定

４－１　結論

脳神経系の修復・代替を目指す人工神経の開発は、他の人工臓器と異なり、単一の神経細胞機能と多数の神経細胞からなるネットワーク機能との両面性克服の困難が伴うが、急速な高齢化の進行する我が国の緊急かつ重要な最先端研究課題である。本研究においては、次の３課題に焦点を合わせ、将来の人工神経開発に役立つ神経機能材料開発のための基盤研究を行なった。第一の課題は、神経繊維伸長活性を持つ蛋白質の機能部位解明とその材料化による神経修復材料開発技術の確立、第二の課題は、シナプス伝達機能を中心とした神経活動制御に関与する分子群の解明、第三の課題は、人工デバイスの脳神経系への組込み技術確立のための神経細胞と人工基板とのインターフェース材料開発のための基盤技術確立を目指したものである。

それぞれの課題について概略すると以下の成果が得られた。

第一課題

・新規神経繊維伸長活性蛋白質をの発見
・上記蛋白質の遺伝子クローニングの成功
・この蛋白質の活性部位解明

第二課題

- 活動依存的シナプス形成の2つの様式の発見
- サイレントシナプスからデュアルコンポーネントシナプスへのシナプス成熟機構解明
- 独自の神経細胞培養系でのシナプス伝達効率の長期的変化の解析に成功
- 上記の長期的変化を誘導する高分子の発見
- シナプス活動変化に伴う神経細胞形態変化の発見
- 新しいチャネル蛋白質の発見と解析
- 海洋微生物ライブラリーからの抗生物質産生菌のスクリーニングの成功とこの物質の精製
- 光制御ペプチド機能材料開発の成功

第三課題

- 神経細胞培養基板のパターニング手法の開発
- 培養基質表面処理による微生物物質生産の制御に成功

これらは本研究の目標に沿った成果であり、期待通りの成果があげられた。さらに、本研究を遂行する過程で研究項目間の相互作用が生じ、当初の予定になかった成果も得られた。神経機能材料という将来の医療福祉分野で重要になる新材料開発につながる基盤研究を、短期間に集中して共同研究の形で進めたことがこれらの実り多い結果の実現に結びついたものと思われる。

第一課題は最も材料化の可能性の高い課題であり、機能部位が限定できたことから生体材料への固定化への発展が期待される。第二課題では機能材料の可能性を秘めた分子が明らかになってきた。特に長期増強誘導因子は広範な応用が期待され、因子同定を早急に進める必要がある。また、光制御ペプチドの世界に先駆けた開発は新たな機能材料開発手法への道を拓いた。第三課題のインターフェースは人工デバイスの新規応用分野開拓に重要である。まだ表面機能の制御・耐久性等に課題は残っているが、本研究で開発した手法の応用可能性は明らかである。

４－２　今後の予定

このような成果は将来の医療福祉技術にかかわる新産業の創生に直結するものと期待される。この期待を現実のものとするためには、本研究の成果に基づき、さらに広範囲の研究者を結集したプロジェクトを早期に開始する必要がある。

このために、我々は、通商産業省工業技術院の産業技術研究開発制度に新たなプロジェクト「脳神経細胞工学の基盤研究」を提案し、平成９年度よりまず先導研究が実施されているところである。先導研究の中でこの分野の技術開発項目を調査し、その結果をもとにプロジェクト研究を提案して行く予定である。

このプロジェクト研究の概要は次頁の図に示した。

この研究は、高齢化福祉社会を支える生命支援技術としての生体機能代行補助技術、すなわち人工臓器のひとつである人工神経の開発のための基盤技術、特にそれに役立つ神経機能材料開発技術の整備を目指している。我が国の高齢化は西暦２０１０－２０１５年にピークを迎えるため、少なくともこの時期以前にこの技術を実用化する必要がある。しかしながら、人工臓器は社会福祉や国民の生活の質向上の観点からは重要な技術であるにも関わらず、大きな需要を生む単一商品とはなりにくい、開発には幅広い分野の最先端技術を結集する必要がある等の理由から民間企業のみでは開発に着手しにくい課題である。したがって、この緊急を要する課題は国家プロジェクトとして強力に推進する必要があり、また、このプロジェクトにより神経機能材料開発に関する基盤技術が整備されれば、民間企業も最終商品化での開発リスクが軽減される。

この研究の提案開発項目からも分かるように、人工神経開発の基盤技術確立には、バイオテクノロジー、生体工学、機械工学、新材料、エレクトロニクスの最先端技術の導入が不可欠である。本研究の遂行は、これら分野の技術レベルの向上、新規技術・新規装置の開発による新しい分野の創製に寄与する。特に、単一細胞レベルの細胞操作技術は動物・植物の個体を用いた微細組織改造を可能にし、治療・品種改良等に新技術を生み、生物を扱う産業界の技術革新に貢献することが期待される。

この研究は産業政策戦略としても重要である。将来の新産業創生を考えた場合、それに先立つ基盤技術整備が必須であることは明白である。我が国に対する基礎研究批判は、我が国に基礎研究能力がないのではなく、多様な基礎研究を体系的に行える仕組みが欠如していた点に留意すべきである。本提案は、人

工神経開発を目指した基盤研究という、世界に先駆けた試みであるところに最大の重要性があり、このような基盤研究の推進によりこの分野の主導権を確保することが可能になる。本研究で生まれる、新しい測定技術、新規機能分子、医療福祉機器開発のアイディアはすべて産業に役立つ知的財産として我が国に蓄積され、国民利益に沿う形で産業界に提供される。

このようなプロジェクト研究の推進、あるいは、個別テーマの研究の大阪工業技術研究所における一層の発展を通じて産業振興、さらには、新しい世紀の快適な人間生活空間創生に寄与して行きたい

産技先導研究「脳神経細胞工学の基盤研究」

研究実施内容と成果の応用可能性

代替人工細胞としての
人工神経の開発

機能代替材料としての
人工神経開発

神経細胞賦活化
神経修復
人工素子導入

微細細胞操作技術に基づく
外科医療技術開発

正確な作用機構知見に基づく
演繹的新薬化合物設計

環境浄化技術

生産プロセス高度化

生理活性物質生産技術

細胞機能改変技術

独創的新医療技術開発

医療ニーズの高度化に対応

次世代型バイオテクノロジー確立

プロジェクト研究内容

単一細胞・単一分子計測操作のための

先端的細胞工学技術開発

細胞機能可視化技術
分子・細胞操作技術
解析プローブ開発
機能分子同定技術
シナプス機能解析技術

人工神経を目指した

神経機能材料開発

生存維持材料
神経修復材料
神経賦活化材料
機能分子
活性部位解明

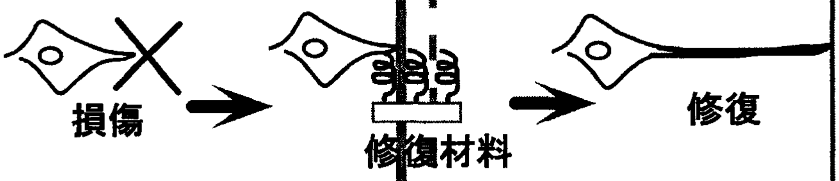

神経機能メカニズム解析・機能分子の解明

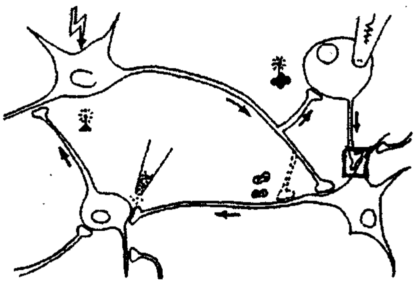

神経回路形成・シナプス可塑性解析

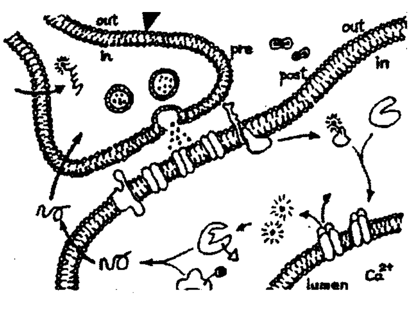

神経細胞内情報伝達解明

第５章　成果発表

５－１　論文発表（２３件）

１．西宗裕史、植田淳子、田口隆久 (1995)
筋由来神経突起伸長因子
実験医学（別冊）（バイオサイエンス用語ライブラリー） 1995:118-119

２． K. Kiyosue, M. Kasai, T. Taguchi (1996)
Two modes of activity-dependent synaptogenesis of cerebral neurons in vitro
Neuroreport, 7:701-704

３． S.B. Sato, K. Kiyosue, T. Taguchi, M. Kasai, S. Toyama (1996)
Okadaic acid gives concentration-dependent reciprocal effects on the fluid phase endosytosis activated by Ca and phorbol 12-myristate 13-acetate
J. Cellular Physiol. 166:66-75

４． S.B. Sato, T. Taguchi, S. Yamashita, S. Toyama (1996)
Wortomannin and Li specifically inhibit clathirn-independent endocytic internalization of bulk fluid
J. Biochem. 119:887-897

５． I.Fujimoto, S.Oike, T.Kondo, T.Katada, H.Kato, T.Taguchi, M.Kasai, Y.Okada, K.Mikoshiba, K.Ikenaka (1996)
GTP-binding protein activation underlies LTP induction by mast cell degranulating peptide Nuerosci. Res. 25:229-237

６． D.V. Nicolau, T. Taguchi, H. Taniguchi, S. Yoshikawa, M. Dusa (1996)
Application of DNQ-based microlithogrphy to patterning bioactive molecules and cells
SPIE 2724:500-511

７． D.V. Nicolau, T. Taguchi, H. Tanigawa, S. Yoshikawa (1996)
Control of the neuronal cell attachment by functionality manipulation of diazo-naphtoquinone/novolak photoresist surface
Biosensors and Bioelectronics, 11:1237-1252

８． Y. Tatsu, Y. Shigeri, S. Sogabe, N. Yumoto, S. Yoshikawa (1996)
Solid-phase synthesis of caged peptides using tyrosine modified with a photo-cleavable protecting group : pplication to hte synthesis of caged neuropeptide Y
Biochem. Biophys. Res. Comm. 227:688-693

９． 田口隆久 (1996)
分子認識を利用した選択的神経細胞培養法の開発
酵素工学ニュース 36:9-11

１０． 田口隆久 (1996)
神経細胞の選択培養を実現するペプチド
通産ジャーナル 304:64-65

１１． D.V. Nicolau, T. Taguchi, H. Taniguchi, S. Yoshikawa (1996)
Bio-microlithography: UV- and E-beam patterning of bioactive molecules
J. Phoropolym. Sci. Tech. 9:645-652

１２． 田口隆久、清末和之、工藤卓 (1996)
培養大脳神経細胞のシナプス形成・可塑性のメカニズム
第１１回生体・生理工学シンポジウム論文集 '96:249-252

１３． K. Kiyosue, M. Kasai, T. Taguchi (1997)
Selective formation of silent synapses on immature postsynaptic cells in cocultures of chick neurons of different ages
Dev.Brain Res.99:201-207

１４． 田口隆久、清末和之、工藤卓 (1997)
大脳皮質ニューロン－シナプス形成・可塑性アッセイ系
神経細胞培養法、p. 158-165 シュプリンガー出版（東京）

１５． 田口隆久 (1997)
ペプチドで純粋培養
神経細胞培養法、p. 78 シュプリンガー出版（東京）

１６． H. Taniguchi, K. Inai, Y.C. Zhu, T. Taguchi, S. Yoshikawa (1997)
Molecular recognition using short peptides and its detection by surface plasmon resonance spectroscopy
Peptide Chem. (in press)

１７． K. Yoshida, T. Ide, K. Inoue, K. Mizuno, T. Taguchi, M. Kasai (1997)
A voltage- and K-dependent K channel from Dictyostelium discoideum membrane fraction enriched in contractile vacuole
Biochim. Biophys. Acta (in press)

１８． S.N. Kudoh, A. Matsuo, K. Kiyosue, M. Kasai, T. Taguchi (1997)
Long-lasting enhancement of synaptic activity in dissociated cerebral neurons induced by brief exposure to Mg-free conditions
Neurosci. Res. (in press)

１９． E.P. Ivanova, E.A. Kiprianova, V.V. Mikhailov, G.F. Levanova, A.D. Garagulya, N.M. Gorshkova, I.Y. Bakunina, G.M. Frolova, D.V. Nicolau, N. Yumoto, T. Taguchi, S. Yoshikawa (1997)
Pseudoalteromonas mytili sp. nov. A new spiecies of marine bacteria isolated from mussels
Int. J. System. Bacter. (in press)

２０． E.P. Ivanova, N. Yumoto, M.G. Petukhov, T. Taguchi, S. Yoshikawa
Antimictobialo peptides synthesized by marine bacteria from the pacific ocean
(submitted)

２１． E.P. Ivanova, D.V. Nicolau, N. Yumoto, T. Taguchi, K. Okamoto, Y. Tatsu, S. Yoshikawa (1997))
The impact of conditions of cultivation and adsorption on antimicrobial activity of marine bacteria.
Marine Biol. (in press)

２２． H. Nishimune, I. Oishi, S. Koyanagi, T. Taguchi
Characterization of neurite-outgrowth promoting factors in the extracto of chick denervated muscle
(submitted)

２３． H. Nishimune, A. Uyeda, M. Nogawa, K. Fujimori, T. Taguchi
Neuroscresin: a novel target derived factor for neurite outgrowth
(submitted)

５－２　口頭発表　（２９件）

1. K. Kiyosue, M. Kasai, T. Taguchi (1995)
Postsynapse-dependent synaptogenesis in dissociated cell culture of chick cerebral neurons
25th Annual Meeting of the Society for Neuroscience, San Diego, USA

2. S.N. Kudoh, K. Kiyosue, M. Kasai, T. Taguchi (1995)
Synaptic plasticity in dissociated chick cerebral neurons induced by Mg-free medium
25th Annual Meeting of the Society for Neuroscience, San Diego, USA

3. H. Nishimune, A. Uyeda, M. Nogawa, T. Taguchi (1995)
A novel neurite outgrowth promoting factor specific to embryonic telencephalic neurons
25th Annual Meeting of the Society for Neuroscience, San Diego, USA

4. T. Taguchi, X.X. Bo, H. Taniguchi, K. Kiyosue, S.N. Kudoh, S. Murase (1995)
Synapse-formation in a glia-free culture of dissocciated chick cerebral neurons
25th Annual Meeting of the Society for Neuroscience, San Diego, USA

5. E. Shimabayashi, K. Kiyosue, M. Kasai, T. Taguchi (1995)
Analysis of long term potentiation in the chick IMHV region
25th Annual Meeting of the Society for Neuroscience, San Diego, USA

6. N. Yumoto, S. Murase, Y. Shigeri, S. Yoshikawa (1995)
Elucidation of structural requirements of neuropeptide Y for recognition by Y2 receptor using acylated and cross-linked analogs.
25th Annual Meeting of the Society for Neuroscience, San Diego, USA

7. 谷口弘志、吉川暹、高山邦明、田口隆久 (1996)
表面プラズモン共鳴法を用いたポルフィリン誘導体の簡便検出法の開発
日本化学会第７０回春期大会，東京

8. D.V. Nicolau, T. Taguchi, S. Yoshikawa (1996)
Laterally Defined Bioactive Molecule Architectures
Bionic Design Workshop/Symp.Molecular Construction, Tsukuba, Japan

9. 田口隆久 (1996)
培養細胞を用いた神経機能解析
大阪大学医学部神経内科教室セミナー（招待講演）、吹田

10. 田口隆久 (1996)
一神経細胞からみた神経活動
大阪工業技術研究所科学技術週間講演会（招待講演）、池田

11. 田口隆久 (1996)
培養神経細胞の用いたシナプス解析
北陸先端科学技術大学院大学　大学院特別講義、小松

12. 清末和之、葛西道生、田口隆久 (1996)
早い発生段階の神経細胞には選択的にサイレントシナプスを形成する
第１９回神経科学学会大会、神戸

13. 工藤卓、清末和之、葛西道生、田口隆久 (1996)
シナプス伝達効率の長期的増強－解離培養細胞による単一ニューロン解析
第１９回神経科学学会大会、神戸

14. 西宗裕史、植田淳子、田口隆久 (1996)
終脳特異的な突起伸長活性を持つ新規因子 Neurite Promoting Factor
第１９回神経科学学会大会，神戸

15. E.P. Ivanova, D.V. Nicolau, T. Taguchi, K. Okamoto, S. Yoshikawa (1996)
Attachment on diffrent polymer surfaces controls a production of anti-microbial peptides by marine bacteria
10th International Biotechnology Symposium, Sydney, Australia

16. D.V. Nicolau, T. Taguchi, H. Taniguchi, S. Yoshikawa (1996)
Laterally organized bioactive molecular architectures built using micro-lithographic materials and techniques
10th International Biotechnology Symposium, Sydney, Australia

17. D.V. Nicolau, T. Taguchi, H. Taniguchi, S. Yoshikawa (1996)
Control of the neuronal cells attachment by surface functionality manipulation of the diazo-naphto-quinone/novolak photoresist
10th International Biotechnology Symposium, Sydney, Australia

18. E.P. Ivanova, N. Yumoto, T. Taguchi, K. Okamoto, S. Yoshikawa (1996)
Production of antimicrobial peptides by marine bacteria from the pacificocean
10th International Biotechnology Symposium, Sydney, Australia

19. M. Petkhov, 湯元昇、吉川暹 (1996)
安定なアルファヘリックス構造をもつペプチドの新しい設計法
第６９回日本生化学会、札幌

20. 谷口弘志、稲井公二、Yao-Can Zhu、田口隆久、吉川暹 (1996)
Molecular Recognition Using Short Peptides and Its Detection by Surface Plasmon Resonance Spectroscopy
第３４回ペプチド化学討論会、筑波

21. 佐藤智、井上敬、田口隆久、清末和之、葛西道生、富山朔二 (1996)
マクロピノサイトーシスの誘導法確立による分子機構の研究
第４９回日本細胞生物学会大会、京都

22. 吉田邦人、井出徹、井上敬、水野孝一、田口隆久、葛西道生 (1996)
収縮胞Ｋチャネル：透過性イオンによるブロック
第３４回日本生物物理学会年会、筑波

23. 工藤卓、清末和之、葛西道生、田口隆久 (1996)
解離培養系における長期増強現象の解析
第３４回日本生物物理学会年会、筑波

24. 清末和之、葛西道生、田口隆久 (1996)
発生依存的なサイレントシナプスの形成と解析
第３４回日本生物物理学会年会、筑波

25. S.N. Kudoh, K. kiyosue, M. Kasai, T. Taguchi (1996)
Long-lasting enhancement of synaptic transmission in dissociated chick cerebral neurons
26th Annual Meeting of the Society for Neuroscience, Washington,D.C. USA

26. H. Nishimune, A. Uyeda, M.Nogawa, Y. Shigeri, K. Hujimori, T. Taguchi (1996)
Functional analysis of neurite promoting factor
26th Annual Meeting of the Society for Neuroscience, Washington, D.C. USA

27. K. Kiyosue, M. Kasai, T. Taguchi (1996)
Postsynaptic regulation of silent-synapse formation in coculture of hetero-aged neurons
26th Annual Meeting of the Society for Neuroscience, Washington, D.C. USA

28. 田口隆久、清末和之、工藤卓 (1996)
培養大脳神経細胞のシナプス形成・可塑性のメカニズム
第１１回生体・生理工学シンポジウム、吹田

29. 田口隆久 (1997)
神経機能材料開発を目指した脳研究 （招待講演）
第８回健康・医療研究会、けいはんな

５－３　特許　（１件）

１．細胞をパターン上に接着するための基板作製法（出願中）

第６章　購入機器一覧

N00101	バイオクリーンベンチ
N00301	超音波細胞破砕機
N00401	精密イオンポリッシャー
N00501	分光分析器
N00601	遺伝子解析装置
N00701	円二色性分散計
N　504	除振台
N　505	製氷装置
N　506	気相インキュベータ
N　507	データ解析コンピュータ
N　522	パソコン
N　550	低温反応槽
N　564	バイオラット
N00201	ミリ RO 05 プラス
N00202	ミリ Q プラス

N00801	INSIGHTPLIS 本体
N00802	空冷アルゴンレーザー
N00803	CCD カメラ
N00804	Hi- 8 ビデオカセットレコーダー
N00805	ビデオプリンタ
N01101	倒立システム顕微鏡本体
N01102	精密マニピュレーター部
N01103	高感度電流増幅器
N01104	神経活動記録装置
N01105	遺伝子増幅装置

あとがき

新エネルギー・産業技術総合開発機構が平成7年度に創設した提案公募型・最先端分野研究開発に採択され、1年5ヶ月にわたり研究を遂行することができた。物心両面の集中的投資により、提案者の考えた大きな研究構想を短期間に実現できたことは研究者として喜びにたえない。同機構の関係者の皆様に甚大なる謝意を表したい。

初めての共同研究形態である本研究の遂行にあたり、格段のご配慮とご協力を頂いた通商産業省工業技術院大阪工業技術研究所の児玉皓雄所長はじめ所員の皆様、特に事務処理の御助言を頂いた総務部の皆様に感謝申し上げる。

はじめに記したように、本研究は同機構から派遣された6名の研究者と大阪工業技術研究所の4名の研究者との共同研究であるが、その他研究の一部をお手伝い頂いた研究者、特に、達吉郎博士、ダン・ニコラウ博士、清末和之博士、西宗裕史研究員、工藤卓研究員、植田淳子研究員、石本哲也研究員、国里篤志研究員に謝意を表す。また、実験補助業務、報告書作成で多大な貢献をして頂いた白井薫氏に謝意を表す。

本研究は平成9年3月で終了したが、ここで得られた成果を生かすべく新たな提案を準備しているところである。今後とも一層のご助言、ご配慮を頂けるようお願い申しあげる。

付録リスト

関連新聞発表

１．	日刊工業新聞	１９９５．１１．２
２．	産経新聞	１９９６．４．２０
３．	日経産業新聞	１９９６．７．１０
４．	化学工業日報	１９９６．７．２９
５．	日経産業新聞	１９９６．１０．２４

参考文献（既発表、及び、発表予定論文）

（論文発表リストの通り）

日刊工業新聞　1995(平成5)年11月2日　7面

人工神経の研究
大工研がスタート
脳細胞修復材を探査

工業技術院大阪工業技術研究所（所長児玉皓雄氏）は一日、「神経機能材料開発のための基盤研究」（プロジェクトリーダー田口隆久氏＝高分子表面化学研究室長）を開始した。新エネルギー・産業技術総合開発機構（NEDO）の提案公募型・最先端分野研究開発制度に基づくもので、人工臓器開発の中で研究が遅れている人工神経を世界に先駆けて開発するための基盤研究。

神経細胞は一個の細胞が機能の単位であると同時に、複数の神経細胞で情報を伝達する二重性があるが、同プロジェクトでは神経機能の修復、代替機能を持つ機能性材料をつくり出すために①神経繊維修復材料②神経活性化材料③神経細胞・人工基板インタフェース材料—の開発について研究する。

修復課題では、神経繊維伸長促進たんぱく質の活性部位を探すとともに、同部位の低分子ペプチド化を試行、再生が難しい脳神経細胞の修復ができる材料の探査を行う。

また活性化材料では、同研究所が開発した培養神経細胞を使ってシナプス活動を活性化する機構を解析し、その主役分子を突き止める。インタフェース技術では、人工基板と脳神経細胞との間の電気信号による情報伝達ができる材料開発を目指す。

化学工業日報(12) '96 7/29

“工学の目”で脳神経細胞探る

工技院が先導研究

通産省工業技術院は「脳神経細胞工学」に着目した研究開発プロジェクトの発足を目指し、来年度から予備的・基礎的な調査研究に乗り出す方針だ。これは、バイオテクノロジー分野で走らせる九七年度の新規先導研究テーマとして候補にあがっているもの。脳は、数百億個にのぼる数多くの神経細胞（ニューロン）から構成されている巨大な情報処理システムといわれる。ニューロンとニューロンがおりなす複雑なネットワークによって、人間にとって重要な認知・思考・感情などといった高次の精神機能をつかさどっている。調査研究では、「脳・神経機能にかかわる機能分子が細胞内でどういう機能を担っているか」に着目。分子レベルから、“一個の生きた細胞”を調べるための基盤技術について検討を進める。さらに脳神経系の機能解明で得られた知見を踏まえて、「切れてしまった神経を自ら修復する神経繊維修復材料」などに着目した神経機能材料開発についても調査する。神経・精神障害の修復予防など、今後の医療ニーズの高度化に対応した独創的新医療技術の開発に先駆けた取り組みとして注目されそうだ。

再生可能な「人工神経」めざし

材料開発にも的

機能を分子レベルで

八月中旬に開かれる産業技術審議会の産業科学技術開発部会で承認されると、今回の「脳神経細胞工学の基盤研究」が新規先導研究課題として正式決定する。工技院の中核実施機関は、大阪工業技術研究所。電子技術総合研究所と生命工学工業技術研究所も、実施機関の候補としてあがっている。調査期間は二―三年。

脳のなかでは膨大な数の神経細胞が相互に結び付いて精緻な神経回路網をつくっている。調査研究では、「脳神経細胞工学」という視点から脳の神経回路網、情報伝達を行うための場であるシナプス、細胞内にアプローチする。

そのアプローチ手法として取り上げるのは、①生きた細胞での機能分子の働きを顕微鏡で高感度に直接計測する「細胞機能可視化技術」②個々の分子や細胞を捕捉・移動・整列させたり、細胞を決まったパターンで培養するための「分子・細胞操作技術」③目的の分子を観測するための標識分子を開発するための技術④注目する活性を持つ微量生体分子を精製・同定する技術⑤シナプスの構造機能相関を解析するための同時解析システムを構築する「シナプス機能解析統合化技術」。これら五つの基盤技術を使って、脳・神経機能を解明する可能性について探る。

脳神経系の解析を踏まえて、人工神経を目指した材料研究にも着手。神経繊維修復材料の研究では、「生まれた後には増えない神経細胞は、工夫すれば再生可能である」点に着目。再生を誘導するたん白質（機能部位）を材料化して、それを損傷部分に埋め込むことにより、神経細胞が自ら再生できるようにする。またシナプス伝達を活性化することは、記憶・学習能力を回復させるために必要。このシナプス伝達機構を制御することも検討課題の一つとなる。具体的には、ある神経細胞に機能を持った分子を置くと弱った細胞が修復され、神経活動が再び回復するようにする「神経活性化材料」を取り上げる。

三つ目に着目するのは、「神経・基板インターフェース材料」。これは情報伝達系のシグナルの流れを回復させるための材料。例えばせき髄の運動神経を損傷した際に、脳から流れ出た情報をこの材料の上（基板上）で受け取って筋肉へ伝えることができれば、神経活動を再生できるという。これら神経機能材料の開発のための基盤研究は、新エネルギー・産業技術総合開発機構（NEDO）の提案公募型・最先端分野研究開発プロジェクトで、大工研が先行的に取り上げていた。

解説

シナプスとは、電気的な信号が一つの神経細胞から情報を受ける次の神経細胞へと伝達されていく際の接続部位。このシナプスでの変化（シナプスの可塑性）が学習や記憶の機能を支えていると考えられている。調査研究は、こうしたシナプス伝達領域を分子レベルから直接解明することが大きな狙い。その解明のためには、生きた細胞内での単一分子の動きを計測する技術など、基盤となる先端的細胞工学技術を確立する必要があった。また、研究が遅れている人工神経を世界に先駆けて進めていくことも求められていた。

1.

筋由来神経突起伸長因子

［別名］mNPF（muscle-derived neurite promoting factor）

歴史とあらまし

発生段階における神経細胞は，さまざまな外部因子の影響を受けており，その神経軸索の誘導に関与する因子が投射経路，または標的組織において発現していることが考えられている．このような因子の１つとして，運動神経細胞に作用する骨格筋由来の神経突起誘導因子の存在が古くから予測されていたが，その同定は未だなされていなかった．1981年Hendersonらにより，ニワトリ胚骨格筋細胞を用いて，条件づけした培養液中に神経突起伸長促進活性が存在することが，脊髄神経細胞の初代解離培養系を用いて示された1)．'83年Hendersonらは，ヒヨコの座骨神経を除神経すると，その神経に支配されていた下腿部骨格筋の抽出液に含まれる神経突起伸長促進活性が上昇することを示した2)．興味深いことに，'87年田口らにより，この除神経筋抽出液中にニワトリ胚の脳神経細胞に対する突起誘導活性も存在することが示された3)．注目すべきことに，この誘導活性は終脳神経細胞に対して特異的に観察された．最近，この終脳特異的な神経突起伸長因子（neurite promoting factor：NPF）が，除神経筋および終脳からクローニングされた（西宗ら，投稿準備中）．

分子構造

機能阻害モノクローナル抗体を用いて，ニワトリ除神経骨格筋cDNAライブラリーから，mNPF（muscle-derived NPF）cDNAがまずクローニングされ，次にそのホモログとしてニワトリ胚終脳から，tNPF（telencephalon-derived NPF）cDNAがRT-PCR法によりクローニングされた．mNPFとtNPFの塩基配列の差はほとんどなく，99％一致する．mRNAのサイズはともに3.7kbである．他の組織における発現は，神経系に比べると非常に弱いが，心臓，肝臓，胃，砂嚢において見受けられる．しかし，肺においては認められない．

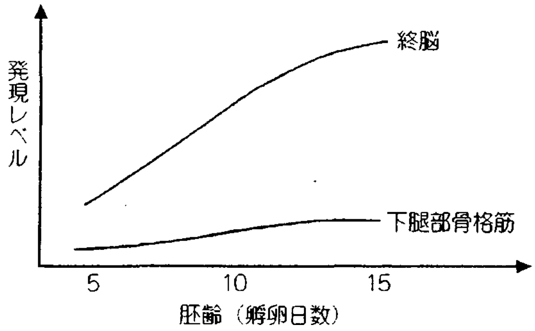

図１　発生段階におけるNPFの発現量調節
イムノブロット法を用いた終脳，下腿部骨格筋における発生段階のNPF発現量の検討．デンシトメーター（NIH-image）による比較

組織中のNPFの分子量は，組換え蛋白質を抗原とした，ポリクローナル抗体を用いたイムノブロットにより，115kDと決定された．発生段階の進行とともに，発現量は下腿部骨格筋，終脳において上昇した（図１）．tNPFとmNPFにおけるアミノ酸配列は完全に一致し，全体的に親水性アミノ酸を多く含み，疎水性アミノ酸からなる膜貫通領域はない．この蛋白質は，*α*-ヘリックスに富む二次構造と，4カ所の糖鎖付加部位の存在が予測される．既知の蛋白質とのホモロジーは低く，ニューロトロフィンファミリーのシステインノットモチーフ，カドヘリン-Ca^{2+}結合領域，フィブロネクチンtypeⅢドメインなどの機能に関連した共通配列は見出されていない．

機能

組換え蛋白質の神経突起誘導活性は，ニワトリ胚脳神経系の初代解離培養において，終脳特異的に観察された（図２）．この活性はC末端30kD領域だけを発現させた場合にも観察され，突起伸長活性に必須な領域はこの部分にあると考えられる．また，*in vitro*の系を用いた実験操作から，NPFは培養基質に接着して活性を発現すること

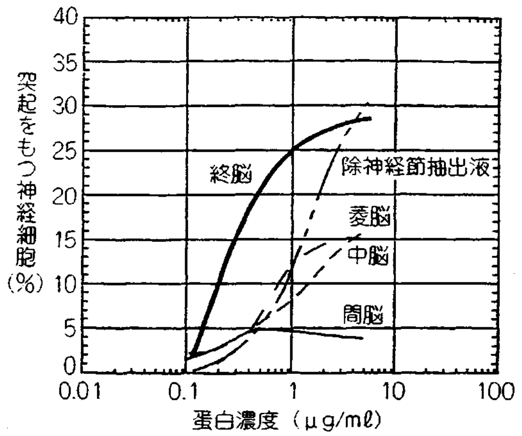

図2　NPFの突起誘導活性
ニワトリ胚初代解離培養系を用いたNPF活性の測定．培養24時間後に細胞体の2倍長以上神経突起を伸長している神経細胞の割合

が示された．大腸菌発現の組換え蛋白質に活性があることから，NPFの終脳特異的な突起誘導活性には糖鎖は必要ないと考えられる．受容体がまだ同定されていないため，分子レベルでの作用機構は明らかではない．しかし，初代解離培養実験に用いた孵卵5日目胚の脳神経細胞（終脳，間脳，中脳，菱脳）は，どの部位もラミニンに対して応答し，活発に突起を伸長することから，NPFレセプターは終脳にのみ発現している可能性がある．

これからの展開

NPFは，ニワトリにおいて骨格筋，終脳においてクローニングされ，その構造がほぼ一致することが証明された（西宗ら，投稿準備中）．哺乳類においても，このような機構を担う類似分子の存在は十分予想され，マウス，ラットからのクローニングが進行中であり，非常にホモロジーの高い部分配列が明らかになっている．Cajalの時代から提唱されてきたように，標的組織または投射経路に存在する組織において発現され，神経突起を誘導する拡散型走化性誘導因子や反発因子として，最近ネトリンやセマフォリンファミリーが注目されている．ここで紹介したNPFの作用メカニズムの解明は，新たな機能分子群の存在を明らかにする可能性が高い．

Database (EMBL/GenBank)

ニワトリ mNPF：D38038

References

1）Henderson, C. E. et al.：Proc. Natl. Acad. Sci. USA, 78：2625-2629, 1981
2）Henderson, C. E. et al.：Nature, 302：609-611, 1983
3）Taguchi, T. et al.：Dev. Brain Res., 37：125-132, 1987

（西宗裕史　植田淳子　田口隆久）

Z.

NeuroReport 7, 701–704 (1996)

Two modes of activity-dependent synaptogenesis of cerebral neurons *in vitro*

Kazuyuki Kiyosue, Michiki Kasai and Takahisa Taguchi[1,CA]

Department of Biophysical Engineering, Faculty of Engineering Science, Osaka University, Toyonaka 560; [1]Department of Organic Materials, Osaka National Research Institute, 1-8-31, Midorigaoka, Ikeda 563, Japan

[CA]Corresponding Author

EFFECTS of transduction activity and transmission activity on synaptogenesis of chick cerebral neurones in dissociated cell culture were studied electrophysiologically using two blockers for these activities, tetrodotoxin (TTX) and 6-cyano-7-nitroquinoxaline-2,3-dione (CNQX), respectively. CNQX inhibited the increase of evoked EPSCs more effectively than TTX, whereas both blockers similarly reduced the increase of miniature EPSCs (Minis). These data indicated that not only transduction-dependent transmission activity but also transduction-independent spontaneous activity regulate the synaptic efficiency. These two activities are suggested to change the quantal amplitude and the number of synaptic sites, respectively.

Key Words: Synaptogenesis; Neurone; Culture; EPSCs; Glutamatergic; Synapse; Transmitter release

Introduction

Elucidating the molecular mechanisms of synaptic plasticity is an essential prerequisite to understanding the higher functions of the brain. The processes of developmental synaptogenesis, including formation, maturation and elimination, are though to re-emerge in synaptic plasticity. Molecular and cellular mechanisms of synaptogenesis have been mainly studied in neuromuscular junctions.[1–3] Synaptogenesis in an activity-dependent manner has been studied in synapses,[4–7] but few studies have been performed in the central nervous system (CNS) due to its complexity.[4]

To analyse synaptogenesis in the CNS at the single cell level, various culture systems have been developed.[8–10] Using cultures of dissociated chick central neurones, we showed electrophysiologically that glutamatergic synaptogenesis is a function of embryonic equivalent days (E.E. days; the sum of embryonic age and days *in vitro*). The glutamatergic spontaneous synaptic currents (SSCs) initially observed at E.E. days 13 abruptly increase in amplitude between E.E. days 15 and 17.[11]

To determine whether the increase in synaptic efficacy seen over this period occurs in an activity-dependent manner, two types of activity, transduction and transmission, were modulated by two blockers, TTX and CNQX, respectively, during the period.

Materials and Methods

Culture: Cell cultures were prepared from cerebral hemispheres of chick embryos (embryonic day 10), as previously described.[11] Briefly, the dissociated cerebral neurons (5×10^5 per dish) were plated on poly-L-lysine-coated 35 mm tissue culture dishes containing 50% of modified Earl's minimum essential medium, 10% fetal calf serum (FCS) and 40% GIT medium (Nihon Seiyaku Co., Ltd, Osaka, Japan). Cells were cultured at 37°C in 5% CO_2/95% air and saturating humidity. Half of the culture medium was changed every 2 days.

Electrophysiology: Whole-cell recording was employed to stimulate presynaptic neurones and to record evoked and miniature synaptic currents from postsynaptic neurones cultured for 6 or 7 days (E.E. days 16 or 17). All electrophysiological experiments were carried out at room temperature (20–25°C). Normal external bath solution contained (in mM) 130 NaCl, 3 KCl, 2 $CaCl_2$, 1 $MgCl_2$, 10 glucose, 0.025 picrotoxin and 10 HEPES-Na (pH 7.3). The solution in the patch pipette contained (in mM) 130 KCH_3SO_4, 10 KCl, 0.2 $CaCl_2$, 2 $MgSO_4$, 1 EGTA, 2 Mg-ATP and 10 HEPES-K (pH 7.3). The pipettes had resistance of between 4 and 6 MΩ. Junction potential was corrected after the pipette entered the bath solution. Evoked synaptic currents were elicited by two stimulation methods as follows. Excitatory postsynaptic currents (EPSCs) in voltage-clamped putative postsynaptic cell were induced by current injection (10–30 ms. duration and 300–500 pA intensity) large enough to evoke action potentials in putative presynaptic cells using a dual whole-cell

© Rapid Science Publishers

recording system with two patch clamp amplifiers (CEZ-2200, Nihon Kohden, Japan). Alternatively, voltage pulse stimulation (duration 80 s, intensity 1–5 V) was provided to putative presynaptic cell to evoke action potentials via a pipette (tip diameter: 10 μm). The postsynaptic currents were measured at –70 mV by stimulation at 0.1 or 0.05 Hz with a low-pass filter at 1 kHz, and the data were digitized at 20 kHz by an A/D converter and stored in a personal computer. The synaptic currents were averaged at 10–30 records. Both input resistance and series resistance were monitored by applying a voltage pulse (30ms) hyperpolarized in 10 mV at the start and end of recording. If these resistances were significantly changed, or synaptic delay was more than 5 ms, the records were discarded. Minis were recorded at –70 mV holding potential for 3 min in a MgCl$_2$-free bath solution supplemented with 1 μM TTX.

Results

In our culture system, the amplitude and frequency of glutamatergic SSCs increased 4-fold and 20-fold, respectively, bewteen E.E. days 15 and 17.[11] To investigate whether these increases depend on neuronal activity, we applied two kinds of blockers, TTX and CNQX, to the dissociated neuronal culture.

At E.E. day 15, 1 μM TTX completely blocked spontaneous neuronal firing caused by transduction signals, but had no effect on minis. When only 5 μM CNQX was added to the culture at the same stage, no spontaneous firing or minis were observed (data not shown). Therefore, TTX blocks transduction-induced synaptic transmission and CNQX blocks all transmission activities via the non-NMDA receptor.

After culturing the neurones with TTX and CNQX between E.E. days 15 and 17, we first confirmed neuronal excitability after washing out these blockers. Following TTX treatment, voltage-gated Na$^+$ and Ca^{2+} spikes that were not evoked by current injection under the voltage clamp mode, appeared fully following the same stimulation after replacement of culture medium by external bath solution. In the case of CNQX treatment, spontaneous firing and excitatory synaptic currents that were not observed in culture medium emerged after replacement of the medium (data not shown). SSCs were then recorded at –70 mV for 3 min from neurones at E.E. day 17. Although averaged maximum amplitudes of each record (Fig. 1) were apparently different from the control, the statistical significance was not large (unpaired *t*-test, $p = 0.15$ for CNQX-treated neurones, $p = 0.6$ for TTX-treated neurones). This is due to the dependency of SSCs on the condition of each neurone and neuronal circuit in the culture.

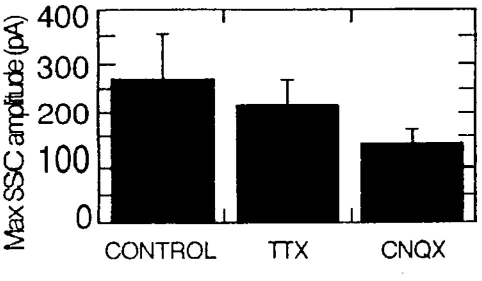

FIG. 1. Effects of TTX and CNQX on the increase in amplitude of SSCs. TTX (1 μM) or CNQX (5 μM) were added to culture medium at E.E. day 15. SSCs were recorded at E.E. day 17, after washing out the blockers from the medium using external bath solution.

To estimate more precisely the action of the blockers, we recorded evoked EPSCs from 21 neurones at E.E. day 16 and from 83 neurones at E.E. day 17. Typical traces of the latter are shown in Figure 2A (traces 1–3). The amplitude of the EPSCs from neurones at E.E. days 16 and 17 were 184 ± 42.2 pA (mean ± s.e., $n = 5$) and 311 ± 35.6 pA ($n = 26$) for control, 96.0 ± 13.3 pA ($n = 5$) and 190.0 ± 38 pA ($n = 25$) for TTX-treated, and 77.4 ± 20.1 ($n = 11$) and 49.7 ± 8.13 pA ($n = 32$) for CNQX-treated neurones, respectively. At E.E. day 16, TTX and CNQX similarly suppressed the increase in amplitude seen in controls (unpaired *t*-test, $p < 0.08$). At E.E. day 17, the suppressive effects of the blockers were more significant (control *vs* TTX: unpaired *t*-test, $p < 0.03$, control *vs* CNQX: unpaired *t*-test, $p < 0.001$) and CNQX showed greater suppression than TTX (unpaired *t*-test, $p < 0.001$) in spite of there being no clear difference at E.E. day 16. The wave-shape of EPSC could be transformed due to a change in the spatial distribution of synaptic sites on the neurone. As to the results, however, this was not the case since the half-time of rise and decay of EPSC traces were not changed after treatments with each blocker (Fig. 2C). In fact, the trace of EPSCs from CNQX-treated neurones (Fig. 2A3) could be superimposed upon controls after fitting the vertical scale (Fig. 2A4). These data suggest that two modes of activity, that is, transduction-induced transmission and transduction-independent spontaneous transmission, both contribute to synapse maturation in different ways.

To elucidate the difference between the modes of activity in synaptogenesis, we next analysed minis from 22 neurones at E.E. day 16 and from 131 neurones at E.E. day 17 (Fig. 3A). The averaged amplitude of minis from neurones at E.E. days 16 and 17 were 17.1 ± 1.95 pA (mean ± s.e., $n = 7$) and 19.2 ± 0.871 pA ($n = 68$) for controls, 13.8 ± 2.37 pA ($n = 5$) and 14.3 ± 0.947 ($n = 42$) for TTX-treated, and 13.5 ± 1.21 and 13.0 ± 0.707 pA ($n = 21$) for CNQX-treated neurones, respectively (Fig. 3B). TTX and CNQX significantly suppressed the amplitude of minis (unpaired *t*-test, $p < 0.005$) at E.E. day 17, but not at E.E. day 16. There was no difference in suppression at E.E. day 17. These results indicate that

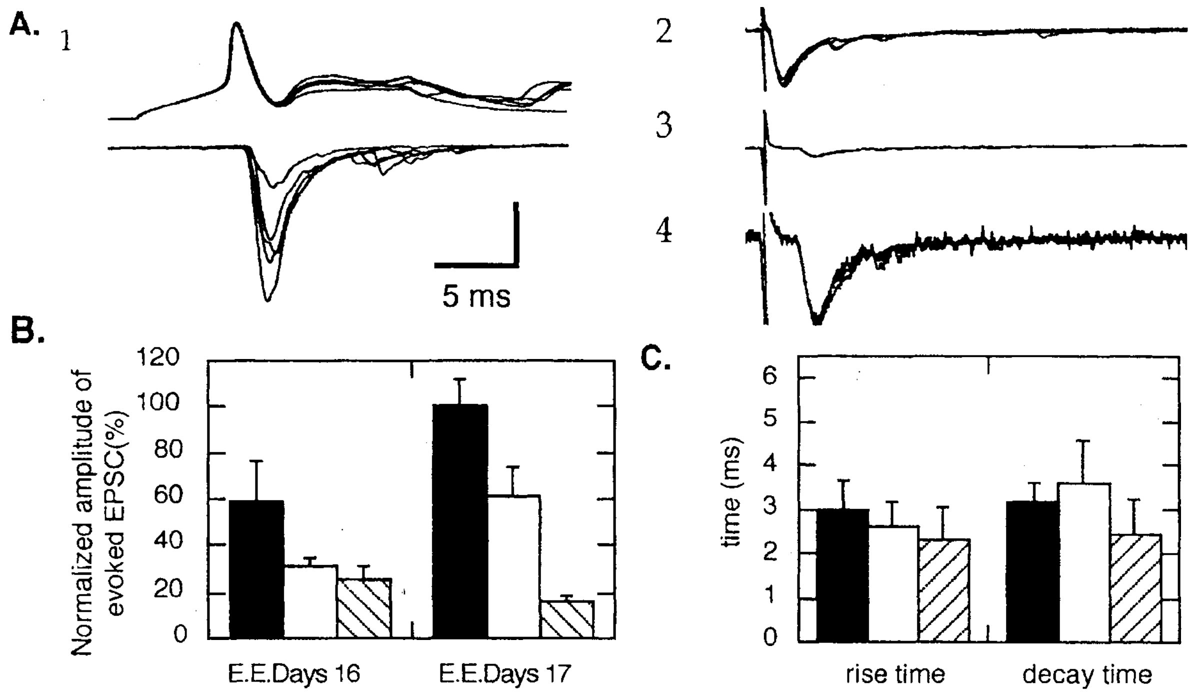

FIG. 2. Effects of TTX and CNQX on amplitude increase of evoked EPSCs. Neurones were treated as describd in the legend to Fig. 1. (**A1**) Evoked EPSCs from control neurones were recorded by dual whole-cell recording method. Upper traces are presynaptic membrane potential in current clamp mode and lower traces are EPSCs (vertical bar: 100 pA). (**A2, A3**) EPSCs evoked by local extracellular stimulation were recorded from TTX-treated neurones (A2) and CNQX-treated neurones (A3) (vertical bar: 100 pA). (**A4**) Vertically expanded traces of A3 are indicated (vertical bar: 10 pA). (**B**) Averaged and normalized amplitudes of evoked EPSCs from control and blocker-treated neurones at E.E. days 16 and 17. The amplitude of control neurones at E.E. day 17 was defined as 100%. (**C**) Averaged rise and decay time of evoked EPSC traces at E.E. day 17. Control, TTX-treated and CNQX-treated neurones are indicated as solid, open and lined columns, respectively.

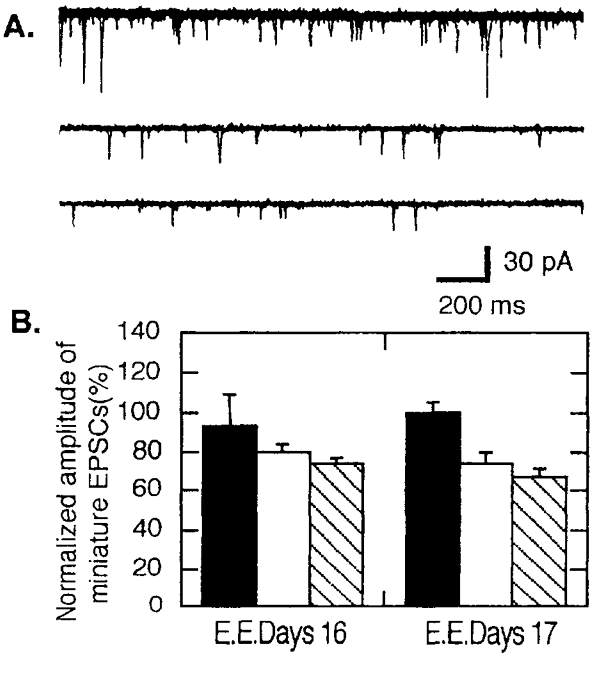

FIG. 3. Effects of TTX and CNQX on the amplitude increase of minis. Neurones were treated as described in the legend to Fig. 1. (**A**) Example of minis from a control (upper), a TTX-treated (middle) and a CNQX-treated (lower) neurone at E.E. day 17. (**B**) Amplitude of mini recorded for 3 min from neurones at E.E. days 16 and 17 in each condition were averaged and normalized. Control, TTX-treated and CNQX-treated neurones are indicated as solid, open and lined columns, respectively.

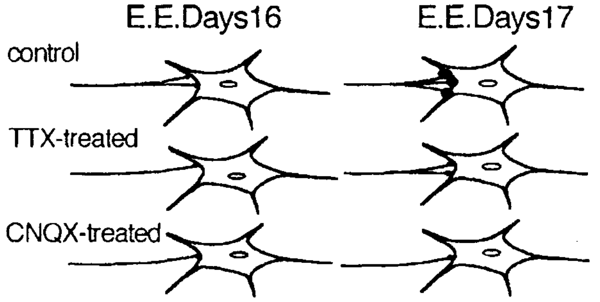

FIG. 4. Schematic diagram of the activity-dependent synaptic change. Note that the synaptic size and the number of synaptic sites correspond to the area of solid circle at terminal and the terminal branches, respectively.

transduction-induced transmission mainly regulates the development of quantal amplitude.

Discussion

The synaptogenesis of cerebral neurones *in vitro* was demonstrated to be dependent on the two modes of neuronal activities: transduction-dependent transmission and transduction-independent spontaneous transmission. In these experiments, the former was blocked by both TTX and CNQX, but the latter was blocked only by CNQX. The plausible explanation of the results (Fig. 4) indicates that the former and the latter activities mainly regulate the size and the number of a single synaptic site, respectively.

The amplitude of minis corresponds to the size of a single synaptic sites that in generally defined by the number of non-NMDA receptors in a postsynaptic sites and/or the glutamate content in a single synaptic vesicle. Since both TTX and CNQX similarly suppressed the amplitude (Fig. 3B), the transduction-dependent activity alone is thought to contribute to development of the size. Unchanged rise and decay times of EPSCs (Fig. 2C) suggest that the increase in size is due to the number of receptors but not to the transmitter content.

Suppression of evoked EPSCs is generally thought to be due to the difference in the size of a single synaptic site, the number of release vesicles at one synaptic site, probability of release of one synaptic vesicle in one presynaptic firing or the number of synaptic sites. The suppression of evoked EPSCs by both TTX and CNQX (Fig. 2B) include the same extent of the reduced size development (Fig. 3B). Considering that only one transmitter release site exists in one bouton in rat hippocampal neurones[12] and in Mauthner cells of the goldfish,[13] the second possibility cannot be the case. Thus, the difference in suppression caused by TTX or CNQX treatment (Fig. 2B) can be explained by the change in the release probability and/or the number of synaptic sites. This large difference reveals the importance of transduction-independent spontaneous transmitter release in synaptogenesis.

Assuming that every synaptic site has the same probability of transmitter release, the number of synaptic sites at E.E. day 17 in control, TTX-treated and CNQX-treated neurones are calculated to be 17.5, 13.3 and 3.8, respectively, using the data in Figures 2B and 3B. The frequency difference in each mini (Fig. 3A) can be due to the difference in the number of sites. Morphological studies of the neuromuscular junction of mutant strains of *Drosophila* have shown that the number and size of synaptic contacts are affected by synaptic activity,[3,14,15] These data indirectly support the hypothesis that CNQX-sensitive synaptogenesis in our culture system involved an increase in synaptic sites (Fig. 4). Our data also indicate that blocking postsynaptic receptor induces presynaptic change, suggesting that a retrograde messenger such as NGF participates in the synaptogenesis of sympathetic neurones[16] while BDNF is involved in hippocampal neurones.[6]

Conclusion

Analysis of synaptogenesis in cultured chick cerebral neurones revealed that the increase in amplitude of EPSCs and minis depends on two modes of activities that are distinguished by the effects of TTX and CNQX. Transduction-independent spontaneous transmitter release and transduction-dependent release contribute to synaptic growth in the period between E.E. days 15 and 17.

References

1. Hall ZW and Sans JR. *Cell* **72** / *Neuron* **10**, 99–121 (1993).
2. Colman H and Lichtman JW. *Dev Biol* **156**, 1–10 (1993).
3. Jia X, Groczyca M and Budnik V. *J Neurobiol* **24**, 1025–1044 (1993).
4. Nelson P, Field R, Yu C *et al. J Neurobiol* **21**, 138–156 (1990).
5. Sanes DH and Takacs C. *Eur J Neurosci* **5**, 570–574 (1993).
6. Zafra F, Hengerer B, Leibrock J *et al. EMBO J* **9**, 3545–3550(1990).
7. Dahm LM and Landmesser LT. *J Neurosci* **11**, 238–255 (1991).
8. Basarsky TA, Parapura V and Haydon PG. *J Neurosci* **14**, 6402–6411 (1994).
9. Kraszewski K and Grantyn R. *Neuroscience* **47**, 555–570 (1992).
10. Nelson PG, Yu C, Fields RD *et al. Science* **244**, 585–587 (1989).
11. Tokioka R, Matsuo A, Kiyosue K *et al. Dev Brain Res* **74**, 146–150 (1993).
12. Perkel DJ and Nicoll RA. *J Physiol* **471**, 481–500 (1993).
13. Korn H, Mallet A, Triller A *et al. J Neurophysiol* **48**, 679–707 (1982).
14. Budnik V, Zhong Y and Wu CF. *J Neurosci* **10**, 3754–3768 (1990).
15. Zhong Y, Budnik V and Wu CF. *J Neurosci* **12**, 644–651 (1992).
16. Campenot RB. *Dev Brain Res* **37**, 293–301 (1987).

Received 24 November 1995; accepted 10 January 1996

General Summary

Synaptogenesis is known to proceed in activity-dependent manner. We developed a system of culture for chick cerebral neurones in which we can analyse synaptogenesis by electrophysiological techniques. Using the system and two blockers of transduction and transmission, we investigated whether these two different neuronal activities are responsible for synaptogenesis. Our results clearly showed that not only transduction-dependent transmission but also transmission-independent spontaneous transmission play important roles in synaptic maturation. The former and latter activity contributed to the increase in the size and the number, respectively, of synaptic sites.

3.

JOURNAL OF CELLULAR PHYSIOLOGY 166:66–75 (1996)

Okadaic Acid Gives Concentration-Dependent Reciprocal Effects on the Fluid Phase Endocytosis Activated by Ca^{2+} and Phorbol 12-Myristate 13-Acetate

SATOSHI B. SATO,* KAZUYUKI KIYOSUE, TAKAHISA TAGUCHI, MICHIKI KASAI, AND SAKUJI TOYAMA

Cell and Information, PRESTO, Research Development Corporation of Japan and Department of Biophysics, Faculty of Science, (S.B.S.) and Institute for Virus Research (S.T.), Kyoto University, Kyoto 606-01, Department of Biophysical Engineering, Faculty of Engineering Science, Osaka University, Toyonaka, Osaka 560 (K.K., M.K.), Department of Organic Materials, Osaka National Research Institute, Ikeda, Osaka 563 (T.T.)

Incubation of a human fibrosarcoma cell line HT-1080 in increasing concentration of Ca^{2+} was found to enhance endocytic internalization of a fluid phase marker, horseradish peroxidase. At 16.8 mM Ca^{2+}, generation of the effect required incubation for more than 45 min. The effect was reversed by removal of the excess ion for 30 min. Monitoring the intracellular concentration showed that the incubation induced a transient large Ca^{2+} influx followed by a recovery to 230 ± 50 nM instead of the normal level of 83 ± 5 nM. The activation was not inhibited by inhibitors of protein kinases nor a cAMP antagonist. In contrast, the effect was prevented by okadaic acid (OKA) at 100 nM without detectable effect on the basal activity. Fluid phase uptake by HT-1080 cells was also enhanced by phorbol 12-myristate 13-acetate (PMA). In contrast to the case with Ca^{2+}, OKA at 100 nM did not prevent the PMA effect but further enhanced the endocytosis. The effect of OKA was concentration-dependent, as the reagent at 1 μM inhibited not only both the activation but also the basal activity. In Ca^{2+}- or PMA-stimulated cells, FITC-dextran was delivered to endosomes that had been labeled with TRITC-transferrin. In contrast, following treatment with a combination of PMA and 100 nM OKA, fluid phase was internalized in vesicular compartments devoid of transferrin labeling. These results suggest that, through differential modifications of protein phosphorylation, endocytosis can be enhanced distinctively either by employing conventional receptor-bearing compartments or generating a new endosomal population. © 1996 Wiley-Liss, Inc.

Eukaryotic cells internalize physiologically important molecules along the endosomal pathway as reviewed by Goldstein et al. (1985) and Courtoy (1991). Although in most cases the endocytic activity of cells in culture occurs without known extracellular stimuli, recent studies have revealed that some endocytic membrane processes employ a mechanism similar to signal transduction. Typically, Robinson et al. (1993) have shown that a large GTPase dynamin involved in early internalization is phosphorylated by protein kinase C (PKC). Rickard and Kreis (1991) and Pierre et al. (1992) have suggested that clip-170, a phosphoprotein which links a certain type of endosomes to microtubles, fulfills its function when it is dephosphorylated. Ca^{2+} assists interactions of protein elements with endocytic compartments. Typically, Emans et al. (1993) have shown that annexin II, a class of Ca^{2+}-dependent phospholipid-binding proteins, is involved in early endosome fusion.

The involvement of protein phosphorylation and Ca^{2+} mechanisms argues that the whole endocytic internalization would be up- or down-regulated by modification of intracellular signaling. Lucocq et al. (1991) have shown that cells treated with okadaic acid, an inhibitor of protein phosphatase (PP) 1 and 2A, inhibits fluid phase endocytosis and some exocytic membrane transport. Woodman et al. (1992) have later shown that the reagent inhibits cell-free endosomal fusion. In exocytosis, studies by Davidson et al. (1992) have revealed that the effect is reversed by applying PP2A to semiintact cells, indicating direct involvement of protein dephosphorylation. In endocytosis, however, it is not clear whether a similar mechanism is involved or if inhibition of protein dephosphorylation is generally inhibi-

© 1996 WILEY-LISS, INC.

Received January 30, 1995; accepted June 8, 1995.

*To whom reprint requests/correspondence should be addressed at Department of Biophysics, Faculty of Science, Kyoto University, Kyoto 606-01, Japan.

tory to the activity. Enhancement of internalization of receptor molecules by PKC-activator phorbol esters has been demonstrated in some cells, as reviewed by Backer and King (1991). Cardone et al. (1994) have demonstrated that, in transcytosis of polymeric IgA, specific Ser-phosphorylation of receptor cytoplasmic tail is involved, and the activity is also enhanced by phorbol myristate acetate possibly by recruiting specific PKC. However, whether the effect is evoked solely by increased protein phosphorylation or other types of reactions such as protein dephosphorylation are involved is not clear yet. Moreover, it is not clear whether Ca^{2+} gives the identical effect as phorbol esters.

In this report, we present evidence that fluid phase endocytosis is stimulated distinctively by Ca^{2+} or PMA. We further show that PMA- or Ca^{2+}-treated cells employ the conventional endocytic route, while in cells treated with PMA in conjunction with 100 nM OKA endocytosis is enhanced employing early compartments devoid of transferrin receptors. In contrast, 1 μM OKA generally inhibited the endocytosis regardless of the treatment with Ca^{2+} or PMA. The results point to variation of protein phosphorylation being one of the key factors that determine the endocytic route and magnitude.

MATERIALS AND METHODS

Reagents

Sodium phosphate-free MEM and DME (low glucose) were purchased from Gibco BRL (Gaithersburg, MD). Staurosporin, genistein, phorbol 12-myristate 13-acetate, okadaic acid (Wako Pure Chemicals, Osaka, Japan) and Rp-cAMPS (Biolog, Bremen, Germany) were purchased from the indicated distributors. Chloride salts of monovalent cations and $CaCl_2\ 2H_2O$ (Wako) were all >99.9%. TRITC-dextran, a fixable Lucifer Yellow CH-labeled dextran (mw. 40,000) and TRITC-labeled human transferrin were purchased from Molecular Probes (Eugene, OR). FITC-dextran (FD20) obtained from Sigma (St. Louis, MO) was purified as described by Preston et al. (1987). Other reagents were obtained from Wako.

Cells

HT-1080, a human fibrosarcoma cell line, was used throughout. The cell line was obtained from ICN Biomedicals (Costa Mesa, CA) and further cloned by limiting dilution. One clone showing an extended morphology, which is typical in the mother culture but at the same time with a larger cell size, was named clone 1. The cells were cultured in DME supplemented with 10% fetal bovine serum (FBS) and used after 2 days.

Treatment of cells with Ca^{2+} and other reagents and assay of fluid phase endocytosis

Cells were washed with prewarmed Na phosphate-free MEM which was reconstituted in ultrapure water prepared by milli-Q plus (Millipore, Bedford, MA) and supplemented with 10 mM Hepes or Mes, 1 mM Na pyruvate, and 2% FBS dialyzed against 150 mM NaCl. They were then incubated in 1 ml of the medium containing various concentrations of $CaCl_2$ with or without other supplemented ions (from 1 M stock) or reagents usually from ×1,000 stock) for 10–60 min at 35°C with gentle shaking in a humidified chamber. For the reversibility, treated cells were washed two times and chased in an appropriate medium. For assay of fluid phase uptake, cells were added to horseradish peroxidase to a final concentration between 0.5 and 2 mg/ml at 35°C. At intervals, cells were washed with ice-cold PBS (145 mM NaCl, 10 mM Na phosphate, pH 7.2) three times on an ice-cold aluminum block. They were then scraped into eppendorf tubes and washed with PBS three times by centrifugation at 3,000g at 4°C for 5 min. In cases with reagents such as 1 μM OKA, which induced cellular rounding, cells were directly scraped in HRP-containing medium and washed seven times by centrifugation. The washed cells were solubilized in 0.45 ml of TBS (150 mM NaCl, 50 mM Tris-HCl, pH 8.0) containing 0.2% NP-40 and 10 μg/ml pepstatin A and 10 μM (*p*-amidinophenyl)-methanesulfonyl fluoride hydrochloride (APMSF) at 0°C for 1 h. After centrifugation at 10,000g for 10 min, the supernatant was triplicately analyzed for protein as described by Bradford (1976) and for the peroxidase activity using tetramethylbenzidine as a substrate. Usually, the enzyme reactions were continued until those in control cells developed the color to OD of 0.3 at 450 nm. The results were normalized for the cellular protein and represented as relative uptake to the control cells.

Measurement of intracellular calcium

Cells grown on coverslips which had been attached to a fitting hole in a culture dish by glue were loaded with either fura-2 AM or indo-1 AM at 10 μM for 0.5–1 h at 37°C. Using fura-2, intracellular calcium concentration ($[Ca^{2+}]_i$) was monitored at room temperature (25°C) in an OSP-3 system (Olympus, Japan) controlled by a 16-bit personal computer with a system software (MICA) which has been developed by the National Institute of Physiological Science (Okazaki, Japan). The ratio of fluorescence at 510 nm excited at 340 and 380 nm was stored one after another. For determination of the steady level of the ion, indo-1 was used. The fluorescence was measured by MPS20 (Zeiss, Germany) using EGTA, ionomycin, and $MnCl_2$ as described by Thomas and Delaville (1991).

Fluorescence microscopy of endosomes

For early endosome labeling, cells pretreated with various reagents in Na phosphate-free MEM-2% FBS were incubated in the same medium containing TRITC-dextran (5–10 mg/ml) at room temperature (23–25°C) for 5 min. For visualization of late compartments, cells were first incubated in the medium containing 5 mg/ml TRITC-dextran in the presence or absence of a reagent of interest at 35°C for 30 min. They were then chased in the medium for 30–60 min. In order to compare the route of the early transport, cells previously incubated in serum-free DME at 37°C for 1 h were incubated with 50–100 μg/ml TRITC-Trf in MEM ± 16.8 mM $CaCl_2$ for 1 h. When the cells were treated with PMA or OKA, they were incubated with the reagent in the TRITC-Trf-containing medium for additional 15 min. After extensive washing with phosphate-free MEM over 5 min, cells were pulsed with 10 mg/ml FITC-dextran (FD) for 5 min and chased for 3 min. The coverslip culture was mounted using phosphate-free

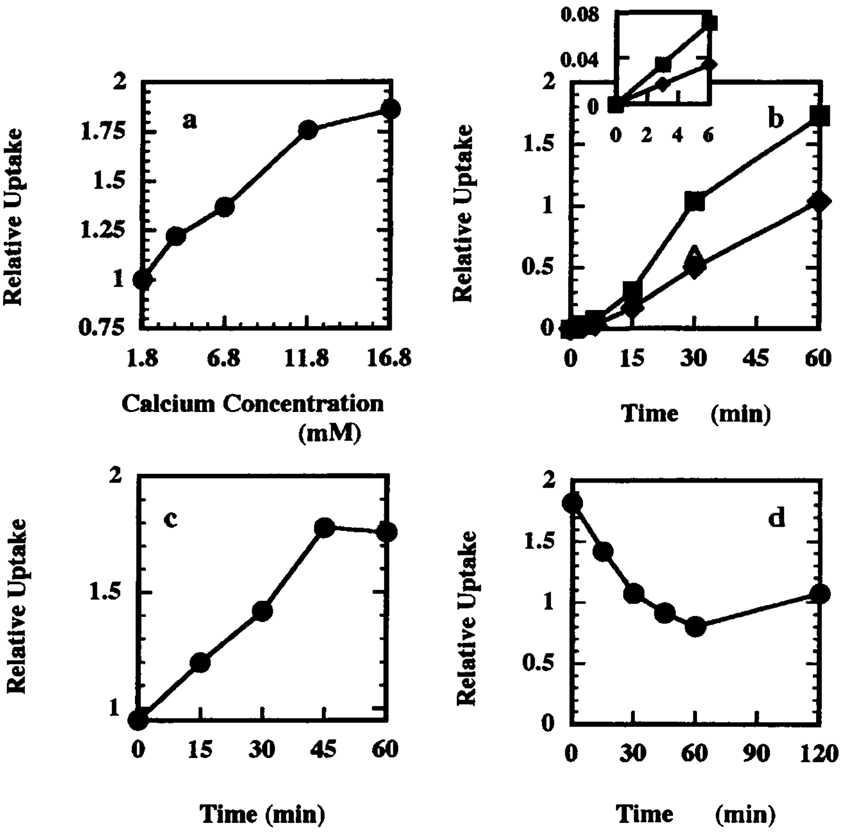

Fig. 1. Enhancement of fluid phase endocytosis by Ca^{2+}. **a:** HT-1080 cells were incubated in Na phosphate-free MEM (1.8 mM Ca^{2+}) supplemented with varying concentrations of $CaCl_2$ at pH 7.4 at 35°C for 1 h. Cells were then added 1 mg/ml HRP for 20 min. After extensive washing, cell-associated HRP was quantified and normalized for the cellular protein. The figure represents the average of three experiments. **b:** Time course of the fluid uptake at 16.8 mM (filled square) and 1.8 mM (filled diamond) Ca^{2+}. Cells were incubated at pH 7.4 at 35°C for 1 h and then with HRP for the indicated periods. The amount of the enzyme in cells in 1.8 mM Ca^{2+} at 1 h was taken as 1. An open triangle indicates the uptake in the presence of 100 µM $LaCl_3$. **Inset:** The uptake at earlier time points. **c:** Enhancement of endocytos requires preincubation of cells. Cells were incubated with 16.8 m $CaCl_2$ at pH 7.4 at 35°C for the indicated periods: then 1.5 mg/n HRP was added for 15 min. The uptake was compared to that of cel without supplemented Ca^{2+}. **d:** The enhanced uptake is reversed b removal of the supplemented Ca^{2+}. Cells were first incubated at 16. mM Ca^{2+} for 1 h and transferred at 1.8 mM Ca^{2+}. At the indicate time points, endocytosis was assayed by adding HRP (1.5 mg/ml) f 15 min. The uptake was compared to that of cells without suppl mented Ca^{2+}. Errors in a–d were within ±15% of the value poin and are not indicated in the figures.

MEM containing 20 mM methylamine hydrochloride in order to visualize otherwise quenched FD fluorescence. Cells were observed by using a confocal laser scanning system (MRC-600; Biorad, Hercules, CA) mounted on an Axiophoto fluorescence microscope (Zeiss).

RESULTS

Enhancement of fluid phase uptake by Ca^{2+}

In a series of tests for an up-regulating mechanism, incubation of HT-1080 cells in an increasing concentration of Ca^{2+} was found to enhance the fluid phase endocytosis (Fig. 1). At 16.8 (=1.8 + 15) mM, the cell-associated HRP amounted to about 1.8 ± 0.3 times that observed when the medium was without the supplemented ion (1.8 mM Ca^{2+}). The activity of the control cells was estimated to be 0.082 ± 0.003 µl/10^6 cells/h, which is comparable to those of other cells as reviewed by Courtoy (1991). Kinetic analysis at 16.8 mM Ca^{2+} indicated that the increase amounted to 1.6–2.5 times at all the time points (Fig. 1b). The effect was reduced by addition of a general calcium antagonist, La^{3+} (10 µM) (triangle in Fig. 1b). Incubation of the cells in phosphate-free medium for avoiding formation of Ca phosphate precipitates did not influence the basal ac tivity (not shown).

Enhancement of endocytosis by Ca^{2+} required prein cubation of the cells for as long as 45 min for saturatio (Fig. 1c). When cells were treated with 16.8 mM Ca^{2} for 15 min and then 1.8 mM for 45 min, no or littl enhancement was obtained (results not shown). Whe the cells incubated in 16.8 mM Ca^{2+} for 1 h were trans ferred into a normal medium, the endocytic activit returned in 30 min to the original level (Fig. 1d).

The enhancement was not inhibited by incubatio with blockers of voltage-gated Ca^{2+} channels such a verapamil (an L-type channel blocker) (5 µM), ω-cono toxin GV1A (L and N types) (1 µM), and amiloride (type), (500 µM) in 16.8 mM Ca^{2+} for 1 h. Incubatio with 100 µM $NiSO_4$, which is also known for blockin the gated flux of the ion, gave no effect either. Neithe

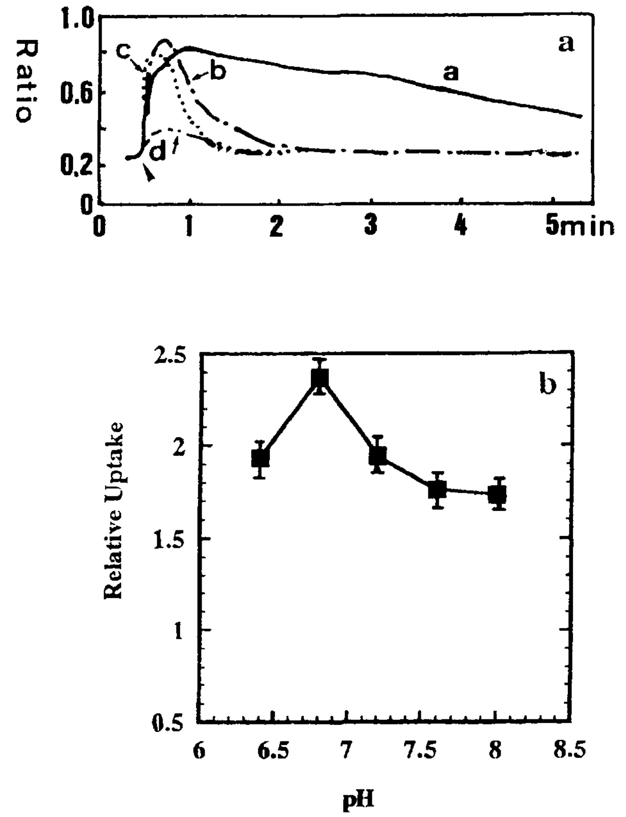

Fig. 2. a: Monitoring the influx of Ca^{2+} in cells loaded with a fluorescent indicator, fura-2. The curves represent the typical results out of at least five different measurements. At the time point indicated by the arrowhead, cells were added to a final concentration of 16.8 mM Ca^{2+} at pH (a) 7.5, (b) 7.1, and (c) 6.4. The magnitude of initial flux did not change, but the following recovery was accelerated by low pH. When 50 mM CsCl was added, the initial influx decreased by more than 70% (d). b: Effect of pH on the fluid phase endocytosis enhanced by Ca^{2+}. Cells were incubated at 16.8 mM Ca^{2+} at the indicated pH for 1 h. Uptake of HRP for 20 min was compared to the activity without supplemented $CaCl_2$ at pH 7.2.

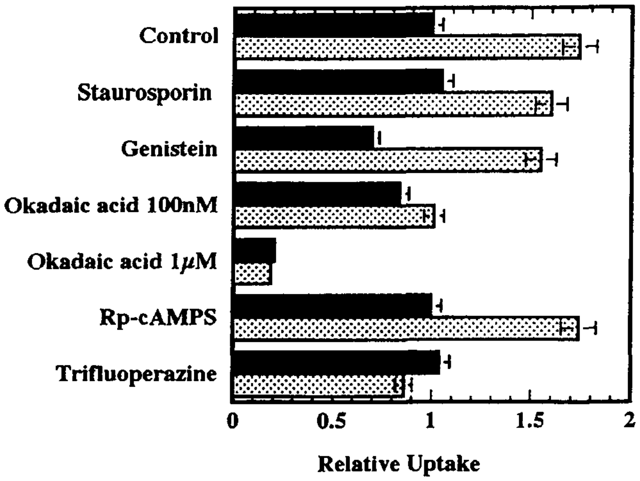

Fig. 3. Effect of various reagents on the fluid phase endocytosis enhanced by Ca^{2+}. Cells were incubated in 1.8 mM (filled bars) or 16.8 mM (dotted bars) Ca^{2+} with either staurosporin (20 nM), genistein (36 µM), okadaic acid (OKA) (100 nM or 1 µM), Rp-cAMPS (100 µM), or trifluoperazine (TFP) (15 µM) at pH 7.2 at 35°C for 1 h. Then 1 mg/ml HRP was added to the cells for 20 min. TFP and 100 nM OKA inhibited the enhancement, while 1 µM OKA inhibited endocytosis regardless of the concentration of Ca^{2+}.

tetraethylamine at 20 mM (a blocker of some K^+ channels) nor tetrodotoxin at 1 µM (a blocker of Na^+ channel) gave any effect.

Incubation in Ca^{2+} induced rapid influx and elevation of stationary concentration of the ion

To assess the action of Ca^{2+}, we monitored intracellular concentration of the ion by using a fluorescent indicator, fura-2. At pH 7.6, exposure of cells to 16.8 mM Ca^{2+} induced a rapid influx of the ion. The increase was then followed by a slower recovery (Fig. 2a, line a). At pH 7.1, the magnitude of the influx did not change, but the recovery was accelerated by a factor of .0 (Fig. 2a, line b). The recovery was further accelerated at pH 6.4 (Fig. 2a, line c). The stationary concentration ($[Ca^{2+}]_i$) at pH 7.2 was 83 ± 5 nM (n = 8) at 1.8 mM Ca^{2+}, while at 16.8 mM it was raised to 230 ± 40 nM (n = 6). When the ionophore, A23187, was added at 40 µM in a normal medium, cellular integrity was lost (not illustrated). When pH dependence of the Ca^{2+} effect was studied, the internalization was more than 1.6-fold at all pH values tested (Fig. 2b). These results suggest that $[Ca^{2+}]_i$ is increased by the influx of the ion but is maintained below the toxic level. This is possibly achieved by the pumping-out activity of Ca^{2+}-ATPase, which can be accelerated by extracellular low pH as revealed by Niggli et al. (1982). When CsCl was supplemented at 50 mM, Ca^{2+} influx was reduced by more than 70%, but the following recovery rate remained unchanged (Fig. 2, line d). The stationary concentration was 115 ± 60 nM (n = 4), suggesting that Cs^+, which has comparable ionic radius as Ca^{2+}, reduced the transmembrane movement of the divalent ion. Concomitantly, the ion reduced the enhancement to the basal level of endocytosis (not illustrated). The activation was similarly reduced by Rb^+, while Na^+ and K^+ gave minor effects. Interestingly, when Li^+ was added, it did not interfere with the Ca^{2+} entry but reduced the enhancement of endocytosis to the basal level. The action of Li^+, which likely modified intracellular reactions, is currently studied.

Enhancement of endocytosis by Ca^{2+} is prevented by okadaic acid but not by protein kinase inhibitors

In order to find the mechanism that is activated by Ca^{2+} on endocytosis, we tested a panel of reagents influencing the intracellular signaling (Fig. 3). We found that okadaic acid (OKA) at 100 nM canceled the enhancement. In the presence of 100 nM OKA, the internalization induced by 16.8 mM Ca^{2+} was similar to the basal level. OKA at this concentration gave no significant effect on the basal activity. In contrast, when cells were treated with 1 µM OKA, the activity was reduced to 20% of the basal level regardless of the concentration of Ca^{2+}. This concentration was the same as in the inhibition of the membrane transport in other cell types reported by Lucocq et al. (1991). At 1 μM but not at 100 nM, the cells showed intense rounding and were easily detached by shaking. Because OKA inhibits PP1 and 2A at different concentration, as reviewed by Cohen et al. (1990), we tested the effect of calyculin A which inhibits both the enzymes at a similar concentration as described by Ishihara et al. (1989). At >1.5 nM, the reagent reduced both the basal and enhanced activities with concomitant cellular rounding. At <1 nM, cells remained extended, but at the same time the reagent had no effect on the activities.

In contrast to the effect of an inhibitor of protein phosphatase, reagents which influence protein phosphorylation had no significant effect. Genistein, an inhibitor of protein tyrosinekinases, reduced uptake in the normal medium by 30–40%, but Ca^{2+} still had an enhancing effect. Likewise, no effects were observed with staurosporin, which inhibits C and also A and myosin light chain (MLC) kinases and with Rp-cAMPS (100 μM), an antagonist of cAMP.

We also found that trifluoperazine (TFP) (15 μM) reduced Ca^{2+}-induced uptake. This reagent also induced intense cellular rounding in the presence of 16.8 mM $CaCl_2$. At lower concentrations without inducing the morphological effect, the reagent was ineffective in interfering with the enhancement (not shown). W-7 also had a similar effect. These reagents are known for inhibiting Ca^{2+}-calmodulin-regulated reactions. However, because studies by Jarrett and Penniston (1977) and Gopinath and Vincenzi (1977) reveal that the Ca^{2+} pump is up-regulated by Ca^{2+}-calmodulin, whether the reagent directly interrupted the endosomal function or if the results reflected increased sensitivity of cellular integrity to the influx of Ca^{2+} was not clear.

Endocytosis is also enhanced by PMA and further by supplementation of OKA at 100 nM

Although the failure of inhibition by staurosporin suggests no involvement of protein kinase C in the Ca^{2+} effect, studies by Siegel et al. (1989) have indicated that diacylglycerol (DAG), which can be released by the ion-induced activation of phospholipase C (PLC), has a potency to induce membrane fusion. When cells were treated with a stable DAG analog phorbol 12-myristate 13-acetate (PMA), enhancement of internalization of HRP also occurred (Fig. 4a). The effect was slightly larger when cells were treated for 15 min than for 60 min (Fig. 4b). When PMA was added at 16.8 mM Ca^{2+} for 1 h, further activation by 1.3–1.5-fold of PMA-stimulated uptake was obtained. This result excludes that PMA was mimicking the Ca^{2+}-induced enhancement.

In contrast to the case with Ca^{2+}, Cs^+ and Rb^+ reduced the PMA effect only slightly (Fig. 5). The result could be explained by a minimum requirement of Ca^{2+} influx in PMA-treated cells. When 100 nM OKA was added, it enhanced the effect of PMA to fourfold over the control (Fig. 5). This result made a very strong contrast to the inhibition of the Ca^{2+} effect. However, when OKA was added at 1 μM, the reagent inhibited the activity to less than 30% of the control. Similar inhibition was obtained by 3 nM calyculin A (not shown). Under these conditions, intense cellular rounding was observed. These results suggest that mild or selective inhibition of PP(s) by OKA, in conjunction with the PMA effect, enhances endocytosis, while OK at 1 μM fully blocked not only the basal but also Ca^{2+} and PMA-induced internalizations. In contrast to th case with Ca^{2+}, the PMA effect was not inhibited b 15 μM TFP, suggesting no involvement of calmodulin dependent processes.

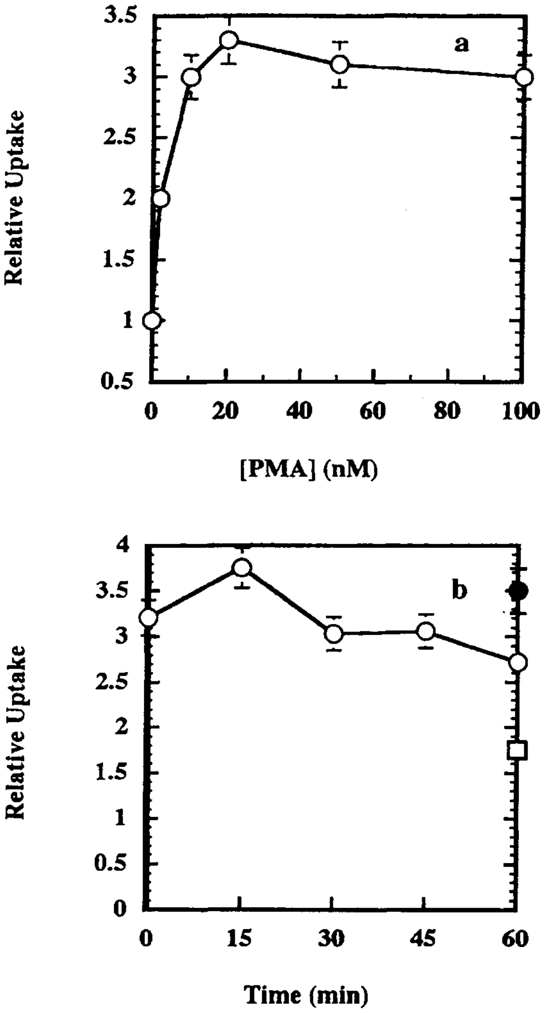

Fig. 4. PMA enhances fluid phase endocytosis by HT-1080 cells. Cells were incubated in MEM (1.8 mM Ca^{2+}) with PMA at the indicated concentrations at pH 7.2 at 35°C for 1 h. After incubation wit HRP (1 mg/ml) for 20 min, cell-associated enzyme was determine b: Time course of the enhancement. Cells preincubated with 20 n PMA for the indicated periods were added to 1 mg/ml HRP in th presence of PMA for 10 min. The uptake was compared to the activit without PMA. When cells were treated in 16.8 mM Ca^{2+} for 1 h (fille circle), the enhancement was strengthened. The square represent endocytosis in 16.8 mM Ca^{2+} alone.

Cells treated with 100 nM OKA in conjunction with PMA employ an altered early transport pathway

The effects of Ca^{2+} and PMA/OKA on the endosoma pathway were examined by confocal fluorescence microscopy of living cells. In the control cells, localizatio of early endosomes revealed by incubation with 5 mi

Backer, J.M., and King, J.L. (1991) Regulation of receptor-mediated endocytosis by phorbol esters. Biochem. Pharmacol., *41:*1267–1277.

Bradford, M.M. (1976) A rapid and sensitive method for the quantitation of microgram quantities of protein utilizing the principle of protein-dye binding. Anal. Biochem., *72:*248–254.

Cardone, M.H., Smith, B.L., Song, W., Mochley-Rosen, D., and Mostov, K.E. (1994) Phorbol myristate acetate-mediated stimulation of transcytosis and apical recycling in MDCK cells. J. Cell Biol., *124:*717–727.

Cohen, P. (1989) The structure and regulation of protein phosphatases. Annu. Rev. Biochem., *558:*453–508.

Cohen, P., Holmes, C.F.B., and Tsukitani, Y. (1990) Okadaic acid: A new probe for the study of cellular regulation. Trends Biochem. Sci., *15:*98–102.

Courtoy, P.J. (1991) Dissection of endosomes. In: Intracellular Trafficking of Proteins. C.J. Steer and Hanover, J.A. eds. Cambridge University Press, London, pp. 103–156.

Davidson, H.W., McGowan, C.H., and Balch, W.E. (1992) Evidence for regulation of exocytic transport by protein phosphorylation. J. Cell Biol., *116:*1343–1355.

Emans, N., Gorvel, J.-P., Walter, C., Gerke, V., Kellner, R., Griffith, G., and Gruenberg, J. (1993) Annexin II is a major component of fusiogenic endosomal vesicles. J. Cell Biol., *120:*1357–1369.

Goldstein, J.L., Brown, M.S., Anderson, R.G.W., Russell, D.W., and Schneider, W.J. (1985) Receptor-mediated endocytosis: Concepts emerging from the LDL receptor system. Annu. Rev. Cell Biol., *1:*1–39.

Gopinath, R.M., and Vincenzi, F.F. (1977) Phosphodiesterase protein activator mimics red blood cell cytoplasmic activator of (Ca^{2+}-Mg^{2+}) ATPase. Biochem. Biophys. Res. Commun., *77:*1203–1209.

Gruenberg, J., and Howell, K.E. (1989) Membrane traffic in endocytosis: Insights from cell-free assays. Annu. Rev. Cell Biol., *5:*453–481.

Haigler, H.T., McKanna, J.A., and Cohen, S. (1979) Rapid stimulation of pinocytosis in human carcinoma cells A431 by epidermal growth factor. J. Cell Biol., *83:*82–90.

Hewlett, L.J., Prescott, A.R., and Watts, C. (1994) The coated pit and macropinocytic pathways serve distinct endosome populations. J. Cell. Biol., *124:*689–703.

Ishihara, H., Martin, B.L., Brautigan, D.L., Karaki, H., Ozaki, H., Kato, Y., Fusetani, N., Watabe, S., Hashimoto, K., Uemura, D., and Hartshorne, D.J. (1989) Calyculin A and okadaic acid: Inhibitors of protein phosphatase activity. Biochem. Biophys. Res. Commun., *159:*871–877.

Jarrett, H.M., and Penniston, J.T. (1977) Partial purification of the Ca^{2+}-Mg^{2+} ATPase activator from human erythrocyte: Its similarity to the activator of 3′:5′-cyclic nucleotide phosphodiesterase. Biochem. Biophys. Res. Commun., *77:*1210–1216.

Lin, H.C., Südhof, T.C., and Anderson, R.G.W. (1992) Annexin VI is required for budding of clathrin-coated pits. Cell, *70:*283–291.

Lucocq, J., Warren, G., and Pryde, J. (1991) Okadaic acid induces Golgi apparatus fragmentation and arrest of intracellular transport. J. Cell Sci., *100:*753–759.

Mayorga, L.S., Colombo, M.I., Lennartz, M.L., Brown, E.J., Rhaman, K.H., Weiss, R., Lennon, P.J., and Stahl, P. (1993) Inhibition of endosome fusion by phospholipase A$_2$ (PLA$_2$) inhibitors points to a role for PLA$_2$ in endocytosis. Proc. Natl. Acad. Sci. U.S.A., *90:*10255–10259.

Niggli, V., Siegel, E., and Carafoli, E. (1982) The purified Ca^{2+} pump of human erythrocyte membrane catalyzes an electroneutral Ca^{2+}-H^{+} exchange in reconstituted liposomal systems. J. Biol. Chem., *257:*2350–2356.

Pierre, P., Scheel, J., Rickard, J.E., and Kreis, T.E. (1992) Clip-170 links endocytic vesicles to microtubles. Cell, *70:*887–900.

Preston, R., Murphy, R.F., and Jones, E.W. (1987) Apparent endocytosis of fluorescein isothiocyanate-conjugated dextran by Saccharomyces cerevisiae reflects uptake of low molecular impurities, not dextran. J. Cell Biol., *105:*1981–1987.

Racoosin, E.L., and Swanson, J.A. (1993) Macropinosome maturation and fusion with tubular lysosomes in macrophages. J. Cell Biol., *121:*1011–1020.

Rickard, J.E., and Kreis, T.E. (1991) Binding of pp170 to microtubules is regulated by phosphorylation. J. Biol. Chem., *266:*17597–17605.

Robinson, P.J., Sontag, J.-M., Liu, J.-P., Fykse, E.M., Slaughter, C., McMahon, H., and Südhof, T.C. (1993) Dynamin GTPase regulated by protein kinase C phosphorylation in nerve terminals. Nature, *365:*163–166.

Siegel, D.P., Banschbach, J., Alford, D., Ellens, H., Lis, L.J., Quinn, P.J., Yeagel, P.L., and Bentz, J. (1989) Physiological levels of diacylglycerols in phospholipid membrane induce membrane fusion and stabilize inverted phase. Biochemistry, *28:*3703–3709.

Simon, S.M., and Llinas, R.R. (1985) Compartmentalization of the submembrane calcium activity during calcium influx and its significance in transmitter release. Biophys. J., *48:*485–498.

Swanson, J.A. (1989) Phorbol esters stimulate macropinocytosis and solute flow through macrophages. J. Cell Sci., *94:*135–142.

Thomas, A.P., and Delaville, F. (1991) The use of fluorescent indicators for measurement of cytosolic free calcium concentration in cell population and single cells. In: Cellular Calcium: A Practical Approach. J.G. McCormack and P.H. Cobbold, eds. IRL Press at Oxford University Press, Oxford, pp. 1–54.

Woodman, P.G., Mundy, D.I., Cohen, P., and Warren, G. (1992) Cell-free fusion of endocytic vesicles is regulated by phosphorylation. J. Cell Biol., *116:*331–338.

4.

J. Biochem. 119, 887-897 (1996)

Wortmannin and Li$^+$ Specifically Inhibit Clathrin-Independent Endocytic Internalization of Bulk Fluid

Satoshi B. Sato,[*,1] **Takahisa Taguchi,**[†] **Shohei Yamashina,**[‡] **and Sakuji Toyama**[§]

[*]Cell and Information, PRESTO, Research Development Corporation of Japan and Department of Biophysics, Faculty of Science, Kyoto University, Kyoto 606-01; [†]Department of Organic Materials, Osaka National Research Institute, Ikeda, Osaka 563; [‡]Department of Anatomy, Kitasato University School of Medicine, Kitasato, Sagamihara, Kanagawa 228; and [§]Institute for Virus Research, Kyoto University, Kyoto 606-01

Received for publication, December 11, 1995

Incubation of a human fibrosarcoma cell line HT-1080 in Li$^+$-containing medium inhibited internalization of a fluid marker, horseradish peroxidase (HRP), by more than 80%. The ion inhibited the activity enhanced by Ca^{2+} or phorbol 12-myristate 13-acetate. We also found that wortmannin (WT), a potent inhibitor of phosphoinositide (PI) 3-kinase (PI 3-k), inhibited the non-stimulated and the two stimulated types of endocytosis to the same extent as Li$^+$. In contrast, neither WT nor Li$^+$ influenced the early internalization of transferrin (Tfn), EGF or platelet-derived growth factor. Neither targeting to early endosomes nor recycling of the once-internalized Tfn was influenced. When the cytoplasmic pH was lowered by chasing cells that had been preincubated with 25 mM NH_4Cl in an amiloride-containing Na$^+$-free medium, more than 90% of internalization of Tfn in HT-1080 cells was inhibited, while that of HRP was reduced by only 35%. In contrast, WT reduced the uptake of HRP by KB cells by 34%, while 60% of the activity was inhibited by the treatment for cytoplasmic acidification. Comparison of other cells *i.e.*, A-549 and a human diploid cell line Miyajima, indicated that cells showing higher sensitivity to WT were less sensitive to low cytoplasmic pH. These results suggest that, in all the cells studied, bulk fluid is internalized either *via* a clathrin-independent/PI 3-k-dependent route or *via* a clathrin-dependent/PI 3-k-independent one, though the ratio varied among them. We also found that internalization of a mAb directed toward the 116 (100)-kDa subunit of vacuolar ATPase [OSW2; Sato and Toyama (1994) *J. Cell Biol.* 127, 39-53] in the fluid phase was inhibited by WT, but the antibody was still internalized in a surface-bound form. Regardless of the treatment with WT, most of the antibody was transported to endosomes that were associated with Tfn receptor. These results suggest that both internalization routes are targeted to the same early endosomal compartments.

Key words: endocytosis, growth factor internalization, PI-3k, PI-turnover, transferrin.

Eukaryotic cells internalize physiologically important molecules by endocytosis. The process employing specific receptors in clathrin-coated pits and vesicles is essential for the internalization of many kinds of protein ligands (*1, 2*). With ligands, the bulk-fluid phase is opportunistically internalized by the vesicles. On the other hand, some toxins and plasma membrane components are internalized independently of clathrin (*3, 4*). The two surface routes appear to be targeted to the common early endosomes (*5, 6*). It has been shown that inhibition of clathrin-polymerization reduces endocytosis of transferrin by rat fetal fibroblasts while the internalization of HRP is much less affected (*7*). Damke *et al.* have demonstrated that induction of a mutant dynamin that lacks GTPase activity in HeLa cells specifically reduces most of the receptor-mediated internalization of protein ligands, but the cells still show a high degree of endocytosis of HRP (*8*). These results imply that the clathrin-independent mechanism(s) takes a large part in the internalization of the bulk fluid in some cells. However, in contrast to clathrin-dependent endocytosis, mechanistic details of the bulk-fluid endocytosis are still unclear (for review, Ref. *9*).

By using wortmannin, which inhibits phosphoinositide (PI) 3-kinase, recent studies have suggested that this enzyme is involved in endocytic activity (*10, 11*). Wortmannin was found to be inhibitory to the internalization of a fluid phase marker, but this was interpreted in terms of the mechanism of clathrin-dependent endocytosis (*10*). In apparent contradiction, Joly *et al.* indicated that a WT-sensitive mechanism is involved in post-endocytic step(s), where the reagent inhibited down-regulation of platelet-derived growth factor receptor (*11*).

We previously found that fluid phase endocytosis in a human fibrosarcoma cell line, HT-1080, was enhanced by Ca^{2+} or phorbol 12-myristate 13-acetate (PMA) (*12*). The fluid phase was transported to compartments that were localized by fluorescent transferrin. In the presence of okadaic acid (OKA) at 100 nM and 20 nM PMA, the fluid phase was targeted to compartments devoid of transferrin-labeling, suggesting that the cells potentially had a clathrin-independent alternate endocytic mechanism(s) (*12*). We

---

[1] To whom correspondence should be addressed. Tel: +81-75-753-4216, Fax: +81-75-791-0271

117

also found that Li^+ inhibited fluid-phase endocytosis activated by Ca^{2+}. In characterizing the effect of the ion, prolonged incubation in Li^+ also inhibited non-stimulated endocytic activity and that activated by PMA. We found that WT inhibits both the basal and activated endocytosis with identical magnitude. We used these two reagents for characterization of receptor-mediated internalization of transferrin (Tfn), epidermal growth factor (EGF) and platelet-derived growth factor (PDGF) and observed no inhibition. Because both reagents interfere with the noncanonical PI-turnover, we suggest that the molecule(s) in the turnover is an essential element in the clathrin-independent endocytosis.

MATERIALS AND METHODS

Reagents—DME and Na phosphate-free MEM were obtained from Gibco BRL (Gaithersburg, MD). Wortmannin (Sigma Chemical, St. Louis, SO) and phorbol 12-myristate 13-acetate (Wako Pure Chemicals, Osaka) were purchased from the indicated distributors. A rabbit antiserum against the p85 subunit of PI 3-k was obtained from UBI (Lake Placid, NY). TRITC-dextran, TRITC-labeled human transferrin (Tfn) and FITC-Tfn were purchased from Molecular Probes (Eugene, OR). ^{125}I-labeled human Tfn, epidermal growth factor (EGF), and platelet-derived growth factor (PDGF)-BB were obtained from Amersham (UK). Non-labeled human Tfn (Chemicon International, Temecula, CA), human recombinant EGF (Wako), and human recombinant PDGF (Genzyme, Cambridge, MA) were purchased from the indicated distributors. Fluorescently labeled antibodies against mouse IgG_1 and IgG_{2b} were obtained from Southern Biotechnology (Birmingham, AL). Other reagents were obtained from Wako.

Cells—HT-1080 clone 1 was as described (*12*). A-549 was obtained from ICN (Costa Mesa, CA). KB-100 was a subclone of KB cells (*13*). MDCK-II was kindly provided by Dr. T. Kobayashi of Tohoku University. A diploid human cell line, Miyajima, was established from a monolayer culture of donor cells. The cells were maintained in DME supplemented with 10% fetal bovine serum (FBS). They were used more than 2 days after culturing on small plastic dishes or on glass coverslips.

Treatment of Cells with Li^+ or Wortmannin—Cells were usually treated in DME-10% FBS containing 50 mM LiCl (>99.9%, from 1 M stock) or 50 nM wortmannin (WT, from ×1,000 stock in DMSO) at 37°C. For treatment with Ca^{2+}, cells were washed with prewarmed Na phosphate-free MEM containing 10 mM Hepes, 1 mM Na pyruvate, and 2% FBS (dialyzed against 150 mM NaCl) at pH 7.2, in order to avoid formation of Ca phosphate precipitates. They were incubated in the medium supplemented with 15 mM $CaCl_2$ (>99.9%, final 16.8 mM, high Ca^{2+}-medium) for 60 min at 37°C with gentle shaking in a humidified chamber. When Li^+- or WT-treated cells were further treated with Ca^{2+}, they were transferred to the high Ca^{2+}-medium containing the reagents 1 h before the assay.

Assay of Fluid-Phase Endocytosis—Duplicate cultures of cells in DME- or MEM-2% FBS ($6\text{-}8 \times 10^5$ cells/small dish) were supplemented with horseradish peroxidase to a final concentration between 0.5-2 mg/ml. They were incubated in a humidified chamber placed in a shaking incubator at 35°C. At intervals, cells were washed with ice-cold PBS (145 mM NaCl, 10 mM Na phosphate, pH 7.2) 3 times, scraped into Eppendorf tubes, and washed with PBS 3 times by centrifugation at $3{,}000 \times g$ at 4°C for 5 min. KB and Miyajima, to which slight background binding of HRP at 0°C was detectable, were treated with 0.01% pronase and sedimented through 0.5 ml of 15% sucrose-PBS. The washed cells were solubilized in 0.45 ml of TBS (150 mM NaCl, 50 mM Tris-HCl, pH 8.0) containing 0.2% Triton X-100 and 10 μg/ml pepstatin A and 10 μM (*p*-amidinophenyl)methanesulfonyl fluoride hydrochloride (APMSF), at 0°C for 1 h. After centrifugation at $10{,}000 \times g$ for 10 min, the supernatant was analyzed in triplicate for protein (*14*) and the peroxidase activity using tetramethylbenzidine as a substrate. The results were normalized for cellular protein and represented as relative uptake to the control cells. Cells were also treated with 25 mM NH_4Cl (Fluka, Switzerland) for 20 min, followed by incubation in K^+-buffer (150 mM KCl, 2 mM $CaCl_2$, 1 mM $MgCl_2$, 10 mM K Hepes, pH 7.0) containing 500 μM amiloride in a similar manner to that described (*15*). Control cells were incubated in DME-10 mM Na Hepes (DME-Hepes) pH 7.2 without serum. After 5 min, cells were incubated with HRP for 10 min and the uptake of the enzyme was determined as described above. The treatments did not change the mechanical stability against the scraping procedure as assessed by membrane permeability to trypan blue.

Assay of Receptor-Mediated Endocytosis—For assay of internalization of transferrin (Tfn), cells were first incubated in serum-free DME for 1.5 h at 37°C, then with 50 nM WT for 30 min. They were incubated in 1 ml of serum-free DME containing 0.5 μg/ml non-labeled Tfn and 1.85 kBq (0.05 μCi)/ml ^{125}I-Tfn at 37°C. Cells were washed with ice-cold DME-Hepes, pH 7.2, 6 times. After removal of surface-bound Tfn by treatment with 50 mM glycine, 100 mM NaCl pH 3.0 for 2 min, 2 times, cell-associated radioactivity was recovered in 2×0.8 ml of 1 N NaOH. When recycling of the ligand was measured, cells depleted of the intrinsic ligand as described above were first incubated with Tfn (1.85 kBq/ml, 0.1 μg/ml) for 1 h at 37°C. WT was added at 50 nM during the next 30 min. The cells were washed and chased in DME containing 50 μg/ml non-labeled Tfn. At intervals, 100 μl aliquots of the chase medium were collected and the radioactivity was determined. For the assay of internalization of EGF or PDGF, cells pretreated with 50 nM WT for 60 min were incubated in DME-5 mM Na Hepes containing 2% dialyzed FBS, 5-10 ng/ml EGF or PDGF and 1.85 kBq/ml ^{125}I-labeled corresponding ligands. At intervals, cells were washed, acid-treated and solubilized in 1 N NaOH. In order to test the effect of WT on the lysosomal degradation, cells were incubated with 2 ng/ml EGF/^{125}I-EGF in DME-2% FBS at 20°C for 1 h. Cells were then treated with WT in the presence of the ligand for 20 min, washed 6 times at 0°C, and chased at 37°C. At intervals, 100 μl of the medium was collected and 100% TCA-0.25% Na deoxycholate was added to give a final concentration of 20%. After incubation in ice for 1 h, the samples were centrifuged at $10{,}000 \times g$ for 5 min and the TCA-soluble count was measured. The radioactivity was determined in a Clinigamma counter (Pharmacia LKB, Uppsala, Sweden).

Fluorescence Microscopy of Endosomes—For labeling of early endosomes with Tfn, cells on coverslips were depleted of the ligand by incubation in serum-free DME-Hepes pH 7.2 at 37°C for 60 min. FITC-Tfn (100 μg/ml) was then added for 1 h. The cells were further incubated with 50 nM WT in the presence of the ligand for 30 min. After having been washed with the medium containing WT over 5 min, the cells were incubated with TRITC-Tfn (50 μg/ml) for 10 min at room temperature (25°C). The coverslips were mounted in DME-5 mM Na Hepes containing 20 mM methylamine for visualization of otherwise quenched FITC-fluorescence. Cells were also incubated with a mAb directed toward the 116(100)-kDa subunit of the vacuolar-type proton pump, OSW2 (IgG$_{2b}$) (*16*), at 100 or 3 μg/ml for 10 min at 37°C. The cells were washed and fixed with 3% paraformaldehyde-PBS for 10 min then permeabilized with 0.05% Triton X-100 in PBS for 1.5 min. After incubation with an anti-human Tfn mAb (IgG$_1$: Chemicon), the antibodies were visualized by fluorescent subtype-specific antibodies. Cells were observed by using a confocal laser scanning system (MRC-600, Biorad, Hercules, CA) mounted on an Axiophoto fluorescence microscope (Carl Zeiss, Germany).

Electron Microscopy—Cells in 8-well Lab-Tek chamber slides (Japan InterMed, Tokyo) were treated with 10 mg/ml HRP at 37°C for 30 min. They were washed with MEM-Hepes pH 7.2, then chased in the presence or the absence of 50 nM WT for 20 min. Cationized ferritin (Sigma) was added to a final concentration of 100 μg/ml for 20 min. Cells were fixed with 0.5% glutaraldehyde in 7% sucrose-PBS at room temperature for 30 min. For visualization of HRP, fixed cells were treated with 0.5 mg/ml diaminobenzidine in TBS and 0.03% H_2O_2. The samples were further fixed in 1% OsO_4. Cells were also stained with ruthenium red in a similar manner to that described (*8*). The cells preincubated with 50 nM WT at 37°C were washed with 150 mM Na cacodylate pH 7.6 and fixed with 1% glutaraldehyde in 100 mM Na cacodylate containing 0.5 mg/ml ruthenium red at room temperature for 1 h. They were then washed with 150 mM Na cacodylate 5 times and further treated with 0.5 mg/ml ruthenium red and 1% OsO_4 in 75 mM Na cacodylate for 3 h. Samples were dehydrated with a graded series of ethanol, and finally embedded in Epon. Ultrathin sections were examined with or without counter-staining by uranyl acetate and lead citrate.

RESULTS

Inhibition of Fluid-Phase Endocytosis by Li$^+$—Fluid-phase endocytosis by HT-1080 was measured by using a non-specific marker, HRP. The activity was 0.081±0.005 μl/h/10^6 cells, which is comparable to that in hepatocytes (*17, 18*). When cells were incubated with 50 mM Li$^+$ for increasing periods, the ion reduced not only the basal endocytosis, but also the activation by Ca^{2+} or phorbol 12-myristate 13-acetate (PMA) (Fig. 1a). When cells preincubated with Li$^+$ for 3 h were returned to a normal medium, the inhibition was reversed nearly to the original level within 3 h (Fig. 1b). Prolonged incubation in Li$^+$ did not induce any evident cytopathic effect. The ion did not change the activity of the marker. The cells remained fully extended even after 18 h. At that time point, the number of cells was 80% of the control, suggesting slight inhibition of multiplication. However, the cells grew normally upon removal of the ion (data not shown).

Fluid-Phase Endocytosis Is Inhibited by WT—Li$^+$ inhibits dephosphorylation of inositol di- and monophosphate, resulting in reduction of a phosphatidylinositol pool. It therefore interferes with both the canonical and non-canonical phosphoinositide (PI)-turnovers (*19-21*). Since Li$^+$ reduced enhancement of fluid-phase endocytosis by Ca^{2+} or PMA, which can mimic some parts of the canonical turnover, we tested the effect of inhibition of non-canonical PI-turnover on the fluid-phase endocytosis by using a potent inhibitor of PI 3-k, wortmannin (WT) (*22, 23*). When cells were incubated with the reagent for 1 h, not only the basal activity, but also that stimulated by Ca^{2+} or PMA were very similarly reduced (Fig. 2a). The concentrations giving 50% inhibition of the original activities were 2 nM for all three cases, which was similar to that inhibiting the partially purified enzyme. In contrast to these effects, incubation of cells with 2,3-dihydroxybenzaldehyde at 5 μg/ml, which inhibits PI 4-k (*24*), did not change the activity.

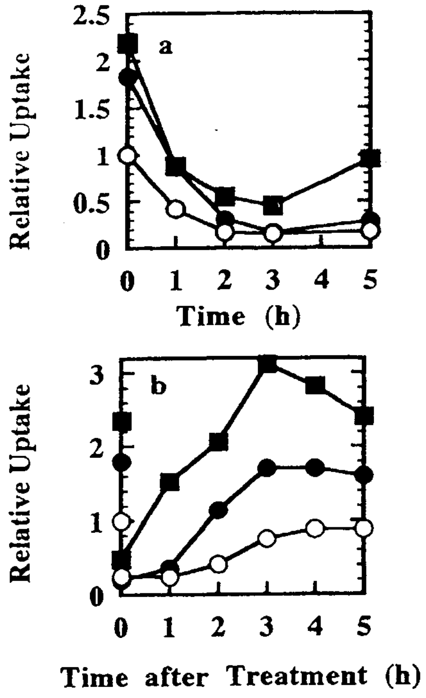

Fig. 1. **Inhibition of fluid phase endocytosis by Li$^+$.** a: Cells were incubated with 50 mM LiCl for indicated periods. During the last 1 h, they were treated with either none (○, 1.8 mM Ca^{2+}), 16.8 mM Ca^{2+} (●) or 20 nM PMA (■) in Na phosphate-free MEM-2% FBS dialyzed against 150 mM NaCl. For treatment with Li$^+$ for longer than 1 h, incubation was initially done in DME-10% FBS. Internalization of HRP was determined by incubating cells with the enzyme at 1 mg/ml at 37°C for 20 min. The uptake at 0 h denotes treatments without Li$^+$. b: Reversibility of the inhibition. Cells previously incubated with 50 mM LiCl in DME-10% FBS for 3 h were chased in the Li$^+$-free medium for indicated periods. During the last 1 h of the chase, medium was replaced with Na phosphate-free MEM (○) or either in the presence of 16.8 mM Ca^{2+} (●) or 20 nM PMA (■). 0 h indicates incubation in Li$^+$-containing DME for 2 h, then in Li$^+$-containing Na phosphate-free MEM for 1 h. Symbols without lines at 0 h indicate the amounts in cells without the Li$^+$-treatment. The results are averages of at least three experiments. Errors, which were less than 15% of each value, are not indicated.

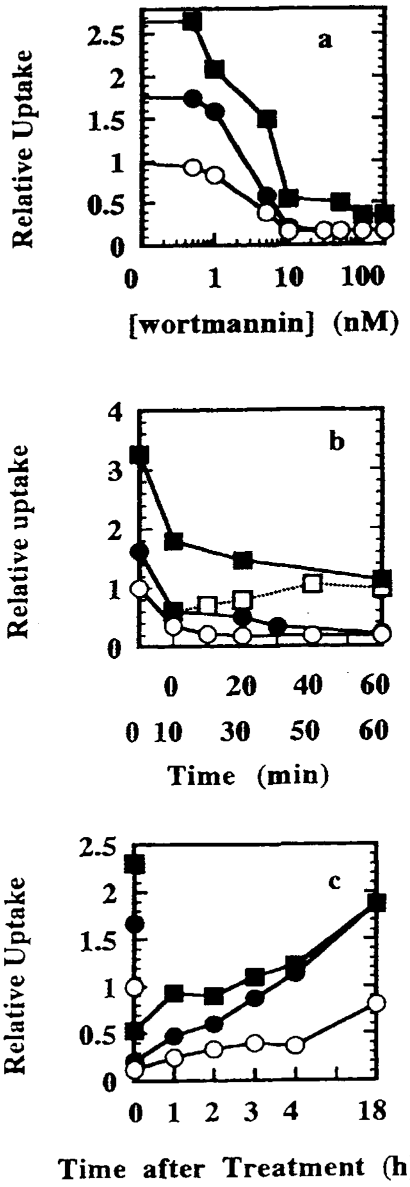

Fig. 2. **Inhibition of endocytosis by wortmannin (WT).** a: Cells were incubated with indicated concentrations of WT for 1 h either in Na phosphate-free MEM (1.8 mM Ca^{2+}, ○), or in the MEM containing 16.8 mM Ca^{2+} (●) 20 nM PMA (■). Endocytosis was then assayed in terms of the uptake of HRP for 20 min. b: Cells preincubated in Na phosphate-free MEM (1.8 mM Ca^{2+}, ○) or in the MEM containing 16.8 mM Ca^{2+} (●) or PMA (20 nM, ■) were treated with 50 nM WT and incubated for the periods indicated in the upper row. They were then assayed for endocytosis by adding HRP (1 mg/ml) for 10 min. The lower row depicts the duration of contact with WT. Open squares with dotted lines denote the internalization of HRP in cells simultaneously treated with PMA and WT. c: Cells were treated with 50 nM WT in DME-10% FBS at 37°C for 1 h. The medium was then replaced with fresh medium lacking WT and incubated for the indicated periods. During the final 1 h, cells were incubated in phosphate-free MEM (1.8 mM Ca^{2+}, ○) or with Ca^{2+} (16. 8 mM, ●) or PMA (20 nM, ■). Cells at the time point of 0 h were directly treated with Ca^{2+} or PMA in WT-containing phosphate-free MEM for 1 h, without subsequent chase. Data points without lines at 0 h indicate internalization without treatment with WT. Endocytosis was assayed for 15 min. The results are averages of at least three experiments. Errors were less than 5% of each value.

Inhibition by WT occurred very rapidly, and more than 60% of the activity was lost when cells made contact with 50 nM WT during the uptake of HRP for 10 min (Fig. 2b). When cells were pretreated with the reagent for 10 min, full inhibition was achieved, suggesting that the reagent inhibited the earliest step. When cells first treated with Ca^{2+} were incubated with WT, the inhibition similarly occurred rapidly. In contrast, when WT was added to cells pretreated with 20 nM PMA for 1 h, the reduction of the full activation by about 65% was significantly lower than the 80% reduction of the activation of WT-treated cells. More inhibition occurred when cells were treated simultaneously with PMA and WT, but the activity then slightly increased. These results suggest that a large part of the PMA-enhanceable process is dependent on a WT-sensitive mechanism, but the cells are able to recruit a certain less sensitive mechanism.

When cells incubated with WT for 1 h were returned to a normal medium, the basal activity was slowly restored. It was 30-40% at 4 h and 80% of the original activity at 18 h

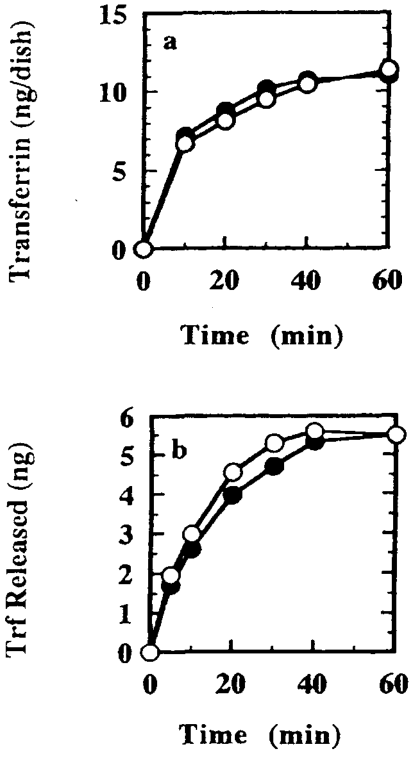

Fig. 3. **Wortmannin does not reduce the internalization (a) or recycling (b) of transferrin.** a: Cells preincubated in a serum-free medium for 1.5 h were further incubated for 30 min in the absence (○) or presence (●) of 50 nM WT. Internalization was assayed by incubating the cells with 0.5 μg/ml Tfn/^{125}I-Tfn in the absence (○) or presence (●) of 50 nM WT at 37°C. At indicated time points, cells were washed with DME and further with 50 mM glycine, 100 mM NaCl (pH 3.5) at 0°C. The cell-associated radioactivity recovered in 0.1 N NaOH was determined. b: Cells preincubated in a serum-free medium were incubated with 0.1 μg/ml Tfn/^{125}I-Tfn for 1 h and for additional 30 min in the absence (○) or presence (●) of 50 nM WT. After having been washed, they were chased in the presence of non-labeled Tfn at 50 μg/ml. At indicated time points 100 μl of the medium was collected and assayed for radioactivity. The amounts represent the sum of the released protein at the time points. The errors were all within 5% and are not shown.

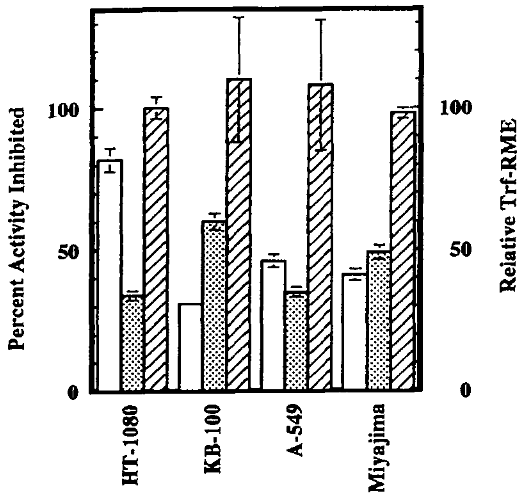

Fig. 10. **Effect of treatment with 50 nM WT (open bars) and that of chase of cells preloaded with 25 mM NH_4Cl in Na^+-free buffer containing 500 μM amiloride (shaded bars) on the internalization of HRP (0.5 mg/ml) at 37°C for 10 min.** The results are expressed as percent of activity lost after the treatments. Cells were also examined for receptor-mediated endocytosis of Tfn/^{125}I-Tfn (Tfn-RME) for 10 min. The results were normalized for the uptake by 8×10^5 cells and are expressed using striped bars as relative activities compared to that of HT-1080.

(OSW2) (*16*) reached endosomes associated with Tfn receptor in 5 to 10 min (Fig. 6). We have also observed that FITC-dextran is similarly transported (*12*). In the absence of WT, some OSW2 was found in small vesicular structures lacking Tfn receptor. These results suggest that, as described in different cells (*4*), the presence of preendosomal intermediate vesicles used for clathrin-independent endocytosis is also the case in HT-1080 cells. Although the vesicles are yet to be characterized *in vitro*, slow recovery from the effect of Li^+ and WT would allow isolation and characterization of vesicles derived from isolated plasma membrane from the treated cells. We are currently addressing the *in vitro* reconstitution of the budding.

In addition to the inhibition of internalization of fluid phase, Li^+ and WT affected the postendocytic transport of EGF. EGF accumulated in cells at 20°C began to be degraded at a similar time point during the chase at 37°C regardless of the treatment with WT (Fig. 5b). In contrast, the degradation thereafter increased in the presence of WT. These results indicate that WT did not change the delivery of the ligand to lysosomes, while the transport of degradation products outside the cell was accelerated. The results are in contrast to the effect of WT on the intracellular transport of PDGF receptor reported by Joly *et al.* (*11*). In that report, a large part of the receptors was exposed to the cell surface even after incubation with the ligand for 90 min in the presence of WT, when the receptors were normal in terms of the PI 3-k binding site. In contrast, treatment with WT slightly reduced the number of mutant receptors that lacked the motif. Although clarification of the reason for the difference between the present result on EGF and that on PDGF receptors awaits further characterization, it is interesting to note that post endocytic traffic of EGF and that of its receptor appear different with respect to the modification of the receptor kinase (*34, 35*).

The present results indicate that WT-sensitive and non-specific fluid-phase endocytosis occurs distinctly from clathrin-dependent and receptor-mediated endocytosis. Although WT has no evident effect on the survival of cells in culture (*22*), the reagent is very toxic to the whole animal (*36*). Because both the clathrin-dependent and -independent endocytosis can be expected to represent non-specific sampling mechanisms, a study on the process involved in internalization of bulk fluid should provide a coherent understanding of the role of fluid-phase internalization in cellular physiology. PI 3-k has been mainly studied in relation to oncogenesis and signal transduction (*22, 23, 37-39*). WT has been mainly employed in relation to signal transduction or cell activation. In contrast, endocytosis is a constitutive process which can be observed in non-stimulated cells. Further study should reveal the functional link through membrane traffic between the resting and stimulated cellular states.

S.B.S. is grateful to the stimulating lecture on "Cell and Information" and encouragement by Dr. Fumio Oosawa, who orginized the research project with the same title. S.B.S. also thanks Dr. Masayuki Otsu for helpful discussions, the PRESTO office of JRDC for generous encouragement and Ms. Yoshiko Iida for her excellent technical help.

REFERENCES

1. Goldstein, J.L., Brown, M.S., Anderson, R.G.W., Russell, D.W., and Schneider, W.J. (1985) Receptor-mediated endocytosis: Concepts emerging from the LDL receptor system. *Annu. Rev. Cell Biol.* **1**, 1-39
2. Anderson, R.G.W. (1991) Molecular motors that shape endocytic membrane in *Intracellular Trafficking of Proteins* (Steer, C.J. and Hanover, J.A., eds.) pp. 13-47, Cambridge University Press, London
3. van Deurs, B., Peterson, O.W., Olsnes, S., and Sandvig, K. (1989) The ways of endocytosis. *Intl. Rev. Cytol.* **117**, 131-177
4. Hansen, S.H., Sandvig, K., and van Deurs, B. (1991) The preendosomal compartments comprise distinct coated and noncoated endocytic vesicle populations. *J. Cell Biol.* **113**, 731-741
5. Hansen, S.H., Sandvig, K., and van Deurs, B. (1993) Molecules internalized by clathrin-independent endocytosis are delivered to endosomes containing transferrin receptors. *J. Cell Biol.* **12**, 89-97
6. Tran, D., Carpentier, J.-L., Sawano, F., Gorden, P., and Orci, L. (1987) Ligands internalized through coated or noncoated invaginations follow a common intracellular pathway. *Proc. Natl. Acad. Sci. USA* **84**, 7957-7961
7. Cupers, P., Veithen, A., Kiss, A., Baudhuin, P., and Courtoy, P.J. (1994) Clathrin polymerization is not required for bulk-phase endocytosis in rat fetal fibroblasts. *J. Cell Biol.* **127**, 725-735
8. Damke, H., Baba, T., Warnock, D.E., and Schmid, S.L. (1994) Induction of mutant dynamin specifically blocks endocytic coated pit formation. *J. Cell Biol.* **127**, 915-934
9. Lamaze, C. and Schmid, S.L. (1995) The emergence of clathrin-independent pinocytic pathways. *Curr. Opin. Cell Biol.* **7**, 573-580
10. Clague, M.J., Thorpe, C., and Jones, A.T. (1995) Phosphatidylinositol 3-kinase regulation of fluid phase endocytosis. *FEBS Lett.* **367**, 272-274
11. Joly, M., Kazlauskas, A., and Corvera, S. (1995) Phosphatidlyinositol 3-kinase activity is required at a postendocytic step in platelet-derived growth factor receptor trafficking. *J. Biol. Chem.* **270**, 13225-13230
12. Sato, S.B., Kiyosue, K., Taguchi, T., Kasai, M., and Toyama, S. (1996) Okadaic acid gives concentration-dependent reciprocal effects on the fluid phase endocytosis activated by Ca^{2+} and phorbol 12-myristate 13-acetate. *J. Cell. Phisiol.* **166**, 66-75
13. Toyama, S., Tiyama, S., and Uetake, H. (1977) Altered cell

fusion capacity of KB cells resistant to Sendai virus-induced cytolysis. *Virology* **76**, 503-515

14. Bradford, M.M. (1976) A rapid and sensitive method for the quantitation of microgram quantities of protein utilizing the principle of protein-dye binding. *Anal. Biochem.* **72**, 248-254
15. Sandvig, K., Olsnes, S., Petersen, O.W., and van Deurs, B. (1987) Acidification of the cytosol inhibits endocytosis from coated pit. *J. Cell Biol.* **105**, 678-689
16. Sato, S.B. and Toyama, S. (1994) Interference with the endosomal acidification by a monoclonal antibody directed toward the 116(100)-kDa subunit of the vacuolar type proton pump. *J. Cell Biol.* **127**, 39-53
17. Ose, L., Ose, T., Reinersten, R., and Berg, T. (1980) Fluid phase endocytosis in isolated rat parenchymal and non-parenchymal liver cells. *Exp. Cell Res.* **126**, 109-119
18. Munniksma, J., Noteborn, M., Kooistra, S., Bouma, J.M.W., Gruber, M., Brouwer, A., Praaning-Van Dalen, D., and Knock, D.L. (1980)) Fluid endocytosis by rat liver and spleen. *Biochem. J.* **192**, 613-621
19. Bansal, V.S. and Majerus, P.W. (1990) Phosphatidylinositol derived precursors and signals. *Annu. Rev. Cell Biol.* **6**, 41-67
20. Majeurs, P.W. (1992) Inositol phosphate biochemistry. *Annu. Rev. Biochem.* **61**, 225-250
21. Berridge, M.J. (1993) Inositol triphosphate and calcium signaling. *Nature* **361**, 315-325
22. Yano, H., Nakanishi, S., Kimura, K., Hanai, N., Fukui, Y., Nonomura, Y., and Masuda, Y. (1993) Inhibition of histamine secretion by wortmannin through the blockage of phosphatidylinositol 3-kinase in RBL-2H3 cells. *J. Biol. Chem.* **268**, 25846-25856
23. Arcaro, A. and Wyman, M.P. (1993) Wortmannin is a potent phosphatidylinositol 3-kinase inhibitor: The role of phosphatidylinositol 3,4,5,-triphosphate in neutrophil responses. *Biochem. J.* **296**, 297-301
24. Nishioka, H., Imoto, M., Sawa, T., Hamada, M., Naganawa, H., Takeuchi, T., and Umezawa, K. (1989) Screening of phosphatidylinositol kinase inhibitors from *Streptomyces*. *J. Antibiot.* **42**, 823-825
25. Miller, K., Shipman, S., Trowbridge, I.S., and Hopkins, C. (1991) Transferrin receptors promote the formation of clathrin lattice. *Cell* **65**, 621-632
26. Pignataro, O.P. and Ascoli, M. (1990) Epidermal growth factor increases the labeling of phosphatidylinositol 3,4-bisphosphate in MA-10 Leydig tumor cells. *J. Biol. Chem.* **265**, 1718-1723
27. Nilsson, J., Thyberg, J., Heldin, K.-H., Westermark, B., and Wasteson, A. (1983) Surface binding and internalization of platelet-derived growth factor in human fibroblasts. *Proc. Natl. Acad. Sci. USA* **80**, 5592-5596
28. Auger, K.R., Serunian, L.A., Soltoff, S.P. Libby, P., and Cantley, L.C. (1989) PDGF-dependent tyrosine phosphorylation stimulates production of novel polyphosphoinositides in intact cells. *Cell* **5**, 167-175
29. Susa, M., Keeler, M., and Varticovski, L. (1992) Platelet-derived growth factor activates membrane-associated phosphatidylinositol 3-kinase and mediates its translocation from the cytosol. *J. Biol. Chem.* **267**, 22951-22956
30. Stephens, L.R., Hughes, K.T., and Irvine, R.F. (1991) Pathway of phosphatidylinositol(3,4,5)-trisphosphate synthesis in activated neutrophils. *Nature* **351**, 33-39
31. Stephens, L., Cooke, F.T., Walters, R., Jackson, T., Volinia, S., Gout, I., Waterfield, M.D., and Hawkins, P.T. (1994) Characterization of a phosphatidylionositol-specific phosphoinositide 3-kinase from mammalian cells. *Curr. Biol.* **4**, 203-214
32. Cross, M.J., Stewart, A., Hodgkin, M.N., Kerr, D.J., and Wakelam, M.J.O. (1995) Wortmannin and its stimulated structural analogue demethoxyviridin inhibit stimulated phospholipase A_2 activity in Swiss 3T3 cells. *J. Biol. Chem.* **270**, 25352-25355
33. Marsh, M. and Helenius, A. (1980) Adsorptive endocytosis of Semliki Forest virus. *J. Mol. Biol.* **142**, 439-454
34. Futter, C.E., Felder, S., Schelessinger, J., Ullrich, A., and Hopkins, C.R. (1993) *J. Cell Biol.* **120**, 77-83
35. Herbst, J.J., Opresko, L.K., Walsh, B., Lauffenburger, D.A., and Wiley, H.S. (1994) *J. Biol. Chem.* **269**, 12865-12873
36. Abbas, H.K. and Mirocha, C.J. (1988) Isolation and purification of a hemorrhagic factor (wortmannin) from *Fusarium oxysporum* (N17B). *Appl. Environ. Microbiol.* **54**, 1268-1274
37. Rodriguez-Viciana, P., Warne, P.H., Dhand, R., Vanhaesebroeck, B., Gout, I., Fry, M.J., Waterfield, M.D., and Downward, J. (1994) Phosphatidylinositol-3-OH kinase as a direct target of Ras. *Nature* **370**, 527-532
38. Kotani, K., Yonezawa, K., Hara, K., Ueda, H., Kitamura, Y., Sakaue, H., Ando, A., Chavanieu, A., Calas, B., Grigorescu, F., Nishiyama, M., Waterfield, M.D., and Kasuga, M. (1994) Involvement of phosphoinositide 3-kinase in insulin- or IGF-1-induced membrane ruffling. *EMBO J.* **13**, 2313-2321
39. Kimura, K., Hattori, S., Kabuyama, Y., Shizawa, Y., Takayanagi, J., Nakamura, S., Toki, S., Matsuda, Y., Onodera, K., and Fukui, Y. (1994) Neurite outgrowth of PC12 cells is suppressed by wortmannin, a specific inhibitor of phosphatidylinositol 3-kinase. *J. Biol. Chem.* **269**, 18961-18967

5.

ELSEVIER

Neuroscience Research 25 (1996) 229–237

NEUROSCIENCE RESEARCH

GTP-binding protein activation underlies LTP induction by Mast Cell Degranulating peptide

Ichiro Fujimoto[a,b], Shigetoshi Oiki[c], Tetsuro Kondo[d], Toshiaki Katada[e], Hiroshi Kato[f], Takahisa Taguchi[g], Michiki Kasai[g], Yasunobu Okada[c], Katsuhiko Mikoshiba[h], Kazuhiro Ikenaka[b,*]

[a]*Department of Physiology, Nagoya City University Medical School, Nagoya 467, Japan*
[b]*Laboratory of Neural Information, National Institute for Physiological Sciences, Okazaki National Research Institutes, 38 Nishigonaka, Okazaki, Aichi 444, Japan*
[c]*Laboratory of Cellular and Molecular Physiology, National Institute for Physiological Sciences, Okazaki National Research Institutes, Okazaki 444, Japan*
[d]*Molecular and Cellular Neuroscience Section, Electrotechnical Laboratory, Tsukuba 305, Japan*
[e]*Department of Physical Chemistry, Faculty of Pharmaceutical Science, University of Tokyo, Tokyo 108, Japan*
[f]*Department of Physiology, Yamagata University School of Medicine, Yamagata 990-23, Japan*
[g]*Faculty of Engineering Science, Osaka University, Osaka 560, Japan*
[h]*Insitute of Medical Science, University of Tokyo, Tokyo 108, Japan*

Received 18 January 1996; accepted 11 April 1996

Abstract

Mast cell degranulating peptide (MCD) induces long-term potentiation (LTP) in the CA1 region of the hippocampus. MCD has been shown to bind to a voltage-dependent A-type potassium channel with high-affinity (less than 1 nM). However, the concentration necessary to induce LTP is more than 500 nM, suggesting that some other functions of MCD are also fundamental to LTP induction. The concentration of MCD required for LTP induction was greatly reduced by preactivating G proteins. This fact suggests that G protein activation by MCD also plays an important role in LTP induction. MCD-binding proteins were purified from rat brain. G proteins were found to exist in a non-denatured state in this affinity-purified fraction. When reconstituted into a planar lipid bilayer membrane, a potassium-selective and voltage-dependent current could be observed. This channel was blocked by MCD at a high concentration equal to the effective concentration for G protein activation. Addition of GTP-γ-S significantly blocked the reconstituted current. Thus, we identified a pathway for LTP induction by MCD in which high concentrations of MCD activate G protein which in turns leads to blocking of a potassium channel.

Keywords: LTP; MCD; Planar lipid bilayer; Voltage-dependent potassium channel; G protein

1. Introduction

Repetitive activation of certain types of excitatory synapses results in long-lasting enhancement of synaptic transmission referred to as 'long-term potentiation (LTP)'. Cherubini et al. (1987) have reported that mast cell degranulating peptide (MCD), purified from bee venom (*Apis mellifera*), induces LTP indistinguishable from NMDA receptor-mediated LTP in the CA1 region of the hippocampus. MCD consists of 22 amino acid residues and is reported to bind with high-affinity to a single set of sites (Kd = 0.15 nM) in mouse synaptosomal membranes (Taylor et al., 1984). A snake venom, dendrotoxin I (DTxI), is known to bind to the same binding sites as MCD. An electric current blocked

---

* Corresponding author. Tel.: +81 564 557841; fax +81 564 557843; e-mail: ikenaka@nips.ac.jp

0168-0102/96/$15.00 © 1996 Elsevier Science Ireland Ltd. All rights reserved
PII S0168-0102(96)01047-4

by addition of DTxI in hippocampal pyramidal neurons has been identified as one of the fast-activating, voltage-dependent, aminopyridine-sensitive potassium currents (Halliwell et al., 1986; Anderson and Harvey, 1988). Thus, the high-affinity binding site for MCD is considered to be a potassium channel. MCD was found to reduce the peak amplitude of fast-inactivating (A-type) currents and to have no effect on non-inactivating (K-type) currents in a whole-cell recording study of hippocampal neurons (Hiroshi Katsuki, personal communication). MCD-sensitive channels, Kv1.1 (RCK1), Kv1.2 (RCK5) and Kv1.6 (RCK2), have already been cloned and identified (Stühmer et al., 1989; Kirsch et al., 1991). However, these channels form a rapidly activating and non-inactivating current when expressed in *Xenopus* oocytes, conflicting with the above-mentioned characteristics of MCD-channels in vivo. Two different subunit structures may explain this contradiction. The first subunit structure is heteromultimer. In the Kv1 (RCK) subfamily, MCD-sensitive channels would form heteromultimer with other Kv1 channels which mediate fast-inactivating currents in vitro (Ruppersberg et al., 1990). The existence of these heteromultimers in vivo has been confirmed by immunoprecipitation, and in the hippocampus they were found to be localized in axons and nerve terminals (Sheng et al., 1993; Wang et al., 1994). Second, a β-subunit of DTx-sensitive potassium channel was purified and cloned from bovine brain, and association of β-subunits with α-subunits was found to confer rapid A-type inactivation on non-inactivating Kv1 channels (delayed rectifiers) in expression systems in vitro (Scott et al., 1994; Rettig et al., 1994).

MCD binding to the high-affinity binding sites seemed to be its most important function in inducing LTP in hippocampal neurons (Kondo et al., 1992). Nevertheless, there is a great discrepancy between the dissociation constant (150 pM) of MCD binding to its receptor and the minimum concentration of MCD (500 nM) needed to induce LTP. We found that the concentration of MCD required for activation of G protein in mast cells is quite close to the concentration required for LTP induction in hippocampal slices (Fujimoto et al., 1991) and that MCD directly stimulates the GTPase activity of Go, Gi in a concentration-dependent manner (Tomita et al., 1991). It has been reported that LTP cannot be induced by tetanic stimulation in the CA1 and CA3 regions of pertussis-toxin (IAP)-treated hippocampal slices (Goh and Pennefather, 1989). These reports indicate that activation of an IAP-sensitive G protein plays an important role in the pathway involved in LTP induction. These findings gave rise to the working hypothesis that activation of G protein as well as binding to the high-affinity binding site is necessary for MCD to induce LTP in hippocampal neurons. In this study, we show that preactivation of G protein reduces the concentration of MCD necessary to induce LTP and that a certain potassium channel may be the target of the G protein activated by MCD in rat brain. Since it has been shown that an endogenous MCD-like substance is present in rodent brain (Cherubini et al., 1987), the results obtained should add to our understanding of the molecular mechanisms underlying synaptic plasticity in the brain.

2. Materials and methods

2.1. Materials

All the chemicals used were of the highest purity commercially available and were purchased from Wako Pure Chemical Industries, unless otherwise noted.

2.2. Electrophysiological assay in the hippocampal slice

Preparation of hippocampal slices from adult guinea pig (or Wistar rats) and the electrophysiological procedures have been described previously (Kondo et al., 1990). A bipolar stimulating electrode was inserted into the stratum radiatum of area CA1 close to CA2-3. Two glass pipettes were used for recording electrical responses, one placed in the pyramidal cell layer of CA1 to record the extracellular population spike and the other in the stratum radiatum, the dendritic region of the former, to record the extracellular field EPSP. Various doses of MCD were applied in a perfusate for 5 min.

2.3. Purification of dendrotoxin I (DTxI) and coupling to Sepharose 4B

Venom from the black mamba, *Dendroaspis polylepis polylepis*, was obtained from Latoxan (France). DTxI was purified from the crude venom in three steps: (1) gel filtration on Sephadex G-50 fine (25 × 600 mm, Pharmacia); (2) ion exchange chromatography on TSK SP-5PW (7.5 × 75 mm, TOSOH); and (3) reverse-phase chromatography on COSMOSIL C_{18} (8 × 250 mm, Nacalai Tesque). Crude venom powder (100 mg) was dissolved in 5 ml of 200 mM NH_4CO_3 and loaded onto the gel filtration column. Void volume fractions were then loaded onto ion exchange HPLC column, equilibrated with 0.1 M NH_4OAc, pH 7.3, and then eluted with a linear gradient between 0.1 M and 1.5 M NH_4OAc. Amino acid composition was determined by an amino acid analyzer (L-8500, HITACHI) for primary identification of DTxI. The structure of DTxI was further confirmed by sequencing the fragments obtained by digesting DTxI with endoproteinase Lys-C and purifying them on reverse-phase HPLC. The amino acid sequence determined was consistent with the published sequence of DTxI (Strydom, 1973). DTxI (4 mg) was coupled to CNBr-activated Sepharose 4B as described previously (Parcej and Dolly, 1989). The A_{280} of the supernatant was measured to determine the amount of DTxI coupled (generally 50–80%).

2.4. Purification and binding assay of DTxI/MCD-binding protein

The synaptic plasma membranes (200 mg) were prepared from rat brain obtained immediately after slaughter (Kondo et al., 1992). It was extracted with 4% (w/v) Lubrol PX and loaded onto a DTxI-Sepharose column (150 × 550 mm). One of the disulfide bonds of DTxI has been shown to be easily reduced by DTT, and alter the conformation of DTxI (Hollecker and Creighton, 1983). DTxI/MCD-binding proteins were eluted by 10 mM DTT as described (Parcej and Dolly, 1989). The adsorbed fractions collected were directly applied to an HPLC ion exchanging column DE-5PW TSK-GEL (5.0 × 50 mm, TOSOH) equilibrated with 25 mM imidazole-HCl (pH 8.2), 100 mM KCl, 1 mM EDTA, 0.2 mM benzamidine, 0.2 mM PMSF, and 0.05% (w/v) Tween 80. After washing to remove DTT, the sample was eluted with 300 mM KCl. The membrane-bound acceptor was assayed by a filtration method using ^{125}I-MCD, ^{125}I-DTxI as described (Bruns et al., 1983).

2.5. Preparation of liposomes

The lipids (1 mg, 13:6:1:2, phosphatidylcholine, phosphatidylethanolamine, phosphatidylserine, ergosterol, (Avanti Polar Lipid Inc)) were mixed in 0.1 ml chloroform. After evaporating the solvent under a stream of nitrogen, the purified DTxI-binding proteins (0.2 ml) were added, and the mixture was bath-sonicated for 15–20 s (Woodbury and Miller, 1990). To remove detergent, the mixture was dialyzed for 48 h at 4°C against 20 mM Na-HEPES, pH 7.2, 120 mM KCl and 1 mM EDTA, and changed six times every 8 h. The resulting liposomes with the reconstituted purified protein were stored in liquid nitrogen.

2.6. Planar lipid bilayer measurement

Planar lipid bilayers were formed by the painting method. A hole on a Teflon septum was made by the shaved method (Wonderlin et al., 1990). The diameter of a hole ranged from 50 to 100 μm. The *cis* and *trans* compartments of 1.2 ml volume were filled with asymmetrical KCl solution, 100 mM and 300 mM, respectively, buffered by Tris-HEPES (10 mM, pH 7.2). A small amount of phosphatidylcholine solution (10 mg/ml *n*-decane, Sigma) was bubbled to the pre-coated hole. The capacitance of the membrane was monitored by application of ramp potential. The *trans* electrode was set to a command voltage relative to the *cis* electrode, which was held at virtual ground. This is the electrophysiological sign convention: the *trans* is the 'intracellular' side with high K concentration.

After thinning of the membrane an L-shaped pipette containing the liposome was placed in the *trans* side of the chamber and was approached close to the membrane under a visual control. Puffing the contents (5 μl) of the pipette rapidly incorporates liposome by fusion and active channels appeared soon after application. Alternative pulses of − 100 and 100 mV were applied continuously until channel activity appeared. The decremental step pulses of 500 ms duration from + 100 to + 20 mV was applied. Current was recorded using a voltage clamp amplifier (Dagan 3900A, Minneapolis). Voltage command pulses were generated and currents were acquired under the control of a 486-based computer, passed through a low-pass filter (500 Hz, 4-pole Bessel, Werner), and sampled (the sampling rate was 500 μs) by DigiData1200 interface. The data were analyzed by pClamp software (version 6.0.2, Axon Instrument). All the current and voltage data were stored on video tape recorder (SANYO) through PCM interface (Instruteck).

All the experiments were performed at room temperature. The Goldman-Hodgkin-Katz equation was used for evaluation of a permeability ratio.

2.7. Western blot analysis

Samples were separated by SDS-polyacrylamide gel electrophoresis (SDS-PAGE) and transferred to a polyvinylidene difluoride membrane at a constant voltage of 50 V for 1 h. The membranes, after being blocked with 2% bovine serum albumin for 1 h, were incubated with polyclonal antibodies, anti-Giα, anti-Goα, anti-βγ complex at 30°C overnight and then treated with horseradish peroxidase-conjugated anti-rabbit IgG. The detection was carried out with a peroxidase immunostain kit (Wako). Go, Gi and their βγ complex were purified from porcine brain according to the method of Katada et al. (1986). The anti-Gil and 2α, anti-Goα and anti-βγ complex antibodies were prepared as described previously (Katada et al., 1987).

2.8. Assay of IAP-catalyzed ADP-ribosylation

Prior to ADP-ribosylation, IAP (1 mg/ml in 2 M urea and 100 mM NaPi) was activated by incubation at 37°C for 10 min with 4 volumes of 50 mM Tris-HCl (pH 7.5) containing 100 mM dithiothreitol and 0.1 mM ATP. A fraction from the rat brain (50 μg of protein) was incubated at 30°C for 30 min with activated IAP (0.5 mg) in 25 ml of a reaction mixture containing 100 mM Tris-HCl (pH 7.5), 2 mM [α-^{32}P]NAD (5000–

10 000 cpm/pmol), 2 mM $MgCl_2$, 1 mM EDTA, 40 mM GDP-γ-S, 0.1 mM NADP, 10 mM thymidine, 1 mM ADP-ribose, and 20 mM nicotinamide. The ADP-ribosylation was terminated by the addition of an equal volume of 2-fold concentrated Laemmli buffer followed by boiling at 90°C for 30 min. Samples were separated by 12% SDS-PAGE and the gel was exposed to Kodak X-Omat AR film for 24–48 h with an intensifying screen at − 80°C.

3. Results

3.1. Dose-response curve for MCD-induced LTP in the CA1 region of the hippocampus shifted after activating G proteins

The amplitude of the population spikes began to increase after MCD perfusion, reaching a maximum about 10 min after MCD application, remaining at that level thereafter (for at least 2 h). The percentage increase in averaged amplitude was plotted against the concentration of MCD circulated. As shown in Fig. 1, MCD enhanced synaptic transmission at a minimum dose of 500 nM, reaching a plateau at 3–10 μM. This concentration is very different from the dissociation constant of high-affinity MCD-binding sites in brain membranes. Since the effective concentration of MCD for LTP induction is similar to the concentration required for G protein activation, G protein activator was used to examine the possible contribution of G protein to LTP. Pretreating the hippocampal slices with compound 48/80 (10 μg/ml) for 2–9 h resulted in a shift in the dose-response curve of MCD toward a concentration two orders of magnitude lower. Thus, high-dose MCD action on a low-affinity site can be replaced by a G protein activator (compound 48/80), but simultaneous binding to a high-affinity site was necessary for LTP induction.

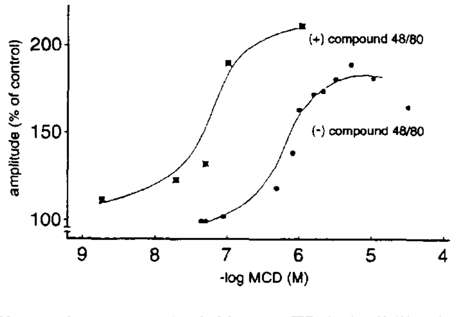

Fig. 1. Effects of compound 48/80 on LTP inducibility by MCD in rat hippocampal slices. Different concentrations of MCD were applied to the hippocampal slice. The mean percentage increase in population spike amplitude is plotted against the concentrations of MCD. Compound 48/80: G protein activator, histamine releaser, condensation product of *N*-methyl-p-methoxy-phenethylamine with formaldehyde.

3.2. Purification of MCD and DTxI-binding proteins

Rat synaptic plasma membranes were solubilized with 4% (w/v) Lubrol PX, and MCD-binding proteins were enriched by DTxI-affinity chromatography (Parcej and Dolly, 1989). DTxI was selected as the ligand of choice due to its higher affinity for MCD-binding sites as well as its ability to induce LTP in hippocampal slices (Kondo et al., 1992). On SDS-PAGE electrophoresis, some blurring bands were seen in the DTT eluate, with Mr values of 70, 60 and 31 K and some minor contaminants whose pattern was similar to that described in the previous report (Parcej and Dolly, 1989). There would be several distinct high- and low-affinity MCD-binding proteins in this fraction.

3.3. Reconstitution of the purified fractions into planar lipid bilayers

Reconstituted liposomes with purified proteins were incorporated into the planar lipid bilayer. Current fluctuations appeared in response to alternative step pulses (± 100 mV) soon after (within 1 min) application of the liposomes. Fig. 2A shows the outward (*trans* to *cis*) currents mediated by reconstituted channels at pulse steps to + 100, + 80, + 60, + 40, + 20 mV from the holding potential of − 100 mV. The channel opened upon application of positive potentials, and it remained open briefly upon returning to the holding potential. The current-voltage relationship of the most frequently observed current is shown in Fig. 2B. The permeability ratio (PCl/PK) was calculated to be 0.1 from the reversal potential of − 23 mV and the chord conductance was 55 pS at + 100 mV. This cationic channel could not be detected in asymmetrical NaCl solution. Thus, this channel is a K-selective channel. The open probability (P_{open}) increased as the membrane potential was increased. P_{open} was 0.5 at + 60 mV. The current disappeared when the steady-state voltage was applied, indicating transient behavior (slow inactivation) of the channel. A channel with opposite polarity (open at negative potentials) was observed, indicating random orientation of the channel in liposomes. Only right-side channels (intracellular side of the channel faces to the *trans* side) are shown in this study.

3.4. The concentration dependence of the block of reconstituted current by MCD

The current produced by this channel was not suppressed in the presence of 50 nM MCD, which was again much higher than the binding constant of the high-affinity binding site of MCD. The channel was blocked, however, by 1 μM MCD (Fig. 3), at which concentration G protein activation and LTP were induced. Therefore, the presence of G protein in the present sample of liposomes was examined.

to the high-affinity binding site is less than 1 nM, more than 500 nM is required for MCD to induce LTP. At this concentration, MCD also activates G protein (Fujimoto et al., 1991). Since both high- and low-affinity binding sites have been shown to be present in rat brain (Bidard et al., 1989), G protein may be the low-affinity binding site for MCD. However, we have not measured the binding constant of MCD to G proteins.

In this study pretreating the hippocampal slices with compound 48/80, a G protein activator, resulted in induction of LTP by MCD at a 100 times lower concentration (Fig. 1). This indicates that MCD acts bifunctionally to induce LTP in the CA1 region of the hippocampus: it activates G proteins, and binds to and blocks the high-affinity binding site, a voltage-dependent potassium channel. During characterization of the MCD-binding sites, we found that one of the targets located down stream of the G protein activated by MCD is also a voltage-dependent cation selective channel. This may be a potassium channel, but not the A-channel which has been reported to be the high-affinity binding site of MCD. We fortuitously found this potassium channel in the purified fraction of MCD-binding proteins and reconstituted it in the planar lipid bilayer (Fig. 2). The channel which was reconstituted in lipid bilayer was not suppressed by 50 nM MCD, but was blocked by addition of a higher concentration of MCD (1 μM) sufficient to activate G protein (Fig. 3). When rKv 1.1 channel was expressed in *Xenopus* oocyte, MCD suppressed it's current at 45 nM concentration (Stühmer et al., 1989). Therefore, this dose of MCD (1 μM) was much higher than that necessary to the block channel activity of MCD-high affinity binding site, and suggested participation of G protein activation. G protein-associated channels are situated very close to each other (Hille, 1992). Thus, this channel protein may be co-purified with G proteins (Go and Gi) in their non-denatured state (Figs. 4 and 5). The channel which was reconstituted in the lipid bilayer was not suppressed at 50 nM MCD, but was blocked by addition of higher concentrations of MCD sufficient to activate G protein. This channel was also blocked by a G protein activator, GTP-γ-S. Therefore, this potassium current was suppressed directly by the action of the G protein (Fig. 6). Furthermore, GTP-γ-S action acts in the right direction: it is effective only when added to the 'intracellular' (*trans*) side, indicating that this reconstituted channel forms an outward current. Many G protein-coupled potassium channels have been found in the brain, but most of them are an inwardly rectifying potassium channel that has been cloned (Kubo et al., 1993; Lesage et al., 1994). These channels are activated via the G protein $\beta\gamma$-subunits and form heteromultimer with members of the same family (Krapivinsky et al., 1995). The mechanisms by which muscarinic acetylcholine receptors modulate potassium channels, both suppressing and activating them, can be divided into two pathways based on G protein activity (ffrench-Mullen et al., 1994). The m1 muscarinic acetylcholine receptor suppress a time- and voltage-dependent potassium channel within sympathetic and hippocampal neurons termed the M-current: suppression of the M-current is responsible for the slow excitatory postsynaptic potentiation of these cells (Stansfeld et al., 1993). Normally this outward potassium current increases as the hippocampal pyramidal neuron is depolarized, with a resulting return of membrane potential toward resting levels. Thus, blocking of this M-current by G protein activation may increase the excitability of the cells and induce LTP. Furthermore, stimulation of the metabotropic glutamate receptors which induce LTP (Bashir et al., 1993) suppresses the same M-current in the CA3 pyramidal neurons of the rat hippocampus (Guérineau et al., 1995). However, the M-current is not suppressed directly by activated G protein. Diffusible cytoplasmic second messengers are also involved in its suppression. The m1 muscarinic acetylcholine receptor utilizes a signal transduction pathway involving PLC-generated signals and cellular tyrosine kinase activity to potently suppress delayed rectifier currents (Guérineau et al., 1994). Thus, the channel we found is novel, and a future challenge will be to characterize and determine the functional significance of the MCD-sensitive currents. Recently, another potassium current suppressed via G protein was discovered in cardiac muscle by Grand (1993). This current was a time- and voltage-dependent transient outward current suppressed by the addition of GTP-γ-S. The relation between the MCD-sensitive A-current and this current should also be investigated.

Suppression of potassium channels is closely correlated with the induction of LTP. In previous studies, the A-current was shown to be important in controlling the pattern of repetitive firing in neurons (Ribera and Spitzer, 1990). The A-current may serve to reduce the effect of delayed depolarization following impulses that can lead to repetitive firing, a finding also observed in MCD-induced LTP in rat hippocampal slices (data not shown), however, blockade of the A-current by 4-AP alone could not induce LTP (Haas and Greene, 1985). LTP can be induced by a specific potassium current blocker, tetraethylammonium (TEA) (Aniksztejn and Ben-Ari, 1991). Blockade of potassium channels by TEA produced powerful activation of quisqualate receptors as a result of the large increase in glutamate release. This leads to depolarization at the dendritic level, which facilitates the activation of voltage-dependent calcium channels and induces LTP (Tsaur et al., 1992). Therefore, suppression of MCD-sensitive G protein-coupled potassium channels may also result in depolarization of resting membrane potentials and, together with blockade of the A-current, induce repetitive firing that lead to LTP induction.

Some of the potassium channel genes expressed in the hippocampus are down-regulated, at least at the mRNA level, following neuron seizure activity (Huang and Malenka, 1993). The fact that regulation of gene expression is required for maintenance of LTP, suggests that regulation of potassium channel gene expression is important for LTP. It is known that some potassium channels in *Hermissenda* are blocked during the process of learning and memory and that these potassium channels are suppressed by G protein activation (Nelson et al., 1990). Therefore, suppression of potassium channels seems to be greatly involved not only in LTP induction, but in the process of learning and memory.

The results of the present study indicate that some potassium currents are suppressed by G protein activated by MCD. It is important to characterize these MCD-sensitive channels in more detail and to explore other signaling pathways following the activation of G protein by MCD.

Acknowledgements

We thank Dr. Hiroshi Katsuki for informing us of his unpublished results on the patch-clamp analysis of hippocampal neurons, and Drs. Kensuke Nakahira and Tetsushi Kagawa for valuable discussions. This study was partly supported by a grant from the Ministry of Education, Science and Culture (Japan).

References

Anderson, A.J. and Harvey, A.L. (1988) Effects of the potassium channel blocking dendrotoxins on acetylcholine release and motor nerve terminal activity. Br. J. Phamacol., 93: 215–221.

Aniksztejn, L. and Ben-Ari, Y. (1991) Novel form of long-term potentiation produced by a K^+ channel blocker in the hippocampus. Nature, 349: 67–69.

Bashir, Z.I., Bortolotto, Z.A., Davies, C.H., Berretta, N., Irving, A.J., Seal, A.J., Henley, J.M., Jane, D.E., Watkins, J.C. and Collingridge, G.L. (1993) Induction of LTP in the hippocampus needs synaptic activation of glutamate metabotropic receptors. Nature, 363: 347–350.

Bidard, J.N., Mourre, C., Gandolfo, G., Schweitz, H., Widmann, C., Gottesmann, C. and Lazdunski, M. (1989) Analogies and difference in the mode of action and properties of binding sites (localization and mutual interactions) of two K^+ channel toxins, MCD peptide and dendrotoxin I. Brain Res., 495: 45–57.

Bruns, R.F., Lawson-Wendling, K. and Pugsley, T.A. (1983) A rapid filtration assay for soluble receptors using polyethyleneimine-treated filters. Anal. Biochem., 32: 74–81.

Cherubini, E., Ben Ari, Y., Gho, M., Bidard, J.N. and Lazdunski, M. (1987) Long-term potentiation of synaptic transmission in the hippocampus induced by a bee venom peptide. Nature, 328: 70–73.

ffrench-Mullen, J.M.H., Plata-Salamán, C.R., Buckley, N.J. and Danks, P. (1994) Muscarinic modulation by a G protein α-subunit of delayed rectifier K^+ current in rat ventromedial hypothalamic neurones. J. Physiol., 474: 21–26.

Fujimoto, I., Ikenaka, K., Kondo, T., Aimoto, S., Kuno, M. and Mikoshiba, K. (1991) Mast cell degranulating (MCD) peptide and its optical isomer active GTP binding protein in rat mast cells. FEBS Lett., 287: 15–18.

Goh, J.W. and Pennefather, P.S. (1989) A pertussis toxin-sensitive G protein in hippocampal long-term potentiation. Science, 244: 980–983.

Grand, B.L. (1993) Regulation of transient outward K^+ current in human atria involves G proteins, Biochem. Biophys. Res. Commun. 196: 1143–1147.

Guérineau, N.C., Bossu, J.L., Gähwiler, B.H. and Gerber, U. (1995) Activation of a nonselective cation conductance by metabotropic glutamatergic and muscarinic agonists in CA3 pyramidal neurons of the rat hippocampus. J. Neurosci., 15: 4395–4407.

Guérineau, N.C., Gähwiler, B.H. and Gerber, U. (1994) Reduction of resting K^+ current by metabotropic glutamate and muscarinic receptors in rat CA3 cells: mediation by G protein. J. Physiol., 474: 27–33.

Haas, H.L. and Greene, R.W. (1985) Long-term potentiation and 4-aminopyridine. Cell. Mol. Neurobiol., 5: 297–301.

Halliwell, J.V., Othman, I.B., Pelchen-Matthews, A. and Dolly, J.O. (1986) Central action of dendrotoxin: selective reduction of a transient K conductance in hippocampus and binding to localized receptors. Proc. Natl. Acad. Sci. USA, 83: 493–497.

Hille, B. (1992) G protein-coupled mechanisms and nervous signaling. Neuron, 9: 187–195.

Hollecker, M. and Creighton, T.E. (1983) Evolutionary conservation and variation of protein folding pathways. J. Mol. Biol., 168: 409–437.

Huang, Y.Y. and Malenka, R.C. (1993) Examination of TEA-induced synaptic enhancement in area CA1 of the hippocampus: the role of voltage-dependent Ca^{2+} channels in the induction of LTP. J. Neurosci., 13: 568–576.

Katada, T., Oinuma, M. and Ui, M. (1986) Two guanine nucleotide-binding proteins in rat brain serving as the specific substrate of islet-activating protein, pertussis toxin. J. Biol. Chem., 261: 8182–8191.

Katada, T., Oinuma, M., Kusakabe, K. and Ui, M. (1987) A new GTP-binding protein in brain tissues serving as the specific substrate of islet-activating protein, pertussis toxin. FEBS Lett., 213: 353–358.

Kirsch, G.E., Drewe, J.A., Verma, S., Brown, A.M. and Joho, R.H. (1991) Electrophysiological characterization of a new member of the RCK family of rat brain K^+ channels. FEBS Lett., 278: 55–60.

Kondo, T., Ikenaka, K., Kato, H., Ito, K., Aimoto, S., Hojo, H. and Mikoshiba, K. (1990) Long-term enhancement of synaptic transmission by synthetic mast cell degranulating peptide and its localization of binding sites in hippocampus. Neurosci. Res., 8: 147–157.

Kondo, T., Ikenaka, K., Fujimoto, I., Aimoto, S., Kato, H., Ito, K., Taguchi, T., Morita, T., Kasai, M. and Mikoshiba, K. (1992) $K+$ channel involvement in induction of synaptic enhancement by mast cell degranulating (MCD) peptide. Neurosci. Res., 13: 207–216.

Kubo, Y., Reuveny, E., Slesinger, P.A., Jan, Y.N. and Jan, L.Y. (1993) Primary structure and functional expression of a rat G-protein-coupled muscarinic potassium channel. Nature, 364: 802–806.

Krapivinsky, G., Gordon, E.A., Wickman, K., Velimirovic, B., Krapivinsky, L. and Clapham, D.E. (1995) The G-protein-gated atrial K^+ channel I_{KACh} is a heteromultimer of two inwardly rectifying K^+-channel proteins. Nature, 374: 135–141.

Lesage, F., Duprat, F., Fink, M., Guillemare, E., Coppola, T., Lazdunski, M. and Hugnot, J.P. (1994) Cloning provides evidence for a family of inward rectifier and G-protein coupled K^+ channels in the brain. FEBS Lett., 353: 37–42.

Nelson, T.J., Collin, C. and Alkon, D.L. (1990) Isolation of a G protein that is modified by learning and reduces potassium currents in *Hermissenda*. Science, 247: 1479–1483.

Parcej, D.N. and Dolly, J.O. (1989) Dendrotoxin acceptor from bovine synaptic plasma membranes. Biochem. J., 257: 899–903.

Rettig, J., Heinemann, S.H., Wunder, F., Lorra, C., Parcej, D.N., Dolly, J.O. and Pongs, O. (1994) Inactivation properties of voltage-gated K^+ channels altered by presence of β-subunit. Nature, 369: 289–294.

Ribera, A.B. and Spitzer, N.C. (1990) Differentiation of IKA in amphibian spinal neurons. J. Neurosci., 10: 1886–1891.

Ruppersberg, J.P., Schroter, K.H., Sakmann, B., Stocker, M., Sewing, S. and Pongs, O. (1990) Heteromultimeric channels formed by rat brain potassium-channel proteins. Nature, 345: 535–537.

Scott, V.E.S., Rettig, J., Parcej, D.N., Keen, J.N., Findlay, J.B.C., Pongs, O. and Dolly, J.O. (1994) Primary structure of a β subunit of α-dendrotoxin-sensitive K^+ channels from bovine brain. Proc. Natl. Acad. Sci. USA, 91: 1637–1641.

Sheng, M., Liao, Y.J., Jan, Y.N. and Jan, L.Y. (1993) Presynaptic A-current based on heteromultimeric K^+ channels detected in vivo. Nature, 365: 72–75.

Stansfeld, C.E., Marsh, S.J., Gibb, A.J. and Brown, D.A. (1993) Identification of M-channels by outside-out patches excised from sympathetic ganglion cells. Neuron, 10: 639–654.

Strydom, D.J. (1973) Protease inhibitors as snake venom toxins. Nature New Biol., 243, 88–89.

Stühmer, W., Ruppersberg, J.P., Schöter, K.H., Sakmann, B., Stocker, M., Giese, K.P., Perschke, A., Baumann, A. and Pongs, O. (1989) Molecular basis of functional diversity of voltage-gated potassium channels in mammalian brain. EMBO J., 8: 3235–3244.

Taylor, J.W., Bidard, J.N. and Lazdunski, M. (1984) The characterization of high affinity binding sites in rat brain for the mast cell degranulating peptide from bee venom using the purified monoiodinated peptide. J. Biol. Chem., 259: 13957–13967.

Tomita, U., Takahashi, K., Ikenaka, K., Kondo, T., Fujimoto, I., Aimoto, S., Mikoshiba, K., Ui, M. and Katada, T. (1991) Direct activation of GTP-binding proteins by venom peptides that contain cationic clusters within their alpha-helical structures. Biochem. Biophys. Res. Commun., 178: 400–406.

Tsaur, M.L., Sheng, M., Lowenstein, D.H., Jan, Y.N. and Jan, L.Y. (1992) Differential expression of K^+ channel mRNAs in the rat brain and down-regulation in the hippocampus following seizures. Neuron, 8: 1055–1067.

Wang, H., Kunkel, D.D., Schwartzkroin, P.A. and Tempel, B.L. (1994) Localization of Kv1.1 and Kv1.2, two K channel proteins, to synaptic terminals, somata, and dendrites in mouse brain. J. Neurosci., 14: 4588–4599.

Wonderlin, W.F., Finkel, A. and French, R.J. (1990) Optimizing planar lipid bilayer single-channel recordings for high resolution with rapid voltage steps. Biophys. J., 58: 289–297.

Woodbury, D.J. and Miller, C. (1990) Nystatin-induced liposome fusion. A versatile approach to ion channel reconstitution into planar bilayers. Biophys. J., 58: 833–839.

6.

PROCEEDINGS REPRINT

SPIE—The International Society for Optical Engineering

Reprinted from

Advances in Resist Technology and Processing XIII

11–13 March 1996
Santa Clara, California

Volume 2724

©1996 by the Society of Photo-Optical Instrumentation Engineers
Box 10, Bellingham, Washington 98227 USA. Telephone 360/676-3290.

Application of DNQ-based microlithography to patterning bioactive molecules and cells

Dan V Nicolau[¥], Takahisa Taguchi[¥], Hiroshi Taniguchi[¥], Susumu Yoshikawa[¥], Mircea V Dusa[$]

[¥]Osaka National Research Institute, Osaka 563, Japan
[$]National Semiconductor, Santa Clara, California 95052-8090

ABSTRACT

Photochemically induced surface functionality manipulation of Diazo-Naphto-Quinone/novolak polymeric films was used for controlling the specificity of the attachment and growth of neuronal cells and biologically active molecules (proteins and peptides) patterning. Different microlithographic techniques (standard positive tone, negative tone Image Reversal based on catalysed decarboxylation, positive tone of Image Reversal resist, and Surface Imaging based on silylation), controlling the surface hydrophobicity and surface concentration of carboxylic groups, were assessed in the view of the suitability as microlithographic techniques for patterning biologically active molecules and cells. It was found that DNQ-based materials and techniques can be easily transferred in bio-microlithography, which is the building of laterally ordered architectures with biological structural elements.

Keywords: cell engineering, molecular engineering, combinatorial chemistry, diazo-naphto-quinone, photoresist, microlithography

1. INTRODUCTION

Techniques for controlling biomolecular architectures on surfaces have a wide range of potential applications in biosensing, cell guidance, and molecular electronics[1]. Advances in constructing on surfaces molecular structures ordered *vertically* incorporating biologically active molecules and cells in their architecture, are followed by a growing interest in ordering these structures *laterally*[2]. This new development will require techniques for *patterning* areas with different surface properties that control the selective attachment of the vertically ordered architectures on the same basal surface. Vertically structured cell engineering found applications in biosensors based on plant and animal tissues[3], and vertically structured biomolecular engineering found applications in creating electronically modulated biological functions[4], while laterally structured cell and biomolecular engineering aim towards multiplication of the functionality of these architectures through selective interaction of the cells or bioactive molecules patterned. on the same substrate

2. NEURONAL CELL ENGINEERING

Due to the importance of their electrical activity, neuronal cells are the most outstanding candidates for bioelectronic devices fabrication. However, so far the research regarding the building of an integrated neuronal cell-semiconductor device relies only marginally on the possibilities offered by the present microlithography. The building of neuronal cell based biodevices would employ two sets of technologies aiming at:

- constructing the basal structure of the biodevice using classical semiconductor technology;

0-8194-2100-6/96/$6.00

- constructing of architectures using neuronal cells this pre-defined basal structure.

The first task requires the design and fabrication of an appropriate electric, magnetic or electronic device which either senses or controls the neuronal cell electrical activity. While in terms of technological complexity this task is rather trivial, as resolution is not a critical element, the design of the basal device might pose some difficulties. The second task requires the precise and preferably biochemically induced positioning of the cells on top of the pre-defined basal device. While in terms of design this task seems trivial, requiring just another mask from the set used for fabrication of the basal device, its technological complexity is high due to the lack of proper understanding of the cell interaction with artificial surfaces.

2.1. Basal devices used for neuronal cells based integrated devices

The basal device used for sensing or controlling the electrical activity of the neuronal cell may be grouped under the category of:

- *ohmic*, using arrays of microelectrodes as ohmic contacts beneath the neuronal cell[5];
- *magnetical*, using magnetic toroids for both neuronal stimulation and detection[6];
- *capacitive effect based*[7].

The ohmic based method, although widely used, is an invasive one. The interference between the cell and the sensing/stimulation device may occur via the current flow that can initiate chemical reactions damaging the cells, or via the cell metabolism reactions that can corrode the electrical contacts and form toxic by-products. The method using magnetical devices, although noninvasive, cannot use planar devices, limiting the applicability to large neuronal cells. Finally, the third method, which uses a FET for detection/stimulation of neuronal cell, relies on manipulation of the neuronal cell on the FET, rather than chemically induced cell patterning. Addressing the issue of biospecific attachment of the neuronal cells, it was proposed[8] the integrated use of microlithography for FET fabrication *and* patterning of the neuronal cells, and recently the use of photoresists as basal substrates for controlling the selectivity of cell attachement'[9]. Ideally the axon of the neuronal cell would lay on the gate of a MOS structure, which will detect or stimulate the electrical activity of the cell (Figure 1.).

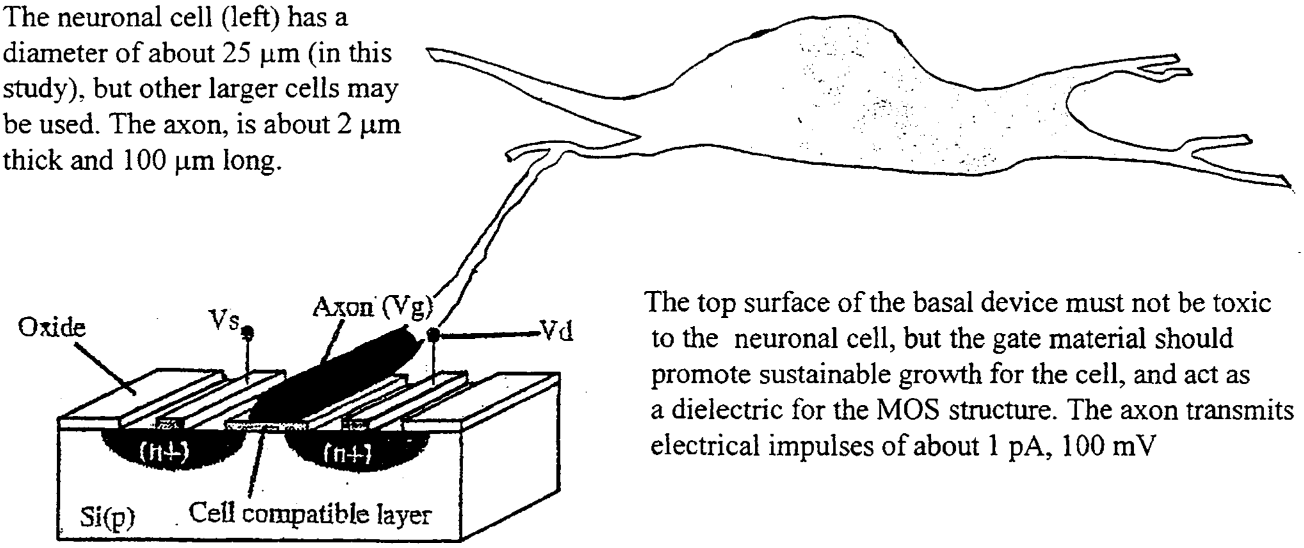

The neuronal cell (left) has a diameter of about 25 μm (in this study), but other larger cells may be used. The axon, is about 2 μm thick and 100 μm long.

The top surface of the basal device must not be toxic to the neuronal cell, but the gate material should promote sustainable growth for the cell, and act as a dielectric for the MOS structure. The axon transmits electrical impulses of about 1 pA, 100 mV

Figure 1. Integrated MOS-neuronal cell biodevice. Only the gate material is cell compatible.

2.2. Patterning of the neuronal cells

Different strategies for controlling neuronal cell selective attachment, using either polymeric surfaces or Self-Assembled-Monolayers (SAMs), are reviewed elsewhere[10]. Our approach was to assess the capabilities of the DNQ-based photoresists in different lithographic modes, that is, standard positive, Image Reversal negative, positive tone processing of Image Reversal resist, and silylation based Surface Imaging.

2.2.1. Experimental details

The base photosensitive material used was a positive tone photoresist, (S1400-17), purchased from Shipley, Co. Image Reversal resist, derived from the former adding imidazole to the polymer solution to reach 2% of the solid content, was used for positive (PIR) and negative (NIR) tone lithography. The 15 mm glass substrates for hydrophobic/hydrophilic contrast (see section 2.2.5.) were made hydrophobic or hydrophilic using the method described in the literature[11]. The photoresist was coated on glass at 0.6 μm thickness, dried for 1 hour at 85° C in a convection oven, then exposed broad band with exposure energies denominated as low (30 mJ/cm^2), medium (60 mJ/cm^2), and high (120 mJ/cm^2). In the case of NIR the substrates were reversal-baked 1 hour in a convection oven at 100° C. Several substrates exposed with the highest energy were silylated with hexamethyldisilazane (HMDS) in a closed chamber at 100° C for 15 min. For cell patterning studies, the films were pattern exposed through an chromium mask at the optimum exposure to obtain the highest contrast, that is 40 mJ/cm^2. The development used a MF-319 developer, diluted to reach 0.237N, and after thoroughly washing the developed features, the remaining photoresist surface was blanket exposed with the energy found as optimum for neuronal cell attachment. The hydrophobicity of the surfaces was quantified measuring the contact angle of 0.5 μl water drops on the unexposed, exposed and silylated polymer surfaces and hydrophilic/hydrophobic glass substrates. The neuronal cells used were either from a short term (for assessing the optimum parameters for selective neuronal cells attachment) or a long term culture of the nervous tissue of chicken embryos. The control surface was poly-hydroxy-styrene from the bottom surface of the cluster dish. Full experimental details will be published elsewhere[10].

2.2.2. Cell attachment on standard photoresist

In the DNQ-novolak standard resist, the DNQ photolysis produces carboxylic groups and releases the hydroxylic groups from the novolak, previously capped in hydrogen bonding with the DNQ acceptor groups. The carboxylic groups are prone to ionization in contact with the slightly basic culture media, creating a negatively charged surface. As the neuronal cells have also negatively charged membranes, attaching preferentially to positively charged surfaces[12], it is expected that the creation of carboxylic groups will negatively affect cell attachment. Superimposed on this phenomenon, photolysis will induce the hydrophilisation of the surface with expected positive effects on cell attachment. Similar studies using SAMs[13], proved that the number of neuronal cells attached on the surface increases with the increase in hydrophilicity. However these studies rely on amino-induced hydrophilicity, and therefore give limited insight regarding the carboxylic- and hydroxylic-induced surface hydrophilicity. Finally, excesive exposure seems to promote surface novolak crosslinking, either through esterification with an excess of ketene, or by further polymerisation induced by O_2 and/or photoradicals in the presence increasing surface hydrophobicity and therefore affecting negatively the cell attachment. This sequence of events explains the evolution of the number of neuronal cells, as well as the evolution of the contact angle vs. exposure energy.

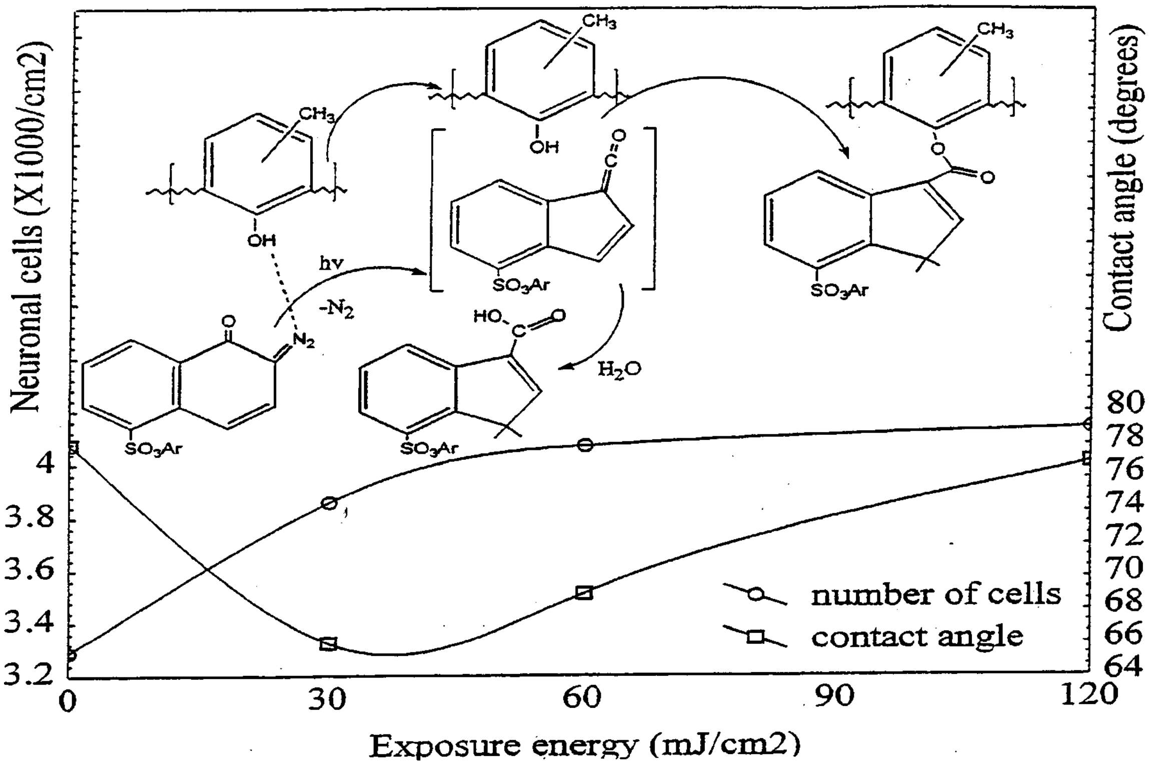

Figure 2. The evolution neuronal cells attachment on standard resist vs. exposure and contact angle.

The overall photochemistry of the standard photoresist with the approximate position vs. the exposure energy coordinate is presented in Figure 2. A higher hydrophobicity obtained by silylation of the fully exposed surface ($\theta = 82^{o}$), depleting the novolak hydroxylic groups as well as photoinduced carboxylic ones, allows the attachment of about 25% less cells as compared to the surface of the unexposed resist.

In any case, the number of neuronal cells on the standard photoresist is about three times lower than that on the control polymeric surface (poly-hydroxy-styrene, $\theta = 39^{o}$), with a considerably higher hydrophilicity, presumably due to a higher concentration of hydroxylic groups on the surface. Hence, apart from the insight on the mechanism of neuronal cell attachment, standard photoresist is not appropriate for cell patterning.

2.2.3. Cell attachment on Negative tone Image Reversal (NIR) photoresist

Image Reversal processing in the negative tone (NIR) produces larger differences in hydrophobicity than standard resist processing, as the hydrogen-bonded hydrophobicity is replaced by the more hydrophobic indene. Hence, NIR should produce higher cell adhesion differentiation between exposed/reversal baked surfaces (hydrophobic) and blanket exposed surfaces (hydrophilic). Indeed, the difference between the number of cells on these two types of surfaces is about three times higher in NIR case as compared to the standard photoresist, but the overall number of attached cells are in a similar range, that is, two times lower than on poly-hydroxy-styrene surface. The NIR resist surface hydrophobicity evolution vs. exposure energy is an overlap of three phenomena, (NIR photochemistry with the approximate position vs. the exposure energy coordinate is presented in Figure 3.):

- the addition of imidazole increases the hydrophilicity once the hydrophilic sites of imidazole are released by photolysis from possible hydrogen bonding; hence a larger number of cells on the resist surface, especially at higher exposure dose;
- the exposure and the subsequent reversal bake produce the decarboxylation of the ICA, catalysed by the presence of imidazole[14]; the indene by-product is hydrophobic, keeping the hydrophobicity variation in the same range as compared to the standard photoresist;
- finally these two effects are superimposed on the novolak crosslinking explaining the leveling of the hydrophilicity at high exposure energies.

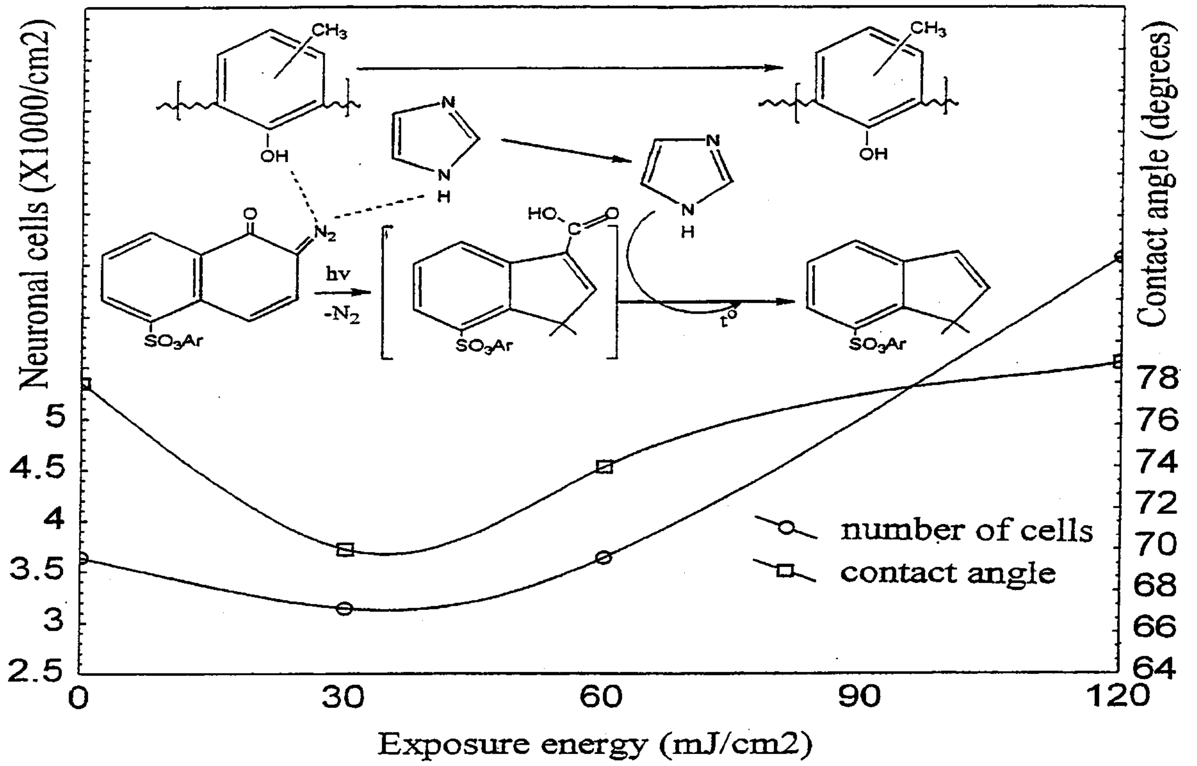

Figure 3. The evolution neuronal cells attachment on NIR resist vs. exposure and contact angle.

The surface hydrophobicity variation vs. exposure on the standard and NIR resist are similar, but a major difference is that the *cell attachment increases with hydrophobicity* rather than hydrophilicity. This feature can be explained by the decreasing concentration of carboxylic groups with exposure as opposed with their increase for standard photoresist surface, keeping the hydrophobicity variation in the same range in both cases. The carboxylic groups on the surface may charge negatively when in contact with the basic culture media, (pH = 7.5), inducing a cell repellent mechanism of the negatively charged neuronal cell membrane. On the other hand, the low pH of the culture media is not able to promote the development. An interesting feature, supporting the beneficial influence of imidazole on cell adhesion is the *higher* number of cells on the silylated resist surface.

However, NIR processing brings insight for the cell adhesion mechanism only, being unsuitable for a proper cell compatible surface.

2.2.4. Cell attachment on Positive tone Image Reversal (PIR) photoresist

The PIR resist processing proceeds on a CEL-like route[15]. A recently proposed mechanism[16] explains this feature of PIR relying on the creation of positive *and* negative charged chemical species *on* the surface of the resist in the early stages of exposure. A similar mechanism was proposed[17] for the BIM technique.

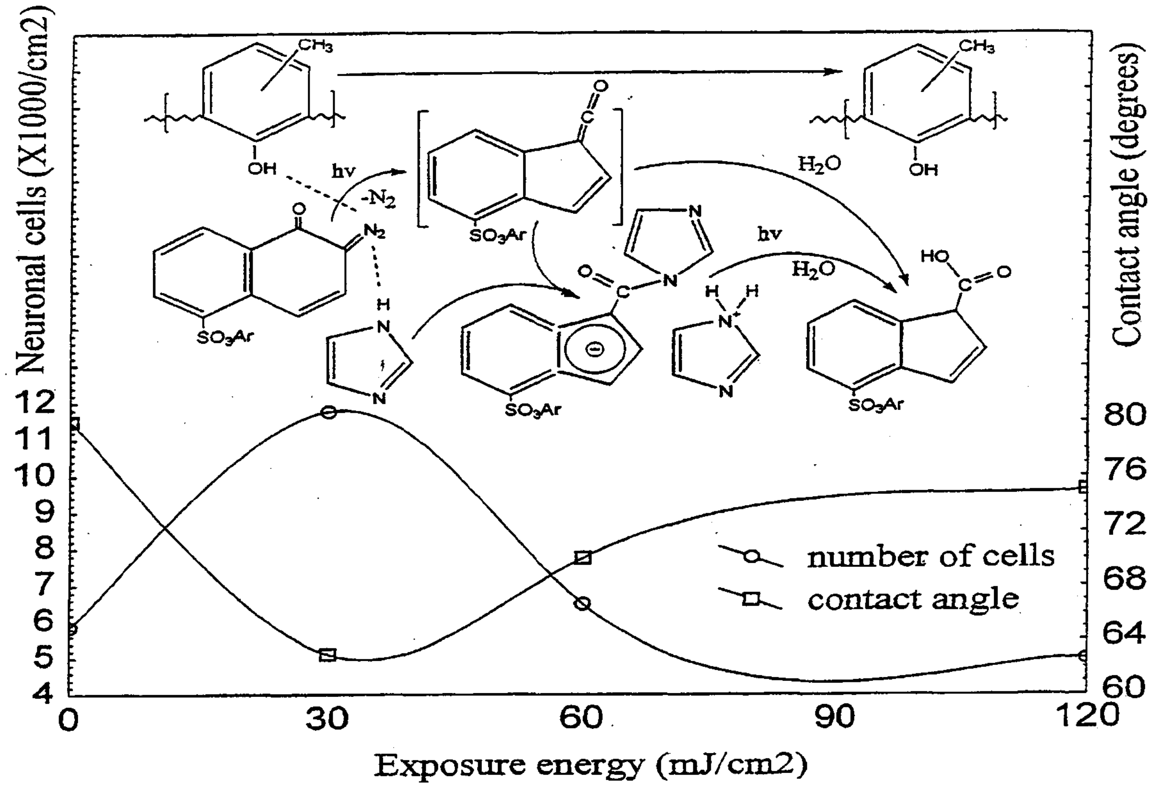

Figure 4. The evolution neuronal cells attachment on PIR resist vs. exposure and contact angle.

In the case of the Image Reversal resist in the positive mode the hydrophobic/hydrophilic balance fails totally in explaining the cell adhesion behaviour. The overall photochemistry of the PIR photoresist with the approximate position vs. the exposure energy coordinate is presented in Figure 4. In the case of PIR, the absence of the post-exposure reversal bake allows the carboxylic groups accumulation with exposure in a similar manner with the standard positive tone photochemistry. Except for the unusual case of low exposure energy, this mechanism is in good agreement with the same or lower number of neuronal cells attached on the exposed surface as compared with NIR photoresist surface. The additional baking steps in the case of NIR can explain the lower number of cells on NIR vs. PIR unexposed surfaces, due to a possible thermo-induced crosslinking of the resist. However, the most striking feature of PIR case is the high number of neuronal cells on the polymer surface when exposed with low energies. This feature can be explained by the formation of the indenyl⊖-imidazolyl⊕ charged species in the first stages of exposures, as proposed earlier[16], as the charged species would have a beneficial effect on the cell attachment behaviour, due to electrostatic double-layer formation.

To this end, an optimum of surface functionality can be found in PIR mode systems for low energy exposure, making PIR surfaces good candidates for cell patterning.

2.2.6. Further experimental studies

Although the chemistry of DNQ/novolak system received an extended treatment in the literature, some aspects of its surface chemistry need further clarification, especially in the frame of surface induced cell engineering. ATR and ESCA spectroscopy studies of the functionalisation of the resist surface are currently pursued.

3. BIOMOLECULAR ENGINEERING

Another front of experiments target the potential of the DNQ/novolak system for patterning biologically active molecules. In the context of the neuronal cell engineering, we aimed at patterning neuroactive peptides[18] which can induce different attachment behaviour of the neuronal and glial cells respectively. However, the results have wide applications as the chemistry involved is a rather general one.

Bioactive molecules patterning[19,20,21,22,23] found application in biosensor fabrication[24,25,26] and neuronal cells guidance[8]. Recently, bioactive molecules patterning received a new incentive from the growing field of combinatorial chemistry[27], reported techniques using light-directed, spatially addressable step-wise chemical synthesis of bioactive peptide[28], being already in use. Although it is recognised that towards-submicron resolution would be beneficial, none of these techniques and applications are able to reach this target, either due to the use of unsuitable imaging layer (e.g. protein layers), or due to the use of unsuitable imaging chemistry (e.g. SAM or triazide photochemistry).

3.1. DNQ potential for patterning bioactive molecules

DNQ photochemistry was largely viewed in the microlithographic community as a vehicle for obtaining higher resolution and higher aspect ratio of the vertically patterned feature. The DNQ chemical flexibility allowed over the years many technological improvements and techniques[29], but due to the emphasis on microlithographic issues, the research was focused on the impact on optical and polymer properties and their distribution throughout the resist layer, rather surface functionality capabilities. However, the DNQ allows many chemical avenues, most of them fairly known[30,31]. In the context of bioactive molecules patterning, three possible chemistries are of interest:

➊ photoinduced creation of carboxylic groups on the polymer surface, (standard processing);
➋ photoinduced creation of ketene groups, when the polymer surface is in contact with the bioactive molecule solution, (in-situ exposure through thin liquid layer); and
➌ destruction of the DNQ moieties and their replacement with amino groups.

The first chemistry would assure the *technological flexibility*, due to the decoupling of the exposure stage from the attachment stage. The exposure can be made on high resolution (projection optics) tools, in conditions of semiconductor-like quality, and the substrates can be transported or stored for further attachment of biologically active molecules to another site. The second chemistry would allow in-situ processing, suitable for step-wise chemical synthesis used in combinatorial chemistry. Finally the third alternative chemistry would allow the portability of the present combinatorial chemistry techniques. However, in terms of their feasibility, the first two chemical and technological routes seem more important, as the reduction of DNQ to amino groups may proceed with several competing parasitic reactions. The overall chemistry of DNQ in the context of bioactive molecules patterning is presented in figure 7.

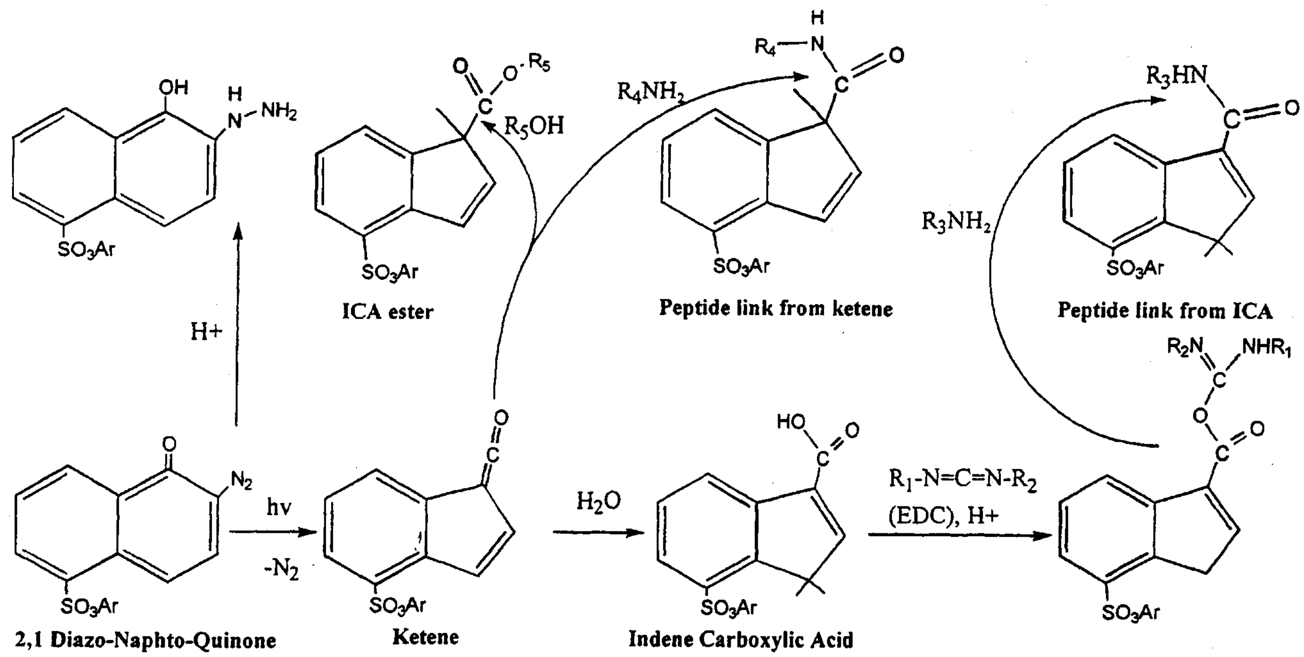
OH
H
N-NH2
SO3Ar
H+
O
O-R5
C
R5OH
SO3Ar
ICA ester
H
R4—N
C
O
R4NH2
SO3Ar
Peptide link from ketene
R3HN
C=O
R3NH2
SO3Ar
Peptide link from ICA
R2N
NHR1
C
O
O
C
O
N2
hv
-N2
SO3Ar
2,1 Diazo-Naphto-Quinone
O
C
SO3Ar
Ketene
H2O
HO
C
O
SO3Ar
Indene Carboxylic Acid
R1-N=C=N-R2
(EDC), H+
SO3Ar

Figure 7. DNQ chemistry associated to bioactive molecule patterning

3.2. Patterning proteins on DNQ-novolak polymeric surfaces

The DNQ-novolak system technological flexibility was used for patterning avidin, a commonly protein used for checking the selectivity of the bioactive molecules attachment. The visualisation of the specific attachment was possible using a fluorescent derivative of avidin, FITC

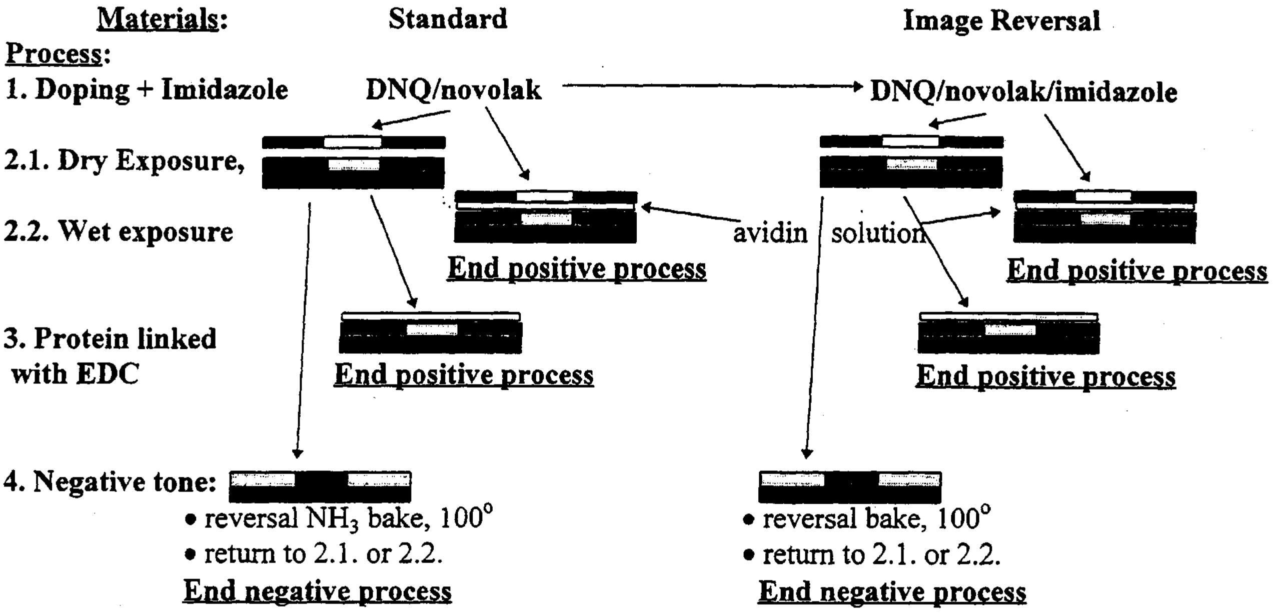
Materials:
Standard
Image Reversal
Process:
1. Doping + Imidazole
DNQ/novolak
DNQ/novolak/imidazole
2.1. Dry Exposure,
2.2. Wet exposure
avidin
solution
End positive process
End positive process
3. Protein linked with EDC
End positive process
End positive process
4. Negative tone:
• reversal NH3 bake, 100°
• return to 2.1. or 2.2.
End negative process
• reversal bake, 100°
• return to 2.1. or 2.2.
End negative process

Figure 8. Processing routes for patterning proteins on DNQ photoresist

3.3. Further experimental studies

Further experimentation is needed for reaching the maximum resolution and for quantifying the amount of bioactive molecule attached on the resist surface vs. processing conditions. Other research is directed towards patterning of neuronal active peptides for neuronal cell engineering. But the most attractive front of research is directed towards implementation of present microlithographic materials and techniques in combinatorial chemistry.

4. CONCLUSION

A wide range of DNQ-based microlithographic materials and techniques were assessed in terms of their potential for patterning of the neuronal cells and bioactive molecules. Neuronal cell engineering can be performed conveniently using positive tone Image Reversal, but other DNQ-based microlithographic techniques can be used as an insight tool for studies concerning cell attachment on polymeric surfaces. The applications of DNQ-based cell engineering span from integrated biodevices fabrication to medical artificial prosthesis. Biomolecular cell engineering can benefit from DNQ-based microlithography through high resolution patterning of the bioactive peptides/proteins on the polymeric surface, by either the linkage to photoinduced inden-carboxylic acid (two-step process), or to addition to photoinduced ketene (single-step process). In the case of DNQ-based biomolecular engineering, the applications span from drug-screening through combinatorial chemistry to biosensors fabrication.

5. ACKNOWLEDGEMENTS

One of the authors (DVN) wishes to acknowledge the thoughtful discussions with Patrick Paniez in the first stages of research.

6. REFERENCES

1. C. Nicolini. *Biosensors & Bioelectronics*, Vol. 10, 1/2, pp. 105-115, 1995.
2. W. Gopel. *Biosensors & Bioelectronics*, Vol. 10, 1/2, pp. 35-45, 1995.
3. D. C. Wijeseruiya, G.A.Rechnitz.. *Biosensors & Bioelectronics*, Vol. 8, pp. 155-160, 1993.
4. M. Aizawa, T. Haruyama, G. F., Kham, E. Kobatake, Y. Ikaryiama. *Biosensors and Bioelectronics*. Vol. 9, pp. 601-610, 1994.
5. for instance, G. W. Gross, B. K. Rhoades, H. M. E. Azzazy, M-C. Wu. *Biosensors & Bioelectronics*, Vol. 10, pp. 553-567, 1995. and, W. L. C., Rutten, T. A. Frieswijk, J. P. A. Smit, T. H. Rozijn, J. H. Meier. *Biosensors & Bioelectronics*, Vol. 10, pp. 141-153, 1995.
6. C. W. Babb, D. R. Coon, G. A. Rechnitz. *Anal. Chem.*, Vol. 67, pp. 763-769, 1995.
7. P. Fromherz, C. O. Muller, R., Weis. *Phys. Rev. Lett.* Vol. 71, 24, pp. 4079-4082, 1993. and P. Fromherz, A. Offenhausser, T. Vetter, J. Weis *Science*, Vol. 252, pp. 1290-1293, 1991.
8. P. Fromhertz, H. Schaden. *European Journal of Neuroscience*, Vol. 6, pp. 1500-1504, 1994.
9. D. V. Nicolau, T. Taguchi, D. E. Nicolau, S. Yoshikawa. *IEEE Intl. Semicond. Conf.*, Vol. CAS 18, pp. 133-136, October, 1995.
10. D. V. Nicolau, T. Taguchi, H. Tanigawa, S. Yoshikawa. *Biosensors & Bioelectronics*, submitted for publication

11. M. Ferreira, J. H. Cheung, M. F. Rubner. *Thin Solid Films,* Vol. 244, pp. 806-809, 1994.
12. E. Yavin, Z. Yavin. *J. Cell Biol.*, Vol. 62, pp. 540-546, 1974.
13. D. A. Stenger, C. J. Pike, J. J. Hickman, C. W. Cotman. *Brain Research,* Vol. 630, pp. 136-147, 1993.
14. M. E. Reuhman-Huisken, C. M. J. Mustaers, F. A. Vollenbroek, J. A. H. M. Moonen. *Microelectronic Eng.,* Vol. 9, pp. 551-554, 1991.
15. D. V. Nicolau, M.. V. Dusa. *Microelectronic Eng.* Vol. 11, pp. 589-592, 1989.
16. D. V. Nicolau, M. Dusa, D. E. Nicolau, S. Yoshikawa. *J. Photopol. Sci. Tech.,* Vol. 8, 187-194, 1995.
17. C. M. J. Mustaers, F. A. Vollenbroek, W. P. M.. Nijssen, R. J. Visser. *Microelectronic Eng.* Vol. 11, pp. 497-500, 1990.
18. T. Taguchi, X.X. Bo, H. Taniguchi, K, Kiyosue, S. Kodoh, N. Yumoto, H. Yamamoto, M. Kasai, S. Yoshikawa.. in M. Ohno (ed.) *Peptide Chem., 1994,* pp. 145-148, Protein Res. Found., Osaka, 1995.
19. S. K. Bhatia, J. J. Hickman, F. S. Ligler, *J. Am. Chem. Soc.,* Vol. 114, pp. 4432-4433, 1992.
20. J. D. Hong, K. Lowack, J. Schmitt, G. Decher, *Progr. Colloid Polym. Sci.,* Vol. 102, pp. 93-102, 1993.
21. D. J. Pritchard, H. Morgan, J. M. Cooper, *Angew. Chem. Int. Ed. Engl.* Vol. 34, pp. 91-92, 1995.
22. P. Connolly. J. Cooper, G. R. Moores, J. Shen, G. Thomson, *Nanotechnology,* Vol. 2, pp. 160-163, 1991. and S. Britland, E. Perez-Arnaud, P. Clark, B. McGinn, P. Connolly, G. Moores. *Biotechnol. Prog.,*Vol. 8, 155-160, 1992.
23. S. K. Bhatia, J. T. Teixeira, M. Anderson, L. C. Shriver-Lake, J. M. Calvert, J. H. Georger, J. H. Hickman, C. S. Dulcey, P. E. Schoen, F.S. Ligler, *Analytical Biochemistry* Vol. 178, pp. 197-205, 1989.
24. D. J. Pritchard, H. Morgan, J. M. Cooper, *Ana. Chim. Acta,* Vol. 310, pp. 251-256, 1995
25. T. Kuriyama, J. Kimura, Y. Kawana, *NEC Res & Dev.,* Vol. 78, pp. 1-5, 1985, F. S. Ligler, T. L. Fare,
26. K. D. Seib, J. W. Smuda, A. Singh, P. Ahl, M. E. Ayers, A. Dalziel, P. Yager. *Med. Instrum.,* Vol. 22, pp. 247-256, 1988.
27. M. A. Gallup, R. W. Barrett, W. J. Dower, S. P. A. Fodor, E. M. Gordon. *J. Medicinal Chemistry,* Vol. 37, pp. 1233-1401, 1994
28. S. P. A. Fodor, J. L. Read, M. C. Pirrung, L. Stryer, A. T. Lu, D. Solas, science, Vol. 251, pp. 767-773, 1991.
29. R. Dammel, *Diazonaphtoquinone-based Resists.*SPIE Opt. Eng. Press., Bellingham, WA, 1993.
30. V. V. Ersov, G. A. Nikiforov, C. R. H. I. de Jonge. *Quinone Diazides.* Elsevier Sci., Amsterdam, 1981
31. T. Ye, M. A. McKervey. *Chem. Rev.* Vol. 94, pp. 1091-1160, 1994.

7.

Biosensors & Bioelectronics Vol. 11. No. 12, pp. 1237–1252, 1996
© 1996 Elsevier Science Limited
Printed in Great Britain. All rights reserved
0956–5663/96/$15.00

Control of the neuronal cell attachment by functionality manipulation of diazo-naphthoquinone/novolak photoresist surface

Dan V. Nicolau, Takahisa Taguchi, Hideo Tanigawa & Susumu Yoshikawa

Osaka National Research Institute, 1-8-31 Midorigaoka, Ikeda, Osaka 563, Japan
Tel: [81] (727) 51 9521 Fax: [81] (727) 51 9628

(Received 2 February 1996; accepted 16 April 1996)

Abstract: The surface of the photosensitive Diazo-Naphto-quinone/novolak film was chemically manipulated through UV exposure and subsequent thermal processes to obtain different surface functionalities (DNQ, carboxylic, imidazole, indene, silylated and charged groups) and hydrophobicities. The neuronal cell attachment is sensitive to chemical functionalization, with favourable influence from charged, imidazole and carboxylic groups, while the hydrophobic/hydrophilic balance of the photoresist surface plays at best a secondary role. The microlithographic techniques assessed (standard positive tone, negative and positive tone image reversal, and surface imaging based on silylation) can be used to gain insight into the cell attachment mechanisms. The positive tone DNQ/novolak/imidazole system was found to be a suitable candidate for cell patterning. © 1996 Elsevier Science Limited

Keywords: cell adhesion, neuronal cells, surface functionalization, photolithography

INTRODUCTION

Techniques for controlling biomolecular architectures on surfaces have a wide range of potential applications in biosensing, cell guidance, and molecular eletronics (Nicolini, 1995). As knowledge regarding architectures ordered vertically incorporating bioactive molecules and cells advanced steadily in the last decade, we witnessed a growing interest in ordering them laterally (Gopel, 1995). This new development requires techniques for patterning areas with different properties that control the selective attachment of the vertically ordered architectures on the same basal surface. Vertically structured cell engineering found applications in biosensors based on plant and animal tissues (Wijeseriya & Rechnitz, 1993), and in creating electronically modulated biological functions (Aizawa *et al.*, 1994). Laterally structured cell engineering aims towards multiplication of these functions on the same substrate.

The neuronal cell's electrical activity makes it an ideal candidate for integration in a bioelectronic device. Although progress has been made in conceiving and building an integrated neuronal-semiconductor device, the technology employed relies only marginally on the possibilities offered by the present state-of-the-art microlithography which is the most dynamic semiconductor technology. In this account we will emphasize the potential of using semiconductor microlithography materials and techniques for building neuronal biodevices, and for cell engineering in general, focusing on the manipulation of neuronal cell attachment by means of photo- and thermally-induced chemical transformations of the surface of the diazo-naphtho-quinone/novolak thin films.

MATERIALS AND METHODS

Materials

The photosensitive material used was a common, positive tone, commercial photoresist, (S1400-17), purchased from Shipley Co. The photoresist is a mixture of a photoactive compound, based on diazo-naphtho-quinone (DNQ), and a novolak based resin, in an approximate proportion of 3:7, dissolved in ethyl cellosolve acetate to reach 30% solid content. The material is sensitive to the g-line of the Hg lamp spectrum (436 nm). Another photosensitive material was derived from the former, adding imidazole to the polymer solution to reach 2% of the solid content. This material (Image Reversal resist) was used for positive tone as well as negative tone lithography. For silylation we used hexamethyldisilazane, (HMDS), as purchased from Aldrich Co.

Substrate preparation

The 15 mm glass substrates were made hydrophobic or hydrophilic using the method described in the literature (Ferreira *et al.*, 1994). The polymer solution was spin coated on 15 mm glass substrates, using a spin coater (Mikasa Co.) for 15 s at a rotation speed of 500 r.p.m. for deposition, and for 1 min at a rotation of 3000 r.p.m. for thinning and drying. This procedure allows the deposition of uniform films approximately 0·6 μm thick. The films were further dried for 1 h at 85°C in a convection oven.

After drying, the polymeric films, both with and without imidazole, were irradiated using a Hg lamp, at exposure energies denominated as low (30 mJ/cm^2), medium (60 mJ/cm^2), and high (120 mJ/cm^2). In the case of imidazole doped resist processed in the negative tone image reversal mode, the substrates were reversal-baked in a convection oven at 100°C for 1 h. Several substrates exposed to the highest energy, both without and with imidazole added, were further exposed to HMDS for silylation of the novolak hydroxylic groups in a closed chamber at 100°C for 15 min.

For studies concerning cell attachment on DNQ/novolak surface, and for increasing the polymer adhesion, the resist was deposited only on hydrophobic glass. For studies concerning cell patterning, the imidazole doped resist was coated on hydrophilic glass slides as well. To obtain the highest contrast, these films were irradiated through an emulsion mask at the optimum exposure energy (40 mJ/cm^2). For the development of the exposed patterns we used a metal-free Shipley developer (MF-319), diluted to reach 0.237 N. The appropriate development time in these conditions is approximately 60 s. After development and thoroughly washing the developed features, the remaining photoresist surface was exposed again at the optimum energy for neuronal cell attachment.

Surface hydrophobicity evaluation

The surface hydrophobicity/hydrophilicity was experimentally evaluated by measuring the water contact angle on respective surfaces. The polymer films were irradiated with the exposure energies as described above, and post exposure baked at 80°C for 30 min to remove the possible polymer tensions. The contact angle of 0.5 μl water drops, deposited on the unexposed, exposed and silylated polymer surfaces, was measured with a Kyowa Kagaku Co. Ltd, anglemeter. The same procedure was used for hydrophilic and hydrophobic glass substrates.

The hydrophobicity of several chemical species encountered in the processing of the DNQ/novolak system was evaluated by computing their log*P* parameter. The log*P* computations used a QSAR (quantitative structure–activity relationships) method (Viswanadham *et al.*, 1989) as implemented in the ChemPlus module of HyperChem molecular modelling software (HyperCube Inc., 1995).

Neuronal cell culture

For the short-term culture, cerebral hemispheres of chick embryos were dissected in Ham's F12 medium. Nervous tissue from one or two embryos was treated for 15 min at 37°C with 0.125%

trypsin in the same medium. Tissues were rinsed in F12 medium supplemented with bovine serum albumin (1 mg/ml), glucose (10 mM), insulin (2.5 μg/ml) and antibiotics, and dissociated in this medium by gentle trituration using a drawn-out Pasteur pipette. The cells (4×10^4 per well) were plated in 16 mm wells of the Clostar cluster dishes, with the previously prepared substrates placed on the bottom of the well. Each well contained 400 μl F12 medium, supplemented with glutamine (2 mM), penicillin (10 IU/ml), streptomycin (100 μg/ml), insulin (2.5 μg/ml) and glucose (10 mM). The cells were cultured at 37°C in 5% CO_2/95% air and saturating humidity. The cultures were observed after 1 day.

The cells for the long-term culture were prepared from cerebral hemispheres of chick embryos (embryonic day 10), as described previously (Tokioka *et al.*, 1993). Briefly, the dissociated cerebral neurons (5×10^4 cm^{-2}) were plated on each control or modified substrate settled in a well of 24 well cluster dish containing 50% of modified Earl's minimum essential medium, 10% foetal calf serum (FCS) and 40% GIT medium (Nihon Seiyaku Co. Ltd.). Cells were cultured for 7 days at 35°C in 5% CO_2/95% air and saturating humidity. Half of the culture medium was changed every 2 days.

RESULTS

Neuronal cell attachment

The neuronal cell adhesion behaviour on photoresist was studied in view of the chemical functionalization of the DNQ/novolak polymeric surface. This functionalization was induced:

- before exposure, through addition of imidazole to the resist;
- during exposure, through several photochemistries; and
- after exposure, through post-exposure reversal bake and silylation.

The overall procedue for assessment of the neuronal cell attachment and patternability potential using DNQ/novolak photoresist surface is presented in Fig. 1.

The control surface was the poly-hydroxy-styrene bottom surface of the cluster dish, either as received or treated with poly-lysine. As the number of neuronal cells on the surfaces with and without poly-lysine treatment is similar in the conditions of our experiments, we will further designate as the control only the poly-hydroxy-styrene surface without poly-lysine.

The assessment of the capabilities of various functionalized photoresist surfaces was based on the observation of the attachment behaviour of the neuronal cells from the short-term culture. Samples of the short-term cell culture on the surface of processed resist films are presented in Fig. 2. The neuronal cells were counted and statistical tests were performed to assure data reliability. The substrates were grouped under the categories of surface type (control, standard, negative and positive tone image reversal resist) and process stage (unexposed, exposed at low, medium, and high energies, functionalized with poly-lysine in the case of the control surface and HMDS for standard and image reversal resist). A class of its own was considered the surface of the positive tone image reversal resist, exposed with low energy, which accidentally peeled-off from the glass substrate. The results on the short-term culture attachment, together with the contact angle values for the respective surfaces, are presented in Table 1. Furthermore, the molecular hydrophobicities (log$P$) of several chemical species encountered during the processing of the DNQ/novolak system (presented in Table 2) are useful in establishing the correlation between surface chemistry and cell adhesion behaviour. Log$P$ (the log of the octanol–water partition coefficient) measures proportionally the molecular hydrophobicity, but it should be noted that QSAR calculations can not take into consideration hydrogen bonding effects.

The attachment behaviour of neuronal cells on the photoresist surface was further assessed for the long-term culture conditions using the same parameters which produced the highest proliferation of cells, that is positive tone image reversal resist exposed with low energy (second row, third column in Fig. 2). A sample of the long-term neuronal cell culture under these conditions is presented in Fig. 3.

Neuronal cell patternability

On the basis of the data from the study on the attachment behaviour of the short-term culture neuronal cells, we attempted their patterning on the photoresist surface from the long-term culture, using the hydrophilic or hydrophobic glass substrate as the contrast surface. As the best candidate

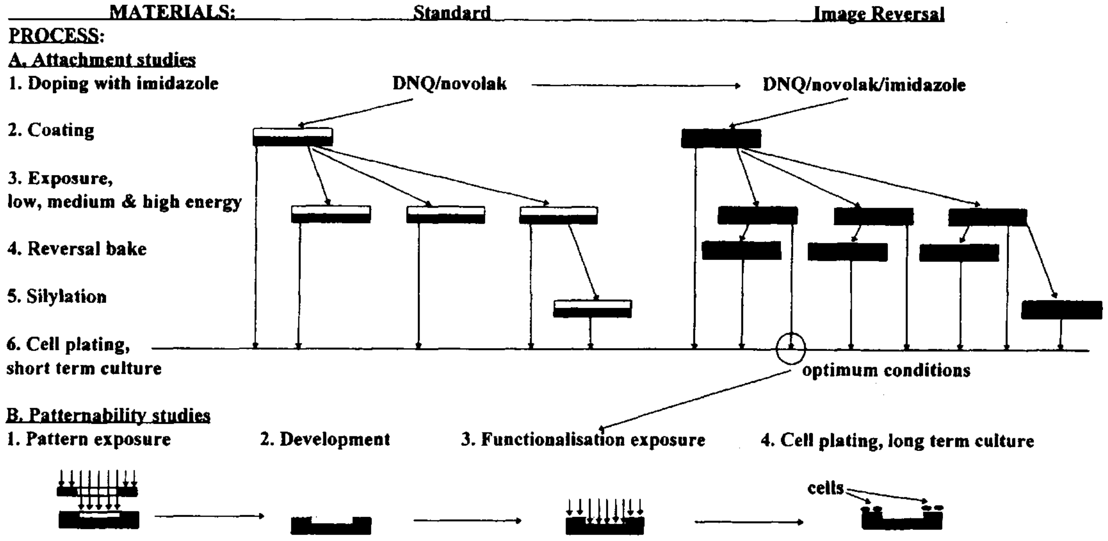
MATERIALS:
Standard
Image Reversal
PROCESS:
A. Attachment studies
1. Doping with imidazole
DNQ/novolak
DNQ/novolak/imidazole
2. Coating
3. Exposure, low, medium & high energy
4. Reversal bake
5. Silylation
6. Cell plating, short term culture
optimum conditions
B. Patternability studies
1. Pattern exposure
2. Development
3. Functionalisation exposure
4. Cell plating, long term culture
cells

Fig. 1. Surface functionality manipulation using DNQ/novolak system for the study of the attachment and patternability of the neuronal cells.

for a selective cell patterning was the image reversal resist in the positive mode exposed at low energies, here we report only the results obtained using this system.

The attachment and growth of the long-term culture neuronal cells on patterned positive tone image reversal resist exposed with low energy may be observed in Figs. 4(a) and (b) (for the case of photoresist on hydrophilic glass) and in Fig. 5 (for the case of photoresist on hydrophobic glass).

DISCUSSION

Neuronal cell engineering

The building of neuronal cell based biodevices would employ two sets of technological tasks aiming at:

- design and fabrication of an appropriate electric, magnetic or electronic device, as the basal structure of the integrated biodevice, either sensing or stimulating the neuronal cell electrical activity; and
- constructing the architecture using neuronal cells on this pre-defined basal structure, requiring the precise and preferably chemically induced positioning of neuronal cells on top of the pre-defined basal device.

As the aim of the present contribution is to progress towards the patternability of neuronal cells using microlithographic techniques and materials employed in semiconductor device fabrication, we will concentrate on previous cell patterning work as well as the technology and chemistry of the DNQ/novolak system. Therefore, the basal devices for sensing and stimulation of the neuronal electrical activity will be only briefly described.

Basal devices used for neuronal cell based integrated devices

The basal devices used for sensing or stimulation of neuronal cell electrical activity may be classified as:

- electrical, using arrays of microelectrodes as contacts beneath the neuronal cell (Gross *et al.*, 1982, 1985, 1993, 1995; Regehr *et al.*, 1988; Connolly *et al.*, 1990; Jimbo & Kawana, 1992; Meister *et al.*, 1991; Gross & Schwalm, 1994; Nisch *et al.*, 1994; Rutten *et al.*, 1995);
- magnetic, using magnetic toroids for both neuronal stimulation and detection (Babb *et al.*, 1995);
- electronic, using the sensing capability of a field-effect transistor (Fromherz *et al.*, 1991, 1993).

An optical technique was also proposed for top detection and visualization of neuronal cell electrical activity (Fromherz & Muller, 1994).

TABLE 1 Number of neuronal cells ($\times 1000/cm^2$) on polymeric substrates with different contact angles, θ.

Substrate modification:	*Unexposed*	*Exposed surface*			*Functionalization*	
			Exposure energy:			
Substrate type		*low*	*medium*	*high*	*HMDS*	*polylysine*
Control surface (poly-hydroxystyrene)	11.57 (±1.01; 8.73%) $\theta = 39°$					11.71 (±1.18; 10.07%)
Standard resist	3.29 (±0.51; 6.13%) $\theta = 78°$	3.86 (±0.81; 20.89%) $\theta = 66°$	4.07 (±0.57; 14.01%) $\theta = 69°$	4.14 (±0.66; 15.94%) $\theta = 77°$	2.43 (±0.49; 20.16%) $\theta = 83°$	
Image reversal resist, negative tone	3.64 (±0.72; 19.78%) $\theta = 80°$	3.14 (±0.56; 17.83%) $\theta = 70°$	3.64 (±0.74; 20.32%) $\theta = 74°$	6.57 (±0.64; 9.74%) $\theta = 79°$	6.78 (±0.74; 10.91%) $\theta = 82°$	
Image reversal resist, positive tone	5.86 (±0.58; 9.90%) $\theta = 80°$	11.78 (±0.85; 7.22%) $\theta = 63°$	6.50 (±0.70; 15.56%) $\theta = 70°$	5.00 (±0.76; 15.2%) $\theta = 75°$	6.81 (±0.71; 10.43%) $\theta = 81°$	
Image reversal resist, positive tone, free surface		65.80 (±2.52; 3.83%)				

The numbers in parentheses are the variance of the number of neuronal cells, in absolute values ($\times 1000/cm^2$) and percentage, respectively, within 95% confidence interval. The contact angles for hydrophobic and hydrophilic glass are 90° and 30°, respectively.

TABLE 2 Computed hydrophobicity (log*P*) for different chemical species encountered during the processing of the DNQ/novolak system.

Process:	*Unexposed*	*Exposed with energy:*		*Post-exposure functionalization*	
Chemical species		*Low/medium*	*Medium/high*	*reversal bake*	*silylation*
Photoactive compound	3.66 (DNQ)	3.04 (ICA)	—	3.71 (indene)	3.91* (silylated ICA)
Base resin, novolak	2.7 (*o*-, *p*-)	—	4.96 (dimerization)	—	3.56† (silylated novolak)
Ester novolak-indencarboxylic acid	—	—	—	5.84	—
Imidazole	−0.04	—	—	—	—

*Due to the lack of parameters for Si, the log*P* for silylated chemical species were computed replacing the Si atom with a C atom. The real values should be higher.

†For comparison, the log*P* value for water is −0.51.

Cell patterning

One strategy for controlling the specific interaction between the cells and the basal substrate is focused on the physico-chemical manipulation of the surface. In this respect, two techniques were used for studying the relation between the adhesion and growth of the cells and the properties and functionality of the polymeric surfaces, that is:

- adsorbing growth-controlling factors on the surface, either before (Ingber *et al.*, 1987; Ingber & Folkman, 1989; Ingber, 1990; Mooney *et al.*, 1992; Bekos *et al.*, 1995) or during cell plating (Taguchi *et al.*, 1987; Ben-Ze'ev *et al.*, 1988; Ingber, 1990); and
- controlling the physical properties of the surface, either through wettability (Letourneau, 1975; Folkman & Moscona, 1978; Li *et*

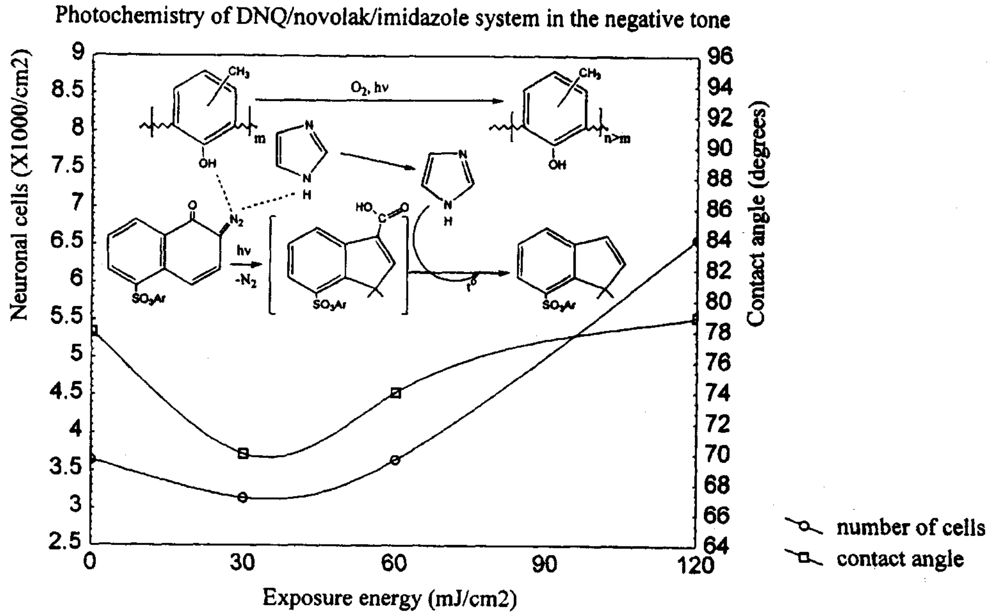

Fig. 7. Neuronal cell attachment (short-term culture), hydrophobicity and photochemistry of the DNQ/novolak system, with 2% imidazole added, processed in the negative tone.

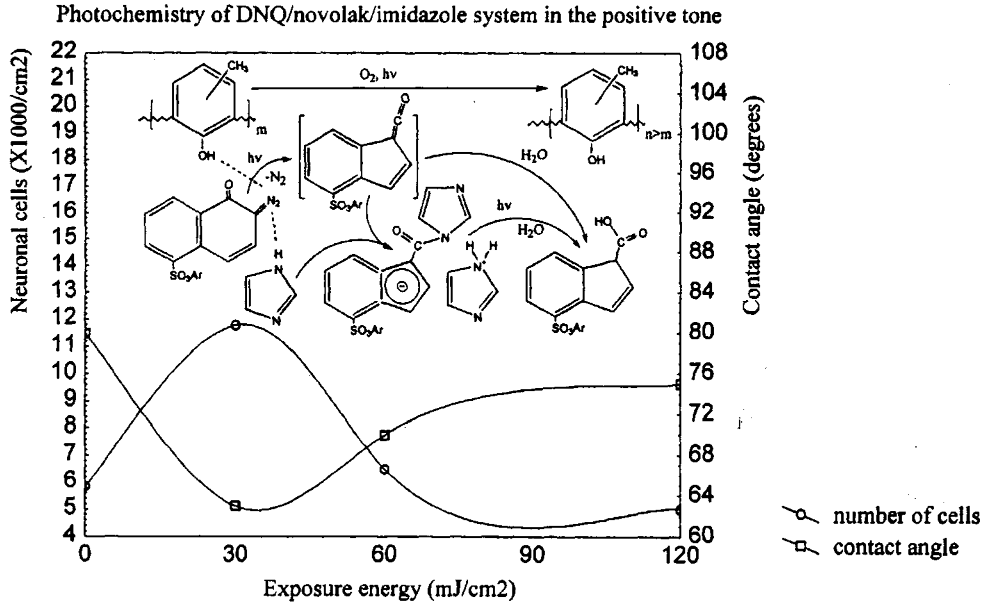

Fig. 8. Neuronal cell attachment (short-term culture), hydrophobicity and photochemistry of the DNQ/novolak system with 2% imidazole added, processed in the positive tone.

show that the surface hydrophilicity decreases again at higher exposure energies. This evolution can be explained by the decrease of hydroxylic groups on the surface, either through esterification with an excess of ketene (Fig. 6, upper right) or due to the crosslinking of the novolak at the surface in the presence of O_2 and photoinduced radicals. Both mechanisms are more effective than DNQ photolyhsis in controlling the surface hydrophobicity as inferred from the log*P* values for both by-products, which are considerably higher than those of the starting novolak (5.84 for esterification and 4.96 for novolak dimerization versus 2.7 for novolak monomer, in Table 2). The former mechanism may prevail for higher power exposure (excess of ketene), while the latter may prevail for higher exposure time (excess of UV radiation). Supporting this overall mechanism, it should be noted that the increase of hydrophilicity appears at energies far from those recommended for the photoresist high resolution patterning. The kinetics of this effect, reported by several groups as a parasitic 'skin effect' inhibition of the development at the photoresist surface (mechanisms reviewed by Dammel, 1993), is expected to be slower than DNQ photolysis, explaining the evolution with a minimum of the contact angle versus exposure energy.

Finally, the surface silylation of the remaining hydroxylic sites, and probably of the carboxylic ones as well, increases the hydrophobicity with an expected increase in the contact angle (Table 1), as both by-products show high log$P$ values (3.56 and 3.91, respectively, Table 2).

Cell attachment behaviour

Other studies regarding the attachment of neuronal cells on SAMs (Stenger *et al.*, 1993; Matsuzawa *et al.*, 1993; Georger *et al.*, 1992) proved that the number of neuronal cells attached to the surface increases with hydrophilicity. However, these studies rely on amino-induced hydrophilicity, and therefore their conclusions, give limited insight regarding the carboxylic- and hydroxylic-induced surface hydrophilicity.

In the conditions of the present study, the cell attachment behaviour on standard photoresist (plotted in Fig. 6 against exposure energies and approximately beneath the proposed responsible surface chemistry) may be explained through the neuronal cell response to the surface functionalization with carboxylic and hydroxylic groups. The levelling of cell attachment is placed close to the same energy range recommended for obtaining the highest microlithographic contrast, i.e. close to the point where all DNQ was photolized and hydroxylic and carboxylic groups on the surface reached their highest concentration. In the view of possible depletion of the hydroxylic groups following novolak crosslinking, it may be inferred that carboxylic and not hydroxylic groups are the prime factor in cell adhesion.

On the other hand, the number of attached cells is also lower than on imidazole doped DNQ/novolak films. This may be explained by the fact that the carboxylic groups, and to a lesser extent hydroxylic ones, may be ionized negatively on the surface when put in contact with the slightly basic culture media (pH 7.5), inducing a cell repellent mechanism of the negatively charged neuronal cell membrane (Yavin & Yavin, 1974). The basicity of the culture media is not able to promote the development of the top resist (the reported pH threshold for triggering the development lies around 12.5, Dammel, 1993).

The hydrophobicity evolution in the conditions of our experiments (measured by contact angle values in Fig. 6) seems to have at best a secondary influence on neuronal cell attachment. However, the overall number of neuronal cells on the standard photoresist is far lower than on the control polymeric surface which has a considerably higher hydrophilicity, presumably due to a higher concentration of hydroxylic groups on the surface.

Finally, the even higher hydrophobicity obtained through silylation of the fully exposed surface allows the attachment of about 25% fewer cells as compared to the surface of the unexposed resist.

The assessment of the short-term neuronal cell culture on the processed surface of standard photoresist proved that, apart from the insight into the mechanism of cell attachment, this system is not appropriate for cell patterning.

Cell attachment on negative tone image reversal photoresist

Surface functionality manipulation

It was reported that image reversal processing in the negative tone produces larger differences in bulk hydrophobicity that standard resist processing (Dammel, 1993). The negative tone image reversal photoresist surface chemistry (presented in Fig. 7, with the approximate position versus the exposure energy coordinate is an overlap of three phenomena:

- The addition of imidazole to the DNQ/novolak system does not increase its hydrophilicity due to the same hydrogen bonding mechanism present in the standard resist. Once the imidazole is released during DNQ photolysis, the contact angle decreases due to the imidazole's high hydrophilicity (log$P = -0.04$, Table 2).
- The exposure and the subsequent reversal

bake induce ICA decarboxylation (catalysed by imidazole, Reuhman-Huisken *et al.*, 1989). The indene by-product is slightly more hydrophobic than DNQ (log*P* values of 3.71 and 3.66, respectively, in Table 2), but does not hydrogen-bind the donor chemical species (imidazole and novolak).

- Finally, these two effects are superimposed on the previously detailed novolak-only chemistry (Fig. 7 presents the second possible mechanism for novolak crosslinking based on methylene bridge formation). Novolak crosslinking decreases the surface concentration of hydroxylic groups and hence should make imidazole molecularly more accessible due to the decreased likelihood of hydrogen bonding.

In image reversal systems, both positive and negative, DNQ partially decomposes due to the addition of imidazole, forming a non-bleacheable azo dye (Nicolau & Dusa, 1989), and therefore the overall chemical processes are delayed by the parasitic light absorption. One important difference of the negative tone image reversal system as compared to the standard and positive tone image reversal ones is the carboxylic-free functionalization. Similarly to the standard system, the silylation increases the surface hydrophobicity, with the difference that in the negative tone image reversal system only the novolak hydroxylic groups are available for silylation.

Cell attachment behaviour

Although the surface hydrophobicity evolution versus exposure energy in standard and negative tone imaged reversal systems looked similar, the neuronal cell attachment behaviour was entirely different, as the number of cells increases with hydrophobicity rather than hydrophilicity. This rather unexpected evolution can be explained in the frame of accessibility to imidazole which increases with exposure energy, firstly due to DNQ photolysis and ICA decarboxylation, and later due to novolak crosslinking. In this context, it is interesting to observe the slight increase in the number of cells of silyated surfaces, probably due to a further decrease of hydrogen bonding between silylated novolak hydroxylic groups and imidazole.

Due to the carboxylic-free surface functionalization, the relation between neuronal cell attachment and the dual influence of the manipulation of the surface hydrophobicity and functionalization using the negative tone image reversal system may be easier to relate with other studies regarding amino-induced hydrophilicity. In the conditions of this study, imidazole functionalization proved beneficial for cell adhesion, analogous to other studies dealing with amino-functionality-induced hydrophilization (Stenger *et al.*, 1993; Matsuzawa *et al.*, 1993; Georger *et al.*, 1992). On the other hand, in the conditions of our study, surface hydrophobicity has a contradictory influence or at best proved to be a secondary factor.

Although the increase in the average number of neuronal cells on negative tone image reversal is about three times higher than on the standard photoresist, this system fails to provide a good environment for neuronal cell patterning, as the number of attached cells is again far from those on the control surface.

Cell attachment on positive tone image reversal photoresist

Surface functionality manipulation

In the case of positive tone image reversal, the absence of the post-exposure reversal bake allows accumulation of the carboxylic groups with exposure in a similar manner to the standard positive tone photochemistry, and at the same time, the increase in accessibility to imidazole as in the negative tone image reversal. The overall hydrophobicity evolution versus exposure energy is then similar to the previous two systems. However, the most important feature of positive tone image reversal is the creation of a coloured complex at low exposure energies (Nicolau & Dusa, 1989). This complex is stable in the dark, but decomposes further when exposed. A recently proposed mechanism (Nicolau *et al.*, 1995) explains this feature through the creation of a pair of positively and negatively charged (indenyl$\ominus$-imidazolyl$\oplus$) chemical species, similar to the mechanism proposed (Mutsaers *et al.*, 1990) for the less stable, ammonia based coloured complex encountered in the built-in-mask technique. The overall photochemistry of the positive tone image reversal photoresist with the approximate position versus the exposure energy coordinate is presented in Fig. 8.

Cell attachment behaviour

The neuronal cell adhesion behaviour on a positive tone image reversal system (with the important exception of the low energy exposed system) may be explained by the overlap of the chemical functionalization valid for the positive standard and negative tone image reversal systems respectively, i.e. imidazole-, carboxylic-, and to a lesser extent hydroxylic-induced cell adhesion mechanism. The higher overall number of cells on positive tone image reversal resist, as compared with the negative one, is explained by the possible bake-induced residual crosslinking of the negative tone image reversal resist surface. Moreover, the cell adhesion behaviour seems to be in good agreement with the surface hydrophilicity evolution, being opposed to the evolution of the number of cells versus hydrophilicity in negative tone image reversal.

The most striking feature of the positive tone image reversal case is the high number of neuronal cells on the polymer surface when exposed at low energies (second column on the third row in Table 1). This feature can be explained by the formation of doubly charged chemical species in the first stages of the exposure, with a beneficial effect on cell adhesion, presumably due to the formation of an electrostatic double-layer between the cell membrane and resist surface. To this end, an optimum of short-term neuronal cell attachment can be found in positive tone image reversal mode systems, for low energy exposure.

A class of its own was the case of neuronal cells attached to positive tone image reversal surfaces which peeled off accidentally from the glass substrate (fifth row in Table 1). The extremely large number of neuronal cells can be explained by the lack of mechanical stress in the polymer floating surfaces, as opposed to fixed-on-the-substrate ones. A similar behaviour was reported and explained by other authors (Emerman & Pitelka, 1977) for mammalian cells on free-standing polymer surfaces. Proper treatment of the glass surface prior to deposition and appropriate pre-exposure bake eliminated the peeling-off effect.

Factors controlling neuronal cell attachment on photoresist surfaces

In the conditions of this study it was found that short-term culture neuronal cell attachment is, in order of importance controlled by: presence of doubly charged chemical species; chemical functionalization with imidazole, carboxylic and hydroxylic groups (in that order); and for the variations found in this study (i.e. ±10° for the contact angle), surface hydrophilicity has a contradictory contribution or a very limited one.

From a similar state of the cells in the short-term culture and in other common conditions (e.g. Tokioka *et al.*, 1993), we conclude that the toxicity of the surfaces is insignificant for cell survivability. Since in the conditions of the short-term, one-day culture all neuronal cells seem to survive irrespective of the surface conditions, we conclude that the survivability of the cells may be further controlled in the long term by their adhesion to the polymeric surface.

Experiments for patterning neuronal cells

The assessment of the capability of the positive tone image reversal surface exposed at low energy to accommodate long-term neuronal cell culture showed (Fig. 3) healthy cells and neurite growth promotion over the period of the culture, which is similar to other common culture media conditions (e.g. Tokioka *et al.*, 1993). One major difference between a long-term culture and short-term one is that the former contains neuronal as well as glia cells.

Following this assessment, the positive tone image reversal photoresist surface exposed at low energy was used to confine the long-term culture neuronal cells. As contrast surfaces, either hydrophobic or hydrophilic glass substrates were presented to the neuronal cells through development of the previously patterned areas.

The neuronal cells seem to be repelled by the highly hydropholic glass substrates presented to the culture through the development of the previously exposed areas (30° as compared with 60–80° for the processed photoresist surface), but can attach directly to the resist surface (in Fig. 4(a), upper right corner). Glia cells on the other hand, do not distinguish to the same degree the different functionalized surfaces, and they may migrate from the resist surface to the hydrophilic glass one (Fig. 4(a), middle left). Still, one can see the alignment of glia cells along the edges of the resist surface (Fig. 4(a), middle right and top end corner). Only if glia cells form a continuum on the highly hydrophilic glass, the neuronal cells may attach to this primary layer (as in Fig. 4(b), top left).

When exposed to hydrophobic glass areas (Fig. 5), glia cells attach indiscriminately onto the surfaces, but neuronal cells still prefer to attach either on the resist (middle bottom in Fig. 5) or, to a lesser extent, on a continuum of glia cells (right top in Fig. 5). The lack of discrimination for glia cell attachment can be connected with the smaller hydrophobicity difference between the resist and hydrophobic glass (average contact angle values of 70° and 90°, respectively) as compared with higher difference for the resist and hydrophilic glass surfaces (average contact angle values of 70° and 30°, respectively). This suggests a different attachment mechanism for glia and neuronal cells, that is, a higher influence of hydrophilicity on glia cells attachment and a more specific influence of chemical functionalization on neuronal cell attachment.

Further experimental studies

Although the chemistry of the DNQ/novolak system received an extended treatment in the literature, some aspects of its surface chemistry need further clarification, especially for the surface functionalization-induced cell engineering. ATR and ESCA spectroscopy studies of the functionalization of the resist surface are currently being pursued.

The chemical versatility of DNQ may allow many other functionalization pathways not explored in the present contribution. The photoinduced reaction ketene, carboxylic group creation and the possible reduction of DNQ to an amino group, may be used as post-exposure functionalization of the resist surface. In particular, our research (Nicolau *et al.*, 1996) proved that the photoinduced production of ketene and carboxylic groups can be used successfully as anchoring sites for linking the amino acid of the bioactive molecules. In this frame, another group of experiments target the potential of the DNQ/novolak system for patterning neuro-peptides which can induce different attachment behaviour of the neuronal and glia cells, respectively (Taguchi *et al.*, 1995).

CONCLUSION

Common microlithographic materials and techniques have been assessed in terms of their potential for patterning of the neuronal cells. The cell attachment is controlled by surface physicochemical properties, mostly by the charged/uncharged species balance and type of chemical functionalization (DNQ, carboxylic, imidazole, hydroxylic, indene and silylated groups), whereas the hydrophilic/hydrophobic balance of the resist surface has a contradictory or at best secondary influence.

The microlithographic techniques assessed (standard positive tone, negative and positive tone image reversal, and silylation) can be used to gain insight into the cell attachment mechanisms. The most suitable surface functionality was obtained using low exposed DNQ/novolak imidazole-doped polymer films, making positive tone image reversal photoresist the best candidate for neuronal cell patterning.

REFERENCES

Aizawa, M., Haruyama, T., Kham, G. F., Kobatake, E.& Ikaryiama, Y. (1994). Electronically modulated biological functions of molecular interfaced enzymes and living cells. *Biosensors & Bioelectronics,* **9**, 601–610.

Aplin, J. D. & Hughes, R. C. (1981). Protein derivatised glass coverslips for the study of cell-to-substratum adhesion. *Anal. Biochem.,* **113**, 144–148.

Babb, C. W., Coon, D. R. & Rechnitz, G. A. (1995). Biomagnetic neurosensors. 3. Nonivasive sensors using magnetic stimulation and biomagnetic detection. *Anal. Chem.,* **67**, 763–769.

Bekos, E. J., Ranieri, J. P., Aebisher, P., Gardela, Jr, J. A. & Bright, F. V. (1995). Structural changes of bovine serum albumin upon adsorption to modified fluoropolymer substrates used for neuronal cell attachment studies. *Langmuir,* **11**, 984–989.

Ben-Ze'ev, A., Robinson, G. S., Bucher, N. L. R. & Farmer, S. R. (1988). Cell–cell and cell–matrix interactions differentially regulate the expression of hepatic and cytoskeletal genes in primary cultures of rat hepatocytes. *Proc. Natl. Acad. Sci.,* **85**, 2163–2165.

Britland, S., Perez-Arnaud, E., Clark, P., McGinn, G., Connolly, P. & Moores, G. (1992a). Micropatterning proteins and synthetic peptides on solid supports: a novel application for microelectronics fabrication technology. *Biotechnol, Prog.,* **81**, 155–160.

Britland, S., Clark, P., Connolly, P. & Moores, G. (1992b). Micropatterned substratum adhesivness: a model for morphogenetic cues controlling cell behaviour. *Exp. Cell Res.,* **198**, 124–129.

Clark, P. (1994). Cell behaviour on micropatterned surfaces. *Biosensors & Bioelectronics,* **9**, 657–661.

Clark, P., Britland, S. & Connolly, P. (1993). Growth cone guidance and neuron morphology on micropatterned laminin surfaces. *J. Cell Sci.,* **105**, 203–212.

Clark, P., Connolly, P. & Moores, G. R. (1992). Cell guidance by micropatterned adhesivness *in vitro*. *J. Cell Sci.,* **103**, 287–292.

Connolly, P., Clark, P., Curtis, A. S. G., Dow,

J. A. T. & Wilkinson, C. D. W. (1990). An extracellular microelectrode array for monitoring electrogenic cells in culture. *Biosensors & Bioelectronics,* **5**, 223–234.

Dammel, R. (1993). *Diazonaphthoquinone-based Resists.* SPIE Optical Engineering Press, Bellingham, Washington.

Dulcey, C. S., Georges, J. M. J., Krauthamer, V., Stenger, D. A., Fare, T. L. & Calvert, J. M. (1991). Deep UV photochemistry of chemisorbed monolayers: Patterned coplanar molecular assemblies. *Science,* **252**, 551–554.

Emerman, J. T. & Pietlka, D. R. (1977). Maintenance and induction of morphological differentiation in dissociated mammary epithelium on floating collagen membranes. *In Vitro,* **13**, 316–327.

Ershov, V. V., Nikiforov, G. A. & de Jonge, C. R. H. I. (1981). *Quinone Diazides.* Elsevier, Amsterdam.

Ferreira, M., Cheung, J. H. & Rubner, M. F. (1994). Molecular self-assembly of conjugated polyions: a new process for fabricating multilayer thin film heterostructures. *Thin Solid Films,* **244**, 806–809.

Folkman, J. & Moscona, A. (1978). Role of cell shape in growth control. *Nature,* 273, 345–349.

Fromherz, P., & Muller, C. O. (1994). Cable properties of a straight neurite of a leech neuron probed by a voltage-sensitive dye. *Proc. Natl. Acad. Sci.,* **91**, 4604.

Fromherz, P., Muller, C. O. and Weis, R. (1993). Neuron transistor: electrical transfer function measured by the patch-clamp technique. *Phys. Rev. Lett.,* **71**, 4079–4082.

Fromherz, P., Offenhausser, A., Vetter, T. & Weis, J. A. (1991). Neuron-silicon junction: a Retzius cell of the leech on an insulated-gate field-effect transistor. *Science,* **252**, 1290–1293.

Georger, Jr, J. H., Stenger, D. A., Rudolph, A. S., Hickman, J. J. Dulcey, C. S. & Fare, T. L. (1992). Coplanar patterns of self-assembled monolayers for selective cell adhesion and outgrowth. *Thin Solid Films,* **210/211**, 716–719.

Gopel, W. (1995). Controlled signal transduction across interfaces of 'intelligent' molecular systems. *Biosensors & Bioelectronics,* **10**, 35–59.

Gross, G. W., Rhoades, B. K., Azzazy, H. M. E. & Wu, M.-C. (1995). The use of neuronal networks on multielectrode arrays as biosensors. *Biosensors & Bioelectronics,* **10**, 553–567.

Gross, G. W., Rhoades, B. K., Reust, D. L. & Schwalm, F. U. (1993). Stimulation of monolayer networks in culture through thin-flim indium-tin oxide recording electrodes. *J. Neurosci. Meth,* **50**, 131–143.

Gross, G. W., Wen, W. Y. & Lin, J. W. (1985). Transparent indium-tin oxide electrode patterns for extracellular, multisite recording in neuronal cultures. *J. Neurosci. Meth.,* **15**, 243–252.

Gross, G. W., Williams, A. N. & Lukas, J. H. (1982). Recording of spontaneous activity with photoetched microlectrode surfaces from mouse spinal neurons in culture. *J. Neurosci. Meth.,* **5**, 13–22.

Gross, G. W. & Schwalm, F. U. (1994). A closed flow chamber for long-term multichannel recording and optical monitoring. *J. Neurosci. Meth.,* **52**, 73–85.

HyperChem^{TM}, Ver. 4 for Windows (1995). HyperCube, Inc., Ontario.

Ingber, D. E. (1990). Fibronectin controls capillary endothelial cell growth by modulating cell shape. *Proc. Natl. Acad. Sci.,* **87**, 3579–3583.

Ingber, D. E. & Folkman, J. (1989). Mechanochemical switching between growth and differentiation during fibroblast growth factor-stimulated angiogenesis in vitro: role of extracellular matrix. *J. Cell Biol.,* **109**, 317–330.

Ingber, D. E., Madri, J. A. & Folkman, J. (1987). Endothelial growth factors and extracellular matrix regulate DNA synthesis through modulation of cell and nuclear expansion. *In Vitro Cellular Devl. Biol.* **23**, 387–394.

Ito, H., Tagawa, S. & Horie, K. (eds) (1994). Polymeric materials for microelectronic applications. Science and Technology. In: *ACS Symposium Series,* Vol. 579. American Chemical Society, Washington, DC.

Jimbo, Y. & Kawana, A. (1992). Electrical simulation and recording from cultured neurons using a planar electrode array. *Biochemistry and Bioenergetics,* **29**, 193–204.

Kleinfeld, K. D., Kahler, K. H. & Hockberger, P. E. (1988). Controlled outgrowth of dissociated neurons on patterned substrate. *J. Neurosci.,* **8**, 4098–4107.

Koshiba, M., Murata, M., Matsui, M. & Harita, Y. (1988). Dissolution inhibition mechanisms of naphthoquinone diazides. *Polym. Eng. Sci.,* **29**, 916–919.

Letourneau, P. C. (1975). Cell-to-substratum adhesion and guidance of axonal elongation. *Dev. Biol.* **44**, 92–101.

Li, L. M., Aggeler, J., Farson, D. A., Hatier, C., Hassel, J. & Bissel, M. J. (1987). Influence of a reconstituted basement membrane and its components on casein gene expression and secretion in mouse mammary epithelial cells. *Proc. Natl. Acad. Sci.,* **84**, 136–140.

MacDonald, S. A., Wilson, C. G. & Frechet, J. M. J. (1994). Chemical amplification in high-resolution imaging systems. *Acc. Chem. Res.,* **27**, 151–158.

Matsuda, M. & Sugawara, T., (1995) Development of a novel protein fixation method with micron-order precision. *Langmuir,* **11**, 2267–2271.

Matsuda, T., Sugawara, T. & Inoue, K. (1992). Two-dimensional cell manipulation technology. Artificial neuronal circuit based on surface microphotoprocessing. *ASAIO Trans.,* **38**, 243–247.

Matsuzawa, M., Potember, R. S., Stenger, D. A. &

Krauthamer, V. (1993). Containment and growth of neuroblastoma cells on chemically patterned substrates. *J. Neurosci. Meth.*, **50**, 253–260.

Meister, W., Wong, R. O. L., Baylor, D. A. & Shatz, C. J. (1991). Synchronous bursts of action potentials in ganglion cells of the developing mammalian retina. *Science*, **252**, 939–943.

Mochitate, K., Pawelek, P. & Grinnel, F. (1991). Stress relaxation of contracted collagen gels: disruption of actin filament bundles, release of cell surface fibronectin, and down regulation of DNA and protein synthesis. *Exp. Cell Res.*, **193**, 198–207.

Mooney, D., Hansen, L., Vacanti, J., Langer, R., Farmer, S. & Ingber, D. (1992). Switching from differentiation to growth in hepatocytes: control by extracellular matrix. *J. Cell. Physiol.*, **15**, 497–505.

Mutsaers, C. M. J., Vollenbroek, F. A., Nijssen, W. P. M. & Visser, R. J. (1990). ImRe, BIM and SUPER using patternwise esterification. *Microelectronic Eng.*, **11**, 497–500.

Nicolau, D. V. & Dusa, M. (1989). The application of the in-situ dyeing effect to an image reversal resist. *Microelectronic Eng.*, **11**, 589–592.

Nicolau, D. V., Dusa, M., Nicolau, D. & Yoshikawa, S. (1995). Nonstandard bleaching behaviour in DNQ systems. Mechanism and lithographic consequences. *J. Photopol. Sci. Tech.*, **8**., 187–194.

Nicolau, D. V., Taguchi, T., Yoshikawa, S. & Dusa, M. V. (1996). Application of DNQ-based microlithography to patterning bioactive molecules/cells. In: *Advances in Resist Technology and Processing XIII*, R. R. Kunz, (ed.). *SPIE Proc.* **2724**, 500–511.

Nicolini, C. (1995). From neural chip and engineered biomolecules to bioelectronic devices: an overview. *Biosensors & Bioelectronics*, **10**, 105–127.

Nisch, W., Bock, J., Egert, U., Hammerle, H. & Mohr, A. (1994). A thin film microelectrode array for monitoring extracellular neuronal activity *in vitro*. *Biosensors & Bioelectronics*, **9**, 737–741.

Regehr, W. G., Chien, C.-B., Kramer, T. J., Crank, D. W., Rutledge, D. B. & Pine, J. (1988). Progress in long-term electrical connections to cultured neurons using integated circuit technology. *IEEE Proc. Conf. Synthetic Microstructures*, pp. 1–20.

Reichmanis, E. & Thomson, L. F. (1989). Polymeric materials for microlithography. *Chem. Rev.*, **89**, 1273–1289.

Reiser, A. (1989). *Photoreactive Polymers: The Science and Technology of Resists.* John Wiley, New York.

Reuhman-Huisken, M. E., Mutsaers, C. M. J., Vollenbroek, F. A. & Moonen, J. A. H. M. (1989). Toward an optimized image reversal process for half micron lithography. *Microelectron Eng.*, **9**, 551–554.

Rutten, W. L. C., Freiswijk, T. A., Smit, J. P. A., Rozijn, T. H. & Meier, J. H. (1995). 3D neuro-electronic interface devices for neuromuscular control: design studies and realisation steps. *Biosensors & Bioelectronics*, **10**, 141–153.

Singhvi, R., Kumar, A., Lopez, G. P., Stephanopoulos, G. N., Wang, D. I. C., Whitesides, G. M. & Ingber, D. E. (1994). Engineering cell shape and function. *Science*, **264**, 696–698.

Stenger, D. A., Georger, J. H., Dulcey, C. S., Hickman, J. J., Rudolph, A. S., Nielsen, T. B., McCort, M. S. & Calvert, M. J. (1992). Coplanar molecular assemblies of amino-perfluorinated alkilsilanes: characterization and geometric definition of mammalian cell adhesion and growth. *J. Am. Chem. Soc.*, **114**, 8435–8442.

Stenger, D. A., Pike, C. J., Hickman, J. J. & Cotman, C. W. (1993). Surface determinants of neuronal survival and growth on self-assembled monolayers in culture. *Brain Res.*, **630**, 136–147.

Sugawara, T. & Matsuda, T. (1995). Photochemical surface derivatization of a peptide containing Ardg-Gly-Asp (RGD). *J. Biomed. Mater.*, **29**, 1047–1052.

Taguchi, T., Bo, X. X., Taniguchi, H., Kyosue, K., Kodoh, S., Yumoto, N., Yamamoto, H., Kasai, M. & Yoshikawa, S. (1995). Analysis of synaptogenesis in vitro by peptides relating to cell adhesion. In: *Peptide Chemistry, 1994*, M. Ohno (ed). Protein Research Foundation, pp. 145–148.

Taguchi, T., Huchet, M., Roa, M., Changeau, J.-P. & Hendersen, C. E. (1987). A subpopulation of embrionic telencephalic neurons survive and develop in vitro in response to factors derived from the periphery. *Devl. Brain Res.*, **37**, 125–132.

Tokioka, R., Matsuo, A., Kiyosue, K., Kasai, M. & Taguchi, T. (1993). Synapse formation in dissociated cell cultures of embryonic chick cerebral neurons. *Devl. Brain Res.*, **74**, 146–150.

Ueda-Yukoshi, T. & Matsuda, T. (1995). Cellular responses on a wettability gradient surface with continuous variations in surface compositions of carbonate and hydroxyl groups. *Langmuir*, **11**, 4135–4140.

Viswanadhan, V. N., Ghose, A. K., Revankar, G. N. & Robins, R. K. (1989). *J. Chem. Inf. Comput. Sci.*, **29**, 163.

Wijeseriya, D. C. & Rechnitz, G. A. (1993). Biosensors based on plant and animal tissues. *Biosensors & Bioelectronics*, **8**, 155–160.

Willson, C. G. (1994). *Introduction to Microlithography*, 2nd Edn, L. F. Thomson, C. G. Willson, M. J. Bowden (eds.). American Chemical Society, Washington, DC, pp. 139–268.

Yavin, E. & Yavin, Z. (1974). Attachment and culture of dissociated cells from rat embryo cerebral hemispheres on polylysine-coated surface. *J. Cell Biol.*, **62**, 540–546.

Ye, T. & McKervey, M. A. (1994). Organic synthesis with α-diazocarbonyl compounds. *Chem. Rev.*, **94**, 1091–1160.

8.

BIOCHEMICAL AND BIOPHYSICAL RESEARCH COMMUNICATIONS 227, 688–693 (1996)
ARTICLE NO. 1570

Solid-Phase Synthesis of Caged Peptides Using Tyrosine Modified with a Photocleavable Protecting Group: Application to the Synthesis of Caged Neuropeptide Y

Yoshiro Tatsu,[1] Yasushi Shigeri,[1] Shinji Sogabe, Noboru Yumoto, and Susumu Yoshikawa

Osaka National Research Institute, AIST, Midorigaoka, Ikeda, Osaka 563, Japan

Received September 17, 1996

A simple method for the synthesis of caged peptides using a novel derivative of tyrosine, *N*-Fmoc-*O*-(2-nitrobenzyl)-tyrosine, is described. The derivative of tyrosine can be incorporated at any position in an amino acid sequence by solid-phase peptide synthesis under the condition for Fmoc chemistry, and caged peptides that contain nitrobenzyl group on the side chain of tyrosine residue can be obtained. The nitrobenzyl group can be photocleaved by UV irradiation and the half life of the intermediate during photolysis is approximately 7 μs. The method was successfully applied to the synthesis of caged neuropeptide Y (NPY). The binding affinity of the caged NPY for the Y1 receptor was one or two orders of magnitude lower than that of intact NPY, but it increased to the value for intact NPY upon irradiation by UV light. © 1996 Academic Press, Inc.

Caged compounds are defined as molecules whose biological activity is controlled by light (1). In studies of fast and/or local biological processes, such as those in muscles and neurons, caged compounds appear to have great potential because illumination can easily be controlled in terms of timing, location and amplitude. Although the term caged implies the total imprisonment of an active molecule inside a large framework, modification of a molecule with photocleavable groups, such as the *o*-nitrobenzyl group, which masks features that are important for biological recognition, is the usual strategy for the synthesis of caged compounds. Most caged compounds reported to date are small molecules, such as caged ATP (2), caged glutamic acid (3), and caged serine (4). There are many natural and synthetic peptides that regulate important biological processes, and the use of caged peptides is expected to yield new information about the spatial range of their actions. However, no efficient method for the synthesis of caged peptides has yet been reported. Preparation of caged peptides and proteins by the chemical modification of amino or carboxyl groups with nitrobenzyl reagents has been reported (5, 6), but when this method is used, it is not possible to control the position and number of modifications. Schultz and coworkers reported a genetic method, using a cell-free translation system, for construction of caged proteins. Caged amino acids were incorporated at a desired site in the amino acid sequence by an amber suppressor tRNA (7). However, it is very difficult to prepare large quantities of caged peptides and proteins in a cell-free translation system.

Here we report a simple approach to the synthesis of caged peptides by Fmoc solid-phase peptide synthesis using a photolabile derivative of tyrosine, which can be incorporated at any

---

[1] To whom correspondence may be addressed. Fax: (+81)-727-51-9628. E-mail: tatsu@onri.go.jp or shigeri@onri.go.jp.

Abbreviations: NPY, neuropeptide Y; AII, angiotensin II; PYY, peptide YY; Tyr(NB), *O*-(2-nitrobenzyl)-tyrosine; Fmoc-Tyr(NB), *N*-(fluorenylmethoxycarbonyl)-*O*-(2-nitrobenzyl)-tyrosine; Fmoc-Tyr(tBu), *N*-(fluorenylmethoxycarbonyl)-*O*-(*t*-butyl)-tyrosine.

0006-291X/96 $18.00
Copyright © 1996 by Academic Press, Inc.
All rights of reproduction in any form reserved.

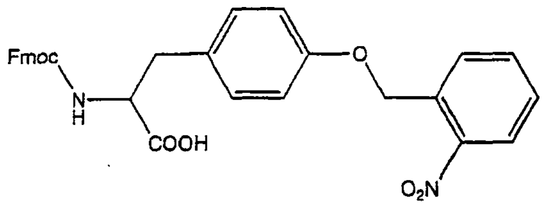

FIG. 1. Fmoc-Tyr(NB).

site in a peptide, and we also demonstrate the effect of caging on the biological activity of neuropeptide Y (NPY) in which the derivative had been incorporated at several sites.

MATERIALS AND METHODS

Materials. L-Tyrosine, 2-nitrobenzylbromide, and fluorenylmethy-succinimidyl carbonate (Fmoc-OSu) were obtained from Tokyo Kasei (Tokyo, Japan), Aldrich, and Kokusan Kagaku (Tokyo, Japan), respectively. Porcine NPY was from the Peptide Institute (Osaka, Japan). Fmoc-amino acids and TentaGel TG-RAM resin were obtained from Shimadzu Co. (Kyoto, Japan). [^{125}I]Peptide YY (PYY) was purchased from Dupont-New England Nuclear (Wilmington, USA). All the other chemicals used were of reagent grade.

Synthesis of nitrobenzyl tyrosine. The derivatives of tyrosine were synthesized as follows. *O*-(2-Nitrobenzyl)-tyrosine [Tyr(NB)] was obtained from the reaction of 2-nitrobenzylbromide with a Cu(II) complex of tyrosine, by reference to the synthesis of dichlorobenzyl tyrosine (8). Nitrobenzyl tyrosine was then made to react with Fmoc-OSu to yield Fmoc-Tyr(NB) (Fig. 1). Full details of the synthesis will be reported elsewhere.

Synthesis of peptide. Caged peptides were synthesized on an automated solid-phase peptide synthesizer (PSSM-8; Shimadzu) and cleaved from the resin by treatment with trifluoroacetic acid (TFA). Crude peptides were purified by semi-preparative HPLC (20 mm × 250 mm; Cosmosil 5C18; Nacalai tesque, Kyoto, Japan) with a gradient phase of 0.1% TFA and acetonitrile. In the case of fractions that contained peptides, the eluate was not passed through the UV monitor to avoid photolysis. The collected peptide was examined by analytical HPLC (4.6 mm × 50mm; ; Cosmosil 5C18; Nacalai tesque) and mass spectrometry (MALDI TOF mass spectrometer; Kratos, Manchester, UK).

Analysis of products of photolysis. The solution of a caged compound was irradiated with a UV lamp (PU-2; Topcon, Japan) and the products were examined by HPLC. Laser flash photolysis was performed as follows. A solution of sample in a quartz cell was irradiated with the third harmonic light pulse of a Nd:YAG laser (GCR-230-10; Spectra Physics, Mountain View CA; FWHM 5 ns; 6.8 mJ). The transient absorption during the laser irradiation was measured with a photomultiplier tube and the monochromatic light from a 500 W xenon lamp.

Study of the binding of NPY to the Y1 receptor. The study of the binding of NPY to the Y1 receptor was performed as described previously (9) with minor modifications. [^{125}I]PYY was used as the radioligand for the receptor instead of [^{125}I]NPY because of the reduced nonspecific binding. SK-N-MC cells were cultured in 12-well culture plates. After 2 to 4 days, the medium was removed and the cells were washed with 20 mM HEPES buffered Hanks' solution (pH 7.4) that contained 1% BSA (binding buffer) and incubated with 0.1 nM [^{125}I]PYY and the appropriate competing peptide or vehicle in 0.5 ml of binding buffer for 60 min at 37°C. The incubation was stopped by removal of the assay mixture and then the cells were washed twice with 1 ml of ice-cold binding buffer. Cells were lysed by two aliquots of 0.75 ml of 1 N NaOH. The solubilized cells were transferred to test tubes and radioactivity was determined with a γ counter. Nonspecific binding was determined in the presence of 10^{-6} M NPY.

RESULTS

Solid-Phase Synthesis of Peptides That Contained Nitrobenzyl Tyrosine

The stability of the *o*-nitrobenzyl group in the reagents for solid-phase synthesis of peptide was examined first. Trifluoroacetic acid (100%) and piperidine (20% in dimethylformamide) were added to Fmoc-Tyr(NB) and to Tyr(NB), respectively, and analysis by HPLC indicated that the nitrobenzyl group was not removed under the experimental conditions used for the Fmoc solid-phase synthesis of peptides (data not shown).

Fmoc-Tyr(NB) was then used for the synthesis of nitrobenzyl NPY and nitrobenzyl angiotensin II (AII), in the same manner as the standard reagent for introduction of Tyr, namely, Fmoc-Tyr(tBu). The solid lines in Figure 2 show the elution of crude products of the synthesis of nitrobenzyl NPY. A dominant peak, with no significant by-products, can be seen in each

167

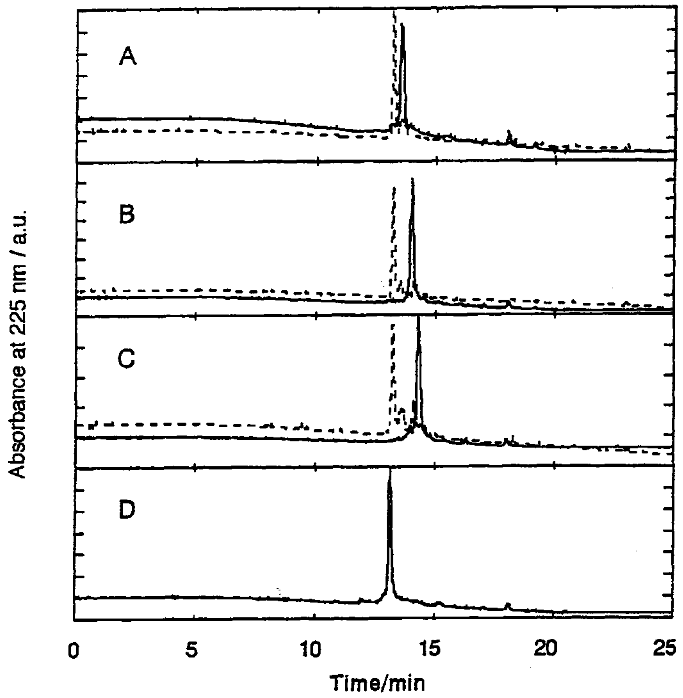

FIG. 2. Results of HPLC of synthetic nitrobenzyl NPYs and the products of photolysis. The elution of crude nitrobenzyl peptides, after cleavage, was monitored after reversed-phase HPLC with a UV detector at 225 nm. Peptides were eluted with a linear gradient of 0.1% trifluoroacetic acid to 80% acetonitrile at 5%/min (solid lines). The purified nitrobenzyl NPYs were irradiated with UV light for 90 min and analyzed under the same conditions (dashed lines). The chromatograms A, B, C, and D were obtained after HPLC of [Tyr(NB)^{1}]NPY, [Tyr(NB)^{36}]NPY, [Tyr(NB)^{1,36}]NPY, and NPY, respectively, and the products of photolysis (except in D).

chromatogram. The purified peptide was identified by mass spectrometry and the molecular weight of the purified peptides agreed with the calculated values within the range of acceptable errors of mass spectrometry: [Tyr(NB)^{1}]NPY, observed 4,391, calculated 4,387; [Tyr(NB)^{36}]-NPY, observed 4,390, calculated 4,387; [Tyr(NB)^{1,36}]NPY, observed 4,520, calculated 4,522; and [Tyr(NB)^{4}]AII, observed 1,183 calculated 1,181. A small peak, assigned to the intact peptide, was also detected in the spectra of the purified nitrobenzyl peptides since the nitrobenzyl group had been partially removed by photolysis during the laser ionization (data not shown).

Photolysis of Nitrobenzyl Groups in Peptides

The photocleavage of the *o*-nitrobenzyl group from Fmoc-Tyr(NB) was first analyzed by HPLC. UV-irradiation caused a decrease in the amount of the Fmoc-Tyr(NB) and the generation of Fmoc-Tyr, which was identified from a comparison with the authentic sample.

The photocleavage of the nitrobenzyl group from peptides was examined next. The UV irradiation caused a decrease in the size of the peak of each nitrobenzyl peptide and the appearance of a peak that could be assigned to the intact NPY (dashed lines in Fig. 2). Small peaks were ascribable to molecules in which there remained one or two nitrobenzyl groups. The evidence for photocleavage of the nitrobenzyl group was also supported by the results of mass spectrometry: the intensity of the peak that corresponded to intact NPY increased after UV irradiation. The results of HPLC and mass spectrometry suggested that no significant side reactions had occurred.

The kinetics of the photocleavage of [Tyr(NB)^{1,36}]NPY were studied by measurements of the transient absorption (Fig. 3). Pulsed UV light caused a rapid increase and a slow decay in the absorption at 420 nm, which could be ascribed to the formation of a *aci*-nitro compound as an intermediate. The half life of the intermediate during photolysis was 6.5 ± 0.9 μs.

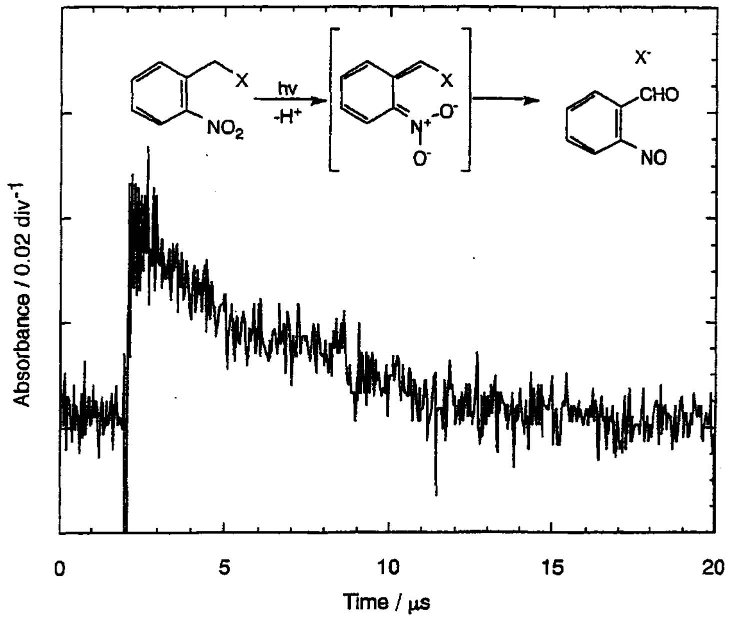

FIG. 3. Changes in absorption of the nitrobenzyl NPY caused by a pulse of UV light. $[Tyr(NB)^{1,36}]$NPY (2.7 mM) in 5 mM TES buffer (pH 7.5) at 23°C was irradiated with the third-harmonic of a Nd:YAG laser. The average of results from 10 experiments is shown. The half life of the absorbing species was calculated to be 6.5 ± 0.9 µs. The inset shows the reaction scheme of the photolysis, where X represents the peptide.

Photo-Control of Biological Activity

We next examined the effects of nitrobenzyl groups on biological activity, namely, the ability of nitrobenzyl NPY to inhibit binding of $[^{125}I]$PYY to Y1 receptors in SK-N-MC cells. Intact NPY inhibited the specific binding of $[^{125}I]$PYY very effectively (IC_{50} value for NPY, 2.0 ± 0.2 nM; open squares in Fig. 4A). Protection of the hydroxyl group of the *N*-terminal or *C*-terminal tyrosine of NPY by a nitrobenzyl group resulted in a significant loss of binding affinity (IC_{50} values for $[Tyr(NB)^1]$NPY and $[Tyr(NB)^{36}]$NPY, 100 ± 10 nM and 55 ± 5 nM,

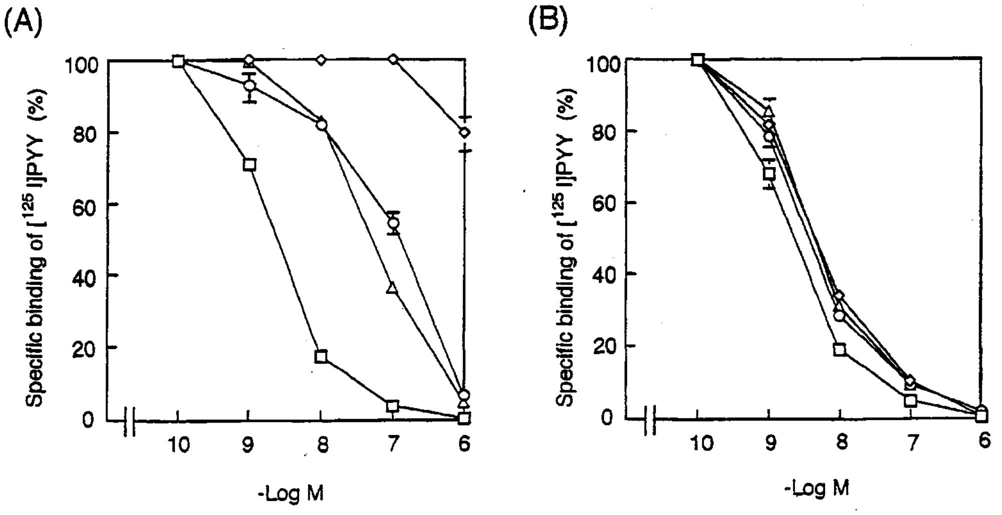

FIG. 4. Effects of nitrobenzyl NPYs (A) and UV-irradiated nitrobenzyl NPYs (B) on the binding of $[^{125}I]$ PYY to the Yl receptor. SK-N-MC cells were incubated for 60 min at 37°C with $[^{125}I]$ PYY and nitrobenzyl NPY, after or without previous irradiation with UV for 90 min. The panels show the results of one representative experiment, which was repeated three times. (□) NPY; (△) $[Tyr(NB)^1]$NPY; (○) $[Tyr(NB)^{36}]$NPY; (◇) $[Tyr(NB)^{1,36}]$NPY.

respectively; mean ± S.E., n = 3). Bisnitrobenzyl NPY, [Tyr(NB)^{1,36}]NPY, even when present at 1 μM, reduced the binding of [^{125}I]PYY by 20% (Fig. 4A). UV irradiation of the nitrobenzyl derivatives of NPY resulted in the recovery of the ability to inhibit the binding of [^{125}I]PYY to the same level as that of intact NPY (Fig. 4B).

We also examined the effect of a nitrobenzyl group on the biological activity of angiotensin II by measuring the inhibition of the binding of [^{125}I]AII to AII receptors in human neuroblastoma SMS-KAN cells (10). However, the protection of the hydroxyl group of tyrosine by a nitrobenzyl group had no effect in the inhibition (data not shown).

DISCUSSION

In this study, a photolabile benzyl group, namely, *o*-nitrobenzyl group, was successfully introduced at the hydroxyl group of tyrosine residues in NPY and AII. It was easy to purify the nitrobenzyl peptides and the yield of nitrobenzyl peptides was as high as that of unmodified peptides. Moreover, the nitrobenzyl peptides eluted later than the unmodified peptides in all cases that we have examined. The latter property is probably due to the hydrophobicity of the nitrobenzyl group.

The nitrobenzyl groups were photocleaved from peptides by UV irradiation without any dependence on position, and the unmodified peptides were generated from the nitrobenzyl peptides. The half life of approximately 7 μs was as high as that for the *o*-nitrobenzyl-type compounds reported to date (1). The rapid release of the intact peptide by photolysis allows experiments with higher time-resolution than those that involve perfusion or pipette injection.

NPY is a 36-amino acid peptide containing five tyrosine residues, which are at the *N*- and *C*-termini and at positions 20, 21 and 27. Studies on the relationship between structure and activity have indicated the possibility that both the *N*-terminal and the *C*-terminal segments of NPY are essential for the activation of Y1 receptors (11). Therefore, we introduced *o*-nitrobenzyl tyrosine into *N*-terminal and/or *C*-terminal tyrosine residues of NPY in order to control its biological activity. The introduction of a nitrobenzyl group at *N*- or *C*-terminal tyrosine residues reduced the activity by about one order of magnitude. The extent of the reduction was almost same for both termini, and an additive effect was observed upon the introduction of nitrobenzyl groups at both termini, supporting the hypothetical model. The restoration of inhibitiory activity in binding assay by UV irradiation showed clearly that the nitrobenzyl group acted as a cage for the biological activity of NPY. Thus, nitrobenzyl NPY can be used as a photolabile precursor of NPY, namely, caged NPY. By contrast, the nitrobenzyl group did not act as a cage for AII, in spite of the larger volume fraction of the nitrobenzyl group in this small, eight-residue, peptide. This result indicates that the tyrosine residue is not involved in binding to the receptor. Thus, nitrobenzyl groups must be introduced at appropriate sites in a peptide that are essential for biological activity if a caged peptide is to be synthesized.

In conclusion, we developed a simple method for the solid-phase synthesis of caged peptides. The biological activity, as well as the chemical structure, of the caged peptides can be controlled by UV irradiation. The temporally and spatially controlled release of intact peptides by UV irradiation provides a versatile tool for studies of biological phenomena (12). We are currently preparing photolabile derivatives of other amino acids to extend this method to other types of side chain.

ACKNOWLEDGMENTS

The authors thank Dr. Keiko Tawa for use of the instrument for flash photolysis and Mses Makiko Nakayama and Yuri Kobayashi for typing the manuscript.

REFERENCES

1. Adams, S. R., and Tsien, R. Y. (1993) *Annu. Rev. Physiol.* **55**, 755–784.
2. Kaplan, J. H., Forbush, B., and Hoffman, J. F. (1978) *Biochemistry* **17**, 1929–1935.

170

3. Wilcox, M., Viola, R. W., Johnson, K. W., Billington, A. P., Carpenter, B. K., McCray, J. A., Gzuikowski, A. P., and Hess, G. P. (1990) *J. Org. Chem.* **55,** 1585–1589.
4. Pirrung, M. C., and Nunn, D. S. (1992) *Bioorg. Med. Chem. Lett.* **2,** 1489–1492.
5. Odaka, M., Furuta, T., Kobayashi, Y., and Iwamura, M. (1995) *Biochem. Biophys. Res. Commun.* **213,** 652–656.
6. Marriott, G. (1994) *Biochemistry* **33,** 9092–9097.
7. Mendel, D., Ellman, J. A., and Schultz, P. G. (1991) *J. Amer. Chem. Soc.* **113,** 2758–2760.
8. Yamashiro, D., and Li, C. H. (1973) *J. Amer. Chem. Soc.* **95,** 1310–1315.
9. Shigeri, Y., and Fujimoto, M. (1992) *Biochem. Biophys. Res. Commun.* **187,** 1565–1571.
10. Shigeri, Y., and Fujimoto, M. (1994) *J. Biol. Chem.* **269,** 8842–8848.
11. Beck-Sickinger, A., and Jung, G. (1995) *Biopolymers* **37,** 123–142.
12. Wang, S. S. H., and Augustine, G. J. (1995) *Neuron* **15,** 775–760.

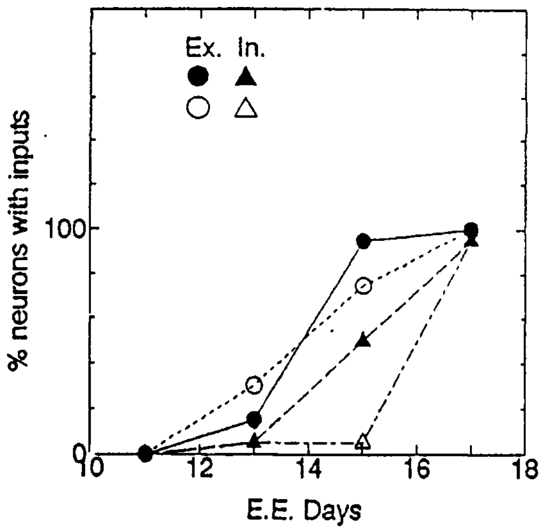

図4　グリア非存在下におけるシナプス形成
横軸は、ニワトリ胚の胚令と培養日数の合計を表す。この例では、胚令10日の胚を用いており、17は培養7日目を示す。たて軸は、計測した神経細胞のうち、シナプス入力の認められた細胞の割合を示す。記号の説明は本文参照。

5．おわりに

ここで述べたように我々は独自の細胞培養系を開発し、シナプス機能の分子メカニズム解析を行っている。この過程には、タンパク質リン酸化酵素をはじめ、多数の酵素が関与しているのは確実である。我々は単一細胞中でのこれらの酵素群解析を試みようとしている。神経のような複雑な系の解析には、いろいろな手法を統合して導入する必要性が高く、超えるべきハードルも多い。酵素工学を専門にされている方々のご助言に期待するところ大である。

文　献

1) Tokioka, R., Matsuo, A., Kiyosue, K., Kasai, M., Taguchi, T.: *Dev. Brain Res.*, **74**, 146 (1993)

2) Autillo-Touati, A., Chamak, J., Vuuillet, J., Araud, D., Glowinski, J., Prochianz, A.: *J. Neurosci.*, **19**, 326 (1988)

3) Rouget, M., Aroud, D., Seite, R., Prochianz, A., Autillo-Touati, A.: *Neurosci. Lett.*, **150**, 85 (1993)

4) Dessi, F., Pollard, H., Ben-Ari, Y., Tremblay, E., Charriaut-Marlangue, C.: *Abst. Soc. for Neurosci*. **24**, 250 (1994)

5) Taguchi, T., Bo, X. X., Taniguchi, H., Kiyosue, K., Kudoh, S., Yumoto, N., Tastu, Y., Yamamoto, H., Kasai, M., Yoshikawa, S.: *Peptide Chem*. **1994**, 145 (1995)

培養細胞を用いた腸管吸収モデルによる吸収促進剤の評価

京大・農　木村幸敬

1．はじめに

薬剤や食品成分の腸管から体内への吸収についての研究手法は、古くは、動物を用いた*in vivo*や*in situ*、摘出した腸管を用いた*in vitro*の系が主流であった。しかし、近年、メンブレンフィルター上に腸管の上皮細胞を培養してその細胞層を隔てた物質の透過を測定することで、吸収過程をモデル化し解析する研究数が急速に増加している[1)]。腸管から体内への物質の吸収過程には、実際、様々な段階での障壁があるわけだが、親水性でしかも難吸収性の物質の吸収過程における一番の障壁は腸管の上皮細胞層である。それ故、上記の培養上皮細胞層モデルでは、これらの物質の吸収過程をよく表現できることが知られている[2)]。この培養細胞を用いた実験系の利点には、1）吸収や代謝過程の迅速な評価が可能、2）実験条件を揃えやすい、3）操作が簡便なので一度に大量の実験が可能、4）細胞内の生理学的な挙動の解析が容易、5）ヒトの細胞での実験か可能、などが挙げられる。

本稿では、難吸収性物質のモデルであるペニシリンやマンニトールの吸収速度を増加させる、中鎖脂肪酸やそのグリセリドの機能について検討した筆者らの研究を中心に紹介する。

2．細胞培養と測定装置

培養細胞にはヒト結腸癌由来の上皮細胞Caco-2[3)]

11

BIO-MICROLITHOGRAPHY: UV- AND E-BEAM PATTERNING OF BIOACTIVE MOLECULES

DAN V NICOLAU, TAKAHISA TAGUCHI, HIROSHI TANIGUCHI, SUSUMU YOSHIKAWA
Osaka National Research Institute, Osaka 563, Japan

UV- and e-beam lithography employing Diazo-Naphtho-Quinone/novolak and poly(tert-Buthyl-Methacrylate)-co-(MethylMethacrylate) respectively as radiation sensitive systems were used to pattern bioactive molecules. Positive and negative tone DNQ based lithography succeed in printing fluorescent avidin up to 2μm resolution, through the linkage of the amino-end of the protein to the photoinduced inden carboxylic acid, either via in-situ addition to ketene, or via NH_2-to-COOH crosslinking mediated by carbodiimide. The carboxylic group produced during e-beam patterning was used as an anchoring site for the same protein. Both UV and e-beam lithography were used for bottom-to-top molecular architecture construction, rather than top-to-bottom classical expose-develop technological sequence. It was found that UV and e-beam lithography materials and techniques can be easily transferred in bio-microlithography, with impact on biodevices fabrication and combinatorial chemistry.

1. Introduction

Advances in constructing on surfaces molecular structures ordered *vertically* incorporating biologically active molecules in their architecture[1], are followed by a growing interest in ordering these structures *laterally*[2]. This new development will require techniques for *patterning* areas with different surface chemistries that control the selective attachment of the vertically ordered molecular architectures on the same basal surface. Vertically structured biomolecular engineering found applications in creating electronically modulated biological functions[3], while laterally structured cell and biomolecular engineering aim towards multiplication of the functionality of these architectures through selective interaction of the cells or bioactive molecules patterned. on the same substrate.

Bioactive molecules patterning[4,5,6,7,8] found application in biosensor fabrication[9,10] and neuronal cells guidance[11]. Recently, bioactive molecules patterning received a new incentive from the growing field of combinatorial chemistry[12], reported techniques using light-directed, spatially addresssable step-wise chemical synthesis of bioactive peptide[13], being already in use. Although it is recognised that towards-submicron resolution would be beneficial, none of these techniques and applications are able to reach this target, either due to the use of unsuitable imaging layer (e.g. protein layers), or due to the use of unsuitable imaging chemistry (e.g. SAM or triazide photochemistry).

2. Biodevice fabrication requires up-side down lithography

The building of bioactive molecular assemblies ordered vertically *and* laterally will comprise several technological steps:

- patterning the photosensitive basal substrate with the first mask, creating an appropriate surface functionality;
- "anchoring" the first bioactive molecule type on the exposed areas, through appropriate crosslinking chemistry. Alternatively the first and second step may be merged, if the exposure generates reactive species *and* if the anchoring sites of the bioactive molecule are present *in situ*.
- cleaning the surface from unreacted, not chemically anchored bioactive molecules;
- return to first step, patterning the second and subsequent masks;
- when the first layer of patterning is complete, sink the uneven topography in a neutral layer of bioactive molecule. This neutral molecule should have the capability of anchoring other molecules with photosensitive end terminal. The top surface should be planar.
- attach *biofunctional* molecules, specifically to patterned first layer bioactive molecules. This step is optional, as the first layer molecules may be biofunctional too.
- repeat step 5.
- anchor molecules with photosensitive end terminal (e.g. photobiotin), to recreate a photosenstive layer.
- return to step 1, for the second and subsequent layers.

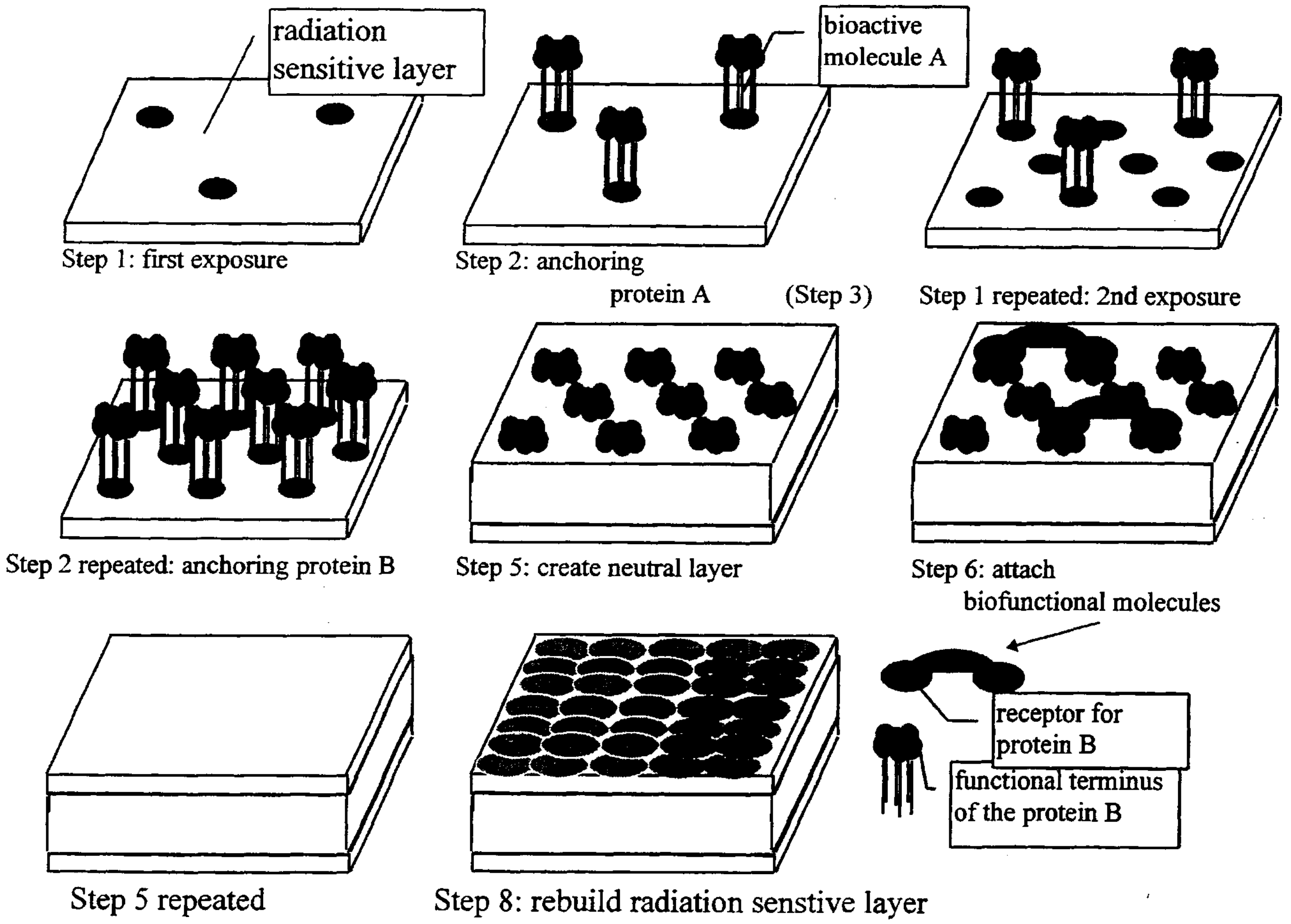
radiation sensitive layer
bioactive molecule A
Step 1: first exposure
Step 2: anchoring protein A
(Step 3)
Step 1 repeated: 2nd exposure
Step 2 repeated: anchoring protein B
Step 5: create neutral layer
Step 6: attach biofunctional molecules
receptor for protein B
functional terminus of the protein B
Step 5 repeated
Step 8: rebuild radiation senstive layer

Figure 1. The overall lithographic process for biodevice fabrication.

3. DNQ potential for patterning bioactive molecules

DNQ photochemistry was largely viewed in the microlithographic community as a vehicle for obtaining higher resolution and higher aspect ratio of the vertically patterned feature. The DNQ chemical flexibility allowed over the years many technological improvements and techniques[14], but due to the emphasis on microlithographic issues, the research was focused on the impact on optical and polymer properties and their distribution throughout the resist layer, rather surface functionality capabilities. However, the DNQ allows many chemical avenues, most of them fairly known[15,16]. In the context of bioactive molecules patterning, three possible chemistries are of interest:

- photoinduced creation of carboxylic groups on the polymer surface, (standard processing);
- photoinduced creation of ketene groups, when the polymer surface is in contact with the bioactive molecule solution, (in-situ exposure through thin liquid layer); and
- destruction of the DNQ moieties and their replacement with amino groups.

The first chemistry would assure the *technological flexibility*, due to the decoupling of the exposure stage from the attachment stage. The exposure can be made on high resolution (projection optics) tools, in conditions of semiconductor-like quality, and the substrates can be transported or stored for further attachment of biologically active molecules to another site. The second chemistry would allow in-situ processing, suitable for step-wise chemical synthesis used in combinatorial chemistry. Finally the third alternative chemistry would allow the portability of the present combinatorial chemistry techniques. The first two chemical and technological routes seem more important, as the reduction of DNQ to amino groups may proceed with several competing parasitic reactions. The overall chemistry of DNQ in the context of bioactive molecules patterning is presented in Figure 2.

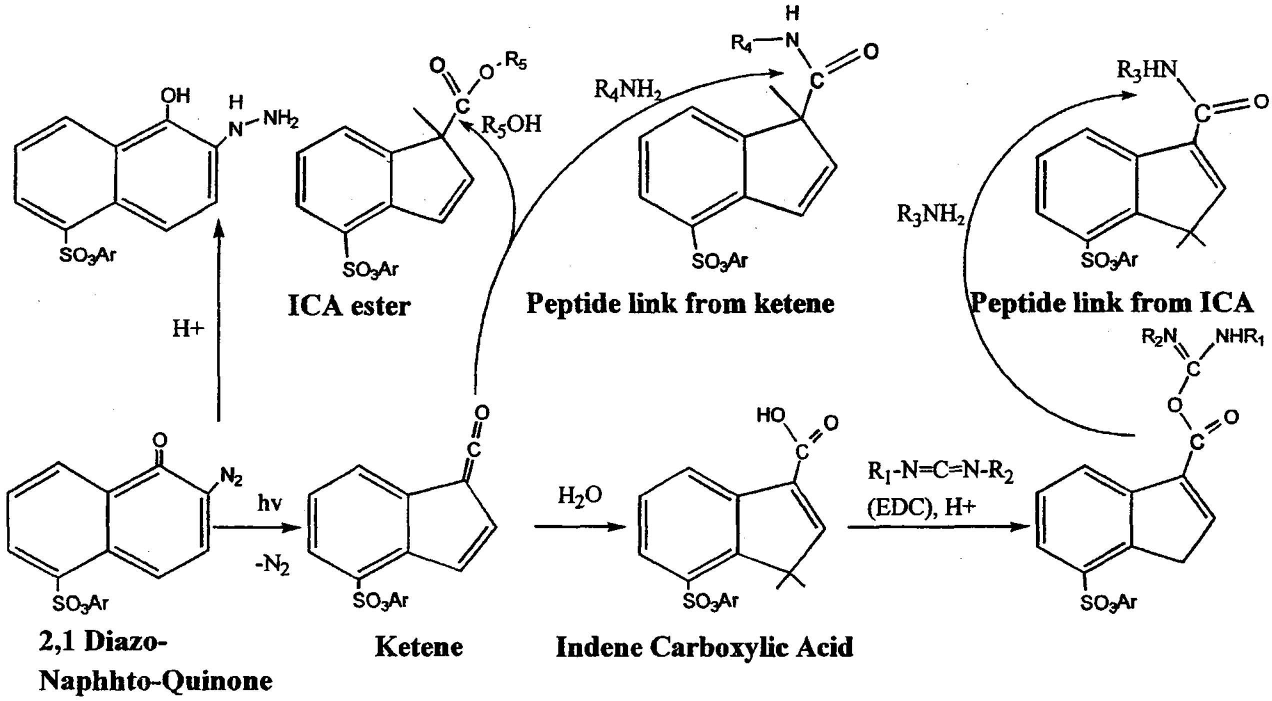

OH
H
N-NH2
SO3Ar
H+
O
O-R5
C
R5OH
SO3Ar
ICA ester
H
R4—N
C
O
R4NH2
SO3Ar
Peptide link from ketene
R3HN
C=O
R3NH2
SO3Ar
Peptide link from ICA
R2N
NHR1
C
O
C
O
O
N2
hv
-N2
SO3Ar
2,1 Diazo-
Naphhto-Quinone
O
C
SO3Ar
Ketene
H2O
HO
O
C
SO3Ar
Indene Carboxylic Acid
R1-N=C=N-R2
(EDC), H+
SO3Ar

Figure 2. Bioactive molecules chemical anchoring to the by-products of the DNQ photolyis

4. Patterning proteins in positive and negative tone lithography

The DNQ-novolak system technological flexibility was used for patterning avidin, a commonly protein used for checking the selectivity of the bioactive molecules attachment. The visualisation of the specific attachment was possible using a fluorescent probe, FITC.

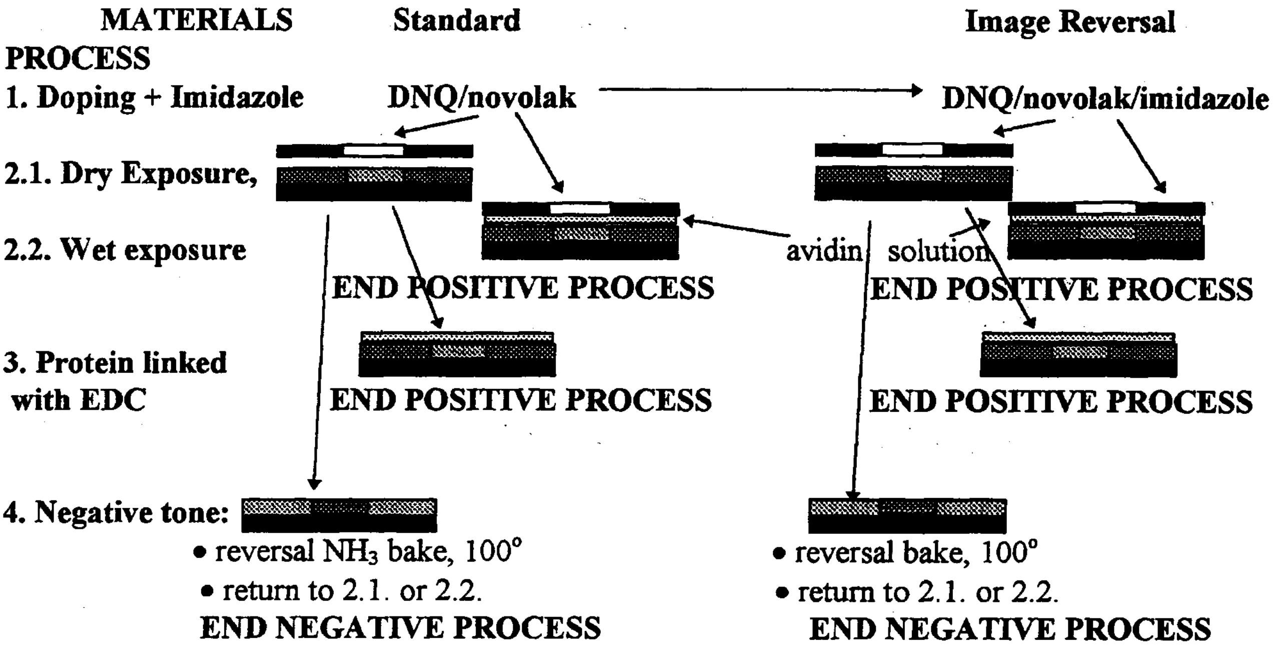
MATERIALS PROCESS
Standard
Image Reversal
1. Doping + Imidazole
DNQ/novolak
DNQ/novolak/imidazole
2.1. Dry Exposure,
2.2. Wet exposure
avidin solution
END POSITIVE PROCESS
END POSITIVE PROCESS
3. Protein linked with EDC
END POSITIVE PROCESS
END POSITIVE PROCESS
4. Negative tone:
• reversal NH$_3$ bake, 100°
• return to 2.1. or 2.2.
END NEGATIVE PROCESS
• reversal bake, 100°
• return to 2.1. or 2.2.
END NEGATIVE PROCESS

Figure 8. Processing routes for patterning proteins on DNQ photoresist

The glass substrates covered with either standard or Image Reversal photoresist, were pattern exposed, either in proximity or projection printing mode, or in contact printing mode through a thin layer of a solution of FITC avidin compressed between the resist surface and the mask. The substrates exposed through proximity or projection *positive* printing mode were incubated in a EDC solution, then incubated in a FITC avidin one, producing positive FITC avidin images. For the substrates intended to be printed in the *negative* tone, the latent images were reversed by ammonia- (for standard resist) or reversal-bake (for imidazole doped resist) at 100° C for 1 hr in a convection oven. Finally, these substrates were blanket exposed, either in proximity/projection printing mode followed by EDC/FITC avidin incubation, or in contact printing mode directly through FITC avidin solution, producing fluorescent negative images of the protein.

The best printing results were obtained using the chemical linkage with the ICA's carboxylic group, probably due to higher yield of COOH-toNH$_2$ linkage. So far, 2 μm FITC avidin patterns were printed, but one can notice the spikes at the corner of the rectangle, (Figure 9), proving that the resolution of the surface-only patterning of the proteins can reach the diffraction limit of the exposure tool. Moreover, this technological route has also the advantage of portability, that is, the patterning step can be handled on a high resolution exposure tool, and the protein attachment step in a different, more bio-oriented facility. Due to its higher definition patterning, EDC mediated, negative tone lithography proved the most promising technological option for single protein patterning.

5. Bio-paterning using e-beam lithography

Although resolution seems not to a critical issue in bio-patterning, the above presented possibilities of mix-and-match lithography can be further expanded through the use of e-beam lithography. On the other hand, as the field of combinatorial chemistry is expanding at a rate similar to the one which was the feature of the semiconductor field at its beginnings, soon the resolution may become a central issue.

As the photogenerated acids proved to be a promising avenue for bio-patterning via carbodiimide crosslinking, we focused our research on the e-beam systems which can produce COOH when exposed to e-beam radiation. A system which fulfilled this requirement was the copolymer between PMMA and Poly(tert-Buthyl-Methyl-Methacrylate). The addition of PtBuMA brings some certain advantages to the classical PMMA, as follows:

- increased sensitivity, from 50 μC/cm^2 to about .5 μC/cm^2.
- change in the chemical properties rather than the decrease of the molecular weight of the polymer. As again development was not intended to be used for protein patterning, this feature allowed a more robust polymer film, on which to "grow" the biomolecular architectures.
- the expected generation of the COOH groups upon exposure, long before the destruction of the polymer network, due to the chemical reactivity of the t-Bu ester group.

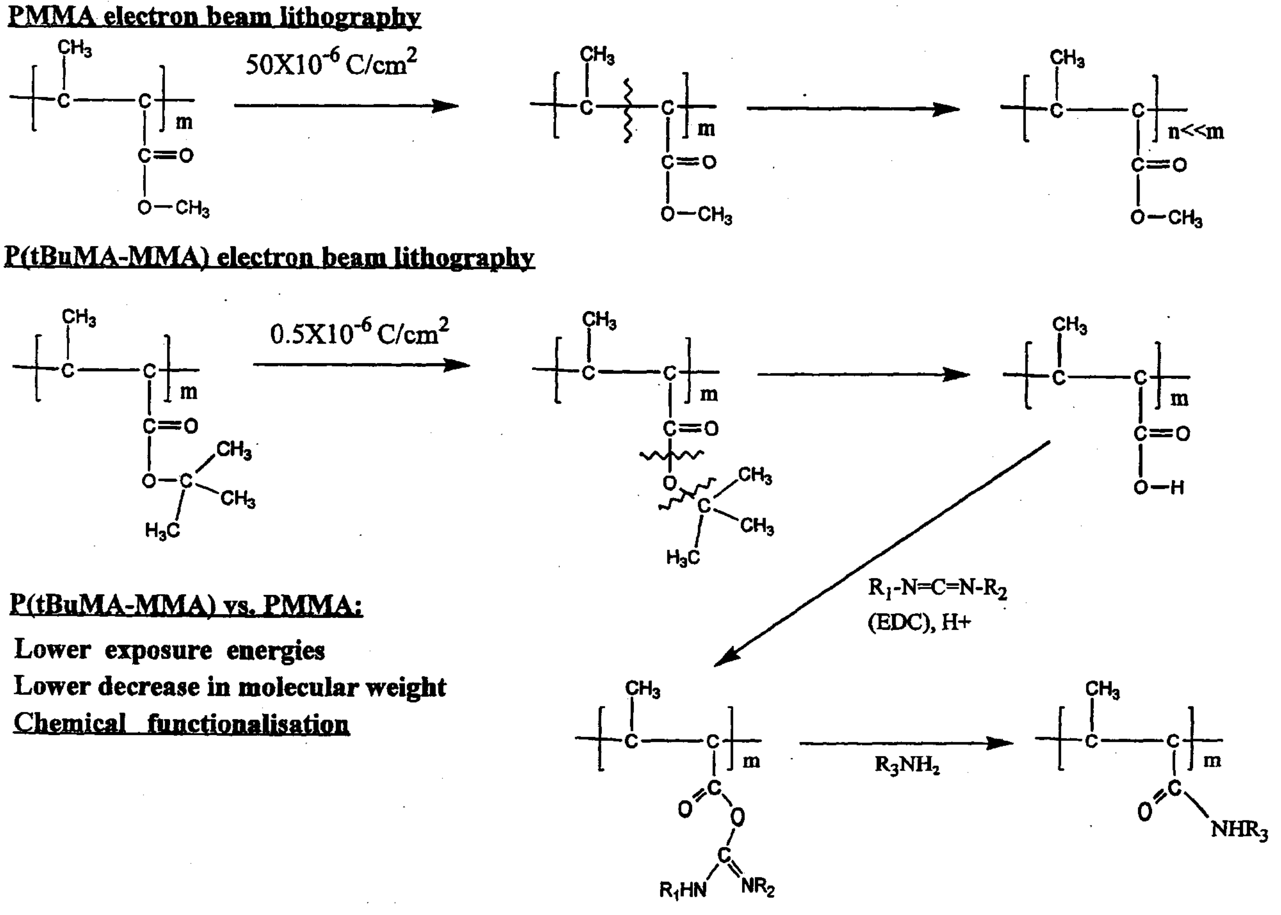
PMMA electron beam lithography
50X10^{-6} C/cm^2
CH$_3$
C=O
O—CH$_3$
m
n<<m
P(tBuMA-MMA) electron beam lithography
0.5X10^{-6} C/cm^2
CH$_3$
H$_3$C
O—H
R$_1$-N=C=N-R$_2$
(EDC), H+
R$_3$NH$_2$
R$_1$HN
NR$_2$
NHR$_3$
P(tBuMA-MMA) vs. PMMA:
Lower exposure energies
Lower decrease in molecular weight
Chemical functionalisation

Figure 11. e-beam induced chemistry for the system P(tertButhyl-Methacrylate)-co-(Methyl-Methacrylate). The linkage to COOH terminus of a bioactive molecule is mediated by EDC.

6. Conclusion

UV- and e-beam lithography were used to pattern bioactive molecules. Positive and negative tone, DNQ- and P(tBuMA)co(MMA)-based lithography respectively, succeed in printing proteins through carbodiimide induced linkage of the protein amino-end to the radiation-induced carboxylic group. In addition the DNQ/UV patterning may proceed in a single step through the addition to the reactive ketene. Our study proved that UV and e-beam lithography materials and techniques can be easily transferred in bio-microlithography, with impact on biodevices fabrication and combinatorial chemistry.

7. Acknowledgements

One of the authors, (DVN), wishes to acknowledge the help of Prof. Iovu during e-beam resist synthesis and Jenoptick research people for assistance during e-beam lithography.

8. References

1. C. Nicolini. *Biosensors & Bioelectronics*, Vol. 10, 1/2, pp. 105-127, 1995.

2. W. Gopel. *Biosensors & Bioelectronics*, Vol. 10, 1/2, pp. 35-59, 1995.

3. M. Aizawa, T. Haruyama, G. F., Kham, E. Kobatake, Y. Ikaryiama. *Biosensors and Bioelectronics*. Vol. 9, pp. 601-610, 1994.

4. S. K. Bhatia, J. J. Hickman, F. S. Ligler, *J. Am. Chem. Soc.*, Vol. 114, pp. 4432-4433, 1992.

5. J. D. Hong, K. Lowack, J. Schmitt, G. Decher, *Progr. Colloid Polym. Sci.*, Vol. 102, pp. 93-102, 1993.

6. D. J. Pritchard, H. Morgan, J. M. Cooper, *Angew. Chem. Int. Ed. Engl.* Vol. 34, pp. 91-92, 1995.

7. P. Connolly. J. Cooper, G. R. Moores, J. Shen, G. Thomson, *Nanotechnology*, Vol. 2, pp. 160-163, 1991.

8. S. K. Bhatia, J. T. Teixeira, M. Anderson, L. C. Shriver-Lake, J. M. Calvert, J. H. Georger, J. H. Hickman, C. S. Dulcey, P. E. Schoen, F.S. Ligler, *Analytical Biochemistry* Vol. 178, pp. 197-205, 1989.

9. D. J. Pritchard, H. Morgan, J. M. Cooper, *Ana. Chim. Acta*, Vol. 310, pp. 251-256, 1995

10. T. Kuriyama, J. Kimura, Y. Kawana, *NEC Res & Dev.*, Vol. 78, pp. 1-5, 1985, F. S. Ligler, T. L. Fare, 26. K. D. Seib, J. W. Smuda, A. Singh, P. Ahl, M. E. Ayers, A. Dalziel, P. Yager. *Med. Instrum.*, Vol. 22, pp. 247-256, 1988.

11. P. Fromhertz, H. Schaden. *European Journal of Neuroscience*, Vol. 6, pp. 1500-1504, 1994

12. 27. M. A. Gallup, R. W. Barrett, W. J. Dower, S. P. A. Fodor, E. M. Gordon. *J. Medicinal Chemistry*, Vol. 37, pp. 1233-1401, 1994

13. S. P. A. Fodor, J. L. Read, M. C. Pirrung, L. Stryer, A. T. Lu, D. Solas, *Science*, Vol. 251, pp. 767-773, 1991.

14. R. Dammel, *Diazonaphthoquinone-based Resists.* SPIE Opt. Eng. Press., Bellingham, WA, 1993.

15. V. V. Ersov, G. A. Nikiforov, C. R. H. I. de Jonge. *Quinone Diazides.* Elsevier Sci., Amsterdam, 1981

16. T. Ye, M. A. McKervey. *Chem. Rev.* Vol. 94, pp. 1091-1160, 1994.

12.

培養大脳神経細胞のシナプス形成・可塑性のメカニズム

The mechanism of synaptogenesis and synaptic plasticity analyzed in cultured cerebral neurons

通産省大阪工業技術研究所　有機機能材料部
○田口隆久、清末和之、工藤卓
Osaka National Research Institute, AIST, Dept. of Organic Materials
○ Takahisa Taguchi, Kazuyuki Kiyosue and Suguru N. Kudoh

Abstract: To understand the mechanism in synaptogenesis and synaptic plasticity at single cell level, the dissociated neuronal culture is an usuful system because of the high accesibility to a synaptic site. We have developed one of the system using cerebral neurons of chick embryos, in which synaptogenesis proceeds in the same time course as in vivo. In the culture, the synaptogenesis completed without any support of glial cells. The maturation of the synapses estimated by amplitudes of postsynaptic currents depended on synaptic activities. The gultamatergic synapse first developed as a site containing only NMDA receptors, even though functional non-NMDA receptors existed in overall membrane of neurons. The mechnism of LTP in the culture included the activation of NMDA receptor and the synthesis of RNA and protein.

1．はじめに

脳神経系における情報は個々の神経細胞を素子とした神経回路網で処理される。したがって、このメカニズムを正確に把握するためには、この素子の動態が観測可能な系を用いて解析する必要がある。この目的には、脳そのもの、あるいは脳スライスは実験材料として構造が複雑すぎるため、培養細胞系、特に解離培養系の活用を試みた。この系においては、形成される回路網はランダムではあるが、個々の神経細胞の計測やそこに存在する機能分子群の解析が可能である。

神経情報処理のメカニズムを理解する場合、神経細胞の性質に関しては、それが増幅器なのか、整流器なのか、抵抗なのかが分かれば、あとは回路網ダイナミックスで情報処理メカニズムは解明可能との議論もあるが、一個の神経細胞の機能が電気回路素子からの類推機能のみに限定されるとは考え難い。個々の神経細胞に注目した精密な解析が未知のメカニズムを明らかにする可能性も十分にある。

我々のグループは情報処理機構の解明のみならず、そこに関与する分子、特に蛋白質、の構造機能相関まで明らかにし、それを神経機能材料開発に結びつけることを目標としている。このためにも解離

培養系の活用が不可欠である。

情報処理メカニズムの解析は広範囲な課題を包含するが、我々は、情報処理とは神経回路網の変化であり、この変化はシナプス伝達効率の増減により規定されると考え、現時点ではこの点に絞って解析を進めている。このシナプス変化としては長期増強現象（ＬＴＰ）が良く知られているが、最近この発現とシナプス形成とのメカニズムの間に共通点が見出されてきており、我々は両者を関連付けながら解析を進めている。

本稿においては、我々の培養系の開発、この系におけるシナプス形成の特徴、ＬＴＰのメカニズム解析について報告する。

２．方法

培養系は以下の方法で調製した。ニワトリ胚（主に孵卵１０日目）の大脳半球（終脳）を取り出し、トリプシン処理で解離した神経細胞を血清を含む培養液中で培養した。７日間の培養でシナプス形成が完了する。

神経細胞の活動はホールセルクランプ法で記録した。３５mmディッシュで培養した神経細胞に倒立顕微鏡下で微小ガラス電極を接触させ、吸引・膜破壊により電極と細胞間のギガシールを形成し、神経細胞の活動に伴う微小電流を増幅・記録した。通常は抑制性シナプスの入力を阻害するためにピクロトキシンを記録外液中に添加した。

３．結果

3-1　培養系のシナプス形成

胚令１０日のニワトリ胚大脳の場合、培養３日目よりシナプス形成が始まり、７日目にかけてシナプス形成率、シナプス入力の頻度・大きさが増大する。興味深いことに、２日若い胚を用いると培養５日目より同様のシナプス形成が始まり、逆に２日遅い胚を用いると培養１日目より始まる。このことは我々の培養系の神経細胞は人工的環境に移した時期に関わらず発生の時間経過が維持されていることを示している。

3-2　シナプス形成のグリア依存性

この培養系は神経細胞とグリア細胞（主にアストログリア）の共存する系である。培養３日目からグリア細胞の増殖が顕著になるため、シナプス形成に対するグリア細胞の寄与が予想された。これの検証には、独自に開発した神経毒性の低いグリアフリー培養系が用いられた。３種のパラメーターで検討したが、この系においても対照群と同じ正常なシナプス形成が観測された。シナプス形成過程にはグリア細胞の関与は不要である。

3-3　シナプス形成の神経活動依存性

我々の培養系のシナプス形成においては、胚令１０日胚を用いた場合、培養５日目から７日目の間に自発的興奮性後シナプス電流（ sEPSC ）が急速に増大する。シナプス接触形成は培養３日目から始まっているため、シナプス成熟に対応するこの増大がシナプス活動に依存する可能性がある。

そこでこの時期に活動電位伝導を阻害する TTX とシナプス後細胞にある nonNMDA 型グルタミン酸受容体のアンタゴ

ニストCNQXを添加し、培養７日目のシナプス電流の大きさの変化をシナプス前細胞を刺激することにより記録した。

この結果、微小EPSCは両者とも対照よりわずかに同程度減少したが、evoked EPSCの場合にはCNQX処理がTTX処理の半分にまで減少した。この結果はミクロに見たシナプス部位の数の増加がCNQX処理で抑制されたことを示唆している。

3-4 シナプス形成のシナプス後細胞膜成熟度依存性

我々の大脳神経細胞培養系における興奮性シナプスはグルタミン酸が伝達物質である。このシナプスにおいてはnon-NMDAタイプのグルタミン酸受容体が主要な脱分極を引き起こす。この成分が培養３日目より現れることは既に記したが、このsEPSCの波形を詳細に解析するとNMDA受容体成分も含まれていることが明らかになった。微小EPSCの解析は両受容体がシナプス部位に存在する可能性を示唆している。

さらに両者の存在比はシナプス後膜の胚令に依存することは胚令の異なる共培養系を用いた解析により明らかになった。興味深いことに、胚令が若い場合には細胞膜表面には両受容体が機能する形で存在するにもかかわらずシナプス部位にはNMDA受容体のみが存在する。胚令の進行とともにここにnon-NMDA受容体が現れるのである。すなわち、発生初期にはNMDA受容体のみのシナプス部位が多数存在し、発生過程におけるこの受容体に活性化により、non-NMDA受容体を伴ったEPSCの大きなシナプスが完成する、という仮説が考えられる。現在この仮説のより直接的な証明を試みている。

この現象はＬＴＰにおける増強発現の説明にも有効であると考えている。

3-5 解離培養系におけるＬＴＰ

胚令１０日の大脳神経細胞を７日間培養した後の、シナプス形成の完了した系を用いてＬＴＰの解析を試みた。この系では多くの神経細胞が同期して活動している。そこでホールセルクランプした２つの細胞への同期した入力のみに注目し、Ｍｇ$^{2+}$のない溶液で１５分間インキュベートすることでＬＴＰを引き起こすことに成功した（図１）。

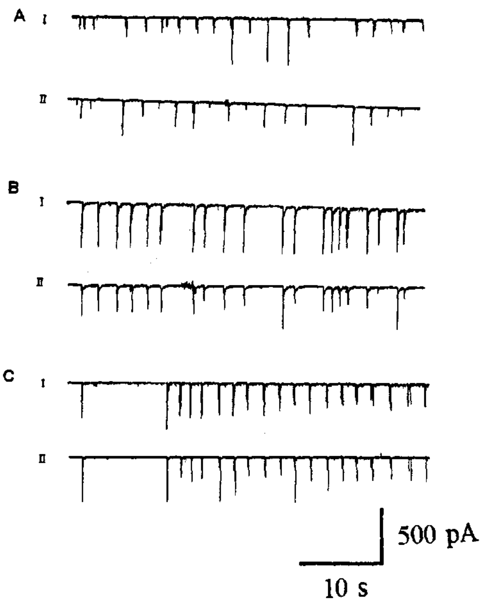

Fig.1. LTP induced by the treatment with Mg^{2+}-free solution. The synchronous sEPSCs were recorded in two cultured neurons (A)before, (B)under and (C) after the treatment.

この増強は４０分以上持続し、この発現にはNMDA受容体の活性化とシナプス伝達が必須であった。この性質はラット海馬CA1領域のＬＴＰと同様である。

さらに、mEPSCの解析を行うと電流の大きさは変わらず、頻度が上昇することが明らかになった。このことはシナプス部位の数の増加で説明ができ、前述したシナプス形成過程と類似したメカニズムの存在する可能性がある。

我々の培養系のＬＴＰは、蛋白合成、あるいはＲＮＡ合成の阻害剤を１５分間のＭｇ$^{2+}$除去処理中共存させると阻害される。このことは長期増強が何らかの新たな分子の発現を要求していることを示している。

3-6　ＬＴＰを誘導する分子

ＬＴＰ発現に際しシナプス部位数が増加する場合、シナプス前膜の変化も考えられる。この場合にはNMDA受容体を通して活性化されたシナプス後細胞内機構の情報が何らかの形で前細胞に伝搬する必要がある。我々の培養系でのＬＴＰ誘導は１５分で完了するので、この時間内に細胞外に放出される物質に注目して解析した。ＬＴＰ誘導のために用いたＭｇ$^{2+}$フリー溶液のＭｇ濃度を１ｍＭに戻した後、これを別の培養細胞に添加するとそれのみでＬＴＰが誘導された。分子の同定は現在進行中であるが、蛋白質である可能性が高い。現時点ではこの分子がシナプス後細胞から放出された証拠はなく、グリア細胞の関与も可能性が残っている。この点についてもグリアフリーの培養系を用いて検討を進めている。

４．まとめ

神経回路網情報処理素過程を解明するためシナプス伝達効率制御機構に焦点を合わせて研究している。シナプス形成過程とシナプス可塑性の類似性に注目した研究から、我々はシナプス機能の変化は機能的なシナプス部位の数の変化によると考えている。この仮説を実証するために電気生理学的手法に形態学的手法を加味した測定システムを開発中である。

本稿では記述していないが、神経回路網形成に重要な役割を果たす分子に神経突起伸長蛋白質がある。我々のグループでも新しい分子（ＮＰＦと命名）を発見し、クローニングした。この分子とシナプス形成との関連は現在研究中である。

ここで述べた解析は単一シナプスに限定した解析が主である。シナプス機能に対する神経回路網活動の影響も重要なテーマであり、培養細胞の優れた２次元特性を生かした解析にも取り組む予定である。

５．参考文献

1. Tokioka,R. et al. (1993) Dev. Brain Res. 74:146-150
2. Kiyosue, K. et al (1996) Neuroreport.7: 701-704
3. Taguchi,T et al. (1995) Peptide Chem. 1994:145-148
4. Kiyosue, K. et al. Dev.Brain Res.in press
5. Kudoh,S.N.et al. submitted
6. 西宗、田口 (1995) 実験医学 13:104-105

13.

Copyright © 1997 Elsevier Science B.V.. All rights reserved.
Tue Jan 28 14:52:26 1997: BRESD: 52319:

Research report

Selective formation of silent synapses on immature postsynaptic cells in cocultures of chick neurons of different ages

Kazuyuki Kiyosue,[a] Michiki Kasai[b] & Takahisa Taguchi[a,*]

[a] *Department of Organic Materials, Osaka National Research Institute, 1-8-31, Midorigaoka, Ikeda 563, Japan*
[b] *Department of Biophysical Engineering, Faculty of Engineering Science, Osaka University, Toyonaka 560, Japan*

Accepted 10 December 1996

Glutamatergic synapses usually contain two types of ionotropic glutamate receptor, *N*-methyl-D-aspartate receptors (NMDARs) and non-NMDA receptors (non-NMDARs), and the ratio of these receptors is thought to be critical for synaptic plasticity. To determine whether or not the ratio of these receptors at synaptic sites is controlled by the developmental stage of postsynaptic neurons, we applied a dual whole-cell recording technique to a culture of dissociated chick cerebral neurons of different ages. We found that formation of synapses that contained both types of receptor required maturation of postsynaptic neurons. Moreover, during the early development of postsynaptic neurons, NMDARs were selectively present at synaptic sites prior to the presence of non-NMDARs, even though both types of receptor were expressed in functional form in the neuronal membranes.

Keywords: Synaptogenesis; Silent synapse; Glutamatergic synapse; NMDA receptor; Non-NMDA receptor; Culture; Development

1. Introduction

Major excitatory synapses in the central nervous system (CNS) use glutamate as a transmitter. Glutamate simultaneously activates two types of ionotropic receptor, *N*-methl-D-aspartate receptors (NMDARs) and non-NMDARs to cause dual-component synaptic currents [1,4,10,14]. We use the term dual-component synapse to refer to the corresponding synapses. The amplitude of synaptic currents at the synapse is determined mainly by the activity of non-NMDARs, which are modified by activation of NMDARs during long-term potentiation (LTP) [3] and in the refinement of neural connections [8,9]. A recent study during critical periods of the thalamocortical synapses indicated that neurons with higher ratio of NMDAR to non-NMDAR components in the evoked excitatory postsynaptic current (EPSC) tend to be associated with greater LTP [5]. Thus, elucidation of the mechanism of incorporation of glutamate receptors into synaptic sites should provide information indispensable for studies of LTP. Since the thalamocortical synapse can alter the ratio of NMDAR to non-NMDAR components in the EPSC with development, analysis of synaptogenesis should help us for characteristic details of synaptic plasticity.

To identify changes in the ratio of the two types of receptor at a developing synaptic site, we studied the functional properties of synapses formed between chick cerebral neurons of different ages. To characterize a synapse between two particular neurons, we developed a method for culture of dissociated neurons in which neurons after 13 days in ovo plus in vitro (embryonic equivalent days 13, or E.E.days 13) start to receive spontaneous synaptic currents (SSCs) and in which, between E.E.days 15 and 17, the amplitude and frequency of SSCs increase rapidly [17].

---

* Corresponding author. Fax: +81 (727) 51-9628. E-mail: taguchi@onri.go.jp

PII: S0165-3806(97)00008-4

2. Materials and methods

2.1. *Cultures*

Neuronal cultures were established as described previously [17]. Whole telencephalic hemispheres of chick embryos were dissected out and incubated in phosphate-buffered saline that contained 0.175% (w/v) trypsin (GIBCO, U.S.A.), 0.007% (w/v) EGTA, 10 mM glucose at 37°C for 30 min, and then they were triturated with a fire-polished Pasteur pipette in culture medium. The culture medium consisted of 50% (v/v) of 2-fold diluted Earl's minimum essential medium, 10% (v/v) fetal calf serum and 40% (v/v) GIT medium (Nihon Seiyaku, Japan), supplemented with 10 mM glucose, 2 mM L-glutamine, 1 mM $CaCl_2$, 25 mM HEPES-Na (pH7.4), 30 mM NaCl, 0.5 mM sodium pyruvate, 25 nM Na_2SeO_3, 50 μM choline-Cl, 50 μM inositol, 100 U/ml penicillin, 100 μg/ml streptomycin and 5 μg/ml insulin. The dissociated neurons were plated on poly-L-lysine-coated (25 μg/ml) 35-mm culture dishes (Corning, U.S.A.) at a density of 520 cells/mm^2. Cocultures containing older (90%) and younger (10%) neurons from embryos of different ages were prepared as follows. After culture of neurons from E10 embryos for 0, 2 or 4 days, we added 10% younger neurons from E6 embryos to the culture dish and continued the culture for 7, 5 or 3 days, respectively. The older neurons corresponded to neurons on E.E.days 17, whereas the three sets of younger neurons corresponded to E.E.days 13, 11 or 9, respectively.

Younger neurons, labeled with the lipophilic fluorescent dye PKH-26, were identified under a fluorescence microscope. They were incubated with 5 μM PKH-26 (Zyaxis Cell Science, U.S.A.) for 2 min at 37°C after dissociation [11]. The suspension of cells was centrifuged to remove unbound dye. The labeled neurons had the same capacity for synaptogenesis as unlabeled ones since we obtained the same results using labeled older neurons and unlabeled younger one as vice versa (data not shown).

2.2. *Electrophysiological recording*

The conventional whole-cell recording technique was used to record synaptic currents from neurons whose membrane potentials were clamped at −60 or +60 mV, except in experiments for which results are shown in Figs. 2 and 4. All experiments were carried out at room temperature (22–25°C). The standard external bathing solution contained: 130 mM NaCl, 3 mM KCl, 2 mM $CaCl_2$, 1 mM $MgCl_2$, 10 mM glucose, 10 mM HEPES-Na (pH 7.3) and 0.025 μM picrotoxin (Sigma, U.S.A.). For recording of inhibitory synaptic currents (Fig. 2), picrotoxin was omitted. The patch pipette contained: 130 mM KCH_3SO_4, 10 mM KCl, 0.2 mM $CaCl_2$, 2 mM $MgCl_2$, 1 mM EGTA, 2 mM Mg-ATP and 10 mM HEPES-K (pH 7.3). The pipettes had a D.C. resistance of 5–7 MΩ. The junction potential was corrected after the pipette had touched the bathing solution. Currents were amplified with an amplifier (CEZ-2400; Nihon Kohden, Japan) filtered at 1 kHz and digitized at 20 kHz with the pClamp or Axotape program (Axon, USA). from

Evoked EPSCs in a single post-synaptic cell were recorded after depolarization or external stimulation of a pre-
VV synaptic cell. For the former stimulation, holding potentials of the pre-synaptic cell were increased form −60 mV to
0 mV for 10 ms to evoke an action potential in axonal processes at 10-s intervals. In the latter case, a glass pipette was
pulled to yield a tip of 2–3 μm in diameter for focal stimulation. After the stimulatory pipette, filled with the external
bathing solution, had been placed slightly above the soma, bipolar pulses of current of 500 μs in duration were applied
[2] at 0.1 Hz through the pipette. The minimal intensity of external stimulation that evoked EPSCs was 1–2 μA [13]. At
the start and end of one recording, the input and series resistance were monitored by application of a step pulse to hyperpolarize the holding potential by 10 mV. If the resistance changed significantly, the recording was discarded.

For recordings at a positive holding potential (Figs. 1 and 3 and 4), the pipette for recording contained cesium ions instead of potassium ions and an increased level of EGTA (5 mM). Glutamate was applied as follows. Glutamate (1 mM) in a glass pipette was applied by pressure ejection (Picopump; World Precision Inc., USA) onto an outside-out patch membrane of the soma via rapid perfusion to prevent desensitization of glutamate receptors. All data relating to synaptic currents were stored on a hard disk and analyzed off-line by personal computer. To analyze formation of synapse, we introduced two parameters, maximum SSCs and input SSCs, which were defined as the largest amplitude in a record of 3-min duration and the product of the averaged amplitude and the number of SSCs observed over a 3-min period, respectively. For analysis of miniature EPSCs (referred to below as minis), events of more than 5 pA were counted.

3. Results

Glutamatergic synapses of E.E.days 17 neurons were confirmed to be dual-component synapses with both NMDARs and non-NMDARs colocalized at the single synaptic site (Fig. 1). EPSCs elicited by one presynaptic cell were recorded as rapidly rising and rapidly decaying currents at a holding potential of −60 mV and rapidly rising and slowly decaying

BRESD: 52319 Copyright © 1997 Elsevier Science B.V. . All rights reserved.

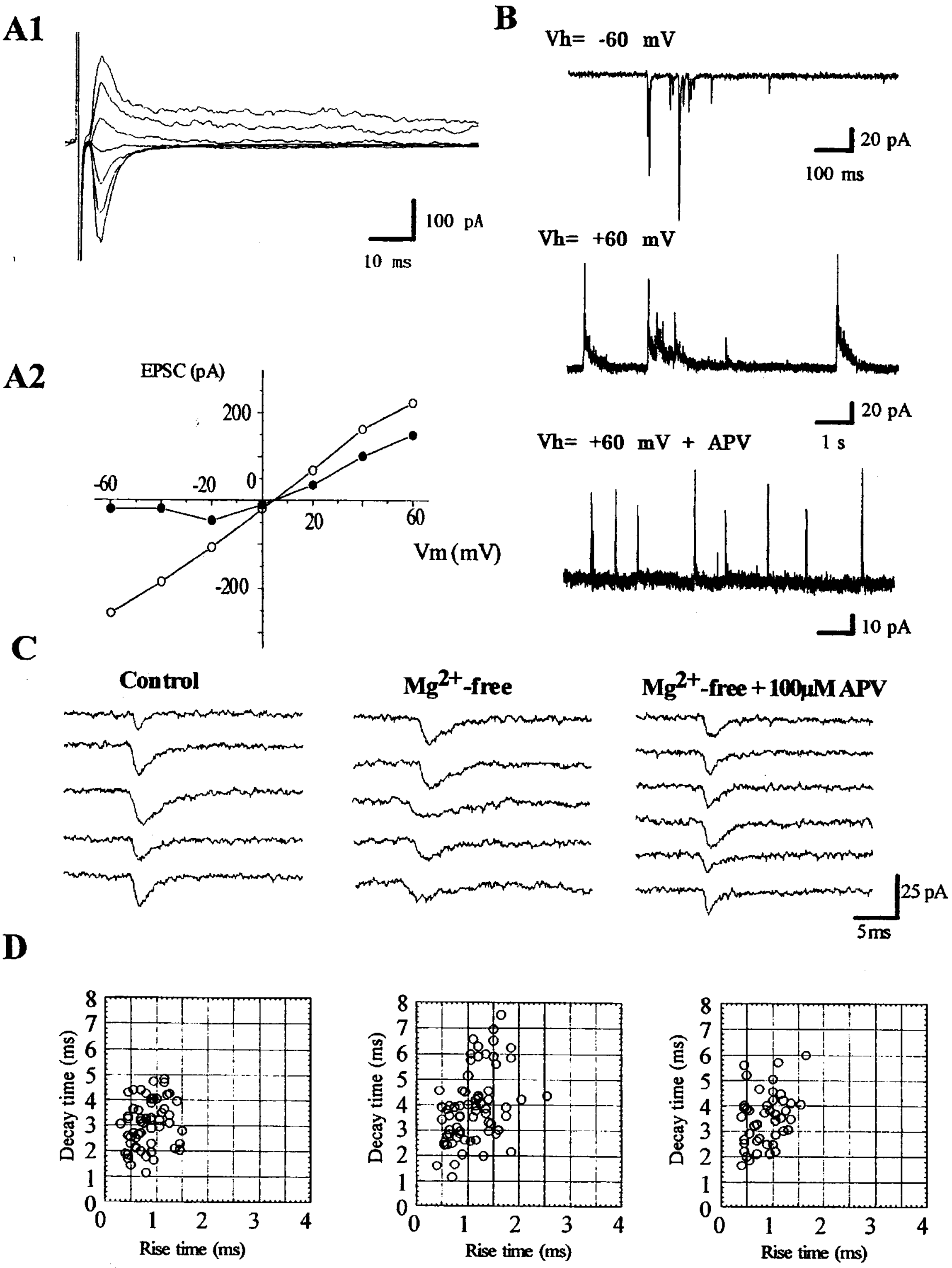

BRESD: 52319 Copyright © 1997 Elsevier Science B.V. . All rights reserved.

Fig. 1. Dual-component synapses in E.E.days 17 neurons. A1: voltage dependency of dual-component EPSCs. EPSCs were recorded from a cell under whole-cell voltage clamp at −60 mV to +60 mV, stepped by 20 mV. Each trace is the average of five successive records. A2: current–voltage relationship of the fast (4.8 ms after stimulation; open circles) and slow (14 ms; solid circles) components of EPSCs. B: two components of SSCs. The top trace shows typical SSCs at a holding potential (Vh) of −60 mV, the middle trace shows that at +60 mV and the bottom trace shows that at +60 mV with 100 μM APV. C: dual-component currents in minis. Typical traces of minis at a Vh of −60 mV were recorded in control bathing solution (left), in a solution with no Mg^{2+} (middle) and in a solution with 100 μM APV and no Mg^{2+} (right). D: relationship between rise and decay times for minis. The recording conditions correspond to those for the minis (Fig. 1C) above each panel. The rise and decay times were defined as the time between 10% and 90% amplitude of each mini.

BRESD: 52319 Copyright © 1997 Elsevier Science B.V. . All rights reserved.

glutamatergic synapses in neurons at E.E.days 17 were dual-component synapses.

To determine whether both types of glutamate receptor are localized at the same synaptic site, we analyzed minis under conditions for activation and blocking of NMDARs (Fig. 1C). The waveforms of minis had significantly slower decay times in bathing solution without Mg^{2+} than those in the control solution and in the presence of 100 μM APV (Fig. 1D). Analysis of a series of records revealed that the mean rise and decay times were 0.829 ± 0.042 ms (mean±S.E., the number of minis (n_m) = 56) and 3.05 ± 0.125 ms (n_m = 56) for controls at −60 mV (Fig. 1D, left), 1.12 ± 0.054 ms (n_m = 67) and 3.90 ± 0.173 ms (n_m = 67) in Mg^{2+}-free bathing solution (Fig. 1D, middle), and 0.861 ± 0.051 ms (n_m = 44) and 4.50 ± 0.162 ms (n_m = 44) with APV (Fig. 1D, right). The differences in rise and decay times under NMDAR-activating and NMDAR-blocking conditions were significant (unpaired t-test, $P < 0.05$). Since similar results had been obtained in five neurons, it was thought that minis were composed of dual synaptic components and that transmitters released in single synaptic vesicles were able to activate both types of glutamate receptor. This colocalization of NMDAR and non-NMDAR at the same single synaptic site resembles observations made in rat hippocampal culture [1].

Using cocultures of differently aged neurons, we examined whether the formation of the dual-component synapse depended, on the degree of maturation of post-synaptic neurons (Fig. 2). The cultures consisted of 90% E.E.days 17 neurons and 10% younger neurons which had been labeled with a fluorescent dye (Fig. 2A). SSCs were recorded simultaneously from E.E.days 13 and 17 neurons by dual whole-cell recordings at −40 mV to distinguish between glutamatergic and GABAergic synaptic currents. Frequent synchronous synaptic inputs revealed that glutamatergic inward currents in E.E.days 17 neurons were significantly larger than in younger neurons, whereas GABAergic outward currents showed no marked difference between the two types of neuron (Fig. 2B). These observations were confirmed quantitatively by cumulative histograms (Fig. 2C). For precise evaluation of synapse formation, we analyzed the SSCs from 77 E.E.days 17 neurons and 75 E.E.days 13 neurons using, as parameters, the maximum SSC and the input SSC over a period of 3 min. The results revealed significant differences between both respective parameters (Fig. 2D). Although E.E.days 13 neurons had acquired the ability to form GABAergic synapses as post-synaptic cells, there was a statistically significant difference between E.E.days 13 and 17 neurons in the ability to make glutamatergic synapses. Since it has been suggested that development of post-synaptic neurons is essential for glutamatergic synaptogenesis (Fig. 2C, D), we examined neurons prior to E.E.days 13 in isolation. The results for E.E.days 11 (n= 19) and 9 (n= 6) neurons confirmed that glutamatergic synaptic currents were hardly ever present in younger neurons (Fig. 2E).

To measure non-NMDAR- and NMDAR-mediated synaptic currents, we recorded SSCs simultaneously from E.E.days 11 and 17 neurons at negative and positive holding potentials (Fig. 3A). At a holding potential of −60 mV, we detected few small SSCs in E.E.days 11 neurons. However, when the potential was raised to +60 mV, synchronous SSCs from neurons of different ages were observed in 18 of 30 paired cells examined (Fig. 3A,). As shown in the right trace in Fig. 3A, SSCs of E.E.days 11 neurons were characteristic in terms of rising phase of waveform. Analysis of rise and decay times for SSCs at +60 mV (Fig. 3B) clearly revealed the large difference in rise times (1.92 ± 0.124 ms, n_s = 65, for E.E.days 17; 25.6 ± 5.17 ms, n_s = 62, for E.E.days 11), suggesting that the SSCs in younger neurons mainly included a slow component. These SSCs were completely blocked by 100 μM APV (Fig. 3C), whereas the fast component remained in E.E.17 neurons (Fig. 1B). These results indicate that NMDARs were exclusively present in synapses formed on E.E.days 11 neurons.

The synchronous SSCs (Fig. 3A, middle) in E.E.days 11 and 17 neurons suggested that NMDARs in the younger neurons might have been located at synapses that functioned in neuronal circuits. To confirm this possibility, we analyzed evoked EPSCs from E.E.days 11 neurons (Fig. 3D). The results obtained from 10 paired cells showed currents typical of NMDAR-mediated synapses at +60 mV but no responses at −60 mV. The absence of non-NMDAR in the synapses of E.E.days 11 neurons can possibly be explained by the absence of expression of these receptors at this stage of development. To examined the possibility, we applied glutamate to excised outside-out patch membranes from soma of E.E.days 11 neurons that had been confirmed to have silent synapses. Responses caused by both NMDAR and non-NMDAR were observed in the traces (Fig. 4A) and the current–voltage relationship (Fig. 4B) was similar to the typical relationship reported previously [16].

4. Discussion

In this study, we showed that the formation of synapse depends on the development of post-synaptic neurons, and this conclusion is consistent with results obtained by immunohistochemical studies of the expression of synapsin-1 in heterochronically cultured neurons [7]. Our data indicate that a synaptic site which is silent at resting membrane potential and composed of functional NMDARs forms first on immature neurons and then non-NMDARs are incorporated or uncovered at this site during development. This scheme has the potential to play an important role in the formation and refinement of neuronal circuits because the silent synapse formed initially can be converted into a dual-component

Copyright © 1997 Elsevier Science B.V. . All rights reserved.

Fig. 2. Post-synaptic maturation-dependent synaptogenesis of glutamatergic and GABAergic synapses in cocultured cerebral neurons. A: Hoffmann modulation (left) and fluorescence (right) images of cocultured E.E.days 13 (fluorescent) and E.E.days 17 (non-fluorescent) neurons. Bar: 25 μm. B: typical traces of SSCs obtained from E.E.days 13 (upper trace) and E.E.days 17 (lower trace) neurons. Synchronous SSCs are indicated by arrowheads. C: cumulative frequency distribution of amplitudes of glutamatergic (left) and GABAergic (right) SSCs. Currents greater than 10 pA were collected for 3 min. D: formation of glutamatergic (open columns) and GABAergic (solid columns) synapses between neurons of different ages. Averaged maximum SSCs (left panel) and input SSCs (right panel) were calculated over periods of 3 min at −40 mV. The input SSC indicates the product of the averaged amplitude and the number of SSCs. The difference between the two open columns in the left is significant (Mann-Whitney *U*-test; $P < 0.001$; max. SSCs) for in E.E.days 17 ($n = 77$) vs. 13 ($n = 75$) neurons, and also in the right panel ($P < 0.05$; input SSCs) for E.E.days 17 ($n = 84$) vs. 13 ($n = 75$). E: effects of postsynaptic maturation on the mean conductance of glutamatergic synapses. The mean conductance was calculated by dividing the maximum SSC amplitude by the holding potential of −40 or −60 mV. E.E.days indicates the age of postsynaptic neurons used for whole-cell clamping. The short vertical lines in the columns in D and E show standard errors (S.E.).

BRESD: 52319 Copyright © 1997 Elsevier Science B.V. . All rights reserved.

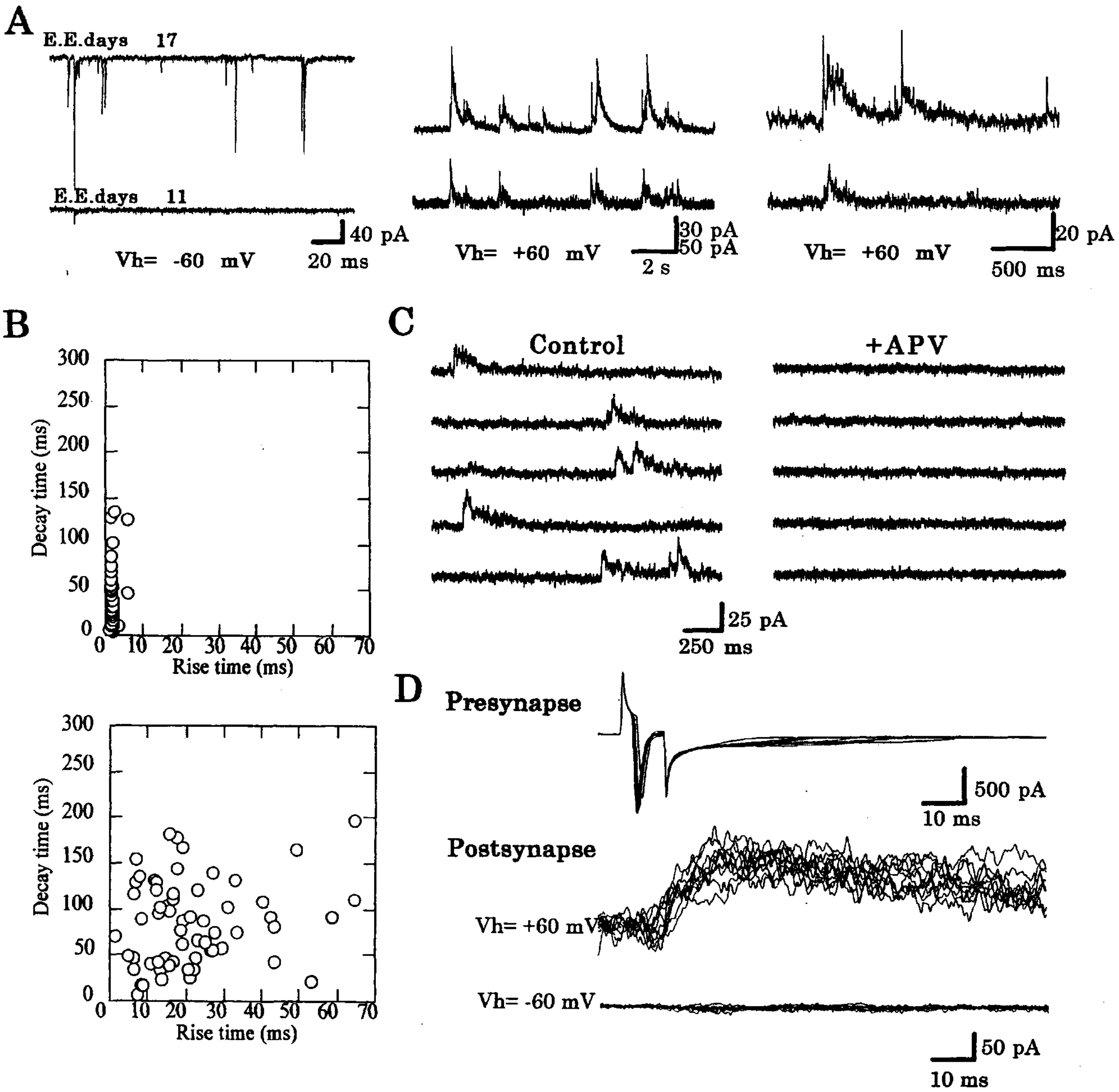

Fig. 3. Prior existence of NMDAR-mediated synapses in E.E.days 11 neurons. A: paired traces of SSCs obtained by dual whole-cell clamp for E.E.days 17 (upper three traces) and 11 (lower ones) postsynaptic neurons. The right and center traces are records at different magnification. B: relationship between rise and decay times of SSCs observed at a holding potential of +60 mV for different aged neurons. The rise and decay times were defined as the time between 10% and 90% maximum SSC for each event. C: effect of APV on SSCs observed at +60 mV in E.E.days 11 neurons. APV was added to the external bathing solution at a final concentration of 100 μM. D: evoked postsynaptic currents from one E.E.days 11 neuron. The superimposed successive traces of postsynaptic currents at a holding potential of −60 mV (lower) and of +60 mV (middle) are shown below the traces of presynaptic currents (upper).

BRESD: 52319 Copyright © 1997 Elsevier Science B.V. . All rights reserved.

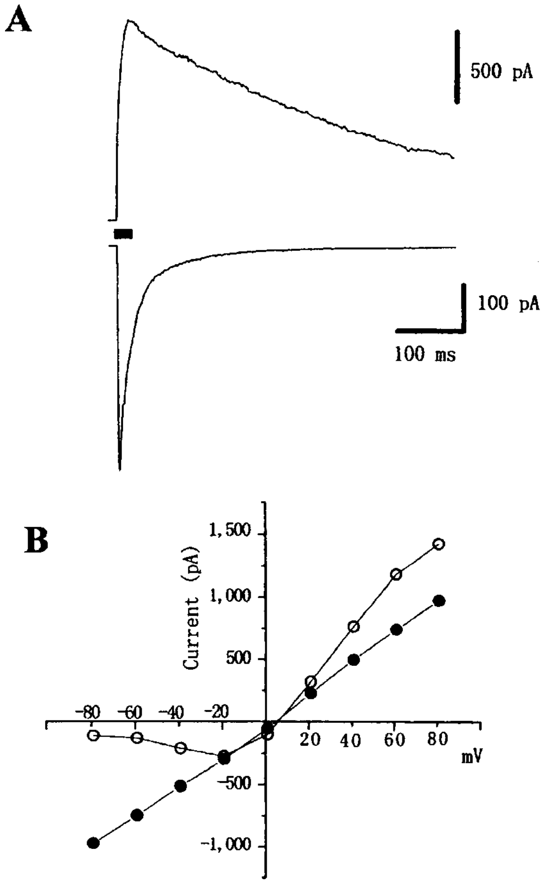

Fig. 4. Functional non-NMDARs in the soma of an E.E.days 11 neuron. A: averaged traces of five successive responses after application of glutamate to an outside-out patch membrane prepared from the soma of E.E.days 11 neuron are shown for holding potentials of +80 (upper) and −80 (lower) mV. B: current–voltage relationships of the glutamate response. The first (solid circles) and the slow (open circles) components of the response were defined as the amplitude 4 ms and 80 ms after the onset of response, respectively. A bar indicates the duration of application of glutamate.

BRESD: 52319 Copyright © 1997 Elsevier Science B.V.. All rights reserved.

responsible for the localization of receptors during synaptogenesis and for synaptic plasticity.

5. Uncited reference

Bekkers [2].

Acknowledgements

The authors thank Drs. D.A.H. Cunningham, S.N. Kudoh and E. Shimabayashi for their helpful comments.

References

[1] Bekkers, J.M. and Stevens, C.F., NMDA and non-NMDA receptors are co-localized at individual excitatory synapses in cultured rat hippocampus, *Nature*, 341 (1989) 230–233.
[2] Bekkers, J.M. and Stevens, C.F., Presynaptic mechanism for long-term potentiation in hippocampus, *Nature*, 346 (1990) 724–729.
[3] Bliss, T.V.P. and Collingridge, G.L., A synaptic model of memory: long-term potentiation in the hippocampus, *Nature*, 361 (1993) 31–39.
[4] Collingrige, G.L., Herron, C.E. and Lester, R.A.J., Synaptic activation of *N*-methyl-D-aspartate receptors in the Schaffer collateral-commissural pathway of rat hippocampus, *J. Physiol.*, 399 (1988) 283–300.
[5] Crair, M. and Malenka, R.C., A critical period for long-term potentiation at thalamocortical synapses, *Nature*, 375 (1995) 325–328.
[6] Durand, D.M., Kovalchuk, Y. and Konnerth, A., Long-term potentiation and functional synapse induction in developing hippocampus, *Nature*, 381 (1996) 71–75.
[7] Fletcher, T.L., De, C.P. and Banker, G., Synaptogenesis in hippocampal cultures: evidence indicating that axons and dendrites become competent to form synapses at different stages of neuronal development, *J. Neurosci.*, 14 (1994) 6695–7706.
[8] Goodman, C.S. and Shatz, C.J., Developmental mechanisms that generate precise patterns of neuronal connectivity, *Neuron*, 10 (1993) 77–78.
[9] Haydon, P.G. and Drapeau, P., From contact to connection: early events during synaptogenesis, *Trends Neurosci.*, 18 (1995) 196–201.
[10] Hestrin, S., Sah, P. and Nicol, R., A, Mechanisms generating the time course of dual component excitatory synaptic currents recorded in hippocampal slices., *Neuron*, 5 (1990) 247–253.
[11] Horan, P.K., Melnicoff, M.J., Jensen, B.D. and Slezak, S.E., Fluorescent cell labeling for in vivo and in vitro cell tracking, *Methods Cell Biol.*, 33 (1990) 469–490.
[12] Issac, J.T.R., Nicoll, R.A. and Malenka, R.C., Evidence for silent synapse: implications for the expression of LTP, *Neuron*, 15 (1995) 427–434.
[13] Jonas, P., Major, G. and Sakmann, B., Quantal components of unitary EPSCs at the mossy fibre synapse on CA3 pyramidal cells of rat hippocampus, *J. Physiol. (Lond.)*, 472 (1993) 615–663.
[14] Jones, A.K. and Baughman, W.R., Both NMDA and Non-NMDA subtypes of glutamate receptors are concentraed at synapses on cerebral cortical neurons in culture, *Neuron*, 7 (1991) 593–603.
[15] Liao, D., Hessler, N.A. and Malinow, R., Activation of postsynaptically silent synapses during pairing-induced LTP in the CA1 region of hippocampal slices, *Nature*, 375 (1995) 400–404.
[16] Nowak, L., Bregestovski, P., Ascher, P., Herbet, A. and Prochiantz, A., Magnesium gates glutamate-activated channels in mouse central neurones, *Nature*, 307 (1984) 462–464.
[17] Tokioka, R., Matsuo, A., Kiyosue, K., Kasai, M. and Taguchi, T., Synapse formation in dissociated cell cultures of embryonic chick cerebral neurons, *Dev. Brain Res.*, 74 (1993) 146–150.

BRESD: 52319 Copyright © 1997 Elsevier Science B.V. . All rights reserved.

14.

3.9 ニワトリ大脳皮質ニューロン――シナプス形成・可塑性アッセイ系

田口隆久, 清末和之, 工藤　卓

記憶・学習・意識に代表される脳高次機能は, 簡単にいえば, ニューロンの作る神経回路網の変更である. この変更が, 主にシナプス部位における構造と機能の変化に依存することは疑いの余地はない. したがって, シナプス変化の分子機構を解明することは現代脳科学における最重要課題の１つである.

この課題に対しては様々なアプローチが考えられるが, 筆者らは, シナプスが２個のニューロン間に形成される局所的構造であり, この場における分子・細胞の動態解析が重要であると考え, 個々のシナプスの解析可能な解離培養系を用いて研究を進めている. この培養系に用いる動物種はいくつか考えられるが, 以下の観点からニワトリ大脳皮質ニューロンを用いている. (1)胚齢の異なる胚の準備が容易(動物飼育室の維持が不要), (2)発生生物学的知見が豊富, (3)胚操作が容易.

実験例に示すように, この系においてはシナプス形成が胚齢等価日数に依存して進行し, このシナプス形成はニューロンの活動に依存し, さらにできあがった回路網においてはシナプスの可塑的現象解析も可能である. 最近, 長期増強(LTP)に代表されるシナプス伝達効率の可塑的変化に伴うシナプスの構造的・機能的変化と, 発生過程のシナプス形成に伴うそれらの変化の間の類似性が注目されるようになってきた. したがって, ここで紹介するニューロン解離培養系は神経情報処理素過程の分子機構解明に大きな貢献をするものと期待される. また, 細胞接着関連ペプチドを用いた手法を用いれば, ニューロンとグリアの相互作用の解析も容易に可能である.

ここではパッチクランプ法を用いた電気生理学的解析に用いているニューロン培養法を紹介する. ニワトリ大脳皮質培養系を用いて, 神経突起伸長活性アッセイやグルタミン酸神経興奮毒性アッセイも行っているが, これらに関しては文献を参照されたい[1~3].

準備するもの

機器類……………………………………………………………………………………

- クリーンベンチ
- 実体顕微鏡(ズーム機能つきが便利)

- 簡易型倒立顕微鏡(細胞数計測用)
- 恒温水槽(37°C 用)
- CO_2 インキュベーター(5% CO_2, 95%空気, 湿度 100%)
- 培養皿(通常は ϕ 35 mm の組織培養用)(Iwaki, 300-035)
- 15 ml 滅菌済み遠心チューブ(Iwaki, 2327-015)
- 滅菌ピペット
- 転卵式インキュベーター(昭和孵卵機)
- 血球計算板(改良ノイバウエル型, 他の型でも可)
- メス
- ピンセット, 精密ピンセット(No. 5)
- 解剖皿(自作, ϕ 60 mm 結晶皿にシリコンゴムを固める)

動物

- ニワトリ白色レグホン有精卵, 1〜5 個(培養規模に依存)
- ニワトリ胚：有精卵を上記転卵式インキュベーターで孵化(37.6°C)し, 適当な日数後に使用(通常は 10 日後)

試薬

- PBS(−)(カルシウム, マグネシウム　除去)
- 90%エタノール(特級エタノールと滅菌水で作成, 70%でも可)
- 改良 MEM 培地：Earle's MEM(GIBCO BRL)を 2 倍希釈し, 以下の試薬を添加

NaCl	60 mM
炭酸水素ナトリウム	2.2 g/l
$CaCl_2$	2 mM
HEPES-Na(pH 7.4)	25 mM
ピルビン酸 Na	1 mM
Na_2SeO_3	0.5×10^{-7}M
塩化コリン	0.1 mM
$ZnSO_4$	0.1 μM
$CuSO_4$	1 nM
ミオ-イノシトール	0.1 mM

- GIT 培地(日本製薬)
- ウシ胎児血清：56°C, 30 分　非働化処理したものを用いる
- 完全培地
  50%改良 MEM, 40% GIT 培地, 10%ウシ胎児血清に 10 mM グルコース, 100 単位/ml ペニシリン, 100 単位/ml ストレプトマイシン, 2 mM グルタミン, 5 μg/ml インスリン添加
- ポリ-L-リジン(Sigma, P1524)(av. MW>300 K)　0.025 μg/ml 溶液

- インスリン(Sigma, I1882)
- トリプシン溶液(GIBCO BRL, 15400-054)
- ペニシリン・ストレプトマイシン溶液(GIBCO BRL, 15140-122)
- L-グルタミン溶液(GIBCO BRL, 25030-016)
- 滅菌水(超純水をオートクレーブしたもの)

プロトコール

培養皿前処理(ポリリジンでコーティング)(すべてクリーンベンチ内で操作)

❶ ϕ 35 mm 培養皿にポリリジン溶液を 1 m*l* 添加.

❷室温で 2 時間放置.

❸ポリリジン溶液を捨てる.

❹滅菌水で 3 回培養皿を洗浄.

❺ UV 滅菌灯下でふたをあけて乾燥(30 分程度)[長時間(2 時間以上)UV 照射は不適].

❻乾燥後の培養皿に 2 m*l* の完全培地を加える.

培養法

❶孵化器から取り出した胚齢 10 日の有精卵(1 個)の表面を 90%エタノールで消毒する.

❷卵の上部を切り取り(約 ϕ 2 cm), 胚をピンセットでつまみ出し, クリーンベンチ内の PBS(−)を入れた滅菌シャーレに置く.

❸頭蓋部を実体顕微鏡下の PBS(−)を入れた解剖皿に置く.

❹精密ピンセットで頭皮を除き, 大脳のみを取り出す.

❺大脳半球ごとに髄膜等の余分な組織を取り除き, メスで 1 mm 幅程度に刻む.

❻ 10 mM グルコース添加 PBS(−)溶液(2 m*l*)の入った 15 m*l* 遠心チューブに大脳組織を移す.

❼ 0.2 m*l* トリプシン溶液を加え, 37°C, 30 分, 恒温水槽に放置.

❽組織が壊れないように静かに溶液を除き, 完全培地(約 1 m*l*)を加え, 軽く撹拌することによって組織を洗浄する.

❾この操作を 4 回繰り返す.

❿完全培地を 2 m*l*(厳密でなくてよい)加え, 滅菌トランスファーピペットでピペッティング

大量のニューロンが必要な場合には，上記の操作を並行して複数の有精卵について行う．同一遠心チューブに上記以上の組織を入れて処理しないこと．

応用実験例1

シナプス形成解析4)

この方法で培養したニューロン間のシナプス形成を，ホールセルクランプ法を用いて確認した．胚齢10日の大脳由来神経細胞の培養7日目の顕微鏡像が図1に示されている．神経線維でつながっている2つのニューロンに微小ガラス電極を適用しホールセルクランプを行い，一方の刺激により他方からシナプス応答をとることができた(図2)．このシナプス形成は胚齢等価日数(胚齢と培養日数の和)依存的に進行することがわかった．このことは，この系においては，*in vivo* から *in vitro* に細胞を移しても同じ時計に従って発生が進行することを示している．詳細な解析から，この系では胚齢等価日数13から15にかけてシナプス形成が進行し，15から17にかけてシナプス成熟，すなわち，シナプス伝達効率が上昇することが明らかになった．

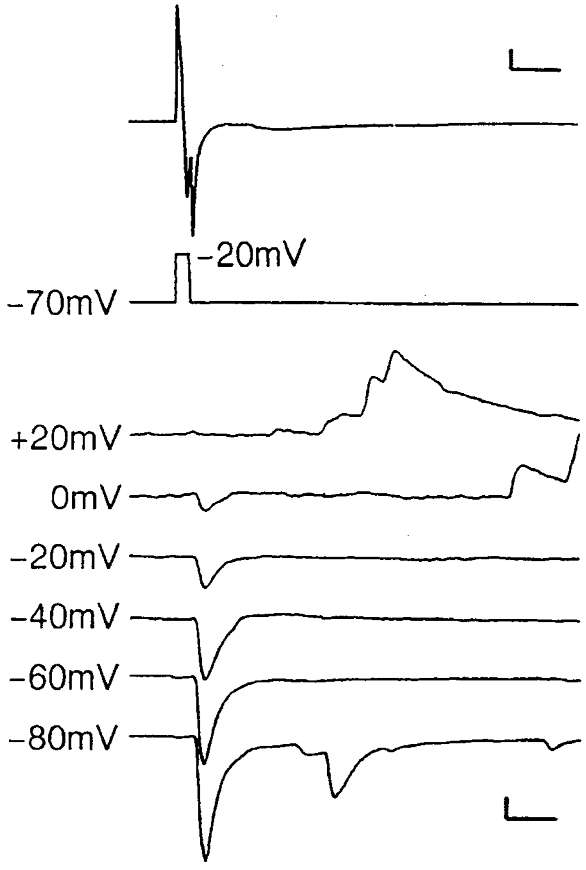

図2 シナプス形成の電気生理学的確認．シナプス形成をしている2つのニューロンにホールセルクランプし，一方の細胞を刺激(上の2トレース)すると，もう一方の細胞から興奮性入力電流(下の6トレース，固定膜電位が各トレース左に示されている)が確認された．この興奮性シナプスの伝達物質はグルタミン酸である．培養日数や胚齢の異なる培養系を用い，このような記録を多数集め，この培養系でのシナプス形成の特性を明らかにした．スケールバーは，250 pA と 10 ms を示す．

応用実験例 2

シナプス成熟過程の活動依存性解析[5]

応用実験例 1 で示された胚齢等価日数 15 から 17 にかけてのシナプス成熟過程に対する神経活動依存性を Na チャンネル阻害剤(テトロドトキシン)と AMPA/kainate 受容体阻害剤(CNQX)を用いて解析した. 微小シナプス後電流の成熟に対する両阻害剤の効果は有意な差はなかったが, 刺激による(evoked)シナプス後電流の発生過程に伴う増大については CNQX の方が有意に大きい抑制効果を示した(図 3). これらの結果は, 局所的に見たシナプス部位の数の制御に自発的伝達物質放出による上記受容体の活性化が重要な役割を果たしていると解釈することができる(図 4).

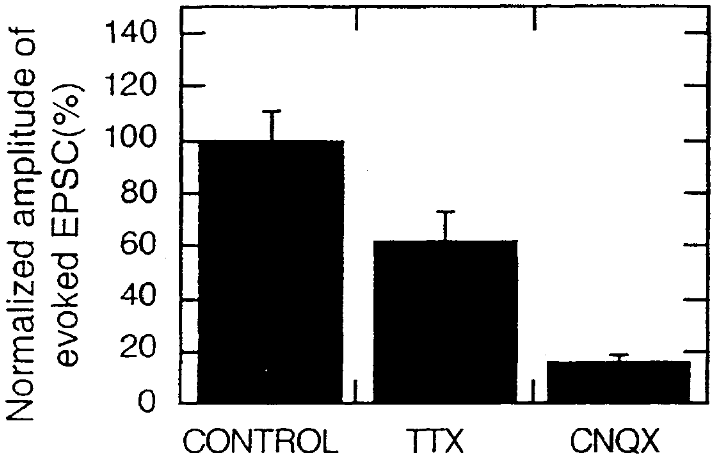

図 3 活動依存性のシナプス成熟. 胚齢等価日数 15 から 17 にかけてシナプス電流が著しく増大する. このシナプス成熟過程に対するニューロン活動の影響を 2 種類の阻害剤, テトロドトキシン(TTX, Na チャンネル阻害剤)と CNQX(AMPA/kainate 受容体阻害剤)を用いて解析した. 興味深いことに, シナプス前細胞の刺激によるシナプス電流増大の阻害程度に両者間で有意な差が認められた.

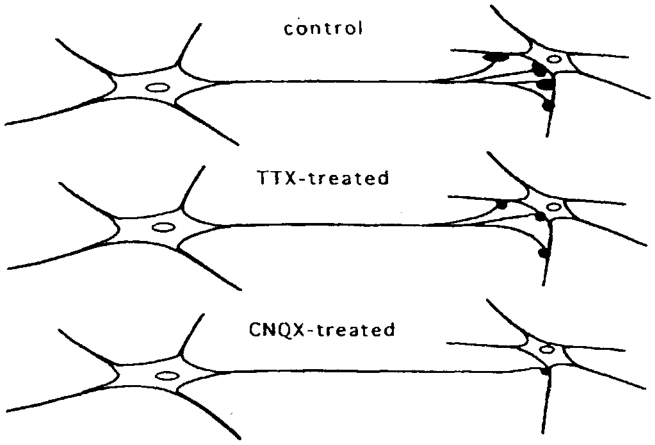

図 4 活動依存的シナプス成熟過程の模式図. 図 3 で示した結果と微小シナプス後電流に対し両阻害剤の効果に差がないという結果と併せて考えると, 最小シナプス部位個々の機能発達は, 対照実験群よりは劣るものの, 両阻害剤間には差はなく, その部位の数に差があるというシナプス成熟モデルを考えることができる.

応用実験例 3

シナプス伝達効率長期増強の解析[6)]

胚齢等価日数 17 でシナプス形成・成熟がほぼ完了するが，この時期の系を用いてシナプスの可塑的変化の解析を試みた．この培養系のニューロンは多くが同期して活動している．2 つのニューロンから同時に電気的活動記録をとることにより，同期した活動のみに注目した．これは，シナプス前細胞刺激によるシナプス解析に近似した解析とみなすことができる．この記録系を用い，培養細胞外液のマグネシウムイオンを 15 分間除く操作により 40 分以上続く増強現象の観測に成功した（図 5）．この増強は NMDA 受容体の活動に依存しており，海馬 CA1 での現象に類似している．さらに，この増強はこの 15 分間の蛋白質合成や RNA 合成に依存していることが明らかになった．

この系を用いた研究の展開

上記の応用例は主にホールセルクランプ法を用いた電気生理学的シナプス解析が主であるが，現在，このシナプス機能に関与する分子群の探索の方向へも研究が広がっている．たとえば，シナプス形成に伴うレセプター分子の動態解析を組織学的手法と高度な光学顕微鏡を用いて行う研究，長期増強に伴う遺伝子発現の分子生物学的研究，細胞内情報伝達系のシナプス機能へ

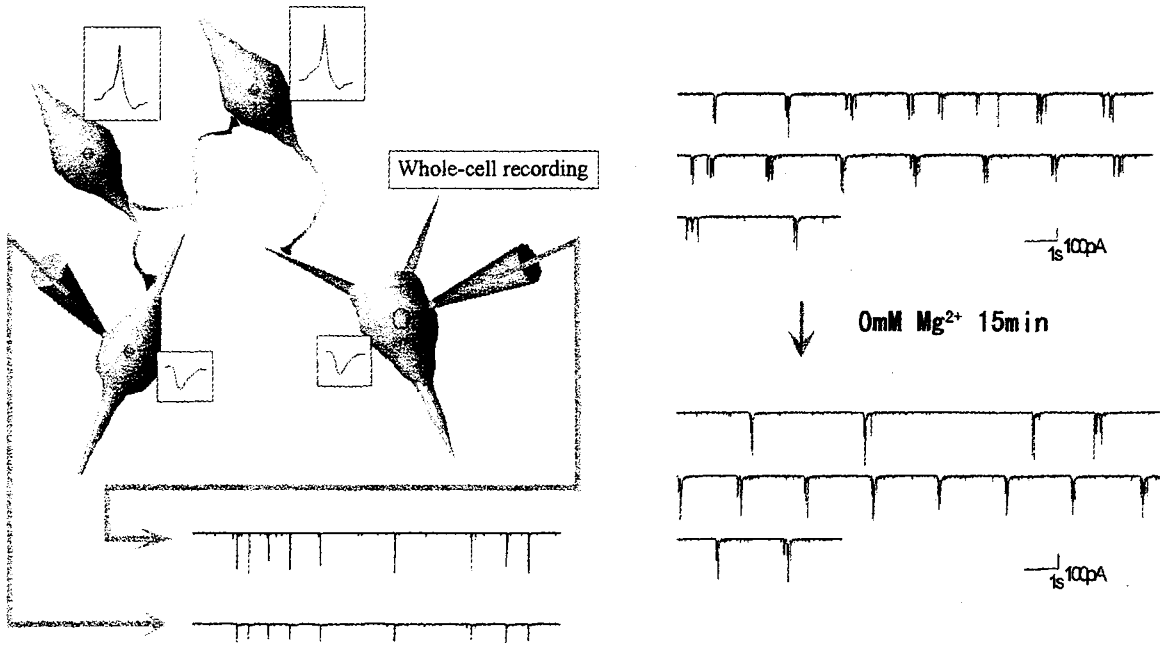

同期して活動するニューロン

図 5　培養系における長期増強解析．同期して活動する 2 個のニューロンにホールセルクランプし，15 分間のマグネシウムイオン除去処理で NMDA 受容体を活性化し，それに引き続く 40 分以上にわたるシナプス後電流の増強を引き起こした．

の関与に関する細胞内灌流法による研究，細胞接着制御によるニューロン・グリア相互作用の研究等がこの培養系を用いて進められている．まだ，準備段階であるが，2次元刺激・活動計測による神経回路網の動態解析もこの系で可能である．

この培養系は，比較的均質な性質を示すが，それでもこの中にはグルタミン酸作動性興奮性ニューロン，GABA作動性抑制性ニューロンの両者が含まれ，またレセプターのサブタイプについては今のところ情報に乏しい．細胞膜表面マーカー探索に基づくニューロンの分類と分別による均質な培養系や，培養基板のパターニング技術開発に基づく制御された培養系の開発が今後の課題である．

文献……………………………………………………………………………………

1. Taguchi T, Huchet M, Roa M, Changeux JP, Henderson CE (1987) A subpopulation of embryonic telencephalic neurons survive and develop *in vitro* in response to factors derived from the periphery. Dev Brain Res 37 : 125-132
2. Yamamoto T, Taguchi T (1992) A muscle-derived factor antagonizes the neurotoxicity of glutamete in dissociated cell cultures of chick telencephalic neurons. Neurosci Lett 139 : 205-208
3. 西宗裕史，田口隆久(1995)注目されるシグナル伝達因子―筋由来神経突起伸長因子．実験医学 13 : 104-105
4. Tokioka R, Matsuo A, Kiyosue K, Kasai M, Taguchi T (1993) Synapse formation in dissociated cell culture of embryonic chick cerebral neurons. Dev Brain Res 74 : 146-150
5. Kiyosue K, Kasai M, Taguchi T (1996) Two modes of activity-dependent synaptogenesis of cerebral neurons *in vitro*. Neuro Report 7 (in press)
6. Kudoh S, Kiyosue K, Kasai M, Taguchi T (1995) Synaptic plasticity in dissociated chick cerebral neurons induced by Mg-free medium. Soc Neurosci Abst 21 : 1321

16.

Molecular Recognition Using Short Peptides and Its Detection by Surface Plasmon Resonance Spectroscopy

Hiroshi Taniguchi[a], Koji Inai[b], Yao-can Zhu[c], Takahisa Taguchi[a], and Susumu Yoshikawa[a]

[a] *Depart. Organic Materials, Osaka National Research Institute, AIST, Ikeda 563, Japan*

[b] *Medical Development Group, Kuraray Co., Ltd., Kurashiki 710, Japan*

[c] *Ion Engineering Research Institute, Hirakata 573-01, Japan*

Although peptides are the potent molecules for specific molecular recognition of some small compounds, there are much difficulties in detecting these molecular complexation directly, since the affinity interactions are too small to detect without using specific markers such as fluorescent probes. For this purpose, we developed a new methodology using surface plasmon resonance spectroscopy for sensitive detection of small molecules by peptides without using any label.

Introduction

Molecular recognition is widely used for assaying biological activities such as immune reaction. In these system, usually the protein interactions are involved for specific binding, which is large enough to detect using ordinal detection methods.

Although peptides are the potent molecules for specific molecular recognition of some small compounds, there are much difficulties in detecting these molecular complexation directly, since the affinity interactions are too small to detect without using specific markers such as fluorescent probes. For this purpose, we developed a new methodology using surface plasmon resonance spectroscopy for sensitive detection of small molecules without using any label.

For finding the pair of molecules with specific binding affinity, we selected to use pentapeptide library method [1] for porphyrin derivatives of rigid structure. The selected peptides were synthesized after GGC sequence attached on these sequence for SPR measurement. Their peptides had a good binding affinity for tetracarboxylic phenyl porphyrin, TCPP. The synthesized peptide was immobilized on the silver coated BK-7. This monolayer of peptide was reacted with TCPP and monitored by SPR.

Result and Discussion

The 5 residue peptide library consisted of 19 natural amino acids except for cysteine, attached on polymer matrix via spacer, with the diameter of about 300μm, being prepared by the split and pool method, giving one petide on one bead. The TCPP molecules (1 μg/ml) was added to this library(50 mg). After reaction for 1 hour at room tempreture, these beads washed with PBS. The reacted beads colored by TCPP. To determined the peptide sequence, the colored bead took out one by one among unreacted beads under microscopic observation. The reacted bead was washed with 6M guanidine hydrochloride and DMSO to remove the receptor complex, and then was determined the peptide sequence on the bead by protein sequencer (model 473A, Perkin Elmer). The selected peptides were synthesized after GGC sequence attached on these sequence for SPR measurement. All peptides were synthesized by the solid-phase method using the Fmoc-strategy on the Shimazu PSSM-8. The peptides were cleaved from the TG-RAM resin and the protection group were simultaneously removed with trifluoroacetic acid / water / thioanisole / ethaneditiol / ethylmethylsulfide / thiophenol (82.5 / 5 / 5 / 2.5 /3 / 2), and then the free peptides were purified by reversed phase HPLC. The purity of peptide was assessed by HPLC and identified by a time-of-light mass spectrometry(TOF-MS) with matrix assisted laser desorption ionization. The mass peak of all purified peptides on the TOF-MS agree with the corresponding calculated value. For finding reaction with TCPP, the dissociation constant of these peptide was measured by capillary electrophoresis method. Table 1 shows the sequences of peptides binding TCPP, synthesized peptide, and their binding affinity.

Table 1. Amino acid sequences of peptides binding TCPP, synthesized peptides and their binding affintiy

Peptide	Sequence of peptide	Sequence of synthesized peptide	Binding affinity
BMP-1	HRFHR	HRFHRGGC	-
BMP-2	MRWNF	MRWNFGGC	+
BMP-3	MIDFR	MIDFRGGC	++
BMP-4	VLIRF	VLIRFGGC	+
BMP-5	LFFAN	LFFANGGC	n.o.
BMP-6	QRRSG	QRRSGGGC	+
BMP-7	WRSTR	WRSTRGGC	+
BMP-8	WRINP	WRINPGGC	n.o.
BMP-9	FRRAQ	FRRAQGGC	-

n.d.:not observed -:weak +:medium ++:strong

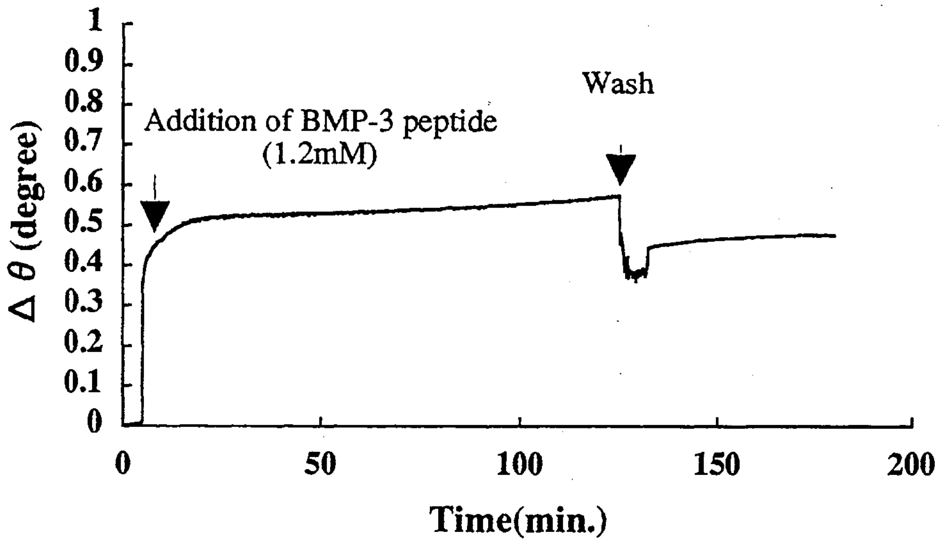

Fig.1 Time-course of BMP-3 peptide binding to Ag surface

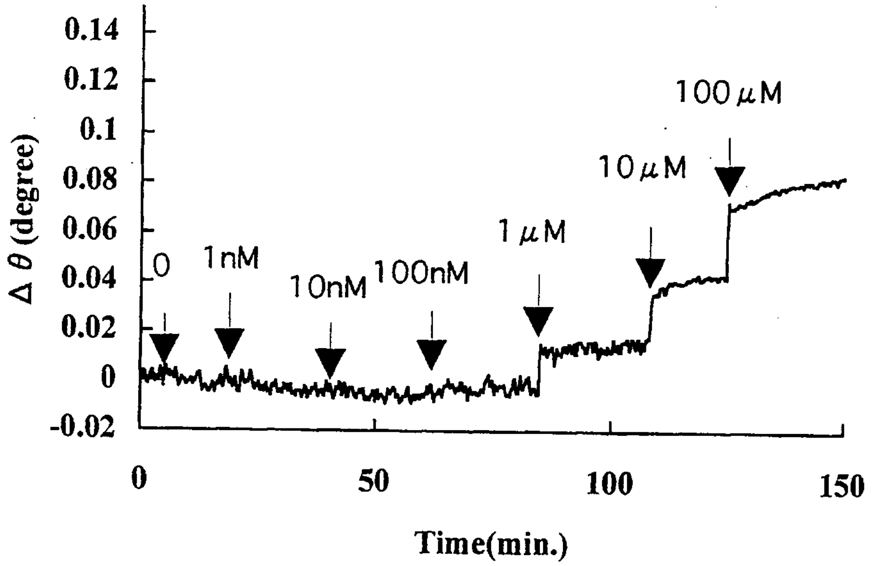

Fig.2 Detection of dose-dependant binding of TCPP by SPR

Out of these porphyrin binding peptides, we selected one of the best associable peptide, BMP-3, for further experiments. The linking of BMP-3 on the silver surface was determined by SPR measurement. Fig. 1 shows the time-course of BMP-3 peptide binding to Ag surface. BMP-3 was linked on Ag surface via SH group of C terminal cysteine forming the covalent bond of Ag-S. This monolayer of peptide was reacted further with TCPP, successfully monitored by SPR.The dose-dependence of TCPP was observed over the concentration ranged form 1 to 100μM. One micro molar of TCPP was detectable within 5minutes.

In conclusion, we found that peptide library is quite a feasible method for finding the affinity pair of molecule and Surface Plasmon Resonace Spectroscopy is a versatile method for detecting the molecular recognition reaction of small molecules.

Acknowledgment

References

1. Kit S. Lam, Sydney E. Salmon, Evan M. Hersh, Victor j. Hruby, Wieslaw M. Kazmierski, and Richard J. Knapp (1991) Nature, **354**, 82-84.

17.

A voltage- and K+-dependent K+ channel from *Dictyostelium discoideum* membrane fraction enriched in contractile vacuole

Kunito Yoshida3*, Toru Ide, Kei Inouye 1, Koichi Mizuno 2, Takahisa Taguchi 3, Michiki Kasai

Department of Biophysical Engineering, Faculty of Engineering Science, Osaka University, Toyonaka 560, Japan

* Corresponding author. Fax: +81 6 8439354
Tel: +81 6 8506542
e-mail: yoshida@bpe.es.osaka-u.ac.jp

1 Department of Botany, Division of Biological Science, Graduate School of Science, Kyoto University, Kyoto 606-01, Japan

2 Department of Biology, Graduate School of Biological Science, Osaka University, Toyonaka 560, Japan

3 Department of Organic Materials, Osaka National Research Institute, AIST, 1-8-31, Midorigaoka, Ikeda, Osaka 563, Japan

Abstract

The contractile vacuole is an intracellular organelle found in fresh-water protozoa and amoebae, whose function is thought to expel water under hypotonic environments. To elucidate the mechanism of this water transport, it is necessary to investigate the ion transport across the organelle membrane. We obtained membrane fraction enriched in contractile vacuole by aqueous-polymer two-phase partitioning, and examined for channel analysis by incorporating it into artificial planar lipid bilayers. We observed single-channel currents of a highly K^+-selective channel with slope conductance of 100 pS and reversal potential of -20.4 mV which corresponded to $P_{K^+}/P_{Cl^-}=7$, in asymmetrical KCl solutions(*cis*, 300 mM/100 mM, *trans*). They showed bursts separated by infrequent quiescent periods. At 0 mV the mean open time was 2.6 ms and the mean closed time was 4.6 ms. Na^+ and Li^+ were impermeant. The permeability ratio P_{Rb^+}/P_{K^+} of almost 1 was obtained from the reversal potential, although the unitary conductance was apparently reduced when the current flowed from the Rb^+ containing side to the other, indicating that Rb^+ is a permeant blocking ion. The open probability within bursts was constantly near 0.5 at the holding potential of the *cis* side positive to the *trans* side, but it decreased to 0 at negative potential. This channel was blocked by 0.2 mM quinine and 30 mM TEA^+. The open probability-voltage relationship showed a striking dependency on the KCl concentration of either side solution. Such voltage- and K^+-dependent gating may play an important role in the water export by this organelle.

Key words: contractile vacuole, planar lipid bilayer, inward rectifier potassium channel, aqueous-polymer two-phase partitioning, *Dictyostelium discoideum,* quinine

Abbreviations: TEA, tetraethylammonium; EDTA, ethylenediamine-N,N,N',N'-tetraaccetic acid; PMSF, phenylmethylsulfonyl fluoride; NBD-Cl, 7-chloro-4-nitrobenzo-2-oxa-1,3-diazole; Tris, tris(hydroxymethyl)aminomethane; FITC, fluorescein isothiocyanate; HEPES, N-2-hydroxyethylpiperazine-N'2-ethanesulfonic acid

1. Introduction

The contractile vacuole is a prominent structure which can be easily recognized in fresh-water protozoa and amoebae. It is believed to accumulate water from the cytosol and excrete it into the extracellular space and this process allows fresh-water organisms to survive under hypotonic environments without losing intracellular essential ions. The great mystery lies in the mechanism that this organelle pumps water in the apparently reverse direction of the osmotic gradient: contractile vacuole takes up water from more hypertonic cytoplasm and excretes it into more hypotonic extraplasmic space. The large amount of water estimated to flow from the cytoplasm into the vacuole suggests the involvement of active transport of salts [1].

Recently, the structure of *Dictyostelium discoideum* contractile vacuole complex was investigated in detail by electron microscopy using a quick-freeze, deep-etch technique and it turned out to be composed of interconnected array of tubules and cisternae highly condensed with 'pegs' which looked like proton pumps [2]. This organelle was isolated by sucrose density gradient centrifugation and turned out to consist of two kinds of vacuoles, the central large vacuole *bladder* and satellite tubules *spongiomes,* as seen in other protozoa [3]. *Spongiome* is highly enriched in V-H^+-ATPases, which seems likely to play an important role in the energetic process of water accumulation. Buoyant membrane fraction highly enriched in V-H^+-ATPases was formerly isolated as *acidosome* [4,5,6], and it seems likely that the fraction at least partly contains *spongiome* although its exact relation to the contractile vacuole complex is under controversy [3, 7]. *Bladders,* more buoyant vacuoles which are enriched in alkaline phosphatase activity [8] and membrane-bound calmodulin [9], and are believed to be the locus where the contractile vacuole complex fuses with the plasma membrane [10]. Interestingly, clathrin heavy chain-deficient mutant cells lack contractile vacuoles, which implies that a certain mechanism common to clathrin-mediated endocytosis plays an important role in generation or retention of this organelle [11].

How can this organelle pump up water from hypertonic cytoplasm into hypotonic extraplasmic space? It has been suggested that the formation of the hypotonic fluid in the vacuole takes place in two steps: osmolytes are transported into the vacuole with water following passively, and the osmolytes are reabsorbed into the cytoplasm leaving hypotonic fluid behind [1,12]. On the other hand, according to his observations, Heuser proposed 'bicarbonate model', which predicts that inexhaustible weak anion HCO_3^- is transported into contractile vacuole driven by proton motive force and plays a role as an osmolyte to drive water in [2]. To understand the mechanism of water-pumping by the contractile vacuole, it is necessary to characterize the ion transport across the organelle membrane. We isolated membrane fraction enriched in contractile vacuole by aqueous-polymer two-phase partitioning [13], and fused it into artificial planar lipid bilayers. We observed many kinds of conductive activities, and among all, investigated the single channel properties of a certain type of K^+ channel which frequently appeared.

The observed channel was highly K^+-selective and voltage-dependent, and showed unusual unique features such that the open probability saturated below 1 whenever a high voltage was applied, and that the open probability-voltage relationship was dependent on the KCl concentration, especially of one side. Such voltage- and K^+-dependency is discussed in view of both biophysical and physiological functions.

2. Materials and methods

2.1. *Cells and fractionation by two-phase system*

D. discoideum strain AX-2 was cultured in HL-5 axenic medium on a gyrorotary shaker at 175 rpm, 23 ℃, to $5\text{x}10^6 \sim 1\text{x}10^7$ cells/ml [14]. To obtain developmental cells, vegetative cells were deprived of nutrition medium, resuspended and shaken in 10 mM Na/K phosphate buffer (pH 6.5) for 5~9 hours at a cell density of $2.0\text{x}10^7$ cells/ml. We observed this 'contractile-vacuole' channel both in vegetative and developed cells, and we combined the data from different stages because no obvious distinction in kinetic characteristics of the channels from different developmental stages, was observed. Cells were pelleted at 800 ×g for 1 min, washed by homogenate buffer(5 mM glycine-NaOH pH 8.5, 0.1 M sucrose) [4,5] and resuspended in homogenate buffer additionally containing 1 mM EDTA and protease inhibitors (1 mM PMSF, 1 μg/ml leupeptin). Cells were lysed by passing through a polycarbonate filter with 5 μm pores. Homogenate was then centrifuged at 1 000 ×g for one minute to remove unlysed cells and at 122 800 ×g for one hour, and the resulting pellet was resuspended in 5 mM potassium phosphate buffer (pH 8.0), containing 0.3 M sucrose. About 5~10 mg protein of the membrane pellet was loaded on aqueous-polymer two-phase system to yield 12-g system in a 15-ml plastic tube with final concentrations of 6.0~6.4%(w/w) dextran T500, 6.0~6.4%(w/w) polyethyleneglycol (PEG 4000), 3 mM KCl, 0.3 M sucrose, and 5 mM potassium phosphate buffer, pH 8.0. Each tube was prepared by weighing contents separately. Membranes were partitioned three times and re-extraction was performed as noted in

[13]. The upper polyethyleneglycol phases and, for marker assays, the first partitioned lower phase also, were collected and diluted 5-10 fold with 10 mM Tris, 20 mM HEPES buffer, pH 7.4. After centrifuged at 122 800 ×g for an hour, the resulting pellet was resuspended in 10 mM Tris, 20 mM HEPES, 0.3 M sucrose, pH 7.4. The final protein concentration was 2~5 mg/ml. The samples were stored in 30~50 μl aliquots at -70 ℃ until use in bilayer experiments.

2.2. *Marker enzyme assays*

Protein concentration was determined with BioRad Protein Assay using bovine serum albumin as a standard [15]. Alkaline phosphatase and NADH oxidoreductase were assayed as described in [16], Acid phosphatase as described in [5], and ATPase activities as described in [4]. NBD-Cl-sensitive ATPase activity as determined as the difference in the activity in the presence and absence of 25 μM NBD-Cl. Vanadate-sensitive ATPase activity was determined as the difference in the presence and absence of 100 μM vanadate. Mitochondrial ATPase activity was measured at pH 9.5.

2.3. *FITC-label of cell surface*

Outer cell surface was labelled by FITC to assay the partitioning of plasma membrane. Cell suspension was washed in 5 mM $NaHCO_3$/NaOH pH 9.5, 0.1 M sucrose, and resuspended in the same solution containing 400 μg/ml FITC at a cell density of approximately 5×10^8 cells/ml [17]. After shaken at 23 ℃ for 5 minutes, cell suspension was diluted at least 30-fold by ice-cold 5 mM glycine-NaOH pH 9.5, 0.1 M sucrose. Then cells were centrifuged and the pelleted cells were resuspended and washed three times in 5 mM glycine-NaOH pH 8.5, 0.1 M sucrose. Most cells did not lyse under these conditions. The specificity of cell surface labeling was evaluated by quenching fluorescence upon acidification to pH 4 by addition of HCl. FITC had an tendency to be taken up into the cell if we allowed pH below 9.5 in the presence of dye. Aliquots of membrane fractionated by two-phase method were suspended in 1 mM Tris, 2 mM HEPES, pH 7.4, 0.1 M sucrose, 0.1 % Triton X-100, and fluorescence was monitored at 520 nm, excited at 495 nm using spectrophotometer. Basal fluorescence of cell lysate without FITC was subtracted from all measurements.

2.4. Electrophysiology

Planar lipid bilayers were formed from asolectin dissolved at 20 mg/ml in n-decane [18]. Prepared samples were mixed with half volume of 3 M KCl (to yield final concentration of 1 M KCl) and fused into the bilayer by pressure application. The recording solutions were composed of designated concentration of salts and 10 mM Tris, 20 mM HEPES, pH 7.4. 50 G Ω-resistative-feedback current-to-voltage converter was built according to [19]. Signals were recorded on videotapes after processing with a digital audio processor (PCM-501ES; SONY Corp.).

2.5. Data analysis

Electrical signals were regenerated from the stored videotapes, filtered at 1 kHz, digitized at 5 kHz, and analyzed by pCLAMP software(Axon Instrument). In this paper, voltages of the *cis* (sample-applying) side relative to the *trans* side are shown, and the sign of the current is positive when it flows from *trans* to *cis*.

For the statsical curve-fitting, the lines and curves were generated by the least-square fitting method using computer softwares (KaleidaGraph 3.0 for Macintosh or Ngraph v.5.31 for NEC PC-9801).

2.6. Materials

Dextran T500 was purchased from Pharmacia, PEG 4000 from Kishida Kagaku (Osaka, Japan), FITC from Dojindo Laboratories(Kumamoto, Japan), and Quinine from Sigma.

3. Results

3.1. Characterization of the sample preparation

Cells were homogenized and separated into two phases by polyethyleneglycol-dextran system as described (*See* Material and methods). The enzyme activities of the upper polyethyleneglycol phases (first and second extraction combined), and the lower dextran phase of the phase system were assayed and shown as percentages of the initial crude membrane fraction (Table. 1). Most of the enzyme activities and protein were predominantly found into the lower phase. However, partitioning of alkaline phosphatase into the upper phase was almost to the same degree of that into the lower phase. Specific activity of alkaline phosphatase was concentrated 6-fold of the initial homogenate. Alkaline phosphatase is a well-established marker for contractile vacuole marker in *Dictyostelium.* So small amount as 6.0 % of vanadate-sensitive ATPase (Table 1), which is a marker enzyme for plasma membrane, and only 3% of the cell-surface label were partitioned into the upper phases (Table. 2). As the SDS-PAGE profile of FITC-labelled cells did not show distinct pattern from that of non-labelled cells (not shown), we thought that the lack of partitioning of FITC-label into upper phases was not brought about by FITC-label itself. From these results, we concluded that our phase system extract contractile vacuole most preferentially from cell homogenate.

Fig. 1 shows the electron micrograph of the negatively stained vesicles from the upper phases. The picture of vesicles resembled those of the previously purified contractile vacuoles, which were featured by large angular holes frequently observed, and smooth and crispy membrane surface.

3.2. Frequency of observing channel activities

When the upper-partitioned membrane vesicles were incorporated into the bilayer, we observed many sorts of conductive activities. For most of them, we could neither discriminate from artifacts, nor apply conventional single-channel analysis to because of too fast gating kinetics to be followed by our recording system. In this paper, we concentrated on a certain kind of channel which appeared in 59 bilayers in total of 2290 trials. This channel showed a strong voltage-dependency such that it opened at a high probability when the *cis* side was positive and closed when negative as described in Fig. 2A. Additionally, in other 9 bilayers, channels which showed similar gating properties with the inverted voltage-dependency (that is, the channel opened when the *cis* side was negative and closed when positive) were observed. We interpreted that they are of the same type channel. For convenience, we shall hereafter call the channel which shows the former voltage-dependency *regular* configuration and the latter *inverted* configuration. The polarity of the voltage and current of the *inverted* channel was made re-inverted to show the corresponding voltage in the *regular* configuration. *Inverted* '*cis*' side is therefore referred to *regular* '*trans*' side, and vice versa.

3.3. Conductance size and ion selectivity

Representative traces of single channel current in the *regular* configuration recorded in asymmetrical (*cis:trans*) 300:100 mM KCl solutions were shown in Fig. 2. The current to voltage relationship revealed the slope conductance of 102.3 ± 2.8 pS and the reversal potential of -20.4 ± 0.8 mV which corresponds to P_{K+}/P_{Cl-} = 7 (Fig.3A, n=5). In asymmetrical (*cis:trans*) 100 mM KCl:100 mM NaCl solutions, the slope conductance shows 57.1 pS at positive holding potentials but the relationship shows non-linearity at negative potentials and the I-V curve never intersects V-axis at less negative potentials than -50 mV (Fig. 3B, open circles). In asymmetrical solution which contains 100 mM KCl in the *cis* side and 80 mM NaCl plus 20 mM KCl in the *trans* side, the relationship was almost linear between -45 and 30 mV, the slope conductance was 57.9 ±1.2 pS, and the reversal potential was -31.5 ±1.7 mV (Fig. 3B, closed symbols, n=2). Fitting into the Goldman-Hodgkin-Katz equation gives the permeability ratio P_{Na+}/P_{K+} almost equal to 0, that is, Na^+ was impermeant ion. In asymmetrical solution (*cis:trans*) 100 mM KCl:80 mM LiCl + 20 mM KCl (Fig. 3C), the slope conductance was 53.3 ±1.2 pS, and the reversal potential was -27.9±2.3 mV, and therefore Li^+ should also be impermeant.

When the proportion of RbCl concentration to the total solution combined with KCl,was variantly raised on the *trans* side with a fixed 100 mM KCl on the *cis* side, the I-V relationship was linear and did not change significantly at positive potentials, whereas the current amplitude was proportionally reduced at negative potentials (Fig. 4A). As seen from the graph, the reversal potential was always around 0 mV. At 80 mM RbCl + 20 mM KCl, actually no current could be observed. The reversal potential, obtained by extrapolation, was 0.75 mV, indicating that the permeability ratio P_{Rb+}/P_{K+} equals approximately 1. The fitted line for positive potentials shows that the slope conductance was 61.1 pS, a slightly higher value than those of impermeant Na^+ and Li^+ ions. On the contrary, when Rb^+ ion was included in the *cis* side solution, the current amplitude did not decrease to so much extent, neither at positive nor negative potentials (Fig. 4B). The corresponding traces are shown in Fig. 4C. These results pointed out that Rb^+ ion is permeant but it blocks this channel effectively at the same time.

3.4. Gating properties

The kinetic properties of this channel shown in Fig. 2 was investigated. The open probability of this channel was nearly 0.5 throughout positive potentials, but it went down to near 0 at negative potentials (Fig. 5A). As seen in Fig. 2B, long silent periods were frequently observed especially at positive potentials. We considered them to be interburst periods and we analyzed open probabilities only within bursts, ignoring closed events longer than 100 msec at positive potentials. It is not clear whether corresponding interburst events exist at negative potentials, but we assumed the absence of events at negative potentials (see Discussion). Open probability did not seem to approach 1 at as highly positive voltages as 60 mV.

As in Fig. 5B, the open time histogram fitted well to a single-exponential curve at each voltage. The reciprocal of the obtained time constant was plotted against voltage in Fig 5C. Inverse of the mean open time approached 0.22 ms^{-1}, corresponding to an open time of 4.5 ms, at positive voltages and increased exponentially towards large negative voltages. The closed time histogram could not be fitted by a single-exponential curve in most cases, although precise number of exponential components necessary for fitting was not determined.

The *trans* side of a bilayer was perfused successively with solutions of varied KCl concentrations. The open probability curve shifted dramatically to the positive direction when the KCl concentration was raised (Fig. 6). The maximal open probability was also lowered when the *trans* KCl concentration was raised from 30 to 300 mM and from 300 to 1000 mM. This decrease in the open probability was reversibly recovered after lowering the KCl concentration to 100 mM.

In Figure 7A, open probability of channels appeared in *cis* 300 mM; *trans* 30 mM, *cis* 300 mM; *trans* 300 mM, and *cis* 30 mM; *trans* 300 mM KCl solution were shown in relation to the applied voltage. The midpoints, estimated by curve-fitting (*See* Discussion), were -23.3 mV, 24.1 mV, and 38.3 mV, respectively, whereas the values of the reversal potential were -44.2 mV, 1.8 mV, and 48.1 mV, respectively (Fig7B). It is obvious that change of *trans* K^+ concentration greatly affects the open-probability-voltage relationship, whereas *cis* K^+ concentration affects only slightly. The maximal open probabilities, estimated by curve-fitting, were 0.63, 0.53, and 0.58, respectively, implying that they were inversely correlated to the total K^+ ion concentration.

3.5. Blockers

Quinine blocked this channel effectively. The critical concentration was near 0.2 mM (Fig. 8A). The ability of TEA^+ to block this channel was also examined. Apparent conductance size was reduced when the concentration of TEA^+ was raised (Fig. 8B, C). The Kd value of TEA^+ block was estimated to be about 30 mM. In both cases, the block was reversible (not shown). TEA^+ seemed to increase the open duration. Charybdotoxin, up to 300 nM, did not block this channel.

3.6. *Regulation by ligands*

We tested effects of 1 mM cyclic AMP, 10 μM cyclic GMP, 2 mM ATP, and 1 μM folic acid on this channel, applied to *cis* or *trans* side. We did not observe any obvious effects of these agents on this channel.

We investigated Ca^{2+}-dependency with changing free Ca^{2+} concentration by addition of calcium or EGTA, but Ca^{2+} did not have any drastic effect on this channel gating (although we could not conclude exactly whether it has any significant effects on gating such as blockade or not). Charybdotoxin, up to 300 nM, also had no effects, applied to *cis* or *trans* side.

4. Discussion

Aqueous-polymer two-phase partitioning is known to enable isolation of right-side-out vesicles of plasma membrane from organelle membrane and inside-out plasma membrane vesicles [13]. We found unexpectedly that samples prepared by this method were poor in the plasma membrane markers, vanadate-sensitive ATPase and cell-surface labels, but instead, highly enriched in alkaline phosphatase activity. In *Dictyostelium,* unlike in other organisms, it was clearly shown by electron microscopy cytochemistry that this enzyme is localized in contractile vacuoles [3,8]. Additionally, the electron micrograph showed that the negatively stained images of our prepared sample was morphologically similar to those of the purified contractile vacuoles, as featured by large holes, and smooth and crispy surface membranes. Therefore, we tentatively concluded that contractile vacuole is preferentially partitioned in upper phase when we apply the two-phase method to *Dictyostelium discoideum* cell homogenate.

The reason why contractile vacuole instead of plasma membrane is partitioned into the upper phase is uncertain. Our preliminary results indicate that prior deprivation of Mg^{2+} ion seems to be essential for preferential partitioning of contractile vacuole into the upper phase, and the partitioning is ascribed to the negative charge of the membrane. On the other hand, *Dictyostelium* plasma membrane is known to be relatively enriched in sterol rather than negatively-charged phospholipid in comparison with other species [6]. These facts may explain the unique way in which the partitioning works with *Dictyostelium* homogenate. Anyway, two-phase partitioning is very complex phenomenon and the method is empirical in essence.

By incorporating these contractile vacuole-enriched upper phases into planar lipid bilayer, we observed single K^+ channel current described as above. We thought that this channel may derive from contractile vacuole membrane. We did not investigate whether other subcellular fractions contain the same K^+ channel activitiy because the lower-partitioned fraction often contains unidentified conductive activities which destabilize the planar bilayer and make the measurements almost impossible. In another preliminary experiment, however, we have fairly often observed the same channel activities in buoyant subcellular fractions isolated by the successive centrifugation in 38% and 12% sucrose solution. Muller previously reported three types of channel activities in the plasma membrane of the aggregative cells with cell-attached patch-clamp [30]. Two of them (DI and DII) were attributed to K^+ channel activities. They were different from ours in the aspects of contductance size and channel kinetics. As for DI, it showed mean open-time within a burst of 21 ms, which was voltage-independent, and discernible from our channel, which showed voltage-dependent mean-open time around 2.6 ms. As for DII, the available information is limited, but judging from the traces, it seems different from ours. As noted in Section 3.1, we observed this channel only 3.0% of the total trials, which was comparable to the percentage of the contaminated membranes recovered in the sample. So far, anyway, we can exclude neither the possibility that this channel also exists in other membranes nor even the possibiliy that it only exists in other membranes. To demonstrate that this channel is indeed localized in the contractile vacuole, it is necessary to identify the channel molecule and raise antibodies against it for immunostaining.

This channel was almost completely impermeable to Na^+ and Li^+ ions, but permeant to Rb^+ ion as judged by the permeability ratio of near 1. However, the conductance size was apparently reduced when the current flowed from Rb^+ containing side to the other. Such a behavior of Rb^+ ion as a permeable blocker was also reported for other K+ channels [20]. Conductance size of this channel is approximately 100 pS, similar to large-conductance Ca^{2+}-activated K^+ (BK) channel. However Ca^{2+} did not have any drastic effect on this channel gating (although we could not conclude whether it has any significant effects on gating such as blockade or not), and charybdotoxin, which is known as a blocker of BK channel, did not block this channel.

The open probability of this channel never approached 1 and saturated at near 0.5. This fact implies that the channel has more than one closed states with one open state. Indeed the open time histogram was well fitted by a single-exponential function, and the closed time histogram needed multiple-exponential function. Assuming that the channel has one open state and two closed states, the channel kinetics would be described by the following model:

$$C_1 \underset{k_1}{\overset{k_{-1}}{\rightleftharpoons}} O \underset{k_{-2}}{\overset{k_2}{\rightleftharpoons}} C_2 \tag{1}$$

The reciprocal of mean open time, that is, the sum of open-to-close rate constants, did not approximate to zero when applied voltage was increased. This means that there are voltage-independent gates and voltage-dependent gates. We assume that one of the gates (gate 1) is voltage-independent and the other (gate 2) is voltage-dependent.

$$\text{gate1:}\quad \frac{O}{C_1} = K_1 = \frac{k_{-1}}{k_1} \tag{2}$$

$$\text{gate2:}\quad \frac{O}{C_2} = K_2 = \frac{k_{-2}}{k_2} = \exp\left\{\frac{-ze\left(V_0 - V\right)}{kT}\right\} \tag{3}$$

where O, C_1, and C_2 designate the probabilities of staying in the corresponding states. K_1 and K_2 are equilibrium constants, k_1, k_{-1}, k_2, and k_{-2} rate constants, z an equivalent valence, V voltage, V_0 the transition voltage, e the elementary charge, k the Boltzmann's constant, and T temperature. In Fig. 5A, the fitted line was drawn according to the equation:

$$P_{open} = \frac{O}{C_1 + O + C_2} = \frac{P_{open}^{max}}{1 + P_{open}^{max} \cdot \exp\left\{\frac{ze\left(V_0 - V\right)}{kT}\right\}} \tag{4}$$

where P_{open}^{max} indicates maximal open probability, which equals $K_1/(K_1+1)$. For this case, $P_{open}^{max}=0.57$ was obtained by curve-fitting, and K_1 was calculated to be 1.33. Concerning the voltage-dependent gate, the equivalent valence z was 1.6, and the midpoint V_0 was 4.34 mV. In Fig. 5C, the reciprocal of the mean open lifetime (1/ τ_{open}) inside bursts was fitted according to the equation,

$$\frac{1}{\tau_{open}} = k_1 + k_2 = k_1 + \kappa_2 \exp\left(\frac{z'eV}{kT}\right) \tag{5}$$

assuming that the rate constant of this channel to shut is composed of the sum of two rate constants, voltage-independent part k_1 and voltage-dependent part $k_2= \kappa_2 \exp(z'eV/kT)$ according to Eyring's rate theory. From this, values of k_1=0.22 ms^{-1}, κ_2= 0.25 ms^{-1}, and z'=-0.56 were obtained.

When the KCl concentration in the each side solution was varied, the voltage-dependence of the open probability of this channel was shifted to the same direction as the changes in the equilibrium potential of potassium ion (E_K). Such voltage-dependent gating with regard to E_K, is well-known for inward rectifier K^+ channels. In our channel, KCl concentration on the *trans* side greatly affected transition voltage (V_o), whereas KCl concentration on the *cis* side showed much weaker effects. It was reported that rectification of inward rectifier K^+ channel in starfish egg depends only on the membrane potential, irrelative to the K^+ equilibrium potential (E_K) when changing the internal K^+ concentration at fixed external K^+ concentration, while it depends on E-E_K when E_K is altered by changing the external K^+ at a fixed internal K^+ concentration [21]. And it has been suggested that K^+ ion may exert a direct influence on the inward rectifier K^+ channel [20,22]. It is quite uncertain whether the voltage- and K^+-dependent gating of our channel is related to the rectification of the inward rectifiers. As for inward rectifiers, voltage-dependent block by intracellular cation such as Mg^{2+} ion or polyamines is considered to be the cause for the rectification. But as we chelated divalent cations during sample preparations and did not add any extra cation (except $Tris^+$), blocking by these cations is unlikely to play a role in the establishment of the gating property of our channel. Then how can we explain the mechanism of K^+-dependency of our channel? We ignorantly think that a hypothesis which involves the voltage-dependent blockade of the permeation pathway by K^+ ion itself (Fig. 9), may explain the following two observations. 1) The maximal open probability (P_{open}^{max}) is suppressed by the increase in KCl concentration of the either side. 2) The transition voltage of open probability apparently depends on the KCl concentration gradient across the bilayer. Furthermore, we showed that Rb+ ion worked as a permeant blocker more effectively from the*trans* side than from the *cis* side. As Rb^+ ion is known to behave in relatively a similar way as K^+ ion in regard to permeating many types of K^+ channels [31], we suggest that there is a Rb^+ binding site in the pore, which may also provide a binding site for K^+ ion itself. (*See* the Fig. 9. legend). Our channel clearly shows discrete gatings and may provide a good model system for studying K^+-dependent mechanism of K^+ channel. Further analysis is necessary to understand the mechanism of K^+-dependent gating.

The physiological roles of this channel in the function of the contractile vacuole are quite unclear. We recently found that inclusion of quinine in hypotonic medium caused the contractile vacuole abnormally swollen and the cell shape round-up (Yoshida et al., manuscript in preparation). It suggests that some quinine-related activities are involved in the normal function of the contractile vacuole. The same concentration of quinine which blocked our channel, was previously shown to exert various effect on physiology of the cell, i.e. cyclic AMP-induced K^+ increase in developmental cell suspension [26,27], cyclic AMP-induced hyperpolarization [28], and formation of long-stalk fruiting body [29]. These phenomena were previously discussed in relation to a presumptive plasma membrane K^+ channel, but can also be attributed to the blockade of the contractile vacuole channel in this study. (Quinine is a membrane-permeable channel blocker.) Our channel was not affected by any signal molecules tested, such as cyclic AMP, but can be somehow indirectly regulated by cyclic AMP in intact cell. Otherwise, change in the partition of K^+ ions between the cytoplasm and the vacuolar lumen, caused by the blockade of the K^+ ion transport by quinine, can affect the activity mediated by the plasma membrane channels. In the fresh water amoebae *Chaos chaos*, it was reported that K^+ ion concentration in the lumen of the contractile vacuole was lower than cytoplasm, whereas Na^+ was higher [23]. The luminal side of the vacuole was found to be mildly acidic [2,9], less acidic than endosomes and lysosomes, and therefore considered to be positively charged relative to the cytoplasmic side [24]. The membrane potential of contractile vacuole was formerly reported in *Amoebae proteus* to be 10 to 20 mV positive luminal side to cytoplasmic side. The presence of inside-positive membrane potential in the contractile vacuole suggests that voltage-dependent channels exist in the membrane. The K^+ channel may work as a pathway for K^+ ion leaking out from inside the vacuole to the cytosol driven by membrane potential set up by H^+-ATPase. The rectifying property of this channel would help not to reverse the direction of the K^+ transport. Identification of the corresponding gene would clarify both the biophysical and physiological functions discussed above.

From both the biophysical and physiological view, this channel seems to be analogous to the inward rectifier K^+ channel found in plasma membrane of other organisms. During the evolution, there seems to be a tendency that the livings in severe environment invaginate their important in-out exchanger system from body surface into inner hidden space to protect it from outer hazards. Possibly, it may not be occasional that a channel related to inward rectifier was observed in upper-partitioned, alkaline phosphatase-enriched membrane fraction in this organism.

Acknowledgements

We are especially grateful for earlier discussions and helpful suggestions to Shigetoshi Oiki, Bert Van Duijn, for earlier encouragements to John Heuser, for facilities of culture and experiments to Koji Okamoto, Mineko Maeda, Atsuko Iwane, Yohko Yamada, Hiroaki Tabuchi, for opportunities to use polarimeter to Tadanao Ando, for suggestions on fluorescence label to Yoshiro Tatsu, for technical advice on perfusion to Manabu Tanifuji, for practical help and suggestions to Kazuyuki Kiyosue, Hiroto Sakamoto, Naohiro Yamaguchi, and Hiroko Yoshida. Part of this work was presented at the 12th International Biophysics Congress, 11-16 August 1996, Amsterdam.

References

[1] Zeuthen, T. (1992) Biochim. Biophys. Acta 1113, 229-258.

[2] Heuser, J., Zhu, Q., Clarke, M. (1993) J. Cell. Biol. 121, 6, 1311-1327.

[3] Nolta, K. V., Steck, T. L. (1994) J. Biol. Chem. 269, 3, 2225-2233.

[4] Padh, H., Lavasa, M., Steck, T. L. (1989) J. Cell Biol. 108, 865-874.

[5] Padh, H., Lavasa, M., Steck, T. L. (1989) Biochim. Biophys. Acta 982, 271-278.

[6] Nolta, K. V., Padh, H., Steck, T. L. (1991) J. Biol. Chem. 266, 27, 18318-18323.

[7] Padh, H., Tanjore, S. (1995) FEBS Lett. 368, 358-362.

[8] Quiviger, B., De Chastellier, C., Ryter, A. (1978) J. Ultrastruct. Res. 62, 228-236.

[9] Zhu, Q., Clarke, M. (1992) J. Cell. Biol. 118, 2, 347-358.

[10] De Chastellier, C., Quiviger, B., Ryter, A. (1978) J. Ultrastruct. Res 62, 220-227.

[11] O'Halloran, T. J., Anderson, R. G. W. (1992) J. Cell Biol. 118, 6, 1371-1377.

[12] Schmidt-Nielsen, B., Schrauger, C. R. (1963) Science 139, 606-607.

[13] Larsson, C., Widell, S., Kjellbom, P. (1987) Methods Enzymol. 148, 558-568.

[14] Sussman, M. (1987) Methods Cell Biol. 28, 9-29.

[15] Bradford, M. M. (1976) Anal. Biochem. 72, 248-254.

[16] Siu, C. H., Lerner, R. A. (1977) J. Mol. Biol. 116, 469-488.

[17] Edidin, M. (1989) Methods Cell Biol. 29, 87-102.

[18] Mueller, P., Rudin, D. O. (1969) in Laboratory Techniques in Membrane Biophysics (Passow, H. and Stepfli, R. eds.) pp. 141-156, Springer-Verlag, Berlin.

[19] Sigworth, F. J. (1983) in Single-channel Recording (Sakmann, B. And Neher, E., eds.), pp. 3-35, Plenum Press, New York.

[20] Silver, M. R., Shapiro, M. S., DeCoursey, T. E. (1994) J. Gen. Physiol.103, 519- 548.

[21] Hagiwara, S., Yoshii, M. (1979) J. Physiol. 292, 251-265.

[22] Kubo, Y. (1995) Prot. Nuc. Acid. Enzym. (in Japanese) 40, 2288-2296.

[23] Riddick, D., H. (1968) Am. J. Physiol. 215, 3, 736-740.

[24] Harvey, W. R. (1992) J. Exp. Biol. 172, 1-17,

[25] Prusch, R., D., Dunham, P., B. (1967) J. Gen. Physiol. 50, 1083.

[26] Aeckerle, S., Wurster, B., Malchow, D. (1985) EMBO J. 4, 39-43.

[27] Aeckerle, S., Malchow, D. (1989) Biochim. Biophys. Acta 1012, 196-200.

[28] Van Duijn, B., Wang, M. (1990) FEBS Lett. 275, 201-204.

[29] Van Duijn, B., Van der Molen, L. G., Ypey, D. L. (1989) Pflugers Arch. 414, (Suppl 1) S148-S149.

[30] Muller, U., Hartung, K. (1990) Biochim. Biophys. Acta 1026, 204-212.

[31] Hille, B. (1991) Ionic Channels of Excitable Membranes 2nd ed., Sinauer Ass., Sunderland.

Table 1.

Characteristics of the crude membrane pellet and the partitioned fraction. Membrane was pelleted from the homogenate of 5 ~ 7-hour developed cells and subsequently partitioned by a two-phase system composed of 6.0% dextran - 6.0 % polyethyleneglycol. Averages of three samples (one of which is FITC-labelled) are shown.

marker	crude (% of homogenate)[a]	upper / lower (% of pellet)[b]	specific activit (upper, nmol/mg/mir
protein	21.9	7.5 / 44.7	-
alkaline phosphatase[c]	26.6	37.7 / 34.4	31(6.0)
NBD-Cl-sensitive ATPase[d]	44.9	3.2 / 102.2	120(0.87)
vanadate-sensitive ATPase[e]	27.9	6.0 / 67.7	140(1.1)

acid phosphatase[f]	66.4	1.4 / 45.3	65(0.63)
NADH oxidoreductase[g]	48.7	1.0 / 72.7	130(0.3)
mitochondrial ATPase[h]	33.4	2.9 / 50.4	290(0.6)

Yields are shown as percentages of [a] the initial homogenate or [b] the crude membrane pellet. In parentheses of the third column, enrichments were calculated as the specific activity of each marker per unit concentration of protein in the upper phases divided by the specific activity of marker per unit concentration of protein in the homogenate. [c] a marker for contractile vacuole, [d] a marker for *acidosome,* [e] a marker for plasma membrane, [f] a marker for endosome/lysosome, [g] a marker for endoplasmic reticulum.

Table 2.

Yield of FITC-surface label in each fraction.

experiment No.	[a]acid-sensitive portion (%)	[b]crude (% of homogenate)	[c]upper phase (% of pellet)	[c]lower phase (% of pellet)
[d]1	95.5	77.8	3.1	63.7
[e]2	83.8	57.1	2.7	43.1

[a] Ratio of acid-sensitive FITC to the total FITC-label was shown in percentage to indicate the degree of the specificity of cell-surface label. Yields are shown as percentages of [b] the homogenate or [c] the crude membrane pellet. Membrane was pelleted from the homogenate and subsequently partitioned by two-phase system which contains, [d] 6.4 %, [e] 6.0 %, each polymer concentration.

Figure Legends

Fig. 1

Negatively-stained electron micrograph of the prepared sample. Bar= (A) 500 nm, (B) 200 nm.

Fig. 2.

(A) Single channel recordings of the *Dictyostelium* K^+ channel. Applied voltages are indicated at the left of each trace. Rightside lines show the baseline current. (*cis:trans*) 300:100 mM KCl, 10 mM Tris-20 mM HEPES, pH 7.4. (B) Same as (A) but in more compressed scale to show the long silent period.

Fig. 3.

Current-voltage relationships of the *Dictyostelium* K^+ channel obtained in different salt solutions. *Cis:trans* = (A) 300 mM KCl:100 mM KCl, (B) 100 mM KCl:100 mM NaCl (open circles), 100 mM KCl:80 mM NaCl + 20 mM KCl (closed symbols), (C) 100 mM KCl:80 mM LiCl + 20 mM KCl, each buffered with 10 mM Tris-20 mM HEPES, pH 7.4. Data from independent (A) 5, (B) 2 (closed circles), (C) 2 bilayers are represented by different symbols. The lines shown here were generated by regression with combination of all the data from different bilayers with the same solution. For (B) (open circles), the curve was generated according to the GHK equation assuming that Cl^- is impermeant.

Fig. 4.

Current-voltage relationships of the *Dictyostelium* K^+ channel obtained in Rb^+ containing solutions.(A) *Cis* side = 100 mM KCl for each, *trans* side =100 mM KCl (circles), 10 mM RbCl + 90 mM KCl (squares), 20 mM RbCl + 80 mM KCl (triangles), 80 mM RbCl + 20 mM KCl (diamonds). Data from independent 2 bilayers for each solution are represented by different colored symbols. (B) *Cis* side =100 mM KCl (circles), 10 mM RbCl + 90 mM KCl (triangles), 20 mM RbCl + 80 mM KCl (squares), with *trans* side =100 mM KCl. All the solutions were buffered with 10 mM Tris-20 mM HEPES, pH 7.4. The lines shown here were generated by regression with combination of all the data from different bilayers with the same solution. (C) The corresponding channel traces. From top to bottom: (*cis* 100 mM KCl / *trans* 100 mM KCl) 30 mV, -30 mV, (*cis* 20 mM RbCl + 80 mM KCl / *trans* 100 mM KCl) 30 mV, -30 mV, (*cis* 100 mM KCl / *trans* 20 mM RbCl + 80 mM KCl) 30 mV, -30 mV.

Fig. 5.

(A) Open probability of the K^+ channel. For voltages more positive than E_K, closed events lasting more than 100 ms were excluded. Data are fitted according to eqn. 4 (*See* Discussion).

(B) An exponential distribution of the duration of the channel open times in the burst period. The histogram shows the number of openings per bin of 0.2 msec width. The continuous line shows an exponential probability density function that has been fitted to the observations (above 0.4 msec) by the maximum likelihood method. It has a time constant of $\tau = 2$ msec at V = 0 mV.

(C) Reciprocal plot of the mean open time obtained by single-exponential curve-fitting as in (B). Data are fitted according to eqn. 5 (*See* Material and Methods, and Discussion).

Fig. 6.

Voltage-dependence of open probabilities shifted by changes in the *trans* concentration of K^+ ion. In one experiment, the *trans* side solution was sequentially exchanged by perfusion from 30 mM (closed circles), to 300 mM (open circles), to 1000 mM (closed triangles), and finally to 100 mM (open triangles) KCl. *Cis* side solution was 300 mM KCl for all records. The values of half-activation voltage were approximately -30 mV in 30 mM *trans* KCl, 10 mV in 300 mM KCl, and 60 mV in 1000 mM KCl, respectively, whereas the values of reversal potential were -50.6 mV, 1.2 mV, and 26.6 mV, respectively (not shown).

Fig. 7.

(A) Voltage-dependence of open probabilities in various concentrations of K^+ ion. (B) The corresponding current-voltage relationship. The means ±S.E.M. are shown. *Cis:trans* solution was 300:30 mM (closed circles, n=8), 300:300 mM (open circles, n=5), and 30:300mM (closed triangles, n=3) KCl. In (A), the data are fitted according to eqn. 4 (*See* Discussion). The values of P_{open}^{max} are 0.63, 0.53, and 0.58, respectively. The values of z are 1.5, 1.7, and 1.5, respectively. The values of V_0 are -23.3, 24.1, and 38.3 mV, respectively. In (B), the values of the reversal potential were, -44.2, 1.8, and 48.1 mV, respectively.

Fig. 8.

The *Dictyostelium* K channel blockade (A) by quinine and (B) TEA^+.

(A) The containing quinine concentration are shown in the left of the trace. *Cis:trans* solution was 300:100 mM KCl. Holding potential = 30 mV.

(B) The containing TEA^+ concentration are shown in the left of the trace. *Cis:trans* solution was 300:100 mM KCl. Holding potential = 30 mV.

(C) Dose-effect relationship of TEA^+ blockade. Data from 2 independent bilayers are represented by different symbols. The curve was drawn such that the conductance ratio relative to the conductance in the absence of TEA^+ related to the TEA^+ concentration. $\gamma / \gamma_0 = 1/(1+[TEA^+]/Kd)$; Kd=30 mM.

Fig. 9.

A hypothetical model proposed to explain the K^+-dependence. Voltage-dependent binding of a Rb^+ or K^+ ion to a blocking site inside the pore prevents permeation of ions. This binding site is vacant during the ordinary permeation process. The energy barrier to access the blocking site is lower for Rb^+ ion than K^+ ion, and therefore blockade by Rb^+ is observed so as to reduce the apparent conductance size (fast block) whereas blockade by K^+ ion is observed as a discrete event. The geometry of the binding site makes it more easily accessible from the*trans* side than from the*cis* side, differntiating the apparent effective concentration from the either side.

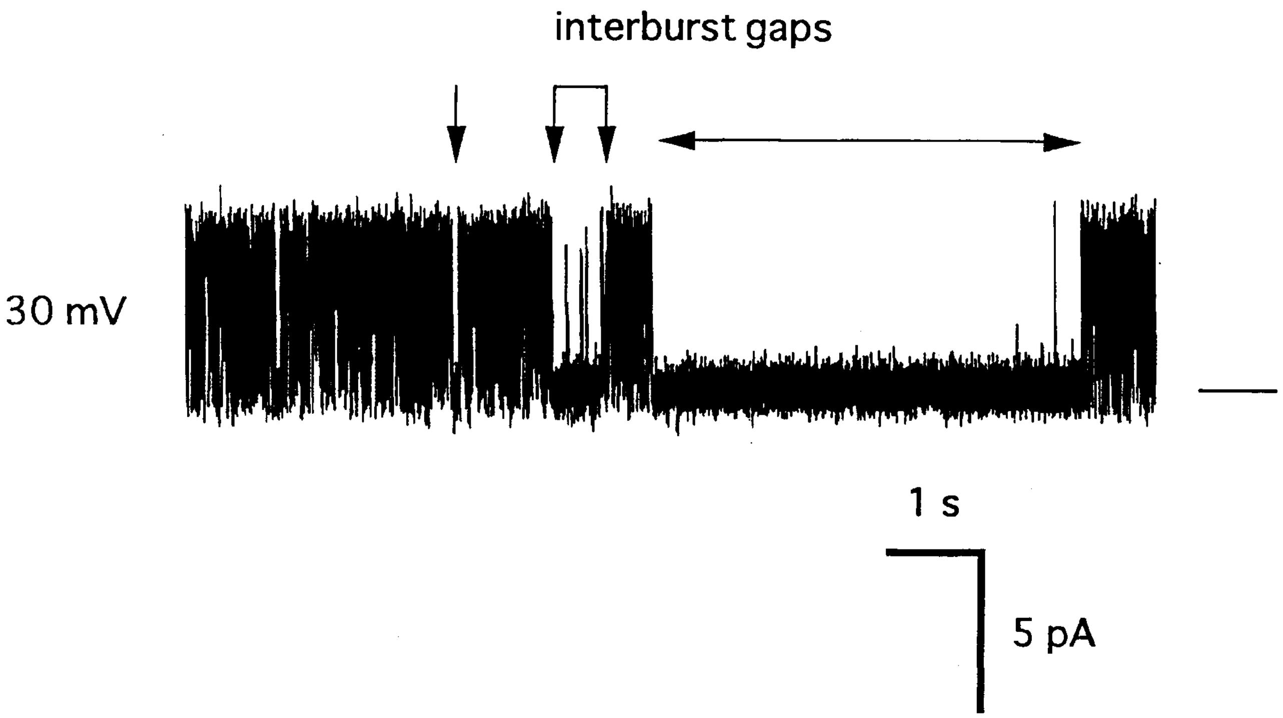
interburst gaps
30 mV
1 s
5 pA

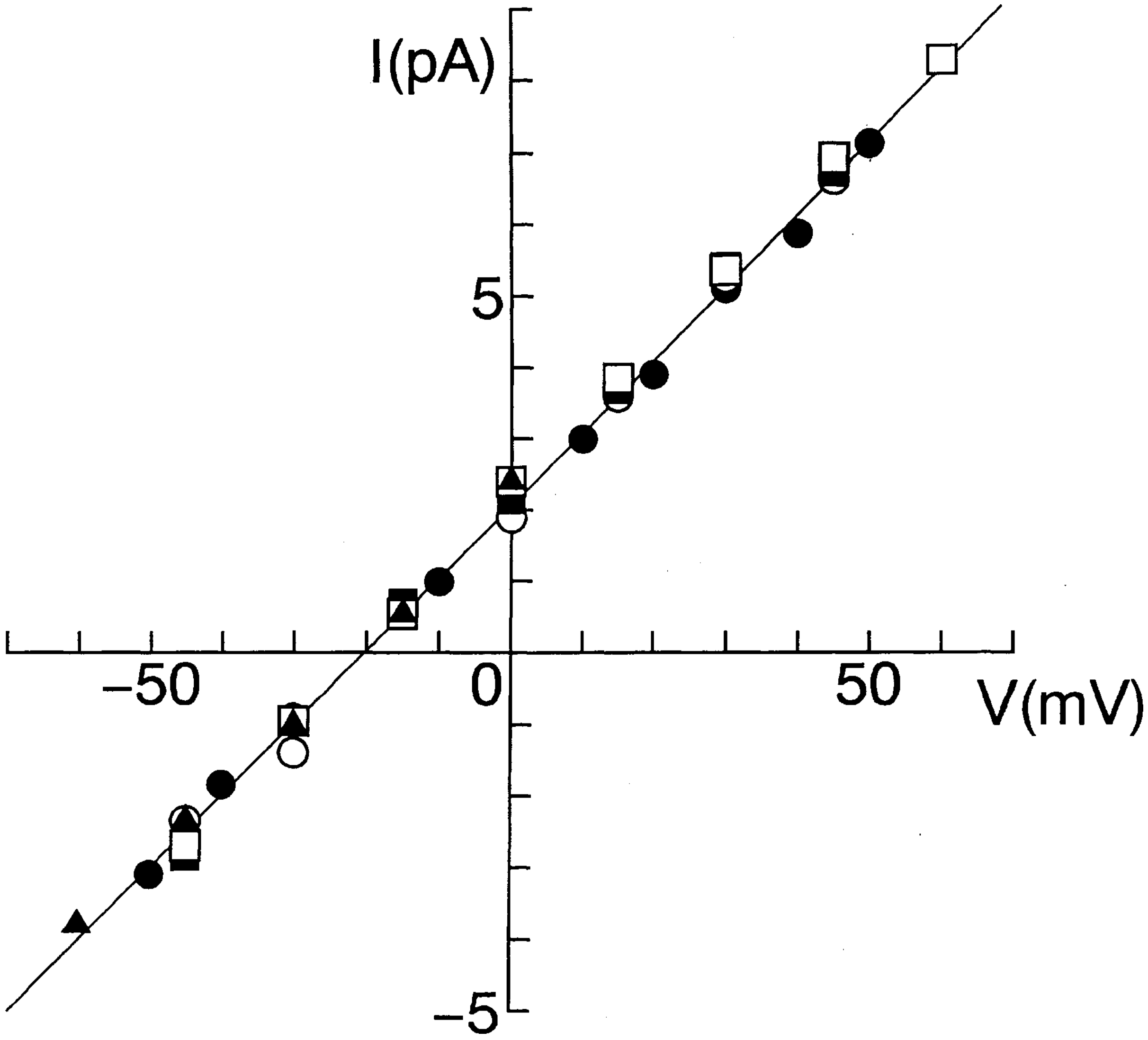
I(pA)
5
−5
−50
0
50
V(mV)

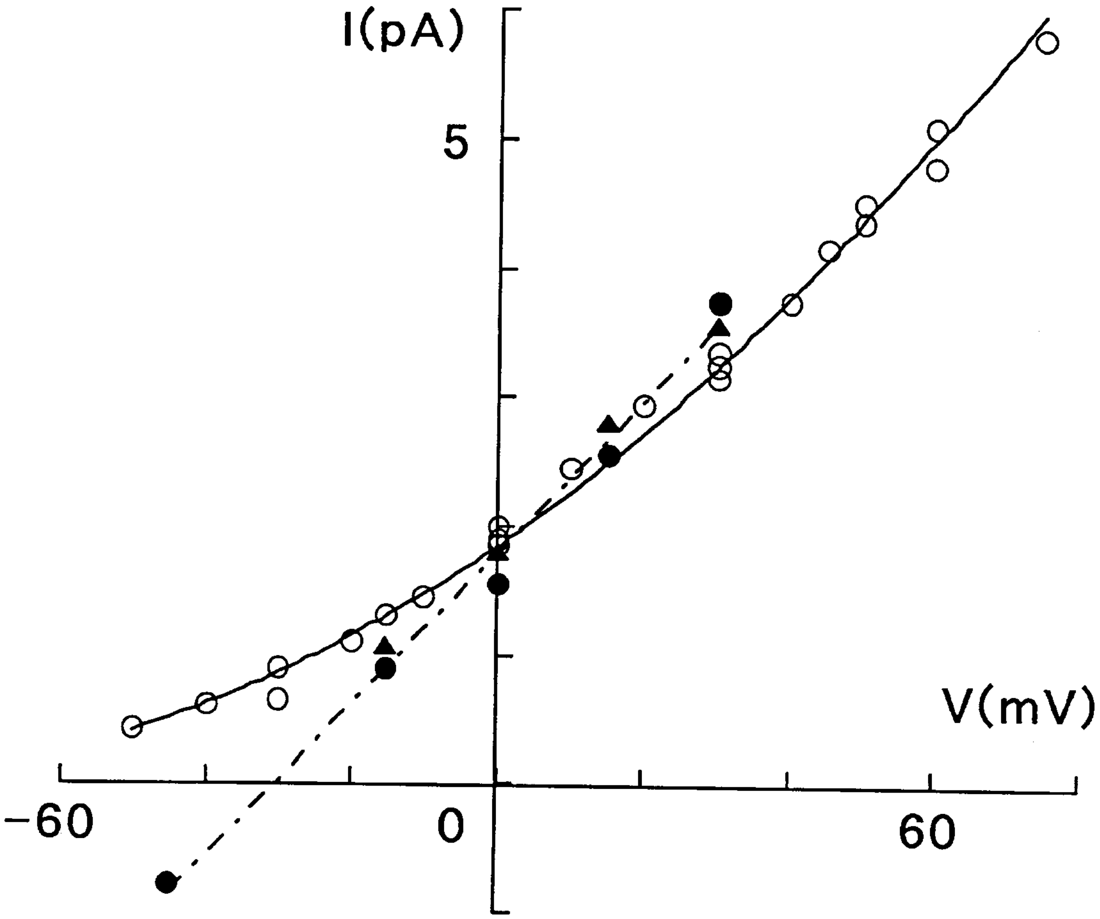
I(pA)
5
V(mV)
-60
0
60

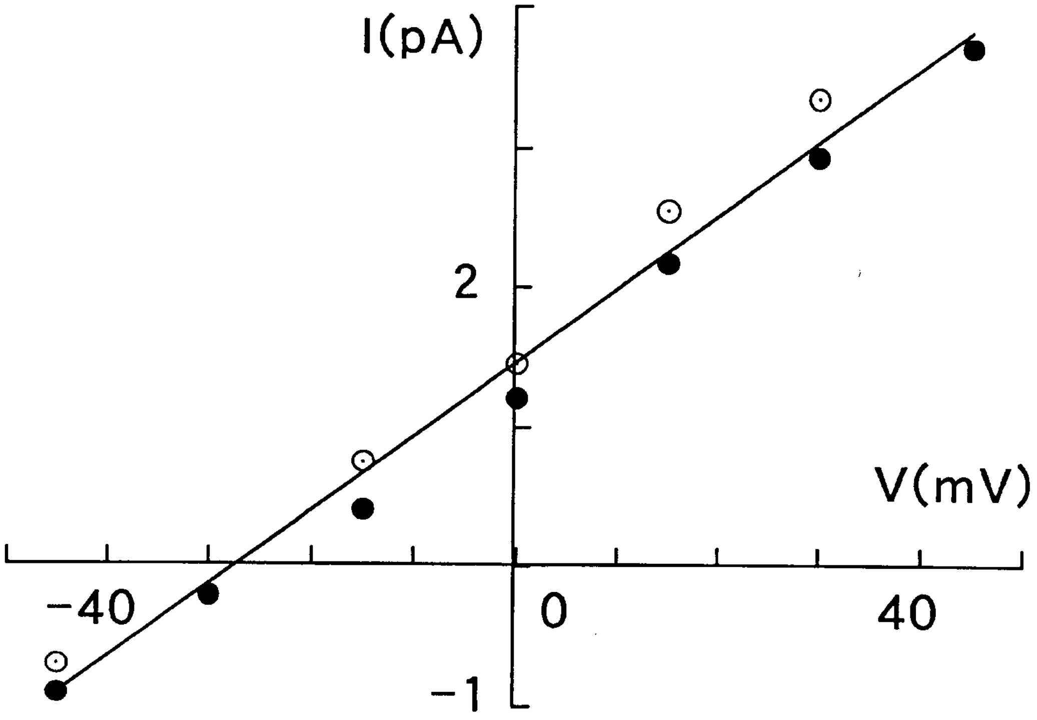
I(pA)
2
−1
V(mV)
−40
0
40

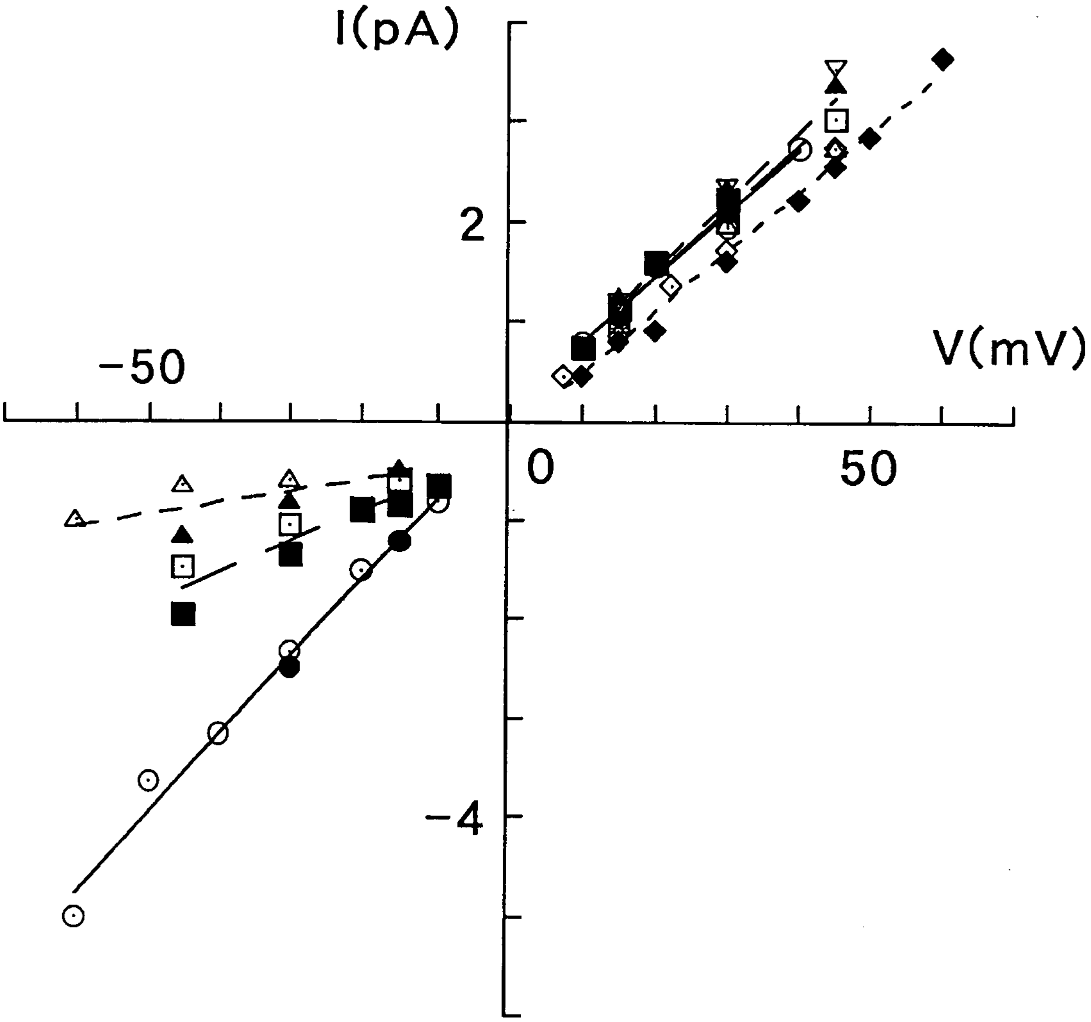
I(pA)
2
-4
V(mV)
-50
0
50

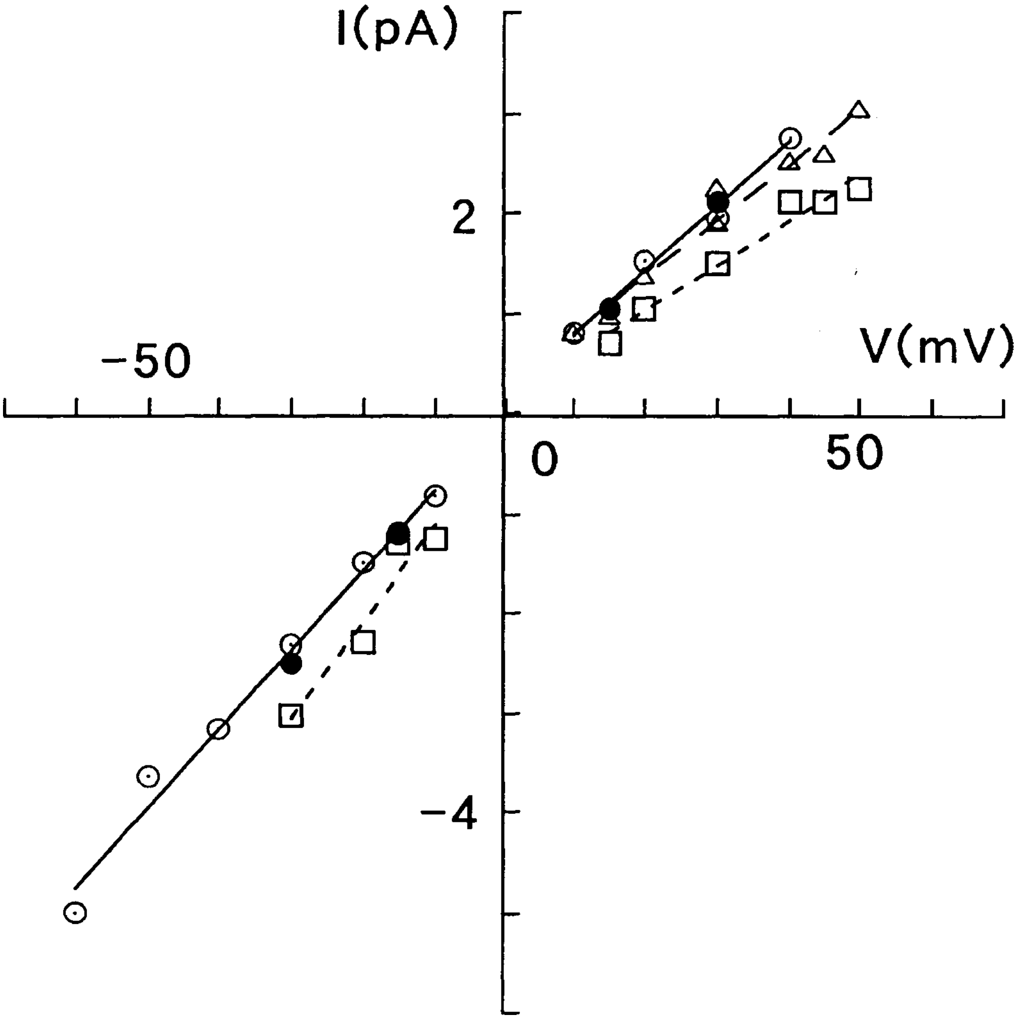
I(pA)
2
-4
V(mV)
-50
0
50

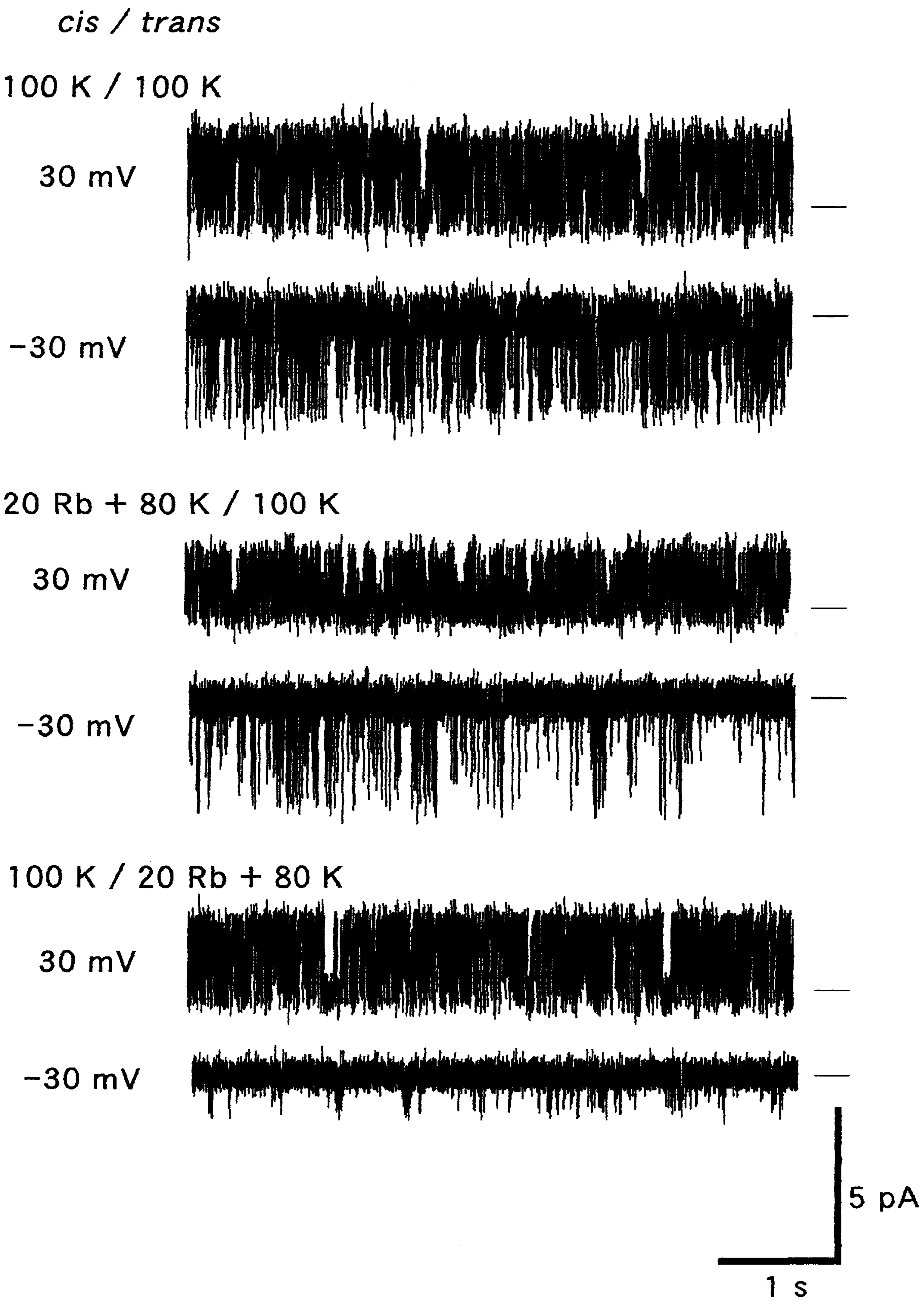
cis / trans
100 K / 100 K
30 mV
−30 mV
20 Rb + 80 K / 100 K
30 mV
−30 mV
100 K / 20 Rb + 80 K
30 mV
−30 mV
5 pA
1 s

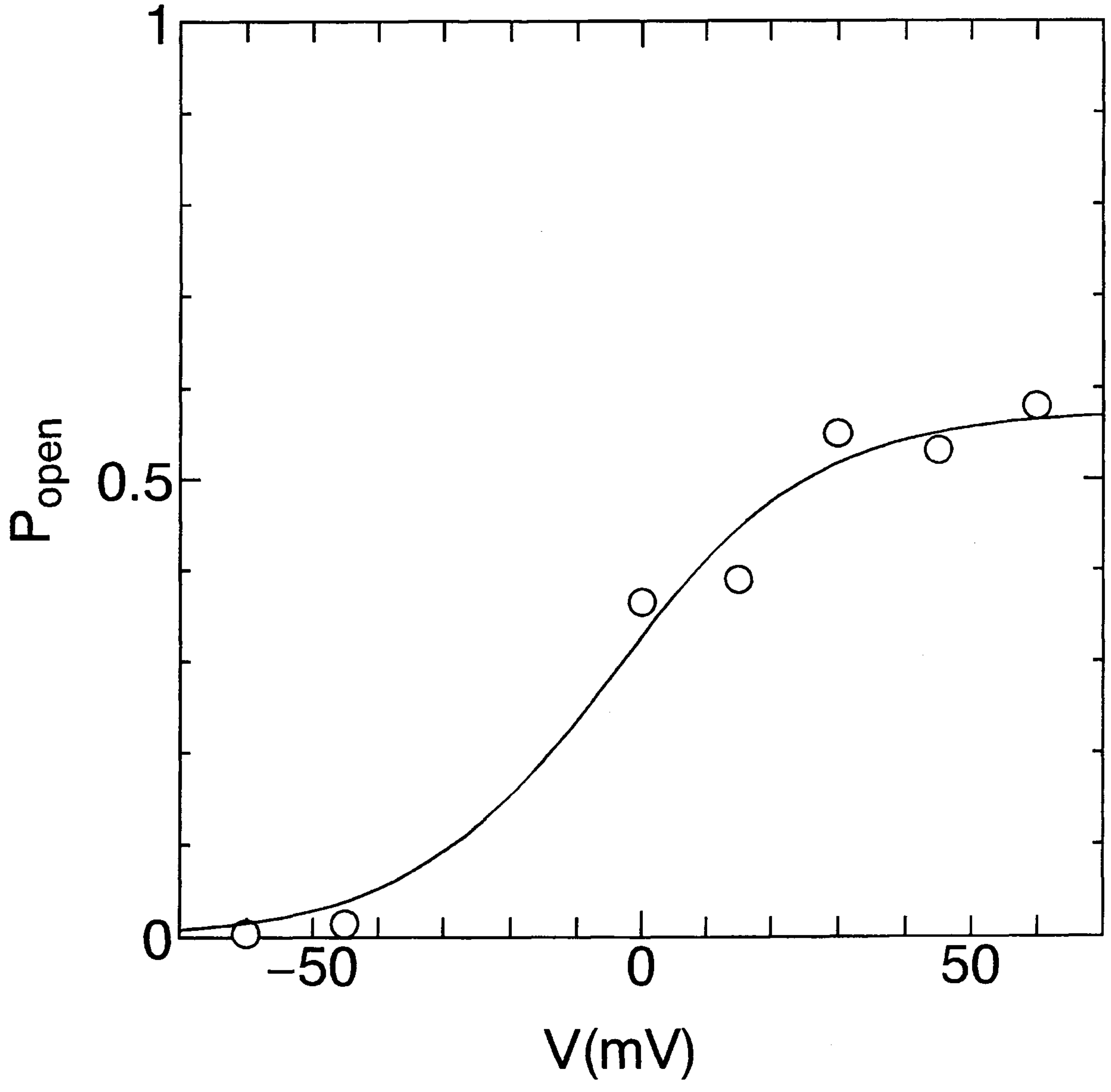
1
0.5
0
Popen
−50
0
50
V(mV)

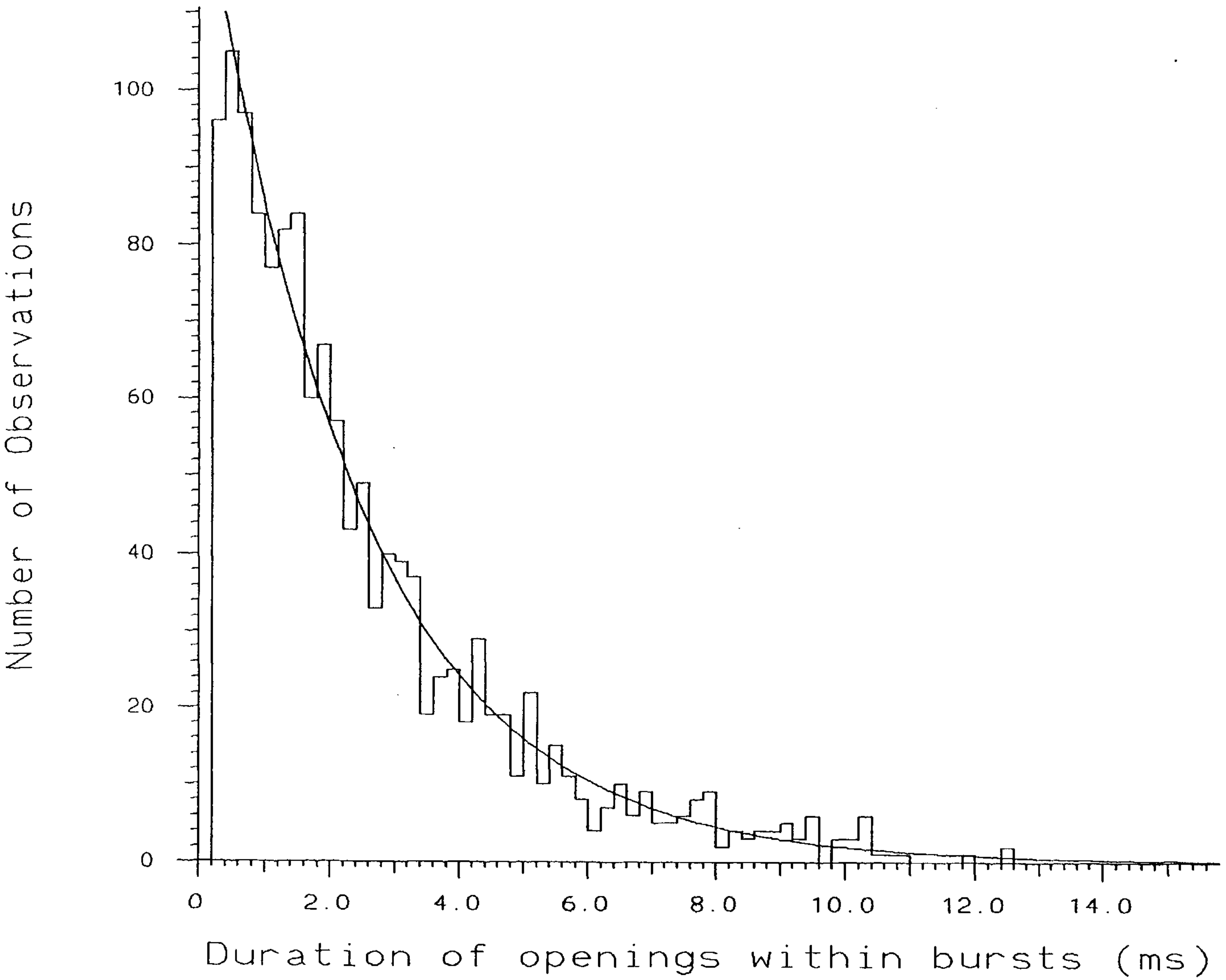
Number of Observations
100
80
60
40
20
0
0
2.0
4.0
6.0
8.0
10.0
12.0
14.0
Duration of openings within bursts (ms)

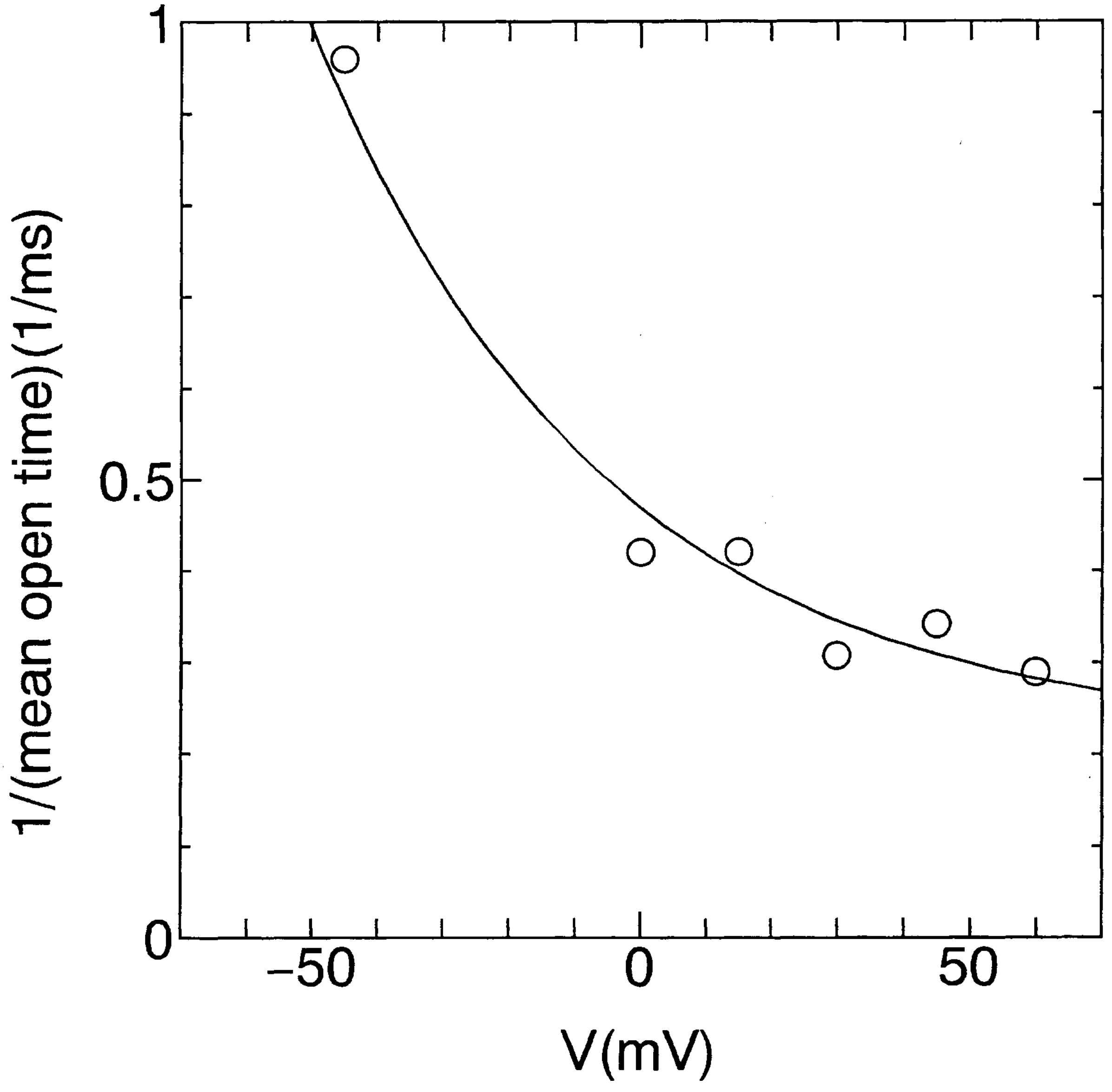
1/(mean open time)(1/ms)
1
0.5
0
-50
0
50
V(mV)

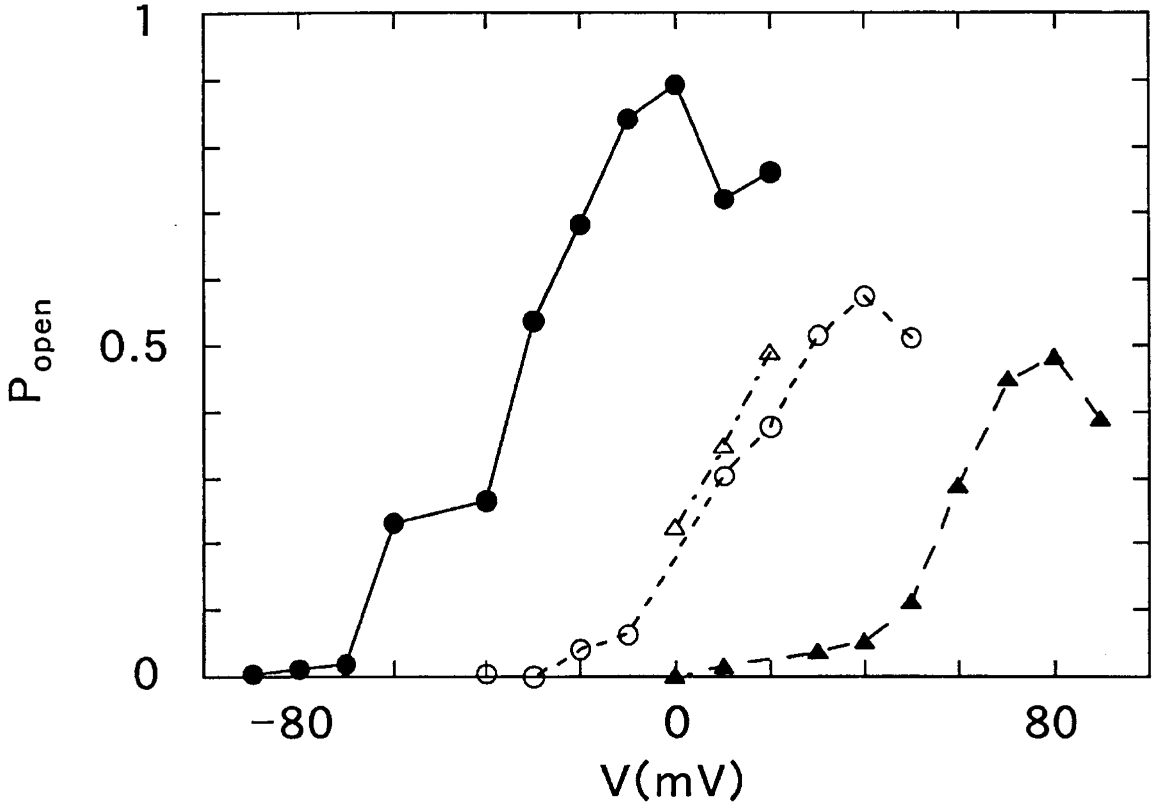
1
0.5
0
P_{open}
−80
0
80
V(mV)

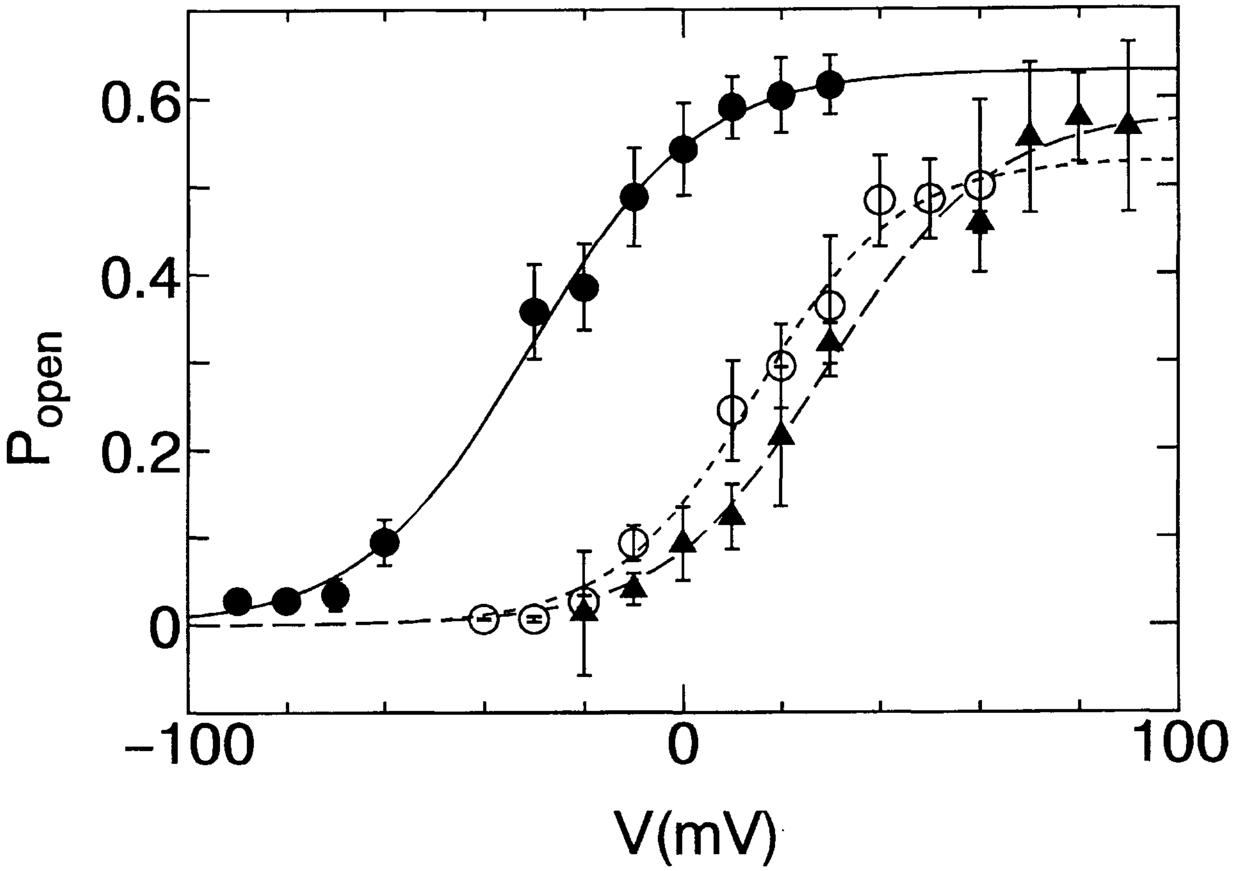
0.6
0.4
0.2
0
P_{open}
−100
0
100
V(mV)

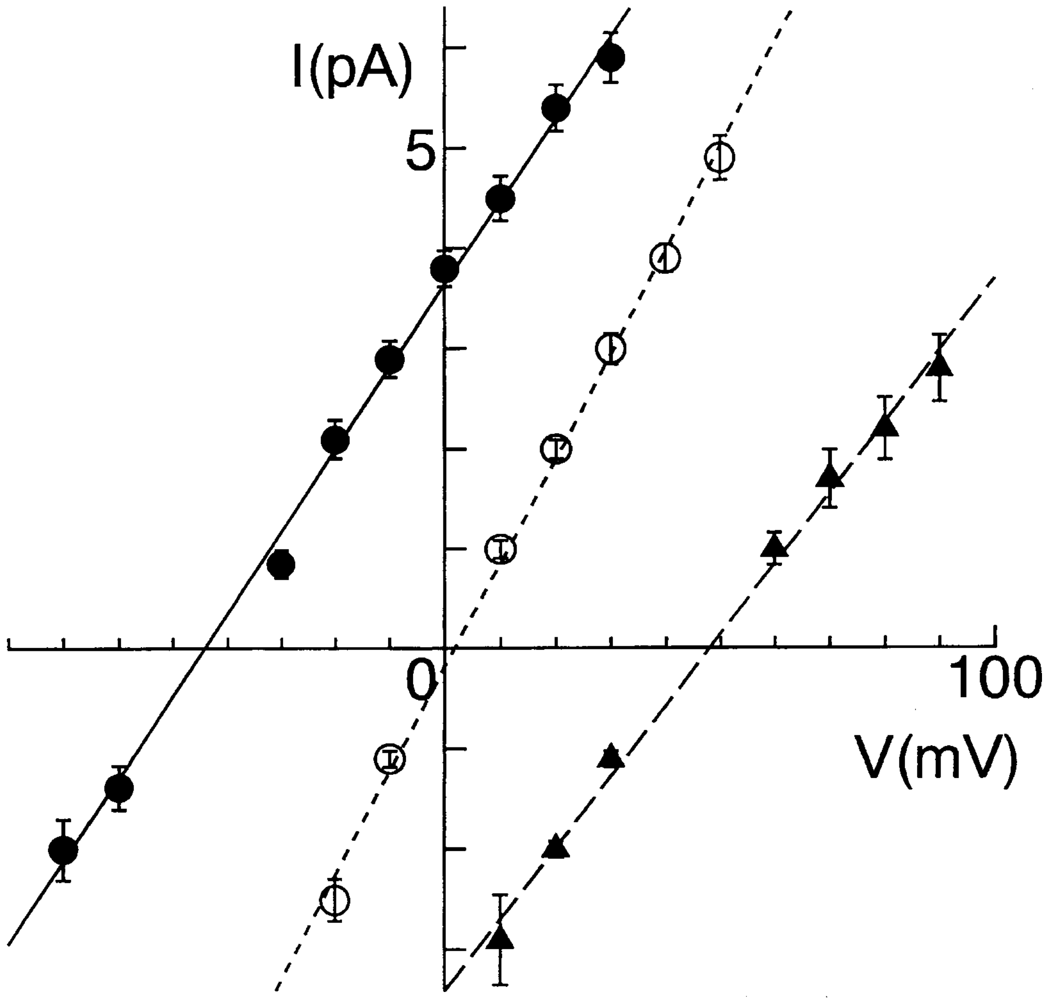
I(pA)
5
0
100
V(mV)

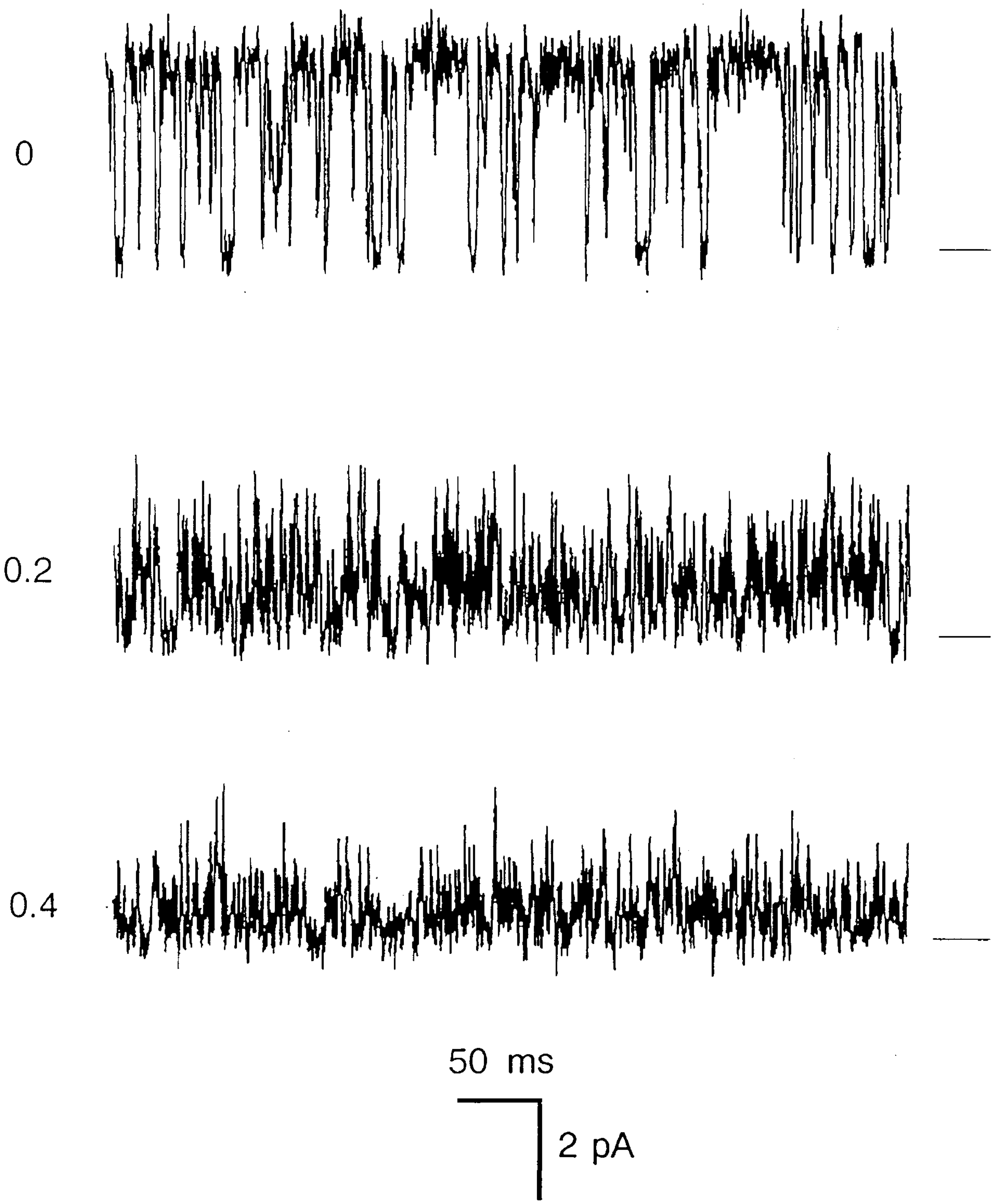
0
0.2
0.4
50 ms
2 pA

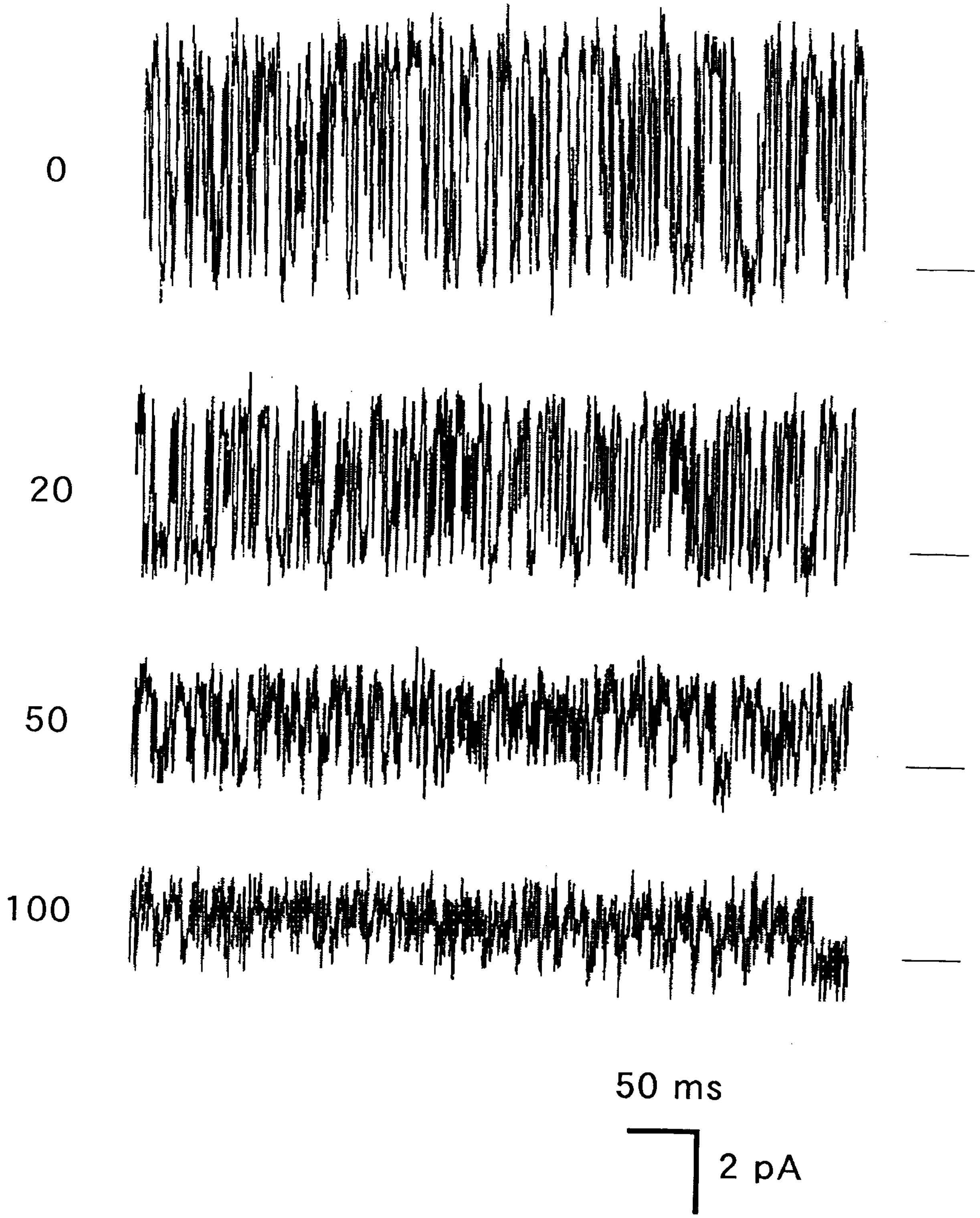
0
20
50
100
50 ms
2 pA

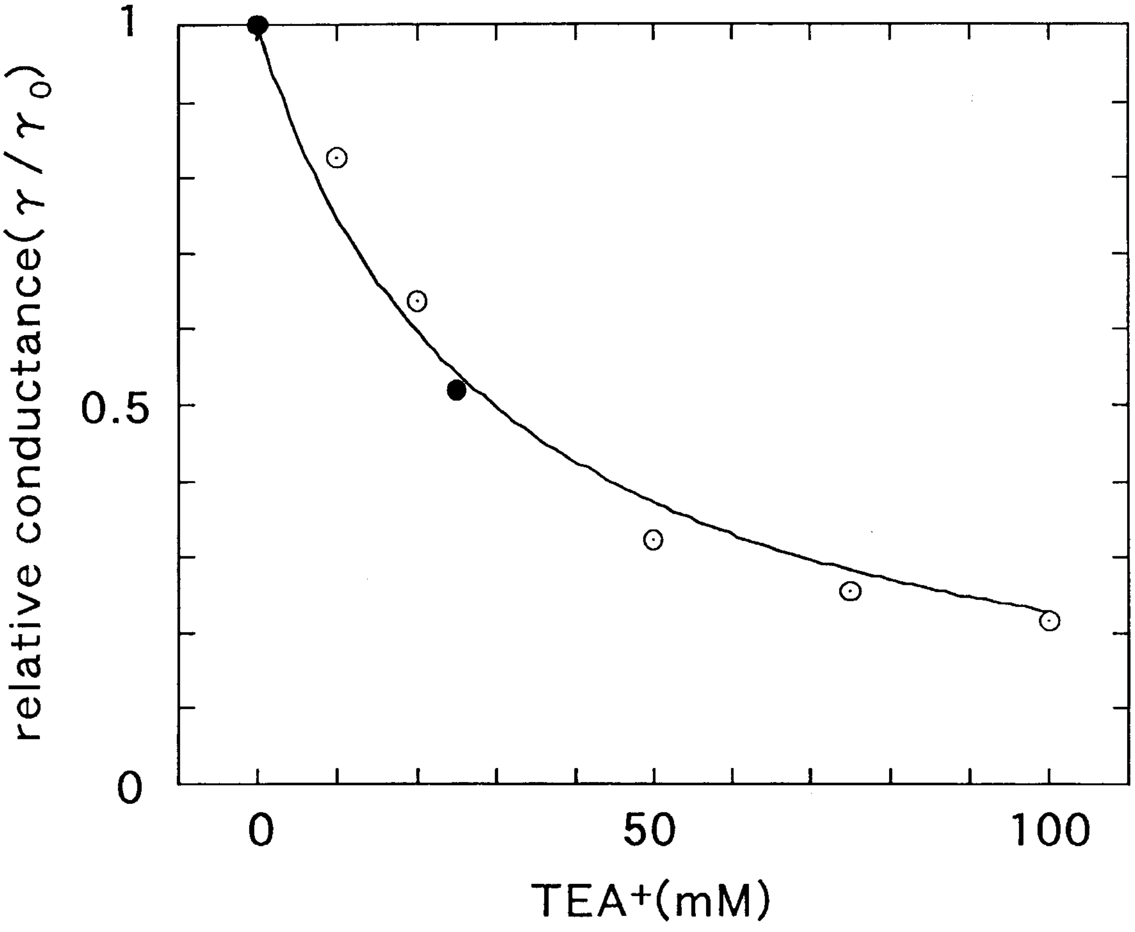
relative conductance(γ / γ_0)
1
0.5
0
0
50
100
TEA+(mM)

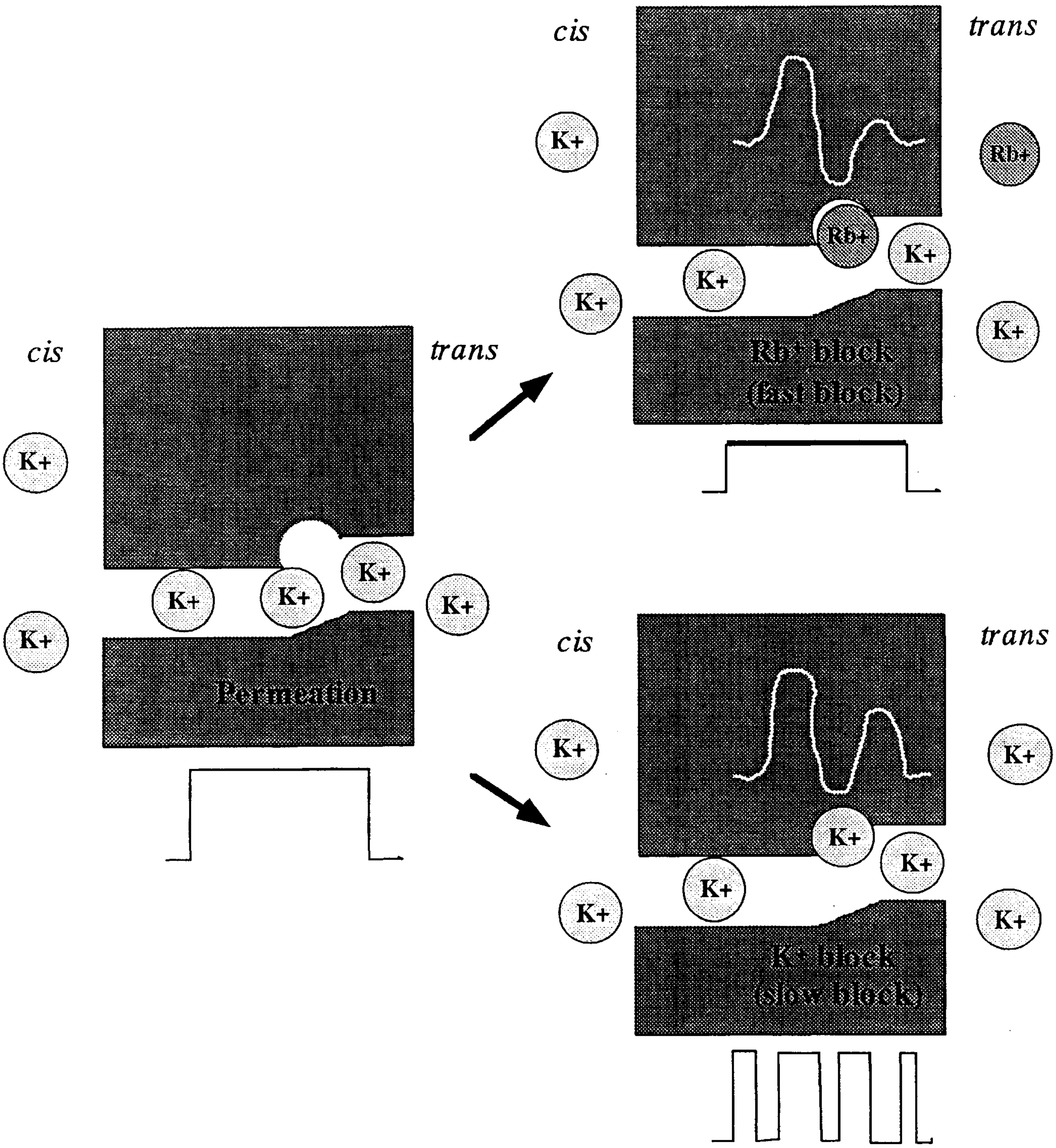
cis
trans
K+
Permeation
cis
trans
K+
Rb+
Rb+ block
(fast block)
cis
trans
K+
K+ block
(slow block)

18.

(Title page)

Long-lasting enhancement of synaptic activity in dissociated cerebral neurons induced by brief exposure to Mg^{2+}-free conditions

Suguru N. Kudoh[1,2], Akira Matsuo[2], Kazuyuki Kiyosue[1], Michiki Kasai[2] and Takahisa Taguchi[1]*

[1]Dept. of Organic Materials, Osaka National Research Institute, Ikeda 563, Japan

[2]Dept. of Engineering Science, Osaka University, Toyonaka 560, Japan

*Corresponding author:

Takahisa Taguchi, Ph.D.

Dept. of Organic Materials

Osaka National Research Institute

1-8-31, Midorigaoka, Ikeda 563, Japan

Tel: (+81) 727-51-9524

Fax: (+81) 727-51-9628

e-mail: taguchi@onri.go.jp

Key words

synaptic potentiation, NMDA receptors, culture, cerebral neurons, synaptic plasticity, gene expression, whole cell clamp

Abstract

The long-lasting enhancement of periodic clusters of spontaneous excitatory postsynaptic currents (SEPSCs) was examined in dissociated chick cerebral neurons that had been transiently exposed to Mg^{2+}-free solution for 15 min. Since the enhancement was diminished by blockade of synaptic transmission, it clearly depended on synaptic activities. A specific antagonist of N-methyl-D-aspartate receptors (NMDARs) also inhibited the potentiations. Furthermore, the presence of inhibitors of protein and RNA synthesis in the Mg^{2+}-free solution blocked the potentiation. In the potentiated neurons, the frequency of miniature excitatory postsynaptic currents (mEPSPs) increased. In addition, a diffusible molecule(s) that promoted the potentiation appeared to be involved in this phenomenon, since conditioned medium of Mg^{2+}-free treated neurons enhanced synaptic activity in other dish.

1. Introduction

Higher functions of the brain, including learning and memory, are thought to be established by plastic changes in the efficiency of synaptic transmission. Among these changes, long-term potentiation (LTP) is the most thoroughly analyzed phenomenon. It can be induced by high-frequency stimuli (Bliss and Lomo, 1973) by application of transmitter (Cormier et al., 1993) or bee venom (Cherubini et.al.,1987; Kauer et al., 1988) and by removal of Mg^{2+} from the extracellular medium (Neuman et al., 1987). In the case of LTP in the CA1 region of the rat hippocampus, high-frequency or paired stimuli that are sufficient to induce depolarization in a postsynaptic neuron allow an exclusion of Mg^{2+} from NMDAR-channels and the entry of Ca^{2+} into the neuron through the receptors (Colino and Malenka, 1993; Lin et al., 1993; Wigstrom and Gustafsson 1986). The molecular mechanism linking entry of Ca^{2+} to potentiation in synapses, remains unknown even though several hypotheses have been proposed, involving, for example, an increase in transmitter release (Arancio et al., 1995; Kamiya et al., 1993), increase in synaptic sites due to the conversion of silent synapses to unsilent ones (Liao et al. 1995; Isaac et al.,1995), a functional change in postsynaptic receptors (Maren et al., 1993), participation of metabotropic glutamate receptors (mGluRs) (Musgrave et al., 1993; Riedel et al., 1995; Zheng, Gallagher, 1992), or calmodulin-dependent protein kinase II (CaMKII) as a target of intracellular Ca^{2+}(Lledo et al., 1995; Wang and Kelly, 1995).

For complete elucidation of the mechanism of LTP, we must analyze not only neuronal activity by electrophysiological methods but also morphological changes at single synaptic sites and the distribution of molecules on synaptic membranes. For such analyses, cultures of dissociated cerebral neurons are useful. We have developed a system for the culture of chick cerebral neurons in which glutamatergic and GABAergic synaptogenesis proceeds with the passage of embryonic equivalent days (E.E. days; the sum of the embryonic age and the number of days *in vitro*) in a manner that is dependent on synaptic activities (Kiyosue et al., 1996; Tokioka et al., 1993). Since recent studies suggest some similarities in the mechanism of synaptogenesis and LTP (Liao et al., 1995; Isaac et al., 1995; Durand et al., 1996; Kiyosue et al., 1997), we think that analysis of developmental synaptogenesis in the culture system will contribute to understand the synaptic plasticity.

In this study, we showed that the enhancement of SEPSCs was induced in the culture system after brief exposure to Mg^{2+}-free medium and we characterized the enhancement of SEPSCs from an electrophysiological, pharmacological and biochemical perspective.

2. Materials and Methods

2.1 Cell culture

Cell cultures were prepared as described previously (Kiyosue et al., 1996; Tokioka et al., 1993). In brief, cerebral hemispheres were dissected from chick embryos on embryonic day 10 (E10) and treated with 0.05% trypsin (Gibco, U.S.A.) in Ca^{2+}, Mg^{2+}-free phosphate-buffered saline (PBS) supplemented with 10 mM glucose. Dissociated neurons (5-6 x 10^5/dish) were cultured for 7 days on 35-mm tissue culture dishes (Corning, U.S.A.) that had been coated with poly-L-lysine (Sigma, U.S.A.) at 37°C in 5% CO_2 / 95% air at saturating humidity. Half of the culture medium was replaced by fresh medium on the third and fifth days of culture. The culture medium contained 50%Earles' minimum essential medium (Gibco, U.S.A), 40% GIT medium (Nihon seiyaku, Japan) and 10% Fetal calf serum, supplemented with 10mM glucose, 2mM L-glutamine,1mM $CaCl_2$, 30mM NaCl, 0.5mM sodium pyruvate, 25μM Na_2SeO_3, 50nM choline-Cl, 50nM inositol, 100u/ml penicilin,100μg/ml streptomycin, 5μg/ml insulin and 25mM Na-HEPES (pH 7.4).

2.2 Electrophysiological measurements

Electrical recordings from neurons that had been cultured for 7 days were performed in the whole-cell clamp mode. The standard external bathing solution contained (in mM) 130 NaCl, 3 KCl, 2 $CaCl_2$, 1 $MgCl_2$, 10 glucose and 10 Na-Hepes (pH 7.3). The Mg^{2+}-free external bathing solution contained the same compounds with the exception of $CaCl_2$ at 3 mM and no $MgCl_2$. The 2ml of standard external bathing solution was perfused at 3ml/min with 5ml of Mg^{2+}-free solution by a peristaltic pump, keeping the volume of bathing solution. The solution in the patch pipette contained (in mM) 130 KCH_3SO_4, 10 KCl, 0.2 $CaCl_2$, 2 $MgCl_2$, 1 EGTA, 2 Mg-ATP and 10 Hepes-K (pH 7.2). To reduce inhibitory synaptic currents, picrotoxin (25μM) was added into the external solution just before measurements. The resistance of the borosilicate glass electrodes (GD1.5; Narishige, Japan) ranged between about 3 and 6 MΩ. Postsynaptic currents, amplified and filtered at 1 kHz, were digitized in a Digidata 1200 A/D system (Axon, U.S.A.). The stored individual current traces were analyzed by Axotape (Axon, U.S.A.). A double whole-cell clamp of distinct two neurons was established within 3 min. All experiments were carried out at 20-25°C at a holding potential of -60 mV. Periodic clusters of SEPSCs recorded from double whole-cell clamped neurons were analyzed if the first EPSC had been above 20pA and the delay of the first SEPSCs in the two clusters recorded simultaneously from these two neurons had been within 10 msec. Series resistance and input resistance of postsynaptic neurons were continuously monitored. The mean series resistance was 37.8 ±12.8 MΩ (n=72), and the mean input resistance was 1.28±0.98 GΩ (n=72). If these parameters deviated more than 20%, data were deleted from records. Each EPSC was observed as a packet composed of multiple sharp SEPSCs. As the first approximation, the amplitude of SEPSC was defined as that of the first EPSC in a packet. All mEPSCs were recorded in the presence of 500 nM tetrodotoxin (TTX, Sigma, U.S.A.).

2.3 preparation of conditioned medium.

After treating cultured neurons with Mg^{2+}-free medium for 15 min, we collected this conditioned medium (CM) and adjusted the concentration of $MgCl_2$ to 1 mM. To examine an effect of the CM on synaptic activity, we applied the CM and concentrated CM in the neuronal culture. Concentration and fractionation of the CM was performed by repetitive centrifugations (1,500 × *g*, 30min) at 4°C using Centriprep (cut off of molecular mass, 30K; Amicon, USA).

3. Results

3.1 Effects of Mg^{2+}-free conditions on grouped firing of neurons

Cerebral cultured neurons prepared from E10 chick embryos start forming glutamatergic synapses on E.E. days 13 (Tokioka et al., 1993). On E.E.days 17, periodic clusters of SEPSCs were frequently observed in paired neurons to which we had applied glass patch-pipette for whole-cell clamping at -60mV in an external solution that contained 25μM picrotoxin (Fig.1). In the culture, it is difficult to record evoked synaptic currents for more than 30min because of rundown in the response of patch-clamped presynaptic neurons, whereas no rundown was observed when presynaptic neurons were stimulated extracellularly. Therefore, to characterize long-lasting enhancement of synaptic activities in cultures of dissociated cells, we analyzed the periodic clusters of SEPSCs before and after activation of neurons under Mg^{2+}-free conditions.

When the standard external solution was replaced by a Mg^{2+}-free solution, the averaged frequency of SEPSCs increased from 0.3 up to 1 Hz and the slow components in each SEPSC became obvious (Fig. 1D). These slow components are due to NMDAR, since they were completely abolished by 25μM APV, antagonist of NMDAR (Kiyosue et al., 1997). Neurons were incubated in the Mg^{2+}-free medium for 15 min in the current-clamp mode. Under these conditions, the membrane potential of the recorded neuron was repeatedly depolarized by synaptic inputs (Fig. 1E). The periodic clusters of SEPSCs were continuously recorded for more than 40 min after the external solution had been replaced once again by the standard solution that contained 1 mM $MgCl_2$.

The mean amplitude of SEPSCs for 3 min, beginning 6 min after the end of the Mg^{2+}-free treatment increased significantly to 192.5% of the averaged amplitude before the treatment and remained at this elevated level for more than 40 min (Figs. 2A and 2C). The enhancement of SEPSCs was observed in eight pairs of cells in nine tests. By contrast, perfusion of cells with the standard external solution caused no significant change in periodic clusters of SEPSCs (n=8, Figs. 2B and 2D). Mg^{2+}-free treatment for 15 min was sufficient to induce the enhancement of SEPSCs and such treatment for up to 40 min made no difference in the results (data not shown). Treatment of 10 min was insufficient for reproducible potentiation.

3.2 Dependence on activity of the potentiation

To confirm that the potentiation was induced by the increase in synaptic activity, we examined the effects of TTX and 6-cyano-7-nitroquinoxaline-2, 3-dione (CNQX) on the potentiation. In the presence of 500 nM TTX, no periodic clusters of SEPSCs evoked by presynaptic activity were observed, whereas smaller SEPSCs of 10 to 50 pA, which were thought to be miniature EPSPs (mEPSPs), were recorded (data not shown). When 5 μM CNQX, an antagonist of non-NMDAR, was added to in the external solution, no spontaneous firing or mEPSC was observed in neurons. The treatment with Mg^{2+}-free solution that included TTX or CNQX resulted in no significant change in the mean amplitude of SEPSCs for 3 min (n=5,Figs. 3A and 3B). These results suggest that the enhancement of the synaptic currents in the cultured cerebral neurons depended on glutamatergic synaptic transmission. Since the treatment of neurons with TTX or CNQX for 15 min had no effect on the amplitude or the frequency of SEPSCs after a change of solution (data not shown), a blocking effects by residual TTX or CNQX on activated neurons can be excluded from consideration.

Removal of Mg^{2+} from the external solution is assumed to facilitate the activation of NMDAR. To examine this issue, we added 25 μM D, L-2-amino-5-phosphonopentanoic acid (D, L-APV), a specific antagonist of NMDAR, to the Mg^{2+}-free solution (n=4, Fig. 3C). D, L-APV abolished the slow component in each SEPSC and blocked the induction of the potentiation under Mg^{2+}-free conditions, (mean amplitude after treatment: 88.9%).

3.3 Involvement of protein synthesis in the potentiation

To determine whether newly synthesized proteins are essential for the induction of enhancement of SEPSCs, we added inhibitors of protein and RNA synthesis to the Mg^{2+}-free solution. After treatment with 1 μM cycloheximide, an inhibitor of protein synthesis, no significant changes were observed in the amplitude and the frequency of SEPSCs (n=4, Fig. 4A), even though the Mg^{2+}-free treatment by itself induced an increase in frequency and in the size of slow component of SEPSCs, as in control experiments. Furthermore, 8 μM actinomycin D, an inhibitor of RNA synthesis, also blocked the enhancement of SEPSCs (n=3, Fig. 4B). Since both inhibitors blocked the enhancement of SEPSCs without disturbing normal synaptic transmission in our system, synthesis of proteins appeared to be required for induction of the potentiation, even at the early stage within 15 min after induction.

As confirmation of the reproducibility of our observations, all data obtained from multiple neurons are summarized in Figure 5.

3.4 Analysis of mEPSCs

Miniature EPSPs after Mg^{2+}-free treatment were analyzed in a TTX-containing bathing solution. The amplitude and frequency of mEPSCs, which were averaged in each neuron, were distributed over the ranges of 10 to 50 pA and 0.025 to 0.1 Hz, respectively (Fig. 6). In the neurons in which the enhancement of SEPSCs had been induced, the frequency of mEPSPs increased significantly (Mann-Whitney test, $P<0.05$, Fig. 7). The mean relative values of mEPSCs in seven neurons, 6 min after the induction of the enhancement of SEPSCs, were 277.4% in terms of frequency, while they were 86.7% in four neurons in control experiments. The decrease of frequency in the control experiments was not significant (Kruskal-Wallis test, $P>0.05$). The increase in frequency was also maintained for more than 30 min (Fig. 7). In control experiments, neurons exposed to a solution that contained Mg^{2+} for 15 min showed no changes in amplitude or in frequency of mEPSCs (data not shown). The mean amplitude of mEPSCs indicated no significant change. However, we did not performed further analysis of their amplitudes and waveshapes, because of few events of mEPSCs under the condition with 1mM Mg^{2+}. The results for mEPSCs suggest that an increase in at least the number of synaptic sites and/or in the probability of transmitter release were involved for the enhancement of SEPSCs in our cultures.

3.5 An enhancement-promoting factor

Our results could be interpreted that induction of the enhancement of SEPSCs in our culture required a secreted factor which increased synaptic activity. To examine this hypothesis, we prepared conditioned medium (CM) as follows. After treating cultured neurons with Mg^{2+}-free medium for 15 min and confirming the potentiation electrophysiologically, we collected the Mg^{2+}-free medium and adjusted in the concentration of $MgCl_2$ to 1 mM. We replaced the medium in another dish of neurons that had been cultured for 7 days by this Mg^{2+}-supplemented CM. The mean amplitude of SEPSCs for 3 min increased significantly within 2 to 5 min (Fig. 8A and 8B) and was maintained at a high level for more than 30 min (Fig. 8B). In six neurons tested with the CM, four neurons showed evidence of the enhancement of SEPSCs and one showed evidence of short-term potentiation that disappeared within 20 min. The amplitudes of SEPSCs were distributed in the range of 120% to 170% of the averaged amplitude before the application of CM, depending on the batch of CM. The conditioned medium prepared from cultures in standard Mg^{2+}-containing bathing solution had no effect on synaptic activity (Fig. 8C). Since concentrated CM by Centriprep (cut off of molecular mass, 30K; Amicon, USA) also enhanced synaptic activity in the same manner (data not shown), the factor may be a relatively large molecule, comparing to ions such as K^+ and amino acids such as glutamate.

4. Discussion

Periodic clusters of SEPSCs from paired neurons were analyzed to characterize the enhancement of synaptic activity *in vitro*. The fact that the enhancement of SEPSCs induced under Mg^{2+}-free conditions was inhibited by TTX (Fig. 5) revealed that the potentiation required presynaptic activity in addition to activation of NMDAR in the post-synaptic membrane. Under the Mg^{2+}-free conditions, SEPSCs increased slightly in frequency up to 3Hz, as a results of activation of NMDA receptors and Ca^{2+} channels. The enhancement certainly occurred at the frequency lower than 1 Hz (Fig. 2A). Thus, the increased frequency may not cause the enhancement by itself. Our results suggest that the enhancement of SEPSCs in our cultures required only activation of NMDA receptors and release of transmitter by action potentials. Voltage clamping of neurons during induction in Mg^{2+}-free condition did not block the enhancement of SEPSCs (data not shown). It suggests that voltage-dependent Ca^{2+} channels in postsynaptic neurons were not required for the enhancement, though it still remains the possibility of the involvement of the channels in synaptic enhancements on other upstream neurons.

Each neuron in a cultured neuronal network receives a packet of multi-presynaptic inputs from different neurons (Fig. 1). Thus, it is possible that the increase in amplitude of SEPSCs after Mg^{2+}-free treatment was due to an increase in the probability of superposition of two EPSCs, each of which had the same amplitude as before the treatment. Comparing the details of wave-forms of SEPSCs at a time-resolution of 1 msec, we found no evidence for such superposition of first SEPSC in a packet, even though a possibility of superposition was not completely excluded (Fig.1 D).

The long-lasting enhancement of SEPSCs analyzed in this study was completely blocked by application of inhibitors of protein and RNA synthesis for 15 min. We have confirmed that these inhibitors had no effects on synaptic transmission in our culture system (Fig. 4). Thus, gene expression was required even at the early stage for expression of this enhancement of SEPSCs. Recently, two kinds of neurotrophins, brain-derived neurotrophic factor (BDNF) and neurotrophin 3 (NT3) were reported to induce LTP in a protein-synthesis dependent manner (Kang and Schuman, 1996). Since the time course of the potentiation was much slower than that of the enhancement of SEPSCs in the present study, the molecular mechanisms for the enhancement might be different in each case. Involvement of NMDA receptors in the mechanism of induction of the enhancement of SEPSCs suggests the important role of Ca^{2+} in the potentiation. Analysis of Ca^{2+}-dependent protein kinases in intraneuronal signaling is now in progress.

Analysis of the effect of TTX on mEPSCs, in an effort to elucidate the mechanism of the enhancement of SEPSCs (Fig. 7), revealed an increase in frequency of mEPSCs, suggesting an increase in the number of synaptic sites and/or in the probability of transmitter release at a synaptic site. It is possible that the increase in the number of synaptic sites was due to the conversion of silent synapses to unsilent ones (Liao et al. 1995; Isaac et al., 1995). In fact, we have reported that silent synapses exist in the early stage of synaptogenesis in our cultured neurons (Kiyosue et al., 1997). The silent synapses may also play an important role both in synaptogenesis and in synaptic

278

plasticity.

We confirmed that the long-lasting enhancement of synaptic activity that depended on activation of NMDAR and synthesis of proteins occurred in the process of developmental synaptic maturation. It was recently suggested that long-lasting enhancement synaptic transmission was involved in the activity-dependent formation of functional glutamatergic synapses in the developing brain (Durand et al., 1996). The phenomena similar to LTP in the mechanism seem to be important for the study on synaptic functions.

Finally, our demonstration of some factor(s) in the conditioned medium that promoted enhancement indicates that interneuronal signaling by a diffusible molecule, such as a retrograde factor, is a key event in the induction of the long-lasting enhancement of SEPSCs. Since the diffusible molecule(s) can control the efficiency of transmission not only of a single synaptic site, but also of adjoining synaptic sites, we propose that the molecule(s) might also be involved in associative enhancement of synaptic activity.

Acknowledgments

The authors thank Ms. E. Shimabayashi and Dr. H. Nishimune for helpful discussions and Ms. K. Shirai for excellent technical support. S. N. K. is a pre-doctoral fellow of JSPS.

References

Arancio, O.,Kandel, E. R. and Hawkins, R. D. (1995) Activity-dependent long-term enhancement of transmitter release by presynaptic 3',5'-cyclic GMP in cultured hippocampal neurons. Nature, 376: 74-80.

Bliss, T. V. P. , and Lomo, T. (1973) Long-lasting potentiation of synaptic transmission in the dentate area of anesthetized rabbit following stimulation of perforant path. J. Physiol. (Lond.), 232: 331-336.

Cherubini, E., Ben Ari, Y., Gho, M., Bidard, J. N. and Lazdunski, M. (1987) Long-term potentiation of synaptic transmission in the hippocampus induced by a bee venom peptide. Nature, 328: 70-73.

Colino, A. and Malenka, R. C. (1993) Mechanisms underlying induction of long-term potentiation in rat medial and lateral perforant paths in vitro. J. Neurophysiol., 69: 1150-1159.

Cormier, R. J., Mauk, M. D. and Kelly, P. T. (1993) Glutamate iontophoresis induces long-term potentiation in the absence of evoked presynaptic activity. Neuron, 10: 907-919.

Durand, G. M., Yury K., and Konnerth, A. (1996) Long-term potentiation and functional synapse induction in developing hippocampus. Nature, 381:71-75

Isaac, J. T., Nicoll, R. A. and Malenka, R. C. (1995) Evidence for silent synapses: implications for the expression of LTP. Neuron, 15: 427-434.

Kamiya, H., Sawada, S. and Yamamoto, C. (1993) Long-lasting potentiation of synaptic transmission in the Schaffer collateral-commissural pathway of the guinea pig hippocampus by activation of postsynaptic N-methyl-D-aspartate receptor. Synapse, 13: 186-194.

Kang H, and Schuman, S. E. (1996) A requirement for local protein synthesis in neurotrophin-induced hippocampal synaptic plasticity. Science, 273: 1402-1406.

Kauer, J. A., Malenka, R. C. and Nicoll, R. A. (1988) NMDA application potentiates synaptic transmission in the hippocampus. Nature, 334: 250-252.

Kiyosue, K., and Kasai, M Taguchi,T. (1996) Two modes of activity-dependent synaptogenesis of cerebral neurons in vitro. Neuroreport, 7: 701-704.

Kiyosue, K., Kasai,M., and Taguchi,T. (1997) Selective formation of silent synapses on immature postsynaptic cells in cocultures of chick neurons of different ages. Dev. Brain Res., *In press*.

Liao, D., Hessler, N. A., and Malinow R. (1995) Activation of postsynaptically silent synapses during pairing-induced LTP in CA1 region of hippocampal slice. Nature 375: 400-404.

Lin, J. H., Way, L. J. and Gean, P. W. (1993) Pairing of pre- and postsynaptic activities in hippocampal CA1 neurons induces long-term modifications of NMDA receptor-mediated synaptic potential. Brain Res., 603: 117-120.

Lledo, P. M., Hjelmstad, G. O., Mukherji, S., Soderling, T. R., Malenka, R. C. and Nicoll, R. A. (1995) Calcium/calmodulin-dependent kinase II and long-term potentiation enhance synaptic transmission by the same mechanism. Proc. Nat. Acad. Sci. U.S.A., 92:

11175-11179.

Maren, S., Tocco, G., Standley, S. Baudry, M. and Thompson, R. F. (1993) Postsynaptic factors in the expression of long-term potentiation (LTP) Increased glutamate receptor binding following LTP induction in vivo. Proc. Natl. Acad. Sci. U.S.A., 90: 9654-9658.

Musgrave, M. L., Ballyk, B. A., and Goh, J. W. (1993) Coactivation of metabotropic and NMDA receptors in required for LTP induction. Neuroreport, 4: 712-714.

Neuman, R., Cherubini, E. and Ben Ari, Y. (1987) Is activation of N-methyl-D-aspartate receptor-gated channels sufficient to induce long-term potentiation? Neurosci. Lett., 80: 283-288.

Riedel, G., Manahan Vaughan, D., Kozikowski, A. P. and Reymann, K. G. (1995) Metabotropic glutamate receptor agonist trans-azetidine-2,4-dicarboxylic acid facilitates maintenance of LTP in the dentate gyrus in vivo. Neuropharmacology,34: 1107-1109.

Tokioka, R., Matsuo, A., Kiyosue, K., Kasai, M. and Taguchi, T. (1993) Synapse formation in dissociated cell cultures of embryonic chick cerebral neurons. Dev. Brain Res., 74: 146-150.

Wang, J. H. and Kelly, P. T. (1995) Postsynaptic injection of CA^{2+}/CaM induces synaptic potentiation requiring CaMKII and PKC activity. Neuron, 15: 443-452.

Wigstrom, H. and Gustafsson, B. (1986) Postsynaptic control of hippocampal long-term potentiation. J. Physiol. (Paris), 81 228-236.

Zheng, F. and Gallagher, J. P. (1992) Metabotropic glutamate receptors are required for the induction of long-term potentiation. Neuron, 9: 163-172.

Legends for Figures

Fig. 1. Potentiation in terms of the amplitude of SEPSCs by treatment with Mg^{2+}-free medium. Oscillating clusters of SEPSCs were recorded from two distinct neurons that had been cultured for 7 days under whole-cell clamp condition at -60 mV. Traces I and II, corresponding to the two neurons, are the records before (A), during (B) and after (C) Mg^{2+}-free treatment which was carried out by replacement of the external bathing solution. Although the treatment was ordinarily performed for 15 min under current-clamp mode, the trace (B) was recorded for the 3 min in the voltage-clamp mode to check the shape of the synaptic currents. Note that slow component of each EPSC, due to activation of NMDAR, became obvious during the incubation under Mg^{2+}-free condition. (D) Waveforms of periodic clusters of SEPSCs. Upper and middle traces represent SEPSCs in solutions with and without 1 mM $MgCl_2$. Lower trace represents SEPSCs after induction of the enhancement. The synaptic currents were recorded at a holding potential of -60 mV. Note that the slow components of the currents increased in Mg^{2+}-free solution. (E) Spontaneous excitatory post-synaptic potentials (SEPSPs) under Mg^{2+}-free conditions. The membrane potential was recorded in the current-clamp mode.

Fig. 2. The enhancement of periodic clusters of SEPSCs induced by Mg^{2+}-free treatment. (A) The enhancement of SEPSCs was induced by perfusion with Mg^{2+}-free external

bathing solution for 15 min. Solid bars indicate the mean amplitude of SEPSCs (pA with S.E.) recorded for 3 min from the time indicated on the horizontal axis. Since each SEPSC was a packet composed of several synaptic inputs, as shown in Fig. 1D, the amplitude of each SEPSC was represented by the first input as the first approximation of SEPSCs. A solid line shows the number of SEPSC events in the 3-min records. Asterisks (*) indicate the statistical significance of the increase, as confirmed by the Mann-Whitney test ($P<0.05$). (B) A control experiment was carried out by perfusion with the standard external solution. No change was detected (Kruskal-Wallis test, $P>0.05$) after perfusion. The data shown in (A) and (B) are one of the two records obtained simultaneously from two neurons. Right-angled arrows in the figure direct to right ordinates. (C, D) Distributions of the amplitudes in 3-min records of SEPSCs. The records are identical to those used to generate Fig. 2. (C) The enhancement of SEPSCs induced by Mg^{2+}-free treatment. (E) Control experiment.

Fig. 3. Effects of TTX, CNQX and D, L-APV on the enhancement of SEPSCs induced by Mg^{2+}-free treatment. Analysis of SEPSCs was performed as described in the legend to Fig. 2. The neurons were treated with Mg^{2+}-free solution that contained 500 nM TTX (A), 5μM CNQX (B) and 25μM D, L-APV (C). Normal synaptic transmission was restored in all three cases after washing out of the reagent but no potentiation was observed (Kruskal-Wallis, $P>0.05$). Right-angled arrows in the figure direct to right ordinates.

Fig. 4. Effects of inhibitors of protein and RNA synthesis on the enhancement of SEPSCs. Analysis of SEPSCs was performed as described in the legend to Fig. 2. The neurons were treated for 15 min with Mg^{2+}-free solution that contained 1μM cycloheximide (A) or 8μM actinomycin D (B). In both cases, no potentiation was detected (Kruskal-Wallis, $P>0.05$). Right-angled arrows in the figure direct to right ordinates.

Fig. 5. Summary of the enhancement of SEPSCs induced in Mg^{2+}-free solution. Each bar shows the average relative value (in % with S.E.) in normalized mean amplitudes of SEPSCs in n (the number of tested neurons shown in the Figure) neurons after induction. The mean amplitude in the initial 3-min was defined as 100%. An asterisk (*) indicates a significant increase (Mann-Whitney test, $P<0.05$).

Fig. 6. The traces of mEPSCs after induction of the enhancement of SEPSCs. The mEPSCs in voltage-clamped neurons at -60 mV were recorded for 3 min in the standard external bathing solution that contained 500 nM TTX 10 min before (A) and 20 min after (B) the induction of the enhancement of SEPSCs under Mg^{2+}-free conditions. A dot in traces indicates a single mEPSC.

Fig. 7. Frequency of mEPSCs after the enhancement of SEPSCs. The mEPSCs were

recorded for 3 min from the time indicated on the horizontal axis. The changes in frequency after the Mg^{2+}-free treatment are shown by solid bars. Note that a significant increase was confirmed. The increase in frequency was blocked by applying an inhibitor of protein synthesis, cycloheximide (CHX) at 1 μM, as shown in the lower panel in.

Fig. 8. The enhancement of SEPSCs induced by application of conditioned medium. (A) Increase in amplitude of SEPSCs upon a change from standard external solution to conditioned medium. The Mg^{2+}-free external bathing solution in which neurons had been incubated to induce the enhancement of SEPSCs was collected from the culture dish and the concentration of $MgCl_2$ was adjusted to 1 mM. This conditioned medium was substituted by perfusion for the medium in another culture dish, in which neuronal activity had been measured in standard external bathing solution. The lower trace was recorded at 15 min after the substitution of medium. (B) The enhancement of SEPSCs induced by conditioned medium. Analysis of SEPSCs was performed as described in the legend to Fig. 2. The bar marked CM shows the duration of application of the conditioned medium. An asterisk (*) indicates the statistical significance of an increase, as confirmed by the Mann-Whitney test ($P<0.05$). Note that the enhancement of SEPSCs was rapidly induced within 5 min. (C) Control experiment. Conditioned medium prepared from standard external bathing solution that contained 1 mM $MgCl_2$ did not induce the enhancement of SEPSCs. Right-angled arrows in the figure direct to right ordinates.

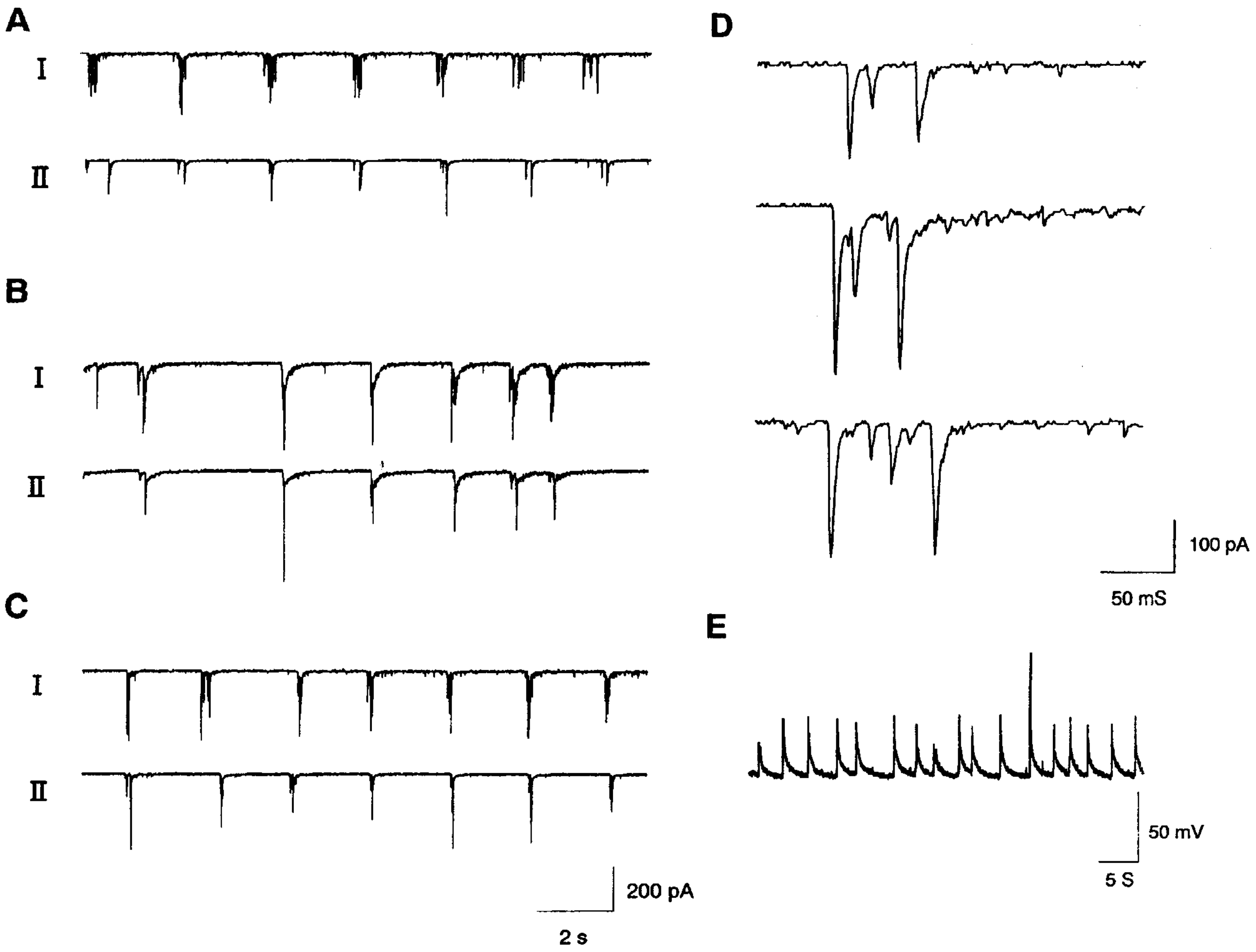
A
I
II
B
I
II
C
I
II
200 pA
2 s
D
100 pA
50 mS
E
50 mV
5 S

Kodah et. al., Fig. [illegible]

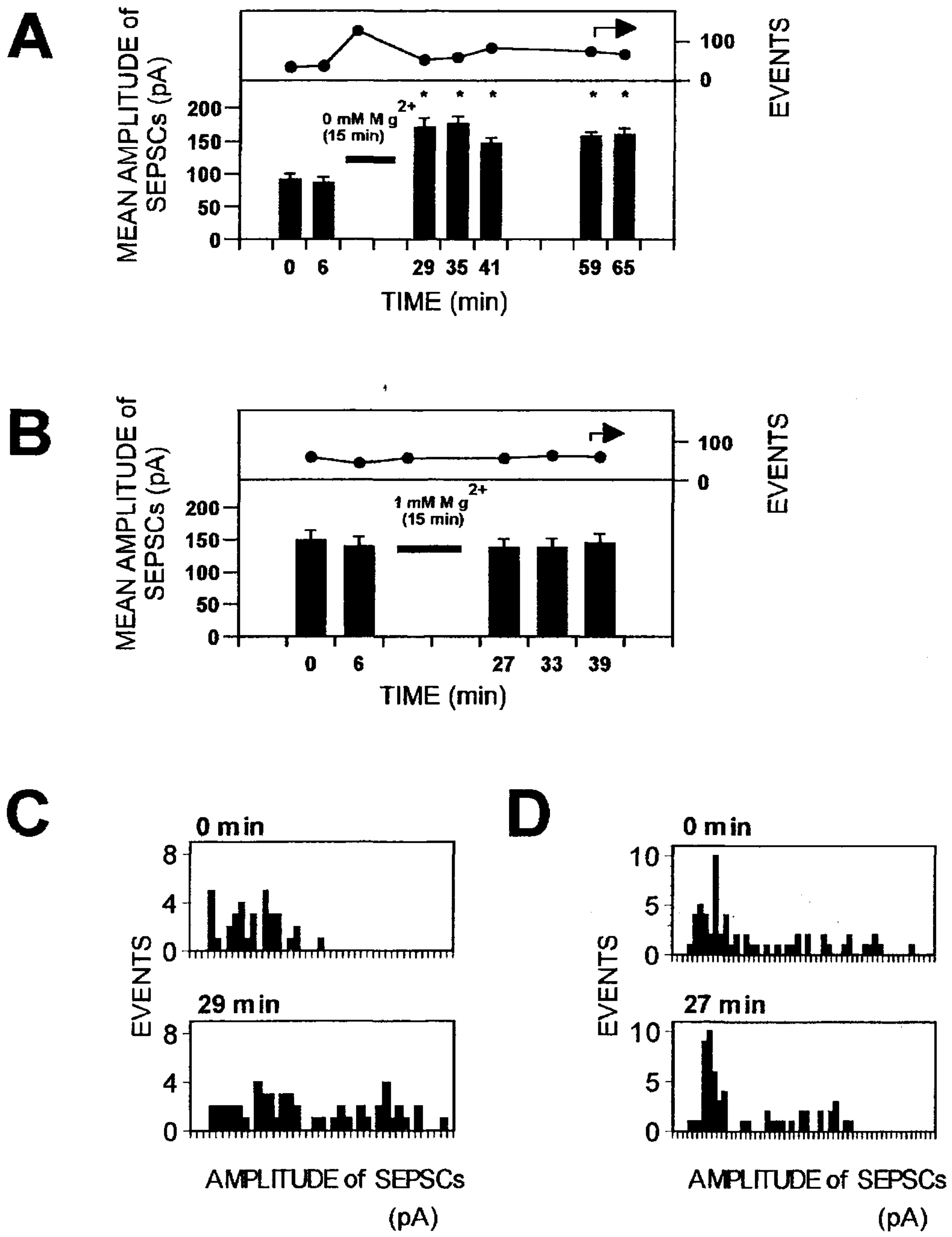

[illegible] et al. Fig. 3-4

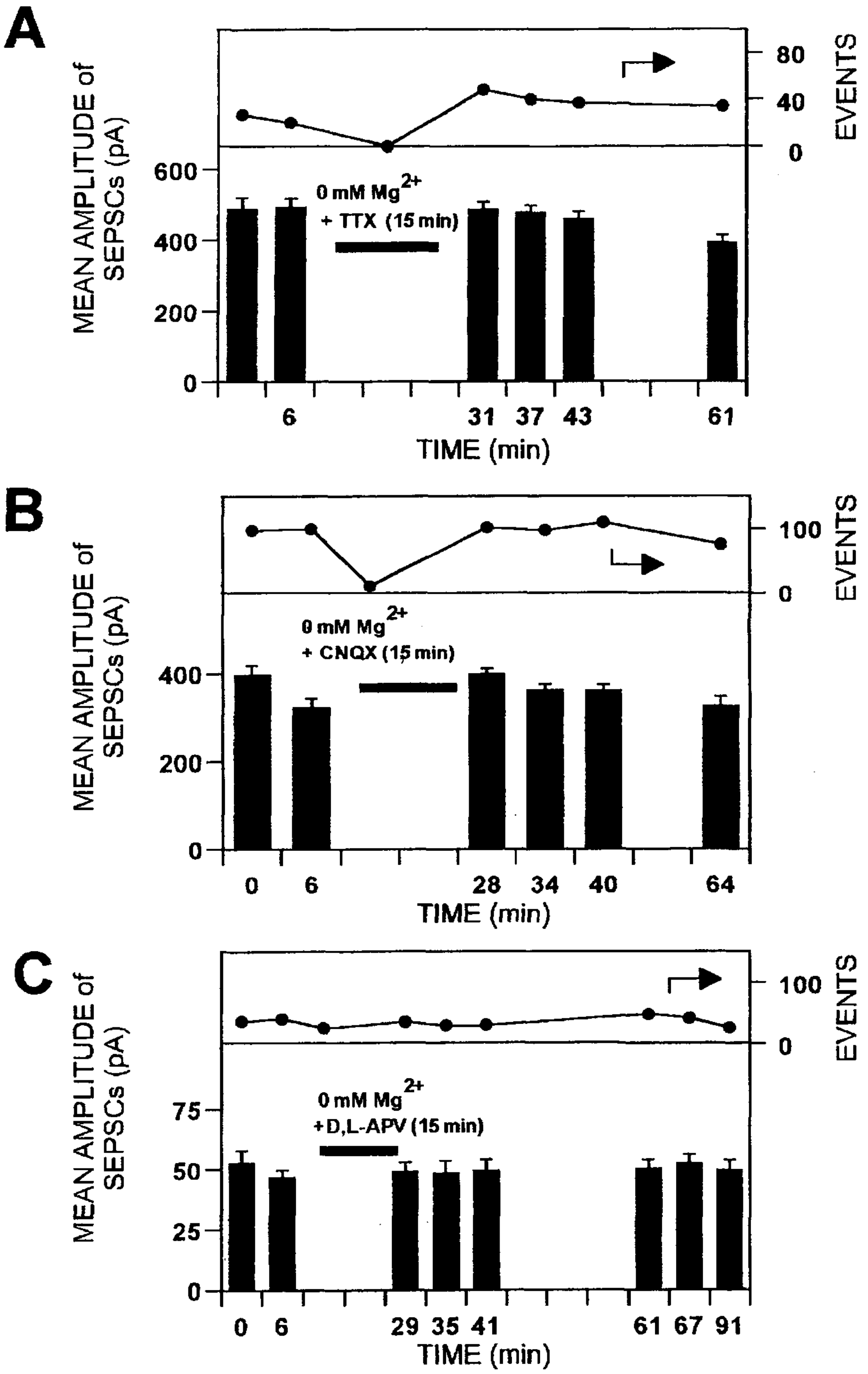
A
MEAN AMPLITUDE of SEPSCs (pA)
0
200
400
600
0 mM Mg^{2+}
+ TTX (15 min)
6
31
37
43
61
TIME (min)
EVENTS
0
40
80
B
MEAN AMPLITUDE of SEPSCs (pA)
0
200
400
0 mM Mg^{2+}
+ CNQX (15 min)
0
6
28
34
40
64
TIME (min)
EVENTS
0
100
C
MEAN AMPLITUDE of SEPSCs (pA)
0
25
50
75
0 mM Mg^{2+}
+D,L-APV (15 min)
0
6
29
35
41
61
67
91
TIME (min)
EVENTS
0
100

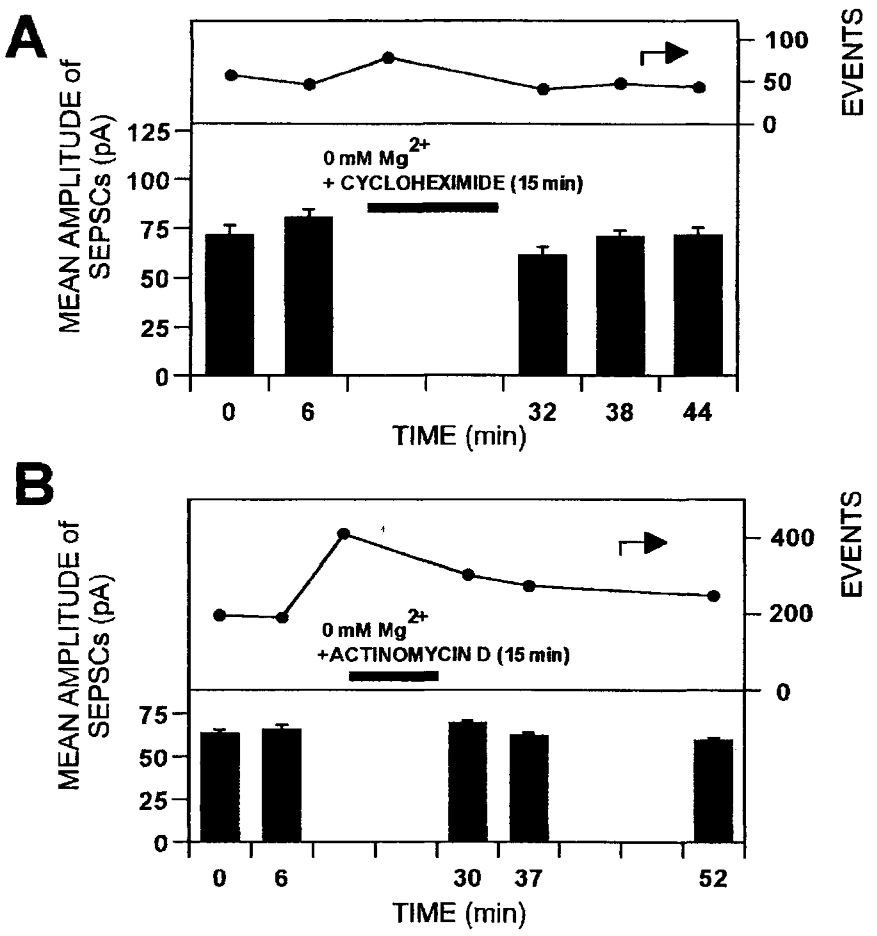
A
MEAN AMPLITUDE of SEPSCs (pA)
0
25
50
75
100
125
0 mM Mg2+
+ CYCLOHEXIMIDE (15 min)
EVENTS
0
50
100
0
6
32
38
44
TIME (min)
B
MEAN AMPLITUDE of SEPSCs (pA)
0
25
50
75
0 mM Mg2+
+ACTINOMYCIN D (15 min)
EVENTS
0
200
400
0
6
30
37
52
TIME (min)

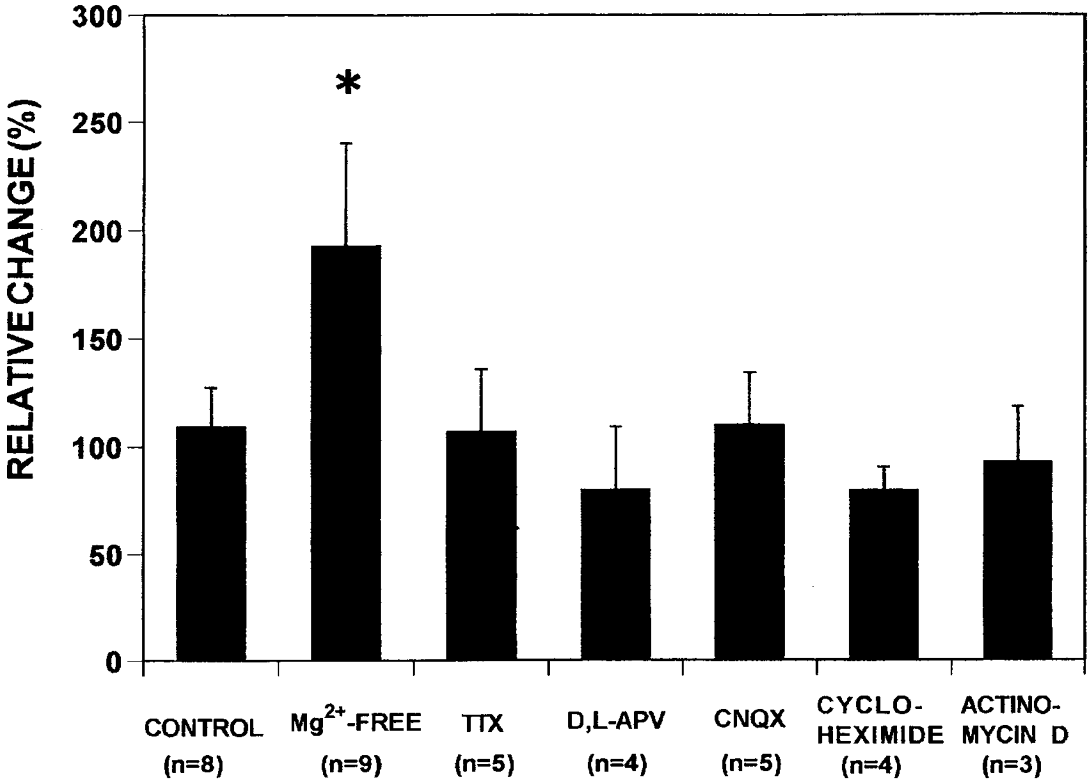
RELATIVE CHANGE (%)
300
250
200
150
100
50
0
*
CONTROL (n=8)
Mg2+-FREE (n=9)
TTX (n=5)
D,L-APV (n=4)
CNQX (n=5)
CYCLO-HEXIMIDE (n=4)
ACTINO-MYCIN D (n=3)

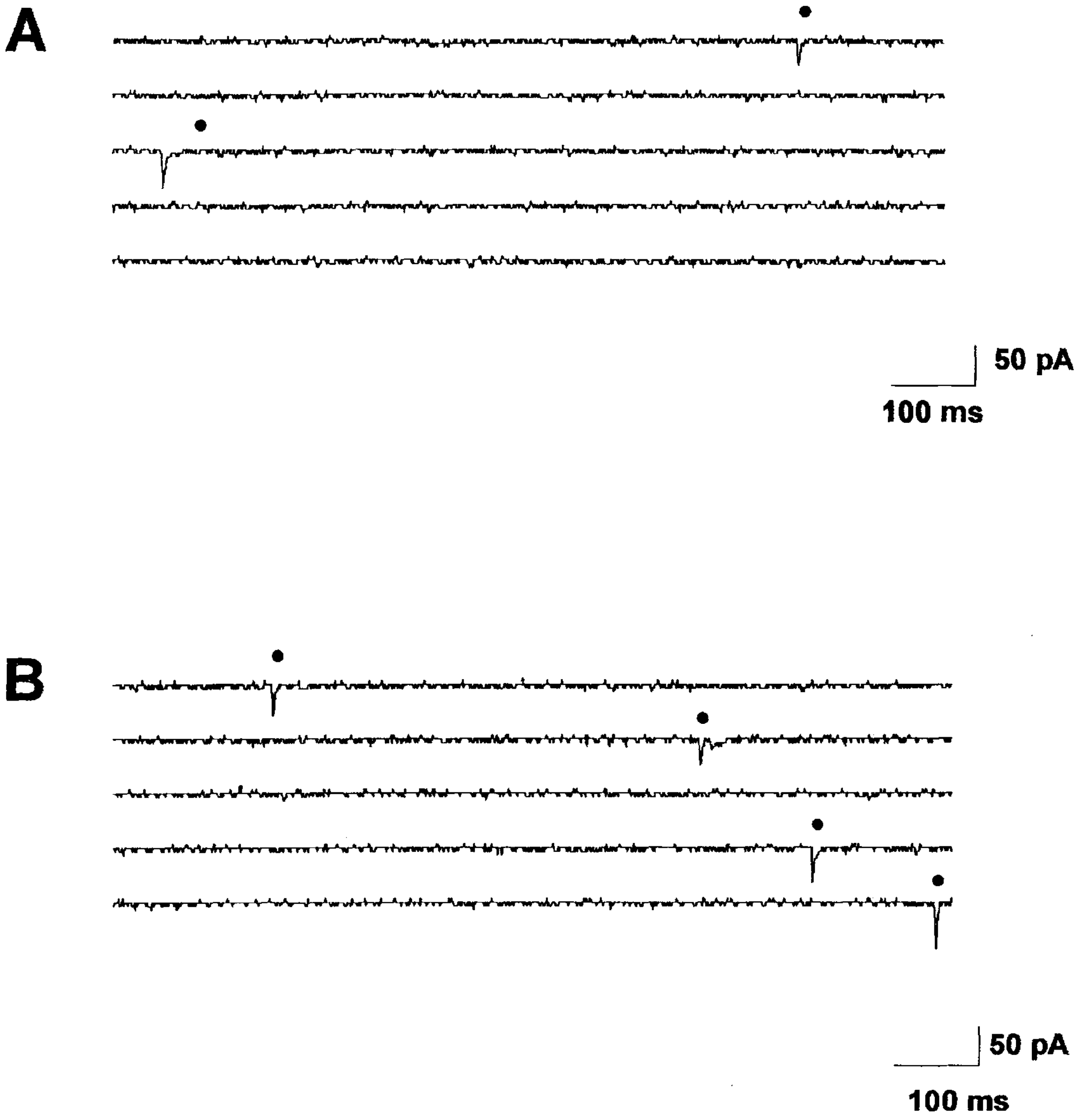
A
50 pA
100 ms
B
50 pA
100 ms

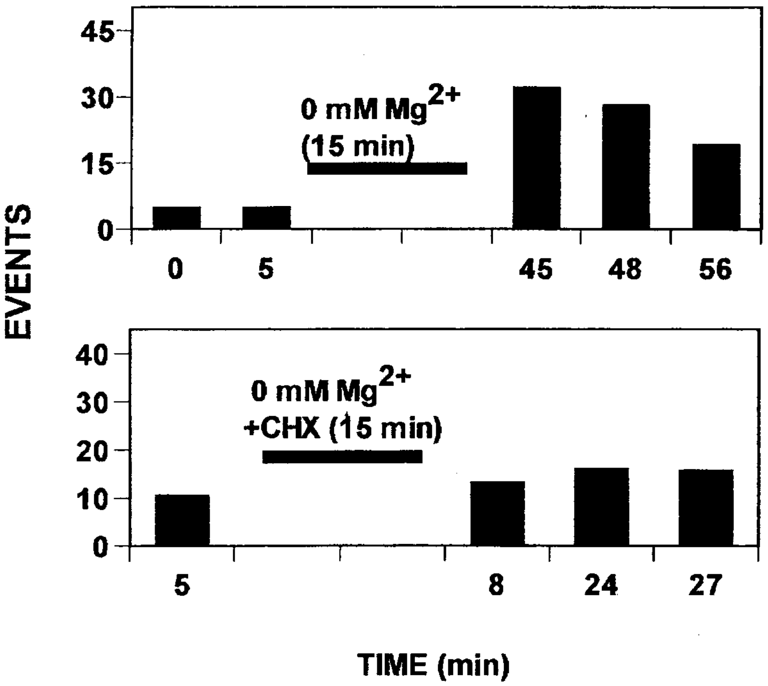
EVENTS
45
30
15
0
0 mM Mg2+
(15 min)
0
5
45
48
56
40
30
20
10
0
0 mM Mg2+
+CHX (15 min)
5
8
24
27
TIME (min)

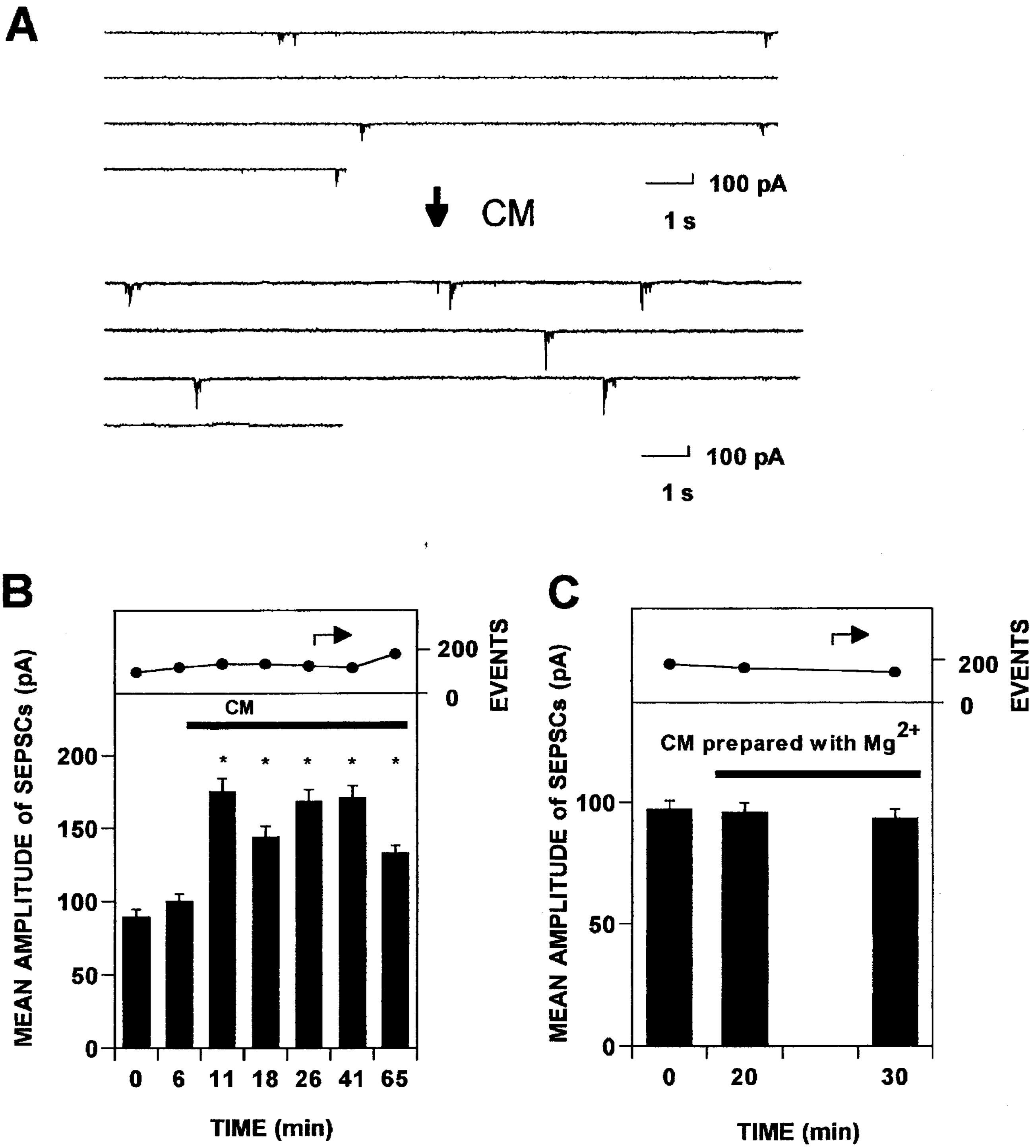
A
CM
100 pA
1 s
100 pA
1 s
B
MEAN AMPLITUDE of SEPSCs (pA)
0
50
100
150
200
CM
*
0
6
11
18
26
41
65
TIME (min)
EVENTS
0
200
C
MEAN AMPLITUDE of SEPSCs (pA)
0
50
100
CM prepared with Mg^{2+}
0
20
30
TIME (min)
EVENTS
0
200

19.

PSEUDOALTEROMONAS MYTILI sp. nov. ~~A NEW SPECIES OF MARINE BACTERIA~~ ISOLATED FROM MUSSELS

PRIVILEGED COMMUNICAT
For Review Only.
IJSB 245-96

Elena P. Ivanova[1,4]*, Elena A. Kiprianova[2], Valery V. Mikhailov[1], Galina F. Levanova[3], Alexandra D. Garagulya[2], Nataliya M. Gorshkova[1], Irina Y. Bakunina[1], Galina M. Frolova[1], Dan V. Nicolau[4], Noboru Yumoto[4], Takahisa Taguchi[4], Susumu Yoshikawa[4]

[1]Pacific Institute of Bioorganic Chemistry, Far Eastern Branch of the Russian Academy of Sciences, 690022, Vladivostok, pr.100 let Vladivostoku, 159, Russia.

[2] Zabolotny Institute of Microbiology and Virology of the Ukrainian Academy of Sciences, 252143, Kiev, Zabolotnogo st.,154, Ukraine.

[3]Institute of Epidemology and Microbiology, 603600, N. Novgorod, Russia.

[4]Osaka National Research Institute, AIST, Ikeda, Osaka 563, Japan.

Key words:marine bacteria, genus *Pseudoalteromonas,* new species

* To whom correspondence should be addressed: Department of Organic Materials, Osaka National Research Institute, AIST, Ikeda, Osaka 563, Japan. Fax: +81-727-51-9628, e-mail:ivep@onri.go.jp

Summary

Four strains of marine, aerobic, agar-decomposing bacteria with one polar flagellum, and with G + C ~~ratio~~ of the DNA ~~at~~ 38.9 to 40.2 mol% were isolated from the Far Eastern mussels *Crenomytilus grayanus* and *Patinopecten jessoensis*. According to carbon utilization tests and the BIOLOG identification system, these bacteria were phenotypically different from other *Pseudoalteromonas* species. High agar-decomposing activity was found in two strains, in one of which agarase, α-galactosidase, pustullanase, and laminarinase had been detected. The level of DNA homology of three of the strains was 70-100%. The fourth isolate was genetically less related to the others (67% of DNA relatedness~~)~~ and phenotypically was more distant from other members of this group. DNA of the strains isolated from mussels showed 40-45% of genetic relatedness with the DNA of *A. atlantica,* 8-36% with DNA of *P. haloplanktis* subsp. *haloplanktis, P. haloplanktis* subsp. *tetraodonis, P. undina, P. nigrifaciens, P. carrageenovora,* and 14-16% with DNA of *Alteromonas macleodii* as determined by DNA-DNA hybridization experiments. These results were confirmed by serological data employing polyclonal antibodies to cell surface antigens. The name *Pseudoalteromonas mytili* is proposed for the new species, and its differentiative characters are given. The type strain KMM 188 (=VKPM B3907) is deposited in the Russian Collection of Industrial Microorganisms (VKPM, Moscow) and in the Collection of Marine Microorganisms of the Pacific Institute of Bioorganic Chemistry (KMM, Vladivostok).

Introduction

Intensive investigations of the genus *Alteromonas* during last few years have resulted in revision and specification of its taxonomic structure on the one hand (1, 2, 11, 12, 28), and broadening of the list of species on the other (8, 10, 17, 24). The resulting data of SSU DNA sequences (12) revealed that the genus *Alteromonas* should be restricted to a single species, *A. macleodii,* while new genus *Pseudoalteromonas* was created for thirteen other species. The latter are common inhabitants of the aquatic environment, and were isolated mainly from seawater (5, 11). *Pseudoalteromonas* strains, typically associated with marine animals, might be of particular interest as a promising source for new species with distinct features. One such feature is a high hydrolytic activity, particularly, in the degradation of array polysaccharides. The agar-decomposing strains were found among *Vibrio spp., Cytophaga spp., Pseudomonas spp.* and some actinomyces. Several years ago Akagawa-Matsushita et al. (1) clarified a taxonomic assignment of a species *"Pseudomonas atlantica",* and described these agar-decomposing bacteria as *Alteromonas (*now *Pseudoalteromonas) atlantica.*

43. The goal of the present report is to describe the new strains of *Pseudoalteromonas* genus isolated from the Far Eastern mussels *Crenomytilus grayanus* and *Patinopecten jessoensis.* Several members of this group proved to hydrolyze agar-agar and other algal polysaccharides.

Materials and Methods

Bacterial strains and isolation procedure. The strains that we used are listed in Table 1. Mussels (*C. grayanus* and *P. jessoensis)* were collected in 1985, 1989, and 1990 at the Pacific Institute Bioorganic Chemistry Marine Experimental Station, Troitza Bay, Gulf of Peter the Great, Sea of Japan. Mussels were collected at a depth of 8 m (salinity, 33%, temperature, 12°C) and were prepared aseptically. The strains were isolated from tissue homogenates by plating on agar plates of marine agar 2216 (Difco) and on plates with medium B, which contained 0.2% (wt/vol) Bacto Peptone (Difco), 0.2% (wt/vol) casein hydrolysate (Merck), 0.2% (wt/vol) yeast extract (Difco), 0.1% (wt/vol) glucose, 0.002% (wt/vol) KH_2PO_4, 0.005% (wt/vol) $MgSO_4 7H_2O$ and 1.5 % (wt/vol) Bacto Agar(Difco), 50% (vol/vol) of natural seawater, and 50% (vol/vol) distilled water at pH 7.5-7.8 as described elsewhere (14). Strains were maintained on the same semisolid B medium in tubes under mineral oil at 4°C. The strains are streaked on agar plates from tubes every six months to control purity and viability.

Bacto

Caps

Phenotypic analysis. The phenotypic properties used for characterization of *Pseudoalteromonas* and related species were ~~determined as~~ previously described (3, 4, 14, 25). Electron micrographs of negatively stained cells were prepared with an JAM-7 electron microscope.

Nutritional tests. The tests for utilization of various organic substrates (listed in Table 2) as sole carbon sources at a concentration of 0.1% (wt/vol) were performed in 10 ml per tube of liquid BM medium (3). The bacteria were grown with shaking on a rotary shaker at 160 rpm for 72 h at 26 to 28°C. To test the bacterial oxidation of 95 carbon sources simultaneously we used the BIOLOG technique. Strains were grown on marine agar plates at 28°C for 24 h. Cell density was adjusted to $A_{590} = 0.3 \pm 0.05$ in a sterile solution of 23.5 g NaCl in 1000 ml of MiliQ water. Three BIOLOG GN microplates (Biolog, Hayward, CA) for each strain were inoculated with150 µl of the cell suspension per well by means of a repeating pipetter. The inoculated plates were incubated at 28°C. The results were read visually as recommended by Rüger&Krambeck (23) after 1, 2, 3 and 5 days of incubation.

A cluster analysis was performed by STATISTICA for Windows software Rel. 4.3 B, StatSoft. Inc. 1993. An unweighted pair-group average method was used to calculate cluster distances, and a dendrogram was drawn by using a per cent disagreement method.

Genetic analysis. The DNA was isolated following the method of Marmur (20). The G+C content of the DNA was determined by the thermal denaturation method of Marmur and Doty (21). DNA-DNA hybridization was ~~studied~~ spectrophotometrically and initial renaturation rates were recorded as described by De Ley et al. (7) and Levanova et al. (19).

Serology. The strains were grown in liquid B medium with shaking for 24 h at 25° C. Cells were harvested by centrifugation for 20 min at 10000xg, washed twice and suspended in 0.85% PBS buffer (pH 7.4) to a final density 1×10^9 cells/ml. Rabbit antiserum for the strains studied was prepared by immunization of rabbits by means of the cells killed with 1% formaldehyde as described by Conway de Macario et al. (6). The Enzyme-Linked Immunosorbent Assay (ELISA) was performed by the methods of Voller et al. (30) and Karaulin et al. (15). The level of antigen relatedness was estimated as described by Conway de Macario et al. (6).

Characterization of pigments. The features of brown melanin-like pigment were tested as described earlier (14). For production of pigment we used B medium (as described above) and BT medium which had the same composition plus L-tyrosine at 1 g/l. The synthetic (S) medium contained (g/l): KH_2PO_4, 0.05; K_2HPO_4, 0.05; $MgSO_4$, 0.05; $CuSO_4$, 0.06; $CaCl_2$, 0.05; L-methionine, 20 mg; DL-t~~h~~ryptophan, 20 mg; α-asparagine, 10 mg; DL-phenylalanine, 10 mg; yeast extract, 2; $(NH_4)_2SO_4$, 1 at pH 7,6. ST medium had the same composition plus L-tyrosine at 1 g/l. Inhibitors of melanogenesis, such as L-cysteine, EDTA and ascorbic acid, were added at 1-10 mM if necessary.

Preparation of cell-free extracts. For preparation of crude enzymes, cells were grown in ~~1-l Erlenmeyer flasks with 0.5 l of~~ liquid B medium with shaking at 160 rpm for 24 h at 25°C. Cells were harvested by centrifugation for 20 min at 10000 xg at 0-4°C. Cells (25 mg of dry weight per ml) were suspended in 0.05 M phosphate buffer (pH 6.8) ~~that contained~~ containing 0.1 M NaCl. ~~The~~ #6 suspension was immersed in a mixture of ~~ice and salt, and cells were disrupted by sonification.~~ The sonicate was stored at 4° C for 18 h, centrifuged at 10000 xg for 40 min and the supernatant was used as the crude preparation of enzymes.

Assays of enzymatic activity. Glycanase activities were assayed by the method of Nelson (22) at 25°C with ~~various~~ p-nitrophenyl glycosides ~~(obtained from Chemacol)~~ dissolved in 0.05 M sodium phosphate buffer, pH 7.0, as substrates. One unit of activity was defined as the amount of enzyme that generated 1 mmol of p-nitrophenol in 1 min per 1 ml of crude enzyme preparation. Carbohydrate-degrading activities were determined using the following substrates: laminarin from *Laminaria cicharoides* (9) and pustulan from *Umbillicaria rossica*, CM-cellulose and starch (Fluka), dextran (Koch-Light Laboratories) and chitosan from the crab *Paralitodes camtschatica,* which was kindly provied by P. Lukyanov (PIBOC FEB RAS). All polysaccharides were dissolved in 0.05 M sodiumphosphate buffer pH 6,8. One unit of enzyme activity was defined as the amount of enzyme that liberated 1 µmol of reducing sugars in 1 min per 1 ml of the preparation of crude enzyme under the given conditions. The concentrations of the reducing sugar were determined by the method of Nelson (22).

Results and Discussion

Identification ~~to the genus level~~. The four strains isolated ~~studied~~ (KMM 157, KMM 188^T , KMM 280, and KMM 327) were gram-negative, strictly aerobic, rod-shaped bacteria with one polar flagellum (Fig.1). None of the bacteria accumulated poly-β-hydroxybutyrate as an intracellular reserve product and had an arginine dihydrolase system. All were oxidase-positive, and all required Na$^+$ ions or seawater for growth. The G+C contents of the DNAs were 39.2-40.2 mol%. Cellular fatty acids were essentially the same as those of *Pseudoalteromonas* species as described by Svetashev et al.(26) and comprised 16:1(n-7), 16:0, 17:1, 18:1(n-7) fatty acids which were the most abundant. All these properties allowed us to assign the isolates from mussels to the genus *Pseudoalteromonas.*

The notable feature of the studied organisms is their phenotypic variability (Table 2). The strain KMM 188 produced a dark brown pigment ~~both~~ in all tested media (in particular at low temperatures), strain KMM 157 produced light-orange pigment in some media, and strains KMM 280 and 327 were colourless in ordinary conditions of cultivation. This fact lead us to examine the formation of pigment on tyrosine-containing media that are optimal for melanogenesis and in media containing its inhibitors (cysteine, EDTA, and ascorbic acid). We found that all of four strains produced brown pigments on tyrosine-containing media and were colorless in presence of inhibitors. The pigments were not extractable with water, alcohols or various polar solvents but were extracted from cells with a 0.5 M ~~N~~ ~~solution of~~ NaOH in ~~water and formed a brown solution~~. The ~~alk~~aline pigment extracted in alkaline solution behaved qualitatively as melanin: it became colorless upon addition of H_2O_2, whereas the addition of $KMnO_4$ gave a green colour ~~solution~~. The absorption maxima of the pigment at 225 and 273 nm were nearly the same as ~~close to~~ those for synthetic melanin (Sigma), namely 223 and 269 nm. The IR spectrum of the pigment had peaks at 1,714, 1,702, 1,672, 1,624, 1,510, 1,486, 1,402 and 1,024 cm^{-1}. All the data confirmed ~~the melanin-like nature of~~ the pigments as melanin.

Strains KMM 188 and 157 hydrolyzed agar, wheseas strains KMM 280 and 327 did not show agarolytic activity. Only one agar-decomposing member of *Pseudoalteromonas* genus, *P. atlantica*, has been described at present, but strains isolated from mussels were distant from this species in their phen properties and level of DNA homology (see below).

The nutritional spectra of strains studied, particularly of KMM 157, are rather diversed. The strain KMM 157 differs from other three members of the group by its ability to utilize 15 different C-sources. At the same time BIOLOG technique based on bacterial oxidation of 95 carbon sources has shown a close similarity between strains KMM 188 and 157 (Fig.2). Accordin~~d~~g to metabolic profiles obtained, strains KMM 188 and 157 were clearly distinguished from other species of the genus Pseudoalteromonas ~~related marine bacte~~ria. The type strains of *Marinomonas vaga* and *Marinomonas communis* #9 phenotypically proved to be distant from the type of *Pseudoalteromonas* species ~~strains~~. On the contrary, type strain of *Alteromonas macleodii* was phenotypically ~~close~~ similar to *Pseudoalteromonas* ~~spp.~~ species, especially *P. haloplanktis*. subsp. *tetraodonis.*

DNA relatedness. The levels of DNA relatedness of strains isolated from mussels and some type species of *Pseudoalteromonas* are presented in Table 3. Four strains studied have shown 67-100% of DNA homology and hence belong to one species (30). Their genetic similarity with the type strain of *P. atlantica* was 40-45%, with other *Pseudoalteromonas* type strains, and *Alteromonas macleodii* was lower, ranging from 8 to 36%.

Serology. The results of the DNA-DNA hybridization experiments were coincided with ~~supported by~~ serological data employing polyclonal antibodies to cell surface determinants. Antiserum to strain KMM 188 did not discernibly react with surface antigens of *P. atlantica, P. macleodii, P. piscicida,* and *P. haloplanktis* subsp. *haloplanktis* and showed 34%, 45%, 46%, and 62% of surface antigen similarity, respectively.

Enzyme activities. The enzyme activities of the strain KMM 188 was studied using a set of carbohydrates including some algal polysaccharides (Table 4). Agarase (4-glycan hydrolase) which catalyzes agar-agar hydrolysis to relatively large fragments and α-galactosidase (α-D-galactoside galactohydrolase) which releases α-galactose from the non-reducing side of oligosaccharides that constitute one of the component of agar-agar, were found as well as pustulanase and laminarinase, enzymes that hydrolyze the brown algae (β-1,6- and β-1,3-glucans). It is of interest to note that the activity of α-galactosidase was twenty times more than agarase. We assume

stronger

the effective hydrolysis of agar-agar by strain KMM 188 was due to the additive effect of agarase and α-galactosidase probably produced at different growth phases.

Description of *Pseudoalteromonas musseli* strains. Our present data give evidence that the strains studied belong to a new species, [although we can not yet find an explaination for the essential phenotypic differences of strain KMM 157 from other members of the group.] See #10 According to the results obtained, we propose a new species *Pseudoalteromonas mytili,* a description of which is given below. [Its differential characteristics (Table 5) are based on properties of three genetically and phenotypically more similar strains of the group.] S. #4

Pseudoalteromonas mytili sp. nov. (my. ti.`li. L. gen. n. *mytili,* of mussels the genus [*Mytilus*]). Cells are Gram-negative, strictly aerobic, motile with one polar flagellum, rod-shaped, 0.5-0.8x1.0-1.5 μm in logarithmic growth phase. Produces cellular melanin-like pigment depending on medium composition and culture conditions. Sodium ions are essential for growth. Amino acids are not required for growth. Temperature range for growth is 4-35°C. Most rapid growth occurs at 28°C. The optimum pH range is 7.0-8.5. Chemoorganotrophs; metabolism is strictly respiratory. Positive for hydrolysis of starch, and gelatin, some strains hydrolyze agar-agar, pustulan, and laminarin. Chitin and Tween-80 are not hydrolyzed. Positive for oxidase and catalase, and levansaccharase. Negative for nitrate reduction, denitrification, luminescence. Glucose, ribose, rhamnose, mannose, fructose, cellobiose, lactose, gluconate, acetate, propionate, butyrate, caproate, succinate, aconitate, glycogen, mannitol, adonitol, ethanol, p-hydroxybenzoate, phenylacetic acid, aspartic acid, glutamic acid, L-arginine, L-ornitine, L-tyrosine, and L-proline are utilized as sole sources of carbon and energy. The following compounds are not utilized: arabinose, maltose, valeriate, glutarate, inositol, threonine and lysine. The strains are sensitive to rifampicin, ampicillin, gentamicin, oxacillin, polymyxin, erythromycin, ofloxacin. The main fatty acids of the cells are palmitoleic, palmitic and *cis*-vaccenic acids.

The G+C content of the DNA is 38.9-40.2 mol%.

Isolated from Far Eastern mussels.

The type strain is strain KMM 188 (=VKPM B 3907).

ACKNOWLEDGMENTS

This study was supported by an individual grant from ISF and Fellowship from the Foreign Researcher Invitation Program of the Agency of Industrial Science and Technology, Japan, The expert assistance of Dr. N. Utkina was greatly appreciated.

References

1. **Akagawa-Matsushita, M., M. Matsuo, Y. Koga, and K. Yamasato.** 1992. *Alteromonas atlantica* sp.nov. and *Alteromonas carrageenovora* sp. nov., bacteria that decomposed algal polysaccharides. Int. J. Syst~~em.~~ Bacteriol. **42**:621-627.

2. **Akagawa-Matsushita, M., Y. Koga, and K. Yamasato.** 1993. DNA relatedness among nonpigmented species of *Alteromonas* and synonymy of *Alteromonas haloplanktis* (ZoBell and Upham 1944) Reichelt and Baumann 1973 and *Alteromonas tetraodonis* Simidu et al. 1990. Int. J. Syst~~em.~~ Bacteriol. **43**:500-503.

3. **Baumann, L., P. Baumann, M. Mandel, and R. D. Allen.** 1972. Taxonomy of aerobic marine eubacteria. J. Bacteriol. **110**:402-429

4. **Baumann, P., and L. Baumann.** 1981. The marine Gram-negative eubacteria; genera *Photobacterium, Beneckea, Alteromonas, Pseudomonas,* and *Alcaligenes,* p. 1302-1330. *In* M. P. Starr, H. Stolp, H. G. Trüper, A. Balows, and H. G. Sclegel (ed.), The prokaryotes. A handbook on habitats, isolation, and identification of bacteria, 1st ed., vol. 2. Springer-Verlag AG, Berlin.

5. **Baumann, P., M. J. Gauthier, and L. Baumann.** 1984. Genus *Alteromonas*. Baumann, Baumann Mandel and Allen 1972, 418; pp. 243-354. *In*: N. R. Krieg, and J. G. Holt (ed.), Bergey`s manual of systematic bacteriology, vol. 1. The Williams & Wilkins Co., Baltimore.

6. **Conway de Macario, E., A. J. L. Macario, and M. J. Wolin.** 1982. Specific antisera and immunological procedures for characterization of methanogenic bacteria. J. Bacteriol. **149**:320-328.

7. **De Ley, J., H. Cattoir, and A. Reynaerts.** 1970. The quantitative measurement of DNA hybridization from renaturation rates. Eur. J. Biochem. 12:133-142.

8. **De Vos, P., A. Van Landschoot, P. Segers, R. Tytgat, M. Gillis, M. Bauwens, R. Rossau, M. Goor, B. Pot, K. Kersters, P. Lizzaraga, and J. De Ley.** 1989. Genotypic relationships and taxonomic localization of unclassified *Pseudomonas* and *Pseudomonas*-like strains by deoxyribonucleic acid: ribosomal ribonucleic acid hybridization. Int. J. Syst. Bacteriol. **39**:35-49.

9. **Elyakova, L. A., and T. N. Zvyagintseva.** 1974. A study of the laminarins of some Far-Eastern brown seaweeds. Carbohydr. Res. 32:241-248.

10. **Enger, O., H. Nygaard, M. Solberg, G. Schel, J. Nielsen, I. Dundas.** 1987. Characterization of *Alteromonas denitrificans* sp. nov. Int. J. Syst. Bacteriol. 37:416-421.

11. **Gauthier, M. J., and V. A. Breittmayer.** 1992. The genera *Alteromonas* and *Marinomonas*, p.3046-3070. *In* A. Balows, H. G. Trüper, M. Dworkin, W. Harder, and K.-H. Schleifer (ed.), The prokaryotes, 2nd ed., vol. 3. Springer-Verlag, New York.

12. **Gauthier, G., M. Gauthier, R. Christen.** 1995. Phylogenetic analysis of the genera *Alteromonas , Shewanella, and Moritella* using genes coding for small-subunit rRNA sequences and division of the genus *Alteromonas* into two genera, *Alteromonas (*Emended) and *Pseudoalteromonas* gen. nov., and twelve new species combinations. Int. J. Syst~~em~~. Bacteriol. 45:755-761

13. **Hansen, A. J., O. B. Weeks, and R. R. Colwell.** 1965. Taxonomy of *Pseudomonas piscicida* (Bein) Buck, Meyers, and Leifson. J. ~~of~~ Bacteriol. **89**:752-761.

14. **Ivanova, E. P., E. A. Kiprianova, V. V. Mikhailov, G. F. Levanova, A. D. Garagulaya, N. M. Gorshkova, N. Yumoto, and S. Yoshikawa.** 1996. Characterization and identification of marine *Alteromonas nigrifaciens* strains and emendation of the description. Int. J. Syst. Bacteriol. **46**:223-228.

15. **Karaulin, A. Yu., B. B. Dzantiev, G. G. Orlova, and A. M. Egorov.** 1990. Some ELISA peculiarities of the bacterial cells. Mikrobiological Journal. 9:12-18.(in Russian).

16. **Kelley, S. K., V. E. Coyne, W. C. Sledjeski, R. M. Fugua, and R. M. Weiner.** 1990. Identification of a tyrosinase from a periphytic marine bacterium. FEMS Microbiol. Letters. **67**:275-280.

17. **Kodama, K., H. Shiozawa, and A. Ishi.** 1993. *Alteromonas rava* sp. nov., a marine bacterium that produces a new antibiotic, thiomarinol. Annu. Rep. Sankyo Res. Lab. **45**:131-136.

18. **Lee, J. V., D. M. Gibson, and J. M. Shewan.** 1981. *Alteromonas putrefaciens* sp. nov. *In* Validation of the publication of new names and new combinations previously published outside IJSB. List N 6. Int. J. Syst. Bacteriol. **31**:215-218.

19. **Levanova, G. F., E. V. Novova,V. N. Sorokina, and E. A. Kiprianova.** 1984. Spectrophotometric method of DNA-DNA molecular hybridization for bacteria of the genus *Pseudomonas.* Biological Sciences. 8:27-32.(In Russian).

20. **Marmur, J.**1961. A procedure for the isolation of deoxyribonucleic acid from microorganisms. J. Mol. Biol. 3:208-218.

21. **Marmur, J., and P. Doty.** 1962. Determination of the base composition of deoxyribonucleic acid from its thermal denaturation temperature. J. Mol. Biol. 5:109-118.

22. **Nelson, T. E.** 1944. A photometric adaptation of Somogyi method for the determination of glucose. J. Biol. Chem. 153:375-380.

23. **Rüger, H.-J., and H.-J. Krambeck.** 1994. Evaluation of the BIOLOG substrate matabolism system for classification of marine bacteria. System. Appl. Microbiol. **17**:281-288.

24. **Simidu, U., K. Kita-Tsukamoto, T. Yasumoto, and M. Yotsu.** 1990. Taxonomy of four marine bacterial strains that produce tetrodotoxin. Int. J. Syst. Bacteriol. **40**:331-336.

25. **Smibert, R. M. and N. R. Krieg.** 1994. Phenotypic characterization, p. 607-654. *In* F. Gerhardt (ed.-in-chief), Methods for General and Molecular Bacteriology. American Society for Microbiology, Washington. D.C.

26. **Svetashev, V. I., M. V. Vysotskii, E. P. Ivanova, E. P., and V. V. Mikhailov.** 1995. Gas-liquid chromatographic analysis of cellular fatty acid methyl esters in *Alteromonas* species. Appl. Syst. Microbiol. **18**:37-43.

27. **Swan, G. A.** 1974. Structure, chemistry and biosynthesis of melanins. Fortschr. Chem. Org. Naturst. **31**:521-582.

28. **Van Landschoot, A., and J. De Ley.** 1983. Intra- and intergeneric similarities of the the rRNA cistrons of *Alteromonas, Marinomonas* (gen. nov.) and some other Gram-negative bacteria. J. Gen. Microbiol. **129**:3057-3074.

29. **Voller, A., D. E. Bidwell, and A. Bartlett.** 1979. Setting up ELISA, p. 38-39. *In* The enzyme-linked immunosorbent assay (ELISA). A guide with abstracts of microplate applications. Guersey-Great Britain, Dynatech Europe.

30. **Wayne, L. G., D. J. Brenner, R. R. Colwell, P. A. D. Grimont, O. Kandler, M. I. Krichevsky, L. H. Moore, W. E. C. Moore, R. G. E. Murray, E. Stackebrandt, M. P. Starr, and H. G. Trüper.** 1987. Report of the Ad Hoc Committee on Reconciliation of Approaches to Bacterial Systematics. Int. J. Syst. Bacteriol. **37**:463-464.

31. **Weiner, R. M., A. M. Segai, and R. R. Colwell.** 1985. Characterization of a marine bacterium associated with *Crassostrea virginica* (the Eastern Oyster). Environm. Appl. Microbiol. **40**:83-90.

See #12

Table 1. List of strains studied

Name	Strain	Other designations	Source
Marinomanas vaga	ATCC 27119^{T}		ATCC
Marinomonas communis	ATCC 27118^{T}		ATCC
Pseudoalteromonas mytili (2)	KMM 157	2GM20	Mussel, *Patinopecten jessoensis,* Sea of Japan, Troitza Bay
Pseudoalteromonas mytili (1)	KMM 188^{T}	32MA	Mussel, *Crenomytilus graynus*; Sea of Japan, Troitza Bay
Pseudoalteromonas mytili	KMM 280	4GM5	Mussel, *Patinopecten jessoensis,* Sea of Japan, Troitza Bay
Pseudoalteromonas mytili	KMM 327	4GM7	-"-
Pseudoalteromonas aurantia	ATCC 33046^{T}		ATCC
Pseudoalteromonas luteoviolacea	ATCC 33492^{T}		ATCC
Pseudoalteromonas rubra	ATCC 29570^{T}		ATCC
Pseudoalteromonas citrea	ATCC 29719^{T}		ATCC
Pseudoalteromonas atlantica	KMM 655$^{T b}$	IAM 12376^{T}, IAM 12927^{T}, NCIMB 301^{T}, ATCC 19262^{T}	M. Akagawa-Matsushita
Pseudoalteromonas nigrifaciens (3)	KMM 160	2MC41	Mussel (*C. grayanus*), Sea of Japan, Troitza Bay,
Pseudoalteromonas nigrifaciens (2)	KMM 156	2ML26	-"-

Pseudoalteromonas nigrifaciens (1)	KMM 298	4ML18	-"-
Pseudoalteromonas nigrifaciens (A)	KMM 661^{T}[b]	LMG 2227^{T}, NCTC 10691^{T}, ATCC 23327^{T}, KMM 662	LMG
Pseudoalteromonas espejiana	ATCC 29659^{T}		ATCC
Pseudoalteromonas nigrifaciens (I)	KMM 662^{T}[b]	IAM 13010^{T}, ATCC 19375^{T}, NCIMB 8614^{T}, KMM 661	U. Simidu
Pseudoalteromonas undina	IAM 12922^{T}	ATCC 29660^{T}	M. Akagawa-Matsushita
Pseudoalteromonas haloplanktis subsp. *haloplanktis*	KMM 460^{T}	IAM 12915^{T}, ATCC 14393^{T}, NCIMB 2084^{T}, Zobell &Upham 545	U. Simidu
Pseudoalteromonas carrageenovora	KMM 656^{T}	IAM 12662^{T}, ATCC 43555^{T}, NCIMB 302^{T}	M. Akagawa-Matsushita
Pseudoalteromonas haloplanktis subsp. *tetraodonis*	KMM 458^{T}	IAM 14160^{T}	U. Simidu
Alteromonas macleodii	KMM 568^{T}	ATCC 27126^{T}, IAM 12920^{T}, NCIMB 1963^{T}	ATCC
Pseudoalteromonas piscicida	LMG 2251^{T}	ATCC 15057^{T}	LMG

[a] ATCC, American Type Culture Collection, Rockville, MD, USA; IAM, Institute of Molecular and Cellular Biosciences (formerly Institute of Applied Microbiology), University of Tokyo, Bunkyo-ku, Tokyo, Japan; KMM, Collection of Marine Microorganisms, Pacific Institute of Bio-Organic Chemistry, Vladivostok, Russia; LMG, Collection of bacteria of the Laboratory of Microbiology, University of Gent, Gent, Belgium; NCIMB, National Collection of Industrial and Marine Bacteria, NCIMB Ltd., Torry Research Station, Aberdeen, Scotland; NCTC, National Collection of Type Culture, London, England.

[b] T = type strain

312

IAM Culture Collection,

[illegible] 12

Table 2. Phenotypic features of *Pseudoalteromonas mytili* strains isolated from mollusks

Characteristic	KMM 188	KMM 327	KMM 280	KMM157
Polar flagellum	+	+	+	+
Oxidase activity	+	+	+	+
Pigmentation	black	-	-	light orange
Na+ required for growth	+	+	+	+
Requirement for organic growth factors	-	-	-	-
Arginine dihydrolase activity	-	-	-	-
Denitrification	-	-	-	-
Production of:				
Agarase	+	-	-	+
Gelatinase	+	+	+	+
Amylase	+	+	+	+
Lipase	-	-	-	+
Chitinase	-	-	-	-
Alginase	nd	nd	nd	nd
Levan	+	+	+	+
Growth at:				
4°C	+	-	-	-
10°C	+	+	+	+
28°C	+	+	+	+
35°C	-	+	+	-
41°C	-	-	-	-
Utilization of:				
D-Glucose	+	+	+	-
D-Ribose	+	+	+	+
D-Xylose	+	-	-	-
D-Arabinose	-	-	-	-

D-Rhamnose	+	+	+	-
D-Mannose	+	+	+	-
D-Galactose	+	-	-	-
D-Fructose	+	+	+	+
Sucrose	+	-	-	+
Trehalose	+	-	-	+
Maltose	-	-	-	+
Cellobiose	+	+	+	-
Lactose	+	+	+	+
Gluconate	+	+	+	-
Salicin	-	+	-	-
Acetate	+	+	+	-
Propionate	+	+	+	+
Butyrate	+	+	+	+
Valerate	-	-	-	+
Caproate	+	+	+	-
Succinate	+	+	+	-
Fumarate	-	+	+	-
α-Glutarate	-	-	-	-
DL-Lactate	-	+	-	+
Citrate	-	-	+	-
α-Ketoglutarate	-	-	-	-
Pyruvate	-	+	+	+
Aconitate	+	+	+	+
Glycerol	+	-	+	-
Caprylic acid	-	-	-	-
Pelargonic acid	-	-	-	-
Glycogen	+	+	+	
Mannitol	+	+	+	+
D-Sorbitol	+	+	-	+
Inositol	-	-	-	+
Adonitol	+	+	+	-
Ethanol	+	+	+	+
p-Hydroxybenzoate	+	+	+	+
Phenylacetic acid	+	+	+	+
L-α-Alanine	+	-	-	+

L-Threonine	+	-	-	+
Aspartic acid	+	+	+	-
Glutamic acid	+	+	+	+
L-Lysine	-	-	-	+
L-Arginine	+	+	+	+
L-Ornithine	+	-	+	+
L-Histidine	-	-	-	-
L-Proline	+	+	+	-
L-Tyrosine	-	+	+	+
L-Phenylalanine	-	-	-	+
Susceptability to:				
Rifampicin (15μg)	+	+	+	+
Rhistomycin (150μg)	-	-	-	-
Kanamycin (10μg)	-	-	-	-
Ampicillin (10μg)	-	-	-	-
Benzyl-penicillin (10μg)	-	-	-	-
Streptomycin (15μg)	-	-	-	-
Neomycin (15μg)	-	-	-	-
Erythromycin (15μg)	+	+	+	+
Gentamicin (10μg)	+	+	+	+
Oxacillin (20μg)	+	+	+	+
Cephalexin (10μg)	-	-	-	-
Polymyxin (50μg)	+	+	+	-
Lincomycin (10μg)	-	-	-	-
Ofloxacin (10μg)	+	+	+	-

[a] +, positive, -, negative, ND, no data;

See #12

Table 3. DNA relatedness among tested strains

		% hybridization with DNA from:		
~~Strain~~ Organism	G+C content (mol%)	KMM 188	KMM 157	KMM 280
P. mytili KMM 188^T	39.2			67
P. mytili KMM 157	40.0	67		
P. mytili KMM 280	40.0	70		
P. mytili KMM 327	39.8			100
P. haloplanktis subsp. *haloplanktis* IAM 12915^T	40.2		42	10
P. haloplanktis subsp. *tetraodonis* IAM 14160^T	36.1	10		8
P. atlantica ATCC 19262^T	39.2		40	45
P. undina IAM 12922^T	42.2	24	16	
P. carrageenovora IAM 12662^T	39.2	36		
P. nigrifaciens IAM 13010^T	39.2	24		8
A. macleodii ATCC 27126^T	44.4		16	14
P. nigrifaciens KMM 156	39.2	48		42
f *P. nigrifaciens* KMM 298	39.5	33		
P. nigrifaciens KMM 160	39.3			32

316

Table 4. Sec # 12

Enzyme activities of strain KMM 188

Enzyme	pH	Enzyme activity, u/ml
α-Galactosidase	7. 0	10
α-N-Acetylgalactosaminidase	7. 0	no
β-N-Acetylhexosaminidase	7. 0	1. 5
β-Galactosidase	7. 0	0. 75
Laminarinase	5. 15	2. 00
Pustulanase	5. 15	0. 40
Cellulase	5. 15	1. 0
Dextranase	5. 15	0. 40
Amylase	5. 15	0. 40
Agarase	7. 0	0. 5
Chitinase	7. 0	no

See #12, #14

[illegible]

Table 5. Differential characteristics of *Pseudoalteromonas species*

	P. mytili KMM 188	*P. haloplanktis* subsp. *haloplanktis* IAM 12915T^{a}	*P. haloplanktis* subsp *tetraodonis* IAM 14160 T^{a}	*P. atlantica* IAM 12975T^{a}	*P. carrageenovora* IAM 12662T^{a}	*P. espejiana* IAM 12640T^{a}	*P. undina* IAM 12922T^{a}	*P. rubra* ATCC 29580 T^{b}	*P. luteoviolacea* ATCC 33492 T^{b}	*P. citrea* ATCC 29719T^{b}	*P. aurantia* ATCC 33046 T^{b}	*P. piscicida* ATCC 15251 T^{c}	*P. denitrificans* ATTC 43337 T^{d}	*P. nigrifaciens* ATCC 19375 T^{e}
Melanin-like dark pigment	d	+	-	-	+	-	-	-	-	-	-	-	-	d[f]
Denitrification with gas formation	-	-	-	-	-	-	-	-	-	-	-	-	+	-
Production of:														
Amylase	+	-	-	+	-	+	+	+	+	+	+	+	+	+
Chitinase	-	-	-	-	-	-	+	-	-	d	-		+	-
Agarase	d	-	-	+	-	-	-	-	-	-	-	-	-	-
Growth at:														
4°C	d	-	-	-	+	-	+	-	d	-	+		+	d
35°C	d	+	+	+	+	+	+	+	+	d	-	+	-	d

Utilization of:														
D-Mannose	+	-	-	+	-	-	-	+	-	+	+	+		+
D-Fructose	+	+	-	+	+	+	-	-	-	+	+	+		+
Sucrose	d	-	+	+	+	+	+	-	-	-	-	+	-	+
Maltose	(-)	+	+			+	+	-	+	-	d		+	+
Cellobiose	+	-	-	+	+	d	-	-	-	-	-			d
Lactose	+	-	+	+	+	+	-	-	-	-	-		-	d
D-Gluconate	+	-	+			-	-	-	-	-	-		-	d
Pyruvate	d	+	+	+	-	+	-	-	-				+	+
Fumarate	d	+	+	+	+	+	-	-	-	-	-		-	-
Glycerol	d	-	-	+	+	+	-	-	-	-	-	-		d
Rhamnose	d	-	-	-	-	-	-					-		d
Citrate	d	+	-	+	+	+	-	-	-	-	-	+		-

[a] Data from reference 1.
[b] Data from reference 5.
[c] Data from reference 12.
[d] Data from reference 10.
[e] Data from reference 13.
[f] d, 11-89% of strains are positive; +, positive; -, negative.

See #15

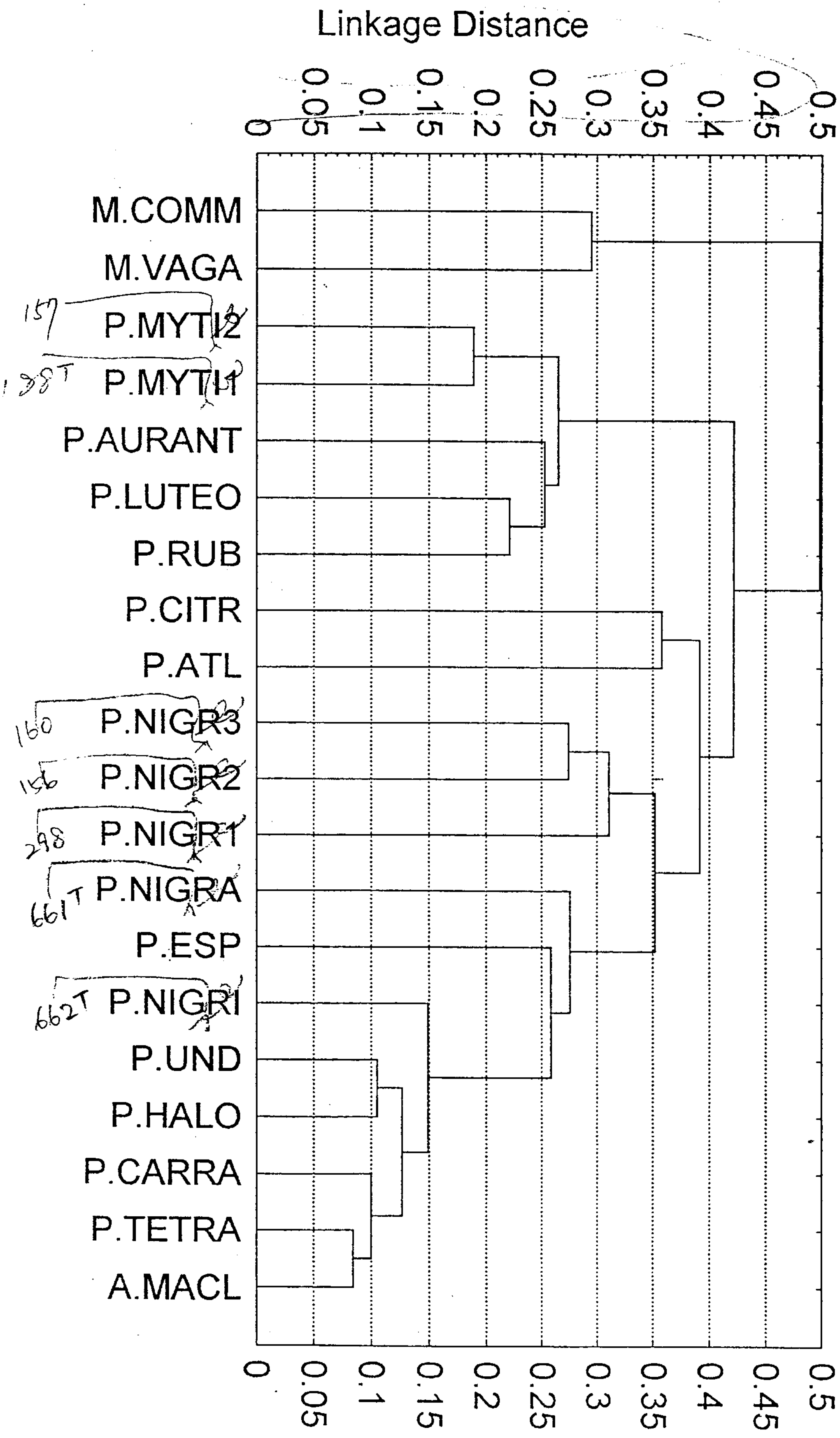

Dissimilarities

Subscription for figures

Figure 1. Electron micrograph of *Pseudoalteromonas mytili* KMM 188. x12000.

Figure 2. Dendrogram showing the clustering of *Pseudoalteromonas spp.* and some related bacteria based on unweighted pair-group average ~~percent disagreement~~ from the BIOLOG assay. All strains are in the same sequences as in Table 1.

linkage cluster analysis.

20.

ANTIMICROBIAL PEPTIDES SYNTHESIZED BY MARINE BACTERIA FROM THE PACIFIC OCEAN

E. P. Ivanova[1,2], N. Yumoto[2], M. G. Petukhov[1,2], T. Taguchi[2],
S. Yoshikawa[2*]

[1]Pacific Institute of Bioorganic Chemistry, Far Eastern Branch of the Russian Academy of Sciences, 690022, Vladivostok, pr.100 let Vladivostoku, 159, Russia.

[2]Osaka National Research Institute, AIST, Midorigaoka 1-8-31, Ikeda, Osaka 563, Japan.

* To whom correspondence should be addressed: Department of Organic Materials, Osaka National Research Institute, AIST, Ikeda, Osaka 563, Japan. Fax: +81-727-51-9628, e-mail: susumu@onri.go.jp

Key words: Marine bacteria; antimicrobial peptides

ABSTRACT.

The ability of free-living and animal-associated marine bacteria to produce antimicrobial peptides was studied in 491 strains isolated from north and south parts of the Pacific Ocean. A total of 26% of strains examined produced antimicrobial compounds, which included peptides. The number and the complexity of the antimicrobial compounds might be a reflection of their diverse functions. Strains of *Bacillus spp.*, *Vibrio spp.* and species in the *Pseudoalteromonas-Pseudomonas* group had the highest proportions of active strains (37.5%, 40%, and 22%, respectively). Species associated with marine invertebrates were more active (from 20% to 40% of all strains) then free-living bacteria.

Twelve strains producing antimicrobial peptides were selected for future analysis. Among them, only one strain, strain of *Bacillus sp.*, was isolated from seawater. The others, strains of *Pseudoalteromonas spp.* and *Bacillus spp.*, were associated with crabs, mussels (*Crenomytilus grayanus* and *Patinopecten jessoensis)*, and sponges (*Haliclona sp.*, *Chonelasma sp*, *Phylospongidae*, and several unidentified species). The antimicrobial spectra of these peptides were similar to those of dermaseptins and plant peptides. Peptides from marine bacteria inhibited the growth of *Candida albicans*, *Staphylococcus epidermidis*, and *Enterococcus faecalis*.

INTRODUCTION

Numerous microorganisms that live in seawater, on benthic substrates and in association with an array of marine animals and algae have been isolated from aquatic environments. In the complex marine communities, the interactions between predator and prey and between different organisms are of a great importance. Recent studies suggest that many of such organisms that have few or no morphological means of defenses defend themselfs by producing chemicals that are toxic to others (Sammarco and Coll 1988; Davis at al. 1989, McClintock and Janssen, 1990, Paul, 1994). One group of such defensive secondary metabolites consists of antimicrobial peptides.

Moreover much evidences exists to support the hypothesis that certain antibacterial peptides play a dual role, being active both in defense and in the development of the organisms (Natori, 1990). Although antimicrobial peptides were usually been isolated by of antibiotic assays, it should be pointed out that many of them have also been reported to exhibit other biological activities, such as the promotion of wound healing (Jacob and Berkowitz, 1991), inhibition of adrenocorticotropic hormone (Zue et al., 1988), inhibition of protein kinase C (Nabayubashi et al., 1990), and stimulation of monocyte chemotaxis (Territo et al., 1989). Antimicrobial peptides isolated mainly from animals, have been separated on a chemical and biochemical basis into five families (Boman, 1994). Particular attention has been paid to study of bioactive peptides from sponges. Most of them have a unique cyclic lipolytic structure and include unusual amino acids, such as α-keto aminoacids, vinylogous amino acids that might be associated with symbiotic microorganisms, in particular with cyanobacteria (Fusetani, and Matsunaga, 1993).

Unlike peptides from animals, several antimicrobial peptides that are produced by soil bacteria have been reported to have complicated ring systems (for example, nisin and subtilin; Sahl, 1994). The only peptide-related compounds from marine bacteria reported to date are halobacillin, a cytotoxic acylpeptide similar to surfactin but without antifungal or antibiotic activity (Trischman et al, 1994), antiviral macrolactins (Gustafson et al, 1989), and bisucaberin (Takahashi et al., 1987). Surprisingly little is known about linear antimicrobial peptides from marine bacteria (Jensen, and Fenical, 1994).

Since antimicrobial peptides are known as defensive secondary metabolites that have been found in different organisms, we initiated a research program to examine free-living bacteria and bacteria associated with marine sponges, ascidians, algae, and mollusks for the production of antimicrobial peptides. The bacteria were isolated from different areas of the Pacific Ocean. Their production of antimicrobial peptides was analyzed and we determined the spectrum of activity of some of them, as well as the conditions required for their biosynthesis during bacterial growth.

MATERIALS AND METHODS

The strains studied and screening for production of antibiotics

The microorganisms studied were taken from the Collection of Marine Microorganisms (KMM) of the Pacific Institute of Bioorganic Chemistry of the Far Eastern Branch of the Russian Academy of Sciences (PIBOC RAS), Vladivostok, Russia.

Antibacterial activities were tested against *Staphylococcus aureus* IFO 14462, *Staphylococcus epidermidis* IFO 12993, *Escherichia coli* IFO 15034, *Proteus vulgaris* IFO 3851, *Proteus mirabilis* IFO 13300, *Enterobacter cloacae* IFO 13535, *Enterococcus faecalis* IFO 3989, *Candida albicans, Bacillus subtilis, Aeromonas hydrophila* subsp. *anaerogenes* IFO 13282, and *Vibrio anguillarum* IFO 13266. Test strains were obtained from the Culture Collection of the Institute for Fermentation, Osaka, Japan.

Bacteria were inoculated in the center of plates and were grown on medium I which contained (w/v): 0.2% Bacto-peptone (Difco), 0.2% casein hydrolysate (Merck), 0.2% yeast extract (Difco), 0.1% glucose, 0.02% KH_2PO_4, 0.005% $MgSO_4$ $7H_2O$, 1.5% Bacto-agar (Difco), 0.1% $CaCl_2$, 0.01% Kbr. The medium was prepared in a mixture of 75% (v/v) natural seawater and 25% distilled water. The pH was adjusted to 7.8 with 10 M NaOH. All plates were incubated for 7 days at 28°C. The test strains were swabbed perpendicularly to the producer strains. Antibacterial effects were apparent as the absence of growth in the region where the test strain coincided with the producer strain by an inhibition zone in the confluence area.

Bioassay of antibacterial activity after treatment with trypsin

The strains that showed apparent antibacterial activity on plates were selected and cultured in tubes that contained 10 ml of liquid medium I of the same composition as describe above for 7 days on a rotary shaker operated at 120 rpm. After incubation, cells were removed by centrifugation at 8000 rpm for 25 min.

The effect of trypsin was evaluated by adding 10 mg trypsin gel (Sigma, St. Louis, MD, USA) to 1 ml of each culture supernatant. After a 1-h incubation at 30°C on a rotary shaker, the enzyme was removed by centrifugation at 15000 rpm for 5 min. Antibacterial activity was assayed by the agar diffusion methods (Gauthier, and Flatau, 1976). Cultures (0.1 ml) of test strains were spread on tryptic soy agar (TSA; Difco) plates in which circular wells (diameter, 10 mm) had been cut. Samples (0.1 ml) were added to the wells and zones of inhibition were measured after incubation for 48 h at 28°C. Supernatants without trypsin treatment were used as appropriate controls.

Preliminary estimations of molecular masses

The bacteria were grown in 500-ml flasks with 100 ml of liquid medium for 2 days on rotary shaker (170 rpm) at 28°C. The first medium was medium I, mentioned above and the second one was medium II, which contained (w/v): 0.2% Bacto-peptone, 0.2% casaminoacids (Merck), 0.1% yeast extract, 0.1% soluble starch, 0.1% $CaCl_2$, and 0.1% NH_4Cl. The medium was prepared in a mixture of 75% (v/v) of natural seawater and 25% (v/v) distilled water. The pH was adjusted to 7.8 with 10 M NaOH. After the incubation the cells were pelleted by centrifugation at 8000 rpm for 25 min.

Preliminary estimations of molecular masses were made by ultrafiltration through low-adsorption, hydrophilic, YM membranes, Centricon-3 and Centricon-10 (Amicon, USA) in accordance with instructions. The antibacterial activity of compounds of less than 3 kDa and 10 kDa substances that had passed through membranes was examined again with an appropriate controls.

The effect of variations in growth conditions on the production of antibacterial compounds

The influence of the duration of cultivation on antibacterial activity was determined in liquid medium after 2, 3, 5, and 6 days of culture in liquid medium by the agar diffusion method. All experiments were repeated twice to ensure reproducibility.

RESULTS

The spectrum of antimicrobial activity

The ability of the various bacteria to produce antimicrobial substances was tested against *Staphylococcus aureus, Staphylococcus epidermidis, Escherichia coli, Proteus vulgaris, Proteus mirabilis, Enterobacter cloacae, Enterococcus faecalis, Candida albicans, Bacillus subtilis, Aeromonas hydrophila* subsp. *anaerogenes* and *Vibrio anguillarum*. The spectra of the antibacterial activities of the studied strains are presented in Figure 1. In all, 126 strains (about 26%) of 491 tested strains inhibited the growth of test strains. No strain inhibited the growth of *Enterobacter cloacae,* and *Escherichia coli* grew weakly in the presence of antibiotics from several strains. Antimicrobial substances produced by marine bacteria were especially active against *Staphylococcus epidermidis, Proteus vulgaris, Enterococcus faecalis* and *Candida albicans.* We note also that 135 strains showed weak antifungal activity (data not shown in Fig. 1).

Prevalence of producers of antimicrobial substances among the strains studied

The bacteria under investigation had different abilities to produce antimicrobial substances (Fig. 2). Strains of *Bacillus spp.* and *Vibrio spp.* yielded the highest proportions of active strains (37.5-40%) and about 22% of the species in the *Pseudoalteromonas-Pseudomonas* group produced antimicrobial substances. It is of interest, that the majority of strains studied were associated with marine invertebrates (Fig. 3), and these species are appeared to be more active (from 20% to 40% of all strains) then free-living bacteria. The representatives of the genus *Bacillus* seem to provide an exception since about half of the bacilli from seawater produced antibacterial substances. Figure 4 shows the significant difference between bacteria from the northern (Japan and Okhotsk seas) and southern (Coral sea, Cook Islands) parts of the Pacific Ocean in terms of production of antimicrobial compounds. Unfortunately, the small number of representatives of *Vibrio, Deleya* and *Flavobacterium* from southern part of the Pacific prevents us from drawing any conclusions at the level of the genera. Nevertheless, among bacilli and the *Pseudoalteromonas-Pseudomonas* group from the southern Pacific, the number of active strains was found to be greater than that from the Japan and Okhotsk seas.

Search for bacteria that produce antimicrobial peptides

After a preliminary screenings we selected 70 strains that had the highest antimicrobial activities. These bacteria were grown in liquid nutrient medium, the culture supernatant was treated with trypsin to confirm the proteinaceous nature of the active materials, and supernatants were subjected to ultrafiltration through Centricon-3 and Centricon-10 membranes. Antimicrobial activity was examined after each step. Twelve strains, isolated from different sources (see Table 1), whose activity disappeared after treatment with trypsin, were then subjected to more detailed analysis to determine the conditions for the expression of antimicrobial activity. Tables 2 and 3 summarize the antimicrobial activity after cultivation on plates or in flasks, after trypsin treatment and after ultrafiltration. Inhibition of the growth of *E. coli* and *P. vulgaris* was noted to be more effective after cultivation in flasks whereas inhibition of the growth of *Enterococcus faecalis* was less effective. The results give evidence that marine bacteria produce a wide range of antibiotics of different chemical composition; the same strain may simultaneously synthesize few antibacterial substances of proteinaceous and non protein nature. For example, the antibiotics produced by strains 114 and 115 (Table 3), and inhibiting the growth of *P. vulgaris* were not inactivated by trypsin and hence didn`t belong to peptides. On the other hand these strains produced the trypsin-sensitive compounds, evidently low molecular peptides, inhibiting growth of *C. albicans* and *S.* epidermidis.

The level of antimicrobial activity in liquid culture was time-dependent and the activity varied among different strains. For example, some strains in Table 2 inhibited the growth of test cultures after a 24-h incubation, other strains were active after 48-74 h.

To evaluate the effect of composition of the culture medium on production of antimicrobial peptides, we cultivated selected strains on the medium II (Table 4). The results showed that medium I was more favourable then medium I for the antibiotics synthesis. These facts suggest also that the strains studied produced different antimicrobial substances dependending on the composition of the medium.

DISCUSSION

The production of antimicrobial compounds by marine bacteria has been investigated for several decades, although most of the structures of such compounds remain unknown (Austin, 1989), and the ecological and physiological significance of bacterial antibiotics is a subject of some discussion (Lemos et al, 1991). It is likely that antibiotic compounds provide producers with a competitive advantage as compared to non-producers. Such compounds can prevent the growth of susceptible bacteria and, consequently, serve as a chemical defense system both for antibiotic-producing strains and associated marine organisms. One group of antimicrobial compounds consists of peptides. To evaluate the production of antimicrobial peptides by marine bacteria, we grew various strains on a seawater based medium, which contained KBr. Our experiments showed that common medium II used for isolation and maintaince of strains failed to induce the production by bacteria of antimicrobial substances. We found that 26% of all studied strains grown on media I had extremely high levels of activity, and about 27% of them had antifungal activity. The anti-yeast activity of marine species of heterotrophic bacteria has previously been reported, but the nature of the active substances has not been elucidated (Bucket et al., 1963), with the exception of that of an intracellular antifungal antibiotic from purple photosynthetic bacteria (Burgess et al., 1991). Among the bacteria studied here, producers of antimicrobial substances were dominant in the *Pseudoalteromonas-Pseudomonas* group and bacilli, which were mainly associated with marine animals and were isolated from the southern Pacific. Twelve strains producing antimicrobial peptides were selected for future study. Among them, only one strain of *Bacillus sp.* had been isolated from seawater. The other strains of *Pseudoalteromonas spp.* and *Bacillus spp.* had been associated with crabs, mussels (*Crenomytilus grayanus* and *Patinopecten jessoensis*), and sponges (*Haliclona sp., Chonelasma sp., Phylospongidae,* and several unidentified species).

The data presented here show that the marine bacteria have wide spectra of antimicrobial activities. Moreover, their activities also varied with the duration of cultivation and media composition. These observations suggest that bacteria produce several active substances at different times. We assume that the diversity of antimicrobial compounds might be a reflection of their diverse functions in, for example, defense, symbiosis, and control of marine bacterial populations.

The antibiotics passed through a Centricon-3 membrane are assumed to belong to antimicrobial peptides. These bacterial peptides inhibited the growth of *Candida albicans, S. epidermidis,* and *Enterococcus faecalis*. Similar spectra of antimicrobial activities have been reported for peptides from plants seeds (Cammue et al., 1994) and for dermaseptins (Mor et al, 1994). These peptides have antifungal activity and are also active against *Enterococcus faecalis, Cryptococcus neoformans, and Aeromonas cavie*, the causative agent of red-leg disease in amphibians. Dermaseptin peptides, such as the bombinins, magainins, and dermaseptins, isolated from the skin and gastrointestinal system of amphibians; and the cecropins from insects were reported to have a linear, cationic (lysine-rich), helical amphipathic structure. The mode of action of these peptides suggests their direct interactions with the lipid groups of the membranes that lead to changes in membrane functions. Future studies of antimicrobial peptides produced by marine bacteria will determine their chemical structure and biological activity, as well as estimate their relatedness to such peptides from plants and animals.

This study was supported by a Fellowship grant from the Foreign Researcher Invitation Program of the Agency of Industrial Science and Technology, Japan.

REFERENCES

Austin B (1989) Novel pharmaceutical compounds from marine bacteria. J Appl Bacteriol 67:461-470

Boman HG (1994) Chairman's opening remarks In: HG Boman, Marsh J, Goode JA (eds) Antimicrobial Peptides. John Wiley & Sons, Chichester, pp. 1-4

Buck JD, Ahearn DG, Roth JFG, Meyers SP (1963) Inhibition of the yeasts by a marine bacterium. J Bacteriol 85;1132-1135

Burgess JG, Miyashita H, Sudo H, Matsunaga T (1991) Antibiotic production by the marine photosynthetic bacterium *Chromatium purpuratum* NKPB 031704: localization of activity to the chromatophores. FEMS Microbiol Lett 84:301-306

Cammue BPA, De Bolle MFC, Schoofs HME, Terras FRG, Thevissen K, Osborn RW, Rees SB, Broekaert WF (1994) Gene-encoded antimicrobial peptides from plants In: HG Boman, Marsh J, Goode JA (eds) Antimicrobial Peptides. John Wiley & Sons, Chichester, pp. 91-101

Davis AR, Tarett NM, McConnel OJ, Young CM (1989) Epibiosis of marine algae and benthic invertebrates: natural products chemistry and other mechanisms inhibiting settlement and overgrowth. In: PJ Scheuer (ed) Bioorganic Marine Chemistry, vol. 3 Springer-Verlag, Berlin, pp. 85-113

Fusetani N, Matsunaga S (1993) Bioactive sponge peptides Chem. Rev. 93:1793-1806

Gauthier MJ, Flatau GN (1976) Antibacterial activity of marine violet-pigmented *Alteromonas* with special reference to the production of brominated compounds. Can J Microbiol 22:1612-1619

Gustafson K, Roman M, Fenical W (1989) The macrolactins, a novel class of antiviral and cytotoxic macrolides from a deep-sea marine bacterium. J Am Chem Soc 111:7519-7524

Jacob LS, Berkowitz B (1991) Wound treatment employing biologically active peptides (US Patent 5,045,531.). US Patent & Trademarks Office, Washington DC 20231

Jacob L, Zasloff M (1994) Potential therapeutic applications of magainins and other antimicrobial agents of animal origin In: HG Boman, Marsh J, Goode JA (eds) Antimicrobial Peptides. John Wiley & Sons, Chichester, pp. 197-223

Jensen, PR, Fenical W (1994) Strategies for the discovery of secondary metabolites from marine bacteria: ecological perspectives. Annu Rev Microbiol 48:559-584

Lemos ML, Dopazo CP, Toranzo AE, Barja JL (1991) Competitive dominance of antibiotic-producing marine bacteria in mixed cultures. J Appl Bacteriol 71:228-232

McClintock JB, Janssen J (1990) Pteropod abduction as chemical defence in a pelagic Antarctic amphipod. Nature 346:462-464

Mor A, Hani K, Nicolas R (1994) The vertebrate peptide antibiotics dermaseptins have overlapping structural features but target specific microorganisms. J Biol Chem 269:31635-31641

Nabayubashi H, Brown JH, Morell JL, Chen HC, Hunang KP (1990) Phosphorylation of magainin 2 by protein kinase C and inhibition of protein kinase C isozymes by a synthetic analogue of magainin 2 amide. FEBS Lett 267:135-138

Natori S (1990) Dual functions of insect immunity proteins in defense and development. Res Immunol 141:938-939

Paul VJ (1994) Chemical defenses of benthic marine invertebrates. In VJ Paul (ed) Ecological Roles of Marine Natural products Cornell University Press, Ithaca and London, pp. 164-188

Sahl H-G (1994) Gene-encoded antibiotics made in bacteria In: HG Boman, Marsh J, Goode JA (eds) Antimicrobial Peptides. John Wiley & Sons, Chichester, pp. 27-42

Sammarco PW, Coll JC (1988) The chemical ecology of alcyonarian corals In PJ Scheur (ed) Bioorganic Marine Chemistry, vol. 2. Springer-Verlag, Berlin, pp. 89-116

Takahashi A, Nakamura H, Kameyama T, Kurasawa S, Naganawa H, Okami Y, Takeuchi T, Umezawa H (1987) Bisukaberin, a new siderophore, sensitizing tumor cells to macropahge-mediated cytolysis. J Antibiotics XL No12:1671-1676

Territo MC, Ganz T, Srlsted ME, Lehrer R (1989) Monocyte-chematactic activity of defensins from human neutrophils. J Clin Invest 84:2017-2020

Trischman J, Jensen P, Fenical W (1994) Halobacillin: a cytotoxic cyclic acylpeptide of the iturin class produced by marine *Bacillus*. Tetrahedron Lett 35:5571-5574

Zue Q, Hu J, Mulay S et al (1988) Isolation and structure of corticostatin peptides from rabbit fetal and adult lung. Proc Natl Acad Sci USA 85:592-596

Table 1. Sources of marine strains with highest antimicrobial acivities

Designation	Taxon	Strain number	Origin	Source	Date of isolation
114	*Pseudoalteromonas sp.*	4ML13	Japan Sea, Troitza Bay	Mussel (*Crenomytilus grayanus)*	Jul, 1990
115	*Marinomonas sp.*	4GM8	Japan Sea, Troitza Bay	Mussel (*Patinopecten jessoensis)*	Jul, 1990
165	*Pseudoalteromonas sp..*	7-77-7/1	Pacific Ocean, Okhotsk Sea	Crab (*Paralithodes camtschatica)*	Jun, 1988
166	*Pseudoalteromonas sp.*	7-77-2	Pacific Ocean, Okhotsk Sea	Crab (*Paralithodes camtschatica)*	Jun, 1988
132	*Pseudoalteromonas sp.*	7-145-19	Pacific Ocean, Coral Sea	Sponge (unident. sp.)	Jul-Nov, 1988
149	*Bacillus sp.*	7-193-11	Pacific Ocean, Coral Sea	Phylospongidae	Jul-Nov, 1988
174	*Pseudoalteromonas sp..*	7-s23-22/1	Pacific Ocean, Okhotsk Sea	Sponge (*Chonelasma sp.)*	Jun, 1988
179	*Pseudoalteromonas sp..*	7-s16-4	Pacific Ocean, Okhotsk Sea	Sponge (*Haliclona p.)*	Jun, 1988
301	*Bacillus sp.*	7-144-4/1	Pacific Ocean, Coral Sea	Sponge (unident. sp.)	Jul-Nov, 1988
307	*Bacillus sp.*	7-165-15	Pacific Ocean, Coral Sea	Sponge (unident. sp.)	Jul-Nov, 1988
361	*Bacillus sp.*	7MB129	Pacific Ocean, Coral Sea	Sea water	Jul-Nov, 1988
458	*Bacillus sp.*	7-248-3	Pacific Ocean , New Zealand	Sponge (unident. sp.)	Jul-Nov, 1988

Table 2. Production of antimicrobial compounds by various marine bacteria.

Antibiotic-producing strain\Test strains	Duration of incubation	Producer strain					
		114	115	149	301	307	458
Staphylococcus aureus	24 h[1]	-[2]	15	18[3]	15	11	-
	48 h	18	20	17	15	13	13
	72 h	25	20	11	11	11	11
	Plates[4]	+[5]	+	20	10	20	+
Staphylococcus epidermidis	24 h	15	25	15	15	15	11
	48 h	25	30	17	15	13	13
	72 h	25	20	11	15-20	11	15-20
	Plates	+	+	10	25	+	+
Aeromonas hydrophila	24 h	-	25	15	18	11	11
	48 h	20	15	17	20	15	-
	72 h	15	11	20	20	18	18
	Plates	+	+	-	+	-	-
Vibrio anquillarum	24 h	17	30	13	25	14	w
	48 h	30	18	11	11	20	11
	72 h	-	-	-	-	-	-
	Plates	+	+	-	-	-	-
Proteus vulgaris	24 h	15	20	11	18	11	11
	48 h	20	30	-	13	13	13
	72 h	-	11	-	-	-	-
	Plates	+	+	-	-	-	-
Proteus mirabilis	24 h	-	-	-	-	-	-

	48 h	-	-	-	-	-	-
	72 h	-	-	-	-	-	-
	Plates	+	-	-	-	-	-
Escherichia coli	24 h	-	11	15	-	-	-
	48 h	17	18	17	-	w	w
	72 h	17	15	-	-	-	-
	Plates	15	-	-	-	-	-
Enterococcus faecalis	24 h	-	-	-	-	-	-
	48 h	-	-	-	-	-	-
	72 h	-	-	-	-	-	-
	Plates	15	10	10	-	-	-
Candida albicans	24 h	21	36	-	-	-	-
	48 h	18	28	11	13	13	13
	72 h	25	20	-	-	-	-
	Plates	+	+	15	10	10	15
Bacillus subtilis	24 h	11	11	11	18	15	11
	48 h	20	18	-	-	-	-
	72 h	-	-	-	-	-	-
	Plates	-	-	25	-	-	30

[1], Antimicrobial activity of the culture fluid tested by agar diffusion assay; [2], no inhibition; [3], diameter of inhibition zone; [4], cultivation on plates of 7 days; [5], total inhibition of growth of the test strain.

Table 3. Differences in antimicrobial activity[1] of marine bacteria culture fluid before and after treatment with trypsin

	Diameter of inhibition zone caused by:											
	non-filtrated culture fluid						culture fluid filtrated through Centricon-3					
Test strains	114/T[2]	115/T	149/T	301/T	307/T	458/T	114/T	115/T	149/T	301/T	307/T	458/T
C. albicans	18/-	28/11	-/-	13/-	13/11	13/-	35/-	40/11	20/-	15/-	13/-	15/-
P. vulgaris	20/20	30/30	-/-	13/11	13/11	13/11	18/20	30/30	-/-	-/-	-/-	18/-
S. epidermidis	25/13	30/15	17/11	15/11	11/-	11/-	25/15	30/15	15/11	13/11	-/-	15/-

[1], 48-h incubation, agar diffusion assay; [2], antimicrobial activity after trypsin treatment

Table 4. Antimicrobial activitiesof marine bacteria cultural gluids obtained after cultivation in medium II

	Diameter of inhibition zone											
Test strains	114/T[2]	115/T	149/T	301/T	307/T	458/T	166/T	167/T	179/T	361/T	174/T	458/T
C. albicans	11/-	-/-	-/-	-/-	11/-	11/-	18/-	20/11	20/-	15/-	20/-	15/-
P. vulgaris	-/-	-/-	-/-	-/-	-/-	-/-	15/-	22/-	20/-	-/-	25/-	18/-
S. epidermidis	18/-	20/-	13/11	11/-	11/-	11/-	25/-	18/	15/-	15/-	15/-	15/-
V. anguillarum	15/-	20/-	15/-	15/-	15/-	13/11	15/15	13/-	13/-	13/-	15/-	-

[1], 48-h incubation, agar diffusion assay; [2], antimicrobial activity after trypsin treatment

Figures legends

Fig. 1. Antibacterial activities of studied strains.

Fig. 2. Microorganisms capable of production of the antibacterial compounds.

Fig. 3. Producers of antimicrobial compounds isolated from seawater and marine animals. Left columns, free-living bacteria; right columns, bacteria associated with marine invertebrates. Dark portions of columns represent numbers of active strains.

Fig. 4. Producers of antimicrobial compounds from the north and south parts of the Pacific Ocean. Light columns, total number of strains studied, dark columns, number of active strains.

21.

FACTORS AFFECTING THE INCREASE OF ANTIMICROBIAL SUBSTANCES PRODUCING BY MARINE BACTERIA

INFLUENCES ON THE ANTIMICROBIAL ACTIVITY OF CULTIVATION AND ADSORBTION CONDITIONS FOR MARINE BACTERIA

E. P. Ivanova[1,2*], D. V. Nicolau[2], N. Yumoto[2] T. Taguchi[2],
K. Okamoto[2], S. Yoshikawa[2]

[1] Pacific Institute of Bioorganic Chemistry, Far Eastern Branch of the Russian Academy of Sciences, 690022, Vladivostok, pr.100 let Vladivostoku, 159, Russia.

[2] Osaka National Research Institute, AIST, Ikeda, Osaka 563, Japan

ABSTRACT. The ability of free-living and animal-associated marine bacteria to produce antimicrobial substances has been studied among 491 strains isolated from northern and southern parts of the Pacific Ocean. A total of 26% (126 out of 491) of the strains examined produced antimicrobial compounds against 11 Test Bacterial Strains (TBS) including fish pathogens, *Aeromonas hydrophila* and *Vibrio anquillarum*. Production of antimicrobial compounds against certain TBS varied within 24-72 hours assuming the presence of several antimicrobial substances both proteinaceous and non-protein nature. The level of antimicrobial activities was increased on culture medium based on natural sea water with Br-ions, and after attachment on diazonaphto-quinone/novolak (DNQ/N) polymeric surfaces. Surfaces with different hydrophobicities estimated by water contact angle measurements were prepared by means of photo- and thermoinduced chemical functionalisation. The production of antimicrobial substances was highly dependent upon type of the polymeric surfaces. The highest antimicrobial activity occurred on standard exposed photo resists (hydrophilic polymeric films) and hydrophilic developed glass surfaces, whereas the number of attached cells was greater on unexposed resist characterized as hydrophobic ones. The results suggest, that the chemical functionalization of the polymeric surfaces rather than hydrophobicity is a major factor affecting the release of antimicrobial compounds of proteinaceous nature.

INTRODUCTION

Numerous microorganisms that are inhabitants of seawater, benthic substrates, and marine macrohydrocoles have been isolated for screening of novel biologically active compounds, many of those become the basis for industrial biotechnological processes. Recent investigations proved that only 'the tip of the iceberg' have been explored

(Vandamme 1994). Diverse antimicrobial compounds encompassing a wide range of chemical structures have been described (Austin 1989, Faulkner 1993, Fenical 1993). In some cases, attempts to isolate and characterize these substances were never made (Jensen and Fenical 1994).

The production of antimicrobial metabolites is a complicated process which depends on various factors. For marine communities, the interactions between different organisms that have a few or no morphological means of defending themselves could cause the production of chemicals that are toxic to others (Sammarco and Coll 1988, Davis et al. 1989, McClintock and Janssen 1990, Paul 1994, Jensen et al. 1996). Moreover, much evidence exists to support the hypothesis that certain antibacterial compounds play a dual role, being active both in defense and in the development of the organisms (Natori 1980). Another significant aspect is a symbiothrophic relationship between macrohydrocoles and microorganisms, when bacteria might produce metabolites ascribed their host-organisms. There are several convincing examples reviewed recently (Jensen and Fenical 1994), although some of the investigations have not yet met with success mostly because of methodological difficulties.

Often marine bacteria are capable for attachment to any sort of objects, sometimes by means of extracellular polymers or specialized structures (Costerton et al 1978) and acquire some advantages as compared to their free-living counterparts (ZoBell 1943, Harvey and Young 1980). Bacterial attachment has received a significant attention, nevertheless due to both bacteria and substratum surfaces heterogeneity, the physicochemistry of bacterial attachment is so far not fully evaluated (Fletcher 1993). On the other hand to best of our knowledge there are no data in literature regarding antimicrobial activity of adsorbed bacterial cells. In this context the aim of the present study was to search the antimicrobial substances producers among free-living bacteria and bacteria associated with marine sponges, ascidians, algae, and mollusks collected from different areas of the Pacific Ocean with attempt to clarify what are some of the main factors affecting the biothynsesis of antimicrobial metabolites. We have determined the spectrum of antibacterial activity, the favorable conditions required for biosynthesis of antimicrobial compounds during bacterial growth, and changes in production of antimicrobial compounds after attachment on photoresist polymeric surfaces.

MATERIALS AND METHODS

The strains studied and screening assay for production of antibiotics

The microorganisms studied were taken from the Collection of Marine Microorganisms (KMM) of the Pacific Institute of Bioorganic Chemistry of the Far Eastern Branch of the Russian Academy of Sciences (PIBOC RAS), Vladivostok, Russia. Several selected producers that showed the highest antimicrobial activity are listed in Table 1.

Antibacterial activities were tested against TBS, namely *Staphylococcus aureus* (IFO 14462), *Staphylococcus epidermidis* (IFO 12993), *Escherichia coli* (IFO 15034), *Proteus vulgaris* (IFO 3851), *Proteus mirabilis* (IFO 13300), *Enterobacter cloacae* (IFO 13535), *Enterococcus faecalis* (IFO 3989), *Candida albicans* (, *Bacillus subtilis*(, *Aeromonas hydrophila* subsp. *anaerogenes* (IFO 13282), and *Vibrio anguillarum* (IFO 13266). TBS were obtained from the Culture Collection of the Institute for Fermentation, Osaka, Japan.

For primary screening bacteria were inoculated in the center of plates and were grown on medium which contained (w/v): 0.2% Bacto-peptone, 0.2% casein hydrolysate, 0.2% yeast extract, 0.1% glucose, 0.02% KH_2PO_4, 0.005% $MgSO_4$ $7H_2O$, 1.5% Bacto-agar, 0.1% $CaCl_2$, 0.01% KBr. The medium was prepared in a mixture of 75% (v/v) natural seawater and 25% distilled water. The pH was adjusted to 7.8 with 10

M NaOH. All plates were incubated for 5-7 days at 28°C. The test strains were swabbed perpendicularly to the producer strains. Antibacterial effects were proved by the absence of growth in the region where the test strains were inoculated.

Bioassay of antibacterial activity after treatment with trypsin

The strains that showed apparent antibacterial activity on plates, were selected and cultured in tubes that contained 10 ml of liquid medium as described above for 3 days on a rotary shaker operated at 120 rpm. After incubation, cells were removed by centrifugation at 8000xg for 25 min.

The effect of trypsin was evaluated by adding 10 mg trypsin gel (Sigma, St. Louis, MD, USA) to 1 ml of each culture supernatant. After a 1-h incubation at 30°C on a rotary shaker, the enzyme was removed by centrifugation at 15000xg for 5 min. Antibacterial activity was assayed by the agar diffusion assay based on method described Barry (1980) slightly modified. Cultures (0.1 ml) of test strains were spread on tryptic soy agar (TSA) plates in which circular wells (diameter, 10 mm) had been cut. Samples (0.1 ml) were added to the wells and areas of inhibited bacterial growth were measured after incubation for 48 h at 28°C. The zones of inhibited growth of the indicator strains surrounding the wells were observed. Mean diameters were measured, and 10 mm subtracted (representing the diameter of the well). Supernatants without trypsin treatment were used as appropriate controls.

The effect of duration of cultivation on the production of antibacterial compounds

The influence of cultivation time on antibacterial activity was determined in a liquid medium after 24, 48, and 72 h of cultivation using agar diffusion method. All experiments were repeated twice to ensure reproducibility.

Polymeric substratum preparation

The photosensitive material used was derived from a common, positive tone, commercial photoresist (S1400-17, purchased from Shipley, Co) adding imidazole to the polymer solution to reach 2% of the solid content. The photoresist was a mixture of a photoactive compound (PAC) based on diazo-naphto-quinone (DNQ) and a novolak resin, in approximate proportion 3:7, respectively, dissolved in ethyl cellosolve acetate, to reach 30% solid content. The material so formulated was sensitive to UV light (436 nm). For silylation we used hexamethyldisilazane (HMDS) as purchased from Aldrich Co.

The 15 mm glass substrata were made hydrophobic or hydrophilic using the method described in the literature (Ferreira 1994). The polymer solution was spin coated on 15 mm glass substrates, using a spin coater, (Mikasa Co.), for 15 seconds at a rotation speed of 500 rpm for deposition, and for 1 min at a rotation of 3000 rpm for thinning and drying. This procedure allows the deposition of uniform films approximately 0.6 μm thick. The films were further dried for 1 hour at 85^{o} C in a convection oven. After drying, the polymeric films were irradiated using a Hg lamp, with band pass filter for bellow 365 nm, at exposure energies denominated as low (30 mJ/cm^2), medium (60 mJ/cm^2) and high (120 mJ/cm^2). In some cases, the photosensitive material was baked in a convection oven at 100^{o} C for 1 hour, in order to decarboxylate the photoinduced created indene carboxylic acid. Several substrates exposed with the highest energy were further exposed to HMDS for silylation of the novolak hydroxylic groups in a closed chamber at 100^{o} C for 15 min. For studies concerning cell patterning, the imidazole doped resist was coated on hydrophilic glass slides. To obtain the highest contrast, these films were irradiated through an emulsion mask at the optimum exposure energy (40 mJ/cm^2). For the development of the exposed patterns we used a metal-free Shipley developer (MF-319), diluted to reach 0.237N. The appropriate development time in these conditions was approximately 60 sec.

The polymer films were irradiated with the exposure energies as above, and post exposure baked at 80° C for 30 min to remove the possible polymer tensions.

Contact angle measurements

The contact angles of 0.5 μl water drop deposited on the polymer surfaces were measured with a Kyowa Kagaku Co. Ltd. anglemeter. The same procedure was used for hydrophilic and hydrophobic glass substrates.

Testing procedure

100 μl of the bacterial suspension of each strain in exponential phase (1.0-2.0×10^{8} cells/ml^{-1}, optical density, at OD_{660}=0.13-0.2) and 400 μl of liquid medium mentioned above composition was applied on each well of the Clostar cluster dishes. Different polymer surfaces prepared previously were plated on bottom of the well. After 4-24 h of incubation the nutrient medium was removed, and antimicrobial activitites were tested. The cells attached to polymers were washed by 200 μl physiological saline and then these solutions were used for detection of antimicrobial activities. Antimicrobial activity was assayed by agar diffusion method as mentioned above against indicator TBS *Staphylococcus epidermidis* (IFO 12993). All experiments were repeated at least twice with appropriate controls.

The number of the cells on the surfaces was calculated visually, using micrographs. The latter were taken at 450X and 900X magnification (400 ASA film, Kodak) in light microscope (Olympus). The results were means of eighty independent calculations ± SD.

RESULTS AND DISCUSSION

The spectrum of antimicrobial activity

The ability of various bacteria to produce antimicrobial substances was tested against *Staphylococcus aureus, Staphylococcus epidermidis, Escherichia coli, Proteus vulgaris, Proteus mirabilis, Enterobacter cloacae, Enterococcus faecalis, Candida albicans, Bacillus subtilis, Aeromonas hydrophila* subsp. *anaerogenes* and *Vibrio anguillarum.* The spectra of the antibacterial activities for the studied strains are presented in Figure 1. In all, 126 strains (about 26%) out of 491 tested strains inhibited the growth of pathogenic, conventionally pathogenic strains, or fish pathogens such as *A. hydrophyla* and *V. anquillarum*. No strain inhibited the growth of *Enterobacter cloacae.* The growth of *Escherichia coli* has been inhibited only by several strains, namely *Pseudoalteromonas spp.* 114, 115, and *Bacillus spp.* 149, 307. The growth of *Proteus mirabilis* has been weakly inhibited by the same strains. Antimicrobial substances produced by marine bacteria were especially active against *Staphylococcus epidermidis, Proteus vulgaris, Enterococcus faecalis* and *Candida albicans.* Besides strains indicated in Fig. 1, a total of 135 other strains showed weak antifungal activity (data not shown).

Although the production of antimicrobial compounds by bacteria from marine environment has been effectively investigated for several decades (Buck et al 1963, Austin 1989, Lemos et al. 1991) to our knowledge there are few reports regarding the proportion of antibiotic producing strains inside selective bacterial communities. For example, among epiphytic bacteria isolated from 5 species of intertidal seaweeds, 16.9% (38 out of 224) bacterial strains displayed anibiotic activity (Lemos 1985). In according to our observations, among bacteria associated with marine invertebrates the number of active strains varied from 20 to 30% for bacterial populations of sponge *Dendrilla sp.* and % for those of mussels (Ivanova, and present study). Among the bacteria studied here, producers of antimicrobial substances were dominant in two bacterial groups such as *Pseudoalteromonas*-related genera, and bacilli, which were mainly associated with marine animals and were isolated from the southern Pacific. Among twelve selected strains only one strain of *Bacillus sp.* had been isolated from seawater. The other strains of *Pseudoalteromonas spp.* and *Bacillus spp.* had been associated with crabs (*Paralithodes camtschatica)*, mussels (*Crenomytilus grayanus, Patinopecten jessoensis*), and sponges (*Haliclona sp., Chonelasma sp., Phylospongidae,* and several unidentified species).

Our results indicated that a production of antimicrobial substances (AS) by bacteria studied was more effective on a seawater based medium, which contained KBr. A common medium used for isolation and maintenance of the same strains failed to induce the production of antimicrobial substances or the antimicrobial activities were weak. The valuable impact of KBr for production of specific marine substances is known, and brompyrrolic antibiotic compounds were described for *Chromobacterium* (Andersen et al 1974), and *Pseudoalteromonas* -related bacteria (Burkholder et al. 1966, Gauthier and Flatau 1976), however the function of halogenated compounds in antibiotic biosynthesis remains unclear yet. The clarification of the structure of active substances produced by strains from the present study is a goal for our further investigations.

After a preliminary screening we selected 70 strains with the highest antimicrobial activities. These bacteria were grown in liquid nutrient medium, the culture supernatants were treated with trypsin to confirm the proteinaceous nature of the active materials. Antimicrobial activity was examined after each step because of differences depending on condition of cultivation. For example. the inhibition of the growth of *E. coli* and *P. vulgaris* was noted to be more effective after cultivation in flasks, whereas inhibition of the growth of *E. faecalis* and *P. mirabilis* was less effective. Twelve strains, isolated from different sources (see Table 1), have been choosen as promissing candidats producing a number of antimicrobial substances. Differences in inhibition of BTS growth after treatment with trypsin are shown in Table 2. The results give evidence that the same strain may simultaneously synthesize a few antibacterial substances of proteinaceous and non-protein nature. For instance, the antibiotics producing by strains 114 and 115, and inhibiting the growth of *A. hydrophila, V. anguillarum,* and in less degree *B. subtilis* were not inactivated by trypsin and might be non protein nature. This suggestion has some support by charts on Fig. 2. which represents the dynamics of antimicrobial activities during 72 hours of incubation of 114 and 115 strains. It is likely that antimicrobial compounds sensitive to treatment with trypsin and inhibiting the growth of *S. epidermides, P. vulgaris,* and *C. albicans* were synthesized by 24 hours, whereas those that inhibited of the growth of *A. hydrophila, V. anguillarum,* and in less degree *B. subtilis* reached their highest values by 48 hours. It seems that antimicrobial activity of these strains might be caused of joint effect of both proteinaceous and non protein antibiotics that could produced at different time of bacterial growth.

The evaluation of the factors that control the biosynthesis of AS remains an important problem. We consider the evaluation of the effect of different adsorbtion condition on the antimicrobial activity as of a particular interest. We have studied the adhesion behaviour of two mentioned above strains with the highest level of antimicrobial activities after attachment on the surfaces with different level of hydrophobicity. Photo- and thermally-induced chemical transformations of the DNQ/N thin polymeric films were the basis for different absorption conditions. Initially, to check the selectivity in AC biosynthesis we tested unexposed, exposed, patterned, and developed polymeric films. The results showed (Fig. 3) that the antimicrobial activities against *S. epidermides* were detected on both unexposed and exposed films. It should be pointed out that the surface of unexposed DNQ/N resist is hydrophobic due to the strong hydrogen bonding between the DNQ acceptor and the hydroxylic donor groups present in the novolak resin (Koshiba et al. 1988), whereas the surface of exposed films is hydrophilic because after exposure the hydrophilicity is increased due to release of the novolak hydroxylic sites and the creation of carboxylic groups.

Therefore for further experiments we have studied how the surface hydrophobicity evolution affect the biosynthesis of AS. It appeared that AS production varied significantly within hydrophilicity variations under exposure energies on exposed polymeric films. The level of antimicrobial activities was greater on the surfaces upon low exposure energies, and less on the same films after highest exposure energies. Contact angle measurements showed that the surface hydrophilicity decreased at highest exposure energies (Fig. 3). This effect might be due to the decrease of hydroxylic groups on the surface, either through esterification with an excess of ketene (fig ? or ref?), or by crosslinking of the novolak in the presence of O2 and photoinduced radicals. The decrease of antimicrobial activities was also detected on exposed surfaces after baking and silylation. In these cases the hydrophilicily decreased due to surface silyation of the remaining hydroxylic and probably carboxylic sites. Similar results were obtained on DNQ/N standard resist with imidazole film. ← what did we use imidazole for ?

[illegible]

To compare the differences in antimicrobial activities on polymeric and glass surfaces we tested hydrophobic, hydrophilic, and charged glasses, and glass as received . In general, the level of antimicrobial activities on glass surfaces was lower as compared to polymeric films. Antimicrobial activities were higher on hydrophilic glass surfaces as compared to hydrophobic and charged surfaces, and absent on glass as received surfaces. As it is shown in Fig. 3, regardless the hydrophilicity for charged glass was about the same as for hydrophilic developed glass, however the antimicrobial activity decreased substantially. This situation is similar to mentioned above on polymeric surfaces, when even after chemical functionalizations the hydrophilicity of the exposed surfaces was close to that for unexposed polymeric films, the antimicrobial activities were lost.

An important point of our experiments was to estimate the correlation between the number of the attached cells, and their antimicrobial activities upon hydrophobicity evolution. The number of the attached bacterial cells (Fig. 4, a, b) was greater on the unexposed polymeric films that were hydrophobic and fewer on exposed surfaces. So even the number of the attached cells on the exposed at low exposure energies films was fewer than on unexposed resist, the antimicrobial activities of the former were a bit higher. This fact allow to suggest that those of the bacterial cells which were attached on exposed resists enriched by carboxylic residues, synthesized AS more activily. According to our considerations, the AS inhibited the growth of *S. epidermides* should be a proteinaceous nature. It is well known that the most common protein-secretion pathway in prokaryotes involves the *sec* secretion system. This system recognizes a characteristic N-terminal secretion signal, consisting of a stretch of hydrophobic residues flanked by basic residues, that is removed during secretion (Bassford et al. 1991, Hendrik and Wickner 1991, Hansen 1993). However what is the substrate requirements for secretion pathway is unclear yet. Probably the presence of carboxylic groups could positively force the AS secretion. In general results obtained suggest that the DNQ/N polymeric films could be a convinient model for study of chemotactic responses of attached bacteria.

REFERENCES

Andersen RJ, Wolfe MS, Faulkner DJ (1974) Autotoxic antibiotic production by a marine *Chromobacterium*. Mar Biol 27:281-285

Austin B (1989) Novel pharmaceutical compounds from marine bacteria. J Appl Bacteriol 67:461-470

Barry AI (1980) Procedures and theoretical considerations for testing antimicrobial agents in agar media. In: Logan V (ed) Antibiotics in laboratory medicine. William&Wilkins, Baltimore, Md, pp 10-16

Bassford P, Beckwith J, Ito K, Kumamoto C, Mizushima S. (1991) The primary pathway of protein export in *E. coli.* Cell 65:367-68

Burkholder PR, Pfister RM, Leitz FN (1966) Production of pirrole antibiotic by a marine bacterium. Appl Microbiol 14:649-653

Buck JD, Aherarn DG, Roth JFG, Meyers SP (1963) Inhibition of the yeasts by a marine bacterium. J Bacteriol 85:1132-1135

Busscher HJ, Sjollema J, van der Mei HC (1990) Relative importance of surface free energy as a measure of hydrophobicity in bacterial adhesion to solid surfaces. In: Doyle RJ, Rosenberg M (eds) Microbial cell surface hydrophobicity. American Society for Microbiology, Washington, DC, pp 335-359

Costerton JW, Geesey GG, Cheng K-J(1978) How bacteria stick. Sci Am 238:86-95

Davis AR, Tarett NM, McConnel OJ, Young CM (1989) Epibiosis of marine algae and benthic invertebrates: natural products chemistry and other mechanisms inhibiting settlement and overgrowth. In: PJ Scheuer (ed) Bioorganic Marine Chemistry, vol. 3. Springer-Verlag, Berlin, pp 85-113

Faulkner DJ (1993) Marine natural products. Natural products reports 10:497-539.

Fenical W (1993) Chemical studies of marine bacteria: developing a new resource. Chem Rev 93:1673-1683

Ferreira M, Cheung JH, Rubner MF (1994) Molecular self-assembly of cojugated polyions: a new process for fabricating multilayer thin film heterostructures. Thin Solid Films 244:806-809

Gauthier NJ, Flatau GN (1976) Antibacterial activity of marine violet-pigmented *Alteromonas* with special reference to the production of brominated compounds. Can J Microbiol 22: 1612-1619

Jensen PR, Fenical W (1994) Strategies for the discovery of secondary metabolites from marine bacteria: ecological perspectives. Annu Rev Microbiol 48:559-584

Jensen PR, Harvel CD, Wirtz K, Fenical W (1996) Antimicrobial activity of extractes of Caribean gorgonian corals. Marine Biol 125:411-419

Fletcher M, Marshall KC (1982) Are solid surfaces of ecological significance to aquatic bacteria? In: Marshall KC (ed) Advances in aquatic microbiology, vol. 6. Plenum Press, New York, pp 199-236

Fletcher M (1993) Physicochemical aspects of surface colonization. In: Guerrero R, Pedros-Alio C (eds.) Trends in microbial ecology. Spanish Society for Microbiology, pp 109-112

Gauthier MJ, Flatau GN (1976) Antibacterial activity of marine violet-pigmented *Alteromonas* with special reference to the production of brominated compounds. Can J Microbiol 22:1612-1619

Gauthier G, Gauthier M, Christen R (1995) Phylogenetic analysis of the genera *Alteromonas , Shewanella, and Moritella* using genes coding for small-subunit rRNA sequences and division of the genus *Alteromonas* into two genera, *Alteromonas* (Emended) and *Pseudoalteromonas* gen. nov., and twelve new species combinations. Int J System Bacteriol 45:755-761

Hansen JN (1993) Antibiotics synthesized by posttranslational modification. Ann Rev Microbiol 47:535-564

Harvey RW, Young LY (1980) Enumeration of particle-bond and unattached respiring bacteria in the salt marsh environment. Appl Environ Microbiol 40:156-160

Hendrick JP, Wickner W (1991) SecA protein needs bith acidic phospholipids and SecY/E protein for functional high-affinity binding to the *Escherichia coli* plasma membrane. J Biol Chem 266:24596-24600

McClintock JB, Janssen J (1990) Pteropod abduction as chemical defence in a pelagic Antarctic amphipod. Nature 346:462-464

Koshiba M, Murata M, Matsui M, Harita Y (1988) Proc. SPIE 1261, 493-501

Lawrence JR, Korber DR (1993) Aspects of macrobial surface colonization behaviour. In: Guerrero R, Pedros-Alio C (eds) Trends in microbial ecology. Spanish Society for Microbiology, pp 113-118

Lemos ML, Toranzo AE, Barja JL (1985) Antibiotic activity of epiphytic bacteria isolated from intertidal seaweeds. Microbial Ecol 11:149-163

Lemos ML, Dopazo CP, Toranzo AE, Barja JL (1991) Competitive domonance of antibiotic-producing marine bacteria in mixed cultures. J Appl Bacteriol 71:228-232

Low CSF, White DC (1989) Regulation of external polyner production in benthic microbial communities. In: Cohen Y, Rosenberg E (eds) Microbial mats. ASM. Wash, D.C.

Natori S (1990) Dual functions of insect immunity proteins in defense and development. Res Immunol 141:938-939

Paul VJ (1994) Chemical defenses of benthic marine invertebrates. In: Paul VJ (ed) Ecological Roles of Marine Natural products. Cornell University Press, Ithaca and London, pp 164-188

Rutter PR, Vincent B (1980) Physicochemical interactions of the substratum, microorganisms, and the fluid phase. In: Marshall KC (ed) Microbial adhesion and aggregation. Springer-Verlag, Berlin, pp 21-38

Sammarco PW, Coll JC (1988) The chemical ecology of alcyonarian corals. In Scheur PJ (ed) Bioorganic Marine Chemistry, vol. 2. Springer-Verlag, Berlin, pp 89-116

Vandamme EJ (1994) The search for novel microbial fine chemicals, agrochemicals and biopharmaceuticals. J Biotechn 37:89-108

ZoBell CE (1943) The effect of solid surfaces upon bacterial activity. J Bacteriol 46:39-56

Table 1. Sources of marine strains with the highest antimicrobial acivities

Designation	**Taxon**	**Strain number**	**Origin**	**Source**	**Date of isolation**
114	*Pseudoalteromonas sp.*	4ML13	Japan Sea, Troitza Bay	Mussel (*Crenomytilus grayanus)*	Jul, 1990
115	*Pseudoalteromonas sp.*	4GM8	Japan Sea, Troitza Bay	Mussel (*Patinopecten jessoensis)*	Jul, 1990
165	*Pseudoalteromonas sp.*.	7-77-7/1	Pacific Ocean, Okhotsk Sea	Crab (*Paralithodes camtschatica)*	Jun, 1988
166	*Pseudoalteromonas sp.*	7-77-2	Pacific Ocean, Okhotsk Sea	Crab (*Paralithodes camtschatica)*	Jun, 1988
132	*Pseudoalteromonas sp.*	7-145-19	Pacific Ocean, Coral Sea	Sponge (unident. sp.)	Jul-Nov, 1988
149	*Bacillus sp.*	7-193-11	Pacific Ocean, Coral Sea	Phylospongidae	Jul-Nov, 1988
174	*Pseudoalteromonas sp.*.	7-23-22/1	Pacific Ocean, Okhotsk Sea	Sponge (*Chonelasma sp.)*	Jun, 1988
179	*Pseudoalteromonas sp.*.	7-16-4	Pacific Ocean, Okhotsk Sea	Sponge (*Haliclona p.)*	Jun, 1988
301	*Bacillus sp.*	7-144-4/1	Pacific Ocean, Coral Sea	Sponge (unident. sp.)	Jul-Nov, 1988
307	*Bacillus sp.*	7-165-15	Pacific Ocean, Coral Sea	Sponge (unident. sp.)	Jul-Nov, 1988
361	*Bacillus sp.*	7MB129	Pacific Ocean, Coral Sea	Sea water	Jul-Nov, 1988
458	*Bacillus sp.*	7-248-3	Pacific Ocean, New Zealand	Sponge (unident. sp.)	Jul-Nov, 1988

Table 2. Antimicrobial activity (mean diam, mm) of marine bacteria against Bacterial Test Strains before (left) and after (right) treatment with trypsin.

Designation	**Taxon**	*S. epidermides*	*S. aureus*	*P. vulgaris*	*P. mirabilis*	*B. subtilis*	*E. feacalis*	*E. coli*	*C. albicans*	*V. anquillaru*	*A. hydrophila*
114	*Pseudoalteromonas sp.*	20/-	15/-	20/-	12	20/15	15/-	13/-	16/-	25/22	15/15
115	*Pseudoalteromonas sp.*	25/-	18/-	25/-	10	18/15	20/-	10/-	23/-	25/23	20/19
166	*Pseudoalteromonas sp..*	15	8	10	-	-	6	-	10	5	7
167	*Pseudoalteromonas sp.*	15	5	10	-	-	-	-	6	10	5
132	*Pseudoalteromonas sp.*	18	13	14	-	13	-	-	15	8	8
149	*Bacillus sp.*	20	15	18	5	25	-	6	25	6	9
174	*Pseudoalteromonas sp..*	15	6	-	-	-	-	-	4	4	12
179	*Pseudoalteromonas sp..*	20	6	15	-	-	-	-	6	6	10
301	*Bacillus sp.*	15	12	8	-	-	-	-	-	-	12
307	*Bacillus sp.*	25	20	18	5	7	6	5	8	-	-
361	*Bacillus sp.*	25	18	-	-	8	8	-	8	-	-
458	*Bacillus sp.*	15	10	-	-	-	4	-	15	-	-

Fig 2 [illegible]

Sheet1 Chart 4

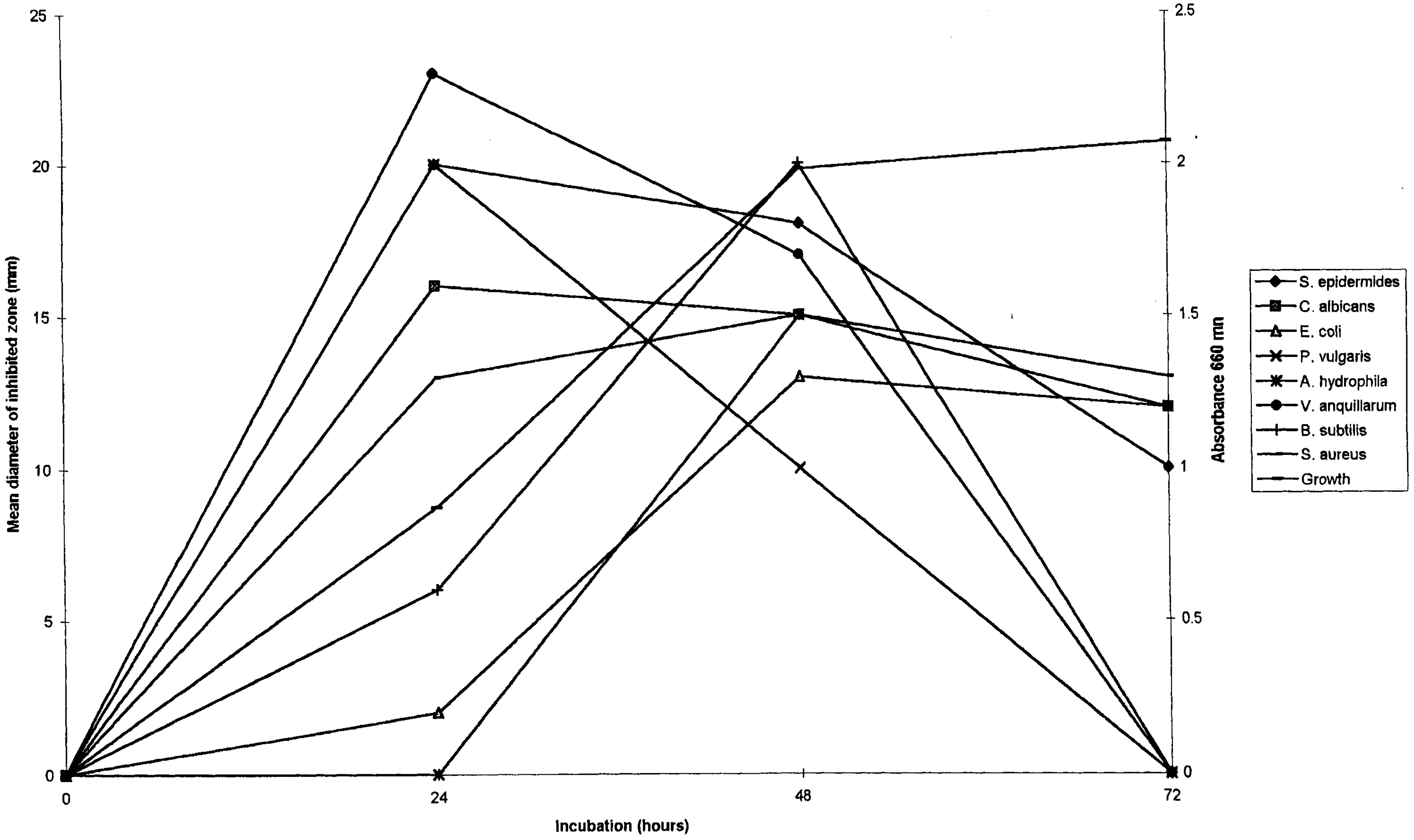

Fig 2.5 (b)

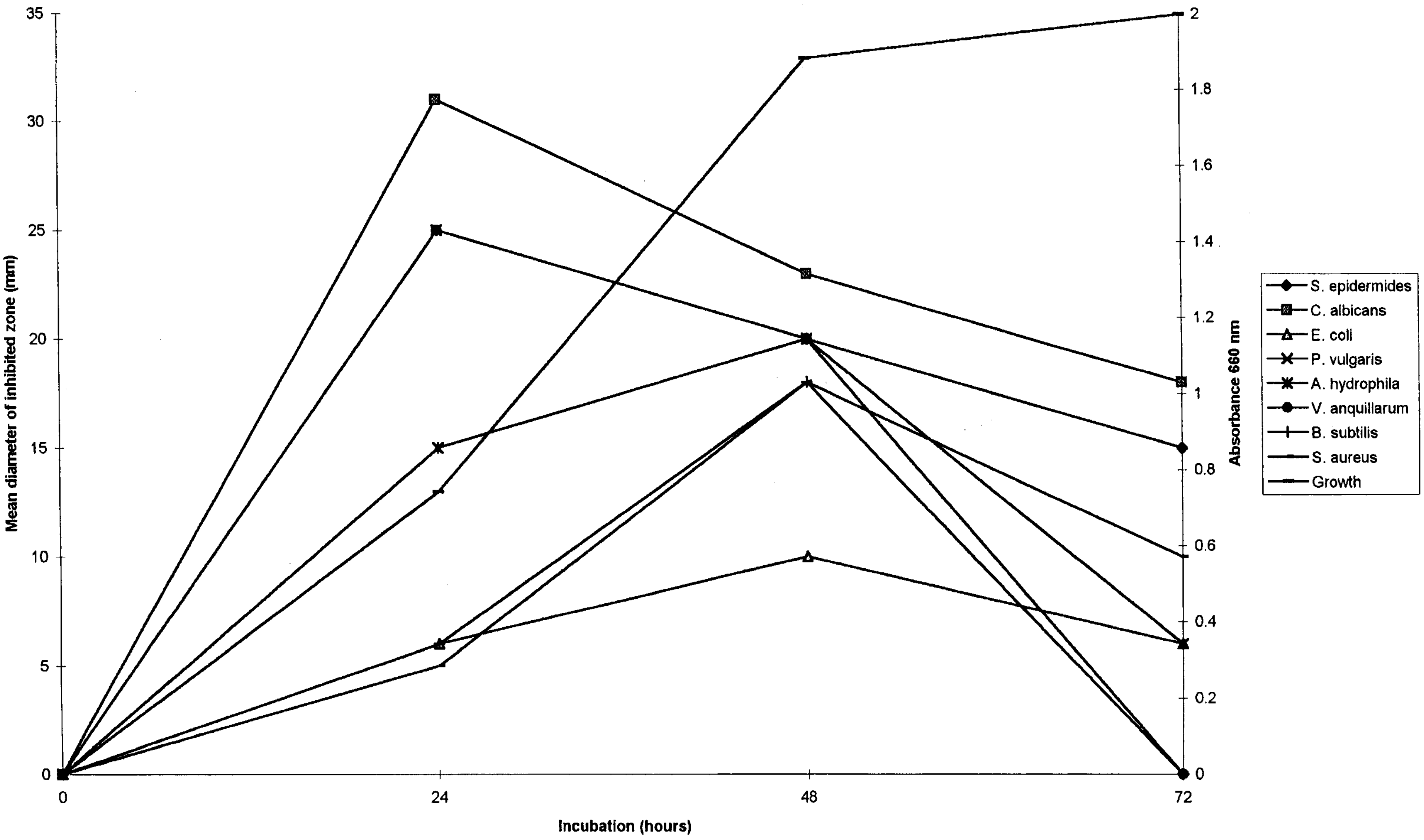
35
30
25
20
15
10
5
0
Mean diameter of inhibited zone (mm)
0
24
48
72
Incubation (hours)
2
1.8
1.6
1.4
1.2
1
0.8
0.6
0.4
0.2
0
Absorbance 660 nm
S. epidermides
C. albicans
E. coli
P. vulgaris
A. hydrophila
V. anquillarum
B. subtilis
S. aureus
Growth

I. POLYMERIC FILMS DIFFERENTIATION

	PHOTO		THERMALLY INDUCED FILMS	
	Unexposed	Exposed	Patterned	Developed
Contact angle, θ	78°	θ ?	θ ?	θ ?
Antimicrobial avtivity	++[1]	++	-	-

II. HYDROPHOBICITY EVOLUTION

Polymeric Standard Surfaces

	Exposed:				
	Low	Medium	High	+bake	+silylation
Contact angle, θ	66°	69°	77°	79°	82°
Antimicrobial avtivity	+++	+	+	-	-

Standard resist + Imidazol, 4%

Unexposed	Exposed:		
	Low	Medium	High
++	+++	+	+

∠ what is θ the

Glass Surfaces

	Hydrophobic	Hydrophilic	Charged	As received
Contact angle, θ	90°	30°	34°	10°
Antimicrobial activity	+	++	+	-

+, diameter of inhibited bacterial growth ≤ 10 mm, ++, ≤ 20 mm, +++, ≤ 30 mm

Fig 4 a)

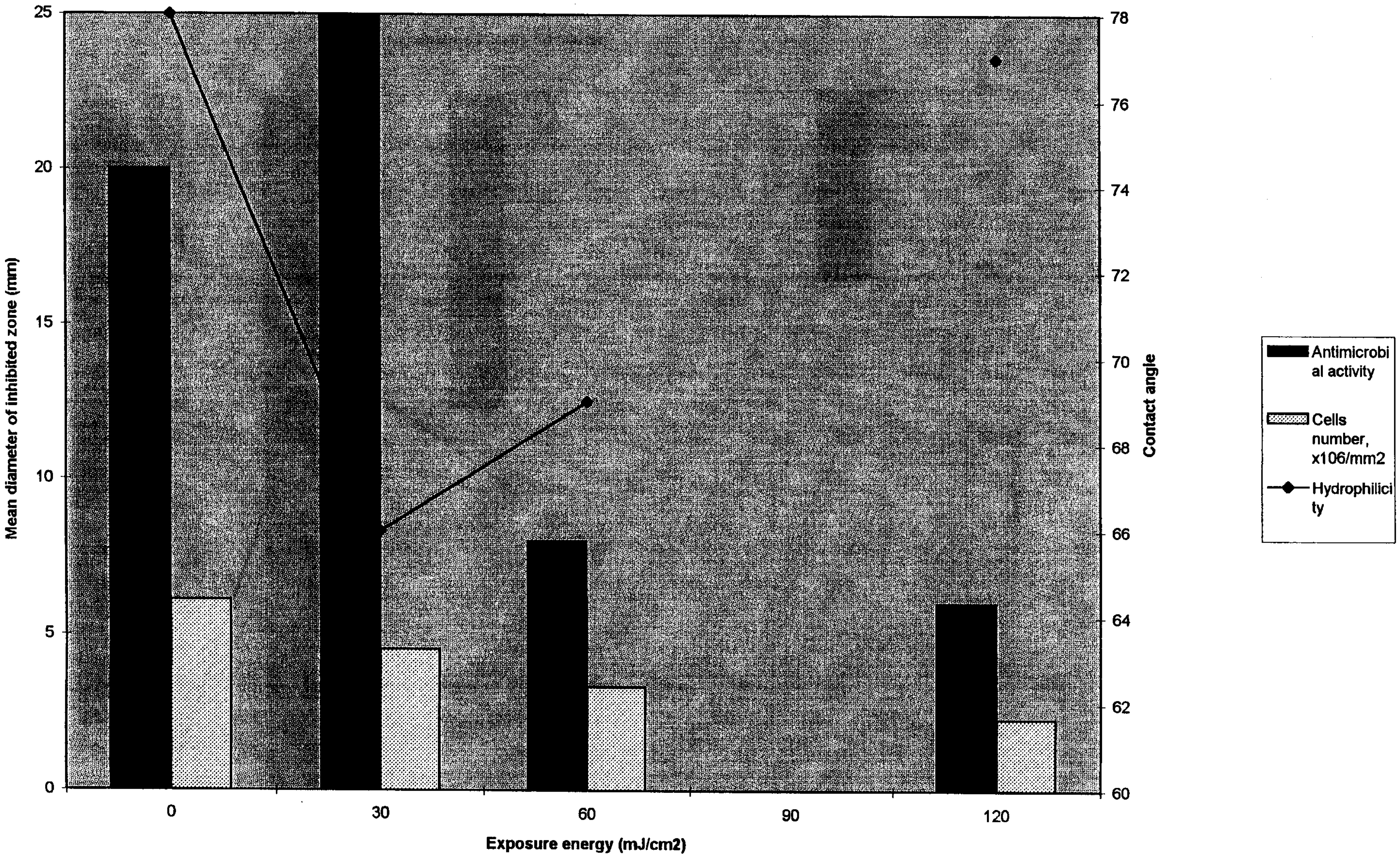
Mean diameter of inhibited zone (mm)
25
20
15
10
5
0
Contact angle
78
76
74
72
70
68
66
64
62
60
0
30
60
90
120
Exposure energy (mJ/cm2)
Antimicrobial activity
Cells number, x106/mm2
Hydrophilicity

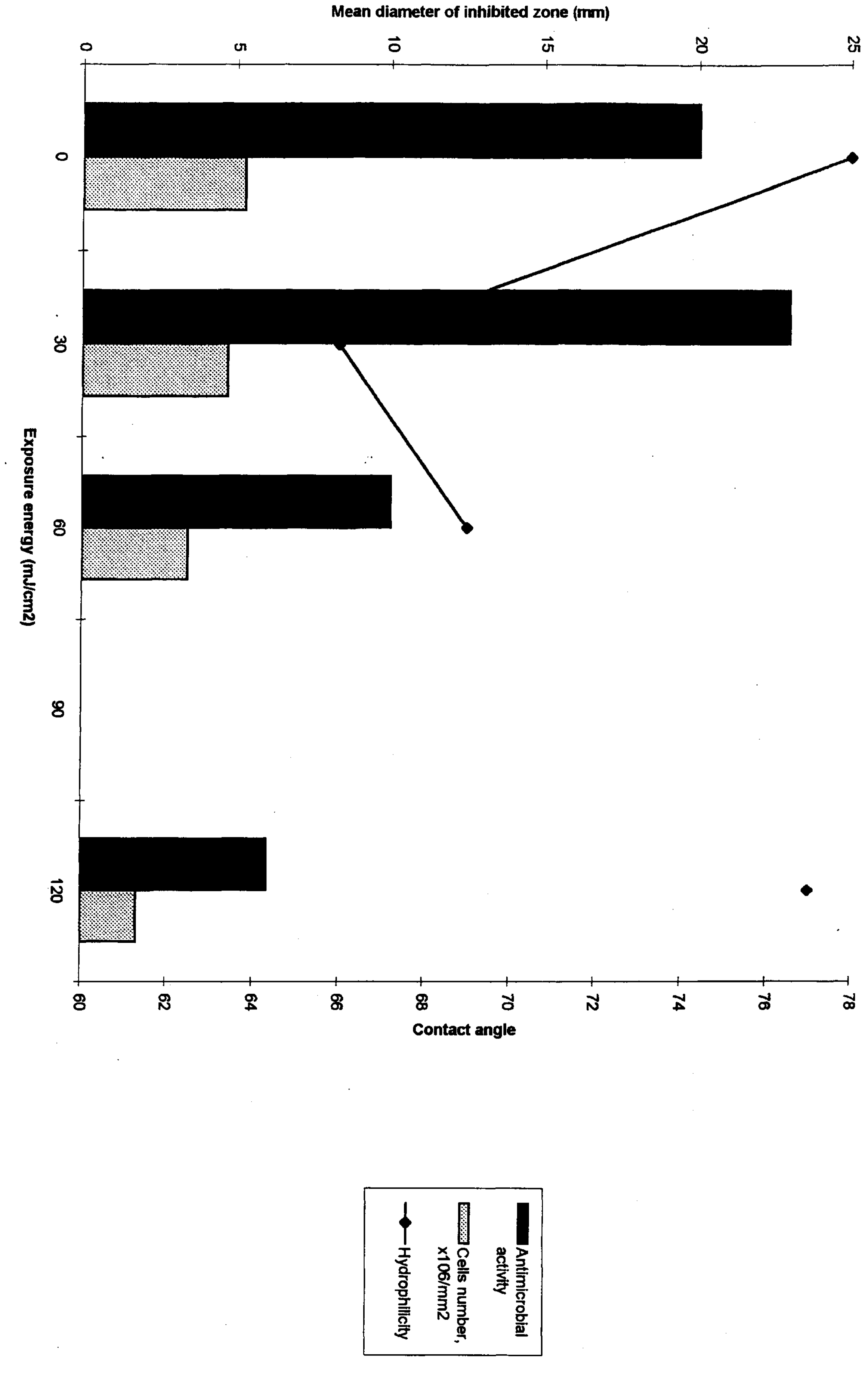
Mean diameter of inhibited zone (mm)
0
5
10
15
20
25
Exposure energy (mJ/cm2)
0
30
60
90
120
Contact angle
60
62
64
66
68
70
72
74
76
78
Antimicrobial activity
Cells number, x106/mm2
Hydrophilicity

Figure legends

Fig. 1. The spectra of antimicrobial activities of marine bacteria against Bacterial Test Strains.

Fig. 2. The dinamics of antimicrobial activities against Bacterial Tast starins during 72 hours of incubation for *Pseudoalteromonas spp.* 114 (a) and 115 (b).

Fig. 3. The differences in antimicrobial activities on polymeric and glass surfaces denending on photo- and thermofunctionalisation.

Fig. 4. The correlation between the number of the attached cells and antimicrobial activities *vs* level of hydrophobicity of the DNQ/N polymeric films for *Pseudoalteromonas spp.*114 (a) and 115(b).

CHARACTERIZATION OF NEURITE-OUTGROWTH PROMOTING FACTORS IN EXTRACTS OF DENERVATED CHICK SKELETAL MUSCLE

Hiroshi Nishimune[1,2], Isao Oishi[2], Satoru Koyanagi[2], and Takahisa Taguchi[1,2,*]

[1] Dept. of Organic Materials, Osaka National Research Institute, AIST, Ikeda, 563, Japan
[2] Faculty of Engineering Science, Osaka University, Toyonaka 560, Japan

Received , 1997

(Abstract)

We reported previously that an extract of denervated skeletal muscle contained an activity that promoted neurite-outgrowth of telencephalic neurons, as well as that of neurons in the spinal cord. In this report, factors with this activity were characterized using primary cultures of dissociated telencephalic neurons from chick embryos. It was only when the factors were attached to the surface of culture dishes that the factors were able to act on neurons. Since proteolytic treatment and binding of lectin reduced the outgrowth-promoting activity, it appeared that the activity was due to a glycoprotein(s). An extract that had been heat-treated at 80℃ for 20 min still contained most of the activity, even after large amounts of denatured proteins had been removed by centrifugation. Among monoclonal antibodies raised against the heat-treated extract, we found five that inhibited the outgrowth of neurite that was promoted promoted by the proteins in the extract. The most potent antibody among the five mainly recognized a protein of 64 kD.

(Main Text)

The neurite-outgrowth is not only the first step in the formation of a neuronal network but it is also indispensable for synaptogenesis and the fine tuning of synaptic function. Terminal sprouting of presynaptic axons (1,2) and competition for target-derived factors (3) are important, respectively, for synaptic plasticity and synaptic maturation (elimination). To elucidate the molecular and cellular mechanisms of synaptic functions, we have established a system of neuronal culture suitable for the analysis of synaptogenesis (4). In this culture system, we have demonstrated activity-dependent synaptogenesis (5), and existence of silent synapse prior to dual component synapse (6). On the basis of the identification of a muscle-derived neurite-promoting activity (7), we have started to characterize factors that promote the outgrowth of neurites in our culture system. An activity that stimulates neurite-outgrowth of chick telencephalic neurons in an extract of denervated skeletal muscle has already been reported (8).

In this study, we characterized the neurite-outgrowth promoting factors in such an extract using biochemical, cell biological and immunochemical approaches and primary cultures of dissociated telencephalic neurons from chick embryos.

MATERIALS AND METHODS

Culture of neuronal cells: Telencephalic regions from chick embryos (White leghorn) at stage 25 (9) were dissected out in Ca^{2+}-, Mg^{2+}-free phosphate-buffered saline (PBS^-) supplemented with 10 mM glucose. The tissues from two or three embryos were treated with 0.0125%(w/v) trypsin (Gibco, USA) in the same solution for 20 min at 37℃. The tissues were then rinsed in Ham's F12 medium supplemented with glucose (10 mM), glutamine (2 mM), insulin (2.5 μg/ml) and antibiotics, and they were dissociated in this medium by gentle trituration with a disposable plastic pipette. Dissociated telencephalic neurons (50,000 cells per well) were plated in 16-mm wells that contained 0.4 ml of the same F12 medium. Neurons were cultured at 37℃ in 5% CO_2 at saturating humidity.

Assay of neurite-outgrowth: To estimate the activity that promoted the neurite-outgrowth, we tested extracts (2 μg/ml, final concentration of protein) in duplicate. The extract plus culture medium was placed in the wells of 24-well culture dishes (Coaster, USA) to allow the proteins to adsorb for 2 hours, unless otherwise specified. After 24 hours of culture, the total numbers of surviving cells and the numbers of cells with one or more neurites with length of more than twice the cell diameter were counted for quantification of neurite-outgrowth.

Preparation of an extract of denervated chick skeletal muscle: The extract was prepared from postnatal chicks as described in our previous report (8).

Biochemical assays: Protein concentrations were determined by the method of Bradford (10) with bovine serum albumin as a standard. Sodium dodecylsulfate-polyacrylamide gel electrophoresis (SDS-PAGE) was performed on 12.5% polyacrylamide gel, as described by Laemmli (11). Immunoblot analysis was performed as described in a previous report (12).

Preparation of monoclonal antibodies (mAbs): The extract was diluted 10-fold and then heated at 80℃ for 20 min. The supernatant after centrifugation of the heated extract (10,000 x *g*, 30 min) was used as the antigen, after concentration by the Centricon system (Amicon, USA). Cloned hybridoma cells derived from dissociated spleen cells and myeloma cells (PAI) were prepared by the conventional method using Balb/c mice. The antibodies produced by these hybridoma cells were screened in an assay for inhibition of neurite-outgrowth from telencephlic neurons, as described below. Proteins (2.5 μg) in the extract of denervated muscle were allowed to adsorb during a 2-hour incubation at 23℃ to the surface of culture dishes coated with 2.5% (w/v) poly-ornithine (Sigma, USA). After an additional 2-hour incubation for reaction of proteins with mAbs in the culture medium of hybridoma cells, the wells were washed and used for the neurite-outgrowth assay, as described above.

RESULTS

Two types of neurite-outgrowth promoting factor have been reported, namely, diffusible factors, such as nerve growth factor (NGF), and components of the extracellular matrix, such as laminin. The former act on neurons as mobile molecules in solution, whereas the latter act as molecules that are attached extracellularly to substrates to which neurons are exposed. To classify the factors in denervated muscle, we varied the timing of the addition of the extract to the primary cultures of neurons (Fig.1A). When the extract was added 2 hours before seeding of telencephalic neurons, full promotion of neurite-outgrowth was observed. If both the extract and neurons were added to wells at the same time, the activity was slightly reduced. By contrast, only a little activity was observed when the extract was added more than 30 min after neurons. Since about 20 min were required for the added neurons to attach to the culture dish (data not shown), these results show that only the factors that had attached to the surface of the culture dish and were located under the cells were active, while factors in the culture medium were much less active.

To confirm the active form of the factor(s), we examined the effect of the duration of the preincubation of the factors on the promotion of neurite-outgrowth (Fig. 1B,C). The activity was tested in dishes in which the medium had been replaced by new medium without the extract after the indicated preincubation time (Fig. 1B). The activity was tested in dishes to which the medium had been transferred from dishes used for preincubations (Fig. 1C). The results confirmed that 2 hours were required for the factors in the extract to adhere to the bottom surface of dishes. Note that Figures 1B and 1C are mirror images.

The adsorption of the active factors to the surface was strong enough to resist repeated washing with PBS, culture medium, 1 M NaCl, or 0.1% (w/v) Triton X-100, since all treated dishes retained the activity (data not shown). This property was useful for characterization of the factors. Exploiting this property, we confirmed that the factors were proteins (Fig. 2A). The neurite-outgrowth activity adsorbed on the surface of dishes decreased with increases in the concentration of trypsin, which degraded surface proteins. Similar results were obtained in experiments with two other proteases, namely α-chymotrypsin (Sigma) and a protease from *Streptomyces griseus* (Sigma; data not shown).

The tightly adsorbed factors on dishes retained full activity, suggesting that the factors acted from outside the neurons. Since such protein factors would have to be secreted extracellularly, we postulated that these factors might be glycoproteins. To confirm our hypothesis, we carried out inhibition experiments using concanavalin A (ConA; Sigma). The activity was dose-dependently blocked by ConA (Fig. 2B) and such inhibition was antagonized in the presence of α-methyl-D-mannoside (Fig. 2C). A similar result was obtained in an experiment with an other lectin, an agglutinin form *Sophora japonic*a (Sigma; data not shown).

The heat stability of the proteins was tested by incubation of diluted extract (0.5 mg protein/ml) in a water bath at 50, 60, 70 or 80℃ for up to 20 min and centrifugation (10,000 x *g*, 30 min) to eliminate denatured proteins. In the subsequent neurite-outgrowth assay, all supernatants retained the same activity as the non-heated control extract (data not shown).

To identify the factors, we prepared monoclonal antibodies (mAbs) against the heat-treated extract and we identified five mAbs that significantly inhibited the outgrowth-promoting activity (Fig. 3A). Further analysis of the most potent mAb (4D2a) revealed that inhibition was dose-dependent (Fig. 3B). Immunoblot analysis indicated that 4D2a mainly recognized a 64 kD protein and also bound weakly to proteins of 108, 96, 59, 53, 48, 45, 41 and 35 kD in the extract of denervated muscle (Fig. 4).

DISCUSSION

The neurite-outgrowth promoting factors in an extract of denervated chick skeletal muscle were revealed to act on neurons, attaching to the substratum to which neurons also adhered (Fig. 1). The fact that preincubation of the neurons with the extract in suspension for up to 50 min did not promote neurite-outgrowth in subsequent culture on non-coated dish for 24 hours (data not shown) supports this interpretation. The adhesiveness of factors from denervated muscle to telencephalic neurons resembled that of a factor in chick muscle extract that promoted neurite-outgrowth from motoneurons (13). The results in Figure 1 indicate that the factors could be classified as components of the extracellular matrix, but the proteins recognized by mAb 4D2a differed from laminin in terms of molecular mass (Fig. 4).

The factors described in this report appeared to be soluble glycoproteins. Since proteins with conjugated sugar residues are secreted or are exposed to the topological exterior of the cell, it is suggested that the factors were secreted extracellularly from muscle cells. Although the factors were recognized by ConA, purification by affinity chromatography on a column of ConA-conjugated Sepharose 4B was unsuccessful, because too many proteins in the extract bound to the lectin. The heat treatment described in Results was rather effective for the partial elimination of proteins other than the factors themselves.

To determine the functional sites on the factors, we examined the activity of attached factors in our bioassay system after modification of sugar residues with neuraminidase (Sigma), β-glucosidase (Sigma), sodium iodoacetic acid (Sigma), β-galactosidase (Sigma), endoglycosidase F (Sigma) and endo-α-N-acetyl galactosaminidase (Sigma). These treatments had no effect on promotion of neurite-outgrowth (data not shown), suggesting that active sites were located in the amino acid core.

The adhesiveness of the muscle-derived factors allowed us to prepare monoclonal antibodies by *in vitro* immunization (14). In four series of preparations, dissociated mouse spleen cells were incubated in culture dishes with adsorbed partially purified proteins from the extract, and then they were fused with myeloma cells. Although quite a few positive clones were obtained, all clones secreted IgM antibodies which have disadvantages in terms of handling and affinity as compared with IgG.

The neurite-outgrowth promoting factors were identified as proteins. Further analysis of the molecular properties of these factors is in progress (15). In the near future, we shall test the ability of these factors to stimulate the regeneration of injured axons.

ACKNOWLEDGMENTS

The authors thank Professor A. Satake for encouragement, Professor M. Kasai and Dr. A. Uyeda for discussions, Dr. S. Fujita for a kind gift of PAI myeloma cells and Ms. K. Shirai for technical assistance. One of the authors (H.N.) is a fellow of Japan Science and Technology Corporation (JST).

REFERENCES

1. Tsukahara, N. (1981) *Annu. Rev. Neurosci.* **4**, 351-379.
2. Bailey, C. H., and Chen, M. (1988) *Proc. Natl. Acad. Sci.* USA, **85**, 2373-2377.
3. Changeux, J.-P., and Danchin, A. (1976) *Nature*, **264**, 705-712.
4. Tokioka, R., Matsuo, A., Kiyosue, K., Kasai, M., and Taguchi, T. (1993) *Dev. Brain Res.* **74**, 146-150.
5. Kiyosue, K., Kasai, M., and Taguchi, T. (1996) *Neuroreport*, **7**, 701-704.
6. Kiyosue, K., Kasai, M., and Taguchi, T. (1997) *Dev. Brain Res.* (in press)
7. Henderson, C. E., Huchet, M., and Changeux, J.-P. (1983) Nature, 302, 609-611.
8. Taguchi, T., Huchet, M., Roa, M., Changeux, J.-P., and Henderson, C. E. (1987) *Dev. Brain Res.* **37**, 125-132.
9. Hamburger, V., and Hamilton, H. L. (1951) *J. Morphol.* **88**, 49-92.
10. Bradford, M. M. (1976) *Anal. Biochem.* **72**, 248-254.
11. Laemmli, U. K. (1970) *Nature*, **227**, 680-685.
12. Nobusada, H., and Taguchi, T. (1992) *Biochiem. Biophys. Res. Commu.* **182**, 39-44.
13. Henderson, C. E., Huchet, M., and Changeux, J.-P. (1984) *Dev. Biol.* **104**, 336-347.
14. Boss, B.D. (1986) *Methods Enzymol.* **121**, 27-33.
15. Nishimune, H., Uyeda, A., Nogawa, M., and Taguchi, T. (1995) *Abst. of Annu. Meeting*

of the Society for Neurosci. **21**, 1772.

FOOTNOTE

(Footnote for the first page)

*To whom correspondence should be addressed at Osaka National Research Institute, AIST, 1-8-31, Midorigaoka, Ikeda 563, Japan. Fax: (+81) 727-51-9628, Tel: (+81) 727-51-9524, e-mail: taguchi@onri.go.jp

FIGURE LEGENDS

Fig. 1 Activation of the neurite-outgrowth from cultured telencephalic neurons by an extract of denervated chick muscles. The promotion of neurite-outgrowth was determined by calculating the percentage of cells with neurites (mean ± range; n=2 dishes). (A) Timing of the extract-addition to the culture medium. The dissociated neurons were plated at time zero in wells with (open circles) and without (solid circles) the extract, which was added at the time indicated on the horizontal axis. (B) The neurite outgrowth in wells preincubated with (open circles) and without (solid circles) the extract. After adsorption of proteins for the indicated time, the medium was transferred to the wells of another dish for use in the experiment for which results are shown in Fig. 1C. The neurons were cultured with the newly added medium without the extract. (C) The neurite-outgrowth in wells with the medium transferred from dishes and used for the preincubation described in the legend to Fig. 1B.

Fig. 2 Characterization of molecules that stimulated neurite-outgrowth. (A) Degradation of proteins adsorbed to wells of culture dish. The proteins adsorbed to the wells were treated with trypsin at the concentrations indicated on the horizontal axis at 37℃ for 30 min. After the wells had been rinsed three times with culture medium, telencephalic neurons were cultured for measurement of the activity, as described in the legend to Fig. 1. The result without the extract is indicated by an open circle. These treatments with trypsin had no effect on neuronal survival. (B) Binding of ConA to molecules adsorbed to the wells of culture dishes. The wells with adsorbed extract were treated with ConA at the indicated

concentrations for 3 hours at 37℃ and used for the assay (solid circles). Since residual ConA was found to be slightly toxic to neurons, the number of surviving cells was counted for calculation of the ratio (open triangles) relative to results in the experiment without ConA. Note that the inhibitory effect of ConA on neurite-outgrowth was significantly greater than that on survival. (C) The effect of α-methy-D-mannoside on the blocking activity of ConA. Wells treated with ConA (250 μg/ml), as described above, were further incubated with a ligand for ConA, α-methyl-D-mannoside (met-mann), at the indicated concentrations at 37℃ for 3 hours and used for the assay (solid circles). As in Fig. 2B, the relative number of surviving neurons (open triangles) was calculated. The open circle and square refer to the neurite-outgrowth in wells with and without the extract in the absence of other treatment, respectively.

Fig. 3 Inhibition of the outgrowth-promoting activity by mAbs. (A) Inhibition of the activity by five mAbs. Among 95 lines of hybridoma cells that secreted IgG, five hybridoma lines were identified that inhibited the activity. Each bar indicates the neurite-outgrowth observed after treatment with a mAb. P.C. and N.C. are the values obtained in wells with and without the extract in the absence of any other treatment, respectively. (B) Dose-dependent inhibition of the activity by the mAb 4D2a. After wells had been treated with (solid circles) or without (open circles) the extract, serial dilutions of complete medium from the hybridoma culture were placed on cells. The complete medium from the hybridoma cells themselves promoted neurite-outgrowth, acting in an additive manner with the extract. When the medium containing 4D2a mAb was substituted for the complete medium in extract-adsorbed wells, a significant inhibition of neurite-outgrowth was observed at high doses (solid squares).

Fig. 4 Immunoblot analysis of proteins in the extract with the mAb 4D2a. Proteins (27 μg) in the extract were denatured under reducing condition with 1% SDS, subjected to SDS-PAGE, blotted on a nitrocellulose filter and analyzed with the mAb 4D2a. The values on the left and right sides indicate molecular masses in kD of standard proteins and of proteins recognized by mAb 4D2a, respectively.

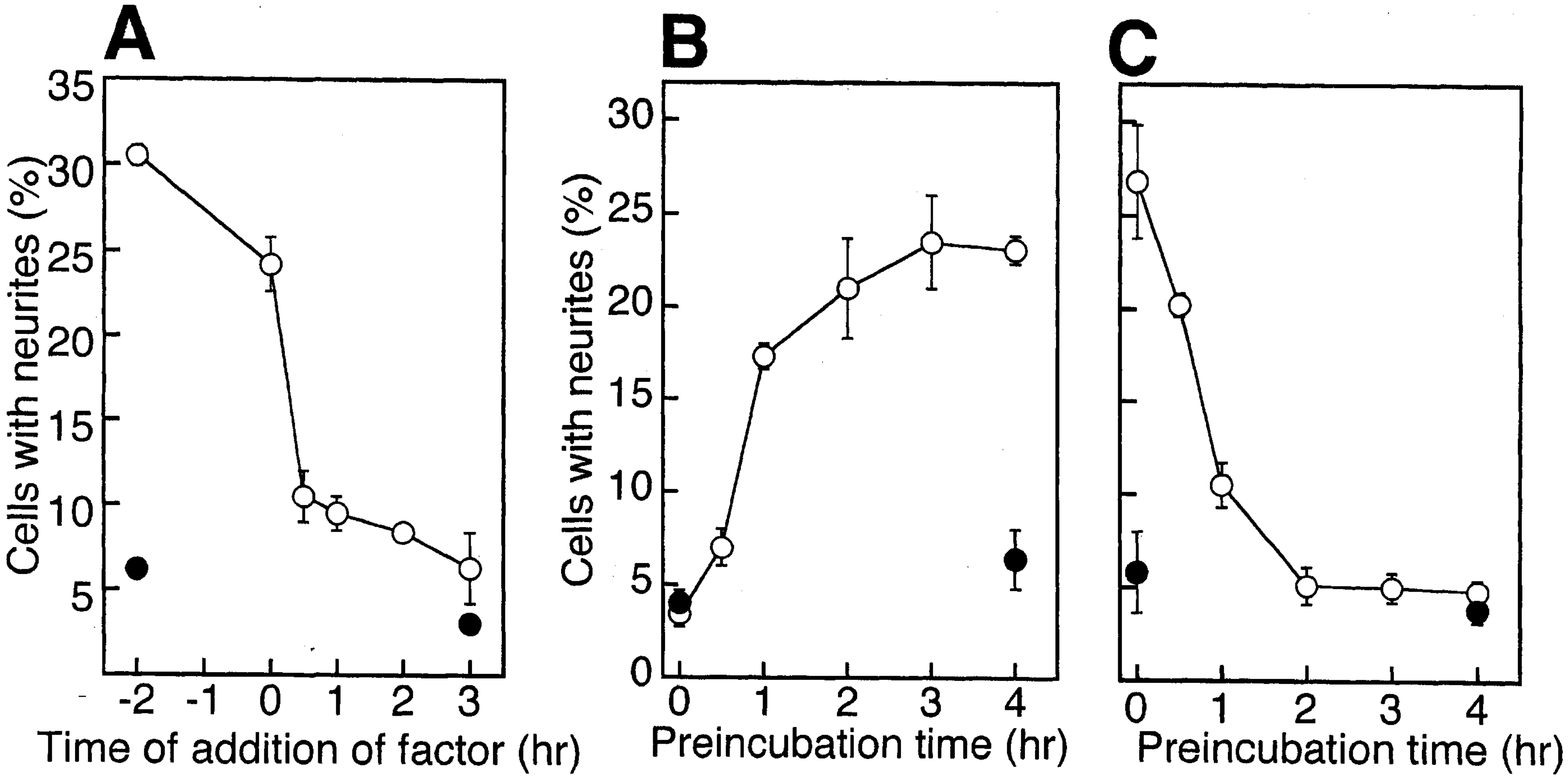
A
B
C
Cells with neurites (%)
35
30
25
20
15
10
5
-2
-1
0
1
2
3
Time of addition of factor (hr)
Cells with neurites (%)
30
25
20
15
10
5
0
0
1
2
3
4
Preincubation time (hr)
0
1
2
3
4
Preincubation time (hr)

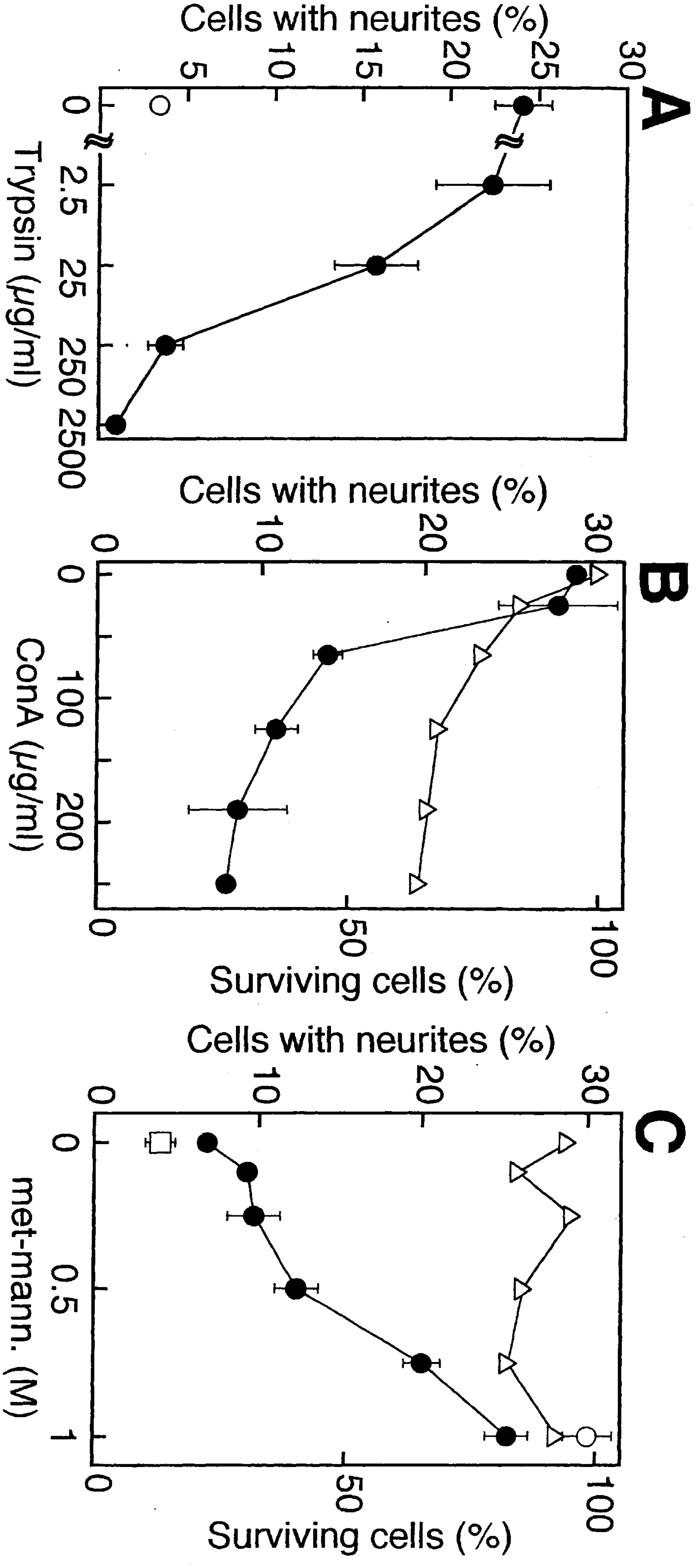
A
Cells with neurites (%)
0
5
10
15
20
25
30
0
2.5
25
250
2500
Trypsin (μg/ml)
B
Cells with neurites (%)
0
10
20
30
0
100
200
ConA (μg/ml)
0
50
100
Surviving cells (%)
C
Cells with neurites (%)
0
10
20
30
0
0.5
1
met-mann. (M)
0
50
100
Surviving cells (%)

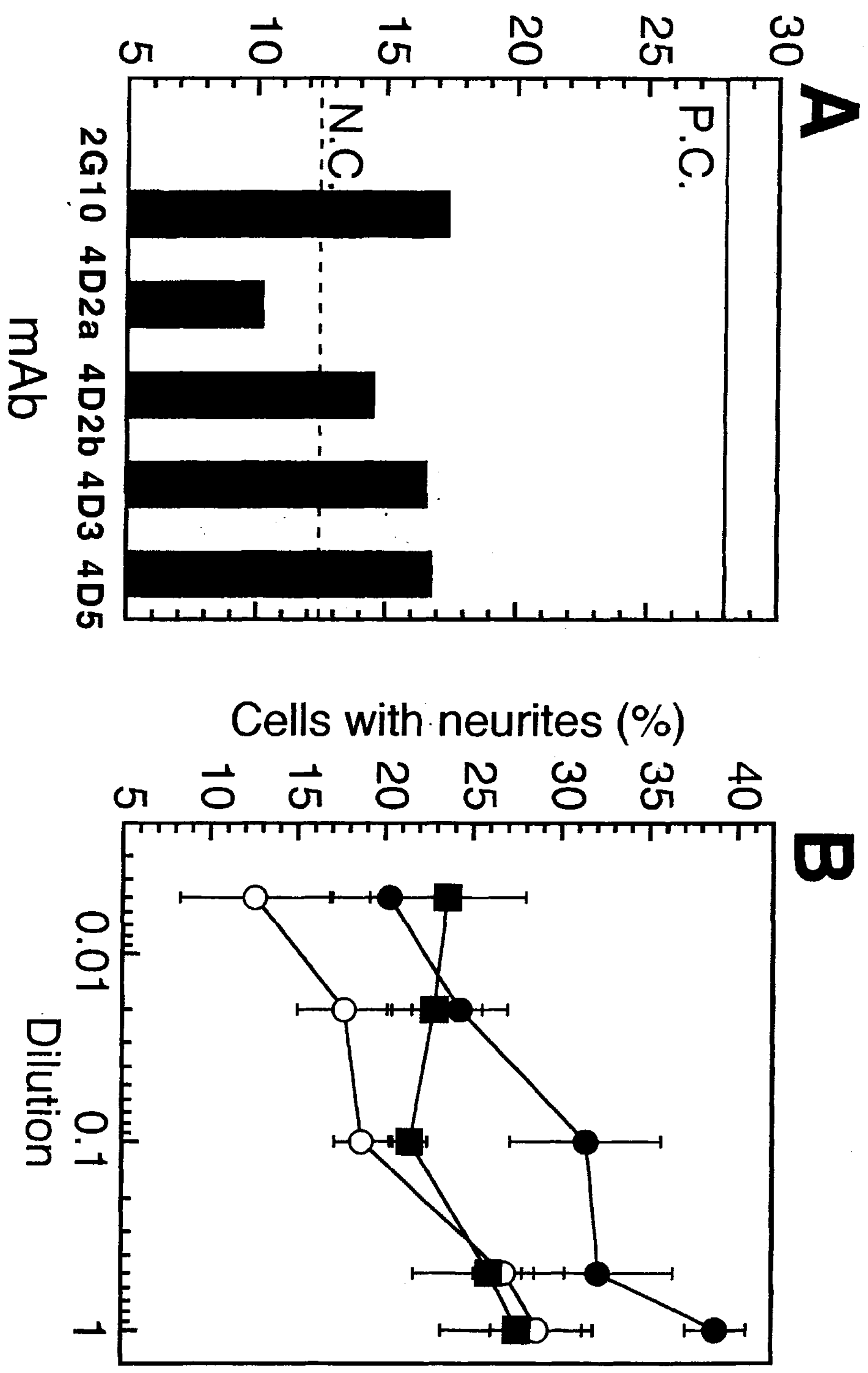
A
Cells with Neurites (%)
5
10
15
20
25
30
P.C.
N.C.
2G10
4D2a
4D2b
4D3
4D5
mAb
B
Cells with neurites (%)
5
10
15
20
25
30
35
40
0.01
0.1
1
Dilution

23.

Neurocrescin: a novel neurite-outgrowth factor secreted by muscle after denervation

Hiroshi Nishimune, *Atsuko Uyeda, *Masaki Nogawa, +Kazuhiro Fujimori & Takahisa Taguchi

Department of Organic Materials, Osaka National Research Institute AIST, Ikeda 563, Japan

*Department of Biophysical Engineering, Osaka University, Toyonaka 560, Japan

+Department of Anatomy, Fukui Medical School, Matsuoka, Fukui 910-11, Japan

Corresponding author : Takahisa Taguchi

Osaka National Research Institute, AIST, MITI

address : 1-8-31 Midorigaoka, Ikeda city, Osaka 563, Japan

telephone : +81-727-51-9524

fax : +81-727-51-9526

e-mail :taguchi@onri.go.jp

377

Neurons extend neurites to form synapses with target cells during the development of nervous systems. Furthermore, sprouting of axons represents one type of synaptic plasticity in mature neuronal circuits[1]. Some cue molecules that participate in these phenomena have recently been identified[2-9]. At neuromuscular junctions, denervation elicits axonal sprouting[10], and extracellularly secreted factors by muscle cells seem to induce sprouting of spinal neurons or elongation of the neurites[11, 12]. We report here the cloning from chick denervated skeletal muscle of a novel factor that promotes the outgrowth of neurites. The factor, designated neurocrescin, promoted the neurite-outgrowth from chick spinal cord and brain neurons. It was expressed predominantly in neural tissue and was secreted extracellularly after intramolecular cleavage. The truncated form was detected in denervated muscle but not in innervated muscle, and also in limb buds and the telencephalon of chicks at early stages of embryonic development but not at later stages. Highly homologous counterparts of chick neurocrescin were also cloned from mouse and rat. Thus, neurocrescin appears to be a novel neurite-outgrowth factor that is secreted in an activity-dependent fashion.

Synaptic connections seem likely to be selectively stabilized in an activity-dependent manner[13]. One form of neuronal plasticity, sprouting of axons, occurs at denervated neuromuscular junctions. This phenomenon can be inhibited by direct stimulation of denervated muscle. Thus the sprouting is promoted by muscle cells in an activity-dependent manner[10]. Moreover, culture medium that has been conditioned by muscle cells promotes the neurite-outgrowth from spinal neurons[11]. The neurite-promoting activity found in a soluble protein fraction of crus muscle was increased after sciatic nerve denervation[12]. These observations suggest the existence of extracellular factors that promote the neurite-outgrowth from spinal neurons. Brain neurons also respond to factors in denervated muscle, indicating that some similar factor(s) is expressed and functional in the brain[14].

To identify factors that promote the neurite-outgrowth, we immunoscreened a cDNA library of denervated muscle with an antibody that inhibited the neurite-promoting activity in an extract of denervated muscle(DM extract) in culture[15]. A recombinant protein encoded by a cloned cDNA exhibited the neurite-promoting activity in a bioassay with cultured spinal or telencephalic neurons, therefore the product of this gene was designated neurocrescin[12, 14] (Fig. 1). The survival of these neurons was similar in culture dishes that contained 1 μg/ml neurocrescin, 1 μg/ml DM extract or no added protein. The number of surviving cells, 24 hr after seeding, normalized to results obtained with neurocrescin, was 90% with the DM extract and 91% in the absence of added protein. A dye-exclusion test for viability using trypan blue revealed that more than 85% of cells were viable under all tested conditions. Thus, neurocrescin promoted the neurite-outgrowth rather than survival.

Since the initially cloned cDNA lacked the 5' end sequence of the mRNA, we isolated a full-length cDNA by rescreening of library and applying the 5'RACE method[16]. The entire cDNA of neurocrescin was 3,336 nt in length and contained a single open reading frame (ORF) that encoded a protein of 782 amino acids (aa) (Fig. 2). The mRNA of neurocrescin revealed by northern blotting analysis corresponded in size to that of the cloned cDNA sequence, indicating that the entire length of the mRNA sequence was cloned (Fig. 4b).

We examined the expression pattern of neurocrescin mRNA in the chick embryo by *in situ* hybridization. The expression of neurocrescin was relatively strong in the brain, spinal cord, dorsal root ganglion, and sympathetic ganglion (Fig. 3a,d). Variations in levels of expression in internal organs of the chick on postnatal day 0 (P0) were examined by northern blotting analysis (Fig. 3g). The levels of expression decreased in the following order: denervated muscle > lung > gaster, gizzard > liver. The bias in levels of expression towards neural tissues suggests the neurite-promoting activity of neurocrescin *in vivo*.

Polyclonal antibody, raised against the recombinant neurocrescin, recognized proteins of 48, 112, 116 and 121 kD in the DM extract (Fig. 4a). Neurocrescin seemed to be modified post-translationally since the molecular mass calculated based on the deduced amino acid sequence of the ORF was 90 kD. Four putative sites for N-glycosylation and two leucine zipper motifs were found in the deduced amino acid sequence of neurocrescin (Fig. 2a). Peptide motifs typical of extracellular matrix proteins, LRE and LDV, were also found in neurocrescin (Fig. 2). These sequences were reported as the neural cell attachment site in laminin-ß2[17] and as integrin-binding site in fibronectin[18], respectively.

The 48-kD protein was only detected in denervated muscle and not in intact or sham-operated innervated muscle (Fig. 4a). Since the size and the level of the mRNA transcript was the same in denervated and innervated muscle (Fig. 4b), it appeared that cleavage of neurocrescin might be controlled posttranscriptionally by muscle activity.

The molecular mass of truncated neurocrescin coincided with the value obtained previously for the partially purified factor[19].

During the embryonic development of the chick, the expression of the truncated form of neurocrescin was also regulated. A 44 kD immunoreactive protein was detected in the limb bud and telencephalon on embryonic day five (E5) but not in the crus muscle and telencephalon on P0 (Fig. 4c). The expression of the immunoreactive 44-kD protein was strictly regulated, whereas the 112-, 116- and 121-kD proteins were expressed at similar respective levels throughout embryonic development.

Neurocrescin lacked a typical signal peptide sequence for secretion. To confirm the extracellular secretion of the protein, we expressed the entire ORF of neurocrescin in COS7 cells. The 48-kD immunoreactive protein was detected only in the conditioned medium (CM) of neurocrescin-expressing COS7 cells (Fig. 4d). The amino-terminal 12 amino acids of the secreted protein were identical to the amino acid sequence (residues 359 to 370) deduced from the ORF for neurocrescin (Fig. 2a). The secreted neurocrescin exhibited significant neurite-promoting activity for neurons from spinal cord and telencephalon (Fig. 1e). The truncated neurocrescin that had been secreted from COS7cells and the 48-kD protein detected in denervated muscle coincided in terms of both molecular mass and structure of the epitope, indicating that neurocrescin was cleaved and secreted after denervation of muscle.

The ability of neurocrescin to promote the neurite-outgrowth of telencephalic neurons suggested the likely expression of homologues in the brain, therefore, we attempted to clone a homologue of neurocrescin from chick brain mRNA by RT-PCR. Two cDNA clones were obtained, one for neurocrescin and one for neurocrescin with a different 5' end region (neurocrescin-β; Fig. 2). The expression of two neurocrescins in crus muscle of the chick (P0) was confirmed by RT-PCR (data not shown). cDNA clones for highly homologous genes that were expressed in the brain of the mouse and the rat were also obtained (Fig. 2). A search of the Genbank database was made for a human homologue of neurocrescin and a gene product designated rabaptin-5[20] was found that exhibited the strongest homology (Fig. 2b). Since the expression of rabaptin-5 in nervous tissue had not been examined, to our knowledge, we confirmed the expression of rabaptin-5 in the human brain by PCR using a whole brain cDNA library of fetal human and sequencing of the amplified product (rabaptin-5 cDNA, nucleotides 263-605 and 709-1044; data not shown). The amino acid sequences encoded by all six cDNAs were highly homologous. Furthermore, the sequence at the site of cleavage found in chick neurocrescin was completely conserved among all four species (Fig. 2b). The strong homology between the homologues of neurocrescin in the chick, rat, mouse and human indicates the conserved biological function of this gene product.

The neurally biased pattern of expression of neurocrescin mRNA suggests an important role for this factor in the nervous system. We revealed the extracellular secretion of neurocrescin, despite the lack of signal peptide sequence for secretion, and the neurite-promoting activity of secreted protein. The mechanism of this secretion may involve the interaction of neurocrescin with Rab proteins, since neurocrescin had strong homology with rabaptin-5[20]. The observation that the truncated form of neurocrescin is only detected on the early embryonic stages suggests the contribution of neurocrescin in neuronal network formation. Furthermore, the truncated form of neurocrescin was detected only after denervation in skeletal muscle. Therefore, this factor is be a target-

382

derived neurite-outgrowth factor, whose extracellular presentation is regulated in a neuronal activity-dependent manner.

Neurocrescin seems to function in innervation during embryonic development, as well as in regeneration during neuromuscular re-innervation. We are now examining roles of neurocrescin in the formation of the neural network in development and in synaptic function, using our culture system designed for analysis of synaptogenesis[21, 22]. Neurocrescin can be expected to contribute to efforts at neural regeneration in attempts to treat neurodegenerative diseases.

Methods

Denervation. Sciatic nerve denervation of chicks on P5 was performed as described previously[12]. Three days after operation, denervated crus muscle was excised for preparation of a tissue extract and of mRNA[14].

cDNA cloning. A cDNA library of denervated muscle was constructed with a Zap-cDNA synthesis kit (Stratagene), and it was immunoscreened with monoclonal antibody 4D2a[15]. The 5' end sequences of cDNAs were obtained with the 5'-Amplifinder RACE kit (Clontech). cDNA for homologues of neurocrescin were obtained by RT-PCR from mRNA isolated from the chick (E8) telencephalon and from the brains of adult ICR mice and adult SD rats. cDNA for human rabaptin-5 was amplified by PCR from a cDNA library of human fetal normal, whole brain (Caucasian, 19-23 weeks gestation; Clontech).

Neurite-outgrowth assay. The promotion of neurite-outgrowth was analyzed *in vitro* in the previously described assay system[12, 14]. In brief, telencephalon and spinal cord were excised from chick embryos (E5), treated with trypsin and dissociated. The cells were plated in 24-well dishes (Coaster) at a density of 40,000 cells per well. For bioassays of neurocrescin, a clone that encoded the carboxyl-terminal 30 kD portion of the protein was used. Recombinant neurocrescin was expressed in *E. coli,* cleaved from the fusion protein and purified to homogeneity using the GST expression system (Pharmacia). The culture medium of transfected COS7 cells was added to the neuronal culture at 5μg/ml protein concentration without purification. Neurons with neurites of more than two cell diameters in length were counted 24 hr after plating. Neurite-promoting activity was expressed as the percentage of cells with neurites relative to the total number of surviving cells.

Expression in COS7 cells. Expression of neurocrescin in COS7 cells was achieved by transfection with cDNA in the pEF-BOS vector[23] using LipofectAMINE reagent (GIBCO BRL). The culture medium was collected and concentrated 14-fold with Centriprep-10 (Amicon). Equal volumes of concentrated medium were used for western blotting analysis. The amino-terminal sequence of the secreted protein was analyzed by Edman degradation with an automated protein-sequencing system (HP G1005A; Hewlett Packard), after purification by SDS-polyacrylamide gel electrophoresis.

Western and northern blotting analysis. Polyclonal antibodies against neurocrescin were raised by immunization of rabbits with the purified recombinant carboxy-terminal 30 kD region of neurocrescin and purified by passage through an antigen-linked affinity column. Soluble fractions of tissue extracts were prepared for western blotting analysis as described previously[15]. For northern blotting analysis, 2 μg of poly(A)$^+$RNA from each sample was subjected to electrophoresis and then transferred to an Immobilon N membrane (Millipore). Blots were probed with RNA probes labeled with [^{32}P]UTP for neurocrescin (nucleotides 1580-2238) and chick glyceraldehyde-3-phosphate dehydrogenase (GAPDH; nucleotides 138-950)[24].

***In situ* hybridization.** Chicks (E8) were fixed in 4% paraformaldehyde and sectioned at 20-30 μm. Sections were processed for *in situ* hybridization as described previously [25]. An antisense RNA probe and a sense RNA probe corresponding to nucleotides 1996 to 2238 and nucleotides 752 to 926, respectively, of the cDNA for chick neurocrescin were labeled with [^{35}S] UTP.

References

1. Tsukahara, N. Synaptic plasticity in the mammalian central nervous system. *Annu. Rev. Neurosci.* **4**, 351-379 (1981).
2. Serafini, T., *et al.* The netrins define a family of axon outgrowth-promoting proteins homologous to C. elegans UNC-6. *Cell* **78**, 409-424 (1994).
3. Kennedy, T.E., *et al.* Netrins are diffusible chemotropic factors for commissural axons in the embryonic spinal cord. *Cell* **78**, 425-435 (1994).
4. Keino-Masu, K., *et al.* Deleted in Colorectal Cancer (DCC) encodes a netrin receptor. *Cell* **87**, 175-185 (1996).
5. Luo, Y., Raible, D. & Raper, J.A. Collapsin: a protein in brain that induces the collapse and paralysis of neuronal growth cones. *Cell* **75**, 217-27 (1993).
6. Cheng, H.J., *et al.* Complementary gradients in expression and binding of ELF-1 and Mek4 in development of the topographic retinotectal projection map. *Cell* **82**, 371-381 (1995).
7. Drescher, U., *et al.* In vitro guidance of retinal ganglion cell axons by RAGS, a

25 kDa tectal protein related to ligands for Eph receptor tyrosine kinases. *Cell* **82**, 359-370 (1995).

8. Chiba, A., *et al.* Fasciclin III as a synaptic target recognition molecule in Drosophila. *Nature* **374**, 166-168 (1995).
9. Schuster, C.M., *et al.* Genetic dissection of structural and functional components of synaptic plasticity. II. Fasciclin II controls presynaptic structural plasticity. *Neuron* **17**, 655-667 (1996).
10. Brown, M.C. & Holland, R.L. A central role for denervated tissue in causing nerve sprouting. *Nature* **282**, 724-726 (1979).
11. Henderson, C.E., Huchet, M. & Changeux, J.-P. Neurite outgrowth from embryonic chicken spinal neurons is promoted by media conditioned by muscle cells. *Proc. Natl. Acad. Sci. USA* **78**, 2625-2629 (1981).
12. Henderson, C.E., Huchet, M. & Changeux, J.-P. Denervation increases a neurite-promoting activity in extracts of skeletal muscle. *Nature* **302**, 609-611 (1983).
13. Changeux, J.-P. & Danchin, A. Selective stabilization of developing synapses as a mechanism for the specification of neuronal networks. *Nature* **264**, 705-712 (1976).
14. Taguchi, T., *et al.* A subpopulation of embryonic telencephalic neurons survive and develop in vitro in response to factors derived from the periphery. *Dev. Brain Res.* **37**, 125-132 (1987).
15. Nishimune, H., *et al.* Characterization of neurite-outgrowth promoting factors in extracts of denervated chick skeletal muscles. *Submitted* .

16. Frohman, M.A., Dush, M.K. & Martin, G.R. Rapid production of full-length cDNAs from rare transcripts: amplification using a single gene-specific oligonucleotide primer. *Proc. Natl. Acad. Sci. USA* **85**, 8998-9002 (1988).

17. Hunter, D.D., *et al.* Primary sequence of a motor neuron-selective adhesive site in the synaptic basal lamina protein S-laminin. *Cell* **59**, 905-913 (1989).

18. Komoriya, A., *et al.* The minimal essential sequence for a major cell type-specific adhesion site (CS1) within the alternatively spliced type III connecting segment domain of fibronectin is leucine-aspartic acid-valine. *J. Biol. Chem.* **266**, 15075-15079 (1991).

19. Taguchi, T. & Henderson, C.E. in *New concepts in Alzheimer's disease* (eds. Briley, M., Kato, A. & Weber, M.) 203-215 (MacMillan, London, 1986).

20. Stenmark, H., *et al.* Rabaptin-5 is a direct effector of the small GTPase Rab5 in endocytic membrane fusion. *Cell* **83**, 423-432 (1995).

21. Tokioka, R., *et al.* Synapse formation in dissociated cell cultures of embryonic chick cerebral neurons. *Dev. Brain Res.* **74**, 146-150 (1993).

22. Kiyosue, K., Kasai, K. & Taguchi, T. Two modes of activity-dependent synaptogenesis of cerebral neurons *in vitro*. *Neuroreport* **7**, 701-704 (1996).

23. Mizushima, S. & Nagata, S. pEF-BOS, a powerful mammalian expression vector. *Nucleic Acids Res.* **18**, 5322 (1990).

24. Dugaiczyk, A., *et al.* Cloning and sequencing of a deoxyribonucleic acid copy of glyceraldehyde-3-phosphate dehydrogenase messenger ribonucleic acid isolated from chicken muscle. *Biochemistry* **22**, 1605-1613 (1983).

25. Simmons, D.M., Arriza, J.L. & Swanson, L.W. A complete protocol for *In Situ*

hybridization of messenger RNAs in brain and other tissues with radio-labeled single-stranded RNA probes. *J. Histotech.* **12**, 169-181 (1989).

Acknowledgments. We thank M. Kasai and C. E. Henderson for helpful discussions, H. Fujimoto for technical assistance, S. Nagata for the pEF-BOS vector, Y. Shigeri for COS7 cells and A. Satake for encouragement. H.N. is a research fellow of JST.

Correspondence and requests for materials should be addressed to T.T. (e-mail: taguchi@onri.go.jp). The DNA sequence has been submitted to DDBJ/GenBank under accession numbers: cNeurocrescin, D38038; cNeurocrescinß, D88828; mNeurocrescin, AB001750; mNeurocrescinß, D86066; rNeurocrescinβ, D85844.

Legends to figures

Figure 1 Neurite-promoting activity of neurocrescin. **a,b,** The activity of the recombinant neurocrescin in culture. Neurocrescin promoted the neurite-outgrowth from neurons isolated from the spinal cord (**a**) and telencephalon (**b**) of the embryonic chick (E5; solid circles). The DM extract, used as a control (solid squares), promoted the neurite-outgrowth from both neurons, as reported previously[12, 14]. No promotion was obserbed in the absence of added protein (open circles). The data are the means ± standard errors of four determinations. **c,d,** The morphology of cultured neurons from the spinal cord (**c**) and telencephalon (**d**) was photographed 24 hr after plating in wells that contained 5 µg/ml recombinant neurocrescin. Scale bar, 50 µm. **e,** The activity of the

secreted neurocrescin from COS7 cells. Culture medium of neurocrescin expressing COS7 cells promoted the neurite outgrowth from neurons isolated from the spinal cord and telencephalon of the embryonic chick (E5; solid bar). Only little promotion was observed by the culture medium of vector transfected COS7 cells(open bar).

Figure 2 Primary structure of chick neurocrescin aligned with homologues. **a,** Amino acid sequences of neurocrescins. The boxed region in chick neurocrescin matched the amino-terminal sequence of the protein secreted from transfected COS7 cells. Four putative sites for N-glycosylation are marked by asterisks. Leucine zipper motifs are underlined. Peptide sequences found in extracellular matrix proteins are doubly underlined. Six neurocrescins were aligned and the matching regions are shaded. Note that only the sequence of chick neurocrescin is given after residue number 23. **b,** Schematic representation of the various ORFs and untranslated regions. Four features of chick neurocrescin are conserved in all six sequences. Identity scores indicated on the right were obtained from comparisons with the region that overlap chick neurocrescin. cNeurocrescin, chick neurocrescin; cNeurocrescinβ, chick neurocrescin-β; mNeurocrescin, mouse neurocrescin; mNeurocrescinβ, mouse neurocrescin-β; rNeurocrescinβ, rat neurocrescin-β.

Figure 3 Intense expression of neurocrescin in the nervous system. **a-f,** Expression of neurocrescin mRNA in chick embryos at E8 as revealed by *in situ*

hybridization. Sagittal section of the chick head (**a**,**b**,**c**) and transverse section of the body (**d**,**e**,**f**) were allowed to hybridize with antisense (**a**,**d**) and sense (**c**,**f**) RNA probes for neurocrescin. Cresyl violet-stained sections corresponding to **a** and **d** are shown in **b** *and* **e**. Scale bar, 2 mm. **g**, Distribution of neurocrescin in the internal organs of the chick (P0) as revealed by northern blotting analysis. The signal of GAPDH was used to monitor the amounts of mRNA loaded in each lane.

Figure 4 Regulated expression of truncated neurocrescin in muscle and its secretion from COS7 cells. **a**, Western blotting analysis of neurocrescin from denervated, intact, and sham-operated (innervated) crus muscle of the chick (P8). **b**, Northern blotting analysis of neurocrescin in denervated and intact crus muscle of the chick (P8). Note that no truncated mRNA was detected. **c**, Developmentally regulated expression of truncated neurocrescin. Immunoreactive 44-kD protein was detected in the limb bud and telencephalon of the embryonic chick (E5). **d**, Secretion of neurocrescin from transfected COS7 cells. Immunoreactive 48-kD protein was detected in the conditioned medium (CM) of neurocrescin-expressing cells. The protein of 92 kD corresponds to the product of the entire ORF for transfected neurocrescin.